

PDF hosted at the Radboud Repository of the Radboud University Nijmegen

The following full text is a publisher's version.

For additional information about this publication click this link.

<http://hdl.handle.net/2066/19012>

Please be advised that this information was generated on 2017-12-05 and may be subject to change.

Nanosized Architectures from Glycoluril Building Blocks

Nanosized Architectures from Glycoluril Building Blocks

EEN WETENSCHAPPELIJKE PROEVE OP HET GEBIED VAN
DE NATUURWETENSCHAPPEN, WISKUNDE EN INFORMATICA

PROEFSCHRIFT

TER VERKRIJGING VAN DE GRAAD VAN DOCTOR
AAN DE KATHOLIEKE UNIVERSITEIT NIJMEGEN,
VOLGENS BESLUIT VAN HET COLLEGE VAN DECANEN
IN HET OPENBAAR TE VERDEDIGEN OP DINSDAG 25 SEPTEMBER 2001
DES NAMIDDAGS OM 1.30 UUR PRECIES

DOOR

JOHANNES ALBERTUS ANTONIUS WILHELMUS ELEMANS

GEBOREN OP 5 JULI 1970 TE NIJMEGEN

Promotor: Prof. dr. R. J. M. Nolte
Copromotor: Dr. A. E. Rowan

Manuscriptcommissie: Prof. dr. ir. J. C. M. van Hest
Dr. J. N. H. Reek (UVA)
Dr. R. P. Sijbesma (TUE)

ISBN 90-9015039-0

Contents

Introduction	1
Chapter 1 The story of glycoluril	3
Chapter 2 Molecular clips with functionalized convex sides	23
Chapter 3 Controlled self-assembly of rigid facial amphiphiles	43
Chapter 4 Controlled self-assembly of metaloclips	57
Chapter 5 Host-guest complexes with tunable solid state structures	81
Chapter 6 Self-assembled molecular clip dendrimers	105
Chapter 7 A conductive molecular clip polymer	133
Chapter 8 Molecular clip porphyrin arrays	141
Chapter 9 Porphyrin clips	175
Chapter 10 Porphyrin clips as epoxidation catalysts	211
Summary	223
Samenvatting	225
List of publications	227
Bedankt...	229
Curriculum vitae	233

Introduction

The spontaneous assembly of simple organic and inorganic molecules into architectures of nanometer size is an extremely challenging area in the field of supramolecular chemistry. Although in recent literature there have appeared many examples of such systems, somewhat surprisingly there is a lack of progress in controlling their precise shape and size. The research described in this thesis mainly deals with the self-assembly of molecular clips into nanosized architectures of such controlled shape and size. The molecular clips (Figure 1a) are derived from diphenylglycoluril. They have a rigid, U-shaped cavity and are ideal hosts for dihydroxybenzene derivatives, *e.g.* resorcinol and catechol. These guests are bound in the cavities due to a combination of hydrogen bonding and π - π interactions (Figure 1b). Over the past two decades, a wide variety of these cavities have been synthesized which possess various functionalities. These clips have been applied in different areas, *e.g.* as supramolecular catalysts, as mesogens forming liquid crystals, and as amphiphiles. Very recently it has been discovered that in the absence of a guest the clips dimerize with one side-wall filling the cavity of its dimeric partner and *vice-versa* (Figure 1c). This propensity to dimerize is utilized in several of the self-assembled architectures that are described in this thesis.

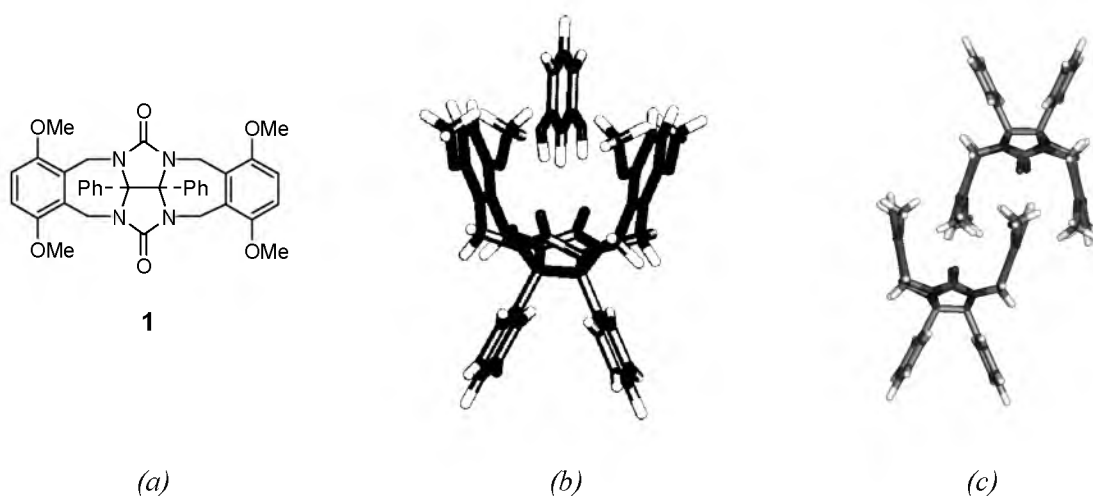


Figure 1 (a) Structure of a molecular clip (**1**) derived from diphenylglycoluril. (b) Computer modelled structure of **1** with a bound 1,3-dihydroxybenzene guest. (c) Structure of a dimer of **1**.

This thesis starts with a review of the basic supramolecular chemistry of glycoluril (Chapter 1). In Chapter 2, the design and synthesis of a new generation of molecular clips with modified convex sides is described. The modifications introduced allow functionalization of the ‘back sides’ of the clips, while their cavities are unaffected and hence remain available for guest binding and dimerization. The behaviour of clips functionalized at their convex side with various groups, which make them water-soluble, liquid-crystalline, etc. is the subject of Chapters 3-8.

In Chapters 3 and 4, the self-assembling properties of water-soluble clips functionalized with benzoic acid substituents and ruthenium bipyridine centers are discussed. The self-association of these molecules in water has been studied in detail with the help of spectroscopic methods and electron microscopy. It is shown that recognition information encoded in these molecules can lead to the formation of various well-defined superstructures of nanometer size.

Chapters 5 and 6 are dealing with the self-assembly of molecular clips in the solid state. Clips functionalized on their convex side with *n*-alkyl tails form lamellar plastic crystals, the properties of which can be fine-tuned by the complexation of guest molecules. Clips functionalized with branched tails self-assemble into cubic liquid crystals with molecular recognition properties.

The synthesis and characterization of a conducting polymer derived from thiophene-functionalized clips are described in Chapter 7. In Chapter 8, several approaches to construct porphyrin arrays based on molecular clips are presented. The first approach involves the complexation of clips provided with *n*-alkyl tails to a tetrafunctional guest porphyrin. The obtained 4:1 complex self-assembles both in solution and in the solid state to give large porphyrin arrays. In a similar approach, four clips functionalized on their convex sides with two porphyrins are complexed to a central porphyrin guest, forming a nonameric porphyrin assembly. The final approach deals with the metal-templated assembly of two basket-shaped clip molecules, functionalized with two pendant porphyrins, around a central tetrapyrrolyl porphyrin, thus forming a capsule-shaped architecture.

The subjects of Chapters 9 and 10 are the synthesis and physical properties of porphyrin capped molecular clips. These turn out to be very strong binders of viologens and pyridines. Manganese derivatives of these porphyrin clips are utilized as catalysts for the epoxidation of simple olefins. It will be shown that, depending on the axial ligand used, a strong increase in catalyst activity or catalyst stability can be accomplished.

Summaries in English and Dutch conclude this thesis.

Chapter 1

The Story of Glycoluril

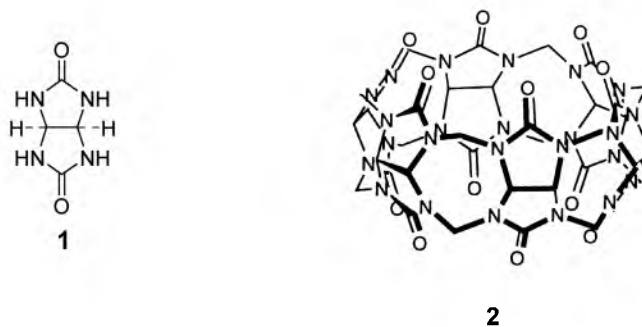
1.1 Introduction

During the last two decades, the concave building block glycoluril **1** has been used as a versatile starting component in the synthesis of a wide variety of molecular receptors. More recently its versatility has been further expanded with its incorporation within well-defined self-assembled nanostructures. This chapter gives an overview of the most recent developments in glycoluril-based supramolecular chemistry. In section 1.2, the properties of the ‘parent’ compound, the hexameric glycoluril macrocycle cucurbituril will be described. Initially used as a receptor for cations, cucurbituril has revealed itself as a stable ring component in the synthesis of oligo- and polyrotaxane architectures. In section 1.3, an overview will be given of the many capsule-like assemblies developed by Rebek’s group over the past couple of years. In the final section (1.4), the most recent developments in molecular clip chemistry will be discussed. Some of this chemistry has served as a base for this thesis.

1.2 Cucurbituril

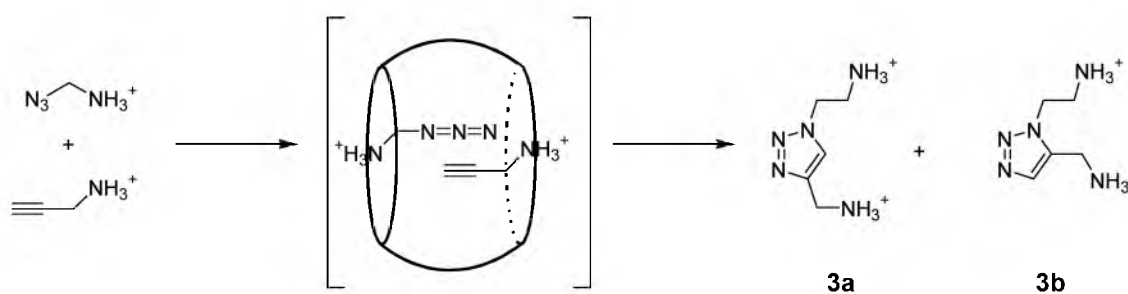
1.2.1 Introduction

'The story of glycoluril' began in 1905, when Behrend *et al.* published the results of an acid-induced condensation reaction of urea, glyoxal and formaldehyde.¹ The product was characterized as $C_{10}H_{11}N_7O_4 \cdot 2H_2O$ (**2**), however no structure was postulated. The compound proved to be very stable towards strong acids and bases, and it was found to form crystalline complexes with a variety of metal salts. It was nearly 80 years later, in 1981, when Freeman *et al.* solved the crystal structure of the calcium bisulfate complex of **2**, that it became clear that the compound was a cyclic hexamer of glycoluril units linked by methylene bridges.² The cyclic hexamer was named 'cucurbituril', because of its resemblance to a pumpkin (latin name: *cucurbita*).³ A remarkable feature of cucurbituril is its internal cavity, which has a diameter of approximately 5.5 Å and is accessible via two portals 4 Å wide. As a consequence of this architecture it has been used as a receptor for a variety of (di-)ammonium ions, as a building block in rotaxane synthesis, and as a macrocyclic component in an interfacial condensation polymerization.⁴



1.2.2 Cucurbituril as a receptor

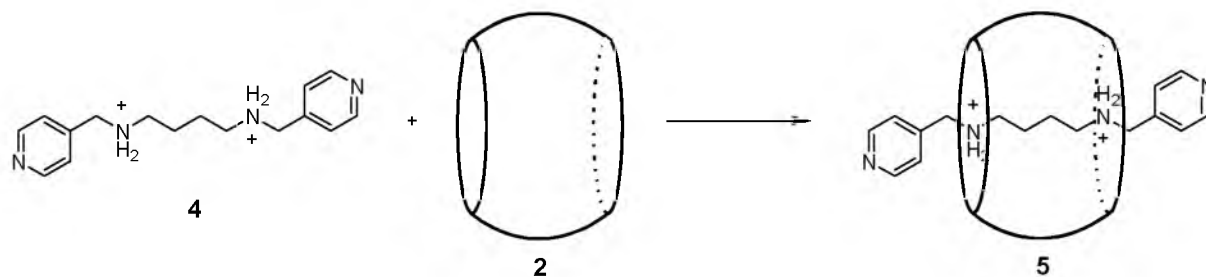
Crystallographic studies⁵ and NMR spectroscopy complexation studies⁶ revealed that cucurbituril binds various small organic compounds in aqueous solution. Although it has been reported that also neutral aliphatic compounds are complexed by **2**,⁷ the macrocycle has been predominantly used to bind alkyl(di)ammonium compounds. Protonated (di-)amines are perfectly suited to interact with the carbonyl groups lining the portals of **2** by means of favourable cation-dipole interactions. When a hydrocarbon chain is attached to the amine, the former is included within the cavity due to a hydrophobic driving force, *i.e.* upon entering the cavity water molecules are liberated which are taken up in the bulk solvent. Binding affinities toward α,ω -diamino-*n*-alkane guests in acidic aqueous solution were found to strongly depend on the length of the alkyl chain. The order of affinity followed the trend $\text{NH}_2(\text{CH}_2)_n\text{NH}_2$, $n = 3 < 4 < 5 < \underline{6} > 7 > 8 > 9 > 10$. For the binding between **2** and 1,6-hexamethylenediamine, an association constant $K_a = 2.5 \times 10^6 \text{ M}^{-1}$ was measured, and NMR studies in $\text{HCOOH-D}_2\text{O}$ solution showed that the host-guest complex and its components exchanged slowly on the NMR timescale. The binding of the guest within the cavity was further confirmed by the observation of upfield shifts for the resonances of all protons of the alkyl chain in the host-guest complex, suggesting shielding by the cucurbituril interior.



Scheme 1.1 1,3-Dipolar cycloaddition between (protonated) propargylamine and (protonated) azidoethylamine, and the proposed intermediate in the reaction catalyzed by **2**.

The internal cavity of **2** is also sufficiently large to accommodate aliphatic and aromatic five-membered rings, and consequently the macrocycle was investigated as a microreactor in 1,3-dipolar cycloaddition reactions.⁸ The uncatalyzed reaction between propargylamine and azidoethylamine yields a mixture of two regioisomeric diazole adducts **3a** and **3b** (Scheme 1.1), which are formed in equal amounts by a standard concerted process. In the presence of a catalytic amount of **2** the rate of this reaction was considerably accelerated (55,000 x). In addition, the 1,4-disubstituted product **3a** was exclusively formed. These results were explained by assuming the formation of a transient ternary complex between cucurbituril and the two

reactants (see Scheme 1.1). The alkyne and azide are bound simultaneously in the portals of **2**, with the acetylene and azide substituents extending into the core of the host. In this way, these reactive groups are perfectly aligned with respect to each other and a quick reaction can occur. Not unexpectedly, the release of the pseudorotaxane product, which has a higher affinity for the host than each of the both reactants, is the rate-limiting step. In more recent work Tuncel and Steinke have shown that this cucurbituril catalyzed Diels-Alder reaction can also be applied in the synthesis of polyrotaxanes.⁹



Scheme 1.2 Synthesis of the cucurbituril derived [2]pseudorotaxane **5**.

1.2.3 Cucurbituril rotaxanes

Due to its 'hole' the cucurbituril macrocycle has been utilized as a cyclic component in the construction of (poly)rotaxanes. The latter structures have received considerable interest in recent years due to their potential application as new materials.¹⁰ Buschmann and coworkers have described the construction of bipyridinium-cucurbituril pseudo-rotaxanes,¹¹ and also the synthesis of polyrotaxanes with cucurbituril as the linear component and polyamides as the linear chain.¹² Kim and coworkers have carried out some very elegant studies on the coupling of cucurbituril pseudo-rotaxanes using transition metal centers. The recurring theme in this work is the very efficient threading of the dication *N,N'*-bis(4-pyridylmethyl)-1,4-diaminobutane dihydronitrate or -chloride **4** in the cucurbituril macrocycle. The pseudo-rotaxane **5**, which is obtained in 83% yield by just stirring the two components in aqueous solution, is the exclusive and stable product (Scheme 1.2).¹³ The pyridine functions on both termini of the linear component allow coordination to transition metals, resulting in the formation of oligo- and polyrotaxanes. The morphology of these rotaxanes is strongly dependent on the metal coordination geometry. Reaction of pseudorotaxane **5** with $\text{Cu}(\text{NO}_3)_2$ gave rise to the formation of a coordination polymer, the chain of which is composed of alternating copper ions and **5**.¹⁴ Its crystal structure showed that the polymer had a 'zig-zag' shape due to the *cis*-coordination of the pyridine ligands at each copper center.

In analogy to the strategy of the synthesis of circular metallo-assemblies by Fujita¹⁵ and Stang,¹⁶ reaction of **5** with $[\text{Pt}(\text{en})](\text{NO}_3)_2$ (*en* = ethylenediamine) resulted in the nearly quantitative one-pot synthesis of a so-called 'molecular necklace', consisting of a cyclic trimer of **5**, *cis*-connected at the corners by the platinum centers (Figure 1.1).¹⁷ Its crystal structure determination confirmed this four-component structure, and suggested furthermore that van der Waals interactions between the outsides of the cucurbituril rings strongly favour the efficient formation of the 'necklace'. A five-component necklace was also prepared, however, using a different approach. 1,10-Phenanthroline was derivatized at the 2- and 9-positions with two linear pyridine-terminated chains to give molecule **6**, which was reacted with two equivalents of cucurbituril. To the resulting L-shaped pseudo-rotaxane $\text{Cu}(\text{NO}_3)_2$ was added, yielding a molecular necklace

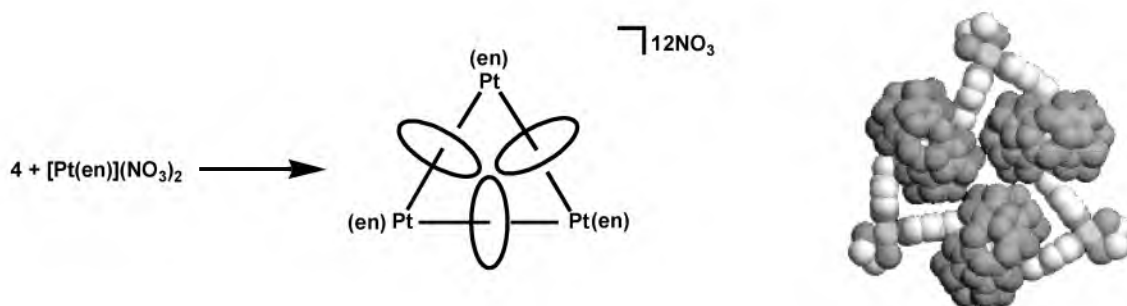


Figure 1.1 (a) Formation of a [4]rotaxane 'molecular necklace'. (b) Crystal structure of this compound.

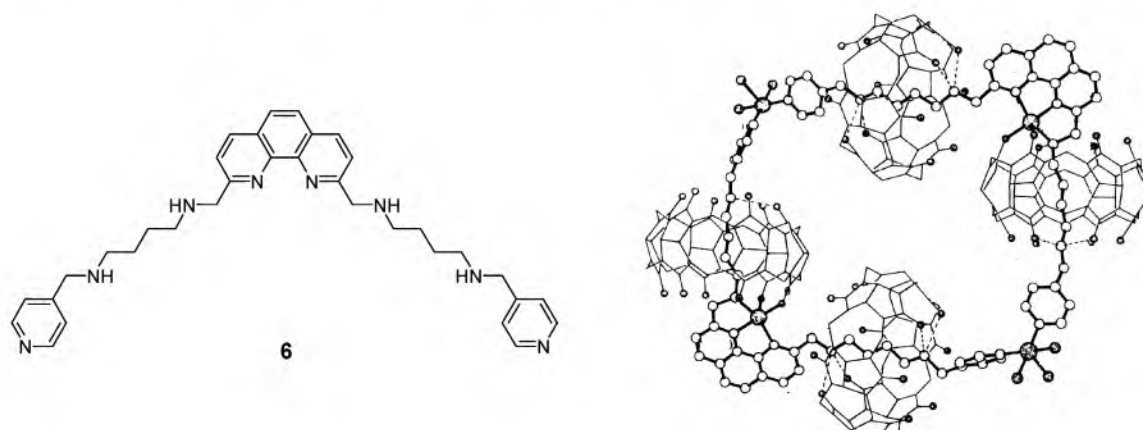


Figure 1.2 Crystal structure of the [5]rotaxane molecular necklace based on the L-shaped linear chain 6.

(Figure 1.2), the structure of which was confirmed by X-ray crystallography.¹⁸ The reaction of **5** with AgNO_3 as the coordinating metal resulted in an entirely different architecture, *viz.* a network consisting of large edge-sharing and chair-shaped hexagons with a silver ion at each corner and a molecule of **4** at each edge connecting two silver ions (Figure 1.3).¹⁹ The polyrotaxane network formed layers which were stacked on top of each other with an interplane separation of 9.87 Å. As mentioned above, variations in metal coordination geometry cause large changes in the resultant rotaxane geometries. If the nitrate anions were substituted by tosylate anions, only a one-dimensional (1D) coordination polymer was formed (Figure 1.3(a)). When the pyridyl groups in the linear unit were connected to the chain at the 3-position instead of the 4-position, a 1D coordination polymer arranged in a helical fashion was generated (Figure 1.3(b)).²⁰ The main key to the successful assembly of these cucurbituril pseudo-rotaxanes is the high affinity between the macrocycle and the diamino linear component. In addition, unlike for example cyclodextrins, which have also been widely used in rotaxane synthesis, the highly symmetrical structure of cucurbituril helps to form polyrotaxanes and networks with a high structural fidelity.

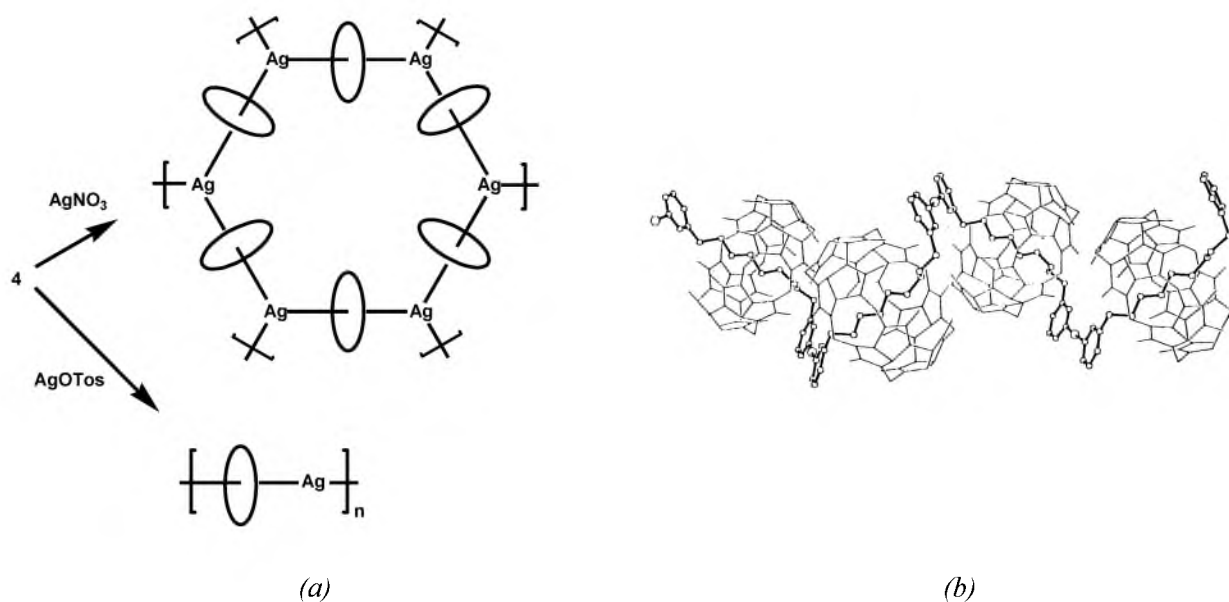


Figure 1.3 Cucurbituril rotaxanes based on Ag⁺ coordination polymers. (a) 2D and 1D polyrotaxanes. (b) Helical polyrotaxane and part of its crystal structure.

1.3 Molecular capsules

1.3.1 Introduction

The insolubility of the cucurbituril macrocycle in most common organic solvents restricts its use as receptor molecule to aqueous solutions. Attempts to solubilize the molecule by derivatizing it at its periphery with lipophilic side-groups, such as methyl or phenyl, were unsuccessful due to steric restrictions. The monomeric glycoluril building block, however, is a very versatile tool for the construction of 3D receptor molecules. During the past 5 years the literature concerning the self-assembly of glycoluril-based host molecules has been dominated by the work of the groups of Rebek²¹ and Nolte.²² The former group initially investigated the self-assembly of a bis-glycoluril building block into a so-called 'molecular tennis ball'.²³ The well-defined, pseudo-spherical capsule consists of two identical building blocks **7** (Figure 1.4), and is prepared by reacting tetrabromodurene with a large excess of diphenylglycoluril. Although the yield of the reaction is relatively low due to the formation of large amounts of polymeric material, the desired product can be obtained in nearly pure form by simple extraction of the crude product with chloroform.

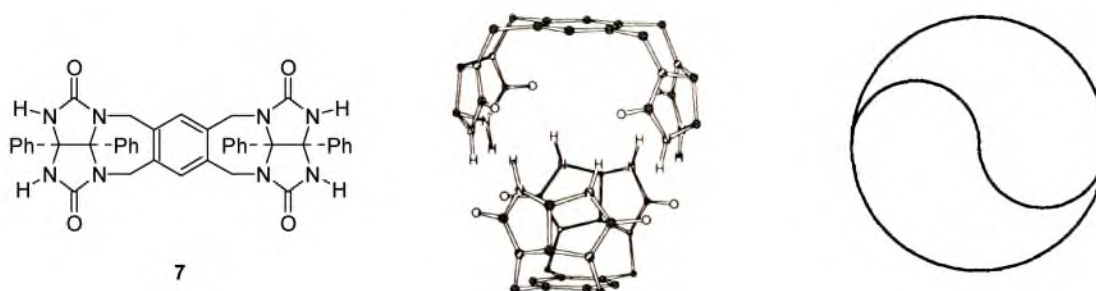
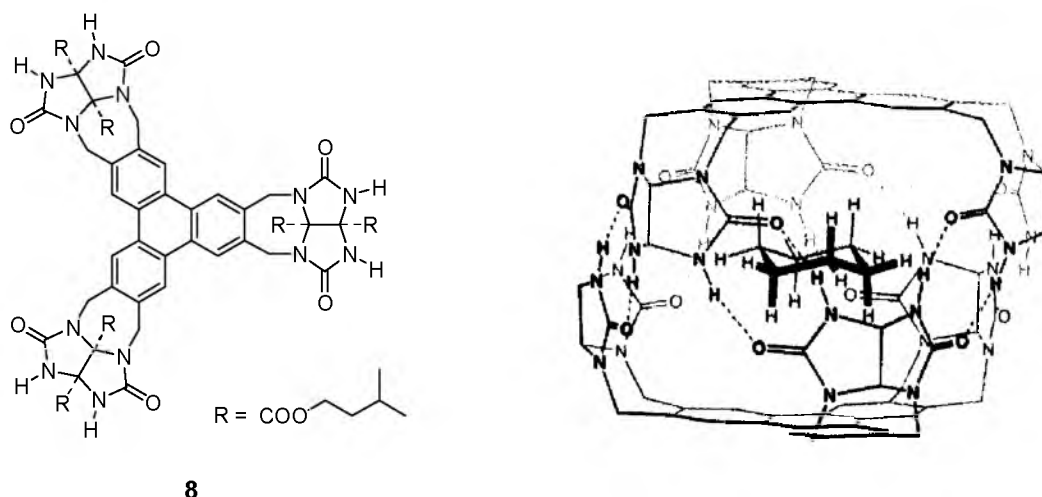


Figure 1.4 Assembly of two molecules of **7** into a dimer resembling a 'tennis ball'.



8

Figure 1.5 Assembly of two molecules of **8** into a dimer resembling a 'jelly doughnut', which can encapsulate a cyclohexane molecule.

1.3.2 Tennis balls, jelly doughnuts and softballs

Building block **7** has several hydrogen bond donor and acceptor functionalities, which in combination with the intrinsic rigid curvature of the molecule allows the formation of a dimeric sphere-like structure by self-assembly. The obtained capsule, **7-7**, is stabilized by a seam of 8 hydrogen bonds, and is formed both in solution and in the solid state.²⁴ In solution, small guests such as methane²⁵ and xenon²⁶ can be included in the cavity, which exhibit properties different from guests outside the capsule. In the development of larger capsules it is important to specifically design molecules which, despite their larger dimensions, can still form self-complementary hydrogen bonding networks. This was accomplished by the group of Rebek using three instead of two glycoluril units coupled to a central aromatic framework (**8**, Figure 1.5).²⁷ Two molecules of **8** were found to self-assemble giving a capsule (**8-8**), with an aromatic roof and an aromatic floor, held together by a seam of 12 hydrogen bonds. This capsule, which was given the name 'jelly doughnut' because of its flattened shape, was predicted to be a perfect host for cyclohexane on the base of molecular modeling calculations. This indeed turned out to be the case with the binding being enthalpically driven by favorable C-H $\cdots\pi$ interactions between the axial hydrogen atoms of the guest and the aromatic surfaces of the capsule. As a result of the inclusion within the capsule the ring-inversion barrier of the encapsulated cyclohexane was found to be 1.25 kJ mol⁻¹ higher than that of free cyclohexane. In an even larger system, **9**, two glycoluril units were connected across 7 rings, of which the central one contains an ethylene bridge function that supplies the required curvature for a hydrogen-bonded dimerization reaction. Structures **9a** and **9b** dimerize forming a capsule resembling a 'softball', held together by 8 hydrogen bonds (Figure 1.6(a)). For these molecules, the molecular programming encoded within the monomer also allows higher order aggregates to form.²⁸ As a consequence, **9c** which possesses four additional hydrogen bonding donors was designed and synthesized. It was found to give a capsule dimer in preference to other assemblies.²⁹ Interestingly, guest encapsulation by **9c-9c** is an entropy-driven process, which was concluded from the fact that the association constant increases with temperature. This was unexpected, since most host-guest complexation processes in organic solution are entropically unfavourable and enthalpy-driven. Upon binding of a guest, *e.g.* adamantane or ferrocene, in **9c-9c**, two molecules of solvent which are present in the cavity are released, resulting in a favourable

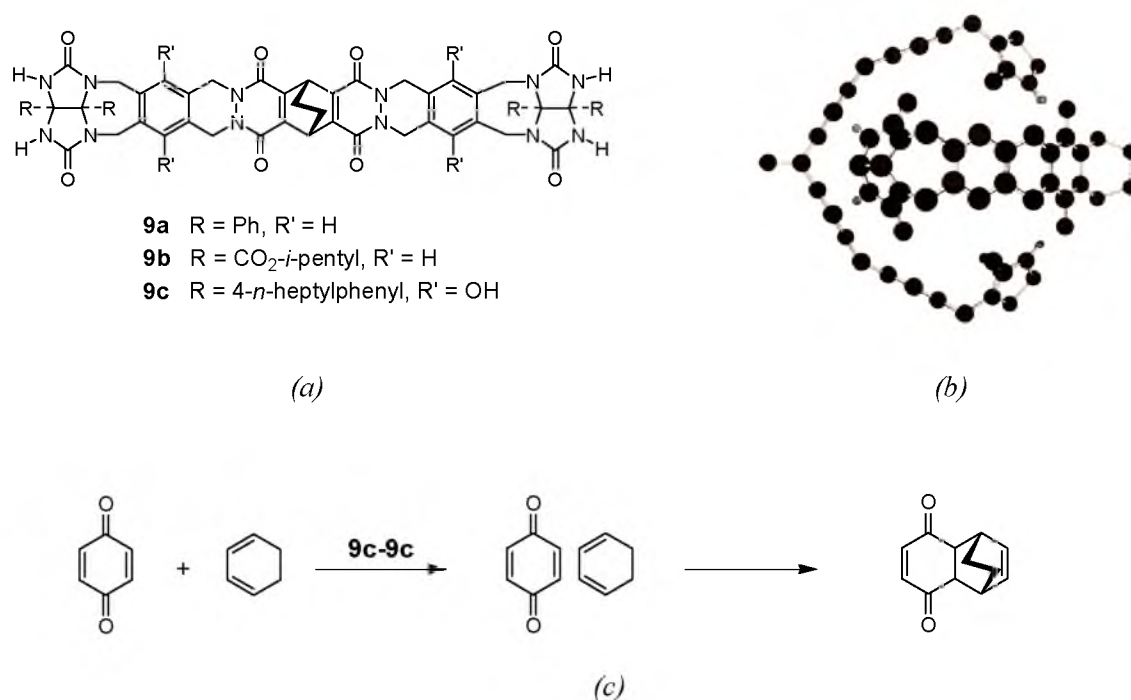
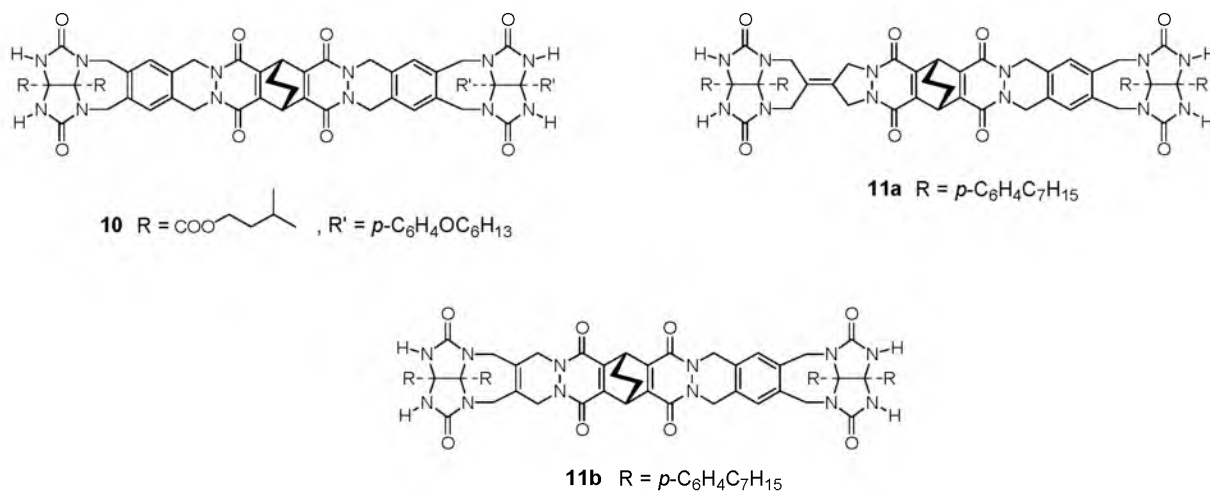


Figure 1.6 (a) Bis-glycoluril compounds which assemble into 'softball'-like dimers. (b) Computer modeled structure of the softball formed from two molecules of **9a**. (c) Schematic representation of the Diels-Alder reaction between cyclohexadiene and *p*-benzoquinone catalyzed by the microreactor **9c-9c**.

increase in entropy. Additional evidence for this binding mechanism came from studies of **9c** in a mixture of fluorobenzene and hexadeuteriobenzene. NMR spectroscopy revealed the presence of three different capsule species, confirming that two solvent molecules occupy the capsule before guest inclusion occurs.

1.3.3 Softballs as microreactors

An interesting application which utilizes the fact that two solvent molecules occupy the cavity, is the exploitation of the softball as a microreactor for bimolecular reactions. An example is depicted in Figure 1.6(b), *viz.* the Diels-Alder reaction between *p*-benzoquinone and cyclohexadiene.³⁰ In *p*-xylene-*d*₁₀ solution, the rate of this reaction is 200 times faster in the presence of the **9c-9c** capsule. This was explained by assuming that both starting compounds are complexed within the capsule and, because of their close proximity, the rate of reaction is enhanced. Due to the restricted space inside the capsule, the *endo*-isomer is favoured as the exclusive product of the Diels-Alder reaction. Control experiments proof that the acceleration of the reaction is solely a result of encapsulation of the reaction components in the capsule. In contrast, if 1,4-naphthoquinone, a molecule that does not fit in the capsule, is used as the dienophile, the reaction is not accelerated. The turnover in this catalytic reaction is low due to product inhibition, since the resulting product fits perfectly within the capsule ($K_a > 10^5 \text{ M}^{-1}$). In order to make the capsule a true catalyst, product release is necessary and this was accomplished by using 2,5-dimethyl thiophene dioxide as the diene in the cycloaddition reaction with *p*-benzoquinone. The resulting Diels-Alder product cannot fit perfectly within the capsule and is thus immediately replaced by new reactants.³¹



1.3.4 Chiral capsules

The most recent achievements in ‘capsule chemistry’ concern the introduction of chirality. The two glycoluril moieties forming the softball were modified with different groups on their convex side (**10**). Upon dimerization, a racemate of two enantiomeric capsules was formed. The chirality introduced at the outside of the capsule had no influence on stereoselective binding of chiral guests. For enantiomeric discrimination, chirality inside the capsule is needed, and this was accomplished by the synthesis of the softball derivatives **11a** and **11b**, which have their glycoluril moieties linked by unsymmetrical spacers.³² The monomers themselves are achiral, but upon dimerization a racemate of two enantiomeric capsules with a chiral inner space is formed. When dimerization is induced by the addition of an enantiomerically pure guest, *e.g.* camphor, one of the enantiomers of the capsule is preferentially formed over the other one. Depending on the shape and size of the guest, host-guest complexes with a diastereomeric excess up to 35% can be formed.



Figure 1.7 Assembly of four molecules of **12** into a tetramer **12₄**, resembling a ‘football’.

1.3.5 Footballs

Capsules which are composed of more than two self-complementary building blocks could be formed by the self-assembly of four molecules of **12** into a cyclic tetramer **12₄**, which is stabilized by a pattern of 16 hydrogen bonds³³ (Figure 1.7). In the resulting assembly, the four molecular units are arranged in a ‘head-to-tail’ fashion which optimizes the orientation and distances between the various hydrogen bond donors and acceptors. Additionally, the most acidic hydrogen bond donors, the sulfamide N-H protons, are paired with the most basic hydrogen bond acceptors, the glycoluril carbonyl oxygen atoms. Unlike in the case of the softball, the tetrameric ‘football’ was not formed in benzene or *p*-xylene solution. Only when an appropriate guest, such as adamantane, was added to a suspension of **12** in dichloromethane, a

capsule was generated which incorporated an adamantane molecule. Dynamic NMR studies of the exchange of free and encapsulated guest indicated an apparent³⁴ association constant of K_a (app.) = 19 M^{-1} . When a guest containing hydrogen bond acceptors, *e.g.* adamantane-2,6-dione was encapsulated, a higher binding constant was measured (K_a (app.) = 3200 M^{-1}). This enhanced binding was attributed to the forming of hydrogen bonds between the guest and the hydrogen bond donor groups in the capsule.

1.4 Recent developments in molecular clip chemistry

1.4.1 Introduction

In the early 1980's the Nolte research group began a study on the possibilities of using cucurbituril as a cage compound for small organic guests. Modification of the cucurbituril macrocycle is inhibited due to the extreme insolubility of the host in most common solvents. In attempts to overcome this problem of solubility by attaching phenyl groups to the glycoluril units, it was discovered that the reaction of diphenylglycoluril **1** with formaldehyde in benzene gave a 'clip-shaped' molecule. This molecule possessed a rigid, U-shaped cavity and several years later it was found that it was an ideal host for dihydroxybenzene derivatives, *e.g.* resorcinol and catechol. These guests are bound in the cavity due to a combination of hydrogen bonding and π - π interactions.³⁵

A wide variety of clip molecules has been developed possessing numerous functionalities. These clips have been applied in different areas, *e.g.* as supramolecular catalysts, liquid crystals, amphiphiles, and as mimics of the photosynthetic reaction center. The most recent developments will be discussed below.

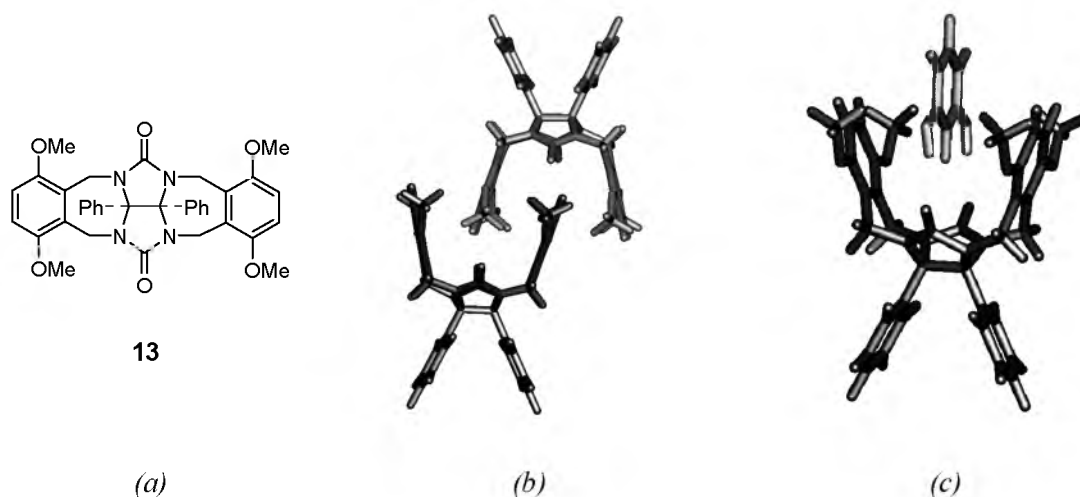


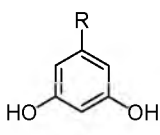
Figure 1.8 (a) Molecular clip **13**. (b) Crystal structure of **13**. (c) Computer modeled structure of the host-guest complex between **13** and **G3** (see Table 1.1).

1.4.2 Binding mechanisms

The crystal structure of the standard molecular clip **13** (Figure 1.8a,b) clearly shows that this host molecule possesses a well-defined preorganized cleft. ¹H NMR studies were the first to reveal that clips are excellent receptors for neutral aromatic (di-)hydroxybenzene guests. The binding

Table 1.1 Association constants (K_a , M^{-1}) and binding free energies (ΔG , $kJ\ mol^{-1}$) of host **13** with guest molecules **G1–G7**.

Guest	R	K_a	ΔG
G1	C ₅ H ₁₁	1500	-18.1
G2	CH ₃	1900	-18.7
G3	H	2600	-19.5
G4	OCH ₃	4400	-20.8
G5	C(O)OCH ₃	16500	-24.1
G6	Cl	16000	-24.0
G7	CN	1×10^5	-28.5



G1 - G7

strength toward these types of guests can reach values over $10^6\ M^{-1}$, depending on the binding functions in the host molecule and the substitution pattern in the guest. The binding is a result of three cooperative effects, *viz.* hydrogen bonding, π - π stacking and a so-called 'cavity effect', which can be simply described as the entropically favourable filling of an empty cavity by the guest. Recent work within the Nolte group³⁶ enabled the separation and quantification of each of these effects. Upon binding of a 1,3-dihydroxybenzene to a clip of type **13** in chloroform solution, two hydrogen bonds are formed simultaneously between the hydroxy groups of the guest and the π -electrons of the urea carbonyl groups of the clip (Figure 1.8c). The strength of these hydrogen bonds is directly correlated to the 5-substituent of the guest, which determines the acidity of the phenolic OH groups. It was found that the ΔG of binding for a series of 5-substituted 1,3-dihydroxybenzenes to clip **13** increased linearly as a function of the Hammett substituent constant $\sigma_m(R)$ (Table 1.1). The contribution of hydrogen bonding to the overall binding was determined by binding experiments of the guests to cyclic ether **14**, a molecule which does not have a cavity (eq. 1). In order to quantify the effect of the other two factors on the overall binding, the urea carbonyl groups were substituted for thiocarbonyl groups.³⁷ Clip **15**, which possesses two thiocarbonyl functions, is still able to weakly bind guests (K_a with **G3** = $51\ M^{-1}$), but only as a result of π - π stacking and a cavity effect (eq. 2). Combining equations 1 and 2 should give the binding of guests to clip **13** (eq. 3). It can be seen below that a good agreement is obtained when eq. 3 is compared with the experimentally determined values (eq. 4).

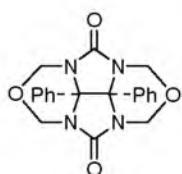
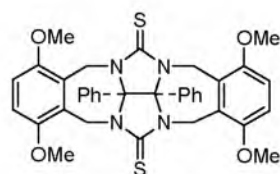
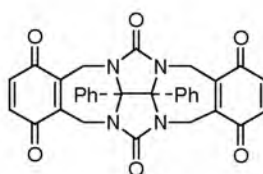
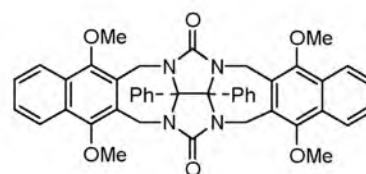
$$\text{Contribution of hydrogen bonding} \quad -\Delta G = 7.8 + 6.3\sigma \quad (1)$$

$$\text{Contribution of } \pi\text{-}\pi \text{ interactions and cavity effect} \quad -\Delta G = 10.4 + 9.1\sigma \quad (2)$$

$$\text{Equations 1 + 2} \quad -\Delta G = 18.2 + 15.4\sigma \quad (3)$$

$$\text{Experimentally determined values for clip } \mathbf{13} \quad -\Delta G = 19.3 + 14.7\sigma \quad (4)$$

The π - π interactions between host and guest can be readily influenced by slight variations in the clip side-walls.³⁸ Altering the 1,4-substituents on the side-walls from methoxy to methyl to hydrogen significantly weakens the π - π interactions, and also reduces the cavity effect because the cavity size is smaller. A host with two *p*-benzoquinone side-walls (**16**) somewhat surprisingly turned out to be a very poor receptor for 1,3-dihydroxybenzene guests (K_a with **G3** =

**14****15****16****17**

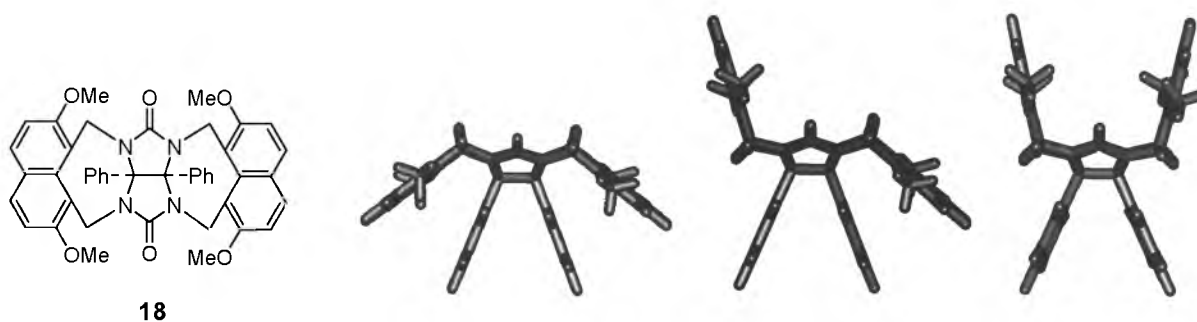


Figure 1.9 Three conformers adopted by clip **18** in chloroform solution.

85 M^{-1}). Although favourable interactions were expected between the electron-poor cavity side-walls and the electron-rich guest, the orientation of the host and the guest, imposed by the hydrogen bonds, is energetically less favourable than that found with clip **13**. Enlargement of the aromatic surface of the side-walls to 1,4-dimethoxynaphthalene (clip **17**) completely inhibited guest binding, due to a combination of unfavourable π - π interactions and steric hindrance from the methoxy substituents.³⁹ Connection of the naphthalene walls at their 1,8-positions removes these constraints. Host **18**, however, exists in three slowly exchanging conformers, of which only the *anti-anti* one possesses a cleft in which substrates can be bound (Figure 1.9). The large aromatic π -surface of the side-walls have favourable interactions with electron deficient guests and metal cations (e.g. silver(I) ions⁴⁰). Binding occurs by an induced-fit mechanism: upon binding the guest, the relative amount of *anti-anti* conformer was found to increase.⁴¹

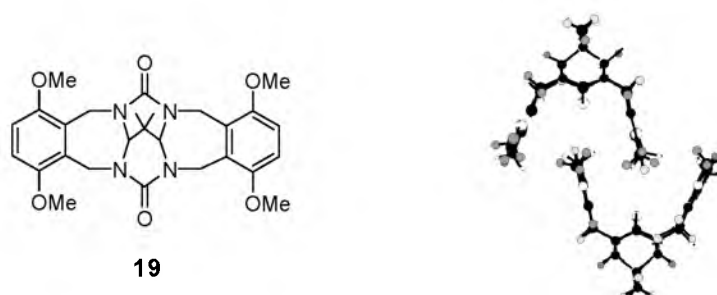


Figure 1.10 Crystal structure of **19**.

All the binding processes described above were determined using clips based on the diphenylglycoluril skeleton. Very recently, this central core was modified and new clip molecules were synthesized based on the propane-diurea skeleton.⁴² The X-ray structure of clip **19** (Figure 1.10) revealed that its cavity resembled the cavities of diphenylglycoluril (DPG) based clips, the only difference being that in the new host the distance between the urea carbonyl groups is slightly shorter (5.2 \AA compared to 5.52 \AA in the case of **13**). As a result of this closer distance, 1,3-dihydroxybenzene guests are bound approximately 10 times stronger to host **19** when compared to clips based on DPG. The exceptionally high binding constants measured for these guests (up to $K_a = 3.4 \times 10^6 \text{ M}^{-1}$ for the complex between **19** and **G7**), highlight the fact that even sub-Ångstrom changes in the host structure can have a dramatic effect on its binding properties.

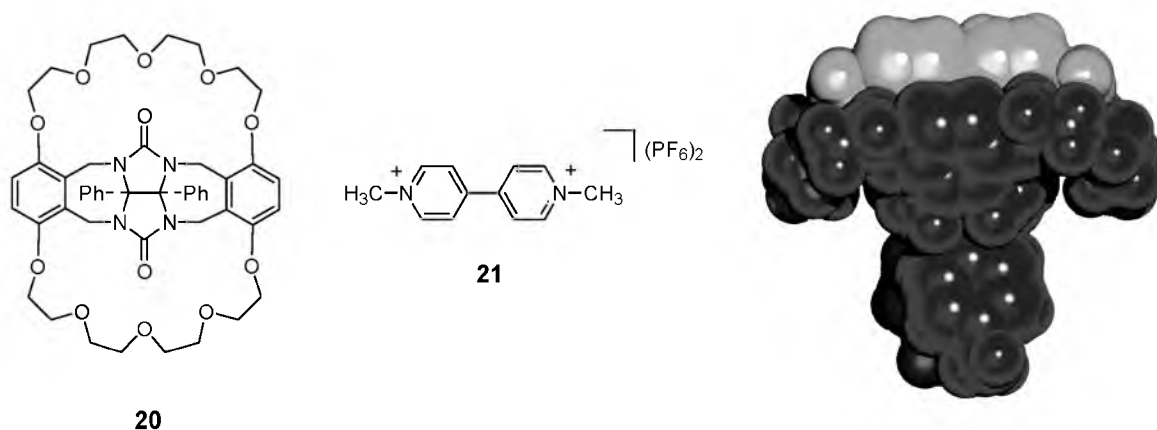


Figure 1.11 Crystal structure of the host-guest complex between basket **20** and paraquat **21**.

Molecular clips derivatized with crown ether moieties, such as **20**, are known as molecular baskets, due to their basket- or bowl-like shape (Figure 1.11). In addition to alkali metal ions and diammonium salts,⁴³ these hosts are also excellent receptors for charged aromatic compounds such as paraquat and polymeric derivatives thereof.⁴⁴ Host **20** binds **21** with a K_a of $5.7 \times 10^4 \text{ M}^{-1}$, which is much stronger than the binding of **21** in the bis(paraphenylene)-[34]-crown-10 macrocycle studied by Stoddart and coworkers.⁴⁵ The redox properties of **21** were found to be modified upon complexation with **20**, *i.e.* bound **21** is 100 mV more difficult to reduce than uncomplexed **21**. Once reduced to its 1+ form, however, **21** is no longer bound by **20**. In the case

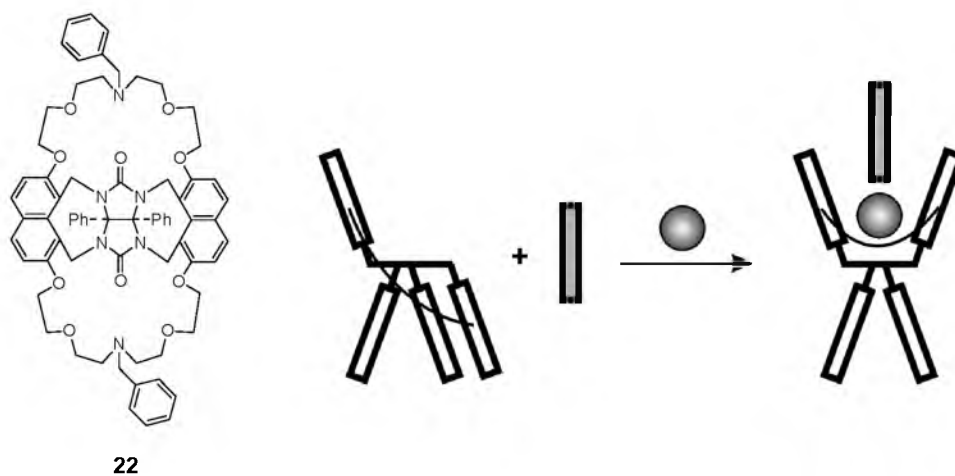


Figure 1.12 Enhanced binding of a 1,3-dinitrobenzene guest in host **22** in the presence of K^+ ions.

of polymeric derivatives of **21**, the electrochemical properties of the polymer can be altered by the addition of host **20**.

Another family of basket-shaped hosts was synthesized containing aza-crown ethers which can act as linking points for functional groups. The naphthalene-walled basket **22** (Figure 1.12) exists in 3 conformations and displays allosteric binding behavior.⁴⁶ Upon the addition of alkali metal ions, the *anti-anti* conformation is induced, which results in a host which is a better receptor for aromatic guests. As a result of this induced change, the binding of 1,3-dinitrobenzene is increased by a factor of 2 to 6 upon the addition of K^+ ions to a solution of **20**. Two K^+ ions are

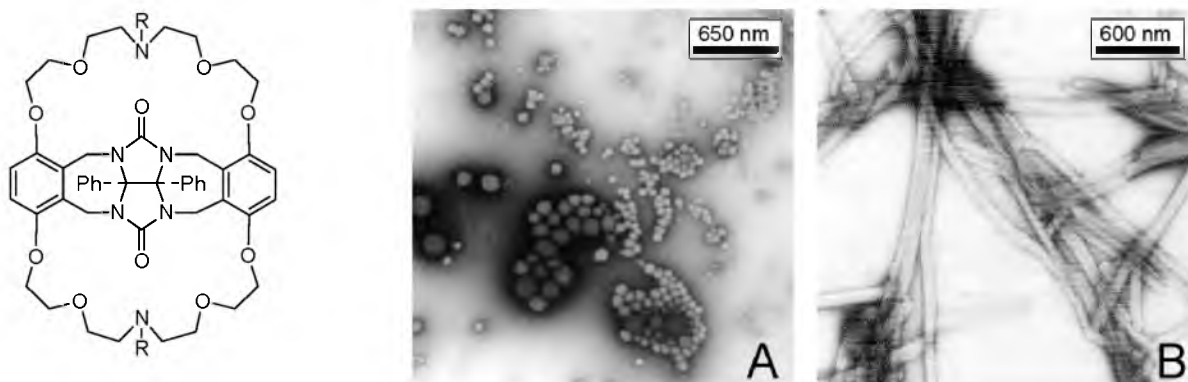
complex guests in its cavity, the host-guest geometry was not ideal and oxidative splitting of the pyridine ligands of the host occurred in preference to oxidation of the guest. Molecular modeling confirmed that in the geometry formed upon O₂ complexation the benzylic protons linking the pyridine functions to the basket are in direct proximity to the bound oxygen. Due to this close proximity, the host is oxidized in preference to the guest.

In addition to oxidative catalytic systems, hydrogenation catalysts have been developed based upon molecular clips. Following a synthetic methodology similar to that used for the preparation of **23** and **24**, a tetrakis(triphenyl)phosphite Rh(I) hydride complex was linked to a molecular basket (**25**).⁵⁰ The resulting supramolecular catalyst was able to selectively catalyze the hydrogenation of guests such as 5-allylresorcinol with a significant rate enhancement compared to non-binding guests such as 5-allyl-1,3-dimethoxybenzene. The catalyst also exhibited many of the features encountered in enzymes, such as Michalis-Menten kinetics, product inhibition and rate enhancement by cooperative binding of a second substrate.

A different strategy used to develop synthetic enzymes was the addition of known catalytic functions to one of the side-walls of a clip.⁵¹ Clip **26**, which has one *p*-dimethoxybenzene side-wall and one nickel-salophen side-wall, and clip **27**, which is functionalized with one quinoxaline-phenanthroline side-wall were prepared.⁵⁵ Unfortunately, the catalytic oxidation of a substrate (3,5-dihydroxystyrene) by molecular oxygen, using **26** as the catalyst, was unsuccessful. Although **26** could still complex substrates, it was concluded that the phenolic OH-groups of the guest act as radical scavengers and inhibit the epoxidation of the alkene.⁵² It was therefore decided to construct an alternative catalyst in which these problems could be circumvented. A new catalyst was designed and synthesized, [Pd(**27**)₂](NO₃)₂. The square planar complex was applied in catalytic hydroformylation reactions of nitrobenzene derivatives. In the solvents in which hydroformylation was carried out (a benzene-methanol mixture), no substrates could, however, be bound in the receptor cavity.⁵²

1.4.4 Golf balls and razorblades

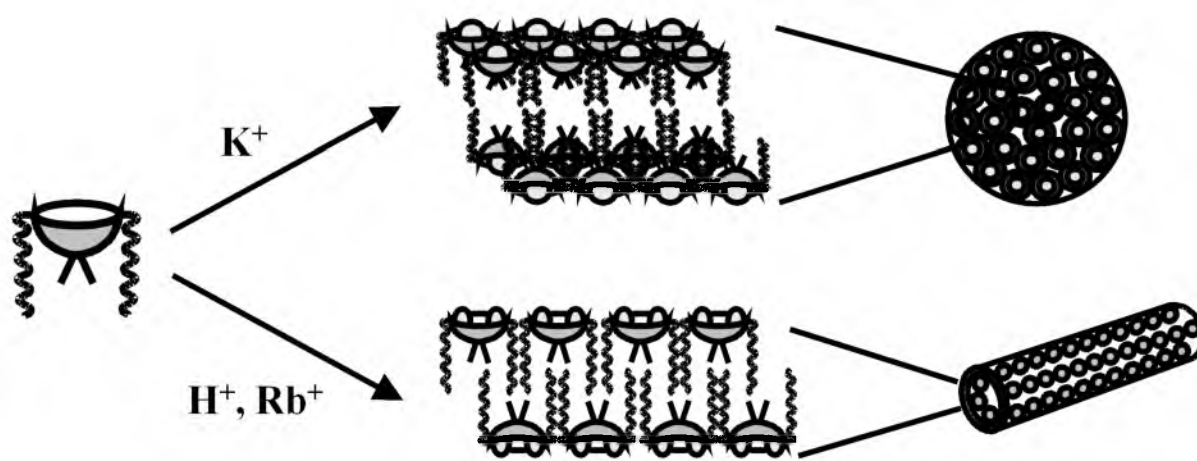
Whilst Rebek's group was beginning their investigations of self-assembling capsules, the group in Nijmegen was investigating the self-assembling behavior of water-soluble clip receptors. The first approach was to attach long hydrocarbon tails which were attached to the nitrogen atoms of azacrown ether functionalized baskets, to give compounds **28** and **29**. Upon dispersion of **28** in water, well-defined vesicles were formed with diameters between 500 and 4000 Å (Figure 1.13).⁵³ It was proposed that in these vesicles the charged receptor cavities are directed toward the water layer, making that the aggregates possess a 'dimpled' exterior. These 'supramolecular golf balls', as they became known, were still able to complex guests, such as magnesium (4-(4-nitrophenylazo)resorcinol) in water. Below the critical aggregation constant (c.a.c.) of the compound UV titrations indicated that a 1:1 host-guest complex was formed ($K_a = 10^6 \text{ M}^{-1}$).⁵⁴ Above the c.a.c., the titration data could only be fitted assuming a 2:1 host-guest complex ratio. This phenomenon was attributed to the fact that above the c.a.c. only the receptors on the outside of the vesicle are able to bind magnesium and that the receptors on the inside of the vesicle can not be accessed by the guests. Basket **29** was found to give tube-like assemblies with a diameter of 100 nm in aqueous HCl, but vesicles in aqueous KCl or NaCl solution.⁵⁵ The morphology of these superstructures could be manipulated by the addition of different alkali metal ions, such as Rb⁺, which resulted in the formation of a mixture of tubes and vesicles, or Cs⁺, which gave only nanotubes.



28 R = C₁₆H₃₃

29 R = (CH₂)₃OC(O)C₁₁H₂₃

(a)



(b)

Figure 1.13 (a) TEM micrographs of aggregates formed by **28** in water (A), and by **29** in aqueous RbCl solution (B). (b) Schematic representation of the proposed structures of the aggregates of **29** in the presence of K⁺ and H⁺ or Rb⁺ ions.

Molecular clips themselves also display association phenomena and ultimately self-assembly to form ordered arrays of molecules. In the absence of guest molecules, clip **13** was found to dimerize in chloroform as a result of cavity filling and favorable intermolecular π - π interactions.⁵⁶ In the dimer, the side-wall of one clip molecule is bound in the cavity of its dimeric partner, and *vice-versa* (see Figure 1.8b). This dimerization, although relatively weak (dimerization constant $K_{\text{dimer}} = 16 \text{ M}^{-1}$, as was calculated from an NMR dilution titration in CDCl₃), is observed also in the crystal structures of a wide range of clip molecules.^{45,57} Work concerning the further exploration of the self-assembly of clips in the solid state will be presented in Chapters 5 and 6 of this thesis. In order to utilize the affinity of clips to dimerize, new water-soluble hosts were designed. It was thought that the dimerization would be enhanced by using the hydrophobic effect as a driving force for self-assembly.⁵⁸ Pyridinium functionalized clip **30** was found to dimerize in water with a dimerization constant $K_{\text{dimer}} = 300 \text{ M}^{-1}$, a value

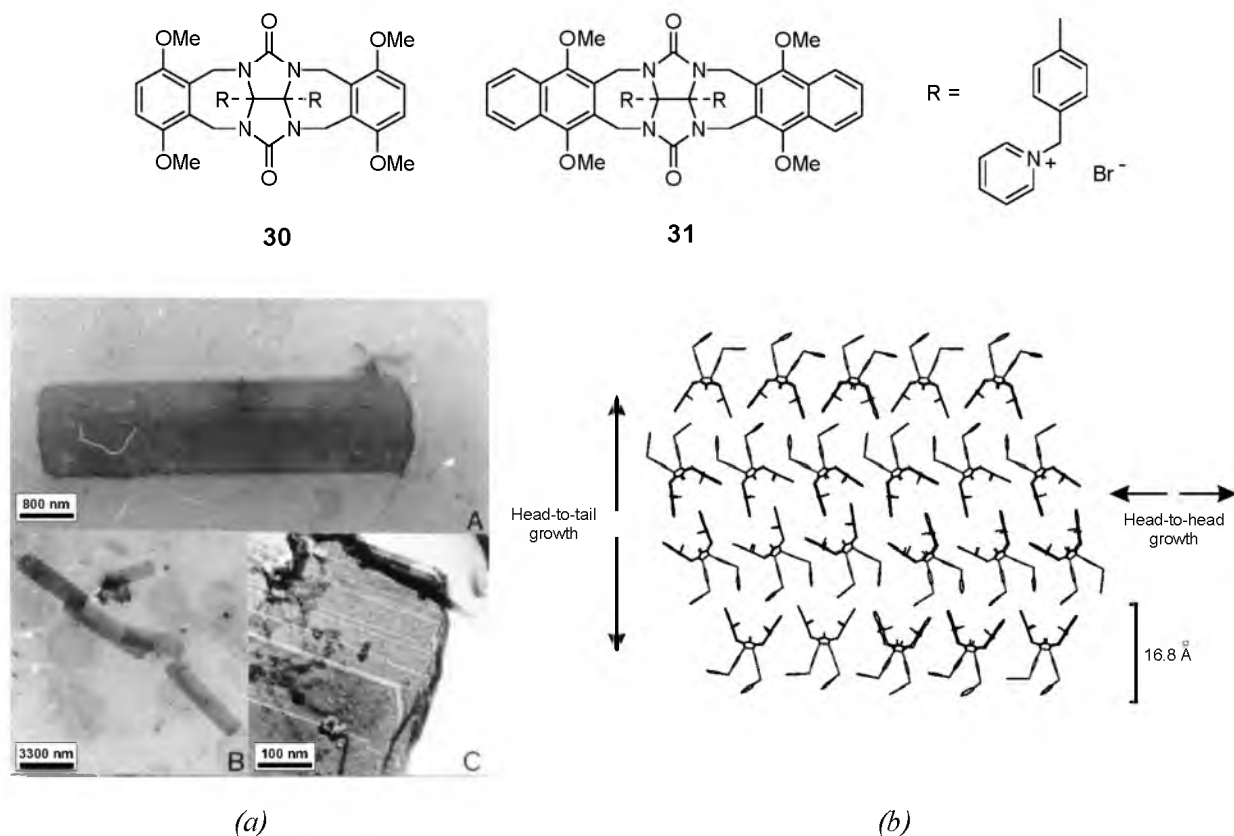


Figure 1.14 (a) 'Razorblade-like' aggregates formed by water-soluble clip **31**: TEM micrographs (A,B), and freeze fracture TEM micrograph (C). (b) Proposed structure of the aggregate showing the combination of head-to-head and head-to-tail growth.

which indeed is much higher than the observed K_{dimer} of **13**.⁵⁹ It was expected that if the cavity was enlarged an even stronger self-association would occur due to a larger hydrophobic driving force. In the case of naphthalene-walled clip **31** a $K_{\text{dimer}} > 5000 \text{ M}^{-1}$ was measured. Remarkably, the observed NMR shifts upon diluting the solution of **31** indicated that two modes of self-association occurred, a 'head-to-head' dimerization and a 'head-to-tail' one, in which the pyridinium groups are docked in the cavities of their neighbours. Upon standing, a pearly-like dispersion gradually formed within the solution. Study of a sample of this dispersion with transmission electron microscopy revealed the presence of well-defined 'razorblade-like' aggregates (Figure 1.14a), which all had approximately the same shape and dimensions ($1.2 \times 8 \mu\text{m}$). Closer inspection of the aggregates showed that they were built up from a limited number of thin layers (approximately 50). Electron diffraction experiments revealed that the structures were not crystals, but a highly ordered array of molecules, with a repeating distance of 16.8 \AA which corresponds to approximately the length of one clip molecule.

There are numerous possible self-assembling pathways for these clip molecules to form finite nano-arrays. NMR and powder diffraction data suggested that initially a 'head-to-head' dimeric 'seed' was formed by hydrophobically dimerizing cavities (Figure 1.14b). This 'seed' can further grow in one dimension because of the presence of strong π - π interactions between the dimers. In an additional process, monomeric clip molecules can attach themselves to the pyridinium moieties at the back of these dimeric 'seeds'. The repeating 16.8 \AA distance observed in the powder diffraction experiment corresponds to this 'head-to-tail' growth. Eventually, 2D lamellar

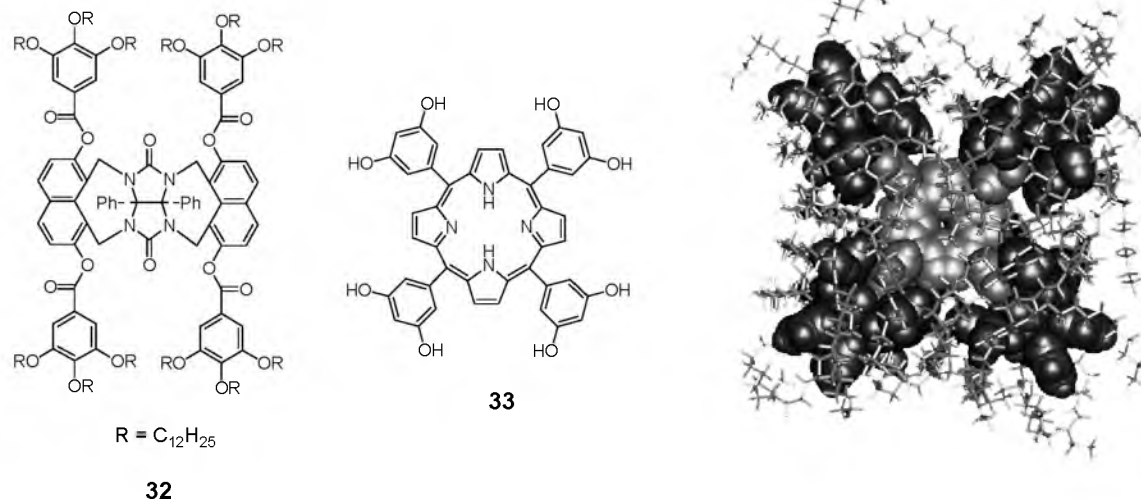


Figure 1.15 Computer modeled representation of the liquid crystalline host-guest complex between tetrakis(3,5-dihydroxyphenyl)porphyrin **33** and four molecules of clip **32**.

multilayers will be generated of which the outside edges are always hydrophilic. Sheets of these lamellar multilayers on top of each other finally may give form to the overall aggregate structure. One of the most intriguing aspects of these aggregates is their precise finite size, and the fact that they stop growing after a certain time. The balance between the molecular recognition processes determining aggregate growth, and the loss in entropy upon self-assembly, are responsible for the defined shape and mono-dispersity of the nanostructures. Studies directed at elucidating the mechanisms determining the self-assembly and the incorporation of metal centers into these defined aggregates will be presented in Chapters 3 and 4.

1.4.5 Liquid-crystalline materials based on molecular clips

An example of a molecular clip or tweezer in Nature is the Gene V protein. This protein, which has a U-shaped structure, binds to single stranded DNA and changes its physical properties.⁶⁰ Using the above protein as a source of inspiration clip **32** was designed, which has twelve hydrocarbon chains connected to its side-walls. It exists predominantly in the *syn-anti* conformation, but upon binding of a guest the *anti-anti* conformation is induced and the resulting complex exhibits liquid crystalline (L.C.) properties.⁶¹ By changing the host-guest ratio, the nature and temperature range of the various L.C. phases could be tuned. The versatility of this concept of supramolecular induction of liquid-crystallinity was demonstrated when multifunctional guests were used. The 4:1 host-guest complex of **32** with porphyrin **33** also displayed L.C. behaviour. If a porphyrin that could not bind was used, no mesophases were formed, which confirmed that the host-guest complex is the mesogenic species (Figure 1.15). Not only were the material properties of the porphyrin changed, but also its redox properties. Electrochemical studies revealed that the porphyrin core is encapsulated in the 48 hydrocarbon tails of the four clips, causing the reduction potentials of the porphyrin to alter in a similar way to certain porphyrin containing enzymes, such as cytochrome C. Through an identical process liquid crystallinity could also be induced in polymers. The host-guest complex of **32** with a copolymer of styrene and 3,5-dihydroxystyrene gave a very stable, discotic-like mesophase. The molecules 'clipped' on the polymer changed its material properties in an analogous manner to the Gene V protein.

1.4.6 Mimic of the photosynthetic reaction center

One of the questions unresolved in the study of electron transfer processes in photosynthetic reaction centers is the role of intervening aromatic amino acid residues.⁶² To study this question, a molecular clip was designed with one zinc-porphyrin side-wall and one 1,4-dimethoxybenzene donor (**34**) or *p*-benzoquinone acceptor (**35**) side-wall (Figure 1.16).⁶³ In a non-polar solvent, such as cyclohexane or CCl₄, the fluorescence quantum yields of **34** and **35** were comparable to that of zinc-tetrakis(*meso*-phenyl)porphyrin, but in a more polar solvent the quantum yield of **35** became much smaller due to solvent mediated electron transfer from the porphyrin donor to the quinone side-wall acceptor. A similar effect was observed when to host **35** in CCl₄ an excess of the guest hexyl 3,5-dihydroxybenzoate was added. Upon binding in the clip, this guest enhanced electron transfer, suggesting that in the natural system the amino acid residues may play a similar role.

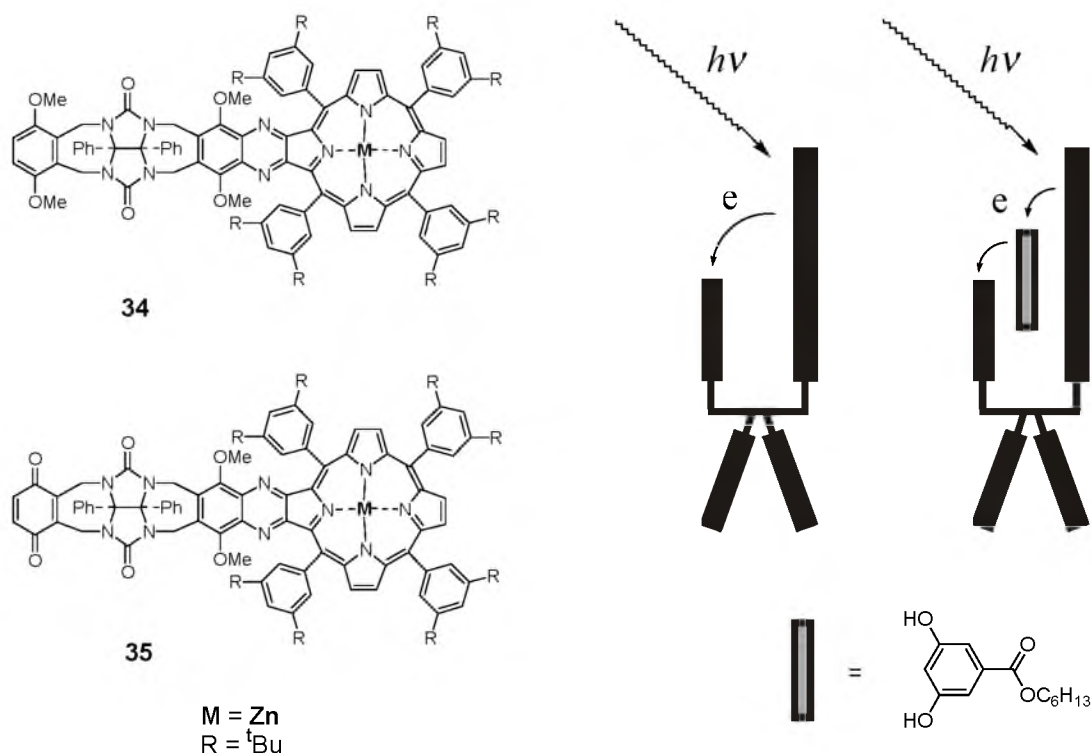


Figure 1.16 Porphyrin-walled clips **34** and **35** and schematic representation of the mediated electron transfer which occurs upon the addition of an aromatic guest to clip **35**.

References and Notes

- Behrend, R.; Meyer, E.; Rusche, F. *Liebigs Ann. Chem.* **1905**, 339, 1.
- Freeman, W.A.; Mock, W.L.; Shih, N.-Y. *J. Am. Chem. Soc.* **1981**, 103, 7367.
- For a review about cucurbituril, see: Mock, W. L. *Top. Curr. Chem.* **1995**, 175, 1.
- Meschke, C.; Buschmann, H. J.; Schöllmeyer, E. *Polymer* **1999**, 40, 945.
- Freeman, W. A. *Acta Crystallogr. Sect. B* **1984**, 40, 382.
- Mock, W. L.; Shih, N.-Y. *J. Org. Chem.* **1983**, 48, 3618.
- Mock, W. L.; Shih, N.-Y. *J. Org. Chem.* **1986**, 51, 4440.
- Mock, W. L.; Irra, T. A.; Wepsiec, J. P.; Manimaran, T. L. *J. Org. Chem.* **1993**, 48, 3619. Mock, W. L.; Irra, T. A.; Wepsiec, J. P.; Adhya, M. *J. Org. Chem.* **1989**, 54, 5302.
- Tuncel, D.; Steinke, J. H. G. *Chem. Commun.* **1999**, 1509.
- For reviews about rotaxanes, see: Sauvage, J.-P. *Acc. Chem. Res.* **1990**, 23, 319. Amabilino, D. B.; Stoddart, J. F. *Chem. Rev.* **1995**, 95, 2725. Philp, D.; Stoddart, J. F. *Angew. Chem. Int. Ed. Engl.* **1996**, 35, 1154.

- 11 Buschmann, H.-J.; Meschke, C.; Schollmeyer, E. *Anales de Química Int. Ed.* **1998**, *94*, 241.
- 12 Meschke, C.; Buschmann, H.-J.; Schollmeyer, E. *Polymer* **1999**, *40*, 945.
- 13 Jeon, Y.-M.; Whang, D.; Kim, J.; Kim, K. *Chem. Lett.* **1996**, 503.
- 14 Whang, D.; Jeon, Y.-M.; Heo, J.; Kim, J. *Am. Chem. Soc.* **1996**, *118*, 11333.
- 15 Fujita, M.; Ogura, K. *Coord. Chem. Rev.* **1996**, *148*, 249 and references cited therein.
- 16 Leininger, S.; Olenyuk, B.; Stang, P. J. *Chem. Rev.* **2000**, *100*, 853 and references cited therein.
- 17 Whang, D.; Park, K.-M.; Heo, J.; Ashton, P.; Kim, K. *J. Am. Chem. Soc.* **1998**, *120*, 4899.
- 18 Roh, S.-G.; Park, K.-M.; Park, G.-J.; Sakamoto, S.; Yamaguchi, K.; Kim, K. *Angew. Chem. Int. Ed.* **1999**, *38*, 638.
- 19 Whang, D.; Kim, K. *J. Am. Chem. Soc.* **1997**, *119*, 451.
- 20 Whang, D.; Heo, J.; Kim, C.-A.; Kim, K. *Chem Commun.* **1997**, 2361.
- 21 Rebek, J., Jr. *Chem. Soc. Rev.* **1996**, 255. Conn, M. M.; Rebek, J., Jr. *Chem. Rev.* **1997**, *97*, 1647. Rebek, J., Jr. *Acc. Chem. Res.* **1999**, *32*, 278.
- 22 See for reviews about molecular clips: Sijbesma, R. P.; Nolte, R. J. M. *Top. Curr. Chem.* **1995**, *175*, 26. Rowan, A. E.; Elemans, J. A. A. W.; Nolte, R. J. M. *Acc. Chem. Res.* **1999**, *32*, 995.
- 23 Wyler, R.; de Mendoza, J.; Rebek, J., Jr. *Angew. Chem. Int. Ed. Engl.* **1993**, *32*, 1699.
- 24 Valdés, C.; Spitz, U.; Toledo, L.; Kubik, S.; Rebek, J., Jr. *J. Am. Chem. Soc.* **1995**, *117*, 12733.
- 25 Branda, N.; Wyler, R.; Rebek, J., Jr. *Science* **1994**, *263*, 1267.
- 26 Branda, N.; Grotzfeld, R. M.; Valdés, C.; Rebek, J., Jr. *J. Am. Chem. Soc.* **1995**, *117*, 85.
- 27 Grotzfeld, R. M.; Branda, N.; Rebek, J., Jr. *Science* **1996**, *271*, 487. O'Leary, B. M.; Grotzfeld, R. M.; Rebek, J., Jr. *J. Am. Chem. Soc.* **1997**, *119*, 11701.
- 28 Meissner, R. S.; Rebek, J., Jr.; de Mendoza, J. *Science* **1995**, *270*, 1485. Meissner, R. S.; Garcias, X.; Mecozzi, S.; Rebek, J., Jr. *J. Am. Chem. Soc.* **1997**, *119*, 77.
- 29 Kang, J.; Rebek, J., Jr. *Nature* **1996**, *382*, 239.
- 30 Kang, J.; Rebek, J., Jr. *Nature* **1997**, *385*, 50. Kang, J.; Hilmersson, G.; Santamaría, J.; Rebek, J., Jr. *J. Am. Chem. Soc.* **1998**, *120*, 3650.
- 31 Kang, J.; Santamaría, J.; Hilmersson, G.; Rebek, J., Jr. *J. Am. Chem. Soc.* **1998**, *120*, 7389.
- 32 Rivera, J. M.; Martín, T.; Rebek, J., Jr. *Science* **1998**, *279*, 1021.
- 33 Martín, T.; Obst, U.; Rebek, J., Jr. *Science* **1998**, *281*, 1842.
- 34 The association constant is an apparent one, because the several dynamic processes involving (de)aggregation of the free host were simplified.
- 35 Sijbesma, R. P.; Nolte, R. J. M. *J. Org. Chem.* **1991**, *56*, 3122. Sijbesma, R. P.; Kentgens, A. P. M.; Nolte, R. J. M. *J. Org. Chem.* **1991**, *56*, 3199. Sijbesma, R. P.; Kentgens, A. P. M.; Lutz, E. T. G.; van der Maas, J. H.; Nolte, R. J. M. *J. Am. Chem. Soc.* **1993**, *115*, 8999.
- 36 Reek, J. N. H.; Priem, A. H.; Engelkamp, H.; Rowan, A. E.; Elemans, J. A. A. W.; Nolte, R. J. M. *J. Am. Chem. Soc.* **1997**, *119*, 9956.
- 37 Gieling, G. T. W.; Scheeren, H. W.; Israel, R.; Nolte, R. J. M. *Chem. Commun.* **1996**, 241.
- 38 Reek, J. N. H.; Elemans, J. A. A. W.; Nolte, R. J. M. *J. Org. Chem.* **1997**, *62*, 2234.
- 39 Sijbesma, R. P.; Bosman, W. P.; Nolte, R. J. M. *J. Chem. Soc. Chem. Commun.* **1991**, 885.
- 40 Reek, J. N. H.; Sijbesma, R. P.; Nolte, R. J. M. *Tetrahedron Lett.* **1994**, *35*, 2801.
- 41 Sijbesma, R. P.; Wijmenga, S. S.; Nolte, R. J. M. *J. Am. Chem. Soc.* **1992**, *114*, 9807. Reek, J. N. H.; Engelkamp, H.; Rowan, A. E.; Elemans, J. A. A. W.; Nolte, R. J. M. *Chem. Eur. J.* **1998**, *4*, 716.
- 42 Jansen, R. J.; Rowan, A. E.; de Gelder, R.; Scheeren, H. W.; Nolte, R. J. M. *Chem. Commun.* **1998**, 121.
- 43 Smeets, J. W. H.; van Dalen, L.; Kaats-Richter, V. E. M.; Nolte, R. J. M. *J. Org. Chem.* **1990**, *55*, 454. Smeets, J. W. H.; Sijbesma, R. P.; van Dalen, L.; Spek, A. L.; Smeets, W. J. J.; Nolte, R. J. M. *J. Org. Chem.* **1989**, *54*, 3710. Smeets, J. W. H.; Visser, H. C.; Kaats-Richter, V. E. M.; Nolte, R. J. M. *Recl. Trav. Chim. Pays-Bas* **1990**, *109*, 147.
- 44 Schenning, A. P. H. J.; de Bruin, B.; Rowan, A. E.; Kooijman, H.; Spek, A. L.; Nolte, R. J. M. *Angew. Chem. Int. Ed. Engl.* **1995**, *34*, 2132.
- 45 Ashton, P. R.; Philp, D.; Reddington, M. V.; Slawin, A. M. Z.; Spencer, N.; Stoddart, J. F.; Williams, D. J. *J. Chem. Soc. Chem. Commun.* **1991**, 1680.
- 46 Sijbesma, R. P.; Nolte, R. J. M. *J. Am. Chem. Soc.* **1991**, *113*, 6695. Sijbesma, R. P.; Nolte, R. J. M. *J. Phys. Org. Chem.* **1992**, *5*, 649.
- 47 For a review about supramolecular catalysis see: Feiters, M. C. *Supramolecular Catalysis*. In: *Comprehensive Supramolecular Chemistry*; Vögtle, F., Ed.; Pergamon/Elsevier Press: New York, **1997**: Vol 10, Chapter 11, p. 267.

- ⁴⁸ Martens, C.F.; Schenning, A. P. H. J.; Klein Gebbink, R. J. M.; Feiters, M. C.; van der Linden, J. G. M.; Nolte, R. J. M. *J. Chem. Soc. Chem. Commun.* **1993**, 88. Martens, C. F.; Klein Gebbink, R. J. M.; Feiters, M. C.; Nolte, R. J. M. *J. Am. Chem. Soc.* **1994**, *116*, 5667.
- ⁴⁹ Klein Gebbink, R. J. M.; Martens, C. F.; Feiters, M. C.; Nolte, R. J. M. *Chem. Commun.* **1997**, 389. Klein Gebbink, R. J. M.; Martens, C. F.; Kenis, P. J. A.; Jansen, R. J.; Nolting, H.-F.; Solé, V. A.; Feiters, M. C.; Karlin, K. D.; Nolte, R. J. M. *Inorg. Chem.* **1999**, *38*, 5755.
- ⁵⁰ Coolen, H. K. A. C.; van Leeuwen, P. W. N. M.; Nolte R. J. M. *Angew. Chem. Int. Ed. Engl.* **1992**, *31*, 905. Coolen, H. K. A. C.; van Leeuwen, P. W. N. M.; Nolte, R. J. M. *J. Org. Chem.* **1996**, *61*, 4739. Coolen, H. K. A. C.; van Leeuwen, P. W. N. M.; Nolte R. J. M. *J. Am. Chem. Soc.* **1995**, *117*, 11906. Coolen, H. K. A. C.; van Leeuwen, P. W. N. M.; Nolte, R. J. M. *J. Organomet. Chem.* **1995**, *496*, 159.
- ⁵¹ Only one of the side-walls was functionalized since functionalization of both side-walls completely blocked the binding of guests. See: Gosling, P. A.; Sijbesma, R. P.; Spek, A. L.; Nolte, R. J. M. *Recl. Trav. Chim. Pays-Bas* **1993**, *112*, 404.
- ⁵² Reek, J. N. H. *Thesis*, **1996**, University of Nijmegen, The Netherlands.
- ⁵³ Schenning, A. P. H. J.; de Bruin, B.; Feiters, M. C.; Nolte, R. J. M. *Angew. Chem. Int. Ed. Engl.* **1994**, *33*, 1662.
- ⁵⁴ It is as yet unclear if the guest binds in the host with its hydroxy groups pointing to the carbonyl groups, or even in the receptor cavity. Recent work has revealed that in aqueous solutions guests also bind on the outside of clip molecules where π -overlap between the aromatic surfaces is maximal, see Chapter 4 of this thesis.
- ⁵⁵ Van Nunen, J. L. M.; Stevens, R. S. A.; Picken, S. J.; Nolte R. J. M. *J. Am. Chem. Soc.* **1994**, *116*, 8825.
- ⁵⁶ Reek, J. N. H.; Rowan, A. E.; Elemans, J. A. A. W.; de Gelder, R.; Nolte, R. J. M. Manuscript in preparation.
- ⁵⁷ Bosman, W. P.; Smits, J. M. M.; de Gelder, R.; Reek, J. N. H.; Nolte, R. J. M. *J. Chem. Cryst.* **1996**, *26*, 365. Bosman, W. P.; Smits, J. M. M.; de Gelder, R.; Reek, J. N. H.; Elemans, J. A. A. W.; Nolte, R. J. M. *J. Chem. Cryst.* **1997**, *27*, 75.
- ⁵⁸ Tanford, C. in: *The Hydrophobic effect*. Wiley Interscience, New York, **1973**.
- ⁵⁹ Reek, J. N. H.; Kros, A.; Nolte, R. J. M. *Chem. Commun.* **1996**, 245.
- ⁶⁰ Folmer, R. H. A.; Nilges, M.; Folkers, P. J. M.; Konings, R. N. H.; Hilbers, C. W. *J. Mol. Biol.* **1994**, *240*, 341.
- ⁶¹ Van Nunen, J. L. M.; Folmer, B. F. B.; Nolte R. J. M. *J. Am. Chem. Soc.* **1997**, *119*, 283. Van Nunen, J. L. M.; Nolte R. J. M. *J. Chem. Soc. Perkin Trans. 2* **1997**, 1473.
- ⁶² *Reaction Centers of Photosynthetic Bacteria*. Michel-Beyerle, M.-E., Ed.; Springer-Verlag, Berlin, **1992**.
- ⁶³ Reek, J. N. H.; Rowan, A. E.; de Gelder, R.; Beurskens, P. T.; Crossley, M. J.; de Feyter, S.; de Schryver, F.; Nolte R. J. M. *Angew. Chem. Int. Ed. Engl.* **1997**, *36*, 361. Reek, J. N. H.; Rowan, A. E.; Crossley, M. J.; Nolte, R. J. M. *J. Org. Chem.* **1999**, *64*, 6653.

Chapter 2

Molecular Clips with Functionalized Convex Sides

2.1 Introduction

Until recently, nearly all the research concerning molecular clips in our group has been concentrated on derivatives of diphenylglycoluril, in particular on the modification and functionalization of the receptor cavities and the side-walls of these molecules (see also Section 1.4). Clips with a variety of different side-walls have been synthesized¹ as well as clips in which the hydrogen bond accepting carbonyl functions have been completely removed or replaced by thiocarbonyl or guanidine functions.² The binding of (di-)hydroxybenzene guest molecules in these clips has been studied in great detail and the factors governing the host-guest binding, *viz.* hydrogen bonding, π - π interactions, and cavity filling effects, have been quantified.³ Functionalization of the clips with catalytically active metal centers on the side-walls has been realized.^{1,4} In another approach, the side-walls have been derivatized with crown ether spacer groups, to which metal complexes such as Rh(I) phosphite,⁵ Cu(II) pyrazole,⁶ and a porphyrin⁷ have been attached.

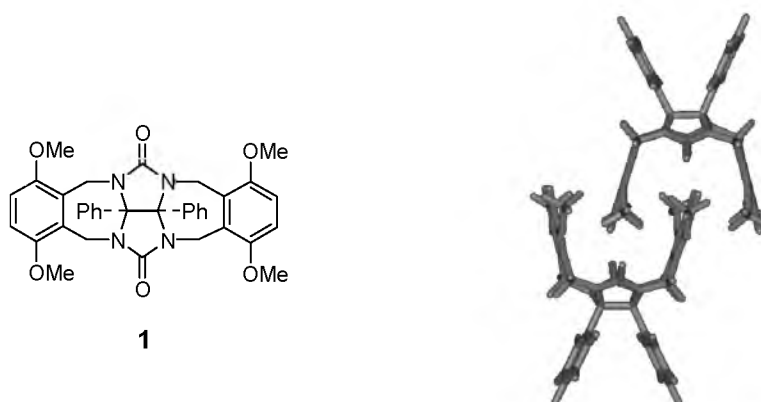
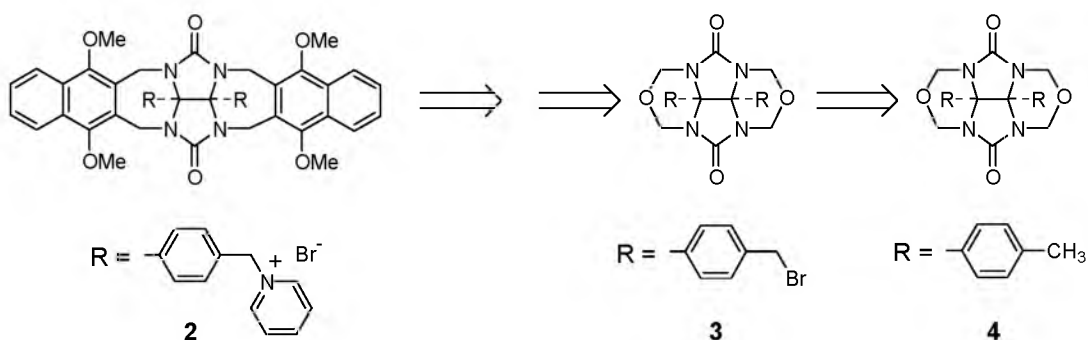


Figure 2.1 Dimerization of two molecules of **1**.

Recently the ability of clip molecule **1** to form dimers was discovered. In these dimers, one of the cavity side-wall of one clip molecule acts as a guest for a second clip molecule and *vice-versa* (Figure 2.1).⁸ This unusual host-guest interaction is relatively weak in organic solvents



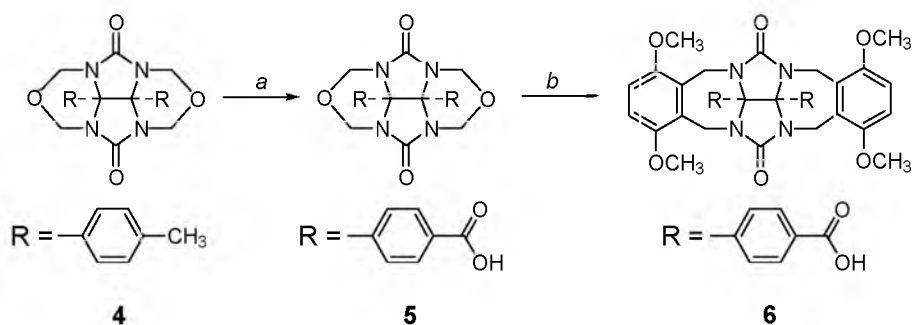
Scheme 2.1 Retrosynthetic procedure for the preparation of water-soluble clip **2**.

(K_{dimer} of **1** in $\text{CDCl}_3 = 16 \text{ M}^{-1}$), but significantly stronger in water because of hydrophobic effects.⁹ Dimers have also been observed in the solid-state structures of many clips.⁸ If water-soluble groups are introduced at the convex side of clips rigid amphiphile-like molecules are formed. Clip **2**, which has a large hydrophobic cavity and two water-soluble pyridinium moieties on its convex side, was found to self-assemble into well-defined ‘razorblade-like’ aggregates when dispersed in water.⁹ The synthesis of this molecule, however, turned out to be quite problematic (Scheme 2.1). It started with the benzylic bromination of cyclic ether **4** to give the dibromide **3**, but during this reaction considerable amounts of the monobromo and tribromo analogues of **3** were formed. Separation of these contaminations from **3** appeared to be impossible, and purification could only be performed in the final step of the reaction, *viz.* by careful crystallization of clip **2**. This troublesome synthetic procedure stimulated us to develop more versatile routes, which would allow for easy functionalization of the convex sides of the clip molecules involving a minimal number of high yield reaction steps and easy purification procedures, for example precipitation or crystallization of the reaction products. In the following sections, such synthetic routes will be presented in which the convex sides of the clip molecules are successfully functionalized with benzoic acid, phenol, and bipyridine groups, respectively.

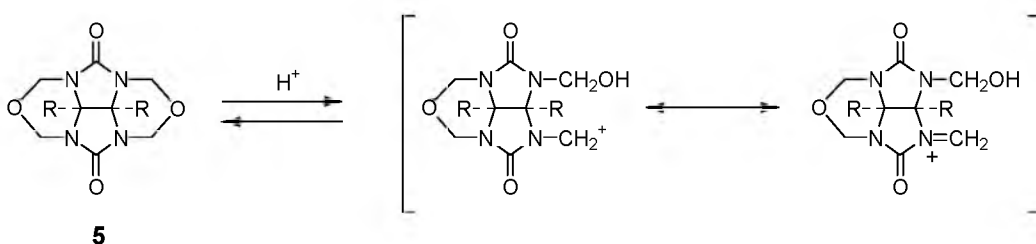
2.2 Convex sides with benzoic acid groups

As starting material for the synthesis of benzoic acid functionalized clip molecules cyclic ether **4** was used (Scheme 2.2).⁹ Its aromatic methyl groups could be oxidized with KMnO_4 in water to give the dicarboxylic acid **5** in a yield of 96%. A standard ureidoalkylation¹⁰ of **5** with *p*-dimethoxybenzene in a mixture of acetic anhydride and trifluoroacetic acid afforded the dicarboxylic acid functionalized clip **6** in 81% yield. This reaction was only completed after 3 days, which is surprising since the analogous reaction to synthesize clip **1** just took 1 hour.¹⁰ The low reactivity of **5** may be attributed to the relatively slow formation of the reactive intermediate, which is believed to be a carbonium-imonium ion (Scheme 2.3).^{11,12} The electron withdrawing carboxylic acid substituents at the glycoluril phenyl groups of **5** apparently disfavour the formation of this intermediate.

For reaction of **5** with other aromatic molecules, *e.g.* benzene, *p*-xylene and 1,4-dimethoxynaphthalene, it was necessary to replace the relatively stable cyclic ether groups by better leaving groups. First, the carboxylic acid functions of **5** were protected by esterification in methanol to give dimethyl ester **7** (Chart 2.1). Apart from the desired compound, considerable amounts of side-products were formed in which one or both of the cyclic ether functions had



Scheme 2.2 Synthesis of benzoic acid functionalized clip **6**. Reagents and conditions: (a) KMnO_4 , H_2O , reflux, 16 h. (b) *p*-Dimethoxybenzene, Ac_2O , TFA, 100°C , 64 h.



Scheme 2.3 The formation of a carbonium-imonium ion from **5**.

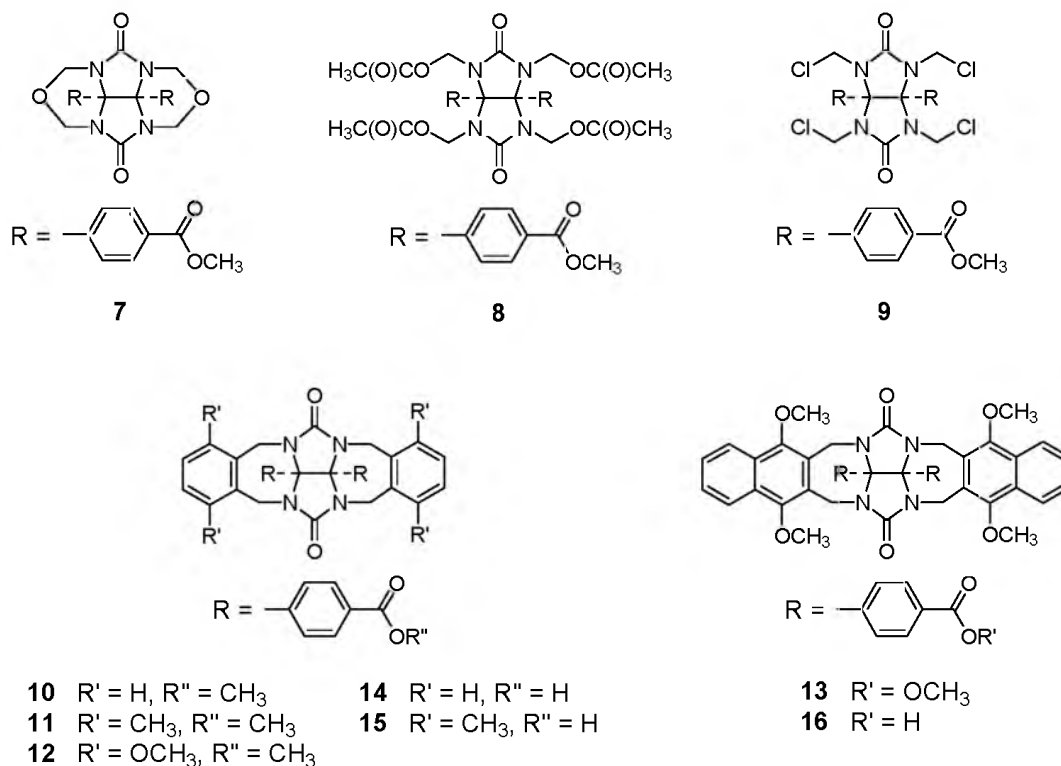
opened to give compounds with methyl ether groups. Compound **7**, however, could be easily isolated from this mixture by column chromatography (yield 56%). It was also possible to use the crude product mixture in the following step, which is the acid-catalyzed acylation with acetic anhydride to give the tetra-acetoxy derivative **8**. This compound was obtained as a single product in 70% yield. The reaction was completed after 40 hours, which is a much longer time than the analogous reaction in the case of the diphenylglycoluril (DPG) derived compound (3 hours). Compound **8** was subsequently treated with thionyl chloride to give the tetrachloride **9** in 84% yield. This activated compound was then used in Lewis acid catalyzed Friedel Crafts alkylation reactions with benzene, *p*-xylene and 1,4-dimethoxynaphthalene as substrates to give clip molecules **10**, **11** and **13** in yields of 36, 34 and 71% respectively, after purification by column chromatography. The yields of **10** and **11** are relatively low because considerable amounts of mono-walled clip compounds were present in the reaction mixtures. Prolonged reaction times and variation of the Lewis acid did not improve the yields. Clip **12** was synthesized directly from cyclic ether **7** and *p*-dimethoxybenzene in a similar way as described for **6**.

Saponification of the methyl ester protected clips **10-13** proceeded smoothly in a mixture of dioxane, methanol and aqueous 4N NaOH^{13} (15:4:1, v/v/v), affording the crude carboxylate disodium salts as precipitates. These could be dissolved in water, whereupon protonation with aqueous 37% HCl gave the benzoic acid functionalized clips **6** and **14-16** as precipitates in nearly quantitative yields.

Crystal structures

Single crystals of **5** were obtained by slow evaporation of an ethanolic solution of the compound. The crystal structure is depicted in Figure 2.2. The unit cell contains four independent molecules of **5** and eight molecules of ethanol. The OH groups of the ethanol molecules are hydrogen bonded to the urea carbonyl oxygen atoms of **5**. The distance between the latter atoms is 5.11 Å, which is slightly larger than the distance between these atoms in the crystal structure of the

Chart 2.1



dimethylglycoluril analogue of **5** (4.98 Å).¹⁴ Single crystals of **12** were obtained by slow diffusion of diethyl ether into a solution of this compound in dichloromethane. The crystal structure is shown in Figure 2.3. The unit cell contains four molecules of **12**, which are arranged in two slightly differing dimers (see Chapter 5 for details about the *intermolecular* interactions in the crystal), and four molecules of dichloromethane. The two *p*-dimethoxybenzene side-walls define a tapering cavity, in which the planes through the side-walls are at a relative angle of 36°. The centers of these side-walls are 6.44 Å apart, which makes the cavity somewhat narrower than that of **1** (distance between the side-walls: 6.67 Å).¹⁵ The distance between the carbonyl oxygen atoms (5.56 Å) is almost identical to the distance between these atoms in the crystal structure of **1** (5.52 Å).

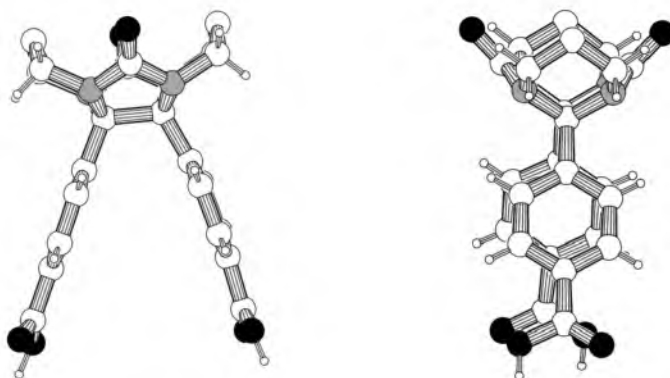


Figure 2.2 PLUTON drawings (front and side-view) of the crystal structure of cyclic ether **5**.

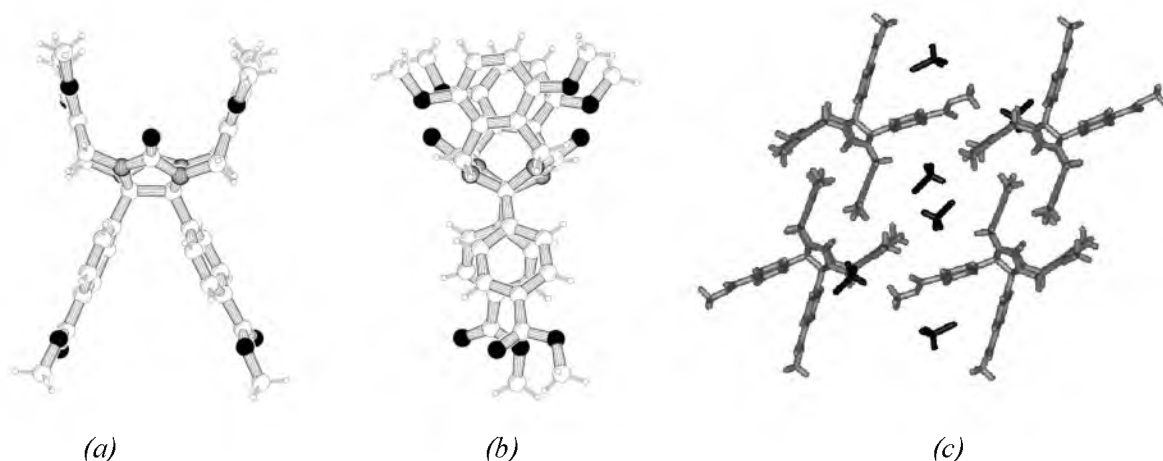
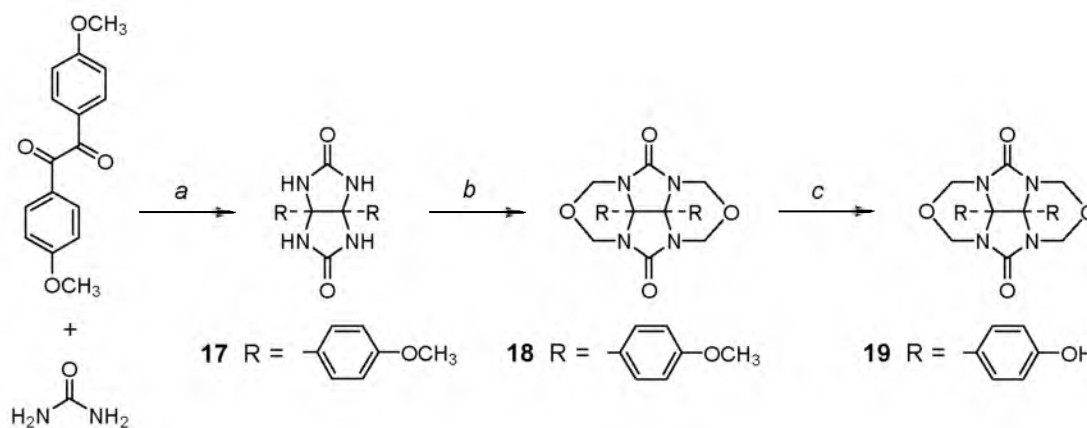


Figure 2.3 PLUTON drawings of the crystal structure of clip molecule **12**. (a) Front view. (b) Side view. (c) Arrangement of the molecules of **12** and solvent molecules (CH_2Cl_2) in the crystal.

2.3 Convex sides with phenol groups

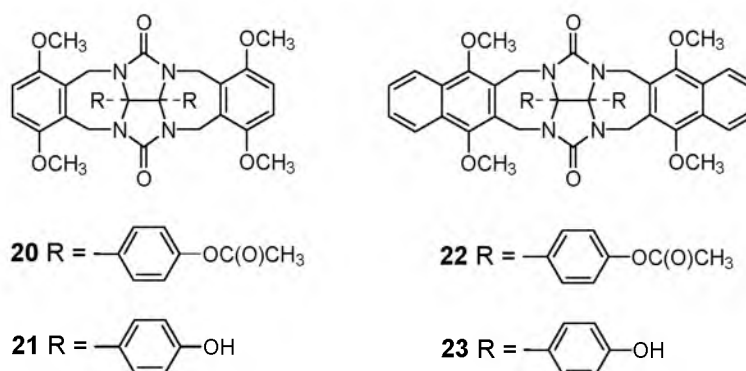
The synthesis of phenol functionalized clip molecules started with the preparation of 4,4'-bis(4-methoxyphenyl)glycoluril **17** which was obtained by condensation of 4,4'-dimethoxybenzil with urea in toluene, using trifluoroacetic acid as a catalyst (70% yield, Scheme 2.4). Subsequent reaction of **17** with paraformaldehyde gave cyclic ether **18** (81% yield), which was demethylated with boron tribromide in dichloromethane.



Scheme 2.4 Synthesis of phenol functionalized cyclic ether **19**. Reagents and conditions: (a) TFA, toluene, reflux, 16 h. (b) $(\text{CH}_2\text{O})_n$, 1N NaOH, DMSO, 16 h, then aqueous 1N HCl, reflux, 2 h. (c) BBr_3 , CH_2Cl_2 , 64 h.

During this reaction, considerable amounts of side-products were formed in which the cyclic ether functions had opened to give hydroxymethylene groups. Refluxing the crude product in a mixture of dichloromethane and aqueous 2N HCl afforded pure **19** in a yield of 94%, after recrystallization from acetic acid. This compound was subjected to an ureido alkylation reaction with *p*-dimethoxybenzene to give clip **20** (yield 83%, Chart 2.2) in which the phenolic hydroxy groups had been converted to acetoxy groups as a result of the applied reaction conditions. The

Chart 2.2

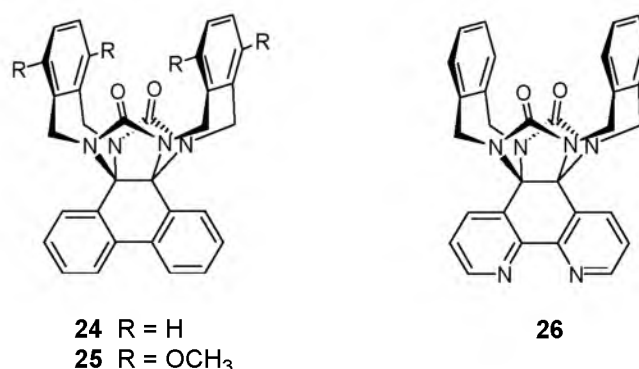


latter groups were removed with aqueous 1N NaOH in dioxane to give clip **21** in 89% yield as a precipitate after acidic workup. Cyclic ether **19** appeared to be sufficiently reactive to undergo an amidoalkylation reaction with 1,4-dimethoxynaphthalene, in the same way as described for the synthesis of **20**. Clip **22** was obtained in a yield of 49%, and it was deprotected as described for **21** to afford **23** in 80% yield.

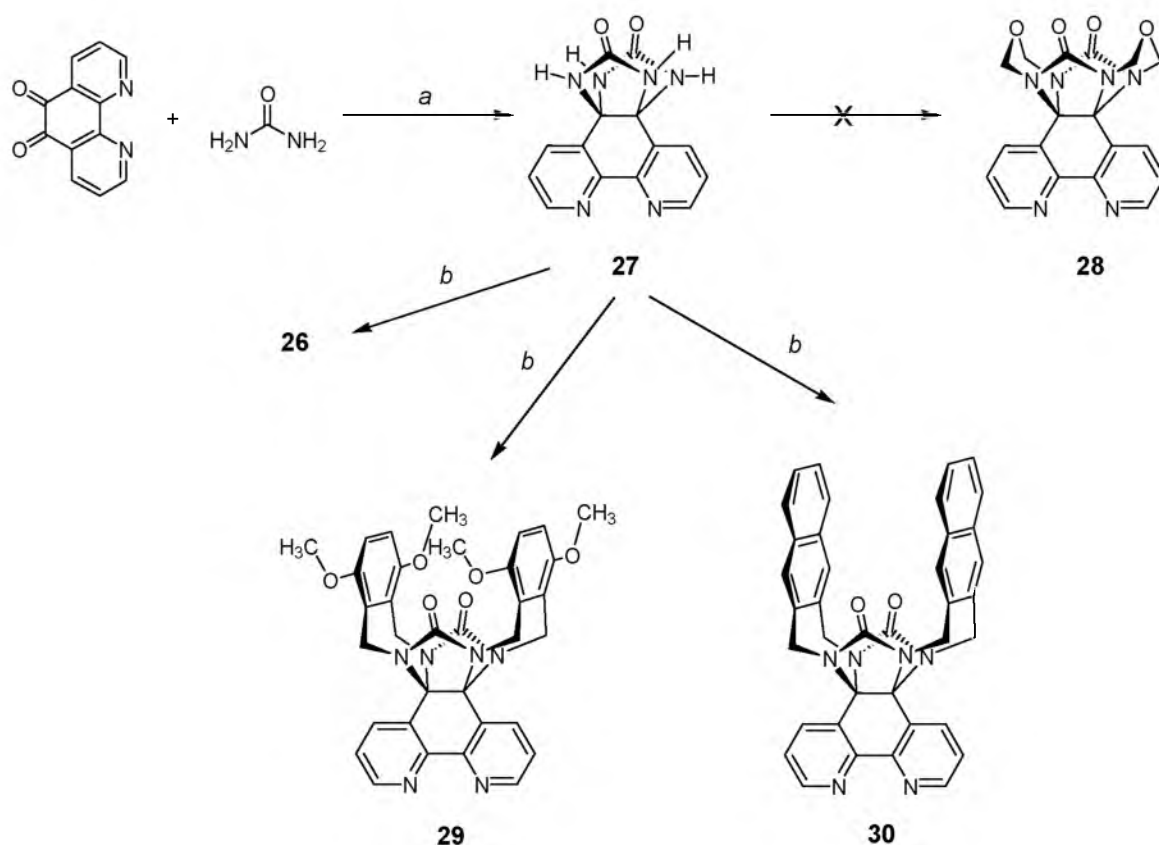
2.4 Convex sides with bipyridine groups

Recently, Murray and Whelan reported the synthesis of molecular clips **24** and **25**, which have a biphenyl group on their convex side (Chart 2.3).¹⁶ The molecules were synthesized from a glycoluril derivative that was prepared from urea and 9,10-dihydro-9,10-phenanthrenedione. The biphenyl groups of **24** and **25**, however, do not have any useful function. Clip molecule **26** was therefore designed, which instead of a biphenyl group has a 2,2'-bipyridine group on its convex side. Alkylation of the bipyridine nitrogen atoms would make the molecule water-soluble - at least in principle - and the bipyridine ligand would allow the complexation of transition metal centers to the clip molecule. Previously metal centers have been connected to the

Chart 2.3



clips *via* crown ether spacers^{5,6} and these centers have also been incorporated in the clip side-walls¹ (see Section 1.4). These clip molecules were designed with the objective to position a catalytically active metal center in close proximity of a receptor cavity, the ultimate goal to achieve substrate selective catalysis. It would, however, also be of interest if metal centers could



Scheme 2.5 Synthesis of bipyridine functionalized clips. Reagents and conditions: (a) TFA, toluene, reflux, 16 h. (b) Appropriate *o*-bis(bromomethyl)arene, KOH, DMSO, 40 h.

be bound to clip molecules *via* the convex side of these molecules. In this way, complexes are obtained of which the properties of the metal center can be influenced by binding of guest molecules in the receptor cavity.

Synthesis

The synthesis of clip molecules with bipyridine ligands started with the acid-catalyzed condensation of urea and 5,6-dihydro[1,10]phenanthroline-5,6-dione in toluene to give bipyridine-glycoluril compound **27** as a solid material in 86% yield (Scheme 2.5). Several efforts were undertaken to convert **27** to cyclic ether **28**, since this type of compound has proven to be a versatile starting material for the synthesis of many molecular clips. Moreover, the cyclic ether compounds are generally more soluble in common organic solvents than compounds of type **27**, which are only sparingly soluble in DMSO. Under standard reaction conditions for the synthesis of cyclic ether compounds¹⁷ (paraformaldehyde in DMSO, aqueous NaOH, then HCl) the desired product **28** was, however, not formed.

It was decided, therefore, to attach the cavity side-walls directly to glycoluril **27**, according to a previously applied procedure.⁹ Alkylation of **27** with 1,2-bis(bromomethyl)benzene in DMSO, using potassium hydroxide as a base, gave clip molecule **26** in a yield of 31%, after recrystallization from methanol. Similar alkylations of **27** with 1,4-dimethoxy-2,3-bis(bromomethyl)benzene and 2,3-bis(bromomethyl)naphthalene gave clip molecules **29** and **30** in yields of 42 and 26%, respectively. NMR spectroscopic studies revealed that in the crude reaction

products no bipyridine *N*-alkylated derivatives were present. The relatively low yields of the alkylation reactions are probably the result of steric shielding of the glycoluril nitrogen atoms for reaction by the 5,5'-bipyridine protons, resulting in the formation of a considerable amount of polymeric material. The ^1H NMR spectra of **26**, **29** and **30** clearly showed the transverse orientation of the bipyridine ligand with respect to the cavity side-walls. The NMR signals of the methylene protons of clip molecules are always expressed as an AB-quartet due to the geminal coupling of the two methylene protons, which, because of the rigidity of the methylene group, are non-equivalent. In clips based on diphenylglycoluril, the methylene *in*-protons, which point toward the shielding phenyl groups at the convex side of the clip, resonate upfield from the methylene *out*-protons. In the clip molecules derived from bipyridine glycoluril, the reverse is the case: the *in*-protons are now deshielded by the edge of the bipyridine moiety.¹⁸

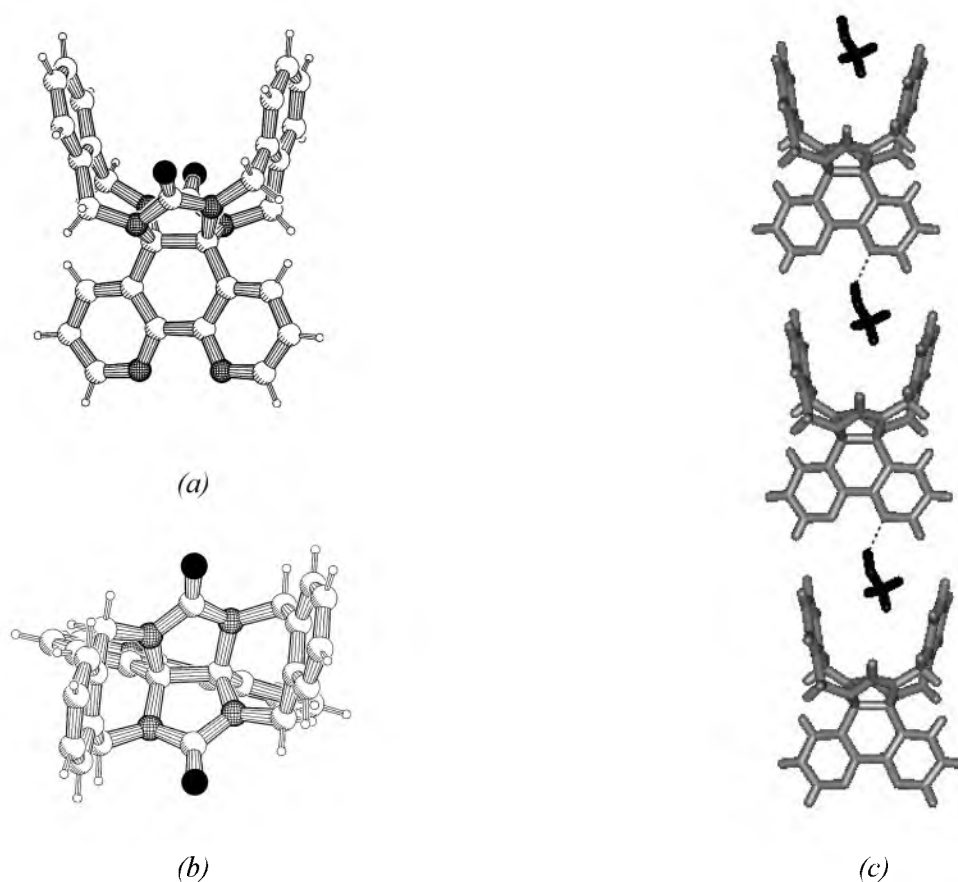


Figure 2.4 Drawings of the crystal structure of clip molecule **26**. (a) Front view. (b) Top view. (c) Arrangement of the molecules of **26** and solvent molecules (CH_3OH) in the crystal.

Crystal structure of **26**

Single crystals of **26**, suitable for X-ray structure analysis, were grown by slow diffusion of methanol into a chloroform solution of this compound. In the crystal structure (Figure 2.4), a severe twist of 26° in the glycoluril framework is visible, which is most clearly expressed in the twisting of the cavity side-walls. Furthermore, the large steric interaction between the 5,5'-bipyridine and methylene protons causes the cavity to be squeezed and narrowed when compared to cavities of clips based on DPG. This is reflected in a relatively small distance between the aromatic side-walls of **26** (6.18 Å, as compared to 6.67 Å in the crystal structure of **1**¹⁵). The

relative angle between the planes through the side-walls is also much smaller than the same angle in **1**, *viz.* 29° compared to 39.5° in **1**. The distance between the carbonyl oxygen atoms (5.59 Å) is similar to the distance between these atoms in **1**. The unit cell contains four independent molecules of **26** and four molecules of methanol, of which the OH groups are hydrogen bonded to one of the bipyridine nitrogen atoms.

Binding properties

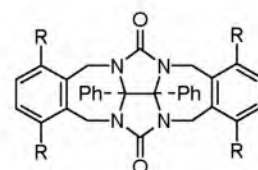
To investigate the consequences of the narrower cavity on the binding properties of the bipyridine functionalized clip molecules, ¹H NMR binding studies were carried out with clip **26** in CDCl₃ solution. Various 5-substituted 1,3-dihydroxybenzene guests were used and the results were compared with similar results obtained for DPG-based clip **31** (Table 2.1). It can be clearly seen in this table that the association constants K_a measured for **26** are significantly smaller than those published for the reference host **31**.³ A similar weak binding was also found by Murray and Whelan for clip **24** (K_a with resorcinol 90 M⁻¹).¹⁶ The calculated Complexation Induced Shift (CIS) values of the aromatic protons of the guests indicate that the geometry of guest binding in **26** is similar to that in **31**, *viz.* with the hydroxy groups of the guest directed to the carbonyl groups of the host. Remarkably, the CIS values of the H-2 protons of the guests are much smaller than those observed for the same protons in the complexes with **31**, which suggests that the guests are bound less deeply in host **26**.

Table 2.1 Association constants K_a (M⁻¹) and calculated CIS values^a (in parenthesis) of complexes between various host and guest molecules in CDCl₃, $T = 298$ K.

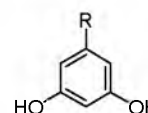
Guest	R	σ_m (R)	Host				
			26 ^b	31 ^c	29 ^b	1 ^c	30 ^d
C ₅ H ₁₁		-0.08	20 (-0.20)	74 (-1.97)	20	1500	< 5
H		0	50 (-0.22)	175 (-2.33)	— ^e	2600	— ^e
OCH ₃		0.12	60 (-0.21)	195 (-2.37)	— ^e	4400	— ^e
Cl		0.37	100 (-0.34)	475 (-2.97)	— ^e	1.65 × 10 ⁴	— ^e
C(O)OCH ₃		0.37	100 (-0.23)	850 (-2.88)	— ^e	1.6 × 10 ⁴	— ^e
C(O)OC ₆ H ₁₃		0.37	— ^e	— ^e	300	1.7 × 10 ⁴	20
CN		0.56	240 (-0.56)	3500 (-3.07)	— ^e	1 × 10 ⁵	— ^e

^aCIS values for the H-2 proton of the guest. ^bEstimated errors 20%.

^cValues taken from ref. 3. ^dEstimated error 50%. ^eNot determined.



1 R = OCH₃
31 R = H



As was observed before in the case of DPG-based clips,³ a Hammett relationship exists between the free energy of binding and the Hammett constant σ_m (R) of the substituent of the guest (Figure 2.5). The slope of the curve is less steep in the case of **26** than in the case of **31**, which is an indication that the K_a values of the complexes with the former host are less dependent on the 5-substituent of the guest than those of the complexes of the latter host. This in turn implies that for **26** binding of the guests is less dependent on the strength of the hydrogen bonds formed between the hydroxy groups of the guests and the carbonyl oxygen atoms of the clip than this is the case for **31**.³ To gain additional information on these hydrogen bonding interactions, CDCl₃¹⁹ solutions of **26** and its host-guest complexes were studied with FTIR spectroscopy. In the spectra of the mixtures, a sharp guest OH stretching vibration corresponding to uncomplexed guest was observed as well as a broad band at lower wavenumbers belonging to complexed guest

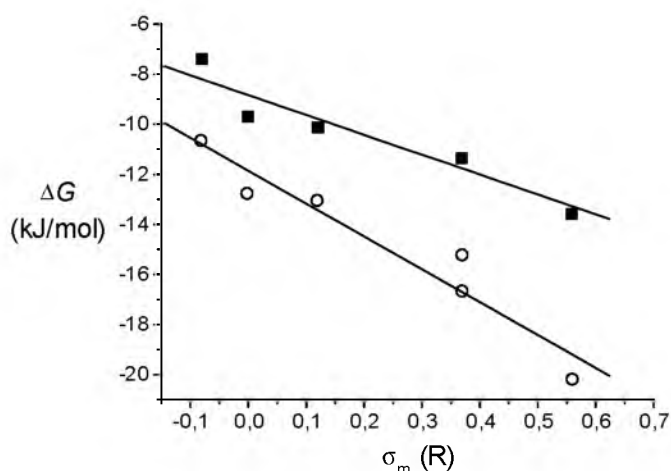


Figure 2.5 Binding free energies (ΔG) of various dihydroxybenzene guest molecules in hosts **26** (■) and **31** (○), plotted as a function of the Hammett constant (σ_m (R), see Table 2.1) of the substituent in the guest.

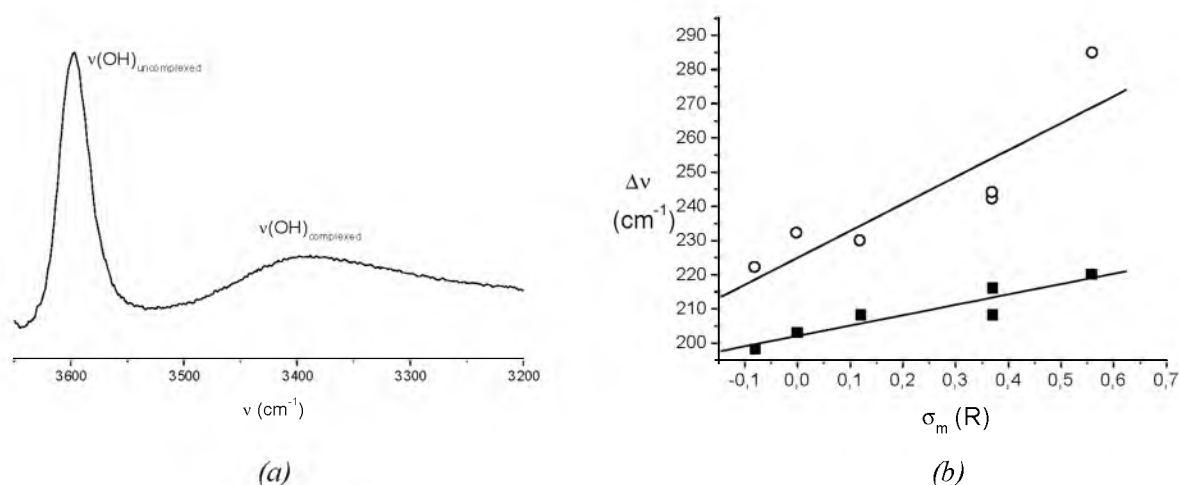


Figure 2.6 (a) Part of the FTIR spectrum of the 1:1 complex of host **26** and resorcinol in CDCl_3 , showing the OH stretching vibration belonging to free and bound guest. (b) $\Delta \nu(\text{OH})$ values as a function of the Hammett constant (σ_m (R), see Table 2.1) of the guest substituent for complexes with hosts **26** (■) and **31** (○).

(Figure 2.6a). When the $\Delta \nu(\text{OH})$ values ($\Delta \nu(\text{OH}) = \nu(\text{OH})_{\text{uncomplexed}} - \nu(\text{OH})_{\text{complexed}}$) observed for each of the complexes were compared to the $\Delta \nu(\text{OH})$ values of the complexes between the guests and host **31** (Figure 2.6b), it was evident that in the case of host **26** the $\Delta \nu(\text{OH})$ values were significantly smaller and less dependent on the 5-substituent of the guest. A smaller $\Delta \nu(\text{OH})$ value corresponds to a relatively longer hydrogen bond, which can be expected when it is assumed that the guests cannot be docked as deeply in host **26** as in host **31**. Clip **29** has 1,4-dimethoxybenzene substituted side-walls and therefore should form stronger host-guest complexes than **26**. Table 2.1 shows that this is hardly the case. As compared to clip **1**, the host-guest binding affinities of **29** are extremely weak, which is a result of the narrow cavity of the latter host. NMR dilution experiments in CDCl_3 showed that **29**, unlike dimethoxybenzene-walled clip **1**, does not dimerize in chloroform solution,²⁰ which is also in line with the aforementioned narrowness of the cavity. The host-guest binding strength of **30** is even lower

than that of **26** and **29**, because of an unfavorable combination of π - π interactions and hydrogen bonding, which has been observed before in clips containing 2,3-connected naphthalene side-walls.³

2.5 Concluding remarks

Several procedures to synthesize clip molecules with modified convex sides have been described in this chapter. The routes to the benzoic acid and phenol functionalized clips lead to high yields of products which are easily purified by precipitation or crystallization. These two types of clips are ideal precursors to water-soluble receptors, because they can be deprotonated and then dissolved in aqueous solutions (see Chapter 3). Furthermore, they can be alkylated with long hydrocarbon chains to generate potentially interesting liquid crystalline materials (see Chapters 5 and 6).

Bipyridine-functionalized clips **26**, **29** and **30** are receptors to which transition metal centers can be easily coupled. In this way it is possible - at least in principle - to influence the physical or catalytic properties of the metal center by the binding of a guest molecule in the cavity of the clip. Furthermore, these clips can also be made water-soluble by protonation or quaternarization of the bipyridine ligand. By allowing the metalloclips to self-assemble in water, interesting metallo-aggregates can be obtained. Studies toward the latter will be presented in Chapter 4.

2.6 Experimental section

2.6.1 Materials and methods

Diethyl ether, toluene and benzene were distilled under nitrogen from sodium benzophenone ketyl. Dichloromethane, chloroform and 1,2-dichloroethane were distilled from CaH₂. MgSO₄, K₂CO₃ and KI were dried in an oven (150°C). All other solvents and chemicals were commercial materials and used without purification. Merck Silica Gel (60H) was used for column chromatography and Merck Silica Gel F₂₅₄ plates for thin layer chromatography. Melting points were determined on a Jeneval polarization microscope THMS 600 hot stage and are uncorrected. Infrared spectra were recorded on a BioRad FTS-25 spectrometer. ¹H NMR and ¹³C{¹H} NMR spectra were recorded on Bruker WM-200, Bruker AM-300, Bruker AM-400, and Bruker AMX-500 instruments. Chemical shifts are reported in ppm downfield from internal (CH₃)₄Si (0.00 ppm) in the case of ¹H NMR spectra in CDCl₃, otherwise the solvent peak was used as a reference (DMSO-d₆: 2.54 ppm). In the case of the ¹³C spectra, the solvent peak was used as a reference (CDCl₃: 77.0 ppm; DMSO-d₆: 43.5 ppm). Abbreviations used are: s = singlet, d = doublet, dd = doublet of doublets, m = multiplet, br = broad. EI and FAB mass spectra were recorded on a VG-7070E instrument. The matrix used for FAB was 3-nitrobenzylalcohol. Elemental analyses were determined with a Carbo Erba Ea 1108 instrument.

2.6.2 NMR titrations

The CDCl₃ solvent used for the titration experiments was dried over P₂O₅ for one week, distilled *in vacuo*, and stored under argon. Association constants were determined by ¹H NMR titrations on a Bruker AMX-500 instrument at 298 K, using optimal concentrations to minimize errors in the fit procedure.¹⁵ For each titration experiment the spectra of at least 10 samples were recorded.

2.6.3 Solution FTIR experiments

Fourier transform infrared solution spectra were recorded on a BioRad FTS-25 spectrometer with a resolution of 2.0 cm⁻¹. Solutions of equimolar amounts of host and guest in CDCl₃ (concentrations approximately 1 mM) were brought in a cuvet between two NaCl plates. The optical bench of the spectrometer was continuously flushed with dry nitrogen gas. For each spectrum 64 scans were recorded. The measured data were corrected for the solvent and analysis was performed using the WIN-IR software.

2.6.4 Syntheses

8b,8c-Di(4-methylphenyl)perhydro-2,6-dioxo-3a,4a,7a,8a-tetraazacyclopenta[def]fluorene-4,8-dione (4):

This compound was prepared according to a slightly modified literature procedure.²¹ Ditoluylglycoluril (7.3 g, 23 mmol) and paraformaldehyde (3.4 g, 113 mmol) were suspended in DMSO (50 mL). Aqueous 1 N NaOH was added dropwise until a pale yellow solution was obtained, and the mixture was stirred for 16 h. The solution was acidified to pH 1 with aqueous 37% HCl and refluxed for 2 h. After cooling, water (10 mL) was slowly added while stirring vigorously and the resulting precipitate was filtered, washed with water (20 mL) and with cold ethanol (50 mL). The product was dried under vacuum to give 8.45 g (92%) of **4** as a white powder.

¹H NMR (CDCl₃, 300.13 MHz) δ 7.04 (d, 4H, ArH *meta* to CH₃, ³J = 6.5 Hz), 6.96 (d, 4H, ArH *ortho* to CH₃, ³J = 6.5 Hz), 5.63 (d, 4H, NCH₂O *out*, ²J = 10.6 Hz), 4.54 (d, 4H, NCH₂O *in*, ²J = 10.6 Hz), 2.21 (s, 6H, CH₃) ppm; ¹³C{¹H} NMR (CDCl₃, 75.47 MHz) δ 159.12 (urea C=O), 139.81 (ArC *ipso* to CH₃), 130.22 (ArC *para* to CH₃), 129.93 (ArC *meta* to CH₃), 128.40 (ArC *ortho* to CH₃), 80.12 (NC(Ar)N), 72.48 (NCH₂O), 21.6 (ArCH₃) ppm.

4-[8b-(4-Carboxyphenyl)-4,8-dioxoperhydro-2,6-dioxo-3a,4a,7a,8a-tetraazacyclopenta[def]fluoren-8-yl]-benzoic acid (5):

A suspension of **4** (5.0 g, 12.3 mmol) and KMnO₄ (10 g, 63 mmol) in water (125 mL) was refluxed for 16 h. After cooling, the brown suspension was filtered over infusorial earth. The residue was washed with aqueous 1 N NaOH (100 mL) and the pale yellow filtrate was acidified to pH 1 with aqueous 37% HCl while stirring vigorously. The precipitate was filtered off, washed with water (200 mL) and dried under vacuum over P₂O₅ to give 5.5 g (96%) of **5** as a white powder. A sample was recrystallized from acetic acid for analysis. Single crystals of **5** were obtained by slow evaporation of an ethanol solution of the compound.

M.p. 302°C (dec.); IR (KBr pellet) ν 3500-3000 (OH), 3069 (ArH), 2938 (CH₂), 1754, 1736, 1702 (C=O), 1467, 1409, 1385 (C=C), 1309, 1293, 1252 (CH₂), 1028 (COC) cm⁻¹; ¹H NMR (CDCl₃/CD₃OD 9:1 (v/v), 300.13 MHz) δ 7.85 (d, 4H, ArH *ortho* to COOH, ³J = 8.2 Hz), 7.30 (d, 4H, ArH *meta* to COOH, ³J = 8.2 Hz), 5.66 (d, 4H, NCH₂O *out*, ²J = 11.1 Hz), 4.57 (d, 4H, NCH₂O *in*, ²J = 11.1 Hz) ppm; ¹³C{¹H} NMR (CDCl₃/CD₃OD 9:1 (v/v), 75.47 MHz) δ 166.44 (COOH), 157.34 (urea C=O), 136.19 (ArC *ipso* to COOH), 131.50 (ArC *para* to COOH), 129.33 (ArC *ortho* to COOH), 127.09 (ArC *meta* to COOH), 78.38 (NC(Ar)C), 71.26 (NCH₂O) ppm; FAB-MS *m/z* 467 (M + H)⁺. Anal. Calcd for C₂₂H₁₈N₄O₈(CH₃COOH): C, 54.76; H, 4.21; N, 10.64. Found: C, 54.76; H, 4.50; N, 10.35.

4-[13b-(4-Carboxyphenyl)-1,4,8,11-tetramethoxy-6,13-dioxo-5,7,12,13b,13c,14-hexahydro-5a,6a,12a,13a-tetraazabenz[5,6]azuleno[2,1,8-*ija*]benzo[*f*]azulen-13-yl]benzoic acid (6):

Method A: Compound **5** (650 mg, 1.39 mmol) and *p*-dimethoxybenzene (580 mg, 4.18 mmol) were dissolved in a mixture of acetic anhydride (1.5 mL) and trifluoroacetic acid (1.5 mL). The mixture was heated at 100°C for 64 h. After cooling, methanol (6 mL) was added dropwise and the precipitate was filtered off, washed with methanol (50 mL) and diethylether (50 mL) to yield 800 mg (81%) of **6** as a white solid.

Method B: Starting from **12** (120 mg, 0.16 mmol) this compound was synthesized as described for **14**. Yield: 112 mg (97%) of **6** as a white solid.

M.p. 309°C (dec.); IR (KBr pellet) ν 3500-3300 (OH), 3046 (ArH), 2937, 2915, 2837 (CH₂), 1727, 1702, 1678 (C=O), 1484, 1467, 1427, 1413, 1360 (C=C), 1305, 1261, 1225 (CH₂), 1080 (COC) cm⁻¹; ¹H NMR (DMSO-*d*₆, 300.14 MHz) δ 7.74 (d, 4H, ArH *ortho* to COOH, ³J = 8.4 Hz), 7.20 (d, 4H, ArH *meta* to COOH, ³J = 8.4 Hz), 6.86 (s, 4H, ArH *side-wall*), 5.43 (d, 4H, NCH₂Ar *out*, ²J = 16.0 Hz), 3.75 (s, 12H, OCH₃), 3.72 (d, 4H, NCH₂Ar *in*, ²J = 16.0 Hz) ppm; ¹³C{¹H} NMR (DMSO-*d*₆, 75.47 MHz) δ 170.57 (COOH), 160.46 (urea C=O), 154.56 (ArC *ipso* to OCH₃), 142.14 (ArC *ipso* to COOH), 134.84 (ArC *para* to COOH), 133.53 (ArC *ortho* to COOH), 132.26 (ArC *meta* to COOH), 131.31 (ArC *ipso* to CH₂N), 116.09 (ArC *para* to CH₂N), 88.24 (NC(Ar)N), 60.57 (OCH₃), 40.26 (NCH₂Ar) ppm; FAB-MS *m/z* 707 (M + H)⁺. Anal. Calcd for C₃₈H₃₄N₄O₁₀: C, 64.58; H, 4.85; N, 7.93. Found: C, 64.64; H, 4.80; N, 7.82.

Methyl 4-8b-[4-(methoxycarbonyl)phenyl]-4,8-dioxoperhydro-2,6-dioxo-3a,4a,7a,8a-tetraazacyclopenta-[def]fluoren-8-ylbenzoate (7):

Compound **5** (5.4 g, 11.6 mmol) was suspended in methanol (300 mL), 98% H₂SO₄ (0.25 mL) was added and the mixture was refluxed for 16 h. After cooling, the solvent was evaporated. The residue was dissolved in CH₂Cl₂ (200 mL) and the organic layer was washed with a saturated aqueous NaHCO₃ solution (200 mL) and with water (200 mL), dried (MgSO₄), filtered and evaporated to dryness. Purification by column chromatography (silica, eluent 1% MeOH in CHCl₃, R_f = 0.16) afforded 3.2 g (56%) of **7** as a white solid.

M.p. 221°C; IR (KBr pellet) ν 3048 (ArH), 2960, 2927, 2854 (CH₂), 1748, 1736, 1714 (C=O), 1475, 1451, 1389 (C=C), 1212, 1290, 1254 (CH₂), 1178, 1110, 1020 (COC) cm⁻¹; ¹H NMR (CDCl₃, 300.13 MHz) δ 7.82 (d, 4H, ArH *ortho* to C(O)OCH₃, ³J = 8.0 Hz), 7.28 (d, 4H, ArH *meta* to C(O)OCH₃, ³J = 8.0 Hz), 5.68 (d, 4H, NCH₂O *out*, ²J =

10.7 Hz), 4.52 (d, 4H, NCH_2O in, $^2J = 10.7$ Hz), 3.87 (s, 6H, COOCH_3) ppm; $^{13}\text{C}\{^1\text{H}\}$ NMR (CDCl_3 , 75.47 MHz) δ 165.90 ($\text{C}(\text{O})\text{OCH}_3$), 158.09 (urea $\text{C}=\text{O}$), 137.52 (ArC *ipso* to $\text{C}(\text{O})\text{OCH}_3$), 131.35 (ArC *para* to $\text{C}(\text{O})\text{OCH}_3$), 130.03 (ArC *ortho* to $\text{C}(\text{O})\text{OCH}_3$), 127.90 (ArC *meta* to $\text{C}(\text{O})\text{OCH}_3$), 79.12 ($\text{NC}(\text{Ar})\text{N}$), 72.06 (NCH_2O), 52.32 ($\text{C}(\text{O})\text{OCH}_3$); EI-MS m/z 494 (M^+). Anal. Calcd for $\text{C}_{24}\text{H}_{22}\text{N}_4\text{O}_8$: C, 58.30; H, 4.48; N, 11.33. Found: C, 58.86; H, 4.03; N, 11.22.

Methyl 4-1,3,4,6-tetra[(acetyloxy)methyl]-6a-[4-(methoxycarbonyl)phenyl]-2,5-dioxoperhydroimidazo[4,5-d]-imidazol-3-ylbenzoate (8):

Compound 7 (3.9 g, 7.9 mmol) and *p*-toluenesulfonic acid monohydrate (0.40 g, 2.1 mmol) were suspended in acetic anhydride (15 mL) and the mixture was stirred at 110°C for 40 h. After cooling, the dark solution was poured into aqueous 1 N NaOH (300 mL) and the product was extracted with CH_2Cl_2 (100 mL). The organic layer was washed with a saturated aqueous NaCl solution (200 mL) and with water (200 mL), dried (MgSO_4) and evaporated to dryness. The residue was dissolved in a minimal amount of CHCl_3 and this solution was added dropwise to stirred diethyl ether. After filtration, 3.9 g (70%) of **8** was obtained as an off-white powder.

M.p. 269°C ; IR (KBr pellet) ν 3050 (ArH), 2925, 2854 (CH_2), 1744 ($\text{C}=\text{O}$), 1616 ($\text{C}=\text{C}$), 1437, 1410, 1367 ($\text{C}=\text{C}$), 1285, 1220 (CH_2), 1114, 1019 (COC) cm^{-1} ; ^1H NMR (CDCl_3 , 300.13 MHz) δ 7.75 (d, 4H, ArH *ortho* to $\text{C}(\text{O})\text{OCH}_3$, $^3J = 8.5$ Hz), 6.97 (d, 4H, ArH *meta* to $\text{C}(\text{O})\text{OCH}_3$, $^3J = 8.5$ Hz), 5.68 (d, 4H, $\text{NCH}_2\text{OC}(\text{O})\text{CH}_3$ out, $^2J = 11.6$ Hz), 5.28 (d, 4H, $\text{NCH}_2\text{OC}(\text{O})\text{CH}_3$ in, $^2J = 11.6$ Hz), 3.89 (s, 6H, $\text{C}(\text{O})\text{OCH}_3$), 2.03 (s, 12H, $\text{C}(\text{O})\text{CH}_3$) ppm; $^{13}\text{C}\{^1\text{H}\}$ NMR (CDCl_3 , 75.47 MHz) δ 169.74 ($\text{C}(\text{O})\text{CH}_3$), 165.52 ($\text{C}(\text{O})\text{OCH}_3$), 156.11 (urea $\text{C}=\text{O}$), 135.71 (ArC *ipso* to $\text{C}(\text{O})\text{OCH}_3$), 131.72 (ArC *para* to $\text{C}(\text{O})\text{OCH}_3$), 129.63 (ArC *ortho* to $\text{C}(\text{O})\text{OCH}_3$), 128.28 (ArC *meta* to $\text{C}(\text{O})\text{OCH}_3$), 86.58 ($\text{NC}(\text{Ar})\text{N}$), 66.69 ($\text{NCH}_2\text{OC}(\text{O})\text{CH}_3$), 52.43 ($\text{C}(\text{O})\text{OCH}_3$), 20.73 ($\text{C}(\text{O})\text{CH}_3$) ppm; FAB-MS m/z 721 ($\text{M} + \text{Na}^+$). Anal. Calcd for $\text{C}_{32}\text{H}_{34}\text{N}_4\text{O}_{14}$: C, 55.01; H, 4.91; N, 8.02. Found: C, 54.91; H, 4.79; N, 8.12.

Methyl 4-1,3,4,6-tetra(chloromethyl)-6a-[4-(methoxycarbonyl)phenyl]-2,5-dioxoperhydroimidazo[4,5-d]imidazol-3-ylbenzoate (9):

Compound **8** (400 mg, 0.66 mmol) was suspended in thionyl chloride (2 mL). One drop of water was added, and the mixture was stirred under argon for 20 h. Diethyl ether (10 mL) was added and the white suspension was stored at 4°C for 2 h. The precipitate was filtered off and dried under vacuum to give 290 mg (84%) of **9** as a white, very hygroscopic powder.

M.p. 258°C (dec.); IR (KBr pellet) ν 3052 (ArH), 2955 (CH_2), 1749, 1729 ($\text{C}=\text{O}$), 1451, 1438, 1410 ($\text{C}=\text{C}$), 1317, 1282 (CH_2), 1115 (COC) cm^{-1} ; ^1H NMR (CDCl_3 , 300.13 MHz) δ 7.85 (d, 4H, ArH *ortho* to $\text{C}(\text{O})\text{OCH}_3$, $^3J = 8.6$ Hz), 7.07 (d, 4H, ArH *meta* to $\text{C}(\text{O})\text{OCH}_3$, $^3J = 8.6$ Hz), 5.35 (d, 4H, NCH_2Cl out, $^2J = 11.4$ Hz), 5.27 (d, 4H, NCH_2Cl in, $^2J = 11.4$ Hz), 3.90 (s, 6H, $\text{C}(\text{O})\text{OCH}_3$) ppm; $^{13}\text{C}\{^1\text{H}\}$ NMR (CDCl_3 , 75.47 MHz) δ 165.50 ($\text{C}(\text{O})\text{OCH}_3$), 153.88 (urea $\text{C}=\text{O}$), 133.73 (ArC *ipso* to $\text{C}(\text{O})\text{OCH}_3$), 132.47 (ArC *para* to $\text{C}(\text{O})\text{OCH}_3$), 130.11 (ArC *ortho* to $\text{C}(\text{O})\text{OCH}_3$), 128.65 (ArC *meta* to $\text{C}(\text{O})\text{OCH}_3$), 86.84 ($\text{NC}(\text{Ar})\text{N}$), 66.65 (NCH_2Cl), 52.50 ($\text{C}(\text{O})\text{OCH}_3$) ppm; FAB-MS m/z 642 ($\text{M} + \text{H}^+$). Anal. Calcd for $\text{C}_{24}\text{H}_{22}\text{N}_4\text{O}_6\text{Cl}_4$: C, 47.70; H, 3.67; N, 9.27. Found: C, 47.91; H, 3.58; N, 9.15.

Methyl 4-13b-[4-(methoxycarbonyl)phenyl]-6,13-dioxo-5,7,12,13b,13c,14-hexahydro-5a,6a,12a,13a-tetraaza-benzo[5,6]azuleno[2,1,8-*ij*a]benzo[*f*]azulen-13-ylbenzoate (10):

A mixture of **9** (1.50 g, 2.48 mmol) and AlCl_3 (2.31 g, 17.3 mmol) in benzene (20 mL) was refluxed under nitrogen for 120 h. After cooling, aqueous 6 N HCl (20 mL) was added and the mixture was refluxed for 1 h. To the dark yellow solution CH_2Cl_2 (100 mL) was added and the organic layer was washed with water (2×200 mL) and evaporated to dryness. The product was purified by column chromatography (silica, $\text{CH}_2\text{Cl}_2/\text{MeOH}$ 197:3, v/v, $R_f = 0.30$) to yield 650 mg (36%) of **10** as a white powder.

M.p. 315°C (dec.); IR (KBr pellet) ν 3050 (ArH), 2956, 2921 (CH_2), 1722 ($\text{C}=\text{O}$), 1454, 1422 ($\text{C}=\text{C}$), 1283 (CH_2), 1115 (COC) cm^{-1} ; ^1H NMR (CDCl_3 , 300.13 MHz) δ 7.83 (d, 4H, ArH *ortho* to $\text{C}(\text{O})\text{OCH}_3$, $^3J = 8.6$ Hz), 7.24 (d, 4H, ArH, $^3J = 8.6$ Hz), 7.29-7.23 (m, 4H, ArH *ortho* to CH_2N), 7.16-7.09 (m, 4H, ArH *para* to CH_2N), 4.81 (d, 4H, NCH_2Ar out, $^2J = 15.8$ Hz), 4.11 (d, 4H, NCH_2Ar in, $^2J = 15.8$ Hz), 3.87 (s, 6H, $\text{C}(\text{O})\text{OCH}_3$) ppm; $^{13}\text{C}\{^1\text{H}\}$ NMR (75.47 MHz, CDCl_3) δ 166.75 ($\text{C}(\text{O})\text{OCH}_3$), 157.45 (urea $\text{C}=\text{O}$), 138.67 (ArC *ipso* to $\text{C}(\text{O})\text{OCH}_3$), 136.31 (ArC *para* to $\text{C}(\text{O})\text{OCH}_3$), 130.80 (ArC *para* to CH_2N), 130.09 (ArC *ortho* to $\text{C}(\text{O})\text{OCH}_3$), 129.48 (ArC *meta* to $\text{C}(\text{O})\text{OCH}_3$), 128.23 (ArC *ortho* to CH_2N), 127.95 (ArC *para* to CH_2N), 84.92 ($\text{NC}(\text{Ar})\text{N}$), 52.07 ($\text{C}(\text{O})\text{OCH}_3$), 45.31 (NCH_2Ar) ppm; FAB-MS m/z 615 ($\text{M} + \text{H}^+$). Anal. Calcd for $\text{C}_{36}\text{H}_{30}\text{N}_4\text{O}_6$: C, 70.35; H, 4.92; N, 9.12. Found: C, 70.73; H, 4.89; N, 8.77.

Methyl 4-13b-[4-(methoxycarbonyl)phenyl]-1,4,8,11-tetramethyl-6,13-dioxo-5,7,12,13b,13c,14-hexahydro-5a,6a,12a,13a-tetraazabenz[5,6]azuleno[2,1,8-*ija*]benzo[*f*]azulen-13-ylbenzoate (11):

Compound **9** (240 mg, 0.40 mmol) was suspended in 1,2-dichloroethane (10 mL). *p*-Xylene (2.5 mL) and SnCl₄ (0.5 mL, 4 mmol) were added and the mixture was refluxed under nitrogen for 64 h. After cooling, aqueous 6 N HCl (15 mL) was added and the mixture was refluxed for 1 h. After cooling, CH₂Cl₂ (100 mL) was added, the organic layer was washed with water (2 × 100 mL) and evaporated to dryness. After purification by column chromatography (silica, CH₂Cl₂/MeOH 397:3, v/v, R_f = 0.21), 60 mg (23%) of **11** was obtained as a white powder.

M.p. 354°C (dec.); IR (KBr pellet) ν 3054 (ArH), 2952, 2930 (CH₂), 1726, 1713 (C=O), 1458, 1422, 1408 (C=C), 1288 (CH₂), 1117 (COC) cm⁻¹; ¹H NMR (CDCl₃, 400.13 MHz) δ 7.78 (d, 4H, ArH *ortho* to C(O)OCH₃, ³J = 8.6 Hz), 7.23 (d, 4H, ArH *meta* to C(O)OCH₃, ³J = 8.6 Hz), 6.85 (s, 4H, ArH side-wall), 5.06 (d, 4H, NCH₂Ar *out*, ²J = 15.7 Hz), 3.86 (s, 6H, C(O)OCH₃), 3.85 (d, 4H, NCH₂Ar *in*, ²J = 15.7 Hz), 2.46 (s, 12H, ArCH₃) ppm; ¹³C{¹H} NMR (CDCl₃, 100.61 MHz) δ 166.18 (C(O)OCH₃), 157.73 (urea C=O), 139.90 (ArC *ipso* to C(O)OCH₃), 135.42 (ArC *para* to C(O)OCH₃), 134.55 (ArC *ipso* to CH₃), 130.50 (ArC *ipso* to CH₂N), 129.86 (ArC *ortho* and *meta* to C(O)OCH₃), 128.18 (ArC *para* to CH₂N), 84.63 (NC(Ar)N), 52.24 (C(O)OCH₃), 40.60 (NCH₂Ar), 20.24 (ArCH₃) ppm; FAB-MS *m/z* 671 (M + H)⁺. Anal. Calcd for C₄₀H₃₈N₄O₆: C, 71.63; H, 5.71; N, 8.35. Found: C, 71.51; H, 5.62; N, 8.18.

Methyl 4-1,4,8,11-tetramethoxy-13b-[4-(methoxycarbonyl)phenyl]-6,13-dioxo-5,7,12,13b,13c,14-hexahydro-5a,6a,12a,13a-tetraazabenz[5,6]azuleno[2,1,8-*ija*]benzo[*f*]azulen-13-ylbenzoate (12):

Starting from **7** (310 mg, 0.63 mmol) and *p*-dimethoxybenzene (220 mg, 1.59 mmol) in a mixture of acetic anhydride (1 mL) and trifluoroacetic acid (1 mL), this compound was synthesized as described for **6** to yield 375 mg (81%) of **12** as a white solid. Single crystals of **12** were obtained by slow diffusion of diethyl ether in a solution of the compound in dichloromethane.

M.p. 336°C (dec.); IR (KBr pellet) ν 3010 (ArH), 2955, 2923, 2851 (CH₂), 1729, 1719 (C=O), 1486, 1465, 1445 (C=C), 1307, 1298, 1281, 1262 (CH₂), 1121, 1078 (COC) cm⁻¹; ¹H NMR (CDCl₃, 300.13 MHz): δ 7.76 (d, 4H, ArH *ortho* to C(O)OCH₃, ³J = 8.5 Hz), 7.17 (d, 4H, ArH *meta* to C(O)OCH₃, ³J = 8.5 Hz), 6.43 (s, 4H, ArH side-wall), 5.54 (d, 4H, NCH₂Ar *out*, ²J = 15.9 Hz), 3.85 (s, 6H, C(O)OCH₃), 3.75 (s, 12H, OCH₃), 3.72 (d, 4H, NCH₂Ar *in*, ²J = 15.9 Hz) ppm; ¹³C{¹H} NMR (CDCl₃, 75.47 MHz): δ 166.22 (C(O)OCH₃), 157.56 (urea C=O), 150.90 (ArC *ipso* to OCH₃), 139.33 (ArC *ipso* to C(O)OCH₃), 130.36 (ArC *para* to C(O)OCH₃), 129.81 (ArC *ortho* to C(O)OCH₃), 128.17 (ArC *meta* to C(O)OCH₃), 126.84 (ArC *ipso* to CH₂N), 111.80 (ArC *para* to CH₂N), 84.85 (NC(Ar)N), 56.62 (ArOCH₃), 52.19 (C(O)OCH₃), 36.94 (NCH₂Ar) ppm; FAB-MS *m/z* 735 (M + H)⁺. Anal. Calcd for C₄₀H₃₈N₄O₁₀: C, 65.39; H, 5.21; N, 7.63. Found: C, 65.62; H, 5.12; N, 7.55.

Methyl 4-5,9,14,18-tetramethoxy-16b-[4-(methoxycarbonyl)phenyl]-7,16-dioxo-6,8,15,16b,16c,17-hexahydro-6a,7a,15a,16a-tetraazanaphtho[2',3':5,6]azuleno[2,1,8-*ija*]naphtho[2,3-*f*]azulen-16-ylbenzoate (13):

Compound **9** (560 mg, 0.93 mmol) and 1,4-dimethoxynaphthalene¹ (520 mg, 2.8 mmol) were dissolved in 1,2-dichloroethane (10 mL). SnCl₄ (1.5 mL, 12 mmol) was added and the mixture was refluxed under nitrogen for 40 h. After cooling, aqueous 6 N HCl (10 mL) was added and the mixture was refluxed for 1 h. After cooling, CH₂Cl₂ (50 mL) was added and the organic layer was washed with water (2 × 100 mL) and evaporated to dryness. After purification by column chromatography (silica, CH₂Cl₂/MeOH 99:1, v/v, R_f = 0.08), 550 mg (71%) of **13** was obtained as an off-white solid.

M.p. 337°C (dec.); IR (KBr pellet) ν 3018 (ArH), 2954, 2848 (CH₂), 1728, 1718 (C=O), 1488, 1460 (C=C), 1296, 1280 (CH₂), 1074 (COC) cm⁻¹; ¹H NMR (CDCl₃, 300.13 MHz) δ 8.00-7.94 (m, 4H, NaphtH-5,8), 7.86 (d, 4H, ArH *ortho* to C(O)OCH₃, ³J = 8.5 Hz), 7.45-7.39 (m, 4H, NaphtH-6,7), 7.31 (d, 4H, ArH *meta* to C(O)OCH₃, ³J = 8.5 Hz), 5.76 (d, 4H, NCH₂Ar *out*, ²J = 15.9 Hz), 4.03 (s, 12H, ArOCH₃), 3.89 (s, 6H, C(O)OCH₃), 3.86 (d, 4H, NCH₂Ar *in*, ²J = 15.9 Hz) ppm; ¹³C{¹H} NMR (CDCl₃, 75.47 MHz) δ 166.45 (C(O)OCH₃), 156.18 (urea C=O), 149.35 (ArC *ipso* to OCH₃), 138.02 (ArC *ipso* to C(O)OCH₃), 130.43 (ArC *para* to C(O)OCH₃), 129.62, 127.99, 127.34, 127.08 (all ArC), 122.32 (ArC *ipso* to CH₂N), 84.12 (NC(Ar)N), 62.64 (ArOCH₃), 52.44 (C(O)OCH₃), 38.87 (NCH₂Ar) ppm; FAB-MS *m/z* 835 (M + H)⁺. Anal. Calcd for C₄₈H₄₂N₄O₁₀: C, 69.06; H, 5.07; N, 6.71. Found: C, 68.88; H, 5.05; N, 6.97.

4-[13b-(4-Carboxyphenyl)-6,13-dioxo-5,7,12,13b,13c,14-hexahydro-5a,6a,12a,13a-tetraazabenz[5,6]azuleno[2,1,8-*ija*]benzo[*f*]azulen-13-yl]benzoic acid (14):

Compound **10** (85 mg, 0.14 mmol) was stirred in a mixture of dioxane, methanol and aqueous 4N NaOH (15:4:1, v/v/v, 8 mL) for 16 h. The precipitate was filtered off, dried and redissolved in water (2 mL). Aqueous 1 N HCl was slowly added until pH = 1 while stirring the mixture vigorously. The formed precipitate was filtered off (small G3 filter, without the application of vacuum), washed with water (1 mL) and dried under vacuum over P₂O₅ to yield 75 mg (95%) of **14** as a white solid.

M.p. 380°C (dec.); ¹H NMR (DMSO-d₆, 300.13 MHz) δ 7.83 (d, 4H, ArH *ortho* to C(O)OH, ³J = 8.6 Hz), 7.24 (d, 4H, ArH *meta* to C(O)OH, ³J = 8.6 Hz), 7.29-7.23 (m, 4H, ArH *ortho* to CH₂N), 7.16-7.09 (m, 4H, ArH *para* to CH₂N), 4.81 (d, 4H, NCH₂Ar *out*, ²J = 15.8 Hz), 4.11 (d, 4H, NCH₂Ar *in*, ²J = 15.8 Hz) ppm; ¹³C{¹H} NMR (75.47 MHz, CDCl₃) δ 166.75 (C(O)OH), 157.45 (urea C=O), 138.67 (ArC *ipso* to COOH), 136.31 (ArC *para* to COOH), 130.80 (ArC *para* to CH₂N), 130.09 (ArC *ortho* to COOH), 129.48 (ArC *meta* to COOH), 128.23 (ArC *ortho* to CH₂N), 127.95 (ArC *para* to CH₂N), 84.92 (NC(Ar)N), 52.07 (C(O)OCH₃), 45.31 (NCH₂Ar) ppm; FAB-MS *m/z* 587 (M + H)⁺.

4-[13b-(4-Carboxyphenyl)-1,4,8,11-tetramethyl-6,13-dioxo-5,7,12,13b,13c,14-hexahydro-5a,6a,12a,13a-tetraazabenzof[5,6]azuleno[2,1,8-*ija*]benzo[*f*]azulen-13-yl]benzoic acid (15):

Starting from **11** (80 mg, 0.12 mmol) this compound was synthesized as described for **14**. Yield: 74 mg (96%) of **15** as a white solid.

M.p. > 400°C (dec.); IR (KBr pellet) ν 3182 (br, OH), 2048 (ArH), 2959, 2924 (CH₂), 1727, 1694, 1674 (C=O), 1475, 1449, 1413 (C=C), 1308, 1266, 1221 (CH₂), 1141 (COC) cm⁻¹; ¹H NMR (DMSO-d₆, 300.13 MHz) δ 7.77 (d, 4H, ArH *ortho* to COOH, ³J = 8.3 Hz), 7.34 (d, 4H, ArH *meta* to COOH, ³J = 8.3 Hz), 6.90 (s, 4H, ArH *side-wall*), 4.95 (d, 4H, NCH₂Ar *out*, ²J = 16.0 Hz), 3.90 (d, 4H, NCH₂Ar *in*, ²J = 16.0 Hz), 2.43 (s, 12H, CH₃) ppm; ¹³C{¹H} NMR (DMSO-d₆, 75.47 MHz) δ 170.62 (COOH), 160.92 (urea C=O), 142.98 (ArC *ipso* to COOH), 140.36 (ArC *ortho* to COOH), 137.82 (ArC *para* to COOH), 135.00 (ArC *ipso* to CH₂N), 133.47 (ArC *meta* to COOH), 132.46 (ArC *para* to CH₂N), 88.07 (NC(Ar)N), 42.18 (NCH₂Ar), 23.72 (ArCH₃) ppm; FAB-MS *m/z* 643 (M + H)⁺. Anal. Calcd for C₃₈H₃₄N₄O₆: C, 71.01; H, 5.33; N, 8.72. Found: C, 71.21; H, 5.55; N, 8.32.

4-[16b-(4-Carboxyphenyl)-5,9,14,18-tetramethoxy-7,16-dioxo-6,8,15,16b,16c,17-hexahydro-6a,7a,15a,16a-tetraazaphtho[2',3':5,6]azuleno[2,1,8-*ija*]naphtho[2,3-*f*]azulen-16-yl]benzoic acid (16):

Starting from **13** (65 mg, 0.078 mmol) this compound was synthesized as described for **14**. Yield: 60 mg (96%) of **16** as a white solid.

M.p. 360°C (dec.); ¹H NMR (DMSO-d₆, 300.14 MHz) δ 7.98-7.92 (m, 4H, NaphtH-5,8), 7.82 (d, 4H, ArH *ortho* to COOH, ³J = 8.4 Hz), 7.55-7.49 (m, 4H, NaphtH-6,7), 7.39 (d, 4H, ArH *meta* to COOH, ³J = 8.4 Hz), 5.58 (d, 4H, NCH₂Ar *out*, ²J = 16.0 Hz), 4.02 (d, 4H, NCH₂Ar *in*, ²J = 16.0 Hz), 3.96 (s, 12H, OCH₃) ppm; ¹³C{¹H} NMR (DMSO-d₆, 50.32 MHz) δ 166.65 (COOH), 156.64 (urea C=O), 149.35 (ArC *ipso* to OCH₃), 138.17 (ArC *ipso* to COOH), 130.08 (ArC *para* to COOH), 129.68, 128.62, 127.54, 126.79 (all ArC), 122.74 (ArC *ipso* to CH₂N), 84.22 (NC(Ar)N), 62.48 (OCH₃), 38.19 (NCH₂Ar) ppm; FAB-MS *m/z* 829 (M + Na)⁺. Anal. calcd for C₄₆H₃₈N₄O₁₀: C, 68.48; H, 4.75; N, 6.94. Found: C, 68.58; H, 4.79; N, 6.81.

3a,6a-Di(4-methoxyphenyl)perhydroimidazo[4,5-*d*]imidazole-2,5-dione (17):

To a suspension of 4,4'-dimethoxybenzil (2.5 g, 9.3 mmol) and urea (1.11 g, 18.5 mmol) in toluene (50 mL) was added trifluoroacetic acid (2.5 mL). The mixture was refluxed for 16 h using a Dean Stark trap to azeotropically remove the formed water. After cooling, the precipitate was filtered off, washed with ethanol (200 mL) and dried under vacuum to give 2.3 g (70%) of **17** as a white solid.

M.p. 354°C (dec.); IR (KBr pellet) ν 3600-3100 (NH), 2980 (CH₂), 1686 (C=O), 1514, 1469 (C=C), 1304, 1258 (CH₂), 1035 (COC) cm⁻¹; ¹H NMR (DMSO-d₆, 300.13 MHz) δ 7.67 (s, 4H, NH), 7.01 (d, 4H, ArH *meta* to OCH₃, ³J = 8.4 Hz), 6.69 (d, 4H, ArH *ortho* to OCH₃, ³J = 8.4 Hz), 3.66 (s, 6H, OCH₃) ppm; ¹³C{¹H} NMR (DMSO-d₆, 75.47 MHz) δ 164.63 (urea C=O), 162.72 (ArC *ipso* to OCH₃), 134.41 (ArC *para* to OCH₃), 132.29 (ArC *meta* to OCH₃), 116.73 (ArC *ortho* to OCH₃), 85.59 (NC(Ar)N), 59.01 (OCH₃) ppm. Anal. Calcd for C₁₈H₁₈N₄O₄: C, 61.01; H, 5.12; N, 15.81. Found: C, 61.64; H, 5.16; N, 15.14.

8b,8c-Di(4-methoxyphenyl)perhydro-2,6-dioxo-3a,4a,7a,8a-tetraazacyclopenta[*def*]fluorene-4,8-dione (18):

Compound **17** (3.8 g, 10.7 mmol) and paraformaldehyde (1.65 g, 55 mmol) were suspended in DMSO (50 mL). Aqueous 1 N NaOH was added until pH = 9. The white suspension was stirred for 16 h. Aqueous 37% HCl was added until pH = 1, and the mixture was refluxed for 2 h. After cooling, water (15 mL) was added dropwise while stirring the suspension vigorously. The product was filtered off, washed with cold ethanol (10 mL) and dried under vacuum to yield 3.8 g (81%) of **18** as a white solid.

M.p. 255°C; IR (KBr pellet) ν 3043, 3008 (ArH), 2934, 2914, 2873 (CH₂), 1747, 1729 (C=O), 1513, 1476, 1412 (C=C), 1310, 1256 (CH₂), 1064, 1034 (COC) cm⁻¹; ¹H NMR (CDCl₃, 300.13 MHz) δ 7.06 (d, 4H, ArH *meta* to OCH₃, ³J = 8.8 Hz), 6.67 (d, 4H, ArH *ortho* to OCH₃, ³J = 8.8 Hz), 5.63 (d, 4H, NCH₂O *out*, ²J = 10.9 Hz), 4.55 (d, 4H, NCH₂Ar *in*, ²J = 10.9 Hz), 3.72 (s, 6H, OCH₃) ppm; ¹³C{¹H} NMR (CDCl₃, 75.47 MHz) δ 160.10 (urea C=O), 158.47 (ArC *ipso* to OCH₃), 129.13 (ArC *meta* to OCH₃), 124.50 (ArC *para* to OCH₃), 113.99 (ArC *ortho* to OCH₃), 79.38 (NC(Ar)C), 71.86 (OCH₃), 55.19 (NCH₂O) ppm. Anal. Calcd for C₂₂H₂₂N₄O₆: C, 60.27; H, 5.06; N, 12.78. Found: C, 60.54; H, 5.06; N, 12.51.

8b,8c-Di(4-hydroxyphenyl)perhydro-2,6-dioxo-3a,4a,7a,8a-tetraazacyclopenta[def]fluorene-4,8-dione (19):

Compound **18** (990 mg, 2.26 mmol) was dissolved in CH₂Cl₂ (50 mL) and BBr₃ (2 mL) was added dropwise. The resulting white suspension was stirred under nitrogen for 1 h, and then an additional amount of BBr₃ (1 mL) was added dropwise. The mixture was stirred for 64 h. The resulting clear solution was cooled on ice and carefully 5 mL of methanol added. Aqueous 2 N HCl (50 mL) was added and the mixture was refluxed for 1 h. After cooling, the suspension was filtered and the residue was recrystallized from acetic acid to yield 875 mg (94%) of **19** as white needles.

M.p. 303°C; IR (KBr pellet) ν 3342 (OH), 3046, 3029 (ArH), 2874 (CH₂), 1735, 1725 (C=O), 1516, 1469, 1447, 1417, 1375 (C=C), 1312, 1275, 1255 (CH₂), 1029 (COC) cm⁻¹; ¹H NMR (DMSO-d₆, 500.14 MHz) δ 9.58 (br s, 2H, OH), 6.97 (d, 4H, ArH *meta* to OH, ³J = 8.3 Hz), 6.59 (d, 4H, ArH *ortho* to OH, ³J = 8.3 Hz), 5.44 (d, 4H, NCH₂O *out*, ²J = 11.0 Hz), 4.57 (d, 4H, NCH₂O *in*, ²J = 11.0 Hz) ppm; ¹³C{¹H} NMR (DMSO-d₆, 75.47 MHz) δ 157.06 (urea C=O), 156.70 (ArC *ipso* to OH), 128.14 (ArC *meta* to OH), 121.66 (ArC *para* to OH), 114.23 (ArC *ortho* to OH), 78.10 (NC(Ar)N), 70.53 (NCH₂O) ppm.

4-13b-[4-(Acetyloxy)phenyl]-1,4,8,11-tetramethoxy-6,13-dioxo-5,7,12,13b,13c,14-hexahydro-5a,6a,12a,-13a-tetraazabenzof[5,6]azuleno[2,1,8-*ija*]benzo[*f*]azulen-13-ylphenyl acetate (20):

A solution of **19** (510 mg, 1.24 mmol) in a mixture of acetic anhydride (1.25 mL) and trifluoroacetic acid (1.25 mL) was stirred at 100°C for 1 h. *p*-Dimethoxybenzene (500 mg, 3.62 mmol) was added and the mixture was stirred for 16 h. After cooling, methanol (5 mL) was added dropwise, the suspension was filtered and the residue was washed with methanol (5 mL) and diethyl ether (10 mL) to yield 760 mg (83%) of **20** as a white solid, which was immediately used in further synthesis.

¹H NMR (CDCl₃, 200.13 MHz) δ 7.08 (d, 4H, ArH *ortho* to OC(O)CH₃, ³J = 8.2 Hz), 6.86 (d, 4H, ArH *meta* to OC(O)CH₃), 6.58 (s, 4H, ArH side-wall), 5.57 (d, 4H, NCH₂Ar *out*, ²J = 15.8 Hz), 3.80 (d, 4H, NCH₂Ar *in*, ²J = 15.8 Hz), 3.73 (s, 12H, OCH₃), 2.24 (s, 6H, OC(O)CH₃) ppm.

13b,13c-Di(4-hydroxyphenyl)-1,4,8,11-tetramethoxy-5,7,12,13b,13c,14-hexahydro-5a,6a,12a,13a-tetraazabenzof[5,6]azuleno[2,1,8-*ija*]benzo[*f*]azulene-6,13-dione (21):

Compound **20** (745 mg, 1.0 mmol) was suspended in a mixture of dioxane (50 mL) and aqueous 1 N NaOH (12 mL). The mixture was stirred for 2 h, and aqueous 2 N HCl was added until pH = 1. The suspension was filtered, washed with water and diethyl ether and dried under vacuum to yield 585 mg (89%) of **21** as a white solid.

M.p. > 400°C (dec); IR (KBr pellet) ν 3467 (OH), 2838 (CH₂), 1690 (C=O), 1572, 1515, 1472 (C=C), 1302, 1259, 1223 (CH₂), 1076 (COC) cm⁻¹; ¹H NMR (DMSO-d₆, 200.13 MHz) δ 9.53 (br s, 2H, OH), 6.80 (s, 4H, ArH side-wall), 6.80 (d, 4H, ArH *meta* to OH, ³J = 7.8 Hz), 6.60 (d, 4H, ArH *ortho* to OH, ³J = 7.8 Hz), 5.37 (d, 4H, NCH₂Ar *out*, ²J = 16.0 Hz), 3.73 (s, 12H, OCH₃), 3.65 (d, 4H, NCH₂Ar *in*, ²J = 16.0 Hz) ppm; ¹³C{¹H} NMR (DMSO-d₆, 50.32 MHz) δ 157.27 (urea C=O), 156.71 (ArC *ipso* to OH), 150.52 (ArC *ipso* to OCH₃), 129.08 (ArC *meta* to OH), 127.63 (ArC *ipso* to CH₂N), 115.42 (ArC *para* to CH₂N), 111.84 (ArC *ortho* to OH), 84.58 (NC(Ar)N), 56.49 (OCH₃), 36.04 (NCH₂Ar) ppm; FAB-MS *m/z* 650 (M + H)⁺.

4-16b-[4-(Acetyloxy)phenyl]-5,9,14,18-tetramethoxy-7,16-dioxo-6,8,15,16b,16c,17-hexahydro-6a,7a,15a,-16a-tetraazanaphtho[2',3':5,6]azuleno[2,1,8-*ija*]naphtho[2,3-*f*]azulen-16-ylphenyl acetate (22):

Starting from **19** (90 mg, 0.22 mmol) and 1,4-dimethoxynaphthalene (90 mg, 0.48 mmol) in a mixture of acetic anhydride (0.5 mL) and trifluoroacetic acid (0.5 mL), this compound was synthesized as described for **20**. Yield: 90 mg (49%) of **22** as an off-white solid, which was immediately used in further synthesis.

¹H NMR (CDCl₃, 300.13 MHz) δ 8.00-7.94 (m, 4H, NaphtH-5,8), 7.45-7.39 (m, 4H, NaphtH-6,7), 7.21 (d, 4H, ArH *ortho* to OC(O)CH₃, ³J = 8.6 Hz), 6.95 (d, 4H, ArH *meta* to OC(O)CH₃, ³J = 8.6 Hz), 5.74 (d, 4H, NCH₂Ar *out*, ²J = 16.0 Hz), 4.02 (s, 12H, OCH₃), 3.95 (d, 4H, NCH₂Ar *in*, ²J = 16.0 Hz), 2.26 (s, 6H, OC(O)CH₃) ppm.

16b,16c-Di(4-hydroxyphenyl)-5,9,14,18-tetramethoxy-6,8,15,16b,16c,17-hexahydro-6a,7a,15a,16a-tetraazanaphtho[2',3':5,6]azuleno[2,1,8-*ija*]naphtho[2,3-*f*]azulene-7,16-dione (23):

Starting from **22** (83 mg, 0.10 mmol) in a mixture of dioxane (5 mL) and aqueous 4 N NaOH (1.5 mL), this compound was synthesized as described for **21**. Yield: 60 mg (80%) of **23** as a white solid.

M.p. > 400°C (dec.); IR (KBr pellet) ν 3428 (OH), 2940, 2849 (CH₂), 1690 (C=O), 1516, 1466, 1430 (C=C), 1356 (CH₂), 1048 (COC) cm⁻¹; ¹H NMR (DMSO-d₆, 300.13 MHz) δ 9.55 (br s, 2H, OH), 7.97-7.91 (m, 4H, NaphtH-5,8), 7.55-7.49 (m, 4H, NaphtH-6,7), 6.98 (d, 4H, ArH *meta* to OH, ³J = 8.5 Hz), 6.66 (d, 4H, ArH *ortho* to OH), 5.52 (d, 4H, NCH₂Ar *out*, ²J = 15.9 Hz), 3.97 (d, 4H, NCH₂Ar *in*, ²J = 15.9 Hz), 3.94 (s, 12H, OCH₃) ppm; ¹³C{¹H} NMR (DMSO-d₆, 75.47 MHz) δ 161.40 (urea C=O), 160.84 (ArC *ipso* to OH), 153.24 (ArC *ipso* to OCH₃), 131.51, 131.17; 130.58, 127.32, 119.50 (all ArC), 88.52 (NC(Ar)N), 66.39 (OCH₃), 41.52 (NCH₂Ar) ppm.

5,6-Dihydro[1,10]phenanthroline-5,6-dione:

This compound was prepared according to a modified literature procedure.²² A solid mixture of 1,10-phenanthroline monohydrate (1.7 g, 8.6 mmol) and KBr (10 g, 84 mmol) was stirred and cooled on an ice bath. H₂SO₄ (98%, 30 mL) was cautiously added over 1 h in small portions (of 1 mL). Then, aqueous 65% HNO₃ (15 mL) was added dropwise over 15 min. The mixture was heated at 90°C for 2 h, and the evolving nitrous vapors were collected in an aqueous 1 N NaOH solution. After cooling, the mixture was poured into water (800 mL). Solid NaHCO₃ was added while stirring the solution until pH 7. The product was extracted with CH₂Cl₂ (2 × 250 mL). The organic layer was evaporated to dryness and the product was recrystallized from methanol to yield 1.3 g (72%) of 5,6-dihydro[1,10]phenanthroline-5,6-dione as a yellow, lachrimating solid.

¹H NMR (CDCl₃, 300.13 MHz) δ 9.13 (dd, 2H, PhenH-2,9, ³J = 4.7 Hz, ⁴J = 1.8 Hz), 8.52 (dd, 2H, PhenH-4,7, ³J = 7.9 Hz, ⁴J = 1.8 Hz), 7.60 (dd, 2H, PhenH-3,8, ³J = 7.8 Hz, ³J = 7.8 Hz) ppm.

Clip molecule 26:

DMSO (10 mL) was purged with argon for 30 min. Powdered KOH (300 mg, 5.3 mmol) was added and the mixture was stirred for another 15 min. Compound **27** (300 mg, 1.0 mmol) and 1,2-bis(bromomethyl)benzene (540 mg, 2.0 mmol) were added while cooling the mixture on a water bath (15°C). The mixture was stirred for 16 h and then poured into a saturated aqueous NaCl solution (150 mL). The product was extracted with CH₂Cl₂ (2 × 100 mL) and the combined organic layers were washed with a saturated aqueous NaCl solution (150 mL) and water (150 mL) and dried (MgSO₄). After filtration, the crude product was recrystallized from methanol (6 mL) to give 160 mg (31%) of **26** as a pale yellow solid. Single crystals of **26** were obtained by slow diffusion of methanol in a solution of the compound in chloroform.

M.p. 354-355°C (dec.); IR (KBr-pellet) ν 3111, 3056 (ArH), 2925, 2853 (CH₂), 1716 (C=O), 1579, 1568, 1461, 1428 (C=C, C=N), 1301, 1282, 1270 (CH₂), 1145, 923, 761 (ArH) cm⁻¹; ¹H NMR (CDCl₃, 300.13 MHz) δ 8.92 (dd, 2H, BipyH-6, ³J = 4.6 Hz, ⁴J = 1.5 Hz), 7.89 (dd, 2H, BipyH-4, ³J = 8.2 Hz, ⁴J = 1.5 Hz), 7.32 (dd, 2H, BipyH-5, ³J = 8.2 Hz, ³J = 4.6 Hz), 7.29 (br s, 8H, ArH side-wall), 4.98 (d, 4H, NCH₂Ar in, ²J = 16.7 Hz), 4.70 (4H, NCH₂Ar out, ²J = 16.7 Hz) ppm; ¹³C{¹H} NMR (CDCl₃, 75.47 MHz) δ 158.53 (urea C=O), 151.44 (BipyC-6), 147.57 (BipyC-2), 136.27 (BipyC-4), 135.38 (BipyC-3), 129.98 (ArC para to CH₂N), 128.06 (ArC ortho to CH₂N), 127.39 (ArC ipso to CH₂N), 123.73 (BipyC-5), 77.42 (NC(Ar)N), 46.25 (NCH₂Ar) ppm; FAB-MS *m/z* 499 (M + H)⁺. Anal. Calcd for C₃₀H₂₂N₆O₂(CH₄O): C, 70.18; H, 4.94; N, 15.83. Found: C, 70.41; H, 5.11; N, 15.44.

Bipyridine-glycoluril 27:

5,6-Dihydro[1,10]phenanthroline-5,6-dione (1.0 g, 4.8 mmol) and urea (580 mg, 9.7 mmol) were suspended in toluene (20 mL). Trifluoroacetic acid (1.5 mL) was added and the mixture was refluxed under nitrogen for 16 h using a Dean and Stark trap. After cooling, the brown lumps were filtered off, suspended in ethanol (20 mL) and the mixture was refluxed for 1 h. After cooling, the yellow precipitate was filtered off, washed with ethanol (50 mL) and diethylether (50 mL) and dried under vacuum to yield 1.2 g of **27** (86%) as a pale yellow solid.

M.p. > 400°C (dec.); IR (KBr pellet) ν 3174 (NH), 1737, 1707, 1689 (C=O), 1481, 1459, 1430 (C=C, C=N), 1143, 1122, 1063, 959 (ArH) cm⁻¹; ¹H NMR (DMSO-d₆, 300.14 MHz) δ 8.72 (dd, 2H, BipyH-6, ⁴J = 1.5 Hz, ³J = 4.5 Hz), 8.35 (s, 4H, NH), 8.13 (dd, 2H, BipyH-4, ⁴J = 1.5 Hz, ³J = 7.2 Hz), 7.60 (dd, 2H, BipyH-5, ³J = 4.5 Hz, ³J = 7.2 Hz) ppm; ¹³C{¹H} NMR (DMSO-d₆, 75.47 MHz) δ 163.5 (urea C=O), 154.2 (BipyC-6), 148.8 (BipyC-2), 139.3 (BipyC-4), 135.1 (BipyC-3), 128.8 (BipyC-5), 77.8 (NC(Ar)N) ppm; FAB-MS *m/z* 295 (M + H)⁺. Anal. Calcd for C₁₄H₁₀N₆O₂(0.5C₂H₆O): C, 56.78; H, 4.13; N, 26.49. Found: C, 56.93; H, 3.73; N, 26.75.

Clip molecule 29:

Starting from **27** (245 mg, 0.823 mmol) and 1,4-dimethoxy-2,3-bis(bromomethyl)benzene²³ (540 mg, 1.67 mmol) in DMSO (10 mL) with powdered KOH (260 g, 4.63 mmol), this compound was synthesized as described for **26**. Yield: 215 mg (42%) of **29** as a pale yellow solid.

M.p. > 400°C (dec.); IR (KBr-pellet) ν 3028 (ArH), 2936, 2836 (CH₂), 1731, 1713 (C=O), 1479, 1464, 1435 (C=C, C=N), 1255 (CH₂), 1073 (COC) cm⁻¹; ¹H NMR (CDCl₃, 300.13 MHz) δ 8.83 (dd, 2H, BipyH-6, ³J = 4.6 Hz, ⁴J = 1.5 Hz), 7.52 (dd, 2H, BipyH-4, ³J = 8.0 Hz, ⁴J = 1.5 Hz), 7.17 (dd, 2H, BipyH-5, ³J = 8.0 Hz, ³J = 4.6 Hz), 6.85 (s, 4H, ArH side-wall), 4.99 (d, 4H, NCH₂Ar in, ²J = 16.9 Hz), 4.67 (d, 4H, NCH₂Ar out, ²J = 16.9 Hz), 3.79 (s, 12H, OCH₃) ppm; ¹³C{¹H} NMR (CDCl₃, 75.47 MHz) δ 164.98 (urea C=O), 151.46 (BipyC-6), 151.06 (ArC ipso to OCH₃), 148.13 (BipyC-2), 137.47 (BipyC-4), 127.31 (BipyC-3), 125.56 (ArC ipso to CH₂N), 123.83 (BipyC-5), 110.63 (ArC para to CH₂N), 77.65 (NC(Ar)N), 56.25 (OCH₃), 39.02 (NCH₂Ar) ppm; FAB-MS *m/z* 619 (M + H)⁺. Anal. Calcd for C₃₄H₃₀N₆O₆: C, 66.01; H, 4.89; N, 13.58. Found: C, 67.32; H, 4.13; N, 13.02.

Clip molecule 30:

Starting from **27** (250 mg, 0.850 mmol) and 2,3-bis(bromomethyl)naphthalene²⁴ (535 mg, 1.70 mmol), in DMSO (15 mL) with powdered KOH (260 mg, 4.63 mmol), this compound was synthesized as described for **26**. Yield 130 mg (26%) of **30** as a pale yellow solid.

M.p. > 400°C (dec.); IR (KBr-pellet) ν 3097, 3060 (ArH), 2956, 2923 (CH₂), 1713 (C=O), 1570, 1565, 1457, 1425, 1407 (C=C, C=N), 1327, 1278 (CH₂), 1125, 937, 789, 746 (ArH) cm⁻¹; ¹H NMR (300.13 MHz, CDCl₃) δ 8.96 (dd, 2H, BipyH-6, ³J = 4.6 Hz, ⁴J = 1.5 Hz), 8.16 (dd, 2H, BipyH-4, ³J = 8.1 Hz, ⁴J = 1.5 Hz), 7.76 (s, 4H, NaphtH-1,4), 7.76-7.70 (m, 4H, NaphtH-5,8), 7.48-7.42 (m, 4H, NaphtH-6,7), 7.36 (dd, 2H, BipyH-5, ³J = 8.1 Hz, ³J = 4.6 Hz), 5.10 (d, 4H, NCH₂Ar in, ²J = 16.7 Hz), 4.92 (d, 4H, NCH₂Ar out, ²J = 16.7 Hz) ppm; ¹³C{¹H} NMR (CDCl₃, 75.47 MHz) δ 158.30 (urea C=O), 151.55 (BipyC-6), 147.71 (BipyC-2), 136.02 (BipyC-4), 133.07 (NaphtC para to CH₂N), 132.44 (NaphtC ipso to CH₂N), 129.35 (NaphtC-1,4), 128.23 (BipyC-3), 127.56 (NaphtC-5,8), 126.63 (NaphtC-6,7), 123.85 (BipyC-5), 79.20 (NC(Ar)N), 46.66 (NCH₂Ar) ppm; FAB-MS *m/z* 599 (M + H)⁺. Anal. Calcd for C₂₈H₂₆N₆O₂(CH₂Cl₂): C, 68.52; H, 4.13; N, 12.36. Found: C, 68.86; H, 4.10; N, 12.05.

2.6.5 X-ray analyses

Single crystals were mounted in air on a glass fibre. Intensity data were collected at room temperature. Unit cell dimensions were determined from the angular setting of 25 reflections. Intensity data were corrected for Lorentz and polarization effects. Semi-empirical absorption correction (Ψ -scans)²⁵ was applied. The structure was solved by the program CRUNCH²⁶ and was refined with standard methods (refinement against F^2 of all reflections with SHELXL97²⁷) with anisotropic parameters for the non-hydrogen atoms. The hydrogen atoms of the solvent molecules were placed at calculated positions and refined riding on the parent atoms. All other hydrogen atoms were initially placed at calculated positions and were freely refined subsequently. Structure determination summaries are given in Table 2.2.

Table 2.2 Crystallographic data for **5**, **12**, and **26**

	5	12	26
Empirical formula	C ₂₆ H ₃₀ N ₄ O ₁₀	C _{41.50} H ₄₁ Cl ₃ N ₄ O ₁₀	C ₃₁ H ₂₆ N ₆ O ₃
Crystal size (mm)	0.49 x 0.14 x 0.10	0.50 x 0.35 x 0.20	0.29 x 0.26 x 0.11
Formula weight	558.54	862.13	530.58
T (K)	293(2)	208(2)	293(2)
Crystal system	Monoclinic	Triclinic	Monoclinic
Space group	P 2 ₁ /n	P -1	P 2 ₁ /n
a (Å)	11.7791(13)	13.9560(5)	10.5690(3)
b (Å)	14.8440(11)	13.9794(4)	18.2221(5)
c (Å)	15.3431(16)	21.5005(7)	12.9211(2)
α (°)	90	93.367(3)	90
β (°)	91.438(8)	99.363(2)	92.241(2)
γ (°)	90	104.256(4)	90
V (Å ³)	2681.9(4)	3990.6(2)	2486.57(10)
ρ_{calcd} (g/cm ³)	1.383	1.435	1.364
Z	4	4	4
Diffractionmeter (scan)	Enraf-Nonius CAD4 (θ -2 θ)	Enraf-Nonius CAD4 (θ -2 θ)	Enraf-Nonius CAD4 (θ -2 θ)
Radiation	Cu-K α	Cu-K α	Cu-K α
Wavelength (Å)	1.54184	1.54184	1.54184
F(000)	1176	1796	1112
θ range (°)	2.88 - 70.09	3.28 - 69.92	4.20 - 69.96
Index ranges	-14 \leq h \leq 14 0 \leq k \leq 18 0 \leq l \leq 18	-17 \leq h \leq 16 0 \leq k \leq 17 -26 \leq l \leq 26	-12 \leq h \leq 0 0 \leq k \leq 22 -15 \leq l \leq 15
Measured reflections	5271	15721	4974
Unique reflections	5076	15055	4710
Observed refl. ($I_o > 2\sigma(I_o)$)	3449	13180	4016
Refined parameters	373	1358	455
Goodness-of-fit on F^2	1.052	1.018	1.019
R ($I_o > 2\sigma(I_o)$)	0.0660	0.0694	0.0410
wR2 (all data)	0.1954	0.2088	0.1078
ρ_{fin} (max/min) (e/Å ³)	0.428 / -0.434	1.139 / -1.442	0.458 / -0.377

References and notes

- ¹ Reek, J. N. H.; Elemans, J. A. A. W.; Nolte, R. J. M. *J. Org. Chem.* **1997**, *32*, 2234.
- ² Gieling, G. T. W.; Scheeren, H. W.; Israel, R.; Nolte, R. J. M. *Chem. Commun.* **1996**, 241.
- ³ Reek, J. N. H.; Priem, A. H.; Engelkamp, H.; Rowan, A. E.; Elemans, J. A. A. W.; Nolte, R. J. M. *J. Am. Chem. Soc.* **1997**, *119*, 9956.
- ⁴ Gosling, P. A.; Sijbesma, R. P.; Spek, A. L.; Nolte, R. J. M. *Recl. Trav. Chim. Pays-Bas* **1993**, *112*, 404. Reek, J. N. H.; Rowan, A. E.; de Gelder, R.; Beurskens, P. T.; Crossley, M. J.; de Feyter, S.; de Schryver, F.; Nolte, R. J. M. *Angew. Chem. Int. Ed. Engl.* **1997**, *36*, 361. Reek, J. N. H.; Rowan, A. E.; Crossley, M. J.; Nolte, R. J. M. *J. Org. Chem.* **1999**, *64*, 6653. Reek, J. N. H. *Thesis*, Nijmegen, **1996**.
- ⁵ Coolen, H. K. A. C.; van Leeuwen, P. W. N. M.; Nolte, R. J. M. *J. Am. Chem. Soc.*, **1995**, *117*, 11906.
- ⁶ Martens, C. F.; Klein Gebbink, R. J. M.; Feiters, M. C.; Nolte, R. J. M. *J. Am. Chem. Soc.* **1994**, *116*, 5667.
- ⁷ Elemans, J. A. A. W.; Claase, M. B.; Aarts, P. P. M.; Rowan, A. E.; Schenning, A. P. H. J.; Nolte, R. J. M. *J. Org. Chem.* **1999**, *64*, 7009.
- ⁸ Reek, J. N. H.; Rowan, A. E.; Elemans, J. A. A. W.; de Gelder, R.; Beurskens, P. T.; Nolte, R. J. M., manuscript in preparation.
- ⁹ Reek, J. N. H.; Kros, A.; Nolte, R. J. M. *Chem. Commun.* **1996**, 245.
- ¹⁰ Sijbesma, R. P.; Nolte, R. J. M. *Recl. Trav. Chim. Pays-Bas* **1993**, *112*, 643.
- ¹¹ Hellman, H. *Angew. Chem.* **1957**, *69*, 463.
- ¹² Zaugg, H. E. *Synthesis* **1970**, *2*, 49. Zaugg, H. E. *Synthesis* **1984**, *16*, 85.
- ¹³ Tesser, G. I.; Bolvert-Geerts, I. C. *Int. J. Peptide Protein Res.* **1975**, *7*, 295.
- ¹⁴ Schouten, A.; Kanters, J. A. *Acta Cryst.* **1990**, *C46*, 2484.
- ¹⁵ Sijbesma, R. P.; Kentgens, A. P. M.; Lutz, E. T. G.; van der Maas, J. H.; Nolte, R. J. M. *J. Am. Chem. Soc.* **1993**, *115*, 8999.
- ¹⁶ Murray, B. A.; Whelan, G. S. *Pure Appl. Chem.* **1996**, *68*, 1561.
- ¹⁷ Niele, F. G. M.; Nolte, R. J. M. *J. Am. Chem. Soc.* **1988**, *110*, 172.
- ¹⁸ The identity of the *in*- and *out*-protons of clips **26**, **29** and **30** was confirmed by 2D NOESY spectroscopy. Very strong nOe contacts were present between the ethylene *in*- and the BipyH-5 protons.
- ¹⁹ CDCl₃ was used as the solvent instead of CHCl₃, because in the former solvent no absorptions are present in the region where the OH stretching vibration resides (3700-3200 cm⁻¹).
- ²⁰ This was concluded from the fact that over a 0.5-20 mM concentration range no shifts were observed in the signals of the side-wall and methoxy protons of **29**.
- ²¹ Reek, J. N. H. *Thesis*, University of Nijmegen, **1996**.
- ²² Yamada, M.; Tanaka, Y.; Yoshimoto, Y.; Kuroda, S.; Shimao, I. *Bull. Chem. Soc. Jpn.* **1992**, *65*, 1006.
- ²³ Jansen, R. J.; Rowan, A. E.; de Gelder, R.; Scheeren, H. W.; Nolte, R. J. M. *Chem. Commun.* **1998**, 121.
- ²⁴ Sisti, A. J.; Meyers, M. *J. Org. Chem.* **1973**, *38*, 4431.
- ²⁵ North, A. C. T.; Philips, D. C.; Mathews, F. S. *Acta Crystallogr.* **1968**, *A24*, 351.
- ²⁶ De Gelder, R.; de Graaff, R. A. G.; Schenk, H. *Acta Crystallogr.* **1993**, *A49*, 287.
- ²⁷ Sheldrick, G. M. SHELXL97. Program for the refinement of crystal structures; University of Gottingen: Germany, **1997**.

Chapter 3

Controlled Self-Assembly of Rigid Facial Amphiphiles

3.1 Introduction

Amphiphilic molecules are essential in the maintenance and function of biological systems, and most of the synthetic amphiphiles that have been studied to mimic these natural systems have a similar topology: a compact, polar head-group, to which one or more long hydrophobic hydrocarbon chains are attached.¹ As a result of this topology, amphiphiles readily aggregate in aqueous solutions, in which they expose their head-groups to the water and dehydrate their tails by clustering them together into a hydrophobic environment. Depending on the nature of the head-group and on the amount and length of the hydrocarbon tails, the morphology of the supramolecular aggregate which is formed can be in many cases rationally correlated to the topology of the amphiphile.² Although these amphiphiles of the "classical type" have received much attention over the past decades, there recently appears to be increasing interest in the development of amphiphiles with a strongly deviating topology.³ Kahne *et al.* were the first to introduce the term "facial amphiphilic" molecules, which are defined as molecules with rigid structures containing separated hydrophilic and hydrophobic "faces".⁴ In Nature, helical peptides are known which exhibit this facial amphiphilicity. They bind to membrane interfaces in order to target peptide sequences to membrane-bound receptors.⁵ These amphiphiles can also cause membrane fusion⁶ and make membranes permeable.⁷ Some examples of synthetic facial amphiphiles are depicted in Figure 3.1.

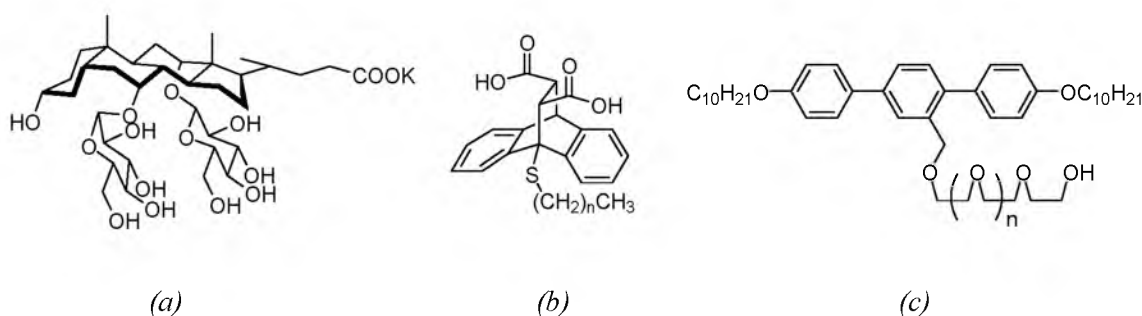


Figure 3.1 Examples of facial amphiphiles synthesized by (a) Kahne, (b) Gelmann, and (c) Tschierske.

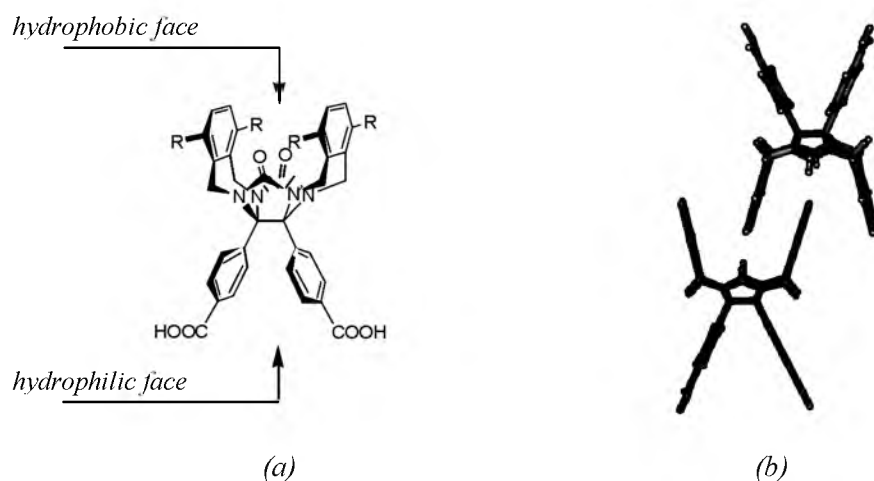


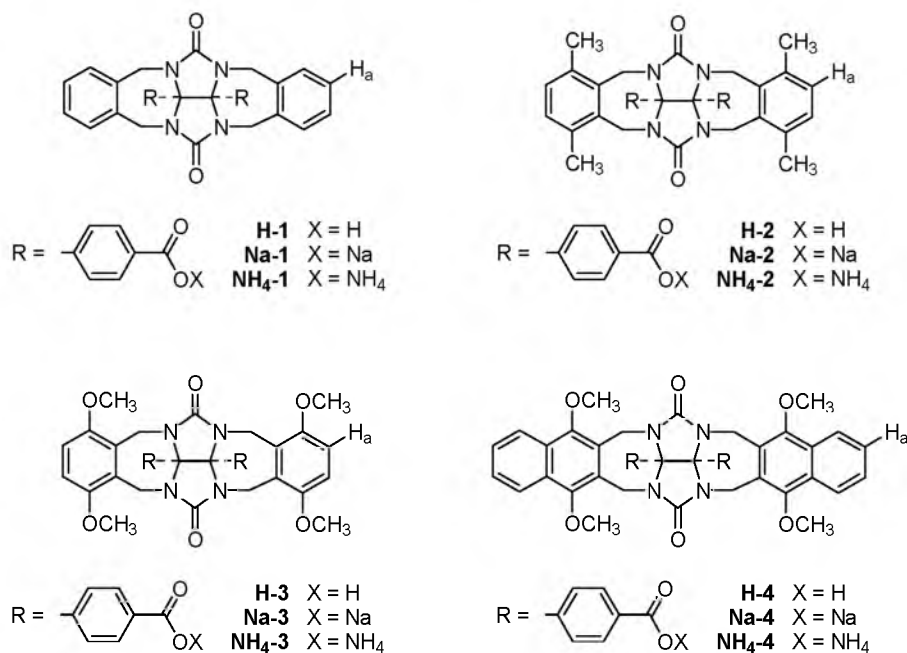
Figure 3.2 (a) Facial amphiphilic character of a glycoluril molecular receptor with two carboxylic acid groups. (b) Computer modeled representation of a dimer of this molecule.

In particular Gellman and coworkers have carried out considerable work on determining the factors that govern the self-association of these types of molecules in water,⁸ and on the ability of their aggregates to include hydrophobic fluorescent probes. No aggregate morphology studies of facial amphiphiles have, however, been reported. It is, therefore, of general interest to investigate whether these molecules are able to form discrete nanometer-sized architectures, and in particular if their unusual topology can be expressed in a unique morphology of their aggregates. In the previous chapter several routes have been described to synthesize molecular clip receptors which are functionalized at their convex side with benzoic acid, phenol, or bipyridine groups. These molecules can, in principle, be considered as rigid, facial amphiphiles with a hydrophobic face formed by the U-shaped receptor cavity and a hydrophilic face formed by the polar groups at the convex side of the clip (Figure 3.2a). Recent work in our group has revealed that clip molecules with water-soluble pyridinium groups at their convex side form well-defined ‘razorblade-like’ aggregates in water (see Section 1.4.4).⁹ A major driving force for the self-assembly of these types of molecules into nanosized structures is the formation of dimeric structures, in which one cavity side-wall of a clip is buried in the cavity of its dimeric partner and *vice-versa* (Figure 3.2b). In this chapter, the amphiphilic properties of the carboxylate salts of compounds **H-1** – **H-4** (Chart 3.1) will be discussed. It will be demonstrated that their self-assembling and aggregation properties in water are strongly dependent on their counter cations, and on the size and substitution pattern of their receptor cavities.

3.2 Synthesis

The sodium salts of dibenzoic acids **H-1** – **H-4** (Chart 3.1) were prepared by suspension of these compounds in demineralized water, to which two equivalents of sodium hydroxide were added. Upon stirring, the compounds completely dissolved, whereafter they were lyophilized. The ammonium salts of **H-1** – **H-4** were prepared by suspension of **H-1** – **H-4** in aqueous ammonia (30%). Again the compounds dissolved upon stirring, whereupon the excess ammonia was evaporated and the products were lyophilized. The sodium and ammonium salts turned out to be very hygroscopic and were therefore stored under nitrogen at -18°C .

Chart 3.1



3.3 Self-association and aggregation in water

3.3.1 NMR experiments

The self-association properties of the carboxylate-functionalized receptors in water were investigated with ¹H NMR dilution studies. There appeared to be large solubility differences between the sodium and the ammonium salts of the molecules, *i.e.* the sodium salts were soluble in water up to relatively high concentrations (> 30 mM), whereas the ammonium salts hardly dissolved at all. For this reason, reliable NMR dilution titrations could only be carried out on the sodium salts. For compounds **Na-1** – **Na-4**, ¹H NMR spectra were recorded of samples of at least ten different concentrations varying between 0.2 and 10 mM. In this concentration range, for all compounds only the signals of the protons of the cavity side-walls and of their 1,4-attached substituents displayed significant upfield shifts (> 0.05 ppm). Increasing the temperature or the addition of acetone caused a decrease in these shifts. The concentration dependent changes in the NMR spectra are in line with the formation of dimeric structures. Average signals were observed for protons in the monomer and the dimer, indicating their fast exchange on the NMR timescale. Only in the case of **Na-4**, the shifting resonances somewhat broadened at concentrations above 5 mM. The signals of the side-wall protons H_a (see Chart 3.1) were monitored versus the concentration, and the titration curves thus obtained were fitted to an equation governing the self-association of two molecules. The calculated dimerization constants (K_{dimer}) and the complexation induced shift (CIS) values of the shifting proton signals are summarized in Table 3.1. The results show that dimerization becomes stronger when substituents are introduced at the 1,4-positions of the cavity side-walls, *i.e.* when the hydrophobic surface of the cavity becomes larger.¹⁰ Without any substituents, dimerization is neglectable (*cf.* the K_{dimer} of **Na-1**). The

Table 3.1 Dimerization constants and CIS-values of clips **Na-1** – **Na-4** in D_2O at 298 K.

Compound	K_{dimer} (M^{-1})	ΔG (kJ mol^{-1})	CIS (ppm) ^a
Na-1	$< 5^b$	— ^b	— ^b
Na-2	145 ^c	-12.3	-1.38
Na-3	630 ^c	-16.0	-1.29
Na-4	1.45×10^4 ^d	-23.7	-1.60

^aValue calculated for the side-wall protons H_a (see Chart 3.1). ^bDimerization too weak to determine a reliable value. ^cEstimated error 10%. ^dEstimated error 20%.

extremely strong dimerization of **Na-4** is attributed to the presence of a large hydrophobic cleft surrounded by the naphthalene side-walls. The observed trend in dimerization strength is similar to that of related substituted receptors in chloroform.¹¹ In water, however, the intermolecular interactions are generally much stronger due to the hydrophobic effect.¹² This is further reflected in the large CIS-values of the H_a -protons, which indicate that the side-walls of the molecules are inserted more deeply within the cavity of their dimeric partner than in the case of their chloroform-soluble analogues.¹¹

Although the strength of dimerization of the ammonium salts of **H-1** – **H-4** could not be determined by dilution titrations, ¹H NMR spectra of low concentrated solutions of these compounds (~0.5 mM) in water showed shifts in the cavity side-wall proton signals which were comparable to those of their sodium salt analogues. This indicates that in the case of both salts self-assembly of the cavity parts of the molecules occurs.

3.3.2 Fluorescence experiments

Due to the low solubility of the ammonium salts **NH₄-1** – **NH₄-4** in water their self-association behaviour could not be investigated by NMR techniques, and instead fluorescence spectroscopy was used. The fluorescence dependence of **NH₄-1** on the concentration of this compound in water is shown in Figure 3.3. Upon excitation of the $\pi \rightarrow \pi^*$ transition band of the aromatic rings in the molecule in the UV-vis spectrum (at 290 nm), a broad emission between 300 and 400 nm was observed, the intensity of which increased until the concentration was raised to $10^{-6} M^{-1}$. A clear drop in intensity was then observed until a minimum was reached at a concentration of approximately $2 \times 10^{-5} M^{-1}$, whereupon the emission started to increase again quickly. This increase coincided with the evolvment of turbidity in the solution. At the same time, in addition to the emission at ~345 nm, a new longer wavelength emission in the fluorescence spectrum became evident. The evolvment of this broad emission between 400 and 450 nm is attributed to the formation of excimers. A similar formation of excimers, although from a different compound *viz.* poly-(*S*)-tyrosine with $\lambda_{\text{em}} = 420$ nm has been reported in the literature and has been taken as evidence for the stacking of *p*-hydroxyphenyl rings.¹³ The dilution titration curve of **NH₄-1** ($\lambda_{\text{em}} = 345$ nm), which is composed from the data presented in Figure 3.3, is shown in Figure 3.4. The maximum and minimum emission are clearly visible at concentrations of 10^{-6} ($I = 300$ a.u.) and 2×10^{-5} M ($I = 95$ a.u.) of **NH₄-1**, respectively. Upon increasing the temperature, this maximum and minimum were found to shift to higher concentration, and simultaneously the emission intensity of the maximum increased (not shown). The observed concentration and temperature effects on the fluorescence spectra of **NH₄-1** point to the formation of assemblies which have

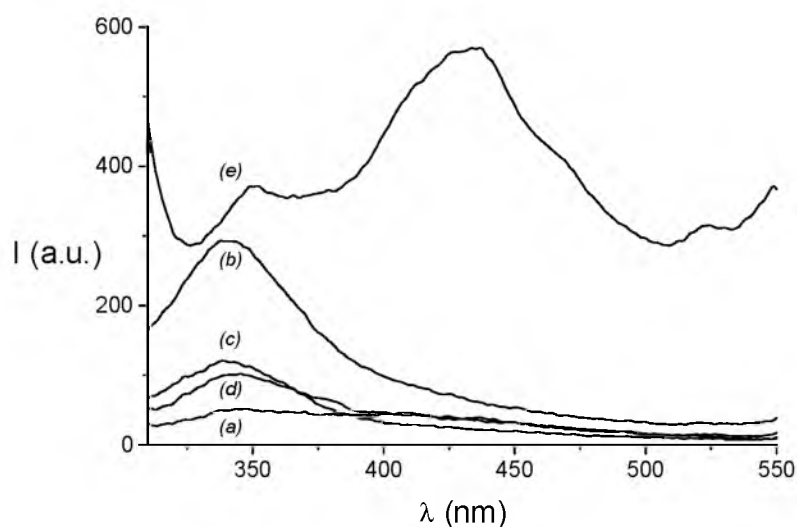


Figure 3.3 Selected fluorescence emission spectra ($\lambda_{ex} = 290$ nm) of $\text{NH}_4\text{-1}$ in water at concentrations of (a) 10^{-8} , (b) 10^{-6} , (c) 5×10^{-6} , (d) 2×10^{-5} , and (e) 10^{-4} M.

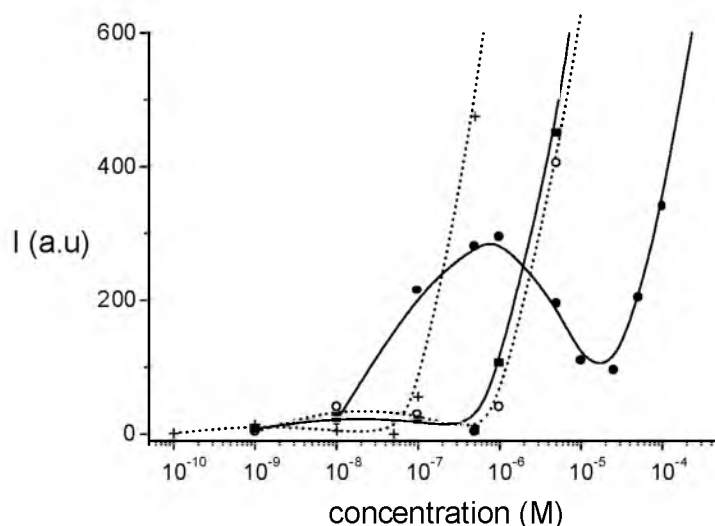


Figure 3.4 Fluorescence dilution curves ($\lambda_{em} = 345$ nm) of compounds $\text{NH}_4\text{-1}$ (\blacksquare , —), $\text{NH}_4\text{-2}$ (\circ , ---), $\text{NH}_4\text{-3}$ (\bullet , —), and $\text{NH}_4\text{-4}$ ($+$, ---) in water at 298 K.

their aromatic rings in close proximity, resulting in their mutual quenching. At concentrations higher than $5 \times 10^{-4} \text{ M}^{-1}$, scattering occurs because of the formation of larger aggregates. A very similar fluorescence behaviour has been reported for the self-assembly of bis(phenylglycine) oxalyl amides in water.¹⁴

Concentration dependent fluorescence studies were also carried out with compounds $\text{NH}_4\text{-2}$ – $\text{NH}_4\text{-4}$. In all cases typical plots of concentration versus fluorescence emission were obtained (Figure 3.4). Upon increasing the concentration of the amphiphile displayed a maximum and a subsequent minimum in emission. These maxima and minima shifted to higher concentration values in the order $\text{NH}_4\text{-4} < \text{NH}_4\text{-3} \approx \text{NH}_4\text{-2} < \text{NH}_4\text{-1}$, whereas the degree of quenching decreased in the same order. In addition, the concentration at which scattering occurred

increased. The fluorescence titration curves thus give a good indication of the self-association and further aggregation behaviour of the ammonium salts of **H-1** – **H-4**. A common approach to determine the critical aggregation constant (c.a.c.) of a surfactant is the application of the ‘pseudo-phase-separation model’, which treats the aggregate as a phase that separates from the solution containing the amphiphile.¹⁵ In the case of the ammonium salts of **H-1** – **H-4**, this occurrence of phase separation coincides with the concentration in the titration curves where the emission reaches a minimum (Figure 3.4). Hence these values were taken as the c.a.c.-values of the compounds (see Table 3.2).

Table 3.2 Properties of the aggregates formed by ammonium carboxylate receptors in water.

Compound	c.a.c. (M) ^a	Average length (nm) ^b	Average width (nm) ^b	Average height (nm) ^b	Aspect ratio (length/width) ^b
NH₄-1	2×10^{-5}	200–250	60–80	50	3.5 ± 1
NH₄-2	5×10^{-7}	1500–2500	200–400	300	9 ± 3
NH₄-3	3×10^{-7}	1500–2500	70–100	75	25 ± 5
NH₄-4	2×10^{-8}	— ^c	— ^c	— ^c	— ^c

^aCritical aggregation constant as determined from the fluorescence titration.

^bDetermined from the dimensions of 200–300 unique aggregates obtained from various samples. ^cNo well-defined aggregates were observed.

3.3.3 Electron microscopy studies

To investigate if the self-association of the carboxylate amphiphiles would result in the formation of assemblies on a mesoscopic scale, solutions and dispersions of the compounds in water were investigated with the help of transmission electron microscopy (TEM). None of the sodium salts was found to form large aggregates, as was already expected from the samples used for the NMR dilution studies, which remained clear up to relatively high concentrations. Even when relatively concentrated samples (30 mM) of **Na-4**, the molecule that dimerized most strongly, were studied, no nanosized structures were observed. In contrast to this, the turbid dispersions of all the ammonium salts in water (0.1% w/v) were indicative of the presence of large aggregates. The addition of acetone to these samples led to the formation of clear solutions, apparently as a result of the dissociation of the assemblies.¹⁶ TEM studies revealed that compounds **NH₄-1**, **NH₄-2** and **NH₄-3** indeed formed well-defined aggregates with a uniform, quasi-rectangular shape and rounded corners (Figure 3.5). Compound **NH₄-4** did not form well-defined structures but rather undefined lumps of material. Electron diffraction experiments indicated that none of the structures were crystalline. The geometrical features of the observed structures are summarized in Table 3.2. As can be seen the length/width aspect ratio increases going from **NH₄-1** to **NH₄-2** to **NH₄-3**. These increases are related to the increase in self-association strength observed from the fluorescence measurements. The shapes or dimensions of the aggregates were not influenced by changes in concentration of the amphiphile used.

3.3.4 Infrared measurements

The fact that compounds **NH₄-1** – **NH₄-4** form nanosized aggregates and **Na-1** – **Na-4** do not, implies that the ammonium ions in the former salts play an important role in the self-assembly process. It is well-known that these ions can form very strong hydrogen bonds with carboxylate anions.¹⁷ They serve as quadruple hydrogen bond donors, whereas each of the carboxylate

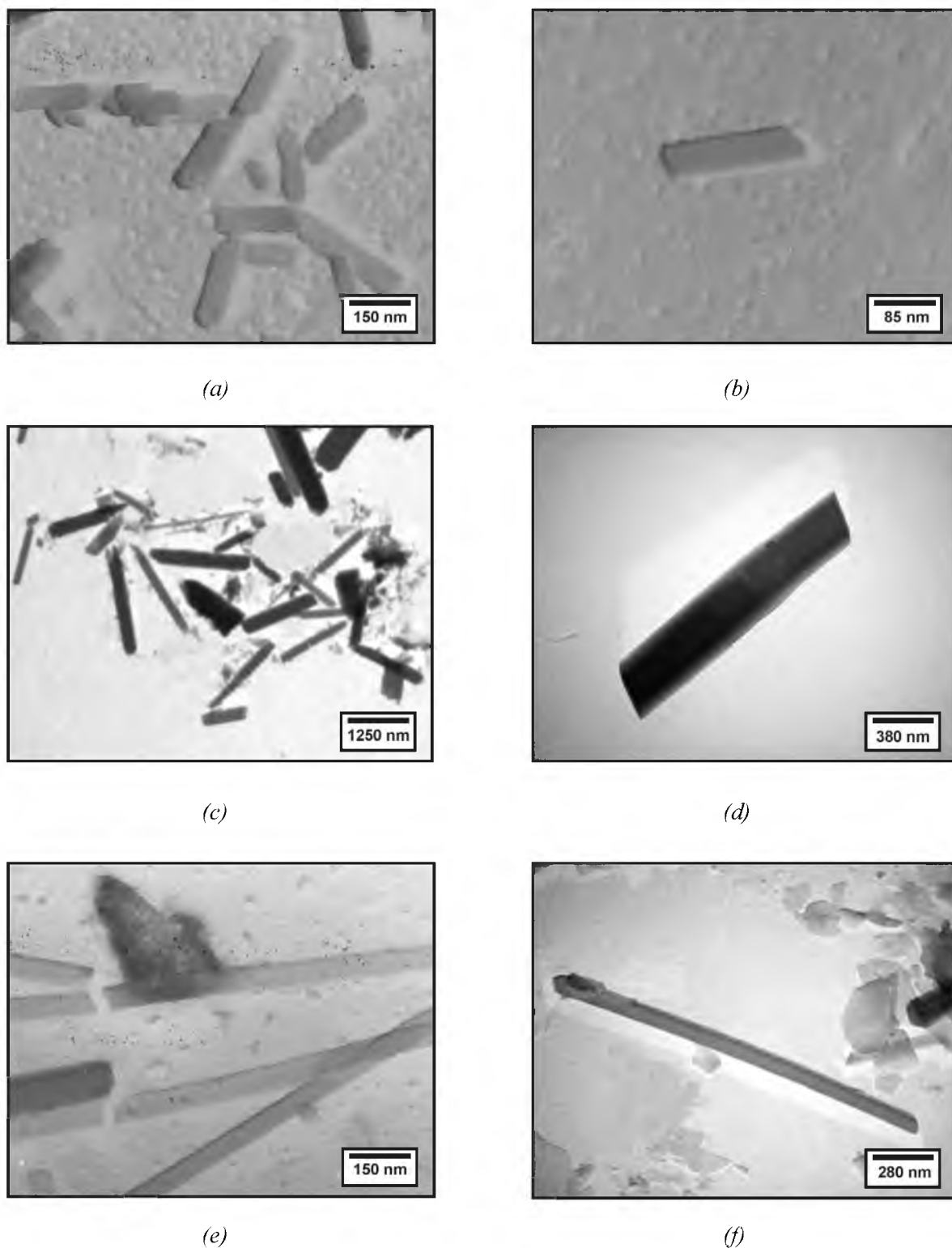


Figure 3.5 TEM images of aggregates formed in water by (a, b) $\text{NH}_4\text{-1}$, (c, d) $\text{NH}_4\text{-2}$, and (e, f) $\text{NH}_4\text{-3}$. All samples are platinum shadowed.

functions in principle can act as multiple hydrogen bond acceptors due to the presence of five lone pairs of electrons.¹⁸ To investigate the role of this hydrogen bonding in the self-assembly of the amphiphiles, cast films of aqueous dispersions of both the sodium and ammonium salts were studied by reflectance infrared spectroscopy. Due to charge delocalization, carboxylate anions

characteristically exhibit a vibration due to the asymmetrical O-C-O stretching motion between 1600 and 1550 cm^{-1} .¹⁹ Indeed, a vibration at approximately 1605 cm^{-1} was present in the spectra of KBr samples of all the sodium salts. In the spectra of the KBr samples of the ammonium salts, however, this asymmetrical O-C-O stretching vibration was absent. Instead, for these compounds a set of superimposed carbonyl vibrations was evident between 1740 and 1660 cm^{-1} . This is an indication that the carboxylate groups are involved in a hydrogen bonding interaction. The N-H stretching vibrations of the ammonium ions were visible as a broad, poorly defined and intense absorption between 3700 and 2700 cm^{-1} . In the cast films of aqueous dispersions (0.5%, w/v) of the sodium salts no significant shifts in the O-C-O stretching vibrations were observed when compared to the spectra of these compounds in KBr. In cast films of aqueous dispersions (0.5%, w/v) of the ammonium salts, however, the set of superimposed carbonyl vibrations observed in the KBr samples had sharpened up and split into two distinct vibrations at approximately 1715 and 1680 cm^{-1} , corresponding to the urea carbonyl and carboxylate functions, respectively. In addition, the N-H stretching vibration of the ammonium ions had narrowed considerably to a stretching vibration of relatively low intensity at 3160 cm^{-1} . These changes in the infrared spectrum are an indication that in the cast films of aqueous dispersions of the ammonium salts, the hydrogen bonding interactions which are present between the ammonium ions and the carboxylate groups are better defined than in the KBr samples of the freshly prepared compound.

3.3.5 Powder diffraction experiments

To get more information about the precise ordering of compounds **NH₄-1** – **NH₄-4** in their aggregates, dried samples of dispersions (0.1%, w/v) of the ammonium carboxylate receptors were investigated by X-ray powder diffraction. For all the compounds, complex powder diffractograms which, however, contained many similar reflections were obtained. This is a strong indication that the aggregates formed by all the ammonium salts are isomorphic.

The powder diffractogram of **NH₄-2** is shown in Figure 3.6. In addition to a strong reflection which can correspond to a repeating distance of 9.75 Å, several small reflections are observed. Calculations to deduce other repeating distances from these reflections are currently in progress.

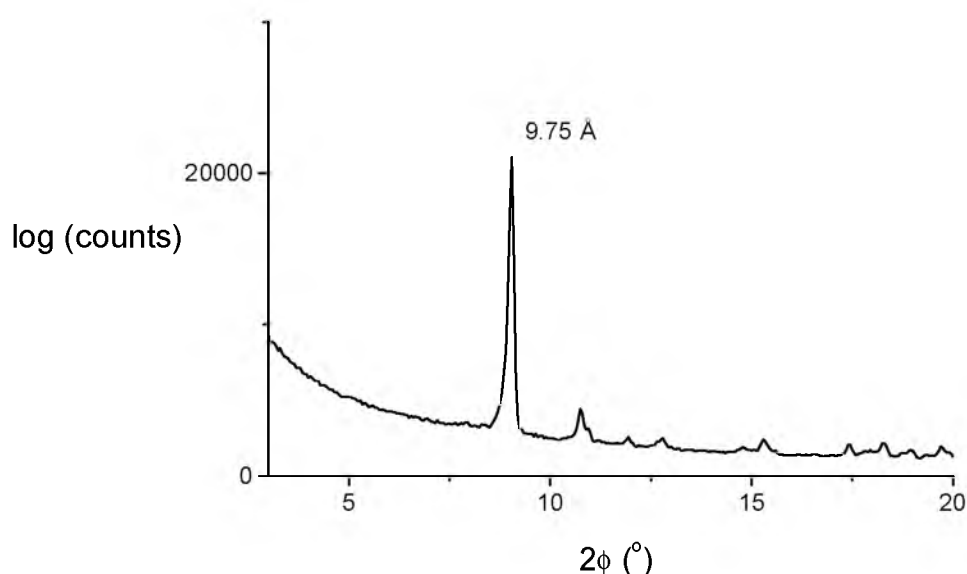


Figure 3.6 Typical powder diffractogram of an aggregate formed by an ammonium carboxylate functionalized receptor (in this case compound **NH₄-2**).

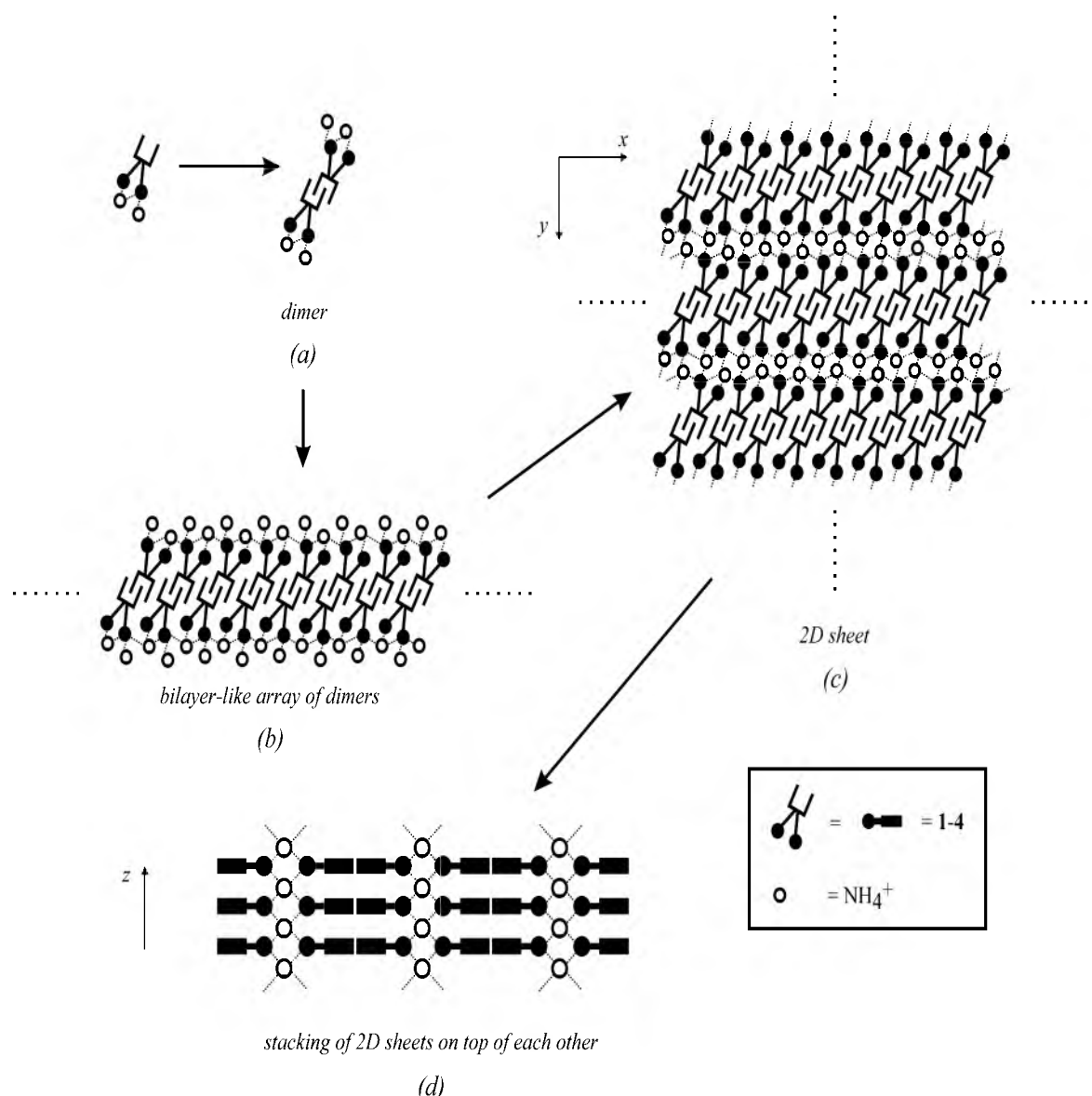


Figure 3.7 Schematic representation of the proposed ordering of facial amphiphiles $\text{NH}_4\text{-1}$ – $\text{NH}_4\text{-4}$. (a) Formation of a dimer. (b) Assembly of dimers in a one-dimensional array. (c) Stitching of bilayers by the NH_4^+ ions resulting in the formation of 2D sheets (top view). (d) Stacking of the 2D sheets on top of each other (side-view).

3.3.6 Proposed ordering of the amphiphiles

In water, the formation of hydrogen bonds between solutes is highly unfavourable unless a *cooperative* self-assembly process between sufficiently large aggregates occurs. Considering the various possible interactions, a self-assembly model for compounds $\text{NH}_4\text{-1}$ – $\text{NH}_4\text{-4}$ is proposed that accounts for such a cooperative process (Figure 3.7). Based on the ^1H NMR data, an important intermolecular interaction is the ‘face-to-face’ dimerization, in which two receptor cavities are mutually filled (Figure 3.7a). In a subsequent process, these dimeric units can form long, one-dimensional arrays, in which their hydrophobic aromatic surfaces are minimally exposed to the aqueous phase and all the hydrophilic carboxylate groups are directed outwards. Hence, a bilayer of facial amphiphiles results (Figure 3.7b). Similar bilayer formation has been observed in the solid state in the case of related receptors functionalized with long aliphatic tails (see Chapter 5).²⁰ In a third process, which probably occurs cooperatively with the growth of the

dimeric array, the ammonium cations can act as a 'glue' and stitch the bilayers together to form a 2-dimensional (2D) sheet by the formation of hydrogen bonds (Figure 3.7c). In the case of **Na-1** – **Na-4**, this stitching cannot occur. Hence, the self-assembly of these molecules stops at the stage of the dimer or the dimeric array and no aggregates on a mesoscopic scale are formed. Finally, it is proposed that the 2D sheets of the ammonium amphiphiles stack on top of each other to give the aggregates their final 3-dimensional shape. Molecular modeling showed that the thickness of one 2D sheet amounts to approximately 9.2-9.5 Å, a value which corresponds reasonably well with the strong reflection observed in the powder diffractogram of **NH₄-2** ($d = 9.75$ Å). A similar stacking of 2D sheets has been observed before for other related receptor molecules.^{9,20} It is not unlikely that the 2D sheets of amphiphiles are also stitched together by the ammonium ions, which can form, apart from hydrogen bonds between the bilayers, additional hydrogen bonds between the carboxylate functions in different layers (Figure 3.7d).

What is unique about the aggregates formed by **NH₄-1** – **NH₄-4** is that their growth stops after a certain point, *i.e.* no infinite assemblies are formed. Another interesting aspect of the aggregates is that their final shape is controlled by the substitution pattern of the cavity side-walls of the amphiphiles. This control over shape and size of self-assembled structures is one of the great challenges of today's supramolecular chemistry.²¹ Calculations have shown that the substitution pattern of the receptor cavity is not only related to the strength of dimerization, but also to the strength of the π - π interactions between the dimers.¹¹ 1,4-Dimethoxy substituted side-walled molecules display stronger intermolecular interactions than 1,4-dimethyl substituted ones, which in turn interact more strongly than unsubstituted benzene side-walls. For the ammonium salts of **H-1** – **H-4**, these differences in interaction strength can be observed in the fluorescence spectra of the compounds, in which the degree of quenching increases going from **NH₄-1** to **NH₄-2** and then to **NH₄-3**. In line with the differences in interaction strength, the dimeric array of molecules of **NH₄-3** in water possibly grows longer than the dimeric array of molecules of **NH₄-2**, which in turn grows longer than the array formed by **NH₄-1**. If the dimeric array growth occurs in the direction of the long sides of the aggregates, this assumption perfectly explains the differences observed in the lengths of the aggregates formed by the ammonium compounds. The other growth processes, *i.e.* the stitching of the bilayers and the stacking of the 2D sheets, are in competition with the growth of the dimeric array. Hence, when the dimerization and self-assembly of the hydrophobic face of the molecules become more favourable, the other growth processes are disfavoured and the length/width aspect ratio increases.

3.4 Concluding remarks

In this chapter it has been demonstrated that a new series of facial amphiphiles, *i.e.* rigid receptor cavities functionalized with carboxylate groups on their convex sides, can form discrete superstructures on a mesoscopic scale. In water the hydrophobic cavities of the molecules form dimeric structures, which in a subsequent process arrange themselves into bilayer-like arrays in which the hydrophobic parts of the molecules are maximally shielded from the aqueous environment. Further growth of these bilayers into nanosized aggregates appears to be strongly dependent on the counter cations of the amphiphiles. When these are sodium ions, no superstructures are formed because the self-assembly stops at the stage of the array of dimers. When, however, ammonium ions are used, these form strong hydrogen bonds with the carboxylate anions and as a result the bilayers are stitched together to form large architectures.

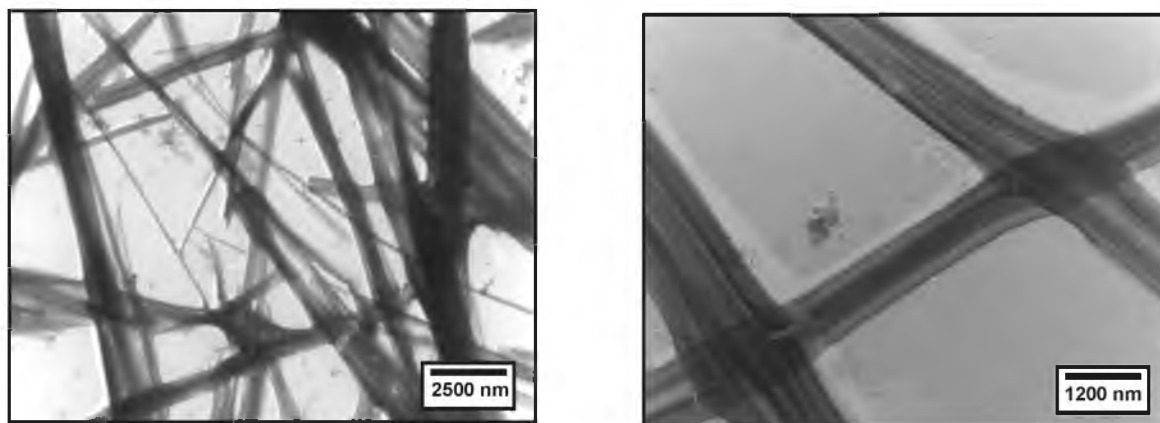


Figure 3.8 TEM images of the hydrogel formed in aqueous 1N NaOH by **Na-3**. Samples are platinum shadowed.

The shape and dimensions of these architectures appear to be directly related to the strength of dimerization of the amphiphiles, which is in turn dependent on the substitution pattern of the cavity side-walls of these molecules. Thus, by introducing small changes in the hydrophobic part of these facial amphiphiles, the size and shape of their final superstructure can be controlled.

The influence of the counter ions on the aggregation behaviour of the amphiphiles opens up many possibilities. Preliminary experiments have, for example, revealed that when **Na-3** is dispersed in aqueous 1N NaOH or 1N NaCl (0.5%, w/v) a stable hydrogel is formed. TEM studies showed that this gel is built up from a network of long fibers (Figure 3.8). Instead of alkali metal ions, it should also be possible to incorporate transition metal centers into the aggregates and as a result provide the latter with a certain function. Finally, since the carboxylate groups at the outside of the aggregates formed by the facial amphiphiles are probably arranged in well-defined arrays, these can in principle serve as a template for the biomineralization of calcium carbonate.²²

3.5 Experimental section

3.5.1 Materials and methods

Unless stated otherwise, all materials were commercially available and used as received. See Section 2.6.1 for a description of general techniques.

3.5.2 NMR experiments

All ¹H NMR experiments in D₂O were carried out in the presence of an external standard (trimethyl phosphate in D₂O, $\delta = 0.00$ ppm). Self-association constants were determined by recording the NMR spectra of at least 10 samples differing in concentration of the host molecule, which varied from the minimum concentration needed for detection by ¹H NMR (~0.1 mM) to approximately 10 mM or the maximum solubility of the compound. The shifts of the probe protons (in Hz) were plotted versus concentration (in mol L⁻¹), and the obtained titration curves were fitted to the following equation, which defines a 1:1 self-association of two molecules (eqn. 1):

$$\delta_{obs} = \delta_m + \frac{(\delta_m + \delta_d) \sqrt{1 + 4cK_{self}} - (1 + 8cK_{self})}{4cK_{self}} \quad (1)$$

In which δ_{obs} and c are the observed shift (in Hz) and the concentration (in M), respectively. From the fitting procedure the self-association constant K_{self} and the CIS value ($\delta_d - \delta_m =$ calculated shift of the dimer minus the calculated shift of the monomer) can be obtained.

3.5.3 Fluorescence measurements

Fluorescence spectra were recorded on a Perkin Elmer luminescence spectrometer LS50B equipped with a thermostatted cuvette holder ($T = 25^{\circ}\text{C}$). Samples of various concentrations of compounds **NH₄-1** – **NH₄-4** in demineralized water in a 1.00 cm 4 mL quartz cuvette were purged with argon to exclude fluorescence quenching by oxygen. The samples were excited at 290 nm, and the emission was recorded between 300 and 550 nm at a scan speed of 60 nm/min. The excitation and emission slits were 5 and 10 nm, respectively.

3.5.4 Electron microscopy studies

An amount of a carboxylate salt was dissolved or dispersed in demineralized water. The dispersion was then sonicated for 30 min. at 25°C in a Branson 2200 Ultrasonic Bath. In the case of the formation of the hydrogel, compound **Na-3** was dispersed in aqueous 1N NaOH, the dispersion was heated to 95°C and allowed to cool to room temperature whereupon a gel was formed. Samples of the dispersions were deposited on Formvar coated copper grids. The excess dispersion was removed after 30 s. The samples were platinum shadowed (layer thickness 2 nm, sputtering angle 45°) and then studied on a Philips TEM 201 instrument operating at 60 kV. In all cases, the results were compared to blanco samples without the amphiphile.

3.5.5 Reflectance infrared experiments

Infrared samples were prepared by evaporation of a drop of an aqueous dispersion of the compound on a gold sputtered cover glass. The resulting thin film was dried in a desiccator. Reflectance infrared spectra of the samples were recorded on a BioRad FTS-25 spectrometer with a resolution of 2.0 cm^{-1} . The angle between the sample and the infrared beam was 30° . For each spectrum 256 scans were recorded, and the optical bench of the IR apparatus was continuously purged with nitrogen. Data analysis was performed using the WIN-IR software.

3.5.6 Powder diffraction experiments

A drop of a sample of a facial amphiphile in water (for sample preparation see section 3.5.4) was deposited on a silicon single crystal, which was then placed in a desiccator containing fresh P_2O_5 as drying agent. The sample was stored *in vacuo* for 24 h, and then placed in a Philips PW1710 diffractometer, which was equipped with a Cu LFF X-ray tube operating at 40 kV and 55 mA (wavelengths (a1,a2): 1.54060, 1.54438).

3.5.7 Syntheses

The syntheses of compounds **H-1**, **H-2**, **H-3** and **H-4** have been described in Chapter 2.

Disodium-4-[13b-(4-carboxylatophenyl)-6,13-dioxo-5,7,12,13b,13c,14-hexahydro-5a,6a,12a,13a-tetraazabenz[5,6]azuleno[2,1,8-*ija*]benzo[*f*]azulen-13-yl]benzoate (**Na-1**):

To a suspension of compound **H-1** (100 mg, 0.17 mmol) in water (10 mL) was added an aqueous NaOH solution (5 mL containing 0.34 mmol of NaOH). The mixture was stirred overnight, whereafter it was lyophilized to yield 108 mg (100%) of **Na-1** as a white foam, which was stored under nitrogen at -18°C .

M.p. $> 400^{\circ}\text{C}$ (dec.); IR (KBr pellet) ν 3050 (ArH), 2922 (CH_2), 1714, 1684 (urea C=O), 1605 (COO^-), 1558, 1471, 1445, 1428, 1407 (C=C), 1309, 1260 (CH_2) cm^{-1} ; $^1\text{H NMR}$ (D_2O , 500.13 MHz, 6.0 mM) δ 7.56 (d, 4H, ArH *ortho* to C(O)O, $^3J = 7.9$ Hz), 7.20 (d, 4H, ArH *meta* to C(O)O, $^3J = 7.9$ Hz), 7.18 (br s, 4H, ArH *ortho* to CH_2N), 7.05 (br s, 4H, ArH *para* to CH_2N), 4.58 (d, 4H, $\text{NCH}_2\text{Ar out}$, $^2J = 16.1$ Hz), 4.20 (d, 4H, $\text{NCH}_2\text{Ar in}$, $^2J = 16.1$ Hz) ppm.

Disodium-4-[13b-(4-carboxylatophenyl)-1,4,8,11-tetramethyl-6,13-dioxo-5,7,12,13b,13c,14-hexahydro-5a,6a,-12a,13a-tetraazabenz[5,6]azuleno[2,1,8-*ija*]benzo[*f*]azulen-13-yl]benzoate (**Na-2**):

Starting from **H-2** (100 mg, 0.156 mmol), this compound was synthesized as described for **Na-1**. Yield: 107 mg (100%) of **Na-2** as a white foam.

M.p. 390°C (dec.); IR (KBr pellet) ν 3048 (ArH), 2924 (CH_2), 1715, 1682 (urea C=O), 1605 (COO^-), 1557, 1475, 1449, 1428, 1405 (C=C), 1308, 1258 (CH_2) cm^{-1} ; $^1\text{H NMR}$ (D_2O , 500.13 MHz, 3.6 mM) δ 7.54 (d, 4H, ArH *ortho* to C(O)O, $^3J = 8.3$ Hz), 7.16 (d, 4H, ArH *meta* to C(O)O, $^3J = 8.3$ Hz), 6.33 (s, 4H, ArH side-wall), 4.84 (d, 4H, $\text{NCH}_2\text{Ar out}$, $^2J = 16.2$ Hz), 3.82 (d, 4H, $\text{NCH}_2\text{Ar in}$, $^2J = 16.2$ Hz), 2.20 (s, 12H, ArCH_3) ppm.

Disodium-4-[13b-(4-carboxylatophenyl)-1,4,8,11-tetramethoxy-6,13-dioxo-5,7,12,13b,13c,14-hexahydro-5a,-6a,12a,13a-tetraazabenz[5,6]azuleno[2,1,8-*ija*]benzo[*f*]azulen-13-yl]benzoate (**Na-3**):

Starting from **H-3** (100 mg, 0.142 mmol), this compound was synthesized as described for **Na-1**. Yield: 106 mg (100%) of **Na-3** as a white foam, which was stored under nitrogen at -18°C .

M.p. 321°C (dec.); IR (KBr pellet) ν 3047 (ArH), 2927, 2841 (CH_2), 1726, 1701 (urea C=O), 1603 (COO^-), 1558, 1472, 1438 (C=C), 1308, 1258 (CH_2), 1080 (COC) cm^{-1} ; $^1\text{H NMR}$ (D_2O , 500.13 MHz, 5.2 mM) δ 7.53 (d, 4H, ArH

ortho to C(O)O, $^3J = 8.2$ Hz), 7.13 (d, 4H, *ArH meta* to C(O)O, $^3J = 8.2$ Hz), 5.94 (s, 4H, *ArH side-wall*), 5.24 (d, 4H, *NCH₂Ar out*, $^2J = 16.3$ Hz), 3.69 (d, 4H, *NCH₂Ar in*, $^2J = 16.3$ Hz), 3.45 (s, 12H, *OCH₃*) ppm.

Disodium-4-[13b-(4-carboxylatophenyl)-1,4,8,11-tetramethoxy-6,13-dioxo-5,7,12,13b,13c,14-hexahydro-5a,6a,12a,13a-tetraazabenz[5,6]azuleno[2,1,8-*ija*]benzo[*f*]azulen-13-yl]benzoate (Na-4):

Starting from **H-4** (100 mg, 0.124 mmol), this compound was synthesized as described for **Na-1**. Yield: 105 mg (100%) of **Na-4** as a white foam, which was stored under nitrogen at -18°C .

M.p. $> 400^\circ\text{C}$ (dec.); IR (KBr pellet) ν 3053 (*ArH*), 2927, 2839 (*CH₂*), 1729, 1707 (urea C=O), 1603 (*COO⁻*), 1559, 1467, 1439, 1392 (C=C), 1306, 1258 (*CH₂*), 1077 (COC) cm^{-1} ; $^1\text{H NMR}$ (D_2O , 300.13 MHz, 2.9 mM) δ 7.63 (d, 4H, *ArH ortho* to C(O)O, $^3J = 7.2$ Hz), 7.31 (d, 4H, *ArH meta* to C(O)O, $^3J = 7.2$ Hz), 6.98 (br s, 4H, *NaphthH-5,8*), 6.05 (br s, 4H, *NaphthH-6,7*), 5.40 (d, 4H, *NCH₂Ar out*, $^2J = 15.8$ Hz), 4.03 (d, 4H, *NCH₂Ar in*, $^2J = 15.8$ Hz), 3.65 (s, 12H, *ArCH₃*) ppm.

Diammonium-4-[13b-(4-carboxylatophenyl)-6,13-dioxo-5,7,12,13b,13c,14-hexahydro-5a,6a,12a,13a-tetraazabenz[5,6]azuleno[2,1,8-*ija*]benzo[*f*]azulen-13-yl]benzoate ($\text{NH}_4\text{-1}$):

Compound **H-1** (100 mg, 0.17 mmol) was dissolved in aqueous ammonia (5 mL, 30%). The mixture was stirred overnight, the excess ammonia was evaporated and the residue was lyophilized to yield 106 mg (100%) of **NH₄-1** as a white foam, which was stored under nitrogen at -18°C .

M.p. 380°C (dec.); IR (KBr pellet) ν 3700–2700 (NH), 2939 (*CH₂*), 1740–1675 (C=O), 1468, 1426 (C=C), 1312, 1280, 1220 (*CH₂*) cm^{-1} ; $^1\text{H NMR}$ (D_2O , 300.13 MHz, 0.8 mM) δ 7.58 (d, 4H, *ArH ortho* to C(O)O, $^3J = 8.0$ Hz), 7.19 (d, 4H, *ArH meta* to C(O)O, $^3J = 8.0$ Hz), 7.18 (m, 4H, *ArH ortho* to *CH₂N*), 7.03 (m, 4H, *ArH para* to *CH₂N*), 4.57 (d, 4H, *NCH₂Ar out*, $^2J = 16.0$ Hz), 4.14 (d, 4H, *NCH₂Ar in*, $^2J = 16.0$ Hz) ppm.

Diammonium-4-[13b-(4-carboxylatophenyl)-1,4,8,11-tetramethyl-6,13-dioxo-5,7,12,13b,13c,14-hexahydro-5a,6a,12a,13a-tetraazabenz[5,6]azuleno[2,1,8-*ija*]benzo[*f*]azulen-13-yl]benzoate ($\text{NH}_4\text{-2}$):

Starting from **H-2** (100 mg, 0.156 mmol) this compound was synthesized as described for **NH₄-1** to yield 105 mg (100%) of **NH₄-2** as a white foam, which was stored under nitrogen at -18°C .

M.p. $> 400^\circ\text{C}$ (dec.); IR (KBr pellet) ν 3700–2700 (NH), 2947 (*CH₂*), 1730–1670 (C=O), 1471, 1448, 1422, 1406 (C=C), 1311, 1218 (*CH₂*) cm^{-1} ; $^1\text{H NMR}$ (D_2O , 400.13 MHz, 0.8 mM) δ 7.60 (d, 4H, *ArH ortho* to C(O)O, $^3J = 8.0$ Hz), 7.25 (d, 4H, *ArH meta* to C(O)O, $^3J = 8.0$ Hz), 6.63 (s, 4H, *ArH side-wall*), 4.95 (d, 4H, *NCH₂Ar out*, $^2J = 16.3$ Hz), 3.91 (d, 4H, *NCH₂Ar in*, $^2J = 16.3$ Hz), 2.32 (s, 12H, *ArCH₃*) ppm.

Diammonium-4-[13b-(4-carboxylatophenyl)-1,4,8,11-tetramethoxy-6,13-dioxo-5,7,12,13b,13c,14-hexahydro-5a,6a,12a,13a-tetraazabenz[5,6]azuleno[2,1,8-*ija*]benzo[*f*]azulen-13-yl]benzoate ($\text{NH}_4\text{-3}$):

Starting from **H-3** (100 mg, 0.142 mmol) this compound was synthesized as described for **NH₄-1** to yield 105 mg (100%) of **NH₄-3** as a white foam, which was stored under nitrogen at -18°C .

M.p. 309°C (dec.); IR (KBr pellet) ν 3700–2700 (NH), 2933 (*CH₂*), 1730–1670 (C=O), 1485, 1465, 1427, 1407 (C=C), 1353, 1299, 1259 (*CH₂*), 1077 (COC) cm^{-1} ; $^1\text{H NMR}$ (D_2O , 400.13 MHz, 0.7 mM) δ 7.58 (d, 4H, *ArH ortho* to C(O)O, $^3J = 8.1$ Hz), 7.18 (d, 4H, *ArH meta* to C(O)O, $^3J = 8.1$ Hz), 6.14 (s, 4H, *ArH side-wall*), 5.29 (d, 4H, *NCH₂Ar out*, $^2J = 16.1$ Hz), 3.76 (d, 4H, *NCH₂Ar in*, $^2J = 16.1$ Hz), 3.54 (s, 12H, *OCH₃*) ppm.

Diammonium-4-[13b-(4-carboxylatophenyl)-1,4,8,11-tetramethoxy-6,13-dioxo-5,7,12,13b,13c,14-hexahydro-5a,6a,12a,13a-tetraazabenz[5,6]azuleno[2,1,8-*ija*]benzo[*f*]azulen-13-yl]benzoate ($\text{NH}_4\text{-4}$):

Starting from **H-4** (100 mg, 0.124 mmol) this compound was synthesized as described for **NH₄-1** to yield 104 mg (100%) of **NH₄-4** as a white foam, which was stored under nitrogen at -18°C .

M.p. 360°C (dec.); IR (KBr pellet) ν 3700–2700 (NH), 2931, 2852 (*CH₂*), 1730–1670 (C=O), 1460, 1427, 1409 (C=C), 1356, 1306 (*CH₂*), 1047 (COC) cm^{-1} ; $^1\text{H NMR}$ (D_2O , 300.13 MHz, 0.4 mM) δ 7.72 (d, 4H, *ArH ortho* to C(O)O, $^3J = 7.8$ Hz), 7.40 (d, 4H, *ArH meta* to C(O)O, $^3J = 7.8$ Hz), 7.20 (br s, 4H, *NaphthH-5,8*), 6.35 (br s, 4H, *NaphthH-6,7*), 5.49 (d, 4H, *NCH₂Ar out*, $^2J = 15.8$ Hz), 4.16 (d, 4H, *NCH₂Ar in*, $^2J = 15.8$ Hz), 3.75 (s, 12H, *ArCH₃*) ppm.

References and notes

- Fendler, J. H. *Membrane Mimetic Chemistry*; John Wiley & Sons, New York, 1982.
- Israelachvili, J. N.; Marcelja, S.; Horn, R. G. *Q. Rev. Biophys.* 1980, 13, 121.

- ³ Nakashima, N.; Asakuma, S.; Kunitake, T. *J. Am. Chem. Soc.* **1985**, *107*, 509. Nusselder, J.-J. H.; Engberts, J. B. F. N. *J. Am. Chem. Soc.* **1989**, *111*, 5000. Muñoz, S.; Gokel, G. W. *J. Am. Chem. Soc.* **1993**, *115*, 4899. Menger, F. M.; Littau, C. A. *J. Am. Chem. Soc.* **1993**, *115*, 10083. Venkatesan, P.; Cheng, Y.; Kahne, D. *J. Am. Chem. Soc.* **1994**, *116*, 6955. Janout, V.; Lanier, M.; Regen, S. L. *J. Am. Chem. Soc.* **1997**, *119*, 640. Broderick, S.; Davis, A. P.; Williams, R. P. *Tetrahedron Lett.* **1998**, *39*, 6083. Nguyen, J. Q.; Iverson, B. L. *J. Am. Chem. Soc.* **1999**, *121*, 2639. Shawaphun, S.; Janout, V.; Regen, S. L. *J. Am. Chem. Soc.* **1999**, *121*, 5860. Vandenburg, Y. R.; Smith, B. D.; Pérez-Payán, M. N.; Davis, A. P. *J. Am. Chem. Soc.* **2000**, *122*, 3252.
- ⁴ Cheng, Y.; Ho, D. M.; Gottlieb, C. R.; Kahne, D.; Bruck, M. A.; *J. Am. Chem. Soc.* **1992**, *114*, 7319.
- ⁵ Kaiser, E. T.; Kezdy, F. J. *Science* **1984**, *223*, 249.
- ⁶ Takahashi, S. *Biochemistry* **1990**, *29*, 6257.
- ⁷ Lear, J. D.; Wasserman, Z. R.; DeGrado, W. F. *Science* **1988**, *240*, 1177.
- ⁸ Stein, T. M.; Gellman, S. H. *J. Am. Chem. Soc.* **1992**, *114*, 3943. McQuade, D. T.; Barrett, D. G.; Desper, J. M.; Hayashi, R. K.; Gellman, S. H. *J. Am. Chem. Soc.* **1995**, *117*, 4862. McQuade, D. T.; Quinn, M. A.; Yu, S. M.; Polans, A. S.; Krebs, M. P.; Gellman, S. H. *Angew. Chem. Int. Ed.* **2000**, *39*, 758.
- ⁹ Reek, J. N. H.; Kros, A.; Nolte, R. J. M. *Chem. Commun.* **1996**, 245.
- ¹⁰ Similar results have been obtained for dimerization of related facial amphiphiles in buffered aqueous solution, see: Isaacs, L.; Witt, D.; Fettinger, J. C. *Chem. Commun.* **1999**, 2549.
- ¹¹ Reek, J. N. H.; Rowan, A. E.; Elemans, J. A. A. W.; de Gelder, R.; Nolte, R. J. M. To be published.
- ¹² Tanford, C. in: *The Hydrophobic Effect*, 2nd edition; Wiley, New York, **1980**.
- ¹³ Lehrer, S. S.; Fasman, G. D. *Biopolymers* **1964**, *2*, 199.
- ¹⁴ Jokić, M.; Makarević, J.; Žinić, M. *J. Chem. Soc. Chem. Commun.* **1995**, 1723.
- ¹⁵ Shinoda, K.; Hutchinson, E. *J. Phys. Chem.* **1962**, *66*, 577.
- ¹⁶ It is well-known that the addition of acetone or methanol strongly reduces hydrophobic interactions.
- ¹⁷ Kinbara, K.; Kai, A.; Maekawa, Y.; Hashimoto, Y.; Naruse, S.; Hasegawa, M.; Saigo, K. *J. Chem. Soc. Perkin Trans 2* **1996**, 247. Kinbara, K.; Hashimoto, Y.; Sukegawa, M.; Nohira, H.; Saigo, K. *J. Am. Chem. Soc.* **1996**, *118*, 3441. Kinbara, K.; Kobayashi, Y.; Saigo, K. *J. Chem. Soc. Perkin Trans. 2* **2000**, 111. Lee, S. B.; Hong, J.-I. *Tetrahedron Lett.* **1996**, *37*, 8501.
- ¹⁸ Matsumoto, A.; Odani, T.; Chikada, M.; Sada, K.; Miyata, M. *J. Am. Chem. Soc.* **1999**, *121*, 11122.
- ¹⁹ Rao, C. N. R. in: *Chemical Applications of Infrared Spectroscopy*, Academic Press, New York and London, **1963**.
- ²⁰ Holder, S. J.; Elemans, J. A. A. W.; Barberá, J.; Rowan, A. E.; Nolte, R. J. M. *Chem. Commun.* **2000**, 355. Holder, S. J.; Elemans, J. A. A. W.; Donners, J. J. J. M.; Boerakker, M. J.; de Gelder, R.; Barberá, J.; Rowan, A. E.; Nolte, R. J. M. *J. Org. Chem.* **2001**, *66*, 391.
- ²¹ Ghadiri, M. R.; Granja, J. R.; Milligan, R. A.; McRee, D. E.; Khazanovich, N. *Nature* **1993**, *366*, 324. Lbotak, P.; Shinkai, S. *Tetrahedron Lett.* **1995**, *36*, 4829. Philp, D.; Stoddart, J. F. *Angew. Chem. Int. Ed. Engl.* **1996**, *35*, 1155. Vreekamp, R. H.; van Duynhoven, J. P. M.; Hubert, M.; Verboom, W.; Reinhoudt, D. N. *Angew. Chem. Int. Ed. Engl.* **1996**, *35*, 1215. Gillard, R. E.; Raymo, F. M.; Stoddart, J. F. *Chem. Eur. J.* **1997**, *3*, 1933. Balagurusamy, V. S. K.; Ungar, G.; Percec, V.; Johansson, G. *J. Am. Chem. Soc.* **1997**, *119*, 1539. Chemseddine, A.; Moritz, T. *Eur. J. Inorg. Chem.* **1999**, 235. Rebek, J., Jr. *Acc. Chem. Res.* **1999**, *32*, 278. Aizenberg, J.; Black, A. J.; Whitesides, G. M. *Nature* **1999**, *398*, 495. Ozin, G. A. *Can. J. Chem.* **1999**, *77*, 2001. Li, M.; Schnablegger, H.; Mann, S. *Nature* **1999**, *402*, 393. Orr, G. W.; Barbour, L. J.; Atwood, J. L. *Science* **1999**, *285*, 1049.
- ²² Naka K.; Tanaka Y.; Chujo Y.; Ito Y. *Chem. Commun.* **1999**, 1931.

Chapter 4

Controlled Self-Assembly of Metalloclips

4.1 Introduction

The ability to have control over the size and shape of self-assembled structures of nanosized dimension is one of the great challenges facing today's supramolecular chemistry.^{1,2} In Nature, self-assembly involves the non-covalent organization of building blocks that contain specific information needed for intermolecular recognition processes, such as hydrogen bonding, π -stacking, van der Waals and electrostatic interactions.³ By using complementarity in shape as a tool and by applying directed intermolecular forces, in combination with entropy-driven processes, Nature is capable of assembling building blocks into nanosized objects and structures of precisely determined shape and dimension. During the last decade many examples have been published of synthetic supramolecular approaches which result in the formation of predesigned architectures. A more recent development is the incorporation of metals into these architectures,⁴ which can, in principle, give a certain function. The ordering of (transition) metals in well-defined positions and at mutually fixed distances may eventually lead to applications in materials science and catalysis.⁵ Most of the supramolecular metallo-assemblies known to date can be divided into two types of architectures: (i) well-defined multi-metal complexes consisting of a relatively small number (< 50) of constituting building blocks which are constructed in solution,⁶ and (ii) infinite solid-state metallo-arrays (metallo-crystals).⁷ The first class of assemblies, which are commonly referred to as 'coordination-directed self-assemblies',⁸ comprises a wide range of systems, *e.g.* metal-containing molecular grids,⁹ metallacycli,¹⁰ helicates,¹¹ metallodendrimers,¹² metallocages and -capsules,¹³ and metallobutubes¹⁴ (Figure 4.1). The properties that these structures have in common are their finite size, but also their *nanoscopic* dimension. Only a limited number of components are usually assembled, the largest discrete metallo-assembly to date being a metallo-dodecahedron which is constructed from 50 components and has a diameter of approximately 8 nm.¹⁵

The limitation in the construction of larger assemblies *via* this approach lies mainly in the thermodynamic parameters of the reaction intermediates and the final product. When such a product is built up from an increasing number of components, indiscrete structures with different geometries may also be formed since they have a similar energy as the desired, discrete product. Approaches to bridge the gap between the small, discrete assemblies mentioned above and the

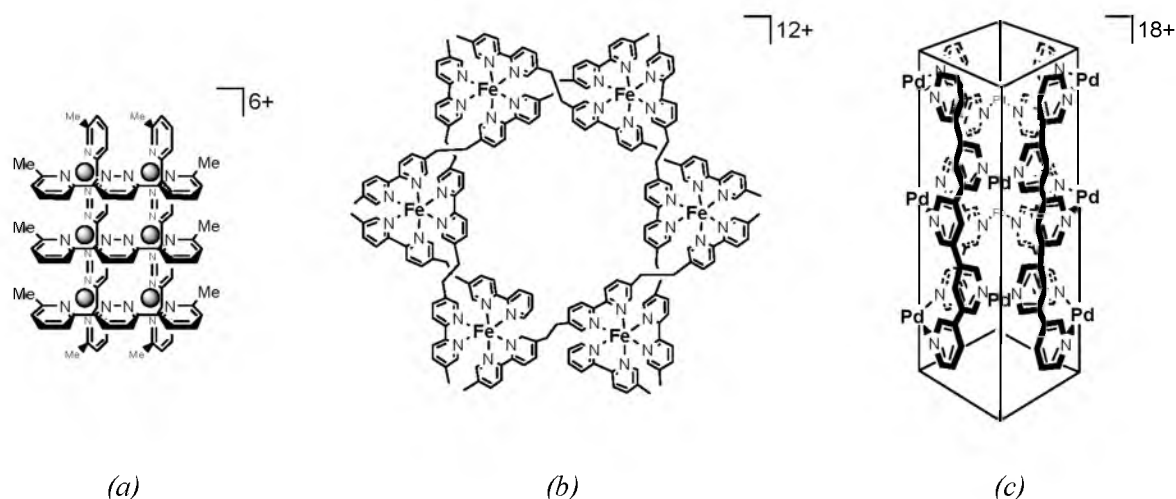


Figure 4.1 Examples of discrete, metal-containing assemblies on a nanoscopic scale. (a) Metallogrid. (b) Metallo-helicite. (c) Metallo-tube.

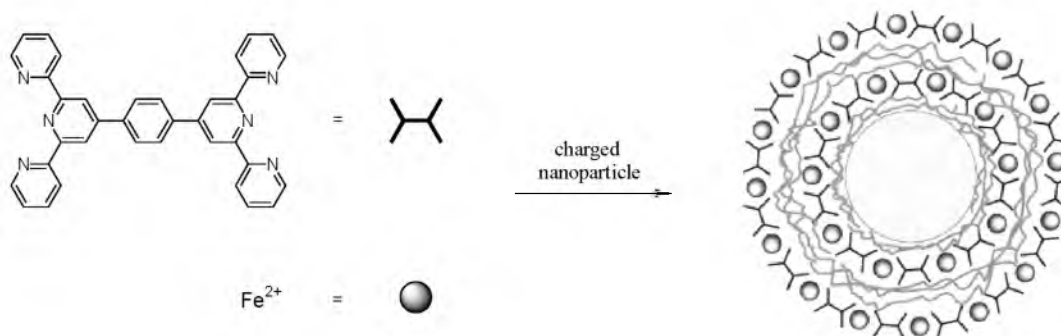


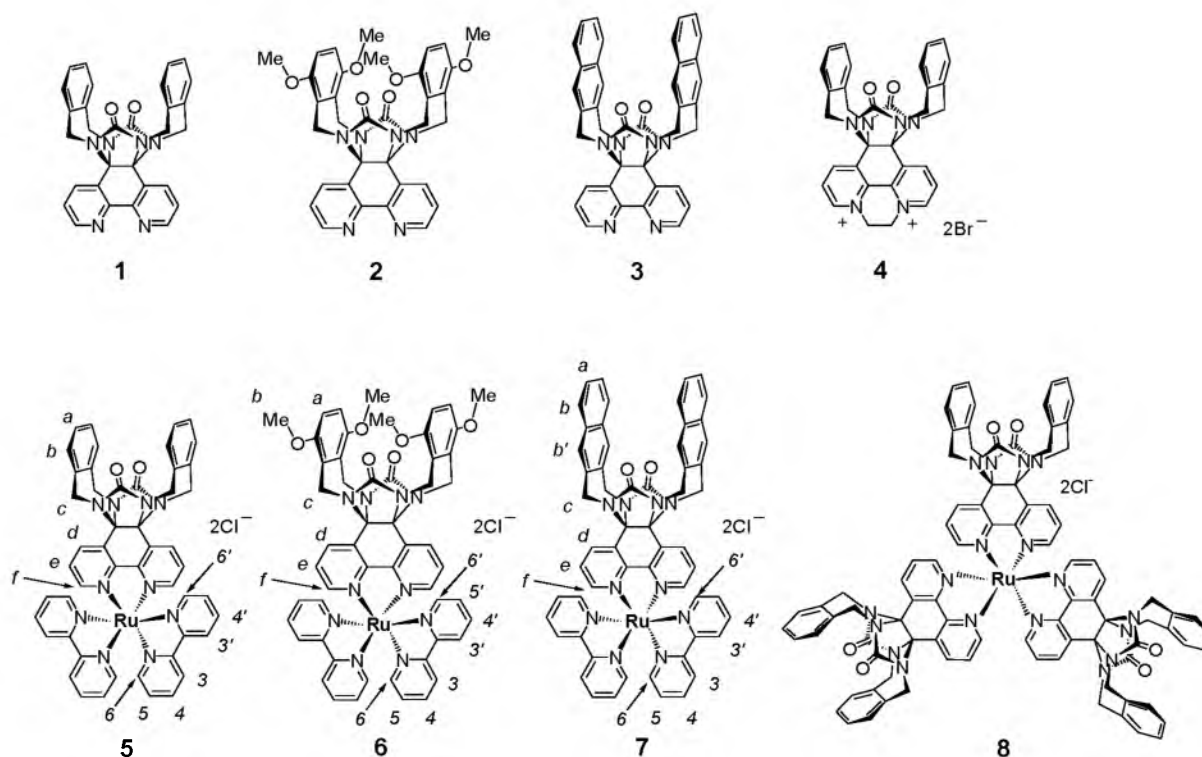
Figure 4.2 Templated deposition of charged coordination complexes around an oppositely charged nanoparticle giving a metallosupramolecular entity of approximately 75 nm size.

extended solid-state architectures have been described only recently. Metallo-superstructures on a *mesoscopic* scale have been constructed by the organization of metal ions with organic counter ions that determine the self-assembled structure. Discrete palladium nanoparticles have, for example, been constructed by liquid-crystalline ordering of their counter ions.¹⁶ These particles exhibited catalytic hydrogenation properties. Other work described the formation of discrete mixed-metal (Pt, Pd, Ni) assemblies in chloroform by the self-assembly of their lipophilic anions.¹⁷ A completely different approach involved the templated deposition of charged coordination complexes around oppositely charged nanoparticles, resulting in the formation of discrete and well-defined metallosupramolecular entities of about 75 nm size (Figure 4.2).¹⁸

This chapter deals with a new approach to construct discrete metallo-assemblies on a mesoscopic scale, which is based on the functionalization of a transition metal center with a ligand that possesses molecular recognition properties. In earlier work it has been demonstrated that water-soluble molecular clips, which are functionalized at their convex side with pyridinium¹⁹ or carboxylate groups,²⁰ form well-defined and discrete nanoarrays upon dispersion in water. The properties of these aggregates could be modified by varying the size and substitution pattern of the receptor side-walls, and by varying the counter ions. Here, the synthesis of new water-soluble metalloclips, *viz.* $[\text{Ru}(\text{bipy})_3]^{2+}$ complexes of which one of the bipyridine ligands has been

functionalized with a molecular clip, is described. Furthermore, the self-assembly of these metalloclips into micrometer-sized aggregates in water is reported, as well as the manipulation of these aggregates by variations in the temperature or the addition of small aromatic guest molecules.

Chart 4.1



4.2 Synthesis and characterization of metalloclips

In Chapter 2, the synthesis of three new molecular clips with a bipyridine ligand at their convex side, **1-3** (Chart 4.1), was described. Alkylation of compound **1** with 1,2-dibromoethane to generate the water-soluble compound **4** (Chart 4.1) was successful, however, the desired product could not be separated from several side-products. It was therefore decided to investigate an alternative approach to prepare water-soluble clips, *viz.* by the coordination of charged metal complexes. Ruthenium-bipyridine complexes were thought to be appropriate candidates, since it is known from literature that these type of complexes are highly water-soluble.

Clip molecules **1**, **2** and **3**, the synthesis of which has been described in Chapter 2, were complexed with $[\text{Ru}(\text{bipy})_2]\text{Cl}_2 \cdot 2\text{H}_2\text{O}$ ²¹ in dimethylformamide to give metalloclips **5**, **6** and **7** (Chart 4.1) in 55, 48 and 87% yields, respectively. Purification of the complexes was accomplished by gradient elution column chromatography on activated neutral alumina using chloroform/methanol mixtures, followed by precipitation of solutions of the products in diethyl ether.²² The compounds had an orange-red colour which is characteristic for $\text{Ru}(\text{bipy})_3$ -derivatives. Several attempts were undertaken to synthesize complex **8** (Chart 4.1), which has three clip molecules **1** coordinated to the central ruthenium center. After refluxing a solution of $\text{RuCl}_3 \cdot x\text{H}_2\text{O}$ and **1** in a mixture of chloroform and ethanol for one night, in the presence of

lithium chloride,²¹ the reaction mixture had turned orange. Analysis by TLC suggested that a new compound (**8**) had been quantitatively formed. This was confirmed by ¹H NMR and FAB mass spectroscopy of a sample of the reaction mixture, which revealed the formation of **8** as a single product. When, however, the compound was left to stand in aqueous or organic solution,²³ the orange colour turned purple within an hour. According to ¹H NMR spectroscopy, after this period an equimolar mixture of a ruthenium complex containing two clips and free ligand **1** was formed. Apparently, at room temperature **8** is unstable in solution. This might be a result of steric crowding of the three ligands around the metal center as suggested by molecular modeling calculations on **8**. Reactions of clips **2** and **3** with RuCl₃·xH₂O gave similar instable products. As a result of the chiral nature of the octahedral ruthenium center, metalloclips **5**, **6**, and **7** are racemic mixtures of their Λ and Δ enantiomers, and as a result they exhibit complicated NMR spectra. With the help of COSY and 2D NOESY techniques (500 MHz) the resonances of all the protons of **5-7** in D₂O solution could be assigned. In addition, the complexes displayed interesting self-association and aggregation behaviour, which will be discussed in the next section.

4.3 Self-association and aggregation of the metalloclips in water

4.3.1 NMR dilution studies

It was expected that metalloclips **5-7** would self-associate in water, since this property was previously observed for other water-soluble clip molecules.¹⁹ The self-association processes were investigated by NMR spectroscopy. The ¹H NMR spectra of **5** in D₂O displayed sharp resonances up to relatively high (>30 mM) concentrations, which enabled a reliable and detailed study of the self-association behaviour of this molecule. Several proton resonances of **5** in the spectra were very sensitive to changes in concentration (when diluted from 30 to 0.5 mM) and temperature. The resonances of the side-wall protons H_a and H_b and the bipyridine protons H₄ and H₅ (see Figure 4.3) exhibited large downfield shifts, whereas the resonances of all the other protons of **5** displayed only relatively small up- or downfield shifts (<0.1 ppm, Figure 4.3). Upon warming a solution of **5** similar shifts as observed upon dilution were visible and no significant proton shifts were seen when similar solutions of [Ru(bipy)₃]Cl₂ in D₂O were diluted or warmed. An NMR dilution titration of **5** in D₂O (using samples which varied in concentration from 0.5 to 10 mM) was carried out, and the chemical shifts of the resonances that displayed the largest shifts (H_a, H_b, H₄ and H₅) were plotted versus concentration. The resulting titration curves (Figure 4.4) could all be fitted to an equation defining a 1:1 self-association process. The self-association constant K_{self} between *two* molecules of **5** was determined to be $53 \pm 6 \text{ M}^{-1}$ (see also Table 4.1). To obtain additional information about the exact geometry of the molecules of **5** in the dimer, 2D NOESY spectra were recorded at different concentrations of the compound in D₂O. At a concentration of 1 mM, only cross peaks were observed resulting from nearest neighbour proton contacts, indicating the presence of (predominantly) non-self-associated **5** in solution. The 2D NOESY spectrum of a 30 mM solution of **5** in D₂O is shown in Figure 4.3. In addition to cross peaks which can be expected because of nearest neighbour contacts, now cross peaks are observed between the signals of side-wall protons H_a/H_b and the set of bipyridine protons H₄/H₅, H₆, H_{6'}, and between the signals of H_a/H_b and H_d/H_e/H_f. These cross peaks can only be the result of *intermolecular* close contacts, which at the used concentration points to dimerization or aggregation of **5**. Furthermore, it was observed that all nOe enhancements in

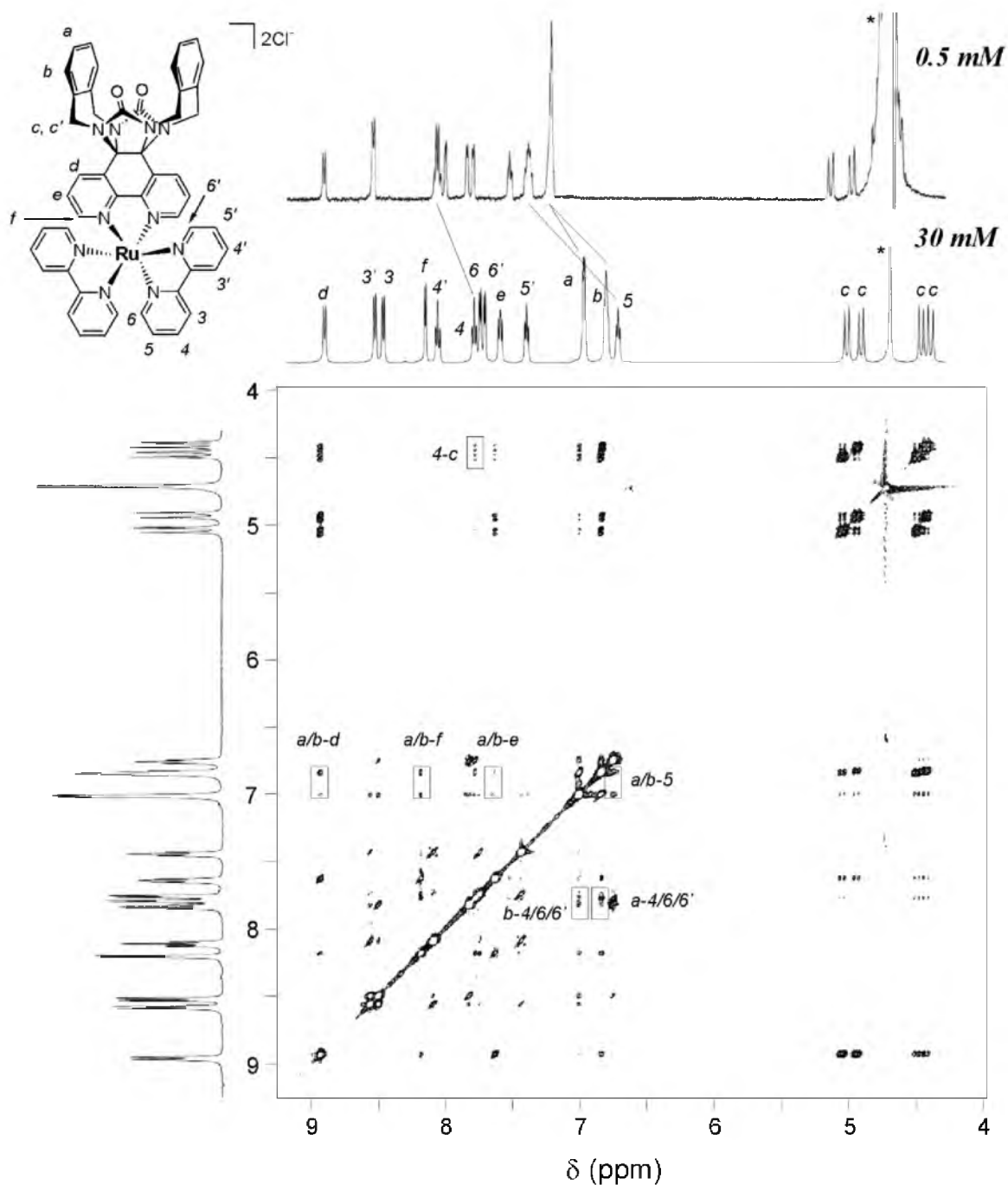


Figure 4.3 ^1H NMR spectra of **5** (D_2O , 298 K, 500 MHz) at concentrations of 0.5 and 30 mM (* = water) and the 2D NOESY spectrum of **5** (30 mM), in which the most important intermolecular *n*Oe contacts are highlighted in rectangles.

the spectrum of the 30 mM sample were negative, in contrast to the enhancements in a 1 mM sample, which were all positive. This implies that in the highly concentrated sample aggregates of **5** are present which have (on average) a molecular weight of at least 2000 amu or higher.²⁴ Combining the results obtained from the NOESY experiment with the complexation induced shift (CIS) values calculated from the dilution titration (Table 4.1), a well-defined ‘head-to-tail’ self-assembly geometry of **5** in water can be proposed. In this assembly the sterically least

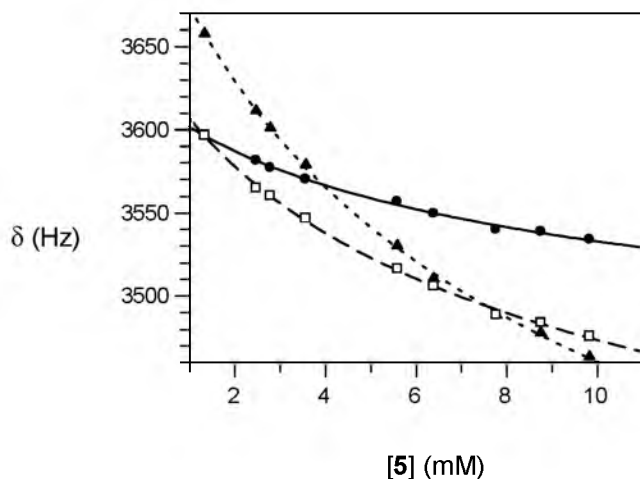


Figure 4.4 ^1H NMR shifts of selected protons during the ^1H NMR dilution titration of **5** in D_2O (500 MHz): H_a (\bullet), H_b (\square), and H_5 (\blacktriangle). The curves are calculated fits of the data points.

Table 4.1 Self-association constants (K_{self} , M^{-1}) and CIS values (ppm) for complexes **5–7** in D_2O at 298 K, calculated using several shifting protons as a probe.

Proton	Host					
	5		6		7	
	K_{self}^a	CIS ^a	K_{self}^a	CIS ^a	K_{self}^b	CIS ^b
H_a	58	-0.85	33	-1.27	21000	-2.07
H_b	55	-0.45			<i>c</i>	<i>c</i>
H_b'					<i>c</i>	<i>c</i>
OCH_3			36	-0.48		
H_4	52	-1.41	19	-0.17	2900	-0.33
H_5	47	-0.58	15	-0.41	2300	-0.27
H_6	<i>d</i>	<i>d</i>	12	-0.76	<i>d</i>	<i>d</i>
H_6'	<i>d</i>	<i>d</i>	20	-0.37	<i>d</i>	<i>d</i>

^aEstimated error approximately 10%. ^bEstimated error approximately 40%. ^cNo reliable value could be obtained due to overlap and broadening of the signals. ^dObserved shift of the resonance too small to calculate a reliable value.

hindered side of one of the bipyridine ligands is clipped between the cavity side-walls of its neighbour. Using the observed intermolecular nOe contacts in combination with molecular modeling, the geometry of this self-associated head-to-tail dimer was calculated (Figure 4.5a,b). In the mode of assembly, a tight fit exists between two adjacent molecules, which combines a maximal cavity filling with a minimal exposure of the hydrophobic aromatic surfaces to water. In the dimer, favourable offset π - π interactions²⁵ are present between the two side-walls and the clamped bipyridine ligand,²⁶ and between one of the side-walls and the other bipyridine ligand, which is positioned in an edge-to-face geometry on top of it. Molecular modeling clearly indicated that simultaneous binding of *both* bipyridine ligands of a molecule of **5** to two clips is

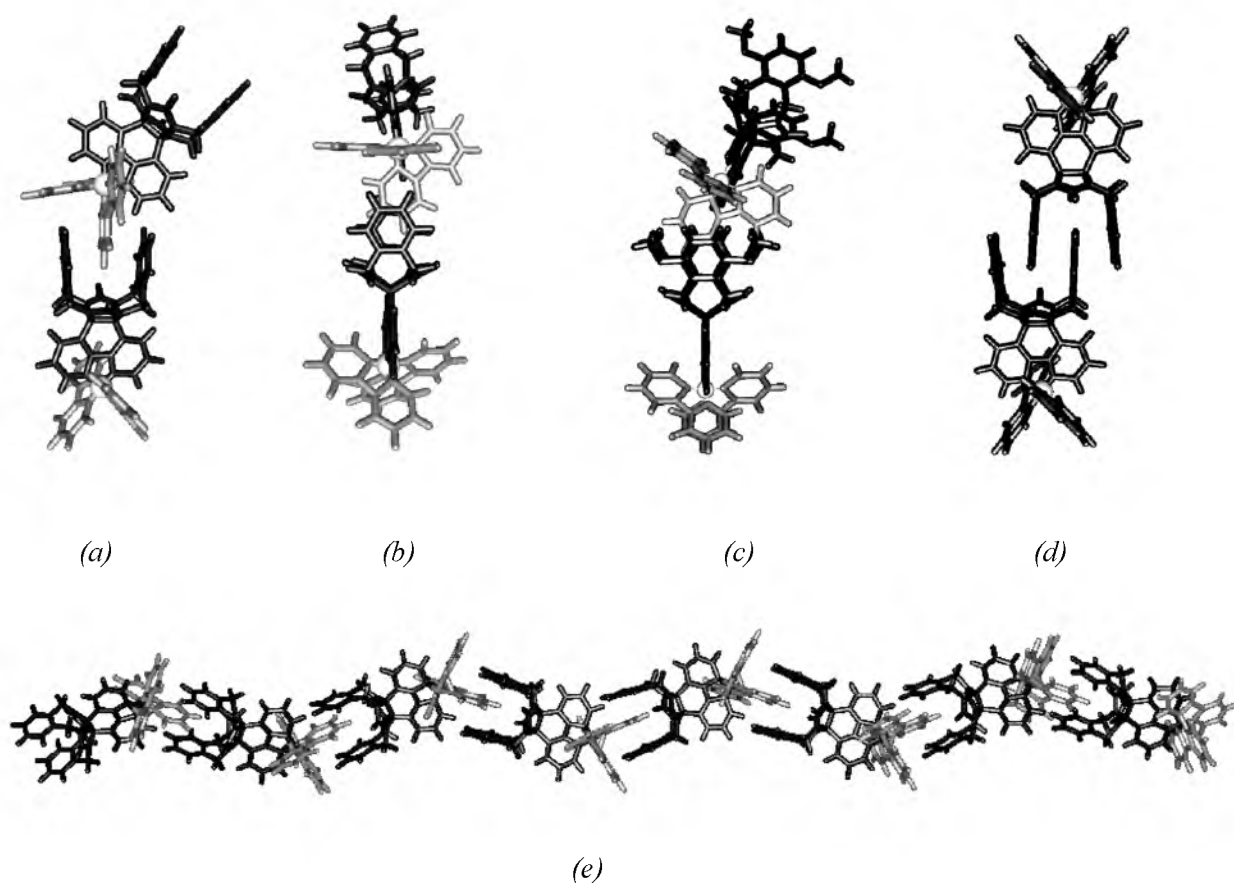


Figure 4.5 Computer modeled structures of the modes of self-association of metalloclips **5** and **6** in water, calculated using the CIS-values from the NMR dilution titrations and the observed intermolecular nOe -contacts. (a, b) Front and side view of the head-to-tail self-association of two molecules of **5**. (c) Side-view of the head-to-tail self-association geometry of **6**. (d) Front view of the competing head-to-head self-association geometry of **6**. (e) Infinite array of molecules of **5** which is a result of a repeated head-to-tail self-association process in water.

not possible due to the occurrence of considerable steric hindering between the molecules in such a 2:1 complex.²⁷ It is, however, expected that self-association of **5** in water is not restricted to the formation of dimers only, since one of the dimeric partners has a free cavity which is available for complexing another molecule of **5**. The binding in the cavity, and the complexation of the bipyridine ligands within the cavity of a neighbouring molecule of **5** are thought to be independent processes. Depending on the concentration, long arrays of **5** can be formed in solution (Figure 4.5e) and the calculated K_{self} clearly is an apparent association constant.

A similar dilution titration was carried out with the methoxy-walled compound **6** in D_2O (0.5-10 mM). Upon dilution, the same proton signals resonances as observed in the titration of **5** exhibited downfield shifts, *viz.* the signals of H_a , H_4 and H_5 (see Chart 4.1), and in addition the signals of the methoxy groups were found to shift. In contrast to **5**, however, the signals of H_3 and $H_{3'}$ also displayed considerable downfield shifts. All the titration curves of the shifting protons gave excellent fits to the equation defining a 1:1 self-association process. When, however, the K_{self} was calculated using the side-wall or methoxy proton signals as probes ($K_{\text{self}} = 35 \pm 5 \text{ M}^{-1}$), the value was substantially different from the value which was calculated using the bipyridine protons as the probe ($K_{\text{self}} = 15 \pm 5 \text{ M}^{-1}$, Table 4.1). Both these values are smaller than the K_{self} observed for **5**. The 2D NOESY spectrum of **6** displayed the same concentration

dependence as the spectrum of **5**. At increasing concentration several new cross peaks were observed, which corresponded to intermolecular nOe contacts between the side-wall and methoxy protons and the set of bipyridine protons H₅, H₄, H₃, and H₃'. From these nOe contacts and the measured CIS-values (Table 4.1), a head-to-tail self-association geometry was calculated using molecular modeling. This geometry differed from the geometry calculated for **5**, in the sense that the bipyridine ligand was clamped between the cavity side-walls of its neighbour in a slightly different orientation (Figure 4.5c). This difference in binding mode is understandable, since when the bipyridine ligand would be bound in the same geometry as in the case of **5**, the methoxy groups of one molecule of **6** would sterically hinder the non-binding bipyridine ligand of its dimeric partner, which is positioned in an edge-to-face geometry with respect to the side-wall of the first-mentioned molecule. This difference in binding angle may be the reason why the head-to-tail K_{self} of **6** is weaker than the K_{self} of **5**. The remarkable fact that two different K_{self} -values were measured for the different sets of protons of **6** suggests that, apart from the calculated head-to-tail geometry, a second self-association geometry occurs, *viz.* a head-to-head one (Figure 4.5d). This geometry, involving dimerization of the two cavities, is commonly observed for 1,4-dimethoxybenzene-walled clips in chloroform²⁸ and in water.^{20,29} The simultaneous existence of both types of geometries, *i.e.* head-to-head and head-to-tail, has been observed before in the case of naphthalene-walled pyridinium-functionalized clips in water.¹⁹ For **6**, the head-to-head self-association will be more favourable than the head-to-tail self-association, since the hydrophobic cavity of **6** is larger than that of **5**.

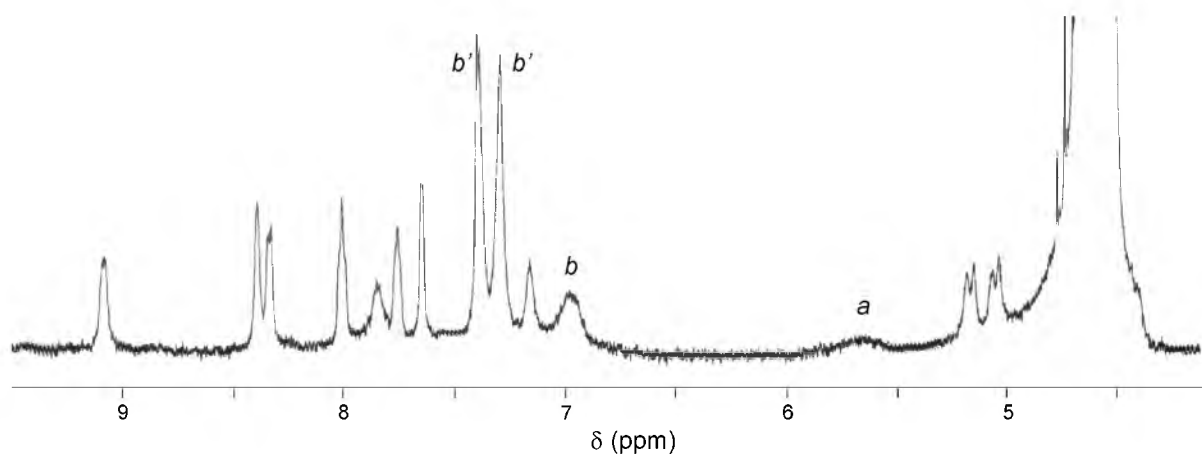


Figure 4.6 ¹H NMR spectrum of compound **7** at a concentration of 1 mM in D₂O. The signals belonging to the side-wall protons are indicated (see for proton numbering Chart 4.1).

Upon diluting compound **7** in D₂O, the resonances of the side-wall protons H_a, H_b and H_c, and of the bipyridine protons H₄ and H₅ (see Chart 4.1) exhibited strong downfield shifts, in particular the signal of the top side-wall protons (H_a). In contrast to **6**, no significant shifts of H₃ and H₃' were observed, suggesting that **7** self-associates in a head-to-tail geometry similar similar to that of **5**. The signals of **7** were significantly broadened even at low concentration (Figure 4.6), and at concentrations above 2 mM the solution gradually turned into a turbid dispersion. An NMR dilution titration carried out using samples varying in concentration between 0.1 and 2 mM revealed a self-association constant which was significantly higher than that calculated for **5** and **6**. Furthermore, the calculated K_{self} using the side-wall protons of **7** as a probe was larger than the

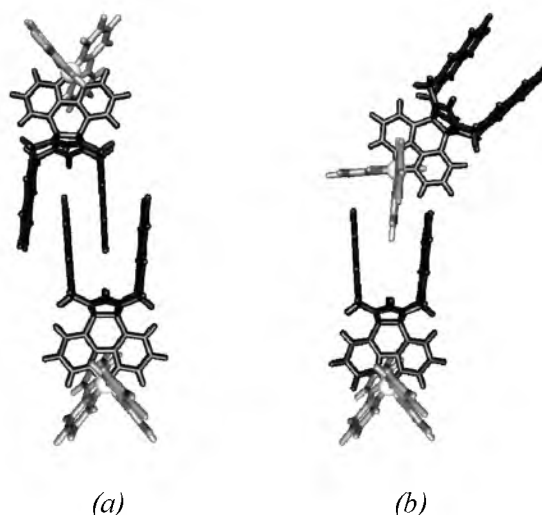


Figure 4.7 Computer modeled structures of the two self-associated dimers by **7** in water. (a) Head-to-head dimer. (b) Head-to-tail dimer.

K_{self} calculated using the bipyridine protons as a probe (Table 4.1). The difference between the two K_{self} -values was far more pronounced for **7** than for **6** (Table 4.1). The K_{self} calculated for the side-wall protons of **7** ($K_{\text{self}} = 21,000 \text{ M}^{-1}$) indeed is very large, and is attributed to the strong self-association of the large naphthalene-walled cavities in a head-to-head geometry (Figure 4.7). This process is dominated by hydrophobic interactions: **7** possesses a much larger hydrophobic cavity than **5** and **6** and hence is expected to form much stronger head-to-head dimers. This phenomenon is further reflected in the very large CIS-value measured for the H_a protons of **7** (-2.07 ppm , Table 4.1). The 2D NOESY spectra of **7** were not very informative, since even at low concentrations the signals were very broad. This broadening is a result of very strong self-association which leads to the formation of larger aggregates. This behaviour is further discussed in section 4.3.3.

4.3.2 UV-vis and fluorescence studies

Ruthenium-bipyridine complexes are well-known for their rich photophysical properties.³⁰ The absorption and emission spectra of **5**, **6** and **7**, and in particular the influence of the aggregation behaviour on these spectra were studied. The absorption and emission spectra of compound **5**, and for comparison also the spectra of $[\text{Ru}(\text{bipy})_3]\text{Cl}_2$ are shown in Figure 4.8. The absorption and emission spectra of **6** and **7** were very similar to those of **5**. In Table 4.2 the data for these compounds are listed. The spectra of the metalloclips exhibit the features commonly observed for ruthenium tris-bipyridine complexes. The broad absorption between 400 and 500 nm in the spectrum of **5** is a low-energy metal-to-ligand charge-transfer (MLCT) band, attributed to the overlap of $\text{Ru}^{\text{II}} \rightarrow \text{bipy}(\pi^*)$, while the strong band at 283 nm is attributed to $\pi \rightarrow \pi^*$ transitions of the naphthalene and bipyridine aromatic rings. Compared to the absorption spectrum of $[\text{Ru}(\text{bipy})_3]\text{Cl}_2$, the MLCT bands of the clip complexes are somewhat broader, which is probably caused by the fact that one of the bipyridine ligands in these compounds is substituted. The emission maxima recorded upon irradiation of the MLCT band are clearly red-shifted with respect to the emission maximum of $[\text{Ru}(\text{bipy})_3]\text{Cl}_2$. This is a commonly observed phenomenon since the wavelengths of the emission maxima are known to be more sensitive to the substitution pattern of the bipyridine ligands than the wavelengths of the absorption maxima.³¹

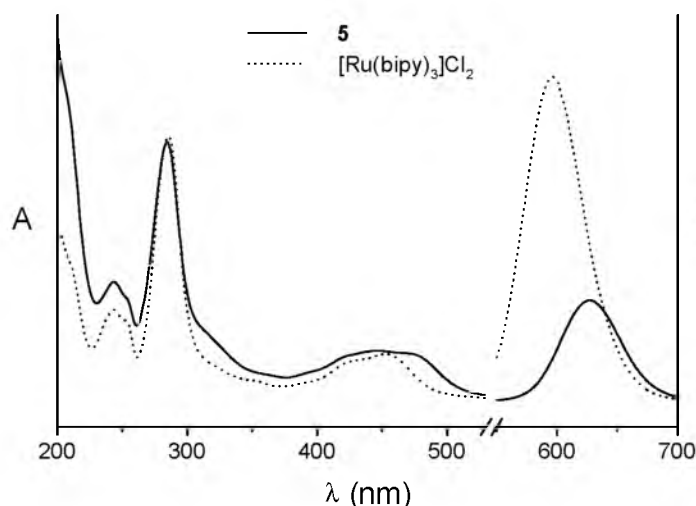


Figure 4.8 Absorption (left part of the graph) and emission spectra (right part of the graph) of **5** (solid lines) and $[\text{Ru}(\text{bipy})_3]\text{Cl}_2$ (dotted lines) in water at a concentration of 10^{-4} M.

Table 4.2 Photophysical properties of $[\text{Ru}(\text{bipy})_3]\text{Cl}_2$, **5**, **6**, and **7** (all 10^{-5} M) in water at 298 K

complex	$\lambda_{\text{max}}(\text{MLCT})/\text{nm}$	$\lambda_{\text{em}}(\text{MLCT})/\text{nm}$	emission intensity/a.u.
$[\text{Ru}(\text{bipy})_3]\text{Cl}_2$	453	596	295
5	447	628	70
6	446	625	62
7	450	625	35

To investigate the influence of the concentration on the absorption and emission spectra, solutions of the ruthenium complexes in water varying in concentration from 10^{-8} to 10^{-4} mM were prepared and measured. These variations in concentration appeared to have no influence on the absorption spectra, indicating that no excitonic interactions between the molecules were present. The observed emission intensities were plotted as a function of the concentration and compared to the emission of $[\text{Ru}(\text{bipy})_3]\text{Cl}_2$ at the same concentrations (Figure 4.9). It appeared that at all concentrations the emission of **5-7** was significantly less intense when compared to the emission of $[\text{Ru}(\text{bipy})_3]\text{Cl}_2$. Apparently, the self-quenching of the metalloclips is stronger than the self-quenching of $[\text{Ru}(\text{bipy})_3]\text{Cl}_2$, which can be attributed to aggregation effects. Further support for this comes from the fact that the emissions of **5-7** increased and became almost equal to the emission of $[\text{Ru}(\text{bipy})_3]\text{Cl}_2$ when a small quantity (5%) of acetone was added to the solutions of the metallo-clips. Acetone is known to cause dissociation of self-assembled clip structures in water.³² Figure 4.9 reveals that the fluorescence of **7** is more quenched than that of **5** and **6**, which is in line with the stronger self-association of the formed compound when compared to the latter ones.

4.3.3 Electron microscopy studies

To investigate whether the self-association of the metalloclips resulted in the formation of large aggregates, samples of **5**, **6** and **7** in water were investigated by transmission electron

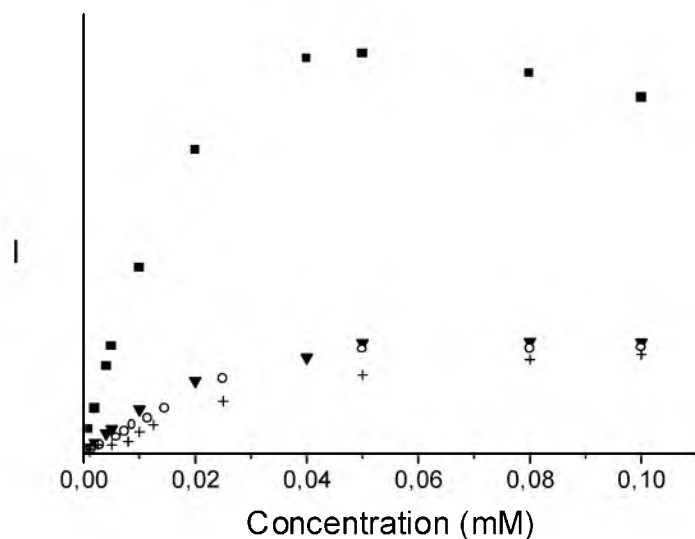


Figure 4.9 Fluorescence dilution curves of $[\text{Ru}(\text{bipy})_2]\text{Cl}_2$ (■), **5** (▼), **6** (○), and **7** (+).

microscopy (TEM). Initially, these studies were carried out without applying shadowing or staining techniques (any observed contrast is the result of the ruthenium centers in the molecules). Solutions of **5** and **6** in water remained clear up to relatively high concentrations ($>30 \text{ mM}^{33}$), suggesting that no large aggregates were present. Samples of these solutions were deposited on a Formvar-coated copper grid and studied with TEM. For both compounds, rather undefined, scroll-like assemblies were observed with lengths up to $10 \mu\text{m}$, and a typical width of approximately 100 nm (Figure 4.10a,b).

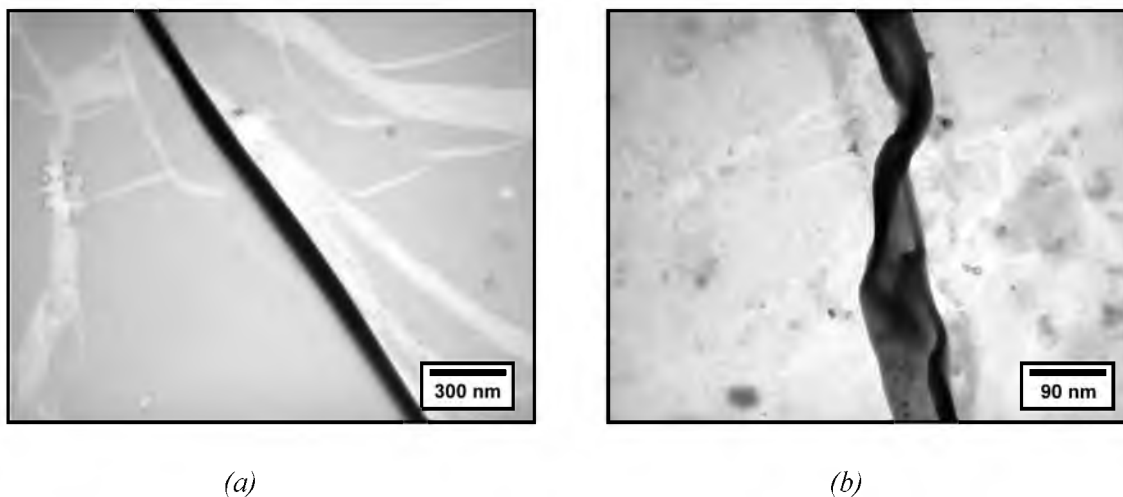


Figure 4.10 (a) TEM image of scroll-like aggregates as typically formed by **5** and **6**. (b) Twist in one of these scrolls. Samples are not shadowed or stained.

When the concentration of **7** in water was increased to approximately 2 mM , the solution transformed into a turbid dispersion. This dispersion remained stable for days without any precipitation. The turbidity suggests that relatively large aggregates are present. Indeed, when

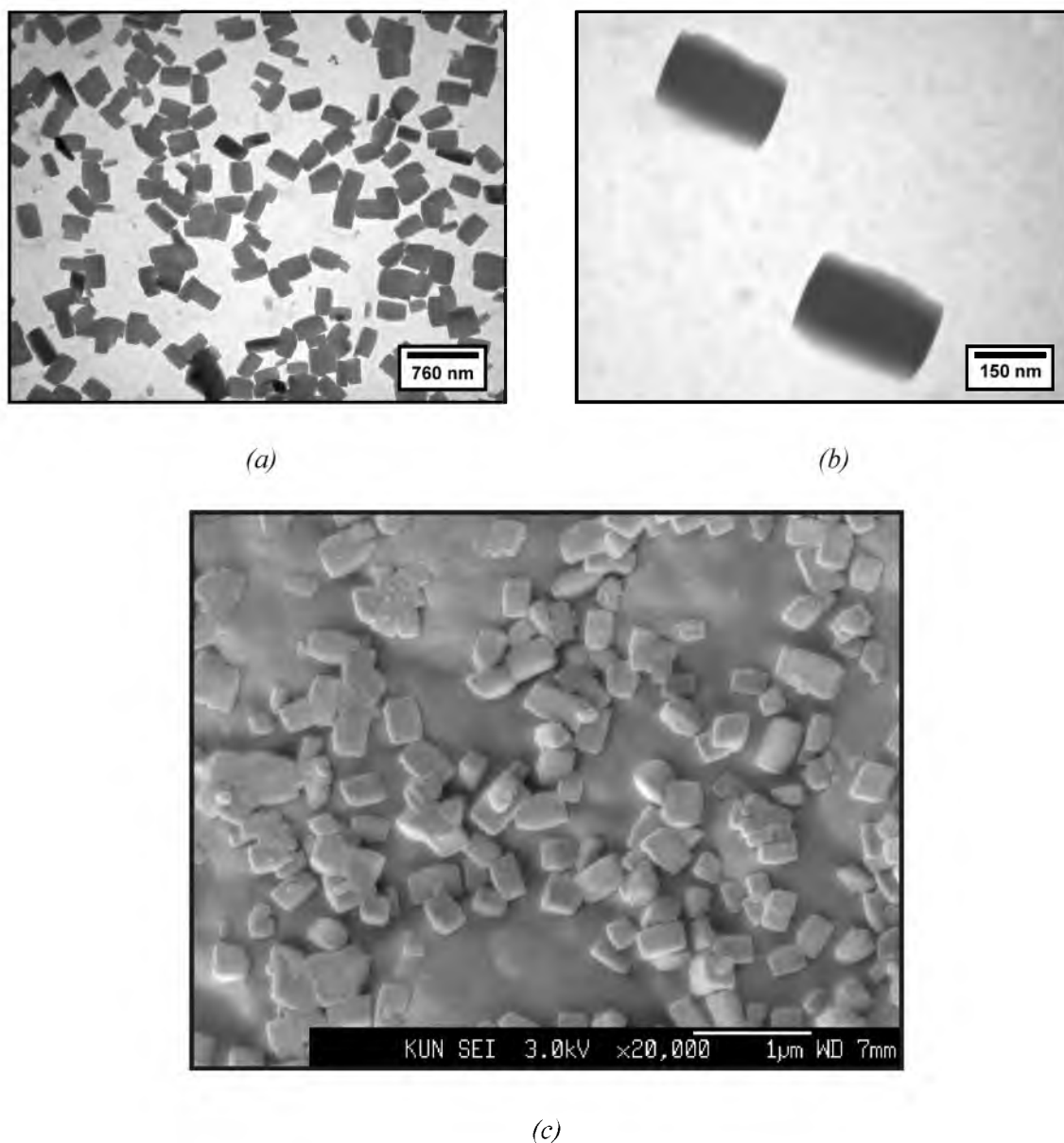


Figure 4.11 (a-b) TEM images of the rectangular aggregates formed by **7**. Samples are not shadowed or stained. (c) SEM image, sample is covered with a thin layer of gold.

samples of a dispersion (0.5% of **7**, w/v) were studied by TEM and scanning electron microscopy (SEM), rectangular aggregates were observed (Figure 4.11), which were very monodisperse in shape and size (typical dimensions 350×150 nm). The grids were subsequently shadowed with platinum under a 45° angle, which allowed the determination of the height of the rectangles. These appeared to be also quite monodisperse in height, *viz.* 75 ± 10 nm.

Somewhat surprisingly, occasionally instead of rectangular structures ‘cigar-like’ aggregates were observed (Figure 4.12a,b), which were an order of magnitude larger (typical dimensions 4000×350 nm) than the rectangular ones. Analysis of these ‘cigars’ revealed that they were also highly monodisperse in both shape and size (aspect ratio length:width = 11 ± 2). Some of the ‘cigars’ displayed transverse cracks (Figure 4.12c), which surprisingly slowly healed when the structure was held for a couple of seconds in the electron beam of the microscope. A closer look

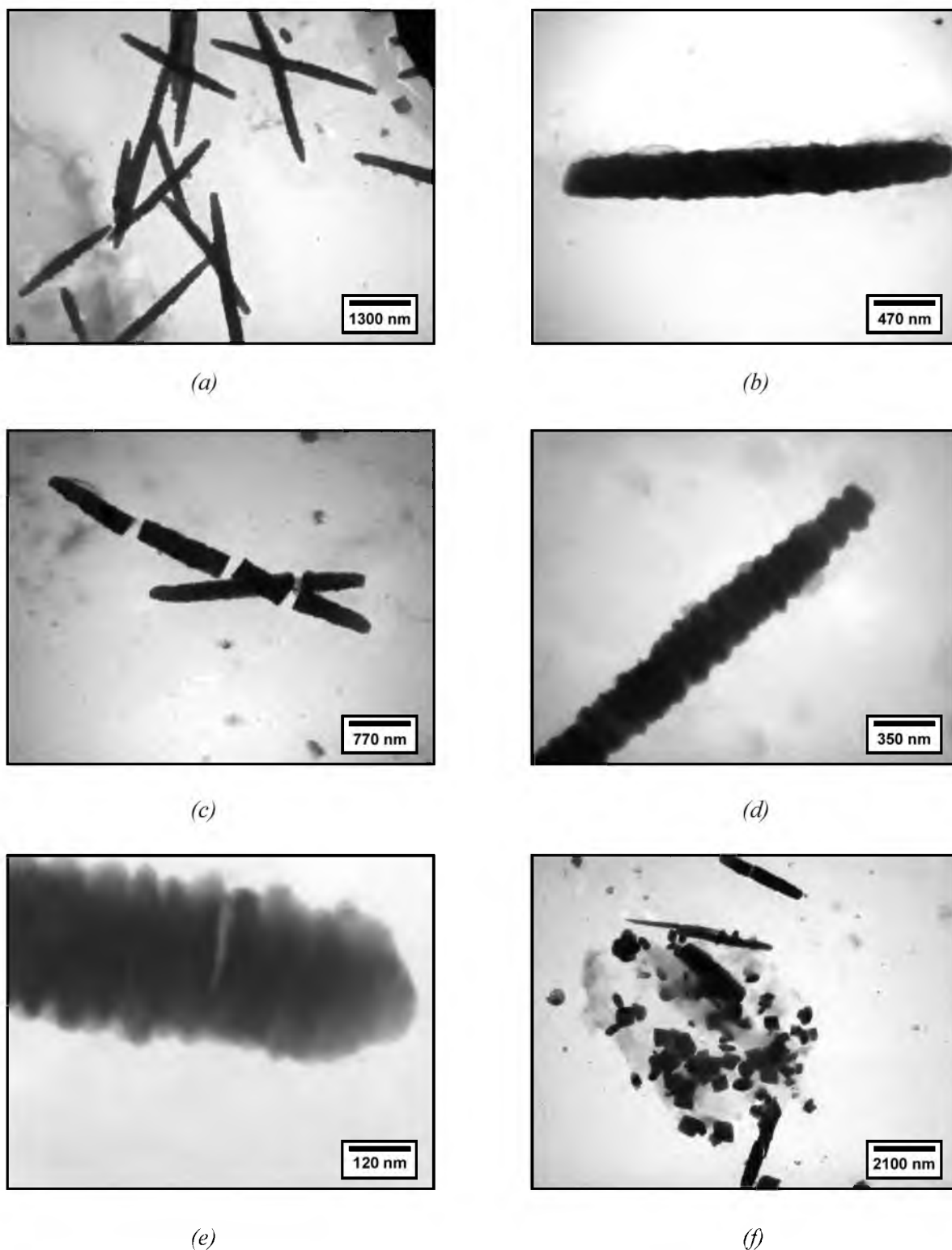


Figure 4.12 (a,b) TEM images of ‘cigar-like’ aggregates formed by 7. (c) ‘Cigars’ displaying transverse cracks. (d,e) Magnification of a ‘cigar’ which shows that it is built up from smaller subunits. (f) Location on the grid where both the ‘cigars’ and their subunits are present. Samples are not shadowed or stained.

at the ‘cigars’ at higher magnification revealed that they were built up from smaller subunits (Figure 4.12d,e). These subunits appeared to have dimensions which were remarkably similar to those of the rectangular aggregates (400 x 75 nm). We propose that the ‘cigars’ are a higher

order assembly, which is constructed from a limited number (40-60) of rectangular aggregates. Only at a few locations on the grids simultaneously the ‘cigars’ and the rectangles were visible (Figure 4.12f). The higher organization of the rectangles into a ‘cigar-like’ superstructure is difficult to induce and, to date, cannot be controlled. On most of the grids studied (> 90%), only rectangles were observed, and neither variations in the concentration of **7**, nor pre-treatment of the dispersions (heating, cooling, or ultrasonication) appeared to induce the hierarchical growth of these aggregates.

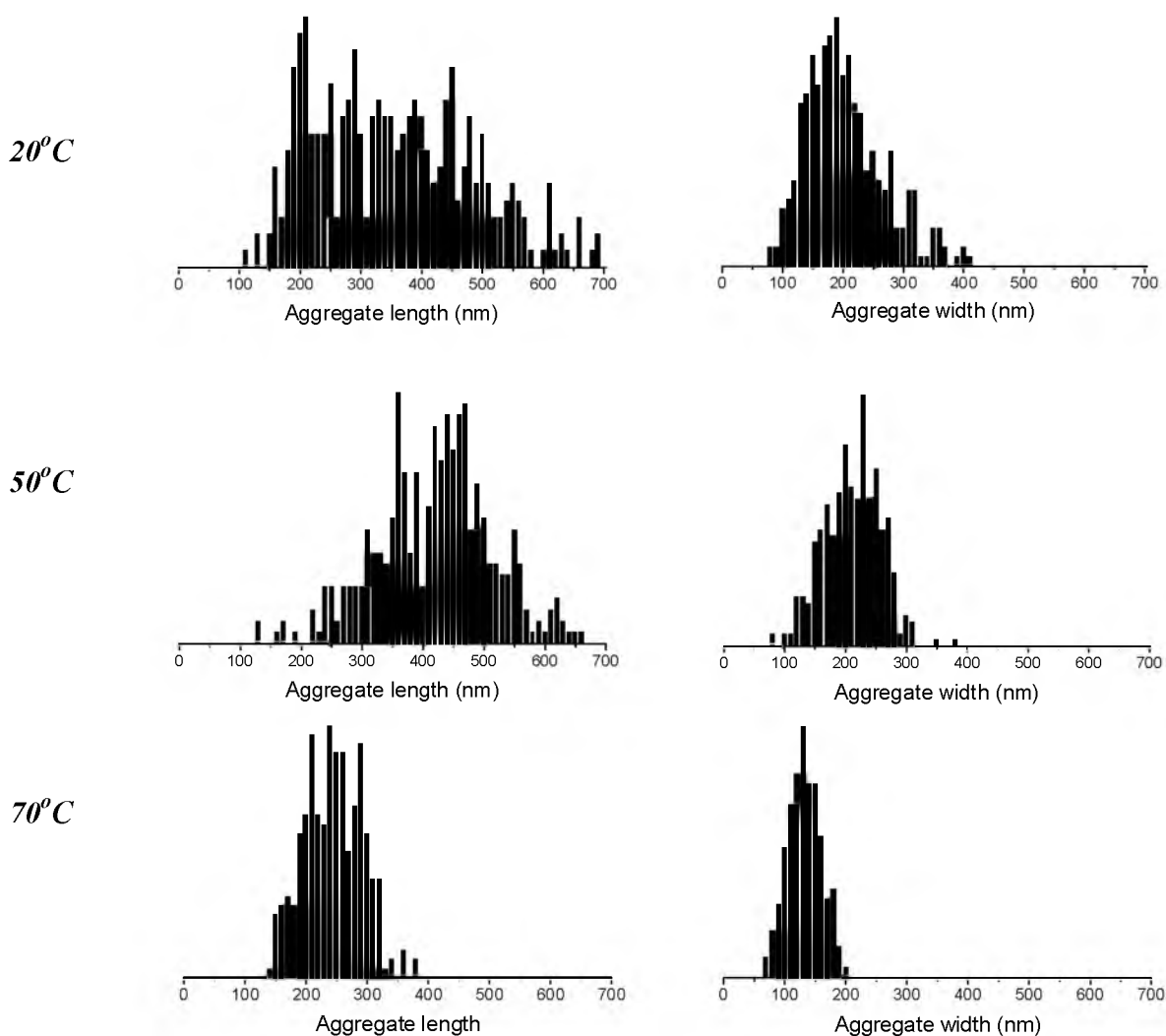


Figure 4.13 Size distribution diagrams of lengths and widths of rectangular aggregates formed by **7** at various temperatures (each diagram contains 300-400 data points).

Effect of the temperature on the aggregate morphology

To study the effect of the temperature on the aggregate morphology, 0.5% (w/v) dispersions of **7** in water were prepared at 20, 50 and 70°C, respectively. Samples of these dispersions were deposited on grids and studied with the help of TEM. In all cases, the observed aggregates were well-defined and rectangular in shape. The observed size dispersity of the structures was, however, dependent on the temperature. For each sample, the lengths and widths of a large number of aggregates (approximately 300-400) were measured and their size distribution plotted (Figure 4.13). From these distributions it can be seen that at higher temperatures the rectangles

are far more monodisperse in size than at lower temperature. In addition, the aggregate size tends to become smaller at higher temperatures. Differential scanning calorimetry (DSC) showed no phase transitions in repeated heating and cooling runs between 0 and 100°C.

4.3.4 Powder diffraction studies

X-Ray powder diffraction on samples of **5-7** revealed only a single, very broad reflection, corresponding to a repeating distance of approximately 10-11 Å. The absence of clear *d*-spacings suggests that the aggregates are built up from molecular units that interact in a very diverse way or assemble in a variety of geometries. Since the complexes are racemic mixtures of Λ and Δ enantiomers, and since in the head-to-tail self-association process one molecule of **5-7** has the possibility to choose between different bipyridine ligands of a neighbouring clip molecule for binding in its cleft and, additionally, has the option to use each of its own bipyridines to hold another clip molecule, such a diversity in binding can be easily envisaged.

4.3.5 Aggregate growth mechanism

The scroll-like aggregates which are formed by **5** and **6** are rather undefined when compared to the rectangular and ‘cigar-like’ structures formed by **7**. Since solutions of the former two compounds in water remained clear and gave sharp NMR spectra up to relatively high concentrations, the observed scrolls probably do not exist in solution, but are a result of drying-in effects upon evaporation of the solvent on the grid. It is, however, still likely that the molecules in these scrolls are to some extent ordered, for example in a head-to-tail fashion as proposed for **5** (Figure 4.5). The observation that **7** assembles into a better defined supramolecular structure than **5** and **6** can be attributed to the much stronger self-association of the former molecule. The naphthalene side-walls in **7** are large hydrophobic surfaces which can significantly enhance the interaction between neighbouring stacked molecules. This may result in a more compact and more well-defined structure at the mesoscopic level.

Based on the ^1H NMR dilution experiments in water and the electron microscopy studies, we propose that the rectangular aggregates grow as is outlined in Figure 4.14. It starts with the formation of a head-to-head dimer, which is the unit corresponding to the strongest interactions between two molecules of **7**. We presume that the dimer then acts as a nucleation point for further growth in two dimensions: as a result of the strong, hydrophobic interactions between the large naphthalene surfaces, the dimers of **7** will stack to form a long, bilayer-like array, which grows away in two directions from the central dimer. In this bilayer array, the so-called ‘dimeric seed’, the hydrophilic ruthenium-bipyridine units are supposed to be directed toward the aqueous phase. An additional process probably takes place simultaneously, in which monomers of **7** attach themselves in a head-to-tail fashion to the bipyridine units of the above mentioned bilayer array of dimers, eventually resulting in the formation of a two-dimensional (2D) sheet. Although this aggregation model only describes growth in two dimensions, it is proposed that growth in the third dimension simply results from the stacking of a number of these 2D sheets on top of each other. The reflection observed in the powder diffractogram of **7**, corresponding to a repeating distance of 10-11 Å, is in good agreement with the thickness of such stacked layers. A similar stacking of layers has been proposed for the ‘razorblade-like’ aggregates formed by pyridinium-functionalized clips in water,¹⁹ and more recently also for the aggregates formed by clips with long aliphatic tails in the solid state³⁴ (see Chapter 5).

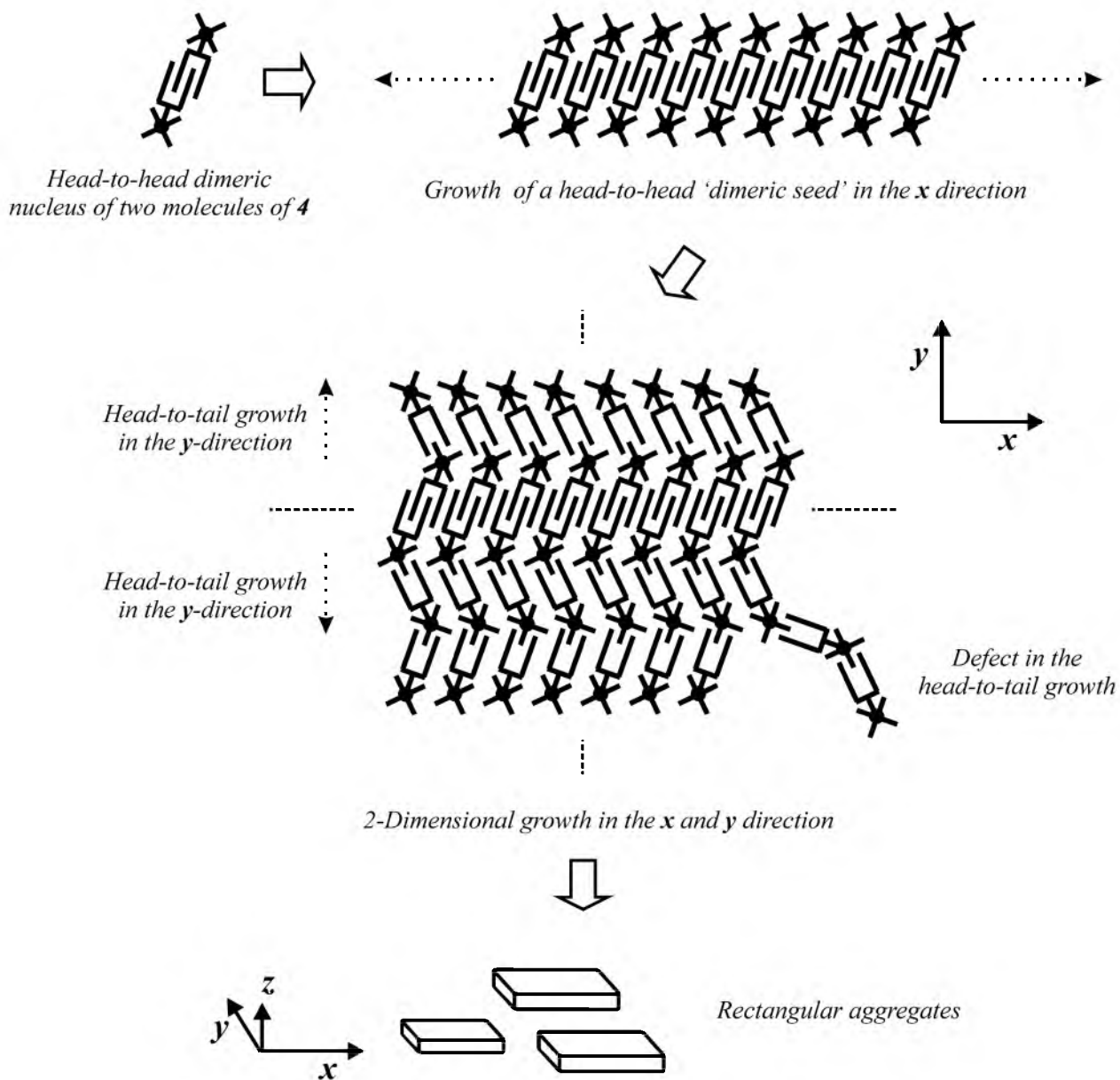


Figure 4.14 Proposed aggregate growth of 7.

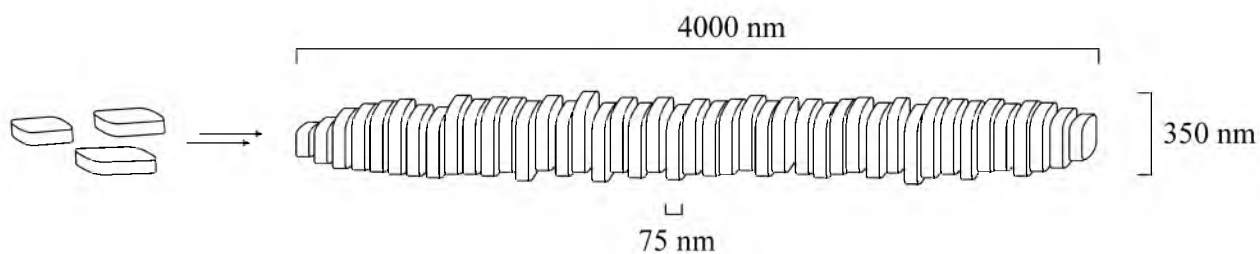


Figure 4.15 Proposed self-assembly of the rectangular aggregates formed by 7 into a 'cigar-like' superstructure.

The unique features of these rectangular aggregates are their finite size and high monodispersity. The fact that the aggregates are not infinite, as they are in the case of **5** and **6**, is attributed to several factors. First, following the proposed growth mechanism it can be expected that in the center of the aggregate the interactions between the molecules are the strongest, both between the two partners of the dimer and between the naphthalene surfaces of neighbouring dimers. In the regions of the aggregate containing the head-to-tail attached molecules, the intermolecular interactions will become weaker, since due to less efficient packing of the molecules the gaps between adjacent arrays become larger. As the aggregate grows, the coherence between the molecules decreases and it can be expected, therefore, that after a certain moment it will be energetically no longer favourable to attach new monomers to the increasingly incoherent and relatively water-soluble exterior of the aggregates of **7**. At this point, the assembly stops growing. The final shape of the architecture is thus governed by a subtle balance between the enthalpy (strength of intermolecular interactions) and the entropy of the self-assembly process. In addition, it is possible that defects which occur in the aggregate growth contribute to a termination of the assembly (see also Figure 4.14).

In the proposed model the sides of the clips form the floor and the roof of the rectangles. Compared to the ruthenium-bipyridine groups at the edges of the rectangles, these sides are hydrophobic. This might be the reason that the rectangles in some cases organize themselves further, tilted on their edges, into a ‘cigar-like’ superstructure, in which all the relatively hydrophobic rectangular faces minimize their exposure to water (Figure 4.15).³⁵

The electron microscopic studies revealed that at high temperature the size of the rectangular aggregates became smaller and more monodisperse. The first effect can be explained by the fact that the strength of the interactions between the molecules of **7**, and as a consequence also the aggregate size, decreases at higher temperature. The higher monodispersity is proposed to be the result of a self-repair process analogous to the repair processes observed in many natural systems. A higher rate of exchange between the attaching monomers and the aggregate enables the assembly process to be more dynamic and to reach thermodynamic equilibrium more easily. Self-association which occurs via the most optimum assembly geometry eventually leads to the most stable structure. Those monomers which assemble in a weaker geometry ‘fall off’ more easily at higher temperatures before further growth occurs.

4.3.6 Manipulation of the aggregate morphology

Mixing experiments

In the previous section it has been demonstrated that benzene-walled clip **5** specifically self-associates in a head-to-tail geometry, in contrast to **7**, which self-associates in both head-to-head and head-to-tail geometries. As a result, the latter molecule forms better defined structures on the mesoscopic scale than the former molecule. To investigate if the morphology of the rectangular aggregates formed by **7** could be manipulated, by mixing this compound with **5**, different mixtures of **5** and **7** in water were prepared. The total concentration of clip molecules was kept constant (0.5%, w/v). The molar ratio **7**:**5** was varied from 8:1 to 1:1 and further to 1:4. Although the ¹H NMR spectra of diluted samples of these mixtures were extremely complex, it was evident that in all cases the position of the broad resonance belonging to the naphthalene side-wall top protons of **7** (H_a) was hardly influenced by the addition of **5**. This suggests that the strong head-to-head dimerization displayed by **7** is not easily disrupted by the addition of **5**. It implies also that **5** probably participates only in the head-to-tail growing parts of the aggregates,

which can be expected because of the specific head-to-tail geometry in which **5** self-associates. To study the influence of the addition of **5** on the aggregate morphology, dispersions of the mixtures were deposited on a grid and studied by TEM. In the 8:1 mixtures of **7** and **5** several of the aggregates no longer were rectangular, but in contrast diamond-shaped (Figure 4.16).

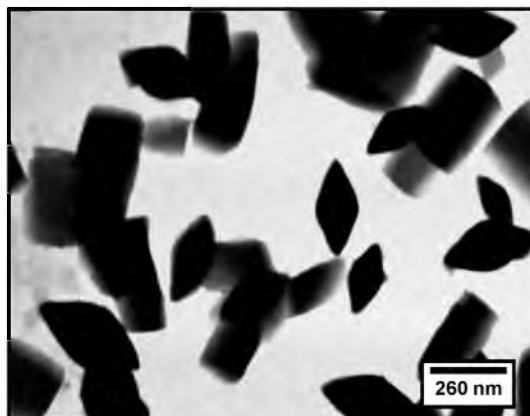


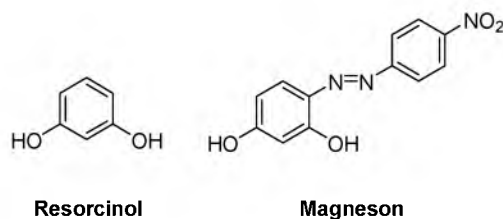
Figure 4.16 TEM image of the aggregates present in a 8:1 molar mixture of **7** and **5** in water. Samples are not shadowed or stained.

In the sample of the 1:1 mixture relatively more of the diamond-shaped aggregates were present, although overall far less aggregates were formed than in the 8:1 mixture. In the sample of the 1:4 molar mixture of **7** and **5**, only scrolls were observed, as in the case of pure **7**.

The diamond-like shape of the structures observed in the 8:1 and 1:1 molar mixtures of **7** and **5** suggests that the rectangular growth of the aggregates is slowed down at the corners. Since the diamonds have dimensions quite similar to the rectangles formed by pure **7**, it is assumed that they mainly consist of molecules of **7**. Apparently, monomers of **5** interfere in the head-to-tail growth process of **7**, and thus weaken the internal cohesion between the molecules. In the 1:4 mixture of **7** and **5**, the ‘tails’ of the head-to-head dimers of **7** probably are directly scavenged by monomers of **5** prohibiting the formation of large aggregates. The exact reason for the change in geometry is as yet unclear.

Effect of the addition of small aromatic guest molecules

In the proposed aggregate growth model of **7**, gaps are present between the molecules of the assembly. Molecular modeling indicated that these gaps are large enough to accommodate small, aromatic guest molecules. To investigate the effect of the addition of such molecules on the aggregate morphology of **7**, preliminary studies were carried out on samples of **7** in water which contained variable amounts of resorcinol or magneson.



At low concentrations of **7** (< 2 mM), when the solutions of the mixtures were still clear, ¹H NMR studies demonstrated that the signals of the side-wall protons H_a and H_b (see Chart 4.1) of

7 were not influenced by the addition of several equivalents of either of the guest compounds. In contrast, H_b, H_e, and in particular H_c and H_d displayed considerable upfield shifts ($\Delta\delta(\text{H}_c) > 0.1$ ppm). This suggests that these protons are shielded by the aromatic rings of the additives. A possible geometry for the complex between 7 and resorcinol is shown in Figure 4.17a. This depicted geometry is stabilized by hydrophobic effects which favour a minimal exposure of the lipophilic aromatic surfaces to water.³⁶

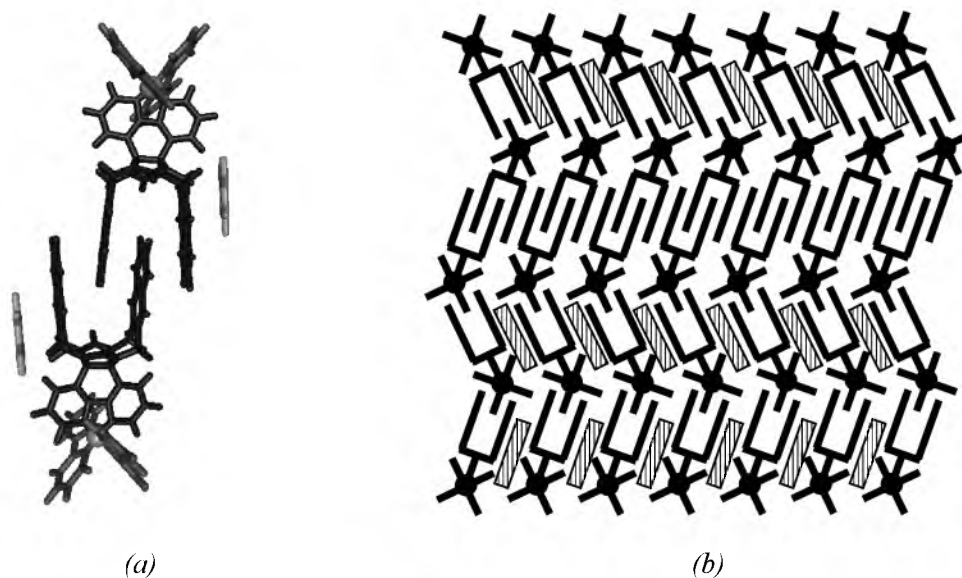


Figure 4.17 (a) Computer modeled structure, based on NMR experiments, of the complexation of the complex of a dimer of 7 and two molecules of resorcinol in water. (b) Proposed mode of inclusion of magneson molecules (dashed rectangles) into the arrays of 7.

To investigate whether the addition of resorcinol and magneson also had an influence on the aggregation process of 7, 0.5% (w/v) samples of this compound containing variable amounts of the additives were prepared and studied with the help of electron microscopy. The addition of resorcinol appeared to have no influence on the aggregation behaviour: similar rectangular structures were observed as in the case of pure 7. The addition of one or more equivalents of magneson to 7 in water, however, gave a completely different self-assembled architecture. Rectangular arrays were no longer observed, instead much larger assemblies were visible (Figure 4.18), which had dimensions in the same order of magnitude (4000-7000 x 400-600 nm) as the 'cigar-like' superstructures of pure 7. In contrast to the latter structures, however, the assemblies of 7 and magneson were far more dispersed in shape and size, and close inspection revealed no segmented structure, *i.e.* there was no indication that they were composed of the rectangular aggregates. It is likely that the addition of magneson to 7 stimulates the rectangular aggregates to grow into larger, less defined structures. This can be explained as follows: as mentioned above, molecular modeling studies indicated that gaps are present between neighbouring arrays of molecules of 7. These gaps weaken the interaction energy between the molecules, resulting in a more easy termination of the growth reaction. Magneson molecules can fill the gaps and hence act as a 'glue' which enhances the interactions between adjacent arrays of 7 (Figure 4.17b). This results in a stimulated growth, eventually leading to less-defined assemblies. We postulate that the increase in interaction energy leads to an assembly process which is less able to 'repair' defects. The fact that the addition of resorcinol had no effect on the aggregate morphology of 7

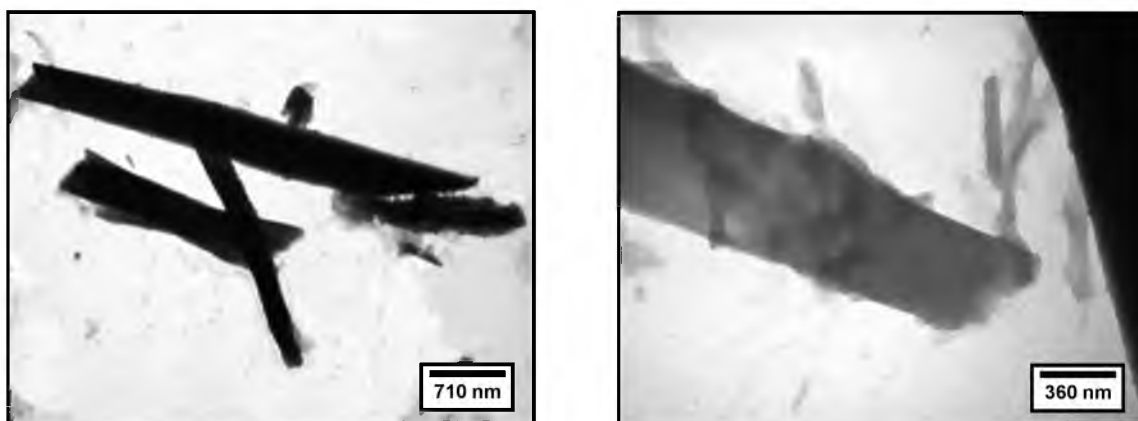


Figure 4.18 TEM images of aggregates present in the 1:1 molar mixture of **7** and magnesium in water. Samples are not shadowed or stained.

suggests that this additive is too small or too hydrophilic to enhance the interactions between the molecules of **7**.

4.4 Concluding remarks

A new series of water-soluble metalloclips, receptor cavities functionalized with a ruthenium-bipyridine center has been synthesized. The ruthenium clips with benzene and methoxybenzene side-walls appear to self-associate in water to form well-defined dimers which further self-assemble to generate undefined mesoscopic assemblies. Enlargement of the side-walls of the metalloclips, *viz.* with naphthalene moieties, increases the interaction between the molecules and as a result well-defined rectangular aggregates and ‘cigar-like’ objects are formed. The rectangular assemblies are very monodisperse in shape, and also relatively monodisperse in size. At higher temperature smaller rectangular architectures are formed with an even greater monodispersity in size. The addition of small aromatic guest molecules enhances the interactions between the metalloclip molecules and as a result larger, less-defined assemblies are generated. The detailed mode of assembly of the metalloclips into rectangular and higher ‘cigar-like’ aggregates is not yet completely understood.

The present work shows that, in order to obtain well-defined nanosized architectures, sufficiently strong interactions between the constituting metalloclips are needed. Both strong head-to-head and head-to-tail growth processes are required to achieve the nanosized architecture. Similar combined growth processes have been observed in the case of pyridinium and carboxylate-functionalized clips molecules.^{19,20}

Future work will be focused on obtaining control over the subtle balance between the enthalpy and entropy factors of the growth process, and on control over the size and shape of the nanostructures, *e.g.* by varying the temperature and by adding guest molecules.

4.5 Experimental section

4.5.1 Materials and general methods

DMF was dried over BaO for one week and then vacuum distilled; the first 30% of the distillate was removed. Diethyl ether was distilled under nitrogen from sodium benzophenone ketyl. All other chemicals were commercial products and were used as received. For column chromatography, neutral alumina purchased from Aldrich was used

which was activated to grade III according to the Brockmann scale.³⁷ To this end, the commercially obtained alumina was dried overnight in an oven at 150°C, then 6% of water (w/w) was added and the mixture was equilibrated by rotation in a round-bottom flask on a closed rotary evaporator for 3 h. Molecular modeling calculations were performed on a Silicon Graphics Indigo II work station using the CHARMM force field.³⁸ For an overview of general techniques see section 2.6.1.

4.5.2 NMR experiments

¹H NMR experiments in D₂O were carried out in the presence of an external standard (trimethyl phosphate in D₂O, δ = 0.00 ppm). 2D NOESY spectra were recorded applying a mixing time of 750 ms. Self-association constants were determined *in duplo* following the procedure described in Section 3.5.2.

4.5.3 Fluorescence measurements

Fluorescence spectra were recorded on a Perkin Elmer luminescence spectrometer LS50B equipped with a thermostatted cuvette holder (T=25°C). Samples of various concentrations of compounds 5-7 and [Ru(bipy)₃]Cl₂ in demineralized water in a 1.00 cm 4 mL quartz cuvette were purged with argon to exclude fluorescence quenching by oxygen. The excitation wavelength was the wavelength of the MLCT band observed in the UV-vis spectra of the compounds. The excitation and emission slits were 15 nm. The emission spectra were recorded from 500 to 750 nm applying a scanning speed of 120 nm min⁻¹.

4.5.4 Electron microscopy studies

A drop of a sample of 5-7 in demineralized water was deposited on a Formvar-coated copper grid. After 45 s, the excess dispersion was removed. The grids were studied on a Philips TEM 201 instrument operating at 60 kV. In some cases, the grids were shadowed with platinum (under an angle of 45°, layer thickness 2 nm). For the variable temperature TEM experiments, which were carried out *in duplo*, samples of 7 having identical concentrations in demineralized water were prepared and then heated to the desired temperature using a water bath. After equilibrating for 30 min, a drop of the sample was deposited on a grid and studied as described above. Size distribution diagrams were obtained by measuring the lengths and widths of 300-400 aggregates. For the SEM measurements, a thin layer of gold (2 nm) was sputtered on the samples.

4.5.5 DSC experiments

The appropriate amount of 7 (0.5 - 3%, w/v) was dispersed in approximately 25 μ L of demineralized water. The DSC samples were prepared in stainless-steel large volume pans (75 μ L). Thermograms were recorded between 0 and 100°C at 5°C/min, and repeated heating and cooling runs were measured.

4.5.6 Powder diffraction studies

A drop of a 5 mM sample of 5-7 in D₂O was placed on a silicon single crystal, which was then placed in a desiccator containing fresh P₂O₅ as drying agent. The sample was stored *in vacuo* for 24 h, and then placed in a Philips PW1710 diffractometer, which was equipped with a Cu LFF X-ray tube operating at 40 kV and 55 mA (wavelengths (a1,a2): 1.54060, 1.54438).

4.5.7 Syntheses

See Chapter 2 for the synthesis of clip molecules 1, 2 and 3. [Ru(bipy)₃]Cl₂ was synthesized according to a literature procedure.²¹

[Ru(bipy)₂]Cl₂·2H₂O

This compound was prepared according to a slightly modified literature procedure.²¹ A mixture of 2,2'-bipyridine (700 mg, 4.49 mmol), RuCl₃·xH₂O (500 mg, 1.91 mmol) and LiCl (550 mg, 13.3 mmol) in DMF (5 mL) was refluxed for 8 h. After cooling, the dark solution was poured into vigorously stirred acetone (50 mL). The resulting mixture was stored overnight at -18°C, filtered, and the residue was washed with water until the washings remained colourless. The product was dried under vacuum over P₂O₅, to yield 810 mg (82%) of [Ru(bipy)₂]Cl₂·2H₂O as a blue-green solid.

¹H NMR (500.14 MHz, DMSO-d₆) δ 10.01 (d, 2H, BipyH-6, ³J = 5.5 Hz), 8.67 (d, 2H, BipyH-3, ³J = 8.0 Hz), 8.52 (d, 2H, BipyH-3', ³J = 8.0 Hz), 8.10 (t, 2H, BipyH-4, ³J = 8.0 Hz), 7.81 (d, 2H, BipyH-5, ³J = 6.0 Hz), 7.72 (t, 2H, BipyH-4', ³J = 7.6 Hz), 7.55 (d, 2H, BipyH-6', ³J = 6.0 Hz), 7.14 (t, 2H, BipyH-5', ³J = 6.0 Hz) ppm.

[Ru(bipy)₂(1)]Cl₂ (5):

A degassed solution of 1 (100 mg, 0.201 mmol) and [Ru(bipy)₂]Cl₂·2H₂O (105 mg, 0.202 mmol) in DMF (15 mL) was stirred under nitrogen at 110°C for 16 h. After cooling, diethyl ether (100 mL) was added while stirring the

mixture vigorously. The purple precipitate was filtered off. The product was purified by column chromatography (alumina act. III, gradient elution, CH₂Cl₂ - CH₂Cl₂/MeOH, 97:3, v/v). The purified compound was dissolved in a minimal amount of methanol, and the resulting solution was added dropwise to stirred diethyl ether. After filtration of the resulting product, 108 mg (55%) of **5** was obtained as an orange-red hygroscopic solid, which was stored under nitrogen at -18°C.

M.p. > 400°C (dec.); IR (KBr pellet) ν 3052, 3017 (ArH), 2978 (CH₂), 1725, 1708 (C=O), 1464, 1445, 1430 (C=C, C=N), 1299, 1272, 1246 (CH₂) cm⁻¹; ¹H NMR (D₂O, 30 mM, 500.13 MHz) δ 8.92 (d, 2H, BipyH-*d*, ³J = 8.0 Hz), 8.55 (d, 2H, BipyH-3', ³J = 8.0 Hz), 8.49 (d, 2H, BipyH-3, ³J = 8.0 Hz), 8.18 (d, 2H, BipyH-*f*, ³J = 5.5 Hz), 8.09 (td, 2H, BipyH-4', ³J = 8.0 Hz, ⁴J = 1.5 Hz), 7.81 (td, 2H, BipyH-4, ³J = 8.0 Hz, ⁴J = 1.5 Hz), 7.77 (d, 2H, BipyH-6, ³J = 5.5 Hz), 7.73 (d, 2H, BipyH-6', ³J = 5.5 Hz), 7.61 (dd, 2H, BipyH-*e*, ³J = 8.5 Hz, ³J = 5.5 Hz), 7.43 (td, 2H, BipyH-5', ³J = 8.0 Hz, ⁴J = 1.5 Hz), 7.03-6.96 (m, 4H, ArH-*a* side-wall), 6.87-6.79 (m, 4H, ArH-*b* side-wall), 6.75 (td, 2H, BipyH-5, ³J = 8.0 Hz, ⁴J = 1.5 Hz), 5.05 (d, 2H, NCH₂-*c*'Ar in, ²J = 17.0 Hz), 4.93 (d, 2H, NCH₂-*c*Ar in, ²J = 17.0 Hz), 4.50 (d, 2H, NCH₂-*c*'Ar out, ²J = 17.0 Hz), 4.42 (d, 2H, NCH₂-*c*Ar out, ²J = 17.0 Hz) ppm, for the proton numbering see the drawing of the molecule in Chart 4.1; ¹³C{¹H} NMR (CD₃OD, 75.47 MHz) δ 159.12, 158.91 (both urea C=O), 154.07, 153.42, 153.05, 152.12, 140.13, 138.20, 137.84, 134.54, 131.99, 131.54, 129.94, 129.66, 129.56, 129.44, 129.39, 126.30 (all ArC), 79.91 (NC(Ar)N), 47.77, 47.42 (both NCH₂Ar) ppm; UV-vis (H₂O) λ /nm, log (ϵ /M⁻¹cm⁻¹) 283 (4.70), 447 (3.99); FAB-MS *m/z* 912 (M - 2Cl)⁺; ESI-MS *m/z* 456 (M - 2Cl)²⁺; FAB-HRMS calcd for [C₅₀H₃₈N₁₀O₂Ru]²⁺: 912.2228. Found: 912.2236.

[Ru(bipy)₂(2)]Cl₂ (**6**):

Starting from **2** (20.0 mg, 0.0324 mmol) and [Ru(bipy)₂]Cl₂·2H₂O (16.8 mg, 0.0324 mmol) in DMF (3 mL), this compound was synthesized as described for **5**. Yield 17 mg (48%) of **6** as an orange-red hygroscopic solid, which was stored under nitrogen at -18°C.

M.p. > 400°C (dec.); IR (KBr pellet) ν 3056 (ArH), 2977, 2963 (CH₂), 1724, 1708 (C=O), 1467, 1450 (C=C, C=N), 1291, 1270, 1245 (CH₂), 1094 (COC) cm⁻¹; ¹H NMR (D₂O, 3.2 mM, 500.14 MHz) δ 8.79 (d, 2H, BipyH-*d*, ³J = 8.3 Hz), 8.53 (d, 2H, BipyH-3', ³J = 8.2 Hz), 8.51 (d, 2H, BipyH-3, ³J = 8.2 Hz), 8.08 (t, 2H, BipyH-4, ³J = 6.5 Hz), 8.06 (t, 2H, BipyH-4', ³J = 6.5 Hz), 7.99 (d, 2H, BipyH-*f*, ³J = 5.5 Hz), 7.87 (d, 2H, BipyH-6, ³J = 5.1 Hz), 7.82 (d, 2H, BipyH-6', ³J = 5.0 Hz), 7.52 (dd, 2H, BipyH-*e*, ³J = 8.3 Hz, ³J = 5.5 Hz), 7.44 (t, 2H, BipyH-5', ³J = 6.0 Hz), 7.39 (t, 2H, BipyH-5, ³J = 6.0 Hz), 6.81 (s, 4H, ArH-*a* side-wall), 5.37 (d, 2H, NCH₂-*c*'Ar in, ²J = 16.7 Hz), 5.22 (d, 2H, NCH₂-*c*Ar in, ²J = 16.7 Hz), 4.72 (d, 2H, NCH₂-*c*'Ar out, ²J = 16.7 Hz), 4.51 (d, 2H, NCH₂-*c*Ar out, ²J = 16.7 Hz), 3.59 (s, 6H, OCH₃-*b*), 3.58 (s, 6H, OCH₃-*b*) ppm, for the proton numbering see the drawing of the molecule in Chart 4.1; ¹³C{¹H} NMR (CD₃OD, 75.47 MHz) δ 154.40, 156.14 (both urea C=O), 152.80, 150.66, 138.15, 136.60, 135.93, 132.77, 131.34, 130.43, 128.70, 127.67, 126.73, 125.62, 124.31 (all ArC), 111.01 (ArC para to CH₂N), 78.18 (NC(Ar)N), 55.69 (OCH₃), 48.04, 37.89 (both NCH₂Ar) ppm; UV-vis (H₂O) λ /nm, log (ϵ /M⁻¹cm⁻¹) 285 (4.54), 446 (3.80); FAB-MS *m/z* 932 (M - 2Cl)⁺. Due to the hygroscopic nature of the compound no satisfactory elemental analysis could be obtained.

[Ru(bipy)₂(3)]Cl₂ (**7**):

Starting from **3** (46 mg, 0.077 mmol) and [Ru(bipy)₂]Cl₂·2H₂O (40 mg, 0.077 mmol) in DMF (6 mL), this compound was synthesized as described for **5**. Yield 72 mg (87%) of **7** as an orange-red hygroscopic solid, which was stored under nitrogen at -18°C.

M.p. > 400°C (dec.); IR (KBr pellet) ν 3050, 3012 (ArH), 2980 (CH₂), 1725, 1707 (C=O), 1467, 1444, 1434 (C=C, C=N), 1298, 1270, 1243 (CH₂) cm⁻¹; ¹H NMR (D₂O, 2 mM, 500.14 MHz) δ 9.12 (br d, 2H, BipyH-*d*, ³J = 6.9 Hz), 8.44 (br d, 2H, BipyH-*f*, ³J = 4.7 Hz), 8.32 (br m, 4H, BipyH-3 and BipyH-3'), 8.00 (br m, 2H, BipyH-4'), 7.88 (br m, 2H, BipyH-4), 7.78 (br m, 2H, BipyH-*e*), 7.64 (br m, 4H, BipyH-6' and BipyH-6), 7.39 (br m, 4H, BipyH-5' and ArH-*b*' side-wall), 7.29 (br m, 2H, ArH-*b*' side-wall), 7.20 (br m, 2H, BipyH), 6.97 (br m, 4H, ArH-*b* side-wall), 5.68 (br m, 4H, ArH-*a* side-wall), 5.20 (d, 2H, NCH₂Ar in, ²J = 16.5 Hz), 5.09 (d, 2H, NCH₂Ar in, ²J = 16.5 Hz), 4.60 (d, 2H, NCH₂-*c*'Ar out, ²J = 16.5 Hz), 4.47 (d, 2H, NCH₂-*c*Ar out, ²J = 16.5 Hz) ppm, for the proton numbering see the drawing of the molecule in Chart 4.1; ¹³C{¹H} NMR (CD₃OD, 75.47 MHz) δ 150.70, 158.31 (both urea C=O), 154.08, 153.63, 152.59, 152.42, 140.02, 139.34, 137.86, 135.50, 134.57, 133.88, 130.77, 130.25, 129.92, 129.46, 128.85, 128.14, 126.13, 125.90 (all ArC), 79.23 (NC(Ar)N), 47.71, 47.51 (both NCH₂Ar) ppm; UV-vis (H₂O) λ /nm, log (ϵ /M⁻¹cm⁻¹) 284 (4.62), 450 (3.89); FAB-MS *m/z* 1011 (M - 2Cl)⁺; ESI-MS *m/z* 506 (M - 2Cl)²⁺; FAB-HRMS calcd for [C₅₈H₄₂N₁₀O₂Ru]²⁺: 1012.254. Found: 1012.209.

[Ru(**1**)₃]Cl₂ (**8**):

A degassed solution of **1** (21 mg, 0.042 mmol), RuCl₃·xH₂O (3.7 mg, 0.014 mmol) and LiCl (1 mg) in a mixture of CHCl₃ (2 mL) and EtOH (2 mL) was refluxed under nitrogen for 6 days. After cooling, the solvent was evaporated.

A dark red solid was obtained which contained **8**. The compound appeared to decompose upon purification by column chromatography or when it was left standing in solution (see text).

^1H NMR (DMSO- d_6 , 200.13 MHz) δ 8.42 (d, 6H, BipyH-4, $^3J = 5.5$ Hz), 7.81 (d, 6H, BipyH-6, $^3J = 8.4$ Hz), 7.31 (dd, 6H, $^3J = 8.4$ Hz, $^3J = 5.5$ Hz), 7.26 (br s, 24H, ArH side-wall, 4.86 (d, 6H, NCH₂Ar in, $^2J = 16.6$ Hz), 4.82 (d, 6H, NCH₂Ar in, $^2J = 16.6$ Hz), 4.61 (d, 6H, NCH₂Ar out, $^2J = 16.6$ Hz), 4.57 (d, 6H, NCH₂Ar out, $^2J = 16.6$ Hz) ppm; FAB-MS m/z 1597 (M - 2Cl)⁺.

References and notes

- ¹ Whitesides, G. M.; Mathias, J. P.; Seto, C. T. *Science* **1991**, *254*, 1312.
- ² Lbotak, P.; Shinkai, S. *Tetrahedron Lett.* **1995**, *36*, 4829. Philp, D.; Stoddart, J. F. *Angew. Chem. Int. Ed. Engl.* **1996**, *35*, 1155. Gillard, R. E.; Raymo, F. M.; Stoddart, J. F. *Chem. Eur. J.* **1997**, *3*, 1933. Chemseddine, A.; Moritz, T. *Eur. J. Inorg. Chem.* **1999**, 235. Rebek, J., Jr. *Acc. Chem. Res.* **1999**, *32*, 278. Aizenberg, J.; Black, A. J.; Whitesides, G. M. *Nature* **1999**, *398*, 495. Ozin, G. A. *Can. J. Chem.* **1999**, *77*, 2001. Li, M.; Schnablegger, H.; Mann, S. *Nature* **1999**, *402*, 393. Orr, G. W.; Barbour, L. J.; Atwood, J. L. *Science* **1999**, *285*, 1049.
- ³ Lehn, J.-M. in: *Supramolecular Chemistry*, VCH, Weinheim, **1995**.
- ⁴ Reviews: Baxter, P. N. W. in: *Comprehensive Supramolecular Chemistry*, Atwood, J. L.; Davies, J. E. D.; MacNicol, D. D.; Vögtle, F.; Reinhoudt, D. N.; Lehn, J.-M. Eds.; Elsevier Science Ltd., Pergamon: Elmsford, **1996**; Vol. 9, p. 165. Fujita, M. *ibid.* p. 253. Constable, E. C. *ibid.* p. 213.
- ⁵ Service, R. F. *Science* **1994**, *265*, 316.
- ⁶ Reviews: Fujita, M. *Chem. Soc. Rev.* **1998**, *27*, 417. Caulder, D. L.; Raymond, K. N. *Acc. Chem. Res.* **1999**, *32*, 975.
- ⁷ Review: Batten, S. R.; Robson, R. *Angew. Chem. Int. Ed.* **1998**, *37*, 1461.
- ⁸ Levin, M. D.; Stang, P. J. *J. Am. Chem. Soc.* **2000**, *122*, 7428.
- ⁹ Baxter, P. N. W.; Lehn, J.-M.; Kneisel, B.; Fenske, D. *Angew. Chem. Int. Ed. Engl.* **1997**, *36*, 1978.
- ¹⁰ Reviews: Stang, P. J.; Olenyuk, B. *Acc. Chem. Res.* **1997**, *30*, 502. Leininger, S.; Olenyuk, B.; Stang, P. J. *Chem. Rev.* **2000**, *100*, 853.
- ¹¹ Hasenknopf, B.; Lehn, J.-M.; Boumediene, N.; Dupont-Geravis, A.; van Dorselaer, A.; Kneisel, B.; Fenske, D. *J. Am. Chem. Soc.* **1997**, *119*, 10956. Withersby, M. A.; Blake, A. J.; Champness, N. R.; Hubberstey, P.; Li, W.-S.; Schröder, M. *Angew. Chem. Int. Ed. Engl.* **1997**, *36*, 2327. Kaes, C.; Hosseini, M. W.; Rickard, C. E. F.; Skelton, B. W.; White, A. H. *Angew. Chem. Int. Ed.* **1998**, *37*, 920. See for a review about helical programming: Rowan, A. E.; Nolte, R. J. M. *Angew. Chem. Int. Ed.* **1998**, *37*, 63.
- ¹² Huck, W. T. S.; Prins, L. J.; Fokkens, R. H.; Nibbering, N. M. M.; van Veggel, F. C. J. M.; Reinhoudt, D. N. *J. Am. Chem. Soc.* **1998**, *120*, 6240. Newkome, G. R.; He, E. F.; Moorefield, C. N. *Chem. Rev.* **1999**, *99*, 1689.
- ¹³ Jacopozzi, P.; Dalcanale, E. *Angew. Chem. Int. Ed. Engl.* **1997**, *36*, 613. Fujita, M.; Yu, S.-Y.; Kusukawa, T.; Funaki, H.; Ogura, K.; Yamaguchi, K. *Angew. Chem. Int. Ed.* **1998**, *37*, 2082. Fox, O. D.; Dalley, N. K.; Harrison, R. G. *J. Am. Chem. Soc.* **1998**, *120*, 7111. Kusukawa, T.; Fujita, M. *J. Am. Chem. Soc.* **1999**, *121*, 1397. Hiraoka, S.; Fujita, M.; *J. Am. Chem. Soc.* **1999**, *121*, 10239.
- ¹⁴ Aoyagi, M.; Biradha, K.; Fujita, M. *J. Am. Chem. Soc.* **1999**, *121*, 7457.
- ¹⁵ Olenyuk, B.; Levin, M. D.; Whiteford, J. A.; Shield, J.; Stang, P. J. *J. Am. Chem. Soc.* **1999**, *121*, 10434.
- ¹⁶ Ding, J. H.; Gin, D. L. *J. Am. Chem. Soc.* **2000**, *122*, 22.
- ¹⁷ Kimizuka, N.; Lee, S. H.; Kunitake, T. *Angew. Chem. Int. Ed.* **2000**, *39*, 389. Kimizuka, N.; Oda, N.; Kunitake, T. *Inorg. Chem.* **2000**, *39*, 2684.
- ¹⁸ Kurth, D. G.; Caruso, F.; Schüler, C. *Chem. Commun.* **1999**, 1579.
- ¹⁹ Reek, J. N. H.; Kros, A.; Nolte, R. J. M. *Chem. Commun.* **1996**, 245.
- ²⁰ Elemans, J. A. A. W.; Slangen, R. R. J.; de Gelder, R.; Feiters, M. C.; Rowan, A. E.; Nolte, R. J. M., manuscript in preparation.
- ²¹ Sullivan, B. P.; Meyer, T. J. *Inorg. Chem.* **1978**, *17*, 3334.
- ²² Many attempts were undertaken to grow single crystals of the metalloclips suitable for crystal structure determination, however, without success.
- ²³ Compound **8** was soluble, although sparingly, in water, dichloromethane, and mixtures of chloroform and ethanol or methanol.
- ²⁴ The sign of a nOe enhancement is related to the correlation time of tumbling and hence to the size of the molecule or the aggregate. See: Neuhaus, D.; Williamson, M. P. *The Nuclear Overhauser Effect*, VCH, Weinheim, **1989**.

- ²⁵ Hunter, C. A.; Sanders, J. K. M. *J. Am. Chem. Soc.* **1990**, *112*, 5525. Reek, J. N. H.; Priem, A. H.; Engelkamp, H.; Rowan, A. E.; Elemans, J. A. A. W.; Nolte, R. J. M. *J. Am. Chem. Soc.* **1997**, *119*, 9956. Breault, G. A.; Hunter, C. A.; Mayers, P. C. *J. Am. Chem. Soc.* **1998**, *120*, 3402. Whitten, D. G.; Chen, L.; Geiger, H. C.; Perlstein, J.; Song, X. *J. Phys. Chem. B.* **1998**, *102*, 10098.
- ²⁶ Clamping of the bipyridine unit of $[\text{Pt}(\text{bipy})(\text{NH}_3)_2](\text{PF}_6)_2$ between the benzene groups of a dibenzocrown ether has been described in the literature. This complex was generated in dichloromethane. The components adopt a different geometry with respect to each other as the molecules in the dimer of **5**. See: Colquhoun, H. M.; Stoddart, J. F.; Williams, D. J.; Wolstenholme, J. B.; Zarzycki, R. *Angew. Chem.* **1981**, *93*, 1093.
- ²⁷ A 2:1 complex was excluded since the data points could not be fitted to an equation defining such a 2:1 complex.
- ²⁸ Reek, J. N. H.; Rowan, A. E.; Elemans, J. A. A. W.; de Gelder, R.; Nolte, R. J. M. manuscript in preparation.
- ²⁹ Isaacs, L.; Witt, D.; Fettingner, J. C. *Chem. Commun.* **1999**, 2549.
- ³⁰ See for a review: Juris, A.; Balzani, V.; Barigelletti, F.; Campagna, S.; Belser, P.; von Zelewsky, A. *Coord. Chem. Rev.* **1988**, *84*, 85.
- ³¹ Issberner, J.; Vögtle, F.; De Cola, L.; Balzani, V. *Chem. Eur. J.* **1997**, *3*, 706.
- ³² Reek, J. N. H. Thesis, University of Nijmegen, **1996**.
- ³³ At higher concentrations the compounds started to precipitate and no dispersions were obtained as in the case of **7**.
- ³⁴ Holder, S. J.; Elemans, J. A. A. W.; Barberá, J.; Rowan, A. E.; Nolte, R. J. M. *Chem. Commun.* **2000**, 353. Holder, S. J.; Elemans, J. A. A. W.; Donners, J. J. J. M.; Boerakker, M.; de Gelder, R.; Barberá, J. Rowan, A. E.; Nolte, R. J. M. *J. Org. Chem.*, **2001**, *66*, 391.
- ³⁵ A similar hydrophobically-driven self-assembly of small aggregates into a higher organized superstructure has been reported for surfactant-coated barium nanoparticles. See: Li, M.; Schnablegger, H.; Mann, S. *Nature* **1999**, *402*, 393.
- ³⁶ It is as yet unclear what the orientation of the hydroxy substituents of the dihydroxybenzenes is, but it can be expected that these substituents are solvated, forming hydrogen bonds with water molecules.
- ³⁷ Brockmann, H.; Schodder, H. *Ber.* **1941**, *74B*, 73.
- ³⁸ CHARMM version 22.0. Revision 920911, Resident and Fellows of Harvard College, **1984**, **1992**, with the use of template charges.

Chapter 5

Host-guest complexes with tunable solid-state structures

5.1 Introduction

The design and construction of synthetic materials with a precise 2D or 3D architecture is an area of great interest. Several routes toward such materials can be followed, the most recent ones make use of molecular recognition processes.^{1,2} The rational design of organized molecular materials is also a fundamental problem in crystal engineering.^{3,4} In theory, since most organic compounds are crystalline, the identification of factors leading to different crystal structures would allow for the generation of a vast range of organic materials. In practice, however, the molecular interactions that generate certain crystal structures are multitudinous and the interpretation of the factors responsible for solid-state self-assembly is very difficult.^{3,5} The rational design of materials becomes even more complicated when two or more distinct molecules are desired in a given solid state structure.⁶ In many cases, this is an elusive process involving accommodation of small guest molecules into a porous crystalline host through rather unselective interactions.⁷ It is therefore of particular interest to design and develop materials in which the different constituting building blocks are oriented in the crystal by making use of well-defined and directed intermolecular interactions, *e.g.* hydrogen bonds and π - π stacking. Excellent examples of such predesigned solid materials are Aoyama's stacked columns⁸ and Wuest's networks,⁹ which both contain small cavities with directed functional groups in which guest molecules can be complexed (Figure 5.1). Other well-defined cavity-containing crystals are those formed by Ghadiri's cyclic peptides,¹⁰ whereas Gin has constructed polymerizable liquid-crystalline nanocomposites containing compartments that can accommodate metal complexes. In the latter example the enclosed metal complexes exhibited unique physical properties different to those of the complexes in the bulk or in solution.¹¹ In addition to these open-framework materials, many lamellar or layered solids are known which possess a spatial ordering of the molecular components in two dimensions.^{7,12} It is of great interest to design similar materials in which guest molecules can be incorporated at discrete positions in the layers. A wide array of potential applications for such lamellar host-guest materials can be envisaged, *e.g.* in photovoltaic or condensator-like devices.

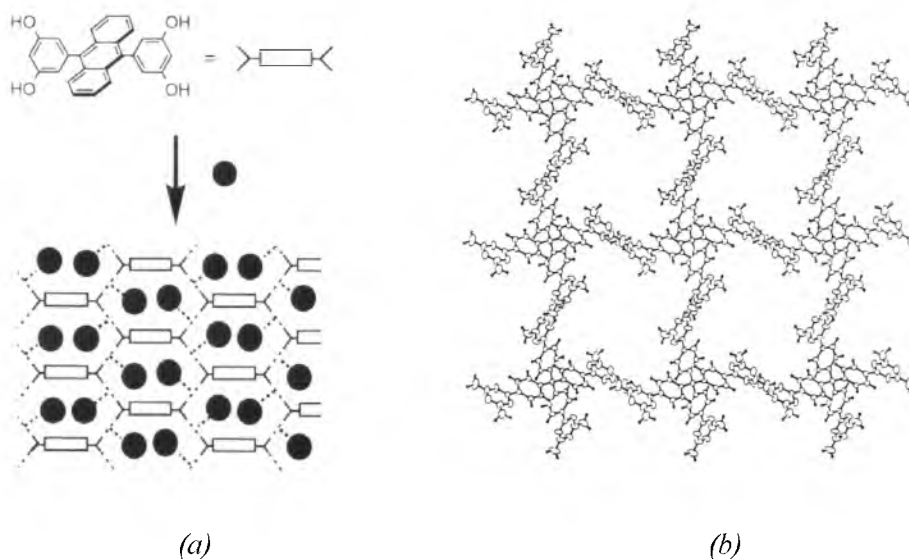


Figure 5.1 Examples of cavity-containing crystals of (a) Aoyama, and (b) Wuest.

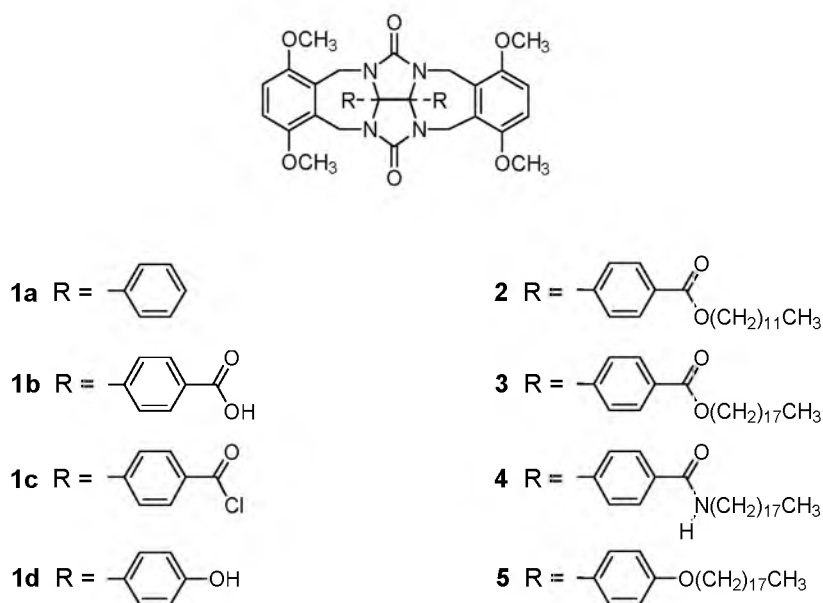
Over the past few years our group has studied the properties of molecular clips of type **1a** (Chart 5.1) mainly as substrate selective receptors for dihydroxybenzene guest molecules in chloroform solution.¹³ Only recently it was discovered that these molecules also can form dimers in organic solution and in the solid state. In these dimers the cavity of one molecule is filled by one of the side-walls of its dimeric partner and *vice-versa*.¹⁴ Analysis of the X-ray structures of a number of different molecular clips¹⁵ has revealed what are the most important factors that determine the ordering of these molecules in the crystal, namely π - π stacking and a 'cavity effect' (the mutual filling of the cavity by the dimeric components). Although dimer formation is relatively weak in chloroform, it can become significant in aqueous solution and lead to arrays of dimers which can further grow into well-defined nanosized aggregates (see also Chapters 3 and 4).¹⁶



Figure 5.2 Calculated structure of a dimer of two clip molecules (**3**) which are functionalized at their convex side with octadecyl hydrocarbon tails.

This chapter deals with the manipulation of clip molecules and their host-guest complexes in the solid state. In Chapter 2 some versatile high yield synthetic routes to clip molecules which are derivatized at their convex sides with benzoic acid and phenol groups have been described. This allows easy functionalization of the 'backside' of the clip, whilst the clip cavities remain open and accessible for dimerization and host-guest complexation. Here we describe the functionalization of these clip molecules with long aliphatic tails, the original goal being that upon dimerization of these new clips a typical rod-like mesogenic structure, *i.e.* a rigid aromatic core surrounded by several flexible hydrocarbon tails, would be generated which could give rise to liquid-crystalline phases (Figure 5.2). In previous research¹⁷ long aliphatic tails had already

Chart 5.1



been attached to the clip side-walls. These molecules themselves were not liquid-crystalline, but liquid-crystallinity could be induced by complexation of an appropriate dihydroxybenzene guest molecule. The new clips described here and their host-guest complexes have been studied in order to obtain insight in the nature of the (self-)assembly processes that can occur in the solid state and, additionally, to probe the capability of the clip molecules to act as host matrices for the ordering and self-assembly of functionalized guest molecules.

5.2 Physical properties of clips with long hydrocarbon tails

5.2.1 Synthesis and characterization

Four new clip molecules **2-5** (Chart 5.1), differing in the hydrocarbon tail length and in the linker between the tail and the clip, were synthesized. Clips **2** and **3**, which have their tails connected *via* ester linkers, were prepared starting from the carboxylic acid functionalized clip **1b** (see Chapter 2). Due to the low solubility of this compound in most common organic solvents, standard coupling methods with an aliphatic alcohol (*e.g.* using dicyclohexylcarbodiimide) turned out to be unsuccessful. Therefore, **1b** was esterified with the appropriate 1-bromoalkane in hot dimethylformamide using potassium carbonate as a base. In this way, clips **2** and **3** were obtained in yields of 73 and 82%, respectively, after recrystallization of the crude reaction products from a mixture of dichloromethane and ethanol. Clip **4**, containing amide linkers, was also synthesized starting from **1b**, which was first converted into the acyl chloride **1c** by treatment with thionyl chloride (yield 82%). This very hygroscopic compound was directly reacted with 1-aminooctadecane in dichloromethane, using triethylamine as a base to give **4** in 72% yield, after recrystallization from methanol. Clip **5**, containing ether linkers, was synthesized in 68% yield from phenol functionalized clip **1d** (see Chapter 2) by alkylation with 1-bromooctadecane in dimethylformamide using potassium carbonate as a base.

^1H NMR dilution experiments revealed that all new clips formed dimers in CDCl_3 solution. The dimerization constants were measured ($K_{\text{dimer}} = 15\text{-}20 \text{ M}^{-1}$ for all compounds) and were found to be in the same order of magnitude as the K_{dimer} which has been reported for the parent compound



Figure 5.3 Typical textures observed with TOPM for clip molecules **2** and **3**. (a) Polychromatic texture. (b) Platelet/mosaic texture.

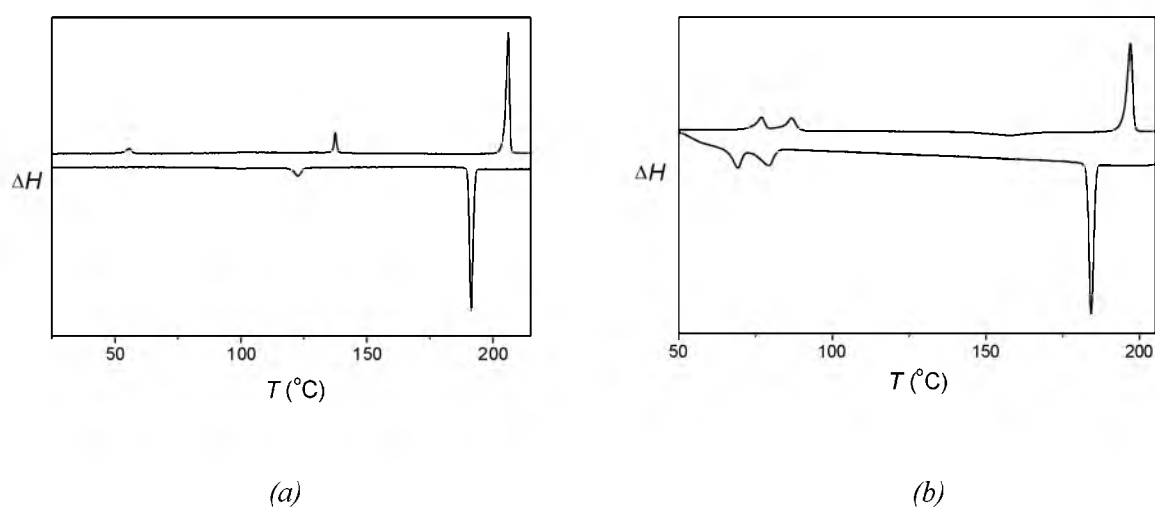


Figure 5.4 DSC thermograms of the first cooling run and second heating run of (a) **2** and (b) **3**.

1a ($K_{\text{dimer}} = 16 \text{ M}^{-1}$).¹⁴ The dimeric structure of the compounds was also observed in the electrospray mass spectra which were recorded for compounds **2** and **3**.

5.2.2 Thermal behaviour

*C*₁₂-ester clip **2**

Analysis of a sample of **2** with thermal optical polarized microscopy (TOPM) showed that a birefringent texture evolved upon cooling from the isotropic melt.¹⁸ Depending on the sample thickness, two different textures were observed: a highly coloured, polychromatic one with no clearly defined pattern, although spherulites were often visible (Figure 5.3a), and a platelet/mosaic texture¹⁹ reminiscent of a smectic liquid-crystalline mesophase (Figure 5.3b).²⁰ Upon cooling, between 191 and 122°C liquid-crystalline-like behaviour was observed in the sense that the birefringence was maintained, and in addition the material was malleable and shearable when pressure was applied to the sample. Prolonged or increased pressure often was found to lead to a certain degree of flow, and small crystallites surrounded by thin layers of isotropic fluid were observed, suggesting that localized melting occurred. Below 122°C, the texture was retained but the material was now completely solid. Differential scanning

Table 5.1 Observed phase transition temperatures and enthalpies of hosts **2-5**.

Host	Transition ^a	<i>T</i> (°C) ^b	ΔH (kJ mol ⁻¹) ^b
2	K → K ¹	137.6 (122.6)	3.0 (-2.9)
	K ¹ → I	206.0 (191.4)	25.3 (-23.6)
3	K → K ¹	36.1 (—) ^c	5.2 (—) ^c
	K ¹ → K ²	79.6 (73.7)	10.4 (-10.0)
	K ² → K ³	89.7 (83.9)	
	K ³ → I	195.4 (185.6)	21.3 (-15.2)
4	K → K ¹	40.3 (32.1)	27.9 (-27.0)
	K ¹ → K ²	58.8 (51.0)	
	K ² → K ³	77.9 (66.8)	
	K ³ → I	242.0 (225.2)	38.2 (-36.4)
5	K → K ¹	85.5 (—) ^c	29.4 (-8.3)
	K ¹ → K ²	104.4 (80.9)	
	K ² → K ³	112.8 (101.1)	
	K ³ → I	212.8 (191.9)	24.3 (-22.3)

^aK, K¹, K², K³: crystalline phases; I: isotropic phase. ^bDetermined by DSC, values obtained from the second heating run; in parenthesis: values obtained from the first cooling run. ^cNo phase transition was observed.

calorimetry (DSC) studies (Figure 5.4a, Table 5.1) showed a phase transition at 122.6°C in the cooling run coinciding with the solidification of the texture observed by TOPM. The (second) heating run revealed the inverse of the cooling behaviour, the material becoming malleable again at 137.6°C up to the isotropization point at 206°C. The enthalpy involved with this last transition was, however, far larger than expected for a mesophase to isotropic liquid transition, suggesting that the material in fact was crystalline, or very highly ordered, throughout the whole temperature range.²¹ This was confirmed by variable temperature X-ray powder diffraction (XRPD) studies, which showed numerous reflections in the middle to high angle regions, indicative of a typical three-dimensional crystalline ordering. The reflection pattern changed with increasing temperature, indicating a crystal-crystal transition, but up to isotropization no pattern ascribable to a mesophase was observed.

*C*₁₈-ester clip **3**

By enlarging the aliphatic tails it was hoped that liquid crystalline behavior would be induced. Upon cooling compound **3**, which has two octadecyl tails, from the melt, two birefringent textures were observed with TOPM which were both very similar to those observed for **2**. Both textures were again malleable over a wide temperature range, *viz.* from 185 to 84°C upon cooling and from 90 to 195°C upon heating. At lower temperatures, the birefringence remained but the material was solid. The large ΔH value of the isotropic melt transition at 195.4°C in the heating run (Figure 5.4b, Table 5.1) suggested that **3**, like **2**, was not mesogenic. The transition from malleable to solid phase in the cooling run at 84°C coincided with an exotherm in the DSC trace, whilst the following heating run showed the inverse of the cooling behaviour.²² XRPD studies confirmed the crystalline nature of the material up to isotropization. A change in the reflection

Table 5.2 *d*-Spacings corresponding to lamellar thicknesses observed for compounds **3-5**.

3		4		5	
<i>T</i> (°C)	<i>d</i> (Å)	<i>T</i> (°C)	<i>d</i> (Å)	<i>T</i> (°C)	<i>d</i> (Å)
20 ^a	39.0	20 ^a	36.9	20 ^a	36.0
20 ^b	28.2	20 ^b	37.7 ± 0.5	20 ^b	38.0
130 ^b	41.3	100 ^b	40.2 ± 0.5	130 ^b	41.0
150 ^b	41.6	150 ^b	40.2		
175 ^b	41.6	180 ^b	40.3		

^aFreshly prepared sample. ^bAfter heating and subsequent cooling of the sample from the isotropic melt.

pattern also confirmed the presence of at least one crystal-crystal transition between 20 and 100°C. More importantly, however, unlike in the case of **2**, for **3** a set of equally spaced reflections (corresponding to first, second, third etc. order reflections) in the low-angle region of all patterns between room temperature and melting was observed, indicating that **3** possessed a layered/lamellar structure.²³ The lamella thickness increased from 28.2 Å at 20°C to 41.3 Å at 130°C, with a further slight increase to 41.6 Å at 175°C (Table 5.2).

*C*₁₈-amide clip **4** and *C*₁₈-ether clip **5**

Unlike in the case of clips **2** and **3**, for clips **4** and **5** only one type of texture was observed with TOPM when the material was cooled from the melt. This texture was similar to the polychromatic one observed for thin samples of **2** and **3**. The DSC traces of both compounds were very similar to the DSC trace of **3**, except that for **4** and **5** the final isotropization temperature was higher than the one observed for **3**. Both textures formed by **4** and **5** displayed a high degree of malleability upon cooling from the melt, whereafter they gradually solidified. The relatively large ΔH values observed for the final isotropization indicated that **4** and **5** were crystalline over the whole temperature range. XRPD measurements of the compounds confirmed their crystalline nature (Table 5.2) and additionally showed a number of low angle reflections corresponding to lamellar order. The layer thicknesses of both **4** and **5** was calculated to be approximately 38 Å at room temperature. This lamellar distance increased only slightly when the samples were heated above 100°C.

5.2.3 Ordering of the clips

The textures observed for clips **2-5** indicate long-range ordering of the molecules in the solid state. To the best of our knowledge, the polychromatic textures can not be assigned to a known structure, the spherulites, however, are indicative of a lamellar organization.²⁴ The more commonly observed platelet/mosaic textures are highly characteristic of a smectic organization in the thin films and the observation of relatively large domains indicates long-range ordering (approaching several millimeters).²⁰

Comparison of the crystal structures of 1a and 1e

A model for the organization of clips **2-5** within the lamellae can be derived on the basis of the crystal structures of clip molecules **1a** and **1e**. In the crystal of **1a**,¹³ the molecules are arranged in infinite arrays in which the cavity of each molecule is filled by the side-wall methoxy groups of two neighbours (Figure 5.5a). The next array of clip molecules is inverted with respect to the

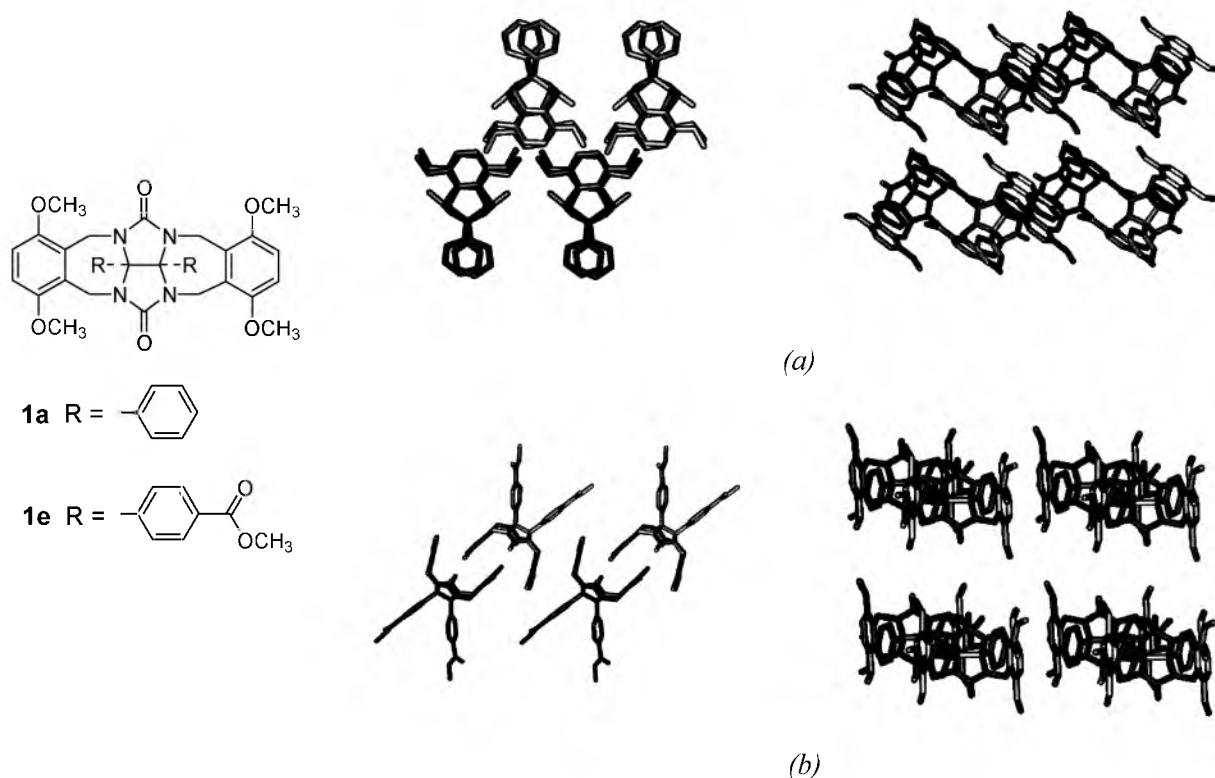


Figure 5.5 (a) Overlapped dimeric arrays of clip molecules in the crystal structure of **1a**. (b) Arrangement of the molecules in the crystal structure of **1e** as discrete, slightly offset dimers.

first row and interacts with this row by π - π interactions. An interwoven network is the result of this molecular ordering. This ordering is substantially different from the ordering of the molecules in the crystal structure of **1e**, which are arranged in slightly offset, but discrete dimers (Figure 5.5b). Calculations have demonstrated that only small energy differences ($\sim 2 \text{ kJ mol}^{-1}$) are involved when the dimeric partners shift up to 1.5 \AA with respect to each other.¹⁴ As a result of the π - π stacking between the aromatic surfaces of adjacent dimers of **1e**, linear arrays of clips are formed which are further arranged in sheet-like structures. Taking the crystal structure of **1e** as a blueprint, it is relatively easy to envisage how the extension of the ester methyl group to a long hydrophobic chain gives rise to a two-dimensional bilayer sheet of clip molecules surrounded by aliphatic tails. This bilayer model is depicted in Figure 5.6 and is supported by the XRPD measurements on compound **3**. The lamella thickness of **3** at 20°C (28.4 \AA , after cooling the sample from the isotropic melt) can be explained by the formation of dimers of **3** which are tilted at an angle of at least 40° , and by assuming that the alkyl chains are fully interdigitized. The proposed 40°C tilt between the dimers is also observed in the crystal structure of **1e** (see Figure 5.5b). The increase in layer spacing, first to 41.3 and then to 42.0 \AA at higher temperatures, is in good agreement with the width of a tilted bilayer of dimers of **3** with almost no alkyl chain interdigitation. The XRPD results on **4** and **5** (Table 5.2) reveal that these compounds have a bilayer thickness at higher temperature which is similar to that of **3**. However, upon cooling this thickness only slightly diminishes suggesting a smaller amount of interdigitation of the hydrocarbon tails in the former compounds when compared to **3**.

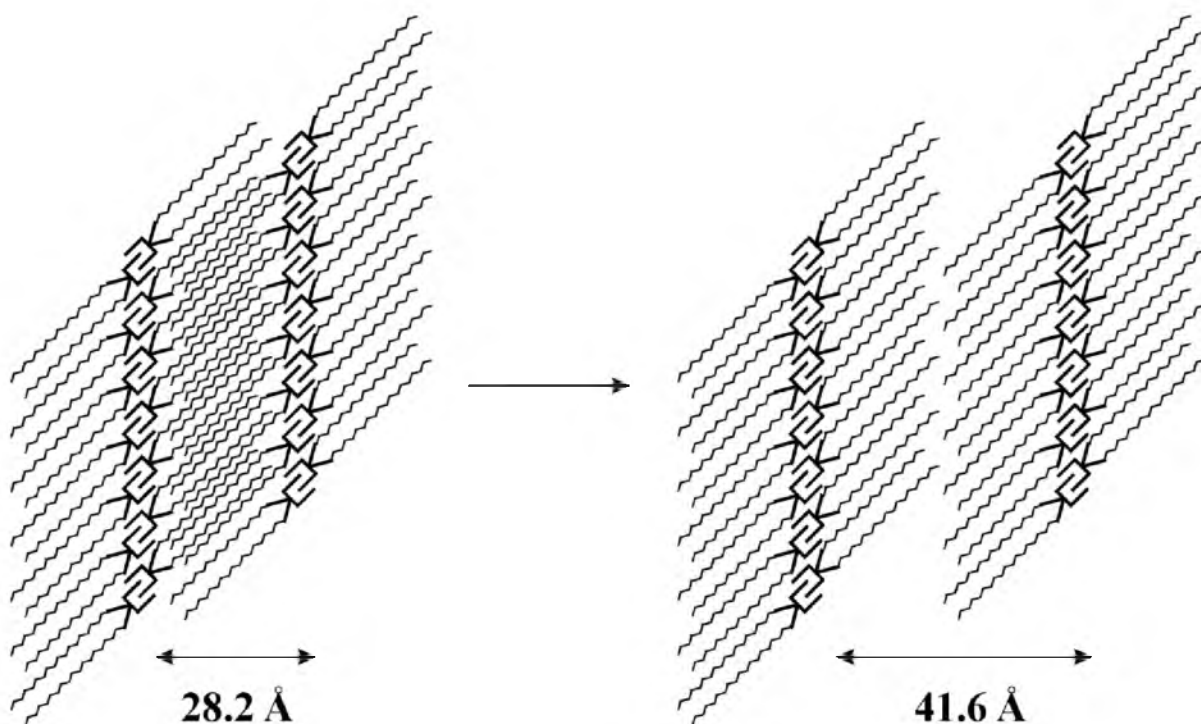


Figure 5.6 Schematic representation of the proposed ordering of bilayers formed by the molecules of **3** at room temperature (left) and in the malleable lamellar phase at higher temperatures (right). The arrows indicate the repeating lamellar distance which was determined by XRPD.

Solid state NMR

To obtain more information about the precise mode of self-assembly of **3** in the solid state, cross polarization magic angle spinning (CPMAS) ^{13}C spectra of this compound were recorded at 20°C and at 150°C (Figure 5.7). All carbon resonances of **3** in these spectra could be assigned using the corresponding ^{13}C and DEPT-135 solution spectra. The carbon nuclei expected to show the greatest difference in their magnetic environment, depending on the mode of dimerization, are the side-wall carbon atoms *e* and the methoxy carbon atoms *c*. Four signals for *e* and four signals for *c* can be expected if **3** exists in discrete, slightly offset dimers, as found in the solid state structure of **1e** (Figure 5.5b). At 150°C , this seems to be the case for **3**. At room temperature, however, for both *e* and *c* fewer signals are observed, indicating a higher degree of symmetry. At this temperature, the clips apparently do not exist as discrete offset dimers, but as molecules in an overlapping structure as observed in the crystal structure of clip **1a** (Figure 5.5a). The resulting interwoven structure then may account for the typically non-malleable crystalline behavior at low temperatures, whereas the presence of discrete dimers at higher temperatures could be the origin of the observed malleability. A further contribution to this malleability may be the decreased interdigitation of the hydrocarbon tails at higher temperatures, as was suggested by the XRPD results. The observed downfield shift of the carbon nuclei in the terminus of the aliphatic chain (*a-b*) upon going from 20 to 150°C , indicating a deshielding of these atoms, is in agreement with this decrease in interdigitation (Figure 5.6). Also in agreement with this is the decrease in the CH_2 main chain peak width at 150°C , indicating a higher degree of conformational mobility of the hydrocarbon chains.

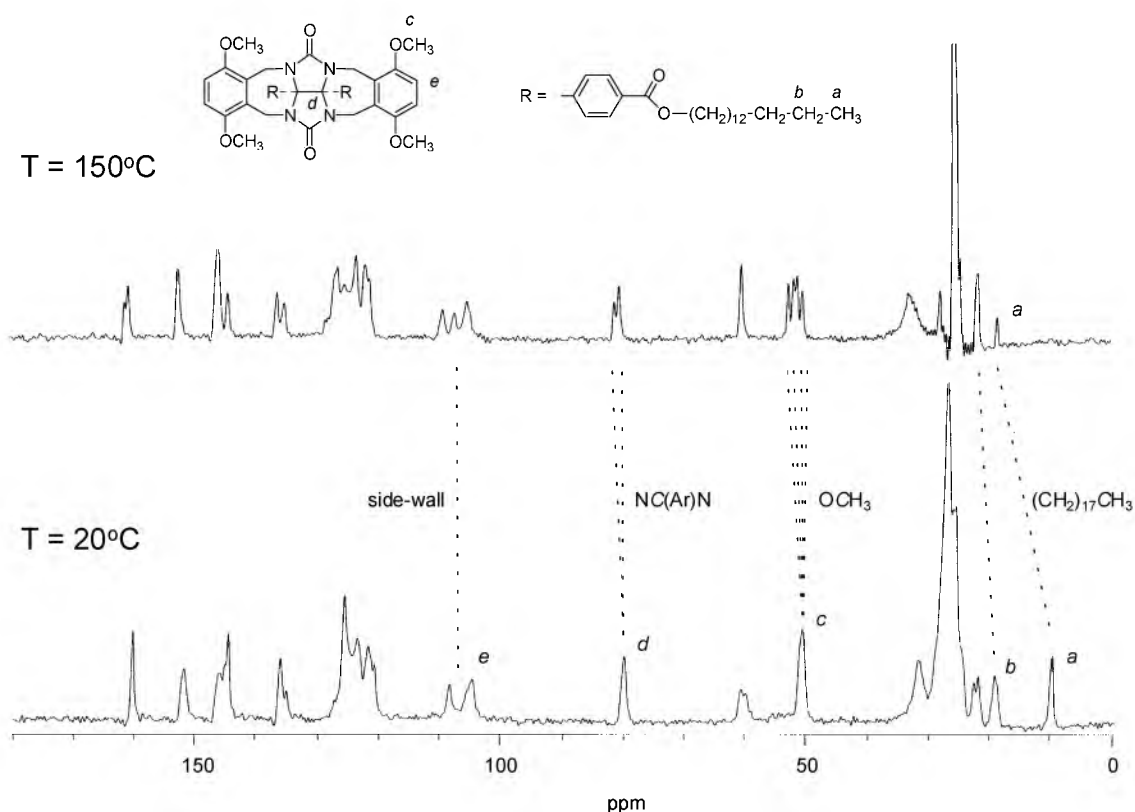


Figure 5.7 ^{13}C CPMAS spectra of **3** at 150 and 20°C.

Table 5.3 Reflectance infrared vibrations (cm^{-1}) of cast thin films of **4** before and after cooling from the isotropic melt.^a

Functional group	Before melting	After melting ^b
N-H	3353 (br)	3450, 3435, 3367, 3326
urea C=O	1737, 1720, 1704 (sh)	1732, 1713 (sh), 1696
Amide I	1665, 1644	1673, 1653
Amide II	1542	1535, 1522 (sh)

^aReflectance angle 30°; br = broad, sh = shoulder. ^bThe cast film was heated to isotropization and then slowly cooled (5°C min^{-1}) to room temperature.

Hydrogen bonding interactions between the lamellae of **4**

In order to investigate what the role of amide hydrogen bonding is in the organization of the molecules of **4** in the lamellar solid, cast films of this compound were studied with reflectance infrared spectroscopy (Table 5.3). The region of the N-H stretching vibration and the

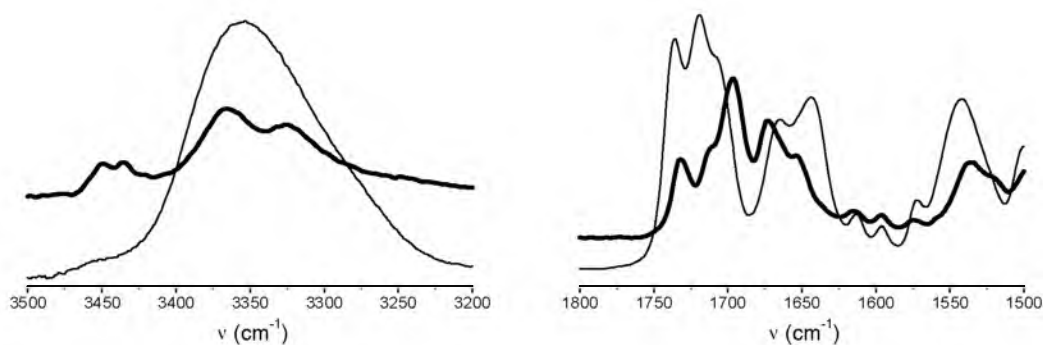


Figure 5.8 Selected regions of the specular reflectance infrared spectra (normalized) of the C_{18} -amide clip **4**. Solid traces: freshly cast film. Bold traces: after slow cooling of the film from the isotropic melt.

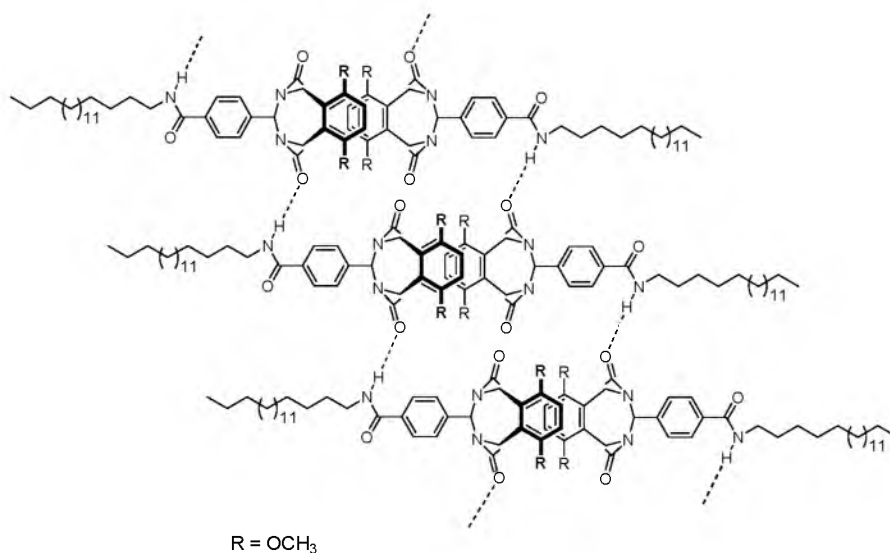


Figure 5.9 Schematic representation of the proposed interlamellar ordering of the molecules of **4** after cooling of the material from the isotropic melt (for clarity reasons only one side of the clip molecules is shown).

carbonyl/amide regions of the spectra are shown in Figure 5.8. In the spectrum of the freshly cast film, one broad N-H stretching vibration is visible at 3353 cm^{-1} , which is an indication that the amide groups are involved in hydrogen bonding.²⁵ The positions of the amide I (C=O stretching) and amide II (N-H bending) vibrations are also indicative of hydrogen bonding. After heating and subsequent cooling the sample from the isotropic melt, the broad N-H stretching vibration splits up into four vibrations, two of which (at 3450 and 3435 cm^{-1}) are due to amide groups that are no longer involved in hydrogen bonding. The shifts of the amide I bands to higher wavenumbers, and the shift of the amide II band to a lower wavenumber, are an indication that the amide groups are less involved in hydrogen bonding, whereas the shifts of the urea carbonyl stretching vibrations to lower wavenumbers suggest that these groups are now more involved in hydrogen bonding. These results can be interpreted as follows. In the freshly cast film, all the N-H functions of **4** are involved in *intermolecular* hydrogen bonding,²⁶ probably only involving amide groups. Upon melting and subsequent cooling, a number of these amide groups start to

form hydrogen bonds with the urea carbonyl groups of neighbouring clip molecules, leaving other amide groups not involved in hydrogen bonding. In the bilayer model proposed for **3**, which according to the XRPD measurements is also applicable to **4**, these intermolecular hydrogen bonds crosslink the two-dimensional lamellae formed by the dimers of **4** (Figure 5.9).

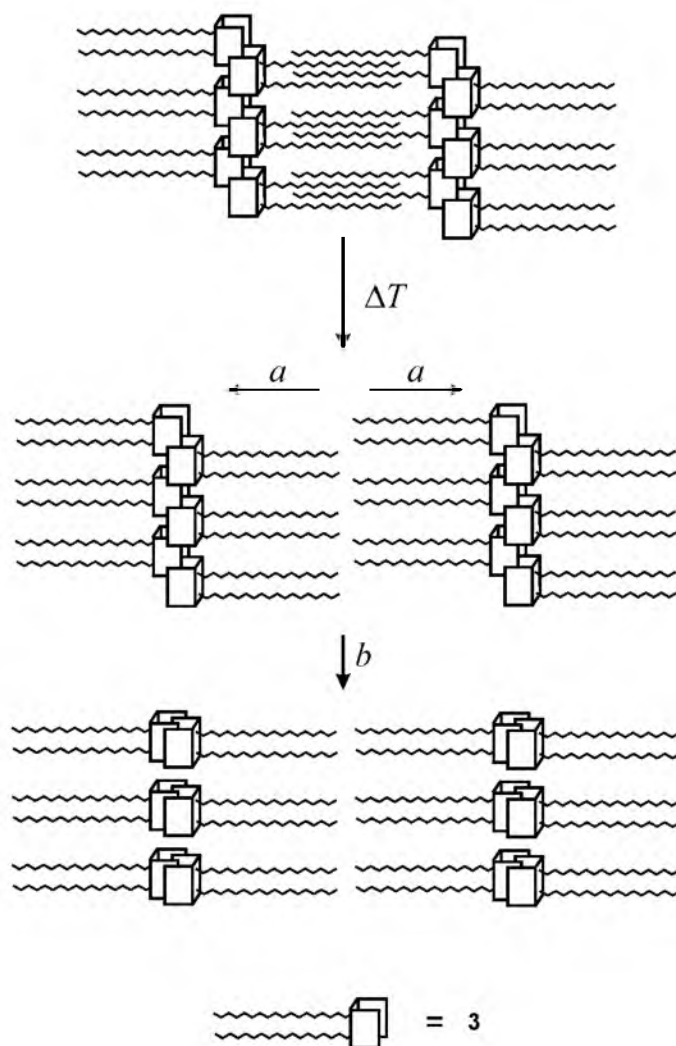


Figure 5.10 Schematic overview of the most important processes that take place when compound **3** is heated from 20°C to 150°C. (a) Separation of the alkyl tails, resulting in an increase in the lamellar distance. (b) Reorganization of the clip head groups from an overlapped polymeric into a discrete dimeric structure.

Origin of the liquid-crystalline-like behavior

The lamellar nature of the materials formed by clips **3-5** may explain the liquid-crystalline-like behaviour observed by TOPM at high temperatures. In the case of **3** this behaviour is attributed to the following factors (Figure 5.10): (i) above the crystal-crystal transition at 90°C the fully interdigitated octadecyl tails become separated resulting in an increased lamellar spacing, (ii) above this transition the octadecyl chains obtain an increased mobility, and (iii) the clip headgroups rearrange from an interwoven array to a structure containing discrete dimers. All these factors will contribute to a weakening of the internal cohesion of the bilayers and as a result lead to an increased malleability of the material.²⁷ The partially separated layers can more readily slide over and along one another in a manner analogous to other layered materials, such

as graphite and talcum powder (Figure 5.11). The ability of the layers to slide over one another seems to contribute most to the malleable nature of the materials. In the lamellar phase, only the π - π interactions between the discrete dimers result and the strength of these interactions, which arrange the dimers in extended two-dimensional sheets, is believed to be the reason for the material to be *non*-mesogenic up to isotropization. At this transition, the interactions between the dimers are most probably broken, but it is yet unknown whether also the dimeric partners themselves are separated.

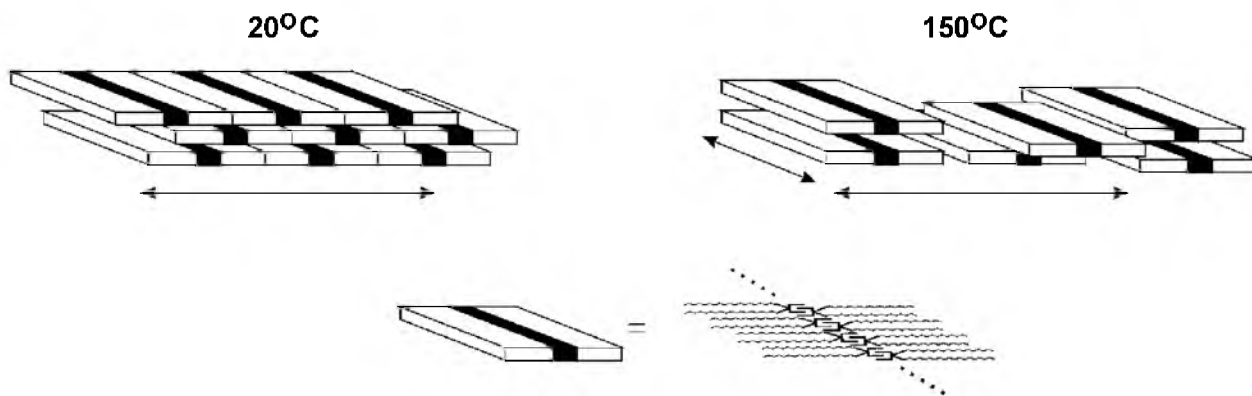


Figure 5.11 Proposed ordering of the lamellae of clips 2-5 at 20°C and at 150°C. At high temperature the bilayer-like layers of clips can more readily slide over one another (the arrows indicate the possible directions of movement).

In the case of the C₁₈-ester clip **3** the lamellar behaviour is evident from the XRPD measurements, while for the C₁₂-ester clip **2** similar behavior is observed although with XRPD no evidence for a layered structure was found. It is well-known that in the case of smectic mesogens an equilibrated balance between the rigid core and the flexible parts of the molecule is needed to obtain liquid crystalline properties. This balance probably also plays a role in the case of **2** and **3**. The tails of **2** apparently are too short to organize the molecules in the material in a well-ordered lamellar structure. The observed higher isotropization temperatures of the C₁₈-amide clip **4** and the C₁₈-ether clip **5** when compared to the C₁₈-ester clip **3** are remarkable. In the case of **4**, it is clear that the presence of hydrogen bonding interactions in the material will result in a higher melting point and in a higher transition enthalpy. The higher melting point of **5** compared to **3** is more difficult to explain, and it is very remarkable that the hydrocarbon tails of both **4** and **5**, in contrast to the tails of **3**, hardly interdigitate at low temperatures, as was evident from the XRPD measurements. It is unlikely that the linkers between the clip and the tails themselves play a significant role in the organization of the molecules. The differences in thermal behavior are therefore attributed to differences in the intermolecular packing of the alkyl chains in the lamellae formed by **4** and **5**. This might be caused by the fact that the tails on the back of **4** and **5** make a different angle with the phenyl groups than the tails on the back of clips **2** and **3**. This may result in a less close packing of these tails in the case of the latter clips, allowing a higher degree of interdigitation. The relatively high enthalpies accompanying the transitions of **4** and **5** into the liquid-crystalline-like phase, when compared to **3**, suggest that the lamellae of the former compounds are less easy to separate than the layers of the latter compound. Further studies are needed to determine the exact ordering of the different phases formed by **2-5**.

5.3 Tuning the lamellar structures by the complexation of guests

5.3.1 Host-guest complex of **3** and methyl 3,5-dihydroxybenzoate

Since the above mentioned bilayer-like ordering of clips **2-5** is supposed to be responsible for the lamellar crystalline nature of the material, it was of interest to investigate the consequences of disrupting the dimeric structure of the clips by adding dihydroxybenzene guest molecules. An equimolar mixture of the C₁₂-ester clip **2** and methyl 3,5-dihydroxybenzoate (**MDB**) was prepared by solvent evaporation of a solution of the two compounds in a mixture of chloroform and methanol (4:1, v/v).²⁸ It was expected that dimerization of the clips would now be prevented and that a 1:1 host-guest complex would be quantitatively formed.²⁹

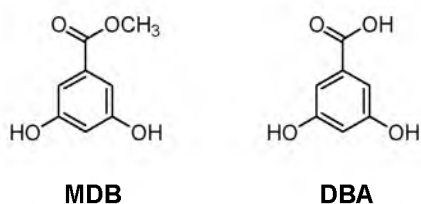


Table 5.4 Observed phase transition temperatures and enthalpies of the 1:1 host-guest complexes of **2** and **3** with **MDB** and **DBA**.

Complex	Transition ^a	<i>T</i> (°C) ^b	ΔH (kJ mol ⁻¹) ^b
2 : MDB	K → I	130.2 (67.6)	32.1 (-8.5)
3 : MDB	K → I	107.3 (53.2)	19.4 (-16.7)
3 : DBA	K → I	170.1 (137.2)	32.4 (-28.8)

^aK: crystalline phase; I: isotropic phase. ^bDetermined by DSC, values obtained from the second heating run; in parenthesis: values obtained from the first cooling run.

The freshly prepared samples initially displayed phase separation, as observed by TOPM and DSC, indicating that complex formation was incomplete. To ensure complete host-guest complexation, the mixture was heated to isotropization and then slowly cooled down, whereupon at 68°C a birefringent, but non-malleable microcrystalline texture began to appear typical of a crystalline organic material. DSC analysis showed that upon cooling a single exotherm at 67.6°C was present, whereas an exotherm due to cold crystallization of the material that had not been crystallized during the cooling run was apparent in the consecutive heating run, followed by isotropization at 130°C (see Table 5.4 and the top trace in Figure 5.12). The absence of phase separation in the mixture was concluded from both TOPM and DSC measurements, suggesting that a complete 1:1 host-guest complexation had taken place. This complexation should prevent dimerization of the clips and the formation of extended 2D sheets. As a result, the energy required for melting is reduced, leading to a dramatic reduction of the melting point. To confirm the formation of a 1:1 host-guest complex, samples containing varying ratios of **2** to **MDB** were

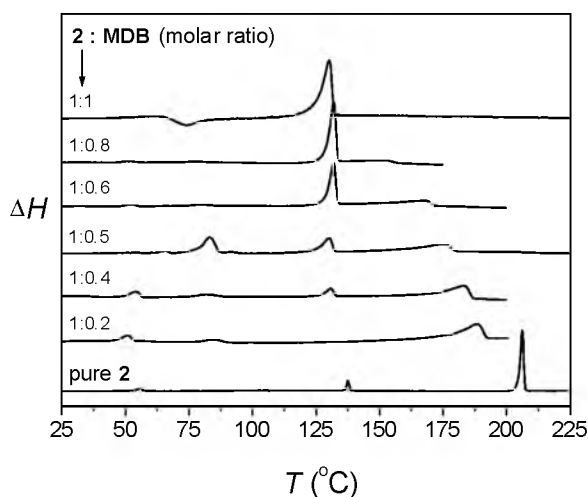


Figure 5.12 DSC thermograms of the second heating runs of the complexes of **2** with various ratios of **MDB**.

Table 5.5 Reflectance infrared vibrations (cm^{-1}) of cast thin films of 1:1 host-guest complexes of **3** with **MDB** and **DBA** before and after cooling from the isotropic melt.^a

Guest	Vibration	ν Free component	ν Host-guest complex	
			before melting	after melting ^b
MDB	ArO-H guest	3379, 3249 ^c	3381	3332
	ester C=O host	1737	1737	1737
	urea C=O host	1722	1722	1719
DBA	ArO-H, acid O-H guest	3600-3000 ^d	3273	3306
	C=O guest	1688	1688	1688
	ester C=O host	1737	1737	1737
	urea C=O host	1722	1721	1718

^aReflectance angle 30° . ^bThe cast film was heated to isotropization and then slowly cooled (5°C min^{-1}) to room temperature. ^cDue to hydrogen bonding with another **MDB** molecule. ^dVery broad peak of overlapping vibrations.

prepared. The DSC traces of the (second) heating runs of these mixtures are also shown in Figure 5.12. As is apparent, the incorporation of progressively lower quantities of **MDB** into the mixtures results in a gradual diminution of the melting endotherm of the 1:1 complex at 130°C . Simultaneously, a second endotherm at progressively higher temperatures and increasing enthalpies, attributable to uncomplexed **2**, becomes apparent. At a ratio of **2**:**MDB** = 1:0.5, stable crystals in an isotropic fluid became visible at 150°C , indicative of phase separation between uncomplexed **2** and the host-guest complex. The endotherms below 100°C in Figure 5.12 are presumed to be crystal-crystal transitions unconnected with the phase separation between the host-guest complex and the clip.

The thermal behaviour of complexes of the C_{18} -ester clip **3** and **MDB** was very similar to that of complexes of **2** and **MDB** (Table 5.4). The freshly prepared samples of the 1:1 **3**:**MDB** mixture again showed a high degree of phase separation in the first heating run. Cooling of the material from the isotropic melt gave a non-malleable birefringent microcrystalline texture at 53°C , while the material melted at 107.3°C in the consecutive heating run. The DSC traces of compound **3**

containing various quantities of **MDB** were similar to the traces observed for the mixtures of **2** and **MDB**, however, the transitions were somewhat broader. It is remarkable that the enthalpy involved with the isotropization of the 1:1 **3:MDB** complex is substantially lower than the corresponding enthalpy for the 1:1 **2:MDB** complex. This suggests a less good packing in the case of the former complex, which apparently is caused by the difference in length of the alkyl tails. The effect of **MDB** on the self-assembly of **3** was further investigated with reflectance infrared spectroscopy (Table 5.5). The infrared spectrum of a thin film of uncomplexed **3** showed two absorptions due to the ester and urea carbonyl groups. In the sample of a thin film of the freshly prepared host-guest complex, neither of these vibrations were initially shifted. After heating of the film to the isotropic melt, followed by slow cooling to 20°C, the ester carbonyl stretching vibration of **3** remained unaffected whereas the stretching vibration of the urea carbonyl function had shifted to a lower wavenumber. This is an indication that the latter group had become involved in a hydrogen bonding interaction. In addition, the absorption due to the OH stretching vibration of **MDB** narrowed considerably, and shifted from 3381 to 3332 cm⁻¹, which is also an indication of a defined hydrogen bonding interaction. The nature of the 1:1 complex was further investigated with XRPD (Table 5.6). The diffractogram at 20°C obtained for the mixture directly after solvent evaporation displayed numerous reflections many of which were similar in position to those observed for uncomplexed **3**. This confirms the phase separation observed by TOPM for freshly prepared samples of the complex in the first heating run. In addition, *d*-spacings corresponding to a lamellar thickness of 37.9 Å were visible in the low-angle region. After recrystallization of the mixture from the melt, a unique diffraction pattern was observed which showed no peaks in the low-angle region anymore, indicating the disappearance of the lamellar structure of **3** (Figure 5.13).

Table 5.6 *d*-Spacings corresponding to lamellar thicknesses observed for 1:1 host-guest complexes of **3** with **MDB** and **DBA**.

3 : MDB		3 : DBA	
<i>T</i> (°C)	<i>d</i> (Å)	<i>T</i> (°C)	<i>d</i> (Å)
20 ^a	37.9	20 ^a	37.9
20 ^b	— ^c	20 ^b	57.8

^aFreshly prepared sample. ^bAfter heating and subsequent cooling of the sample from the isotropic melt. ^cNo *d*-spacing was observed.

5.3.2 Host-guest complex of **3** and 3,5-dihydroxybenzoic acid

If **MDB** complexation prevents **3** to form dimers and to adopt a lamellar organization, complexation of a guest which again allows dimerization of the resulting host-guest complex should restore the lamellar behaviour. In order to investigate this, the 1:1 complex of **3** and 3,5-dihydroxybenzoic acid (**DBA**) was prepared. This guest can complex with its phenolic hydroxy groups to the carbonyl groups of **3**, and additionally form a dimer with another **3:DBA** host-guest complex *via* its carboxylic acid group. Upon cooling from the melt, the complex of **3** and **DBA** displayed a clearly spherulitic birefringent texture at 137°C. As for uncomplexed **3**, the film of the complex was malleable. This property disappeared below 100°C but the texture remained. Unlike in the case of uncomplexed **3**, no clear transition from solid crystal to malleable crystal was visible by DSC (Table 5.4). XRPD measurements on the freshly prepared sample again showed many reflections which coincided with those observed for uncomplexed **3**

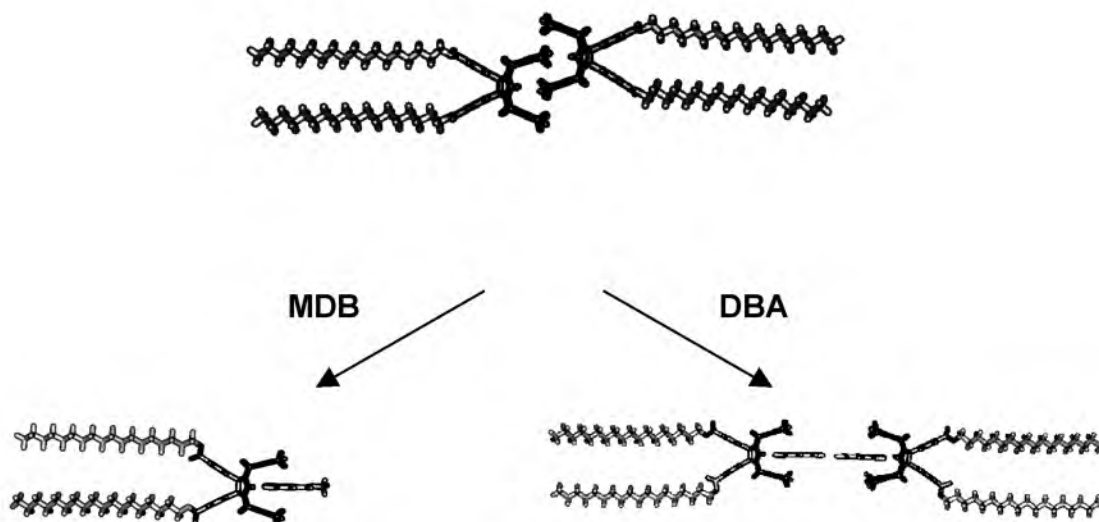


Figure 5.13 Computer modeled structures of a dimer of **3** and the 1:1 host-guest complexes of **3** with **MDB** and **DBA**.

(Table 5.6). After recrystallization from the melt a unique pattern was observed, which showed reflections in the small angle region arising from first, second and third order reflections corresponding to a lamellar thickness of 57.8 Å. This value is in agreement with a model in which the complexes are self-assembled in an 'extended dimeric' structure, as is depicted in Figure 5.13. The increase in isotropization point of the complex, when compared to the 1:1 complex of **3** and **MDB**, and the increase in enthalpy involved with this transition, confirm the formation of the lamellar structure. Further evidence for this structure came from the infrared spectrum of the thin film of the complex (Table 5.5). As for the complex of **3** with **MDB**, the complex of **3** with **DBA** showed a urea carbonyl stretching vibration indicative of a hydrogen bonding interaction between **3** and the guest. The absorption due to the OH stretching vibration of the hydroxyl groups of the **DBA** guest narrowed considerably upon complexation, again indicating a well-defined hydrogen bonding interaction with **3**. Most importantly, however, the carbonyl stretching vibration at 1688 cm^{-1} which can be attributed to the dimeric benzoic acid structure was preserved in the lamellar crystalline complex, implying that this function is not involved in any other hydrogen bonding interaction.

5.4 An approach to self-assembled dendritic host-guest architectures

In the previous section it was shown that by two orthogonal supramolecular interactions, *i.e.* host-guest binding and guest-guest dimerization, a well-defined self-assembled structure can be generated. This stimulated us to investigate if this concept would work for the self-assembly of even larger complexes. A new host, **6**, was designed which has on its convex side two dihydroxybenzene moieties (Figure 5.14a). As a result, this molecule can form host-guest complexes with other molecules leading to - at least in principle - large, dendritic architectures (Figure 5.14b). It was, however, our intention to investigate whether these molecules would generate self-assembled lamellar structures generated when applying the melt-processing technique described in the previous section.

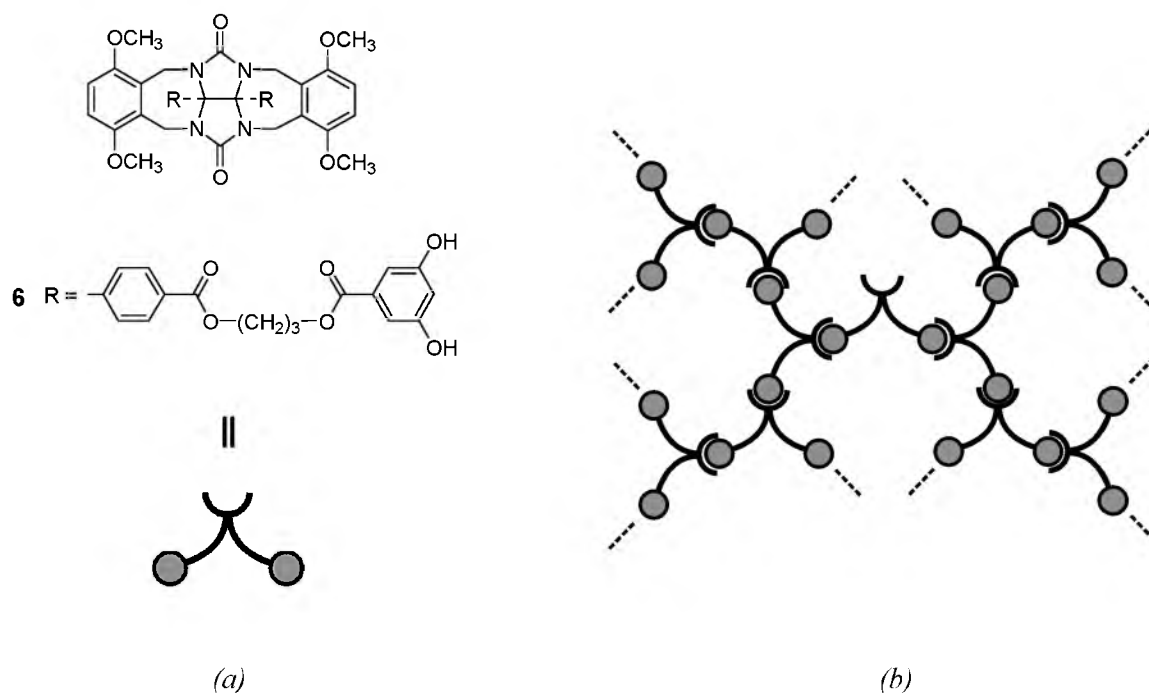
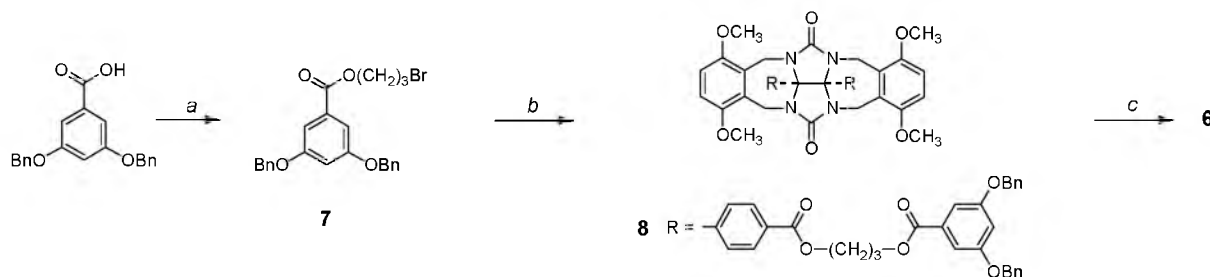


Figure 5.14 (a) Schematic representation of **6**. (b) Schematic picture of a possible mode of self-complexation of **6** and the resulting dendritic architecture which is generated.



Scheme 5.1 Reagents and conditions: (a) 1,3-Dibromopropane, K_2CO_3 , DMF, 16 h, $20^\circ C$. (b) **1c**, DMF, K_2CO_3 , KI, 64 h, $20^\circ C$. (c) 33% HBr/AcOH, 16 h, $20^\circ C$.

5.4.1 Synthesis

The synthesis of **6** started with the alkylation of 3,5-di(benzyloxy)benzoic acid using an excess of 1,3-dibromopropane in dimethylformamide and potassium carbonate as a base (Scheme 5.1). Compound **7** was obtained in a yield of 81% after recrystallization from diisopropyl ether. It was subsequently reacted with clip **1c** in dimethylformamide using potassium carbonate as a base to give **8** in 87% yield, after recrystallization from a mixture of dichloromethane and methanol. Compound **8** was deprotected by stirring it in 33% bromic acid in acetic acid to give, after purification by column chromatography, compound **6** in 32% yield.³⁰

5.4.2 Thermal behaviour

To investigate whether **6** could be incorporated in a lamellar structure, both its dihydroxybenzene groups were endcapped with molecules of **3**. An amount of **6** was mixed with two equivalents of C_{18} -ester clip **3** following the procedure described for the generation of the complex between **3** and **MDB**. A sample of the resulting mixture was heated to the melt. At

181°C, TOPM revealed an isotropic liquid in which some small crystals remained, indicating phase separation. Upon cooling, a birefringent spherulitic malleable texture evolved at 152°C which was very similar to textures observed for uncomplexed **3**. After several repeated heating and cooling runs no phase separation was observed anymore upon melting, and further heating and cooling runs were identical. DSC analysis confirmed the TOPM observations and revealed that *four* consecutive heating and cooling runs were required until reversible thermal behavior was observed (Table 5.7).

Table 5.7 Observed phase transition temperatures and enthalpies of the 2:1 complex of hosts **2** and **6**.

Transition ^a	<i>T</i> (°C) ^b	ΔH (J g ⁻¹) ^{b, c}
K → K ¹	84.2 (71.6)	} 5.5 (-11.8)
K ¹ → K ²	95.8 (80.3)	
K ² → I	180.1 (146.1)	15.8 (-8.0)

^aK, K¹, K²: crystalline phases; I: isotropic phase. ^bDetermined by DSC, values obtained from the fifth heating and cooling runs (in parenthesis). ^c ΔH values are given in J g⁻¹ because the exact structure of the complex is unknown (see text).

5.4.3 Ordering of the complex

The observed texture, in combination with the malleability of the sample and the ΔH values measured with DSC, suggest that the 2:1 complex of **3** and **6** has a lamellar crystalline structure similar to that observed for uncomplexed **3**. However, we have as yet no firm evidence, *e.g.* X-ray data, confirming such a lamellar structure. The observation that it requires several heating and cooling runs before the thermal behaviour is reversible is an indication that the different components have difficulties to reorganize themselves into an ordered matrix.³¹ The assembly which is eventually formed, is stable and homogeneous. Interestingly, the observed isotropization and crystallization temperatures are similar to those found for the lamellar 1:1 complex between **3** and **DBA**. If it is assumed that all dihydroxybenzene functions are involved in host-guest binding, and that the clips possessing the tails are located at the periphery of the lamella, still several different structures are possible. Examples of such structures are shown in Figure 5.15. XRPD and FTIR measurements will be required to unravel the exact identity of the assembly.

5.5 Concluding remarks

The attachment of long alkyl tails to the convex side of molecular clips leads to interesting self-assembled architectures. The clip molecules adopt a bilayer structure through a mutual cavity filling process (dimerization) which in combination with intermolecular π - π stacking interactions generates malleable crystalline films. Between room temperature and the melting temperature to the isotropic liquid the clips undergo a number of crystal-crystal phase transitions. The last of these transitions results in a lamellar crystal with expanded interlayer distances, in which the self-assembled clip molecules have adopted a rearranged structure. In combination with an increased mobility of the alkyl tails, this leads to a liquid-crystalline-like behaviour. The length of the alkyl tail and the nature of the linker between the clip and the tail

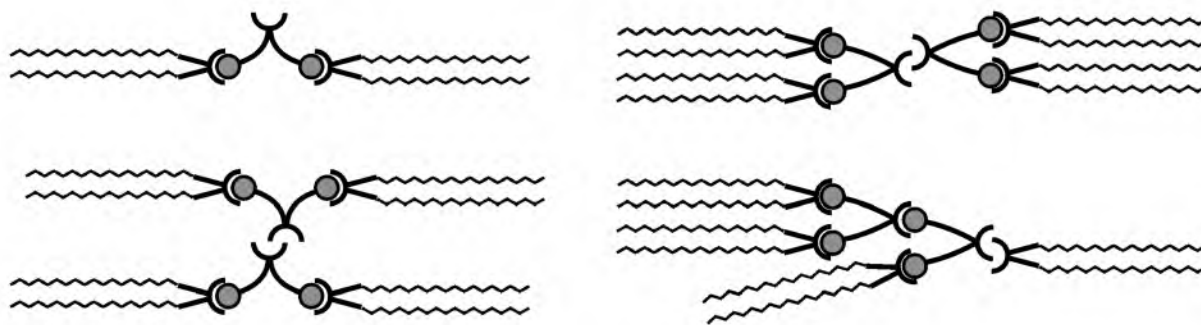


Figure 5.15 Schematic overview of the lamellar structures that can be formed when hosts **3** and **6** are mixed in a 2:1 molar ratio.

were found to influence the temperature range and melting point of the lamellar crystalline phase. Host-guest complexes of the clips can be generated by melt-processing stoichiometric quantities of the clips and aromatic guest molecules, like **MDB** and **DBA**. Upon complexation, the **MDB** guest inhibits the self-assembly process of the clip molecules. As a result, the bilayer structure is disrupted and a host-guest complex is formed with no higher structural order. In the case of **DBA**, the guest also inhibits the above-mentioned self-assembly of the host, but another self-assembly process is possible, *viz.* via the formation of acid dimers. The consequence of the latter is that the bilayer structure is restored and that the material becomes liquid-crystalline-like again.

The self-organization of host-guest complexes by means of the melt-processing technique can also be applied to larger building blocks. A clip functionalized at its convex side with two dihydroxybenzene groups was co-melted with two equivalents of a clip with long hydrocarbon chains. After several repeated meltings, a well-defined material was obtained which displayed similar lamellar crystalline behaviour as **3** and the 1:1 host-guest complex of **3** and **DBA**.

The ability of compounds **2-5** to form highly ordered lamellar structures from the melt and the possibility to fine-tune these structures by adding guest molecules opens the way to design new, functional materials that are easily melt-processed. Further research will be focussed on the incorporation of functional guests. An approach to include porphyrin guests into the lamellar solids is described in Chapter 8.

5.6 Experimental section

5.6.1 Materials and methods

DMF was dried over BaO for one week and then vacuum distilled; the first 30% of the distillate was discarded. Dichloromethane was distilled over CaH₂. Triethylamine was dried on KOH. K₂CO₃ and KI were dried in an oven (150°C). Methyl 3,5-dihydroxybenzoate and 3,5-dihydroxybenzoic acid were recrystallized from chloroform. All other chemicals were used without further purification. Thermal behavior was observed under crossed polarizers with a Jeneval polarizing optical microscope connected to a Linkam THMS hot stage. Differential scanning calorimetry thermograms were recorded on a Perkin Elmer DSC 7 instrument. ESI-MS spectra were recorded on a Perkin Elmer-Sciex API 300 MS/MS mass spectrometer. For a description of the other general techniques see Section 2.6.1.

5.6.2 Thermal polarized optical microscopy and differential scanning calorimetry experiments

Approximately 5-10 mg of a clip was used in the DSC experiments. In the case of host-guest complexes, an amount of 5-10 mg of clip and an equimolar quantity of guest were dissolved in a mixture of CHCl₃ and MeOH (4:1, v/v). The solvent was evaporated overnight under a stream of nitrogen while maintaining the mixture in a water bath at

40°C. Samples were studied under a polarizing optical microscope with crossed polarizers. DSC samples were prepared in stainless-steel large volume pans (75 μ L). Thermograms were recorded at 10°C/min and repeated heating and cooling runs were measured to study the stability of the material and the reproducibility of the transitions. In general, transition temperatures and enthalpies were determined from the first cooling and second heating scans.

5.6.3 X-ray powder diffraction experiments

X-ray powder diffraction experiments were carried out on powder samples in a pinhole camera (Anton-Paar) operating with a Ni-filtered $\text{Cu}_{K\alpha}$ beam. The samples were held in Lindemann glass capillaries (1 mm diameter), and the X-ray patterns were collected on flat photographic film.

5.6.4 Reflectance infrared experiments

Infrared samples of the clips and their host-guest complexes were prepared by evaporation of a drop of a CHCl_3 solution (2 mM) of the compound or complex on a gold sputtered cover glass. The resulting thin film was dried in a desiccator. Reflectance infrared spectra of the samples were recorded on a BioRad FTS-25 spectrometer with a resolution of 2.0 cm^{-1} . Spectra of the sample were taken before and after heating and subsequent cooling of the sample from the isotropic melt, which was carried out on the polarization microscope as described in Section 5.6.2. The angle between the sample and the infrared beam was varied between 15 and 65°. For each spectrum 64 scans were recorded, and the optical bench of the IR apparatus was continuously purged with nitrogen. Data analysis was performed using the WIN-IR software.

5.6.5 Syntheses

The syntheses of clip molecules **1b** and **1d** have been described in Chapter 2. 3,5-Di(benzyloxy)benzoic acid was synthesized as described in the literature.¹⁷

4-[13b-(4-Chlorocarbonylphenyl)-1,4,8,11-tetramethoxy-6,13-dioxo-5,7,12,13b,13c,14-hexahydro-5a,6a,12a,-13a-tetraazabenz[5,6]azuleno[2,1,8-*ija*]benzo[*f*]azulen-13-yl]-1-benzenecarbonyl chloride (**1c**):

Compound **1b** (1.0 g, 1.4 mmol) was suspended in SOCl_2 (30 mL). The mixture was refluxed under nitrogen for 16 h, and after cooling it was added dropwise to stirred diethyl ether (250 mL). After filtration, 860 mg (82%) of **1c** was obtained as a white, very hygroscopic solid which was immediately used in further synthesis.

^1H NMR (CDCl_3 , 300.13 MHz) δ 7.84 (d, 4H, *ArH ortho* to $\text{C}(\text{O})\text{Cl}$, $^3\text{J} = 8.5$ Hz), 7.25 (d, 4H, *ArH meta* to $\text{C}(\text{O})\text{Cl}$, $^3\text{J} = 8.5$ Hz), 6.48 (s, 4H, *ArH side-wall*), 5.48 (d, 4H, $\text{NCH}_2\text{Ar out}$, $^2\text{J} = 15.7$ Hz), 3.82 (d, 4H, $\text{NCH}_2\text{Ar in}$, $^2\text{J} = 15.7$ Hz), 3.72 (s, 12H, OCH_3) ppm; $^{13}\text{C}\{^1\text{H}\}$ NMR (CDCl_3 , 75.47 MHz) δ 167.49 (acyl $\text{C}=\text{O}$), 157.47 (urea $\text{C}=\text{O}$), 150.95 (*ArC ipso* to OCH_3), 143.10 (*ArC ipso* to $\text{C}(\text{O})\text{Cl}$), 133.53 (*ArC para* to $\text{C}(\text{O})\text{Cl}$), 132.10 (*ArC ortho* to $\text{C}(\text{O})\text{Cl}$), 128.65 (*ArC meta* to $\text{C}(\text{O})\text{Cl}$), 126.37 (*ArC ipso* to CH_2N), 111.91, 84.59 ($\text{NC}(\text{Ar})\text{N}$), 56.63 (OCH_3), 37.12 (NCH_2Ar) ppm.

Dodecyl 4-(13b-4-[(dodecyloxy)carbonyl]phenyl-1,4,8,11-tetramethoxy-6,13-dioxo-5,7,12,13b,13c,14-hexahydro-5a,6a,12a,13a-tetraazabenz[5,6]azuleno[2,1,8-*ija*]benzo[*f*]azulen-13-yl)benzoate (**2**):

Compound **1b** (200 mg, 0.283 mmol), 1-bromododecane (285 mg, 1.71 mmol), K_2CO_3 (400 mg, 4.27 mmol) and KI (5 mg) were added to degassed DMF (10 mL) and stirred under nitrogen at 100°C for 64 h. After cooling, the mixture was evaporated to dryness and the residue was suspended in CH_2Cl_2 (100 mL). This solution was extracted with aqueous 1 N HCl (2 \times 100 mL), with water (200 mL) and evaporated to dryness. The residue was recrystallized from a mixture of CH_2Cl_2 and ethanol (1:9, v/v) to yield 215 mg (73%) of **2** as a white powder.

M.p. 206°C; IR (KBr pellet) ν 2980-2840 (CH_2), 1737 (ester $\text{C}=\text{O}$), 1722 (urea $\text{C}=\text{O}$), 1576, 1559, 1540, 1486, 1459, 1438, 1425 ($\text{C}=\text{C}$), 1307, 1264, 1218 (CH_2), 1108, 1080 (COC) cm^{-1} ; ^1H NMR (CDCl_3 , 300.13 MHz) δ 7.77 (d, 4H, *ArH ortho* to $\text{C}(\text{O})\text{OC}_{12}\text{H}_{25}$, $^3\text{J} = 8.4$ Hz), 7.17 (d, 4H, *ArH meta* to $\text{C}(\text{O})\text{OC}_{12}\text{H}_{25}$, $^3\text{J} = 8.4$ Hz), 6.45 (s, 4H, *ArH side-wall*), 5.56 (d, 4H, $\text{NCH}_2\text{Ar out}$, $^2\text{J} = 15.9$ Hz), 4.24 (t, 4H, $\text{C}(\text{O})\text{OCH}_2$, $^3\text{J} = 6.7$ Hz), 3.73 (d, 4H, $\text{NCH}_2\text{Ar in}$, $^2\text{J} = 15.9$ Hz), 3.71 (s, 12H, OCH_3), 1.79-1.67 (m, 4H, $\text{C}(\text{O})\text{OCH}_2\text{CH}_2$), 1.44-1.17 (m, 36H, $(\text{CH}_2)_9\text{CH}_3$), 0.88 (t, 6H, CH_2CH_3 , $^3\text{J} = 6.4$ Hz) ppm; $^{13}\text{C}\{^1\text{H}\}$ NMR (CDCl_3 , 75.47 MHz) δ 165.85 (ester $\text{C}=\text{O}$), 157.56 (urea $\text{C}=\text{O}$), 150.91 (*ArC ipso* to OCH_3), 139.09 (*ArC ipso* to $\text{C}(\text{O})\text{OC}_{12}\text{H}_{25}$), 130.77 (*ArC para* to $\text{C}(\text{O})\text{OC}_{12}\text{H}_{25}$), 129.81 (*ArC ortho* to $\text{C}(\text{O})\text{OC}_{12}\text{H}_{25}$), 128.16 (*ArC meta* to $\text{C}(\text{O})\text{OC}_{12}\text{H}_{25}$), 126.91 (*ArC ipso* to CH_2N), 111.83 (*ArC para* to CH_2N), 84.90 ($\text{NC}(\text{Ar})\text{N}$), 65.40 ($\text{C}(\text{O})\text{OCH}_2$), 56.64 (OCH_3), 36.92 (NCH_2Ar), 31.89 ($\text{CH}_2\text{CH}_2\text{CH}_3$), 29.51, 29.32,

28.57, 25.95 ((CH₂)₈CH₂CH₂CH₃), 22.67 (CH₂CH₃), 14.10 (CH₂CH₃) ppm; ESI-MS *m/z* 1043.9 (M)⁺, 1065.6 (M + Na)⁺, 2109.4 (M + M + Na)⁺. Anal. Calcd for C₆₂H₈₂N₄O₁₀: C, 71.37; H, 7.92; N, 5.37. Found: C, 71.34; H, 7.97; N, 5.35.

Octadecyl 4-(1,4,8,11-tetramethoxy-13b-4-[(octadecyloxy)carbonyl]phenyl-6,13-dioxo-5,7,12,13b,13c,14-hexahydro-5a,6a,12a,13a-tetraazabenz[5,6]azuleno[2,1,8-*ija*]benzo[*f*]azulen-13-yl)benzoate (3):

Starting from **1b** (300 mg, 0.425 mmol), 1-bromooctadecane (566 mg, 1.70 mmol), K₂CO₃ (590 mg, 4.27 mmol) and KI (5 mg) in DMF (15 ml), this compound was synthesized as described for **2** to yield 420 mg (82%) of **3** as a white powder.

M.p. 195°C; IR (KBr pellet) ν 2960-2840 (CH₂), 1737 (ester C=O), 1722 (urea C=O), 1611, 1597, 1577, 1487, 1468, 1438, 1425, 1407 (C=C), 1305, 1275, 1266 (CH₂), 1120, 1106, 1077 (COC) cm⁻¹; ¹H NMR (300.13 MHz, CDCl₃) δ 7.76 (d, 4H, *ArH ortho* to C(O)OC₁₈H₃₇, ³J = 8.5 Hz), 7.17 (d, 4H, *ArH meta* to C(O)OC₁₈H₃₇, ³J = 8.5 Hz), 6.54 (s, 4H, *ArH side-wall*), 5.55 (d, 4H, NCH₂Ar *out*, ²J = 15.9 Hz), 4.23 (t, 4H, C(O)OCH₂, ³J = 6.7 Hz), 3.76 (d, 4H, NCH₂Ar *in*, ²J = 15.9 Hz), 3.74 (s, 12H, OCH₃), 1.70 (m, 4H, C(O)OCH₂CH₂), 1.45-1.19 (m, 60H, (CH₂)₁₅CH₃), 0.88 (t, 6H, CH₂CH₃, ³J = 6.4 Hz) ppm; ¹³C{¹H} NMR (75.47 MHz, CDCl₃) δ 165.83 (ester C=O), 157.55 (urea C=O), 151.09 (*ArC ipso* to OCH₃), 139.18 (*ArC ipso* to C(O)OC₁₈H₃₇), 130.61 (*ArC para* to C(O)OC₁₈H₃₇), 129.76 (*ArC ortho* to C(O)OC₁₈H₃₇), 128.16 (*ArC meta* to C(O)OC₁₈H₃₇), 127.14 (*ArC ipso* to CH₂N), 111.95 (*ArC para* to CH₂N), 84.83 (NC(Ar)N), 65.38 (C(O)OCH₂), 56.84 (OCH₃), 36.97 (NCH₂Ar), 31.91 (CH₂CH₂CH₃), 29.69, 29.34, 28.58, 25.97 ((CH₂)₁₄CH₂CH₂CH₃), 22.68 (CH₂CH₃), 14.11 (CH₂CH₃) ppm; ESI-MS *m/z* 1211.9 (M)⁺, 1234.1 (M + Na)⁺, 2445.4 (M + M + Na)⁺. Anal. Calcd for C₇₄H₁₀₆N₄O₁₀: C, 73.48; H, 8.67; N, 4.63. Found: C, 73.35; H, 8.82; N, 4.62.

***N*-1-octadecyl-4-(1,4,8,11-tetramethoxy-13b-4-[(octadecylamino)carbonyl]phenyl-6,13-dioxo-5,7,12,13b,13c,14-hexahydro-5a,6a,12a,13a-tetraazabenz[5,6]azuleno[2,1,8-*ija*]benzo[*f*]azulen-13-yl)benzamide (4):**

Compound **1c** (850 mg, 1.14 mmol), 1-aminooctadecane (1.25 g, 4.65 mmol) and triethylamine (1 mL) in CH₂Cl₂ (50 mL) were stirred under nitrogen for 16 h. The suspension was extracted with a saturated aqueous NaCl solution (200 mL), with water (2 x 200 mL) and evaporated to dryness. The residue was recrystallized from methanol to yield 1.0 g (72%) of **4** as a white solid.

M.p. 242°C; IR (KBr pellet) ν 3353 (NH), 3042 (*ArH*), 2925, 2854 (CH₂), 1736, 1719 (urea C=O), 1665, 1644 (amide I), 1613, 1596, 1573 (C=C), 1542 (amide II), 1485, 1462, 1439 (C=C), 1305, 1260 (CH₂), 1080 (COC) cm⁻¹; ¹H NMR (CDCl₃, 300.13 MHz) δ 7.51 (d, 4H, *ArH ortho* to C(O)NH, ³J = 8.4 Hz), 7.13 (d, 4H, *ArH meta* to C(O)NH, ³J = 8.4 Hz), 6.65 (s, 4H, *ArH side-wall*), 6.25 (t, 2H, NH, ³J = 5.5 Hz), 5.56 (d, 4H, NCH₂Ar *out*, ²J = 15.9 Hz), 3.72 (d, 4H, NCH₂Ar, ²J = 15.9 Hz), 3.70 (s, 12H, OCH₃), 3.37 (q, 4H, C(O)NHCH₂, ³J = 6.5 Hz), 1.57 (m, 4H, C(O)NHCH₂CH₂), 1.40-1.18 (m, 60H, (CH₂)₁₅CH₃), 0.88 (t, 6H, CH₂CH₃, ³J = 6.4 Hz) ppm; ¹³C{¹H} NMR (CDCl₃, 75.47 MHz) δ 166.68 (amide C=O), 157.55 (urea C=O), 150.95 (*ArC ipso* to OCH₃), 137.46 (*ArC ipso* to C(O)NHC₁₈H₃₇), 135.31 (*ArC para* to C(O)NHC₁₈H₃₇), 128.33 (*ArC ortho* to C(O)NHC₁₈H₃₇), 127.23 (*ArC meta* to C(O)NHC₁₈H₃₇), 127.03 (*ArC ipso* to CH₂N), 111.80 (*ArC para* to CH₂N), 84.97 (NC(Ar)N), 56.66 (OCH₃), 40.23 (C(O)NHCH₂), 36.93 (NCH₂Ar), 31.91 (CH₂CH₂CH₃), 29.69, 29.57, 28.58, 27.04 ((CH₂)₁₄CH₂CH₂CH₃), 22.67 (CH₂CH₃), 14.10 (CH₂CH₃) ppm; FAB-MS *m/z* 1209 (M + H)⁺. Anal. Calcd for C₇₄H₁₀₈N₆O₈: C, 73.47; H, 9.00; N, 6.95. Found: C, 73.66; H, 8.60; N, 7.16.

5,7,12,13b,13c,14-Hexahydro-1,4,8,11-tetramethoxy-13b,13c-bis(4-octadecyloxyphenyl)-6H,13H-5a,6a,12a,-13a-tetraazabenz[5,6]azuleno[2,1,8-*ija*]benz[*f*]azulene-6,13-dione (5):

Starting from **1d** (80 mg, 0.12 mmol), 1-bromooctadecane (165 mg, 0.492 mmol), K₂CO₃ (170 mg, 1.20 mmol) and KI (5 mg) in DMF (5 mL), this compound was synthesized as described for **2**. The crude product was recrystallized from methanol to afford 96 mg (68%) of **5** as a white powder.

M.p. 213°C; IR (KBr pellet) ν 3050 (*ArH*), 2919, 2851 (CH₂), 1733, 1715 (C=O), 1610, 1510, 1488, 1461, 1426 (C=C), 1311, 1266, 1250 (CH₂), 1171, 1075 (COC) cm⁻¹; ¹H NMR (CDCl₃, 200.13 MHz) δ 6.94 (d, 4H, *ArH meta* to OC₁₈H₃₇, ³J = 8.8 Hz), 6.65 (s, 4H, *ArH side-wall*), 6.62 (d, 4H, *ArH ortho* to OC₁₈H₃₇, ³J = 8.8 Hz), 5.57 (d, NCH₂Ar *out*, ²J = 16.0 Hz), 3.76 (d, 4H, NCH₂Ar *in*, ²J = 16.0 Hz), 3.82 (t, 4H, ArOCH₂, ³J = 6.4 Hz), 1.69 (m, 4H, ArOCH₂CH₂), 1.48-1.18 (m, 60H, (CH₂)₁₅CH₃), 0.88 (t, 6H, CH₂CH₃, ³J = 6.0 Hz) ppm; ¹³C{¹H} NMR (CDCl₃, 50.32 MHz) δ 159.05 (urea C=O), 157.73 (*ArC ipso* to OC₁₈H₃₇), 129.43 (*ArC meta* to OC₁₈H₃₇), 127.82 (*ArC para* to OC₁₈H₃₇), 125.71 (*ArC ipso* to CH₂N), 114.48 (*ArC para* to CH₂N), 111.82 (*ArC ortho* to OC₁₈H₃₇), 85.14

(NC(Ar)N), 68.00 (OCH₂CH₂), 56.89 (OCH₃), 36.74 (NCH₂), 31.91 (CH₂CH₂CH₃), 29.69, 29.38, 29.11, 25.97 ((CH₂)₁₄CH₂CH₂CH₃), 22.68 (CH₂CH₃), 14.12 (CH₂CH₃) ppm; FAB-MS *m/z* 1156 (M + H)⁺. Anal. Calcd for C₇₂H₁₀₆N₄O₈: C, 74.83; H, 9.25; N, 4.85. Found: C, 74.80; H, 9.23; N, 4.90.

3-((1-(3,5-Dihydroxyphenyl)vinyl)oxy)propyl 4-(13b-(4-((3-((1-(3,5-dihydroxyphenyl)vinyl)oxy)-propoxy)carbonyl)phenyl)-1,4,8,11-tetramethoxy-6,13-dioxo-5,7,12,13b,13c,14-hexahydro-5a,6a,12a,13a-tetraazabenz[5,6]azuleno[2,1,8-*ija*]benzo[*f*]azulen-13-yl) (6):

A solution of 7 (50 mg, 34.4 μmol) was stirred in a 33% HBr solution in acetic acid (0.5 mL) under nitrogen for 16 h. EtOAc (10 mL) was added, the organic layer was extracted with water (100 mL) and evaporated to dryness. The crude product was purified by column chromatography (CH₂Cl₂/EtOH, 95:5, v/v, R_f = 0.09) to yield 12 mg (32%) of 6 as a white and hygroscopic solid which was stored under argon at -18°C.

M.p. 330°C (dec); ¹H NMR (CDCl₃/CD₃OD 4:1, v/v, 500.14 MHz) δ 7.78 (d, 4H, ArH glycoluril *ortho* to C(O)O, ³J = 8.5 Hz), 7.16 (d, 4H, ArH glycoluril *meta* to C(O)O, ³J = 8.5 Hz), 6.99 (d, 4H, ArH *para* to OH, ⁴J = 2.5 Hz), 6.72 (s, 4H, ArH side-wall), 6.54 (t, 2H, ArH *ortho* to OH and *para* to C(O)O, ⁴J = 2.5 Hz), 5.54 (d, 4H, NCH₂Ar *out*, ²J = 16.0 Hz), 4.43 (m, 8H, C(O)OCH₂), 3.79 (s, 12H, OCH₃), 3.75 (d, 4H, NCH₂Ar *in*, ²J = 16.0 Hz), 2.22 (m, 4H, CH₂CH₂CH₂) ppm, the OH-protons were not detected; ¹³C{¹H} NMR (CDCl₃/CD₃OD 4:1, v/v, 500.14 MHz) δ 164.66, 160.87 (2 × ester C=O), 157.56 (urea C=O), 156.75 (ArC *ipso* to OH), 137.99, 131.00, 129.59, 126.33, 111.50, 107.64, 107.00 (all ArC), 84.17 (NC(Ar)N), 62.10, 61.65 (2 × C(O)OCH₂), 55.99 (OCH₃), 35.47 (NCH₂Ar), 27.54 (CH₂CH₂CH₂) ppm; FAB-MS *m/z* 1095 (M + H)⁺. No satisfactory elemental analysis could be obtained.

3-Bromopropyl-3,5-di(benzyloxy)benzoate (7):

A solution of 3,5-di(benzyloxy)benzoic acid (2.54 g, 7.6 mmol) and 1,3-dibromopropane (15 g, 74 mmol) in DMF (150 mL) was purged with argon for 30 min. K₂CO₃ (2.5 g, 18 mmol) was added and the mixture was stirred for 16 h. The solvent was evaporated and the residue was suspended in CHCl₃ (100 mL). This solution was extracted with aqueous 1 N HCl (150 mL), with a saturated aqueous NaHCO₃ solution (150 mL) and evaporated to dryness. The residue was recrystallized from diisopropyl ether to yield 2.8 g (81%) of 7 as white needles.

¹H NMR (CDCl₃, 300.13 MHz) δ 7.46-7.22 (m, 10H, ArH benzyl), 6.81 (d, 2H, ArH *ortho* to C(O)O, ⁴J = 2.3 Hz), 6.81 (t, 1H, ArH *para* to C(O)O, ⁴J = 2.3 Hz), 5.06 (s, 4H, CH₂Ph), 4.43 (t, 2H, C(O)OCH₂, ³J = 6.0 Hz), 3.50 (t, 2H, CH₂Br, ³J = 6.6 Hz), 2.28 (m, 2H, CH₂CH₂CH₂) ppm; ¹³C{¹H} NMR (CDCl₃, 75.47 MHz) δ 165.97 (ester C=O), 159.75 (ArC *ipso* to OCH₂), 136.37 (benzyl C *ipso* to CH₂OAr), 131.83 (ArC *ipso* to C(O)O), 128.61, 128.11, 127.53 (benzyl C *ortho*, *meta*, *para* to CH₂OAr), 108.44 (ArC *ortho* to C(O)O), 107.13 (ArC *para* to C(O)O), 70.29 (ArOCH₂), 62.79 (C(O)OCH₂), 31.74 (CH₂Br), 29.39 (CH₂CH₂CH₂) ppm.

3-((1-(3,5-Di(benzyloxy)phenyl)vinyl)oxy)propyl 4-(13b-(4-((3-((1-(3,5-di(benzyloxy)phenyl)vinyl)oxy)-propoxy)carbonyl)phenyl)-1,4,8,11-tetramethoxy-6,13-dioxo-5,7,12,13b,13c,14-hexahydro-5a,6a,12a,13a-tetraazabenz[5,6]azuleno[2,1,8-*ija*]benzo[*f*]azulen-13-yl) (8):

A suspension of 1b (450 mg, 0.64 mmol) and 7 (1.15 g, 2.53 mmol) in DMF (30 mL) was purged with argon for 30 min. K₂CO₃ (900 mg, 6.5 mmol) and KI (10 mg) were added and the mixture was stirred under argon for 64 h. The solvent was evaporated, the residue was suspended in CH₂Cl₂ (100 mL) and this suspension was extracted with aqueous 0.1 N HCl (200 mL), with a saturated aqueous NaCl solution (200 mL) and evaporated to dryness. The residue was recrystallized from CH₂Cl₂/MeOH (1:5, v/v) to yield 810 mg (87%) of 8 as an off-white solid.

M.p. 185°C; ¹H NMR (CDCl₃, 500.14 MHz) δ 7.74 (d, 4H, ArH glycoluril *ortho* to C(O)O, ³J = 8.4 Hz), 7.42-7.34 (m, 24H, ArH benzyl and ArH *para* to OCH₂Ph), 7.12 (d, 4H, ArH glycoluril *meta* to C(O)O, ³J = 8.4 Hz), 6.77 (br s, 2H, ArH *para* to C(O)O), 6.69 (s, 4H, ArH side-wall), 5.51 (d, 4H, NCH₂Ar *out*, ²J = 15.9 Hz), 5.04 (s, 8H, CH₂Ph), 4.43-4.36 (m, 8H, C(O)OCH₂), 3.78 (s, 12H, OCH₃), 3.76 (d, 4H, NCH₂Ar *in*, ²J = 15.9 Hz), 2.18 (m, 4H, CH₂CH₂CH₂) ppm; ¹³C{¹H} NMR (CDCl₃, 75.47 MHz) δ 165.98, 165.73 (2 × ester C=O), 159.75 (urea C=O), 157.51 (ArC *ipso* to OBn), 151.04 (ArC *ipso* to OCH₃), 139.48, 136.41 (2 × ArC *ipso* to C(O)O), 131.90, 130.25, 128.84, 128.20, 128.10, 127.53, 127.04 (all ArC), 111.91 (ArC *para* to CH₂N), 107.08 (ArC *para* to OBn), 106.49 (ArC *ortho* to OBn), 84.98 (NC(Ar)N), 70.27 (ArOCH₂Ph), 61.95, 61.85 (2 × C(O)OCH₂), 56.78 (OCH₃), 36.95 (NCH₂Ar), 28.07 (CH₂CH₂CH₂) ppm; FAB-MS *m/z* 1456 (M + H)⁺. Anal. Calcd for C₈₆H₇₈N₄O₁₈: C, 70.96; H, 5.40; N, 3.85. Found: C, 70.91; H, 5.35; N, 3.95.

References and notes

- ¹ Lehn, J.-M. *Supramolecular Chemistry - Concepts and Perspectives*; VCH, Weinheim, **1995**, Chapter 9 and references therein.
- ² Whitesides, G. M.; Mathias, J. P.; Seto, C. T. *Science* **1991**, *254*, 1312. Martin, C. R. *Chem. Mater.* **1996**, *8*, 1739. Stupp, S. I.; Braun, P.V. *Science* **1997**, *277*, 1225.
- ³ Desiraju, G. R. *Crystal Engineering: The Design of Organic Solids*; Elsevier, Amsterdam, **1989**.
- ⁴ Reviews: Gavezotti, A. *Acc. Chem. Res.* **1994**, *27*, 309. Russell, V. A.; Ward, M. D. *Chem. Mater.* **1996**, *8*, 1654. Desiraju, G. R. *Chem. Commun.* **1997**, 1475. Ashton, P. R.; Fyfe, M. C. T.; Hickingbottom, S. K.; Menzer, S.; Stoddart, J. F.; White, A. J. P.; Williams, D. J. *Chem. Eur. J.* **1998**, *4*, 577.
- ⁵ Lehn, J.-M. *Angew. Chem. Int. Ed. Engl.* **1990**, *29*, 1304. Garcia-Tellado, F.; Geib, S. J.; Goswami, S.; Hamilton, A. D. *J. Am. Chem. Soc.* **1991**, *113*, 9265. Mathias, J. P.; Stoddart, J. F. *Chem. Soc. Rev.* **1992**, *21*, 215. Aakeröy, C. B.; Hughes, D. P.; Niewenhuyzen, M. *J. Am. Chem. Soc.* **1996**, *118*, 10134.
- ⁶ Bishop, R. *Chem. Soc. Rev.* **1996**, *25*, 311.
- ⁷ Mallouk, T. E.; Gavin, J. A. *Acc. Chem. Res.* **1998**, *31*, 209.
- ⁸ Endo, K.; Sawaki, T.; Koyanagi, M.; Kobayashi, K.; Masuda, H.; Aoyama, Y. *J. Am. Chem. Soc.* **1995**, *117*, 8341. Aoyama, Y.; Endo, K.; Anzai, T.; Yamaguchi, Y.; Sawaki, T.; Kanehisa, N.; Hashimoto, H.; Kai, Y.; Masuda, H. *J. Am. Chem. Soc.* **1996**, *118*, 5562. Dewa, T.; Endo, K. Aoyama, Y. *J. Am. Chem. Soc.* **1998**, *120*, 8933.
- ⁹ Brunet, P.; Simard, M.; Wuest, J. D. *J. Am. Chem. Soc.* **1997**, *119*, 2737.
- ¹⁰ Ghadiri, M. R.; Granja, J. R.; Milligan, R. A.; McRee, D. E.; Khazanovich, N. *Nature* **1993**, *366*, 324. Kim, H. S.; Hartgerink, J. D.; Ghadiri, M. R. *J. Am. Chem. Soc.* **1998**, *120*, 4417. Vollmer, M. S.; Clark, T. D.; Steinem, C.; Ghadiri, M. R. *Angew. Chem. Int. Ed.* **1999**, *38*, 1598.
- ¹¹ Smith, R. C.; Hu, S.; Juang, E.; Gin, D. L. *J. Am. Chem. Soc.* **1997**, *119*, 4092. Gray, D.H.; Gin, D. L. *Chem. Mater.* **1998**, *10*, 1827. Deng, H.; Smith, R. C.; Gin, D. L. *J. Am. Chem. Soc.* **1998**, 3522. Miller, S. A.; Kim, E.; Gray, D. H.; Gin, D. L. *Angew. Chem. Int. Ed.* **1999**, *38*, 3022.
- ¹² Lee, K. M.; Lee, C. K.; Lin, I. J. B. *Angew. Chem. Int. Ed. Engl.* **1997**, *36*, 1850. Sharma, C. V. K.; Bauer, C. B.; Rogers, R. D.; Zaworotko, M. J. *Chem. Commun.* **1997**, 1559.
- ¹³ Sijbesma, R. P.; Kentgens, A. P. M.; Lutz, E. T. G.; van der Maas, J. H.; Nolte, R. J. M. *J. Am. Chem. Soc.* **1993**, *115*, 8999. Reek, J. N. H.; Priem, A. H.; Engelkamp, H.; Rowan, A. E.; Elemans, J. A. A. W.; Nolte, R. J. M. *J. Am. Chem. Soc.* **1997**, *119*, 9956.
- ¹⁴ Reek, J. N. H.; Rowan, A. E.; Elemans, J. A. A. W.; de Gelder, R.; Nolte, R. J. M. manuscript in preparation.
- ¹⁵ Bosman, W. P.; Smits, J. M. M.; de Gelder, R.; Reek, J. N. H.; Nolte, R. J. M. *J. Chem. Cryst.* **1996**, *26*, 365. Bosman, W. P.; Smits, J. M. M.; de Gelder, R.; Reek, J. N. H.; Elemans, J. A. A. W.; Nolte, R. J. M. *J. Chem. Cryst.* **1997**, *27*, 75. Reek, J. N. H.; Rowan, A. E.; de Gelder, R.; Beurskens, P. T.; Crossley, M. J.; de Feyter, S.; de Schryver, F.; Nolte, R. J. M. *Angew. Chem. Int. Ed. Engl.* **1997**, *36*, 361.
- ¹⁶ Reek, J. N. H.; Kros, A.; Nolte, R. J. M. *Chem. Commun.* **1996**, 245. Elemans, J. A. A. W.; de Gelder, R.; Rowan, A. E.; Nolte, R. J. M. *Chem. Commun.* **1998**, 1553.
- ¹⁷ Van Nunen, J. L. M.; Folmer, B. F. B.; Nolte, R. J. M. *J. Am. Chem. Soc.* **1997**, *119*, 283. Van Nunen, J. L. M.; Nolte, R. J. M. *J. Chem. Soc. Perkin Trans. 2* **1997**, 1473.
- ¹⁸ It should be mentioned here that heating of samples of the clips described in this chapter to temperatures more than $\sim 10^\circ\text{C}$ above their melting point was often observed to result in the decomposition of the compounds.
- ¹⁹ The platelet texture was predominantly observed when the film was thinner. Strong evidence that both textures result from the same crystal structure comes from the fact that the melting and crystallisation temperatures of the two textures always coincided on heating and cooling runs. Further evidence is the observation that the polychromatic texture often merges with the platelet texture in the same sample, particularly at the sample edges where the sample was thinner.
- ²⁰ Gray, G. W.; Goodby, J. W. G. in: *Smectic Liquid Crystals - Textures and Structures*, Leonard Hill, Glasgow, **1984**.
- ²¹ Similar high isotropization ΔH values have been observed for structurally related mesogenic gold(I) dicarbene complexes, however for these molecules the ΔH values for the transition from crystalline to mesophase amounted to approximately 100 kJ mol^{-1} . See: Lee, K. M.; Lee, C. K.; Lin, I. J. B. *Angew. Chem. Int. Ed. Engl.* **1997**, *36*, 1850.

- ²² The exotherm observed at 162°C in the heating run is due to a cold crystallization, caused by incomplete crystallization in the cooling run due to too a rapid cooling process (10°C min⁻¹). No exotherm was visible in the heating run when the sample was cooled at 1°C min⁻¹ from the isotropic melt.
- ²³ In addition to the set of maxima corresponding to lamellar ordering there were a high number of other reflections in the middle to high angle region corresponding to intra-layer ordering, as well as crossed reflections, *i.e.* reflections with Miller indices *h, k, l* simultaneously different from zero, which indicates the existence of three-dimensional ordering.
- ²⁴ Billmeyer, Jr., F. W. in: *Textbook of Polymer Science*, John Wiley and Sons, New York, **1984**.
- ²⁵ Rao, C. N. R. in: *Chemical Applications of Infrared Spectroscopy*, Academic Press, New York and London, **1963**.
- ²⁶ Inspection of a CPK model reveals that the amide groups in a molecule of **4** are too far apart (~5 Å) to form an *intramolecular* hydrogen bond.
- ²⁷ Whereas a simple lamellar structure with weak interactions between bilayers of clip molecules explains the malleability of the material, it does not explain the appearance of an isotropic fluid component which was observed upon the application of pressure. A possible explanation for this phenomenon is that due to the applied pressure Van der Waals attractions responsible for the bilayer cohesion are broken. Without the latter attractions, the monomers or dimers will melt and form an isotropic liquid.
- ²⁸ Methanol was added in order to fully dissolve both the clip and guest components.
- ²⁹ This assumption is based on the relative strengths of the dimeric host-host and the host-guest complexes in chloroform solution; the K_a of the **2:MDB** complex is found to be several orders of magnitude higher (1.0×10^4 M⁻¹) than the K_{dimer} (18 M⁻¹) of **2**.
- ³⁰ The deprotection of **8** appeared to be troublesome and several side-products were formed. Other methods of deprotection were not tried.
- ³¹ Another possibility is that it takes several heating and cooling runs to 'dissolve' **6**. In contrast to **MDB** and **DBA**, **6** has a melting point which is higher than that of **3**, which implies that it can only be incorporated in the lamellar structure when it is 'dissolved'.

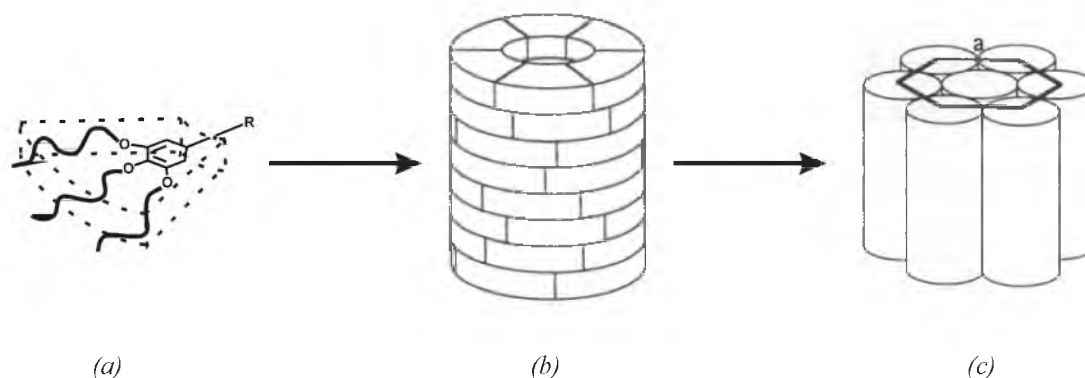


Figure 6.1 Schematic representation of the self-assembly of tapered monodendron **MD-G1**. (a) Tapered monodendron, $R = \text{COOH}$, COOMe , etc. (b) Columnar structure formed by **MD-G1** (c) Orientation of the columns in (b) into a hexagonal lattice.

relatively small but well-defined building blocks, the so-called ‘monodendrons’. During the past decade, the group of Percec has extensively studied this research area. This group uses a monodendron structure which is based on the gallic acid (3,4,5-trihydroxybenzoic acid) building block. It has been demonstrated that derivatives of this molecule can self-assemble into predictable macroscopic structures in the crystalline and liquid-crystalline state. The molecular order in these assemblies has been analyzed by X-ray diffraction techniques, which can provide direct information about the size and the 3-dimensional shape of the constituting monodendritic building blocks.⁶ The shape of the monodendrons was predicted by Percec and coworkers with the help of molecular modeling calculations, and confirmed by ^1H NMR measurements.⁷ The first generation monodendron, a gallic acid substituted with three dodecyl groups (**MD-G1**), forms a flat, tapered disk (Figure 6.1a). Its tapered shape (comparable to a slice of pizza) is expressed in the supramolecular architectures formed by the compound upon self-assembly: upon heating to the isotropic melt, the molecules organize themselves into columnar structures, which further arrange into a hexagonal lattice (Figure 6.1b-c).⁸ The coupling of three **MD-G1** building blocks to another gallic acid derivative yields the second generation monodendron (**MD-G2**). In this molecule, for steric reasons only a restricted and cooperative rotation of the benzyl ether groups is allowed, which requires the two external benzyl ether moieties to be positioned orthogonal to the internal one, resulting in an overall conical shape (Figure 6.2a). Upon cooling from the isotropic melt, these conical monodendrons self-assemble into spherical structures, which have become known as ‘supramolecular dendrimers’. These can organize further into a cubic liquid-crystalline lattice (Figure 6.2b-c). In contrast to the wide abundance of lyotropic systems which exhibit such a cubic symmetry,⁹ there are relatively few examples known of thermotropic systems exhibiting cubic phases.¹⁰ The higher order equivalent of **MD-G2**, *i.e.* the third and fourth generation monodendrons also self-assemble into supramolecular dendrimers and then further into a cubic lattice.⁷ Extensive X-ray diffraction experiments, in combination with molecular modeling and density measurements, have revealed that the aforementioned dendrimers are built up from 12 second generation, 6 third generation, and 2 fourth generation monodendrons. The cylindrical and spherical form of the respective assemblies could be directly visualized by scanning force and transition electron microscopy techniques.¹¹

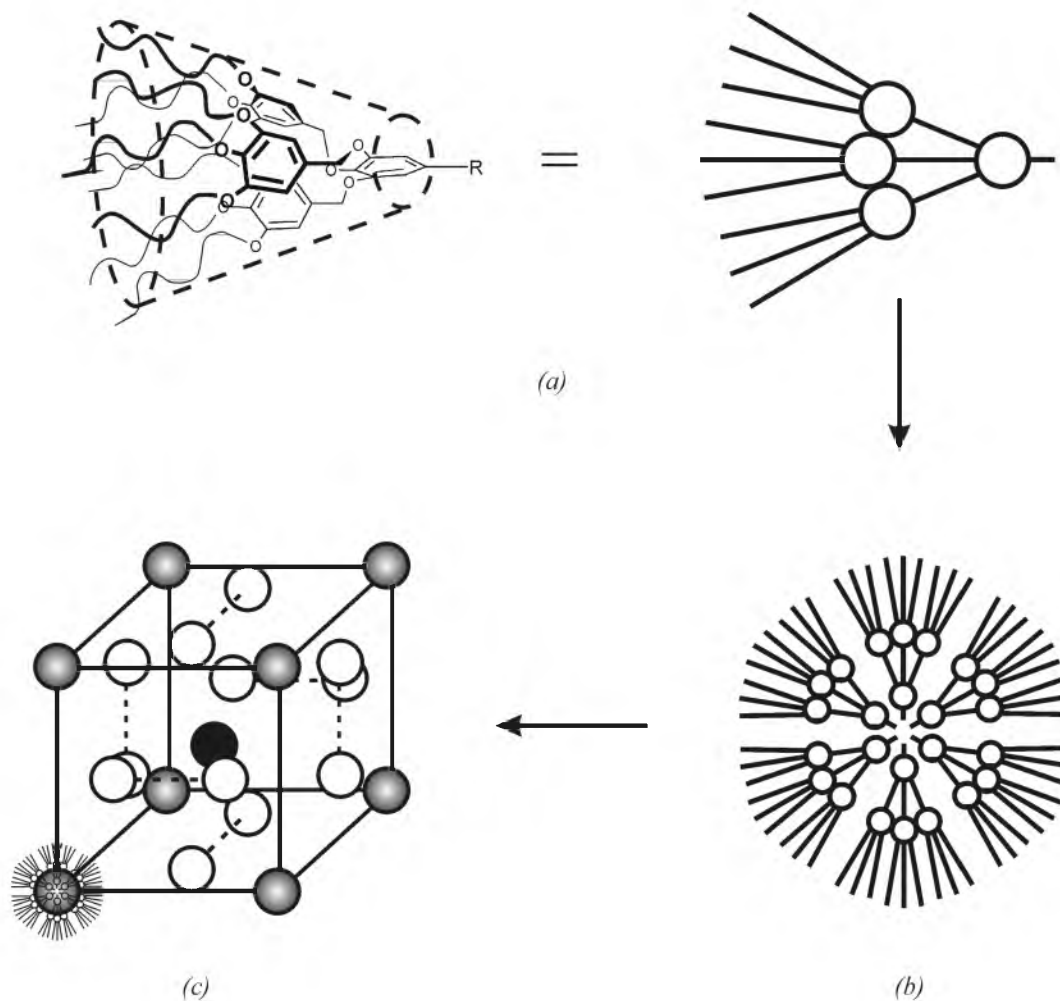


Figure 6.2 Schematic representation of the self-assembly of conical monodendron **MD-G2**. (a) Conical monodendron, $R = \text{COOH}$, COOMe , etc. (b) Two-dimensional cross-section of a supramolecular dendrimer. (c) Orientation of the supramolecular dendrimers in a cubic lattice.

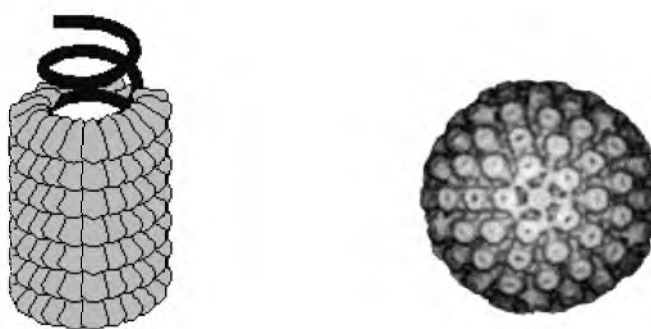


Figure 6.3 Natural self-assembled systems with cylindrical or spherical shape. (a) Tobacco Mosaic Virus. (b) An icosahedral virus.

In processes reminiscent of the construction of viruses in Nature, e.g. the Tobacco Mosaic Virus (Figure 6.3a), the polymerization of tapered monodendrons functionalized with a methacrylate group gave cylindrical structures in which the polymer backbone had adopted a helical

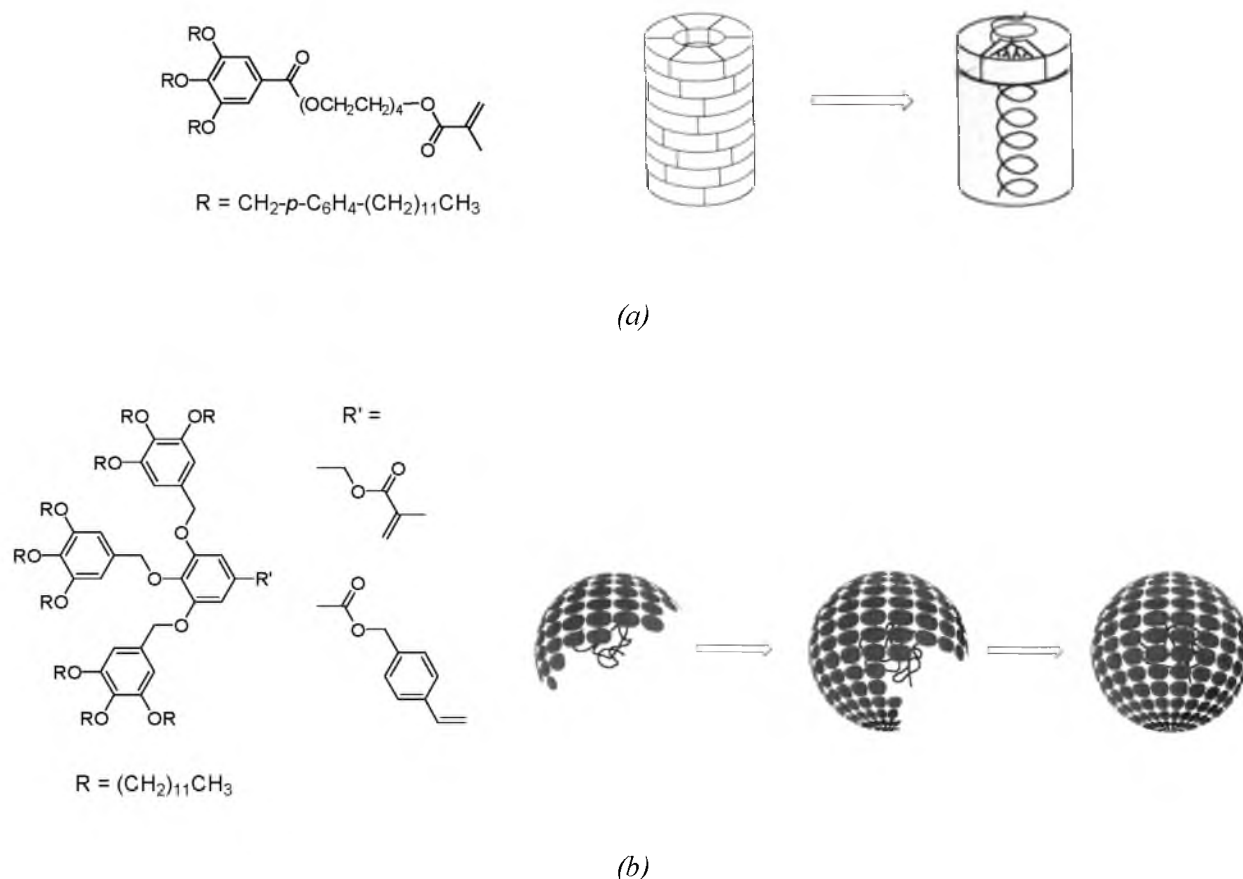


Figure 6.4 (a) Polymerization of tapered monodendrons into a columnar aggregate containing a helical inner polymer chain, resembling the Tobacco Mosaic Virus. (b) Polymerization of conical monodendrons into a spherical aggregate, resembling an icosahedral virus.

conformation (Figure 6.4a).¹² When similar polymerizations were carried out with conical monodendrons functionalized with methacrylate or styrene groups, spherical virus-like assemblies (Figure 6.3b) incorporating a random coil polymer backbone were again formed (Figure 6.4b), however, only when the degree of polymerization (DP) was low (< 20).¹³ At higher DP-values cylindrical assemblies with helical polymer backbones were formed.

In this chapter, the synthesis and self-assembling behaviour of molecular clips, which are functionalized with two first (**MD-G1**) or second (**MD-G2**) generation monodendrons, will be described. The physical properties of the clip-dendrimers will be compared with the properties exhibited by the monodendrons studied by the group of Percec.

6.2 Design

In the previous chapter it was demonstrated that molecular clip **1**, which is functionalized at its convex side with two octadecyl tails, can dimerize via a mutual cavity filling process. The dimers form extended two-dimensional sheets as a result of strong π - π interactions between the dimeric clip molecules (Figure 6.5a).¹⁴ The material has an extended lamellar structure and behaves as a crystalline but malleable solid. One of our objectives was to make clip molecule **1** truly liquid-crystalline. To achieve this goal we reasoned that it would be necessary to break the

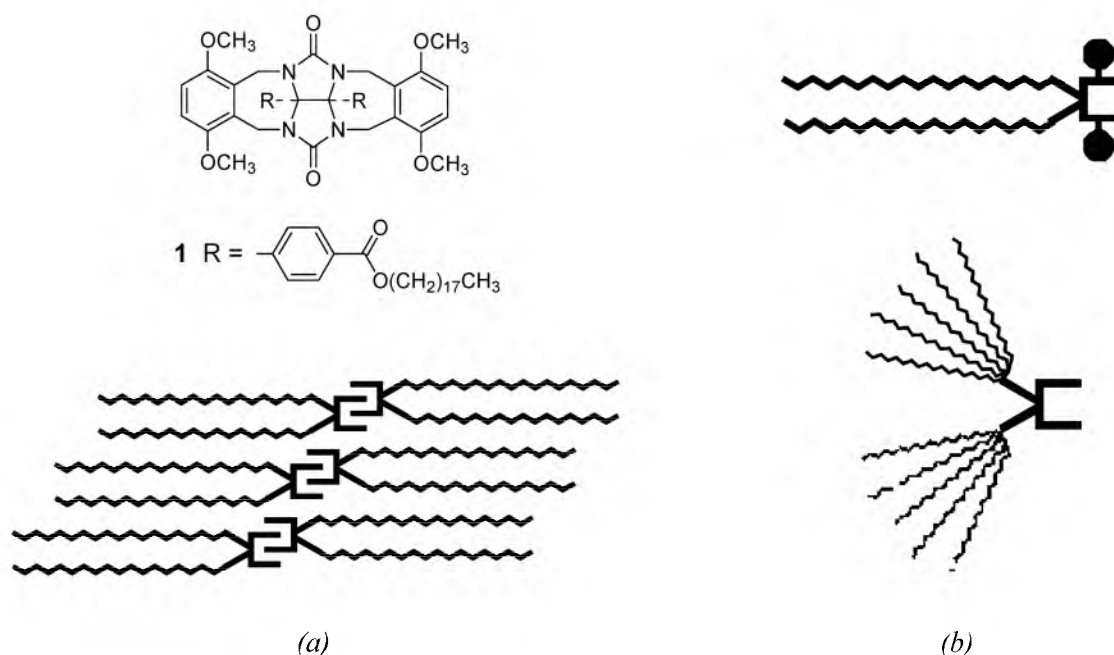


Figure 6.5 (a) Schematic drawing of the lamellar structure formed by molecules of **1**; note the strong π - π interactions between the clip head-groups. (b) Schematic drawing showing how the strong π - π interactions between the dimers can be broken by the attachment of bulky substituents to the side-walls of the clips (top), or by increasing the steric bulk of the aliphatic tails (bottom).

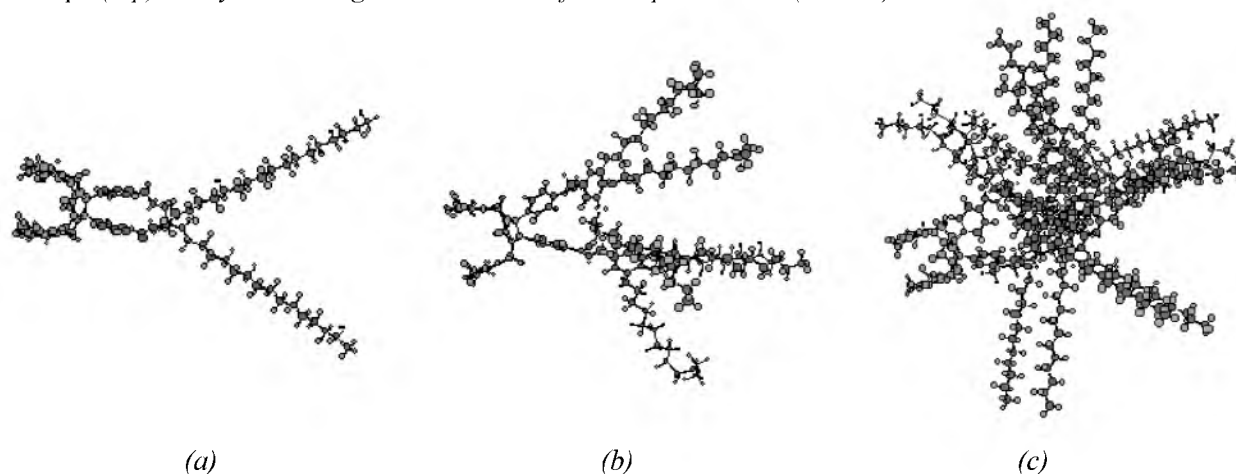
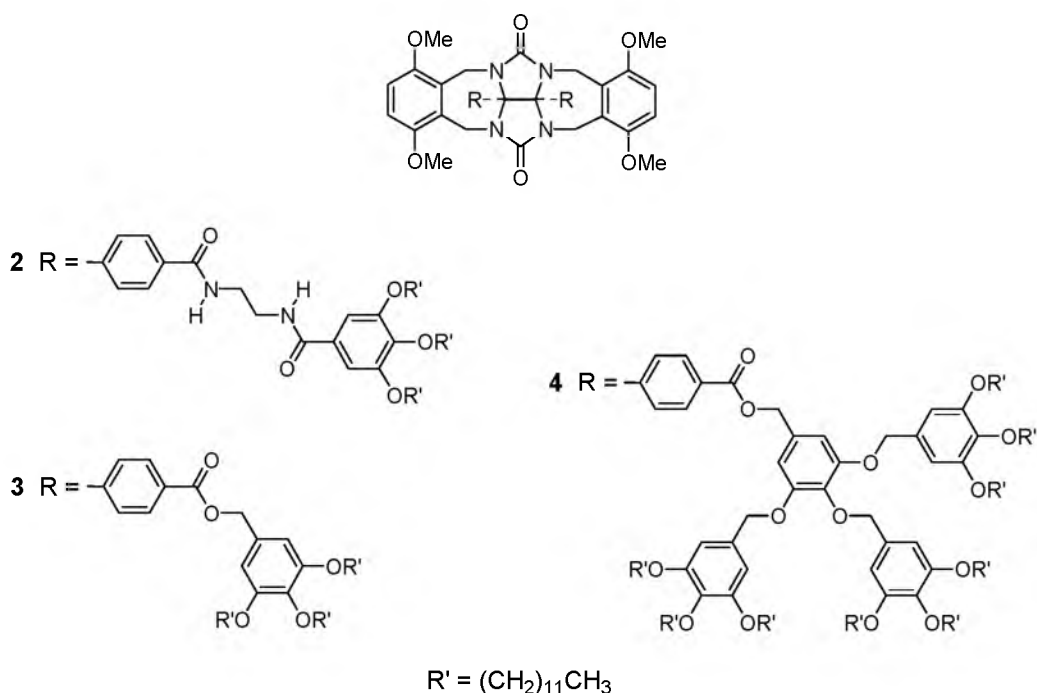


Figure 6.6 Computer modeled representations of (a) clip **1**, (b) clip **3**, and (c) clip **4** (see Chart 6.1). The increase in steric bulk imposed by the increase in monodendron generation number is clearly visible.

lamellar architectures formed by the dimers. This can be accomplished, at least in principle, by attaching bulky substituents (e.g. *tert*-butoxy groups) to the side-walls of the clip (Figure 6.5b). The bulkiness near the cavity of the clips would, however, also inhibit clip dimerization and the complexation of guest molecules. An alternative and more feasible approach would be to increase the bulkiness at the convex side of the clip (Figure 6.5b). Following the latter approach, clip molecules were designed which are functionalized at their convex side with two tapered (**2** and **3**) or conical monodendrons (**4**) (Chart 6.1). Molecular modeling calculations on **3** and **4**

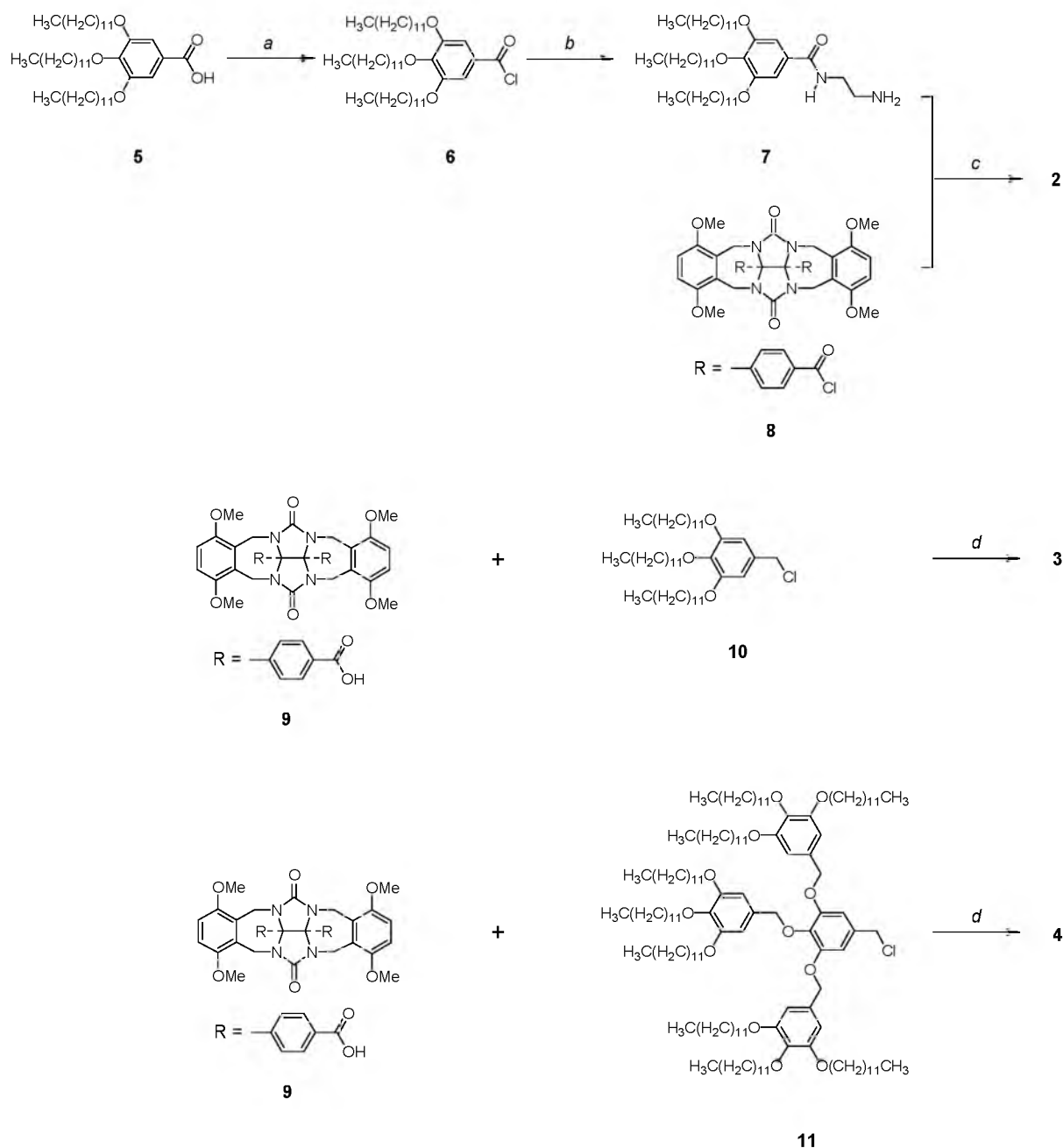
Chart 6.1



clearly showed that the increase in steric bulk imposed by the tails (Figure 6.6) should inhibit a close packing of the dimers.

6.3 Synthesis of monodendron functionalized clips

Clips **2** and **3** (Chart 6.1) have two tapered monodendritic tails and differ in the linker between the clip and the tail. Tapered monodendron **7** was synthesized in nearly quantitative yield by chlorination of carboxylic acid **5**¹⁵ with thionyl chloride to give **6**, followed by a reaction of this compound with a 40-fold excess of 1,2-ethylenediamine in dichloromethane using triethylamine as a base (Scheme 6.1). Compound **7** was coupled to the benzoyl chloride functionalized clip **8** (see Chapter 5) in dichloromethane, using triethylamine as a base, to afford **2** in 38% yield, after purification by column chromatography. Clip **3** was synthesized starting from carboxylic acid functionalized clip **9** (see Chapter 5) by esterification with four equivalents of benzyl chloride derivative **10**¹⁵ in dimethylformamide using potassium carbonate as a base. Pure **3** was obtained in 33% yield after recrystallization of the crude product from methanol. In a similar manner as described for **3**, clip **4** was obtained from **9** and the benzyl chloride derivative **11**¹⁵ in 42% yield, after purification by column chromatography and recrystallization from acetone. The reason for the relatively low yield of **2** is unknown; the low yields of **3** and **4** can be attributed to the limited solubility of **9**, **10** and **11** in DMF¹⁶ and to the relatively poor leaving group abilities of the chloride anions of the tails. Addition of a small amount of potassium iodide to the mixtures, in order to improve the leaving group ability via catalytic anion-exchange, did, however, not result in improved yields, neither had the use of a different base, such as cesium carbonate, the desired effect. Four equivalents of **10** or **11** were required to complete the esterification reaction. When less equivalents of the tails were used, analysis of the crude reaction product by NMR spectroscopy indicated that in addition to the desired product a considerable amount of mono-tailed clip and benzyl alcohol monodendron were formed.



Scheme 6.1 Reagents and conditions: (a) SOCl_2 , reflux, 2 h. (b) $\text{NH}_2\text{CH}_2\text{CH}_2\text{NH}_2$, Et_3N , CH_2Cl_2 , 48 h. (c) Et_3N , CH_2Cl_2 , 18 h. (d) K_2CO_3 , KI , DMF , 100°C , 16 h.

6.4 NMR studies

The structures of clips **2-4** in CDCl_3 were investigated with the help of ^1H NMR spectroscopy. The ^1H NMR spectra of both **2** and **3** displayed two overlapping triplets in a 2:1 ratio at ca. 3.95 ppm, corresponding to the aryloxymethylene protons in the *meta* and *para* positions, respectively. The slightly upfield shifted signal of the latter protons is attributed to electronic factors.⁷ Compared to the signals of model compound **10**, the aryloxymethylene proton signals of **2** and **3** displayed no significant shifts, indicating that the two monodendron units of the clips in solution are not in close proximity. The ^1H NMR spectrum of **4** in CDCl_3 displayed three triplets at 3.92, 3.86, and 3.72 ppm for H_{a} , H_{a} and H_{a} (Figure 6.7a), with integrals in the ratio 4:3:2,

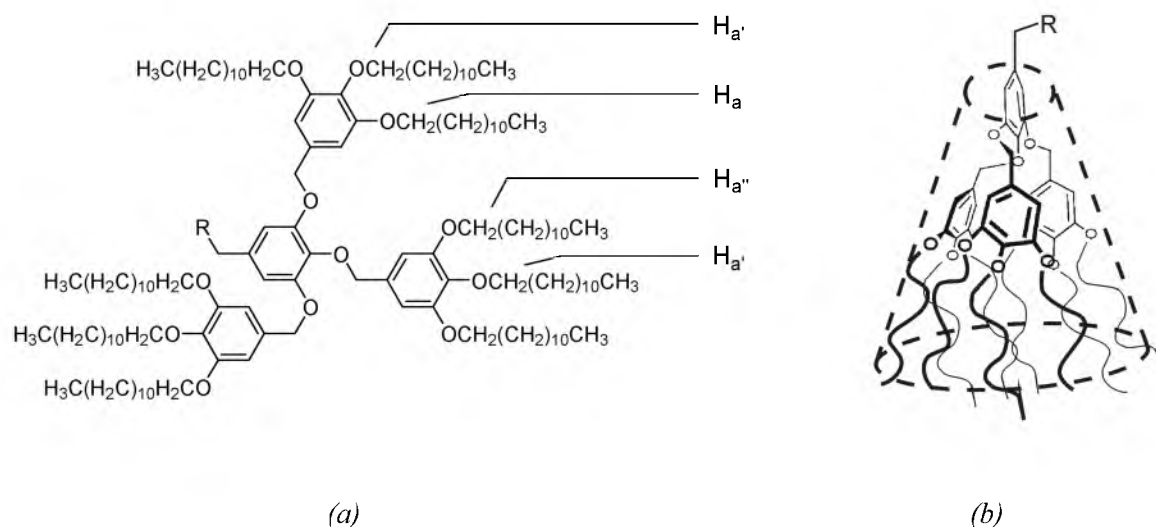


Figure 6.7 (a) Proton numbering of the second generation monodendron substituent of clip **4**. (b) Cone-like shape of this substituent.

respectively. The signal arising from $H_{a'}$ at 3.92 ppm is slightly shifted upfield compared to the signal in the model compound **10**, whereas the remaining signals are shifted upfield by 0.07 (H_a) and 0.21 ($H_{a''}$) ppm, respectively. These nuclei are shielded due to their close proximity ($< 5 \text{ \AA}$ based on molecular models) to the center of the anisotropic shielding zone of the two flanking aromatic units. A similar effect plays a role in the case of the H_a protons in relation to the central aromatic ring. However, in this case the magnitude of the shielding is decreased due to the free rotation of the peripheral aromatic rings around their $C_{Ar}-CH_2$ bonds, which increases the average distance of H_a from the central aromatic ring.⁷ These results provide strong evidence that the monodendron attached to **4**, in contrast to those attached to **3**, adapt a conical shape in solution (Figure 6.7b).

The self-association properties of the clips in solution were investigated by ^1H NMR dilution titrations in chloroform. Clips **3** and **4** appeared to dimerize through mutual cavity filling. The dimerization constants, $K_{\text{dimer}} = 16 \pm 5 \text{ M}^{-1}$ for **3**, and $K_{\text{dimer}} = 18 \pm 5 \text{ M}^{-1}$ for **4**, are similar to the dimerization constant of **1** in CDCl_3 ($K_{\text{dimer}} = 18 \pm 5 \text{ M}^{-1}$). The self-assembling behaviour of **2** in CDCl_3 appeared to be more complex. An unusually high self-association constant $K_{\text{self}} = 190 \pm 50 \text{ M}^{-1}$ was measured. It is not likely that the cavity of **2** differs structurally from the cavities of **1**, **3** and **4**, hence additional interactions between the molecules of **2** must play a role. During the titration shifts in the signals of the NH protons were observed and it is proposed, therefore, that intermolecular hydrogen bonding interactions are the reason for the increase in self-association strength. This was confirmed by molecular modeling calculations, which revealed that multiple hydrogen bonding interactions are possible between the diamide linkers of adjacent dimers of **2** (Figure 6.8), and hence arrays of clip molecules can be formed.

6.5 Physical properties of clips with tapered monodendrons

6.5.1 Thermal behaviour

Upon cooling a sample of **2** from the isotropic melt, thermal optical polarized microscopy (TOPM) revealed the very slow formation (only observed at a cooling rate of 1°C min^{-1}) of a microcrystalline texture reminiscent of a highly ordered smectic mesophase.¹⁷ However, only a

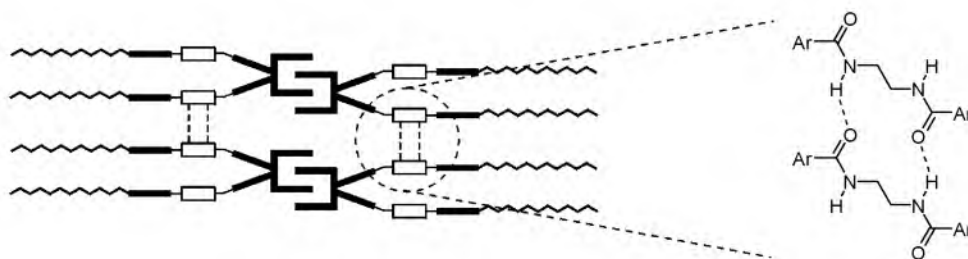


Figure 6.8 Schematic representation of the proposed self-assembly of molecules of **2** in CDCl_3 via cavity dimerization and intermolecular hydrogen bonding. In principle, in this way long chains of hydrogen-bonded dimers can be formed.

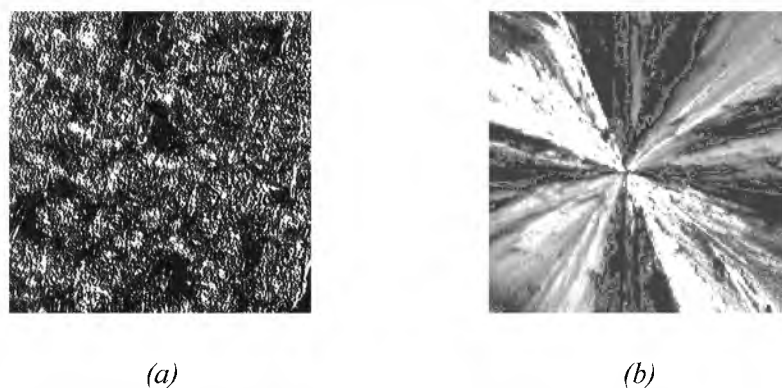


Figure 6.9 Textures observed by thermal optical polarized microscopy for (a) clip **2** and (b) clip **3**.

Table 6.1 Phase transition temperatures and enthalpies of hosts **2** and **3**, and of the 1:1 host-guest complex of **3** and **MDB**.

Host	Transition ^a	T ($^{\circ}\text{C}$) ^b	ΔH (kJ mol^{-1}) ^b
2	$\text{K} \rightarrow \text{I}$	191.3 (—) ^c	51.90 (—) ^c
3	$\text{K} \rightarrow \text{K}^1$	-33.1 (-39.7)	14.92 (-57.69)
	$\text{K}^1 \rightarrow \text{I}$	134.0 (71.5)	34.04 (-14.58)
3:MDB	$\text{K} \rightarrow \text{K}^1$	-14.0 (-25.2)	6.44 (-6.59)
	T_g	24 (—) ^c	
	$\text{K}^1 \rightarrow \text{I}$	106.0 (52.3)	28.66 (-5.05)

^a K , K^1 : crystalline phases; I : isotropic phase. ^bDetermined by DSC at a temperature rate of $1^{\circ}\text{C min}^{-1}$, values obtained from the second heating run; in parenthesis: values obtained from the first cooling run. ^cNo transition was observed.

relatively low birefringence was observed (Figure 6.9a). Upon heating the sample from room temperature, isotropization occurred at 192°C . Over the whole temperature trajectory up to isotropization, the material remained completely solid upon shearing. The corresponding DSC thermogram showed only one broad endotherm in the heating run at 191.3°C , whereas in the cooling run no transitions were observed (Table 6.1).

Upon cooling a sample of **3** from the isotropic melt at a rate of $10^{\circ}\text{C min}^{-1}$, TOPM showed no evolution of a texture. Instead, the viscosity of the material gradually increased until

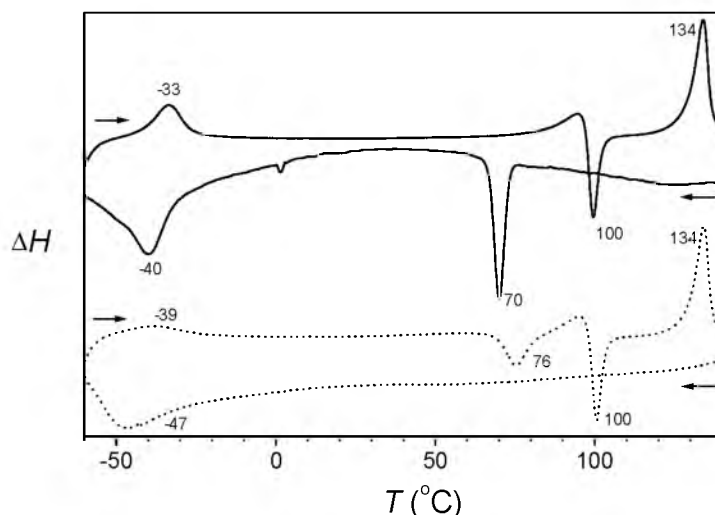


Figure 6.10 DSC thermograms of the first cooling run and second heating run of clip **3** taken at temperature rates of $2^{\circ}\text{C min}^{-1}$ (solid line) and at $10^{\circ}\text{C min}^{-1}$ (dashed line).

solidification into a glassy material occurred at approximately 75°C . When, however, upon cooling the sample was extensively annealed (> 24 h) at 125°C , a birefringent, spherulitic texture, which at the edges was surrounded by viscous glassy domains very slowly evolved (Figure 6.9b). The material was not malleable, and upon sheering the thin film cracked, indicating a crystalline nature of the material. Upon further cooling (at $10^{\circ}\text{C min}^{-1}$) after annealing, the viscous glassy domains surrounding the texture solidified at 75°C . In the consecutive heating run, the material became slightly malleable at 74°C , whereafter at 78°C polymorphous regions evolved at the edges of the glassy domains and solidification of the sample occurred. At 97°C the material became fully malleable, and at slightly higher temperature the glassy domains turned into a smectic-like texture. Isotropization occurred at 133°C . The DSC thermogram of **3** recorded at a temperature rate of $10^{\circ}\text{C min}^{-1}$ (Figure 6.10, dashed traces) showed only one transition in the first cooling run, *viz.* at -47°C . Upon heating, the TOPM-observed solidification at 78°C was visible as a negative peak (cold crystallization) at 76°C in the DSC spectrum. The second cold crystallization exotherm visible at 100°C is related to the malleable structure observed by TOPM at 97°C and was followed by isotropization at 134°C . The two cold crystallization exotherms indicate that the material was cooled at a too fast rate to allow a complete ordering of the molecules. When the DSC thermogram was recorded at a temperature rate of $2^{\circ}\text{C min}^{-1}$, a different thermal behavior was observed (Figure 6.10, solid traces). In the cooling run, a clear exotherm related to the TOPM-observed solidification was observed at 70°C . In the subsequent heating run, only one of the two exotherms due to cold crystallization remained (at 100°C), and isotropization occurred at 134°C . The remaining cold crystallization exotherm could be further reduced by carrying out the cooling and heating run at an even lower temperature rate, (*i.e.* $0.5^{\circ}\text{C min}^{-1}$).

The large endotherm involved with isotropization suggests that **3** is crystalline throughout its whole temperature range. This was confirmed by variable temperature X-ray powder diffraction (XRPD) measurements of the compound, which showed sharp, complex X-ray patterns characteristic of crystalline materials. When the sample was quickly cooled from the isotropic melt (at a rate of $10^{\circ}\text{C min}^{-1}$), a more simple X-ray pattern resulted with a relatively low number of reflections. Upon heating the sample to 100°C a complex diffraction pattern was obtained

again, indicative of a rearrangement of the molecules into a more organized state. This apparent ordering corresponds to the second cold crystallization exotherm observed in the DSC thermogram. When the sample was slowly cooled ($1^{\circ}\text{C min}^{-1}$) from the isotropic melt, a complex diffraction pattern with many reflections was obtained. Although several low-angle reflections were found, neither a set of equally spaced reflections, indicative of a long-range lamellar ordering similar to that observed for **1**, nor low-angle reflections in a spacing ratio of 1: $1/\sqrt{3}$: $1/2$, attributable to an ordering in a hexagonal lattice, were observed.

6.5.2 Ordering of the clips

Ordering of the molecules of 2

The smectic-like texture in combination with the non-malleability of **2** suggests that the material is highly ordered and crystalline. This behaviour was confirmed by the enthalpy change involved with isotropization of the compound, which is even higher than the isotropization enthalpy of clip **1**¹⁴ and of the related compound **3** (Table 6.1). The high enthalpy value can be explained if the amide functions of **2** form extended intermolecular hydrogen bonding networks.¹⁸ Well-defined intermolecular hydrogen bonding has been reported for other diamide functionalized tapered monodendrons,¹⁹ and support for such interactions between the molecules of **2** comes from the ^1H NMR studies of **2** in chloroform (see section 6.4). Upon dilution or addition of methanol to the solution, much simpler NMR spectra were obtained. In the solid state, hydrogen bonding interactions were confirmed by reflectance infrared spectroscopy studies on a thin film of the compound. After cooling the sample from the isotropic melt, four N-H stretching vibrations were visible at 3450, 3435, 3370 and 3322 cm^{-1} , of which the latter two vibrations suggest hydrogen bonding.²⁰ Also the wave number of the urea carbonyl stretching vibration (1718 cm^{-1}) indicated the occurrence of hydrogen bonding interactions between the molecules of **2**. These results indicate that the self-assembly pattern of **2** in the solid state is very complex. Powder diffraction experiments will be needed to further elucidate the exact ordering of the molecules of **2**.

Ordering of the molecules of 3

The large enthalpy involved with isotropization of **3** indicates that this compound is crystalline. From the observed spherulitic texture and malleability of the material it may tentatively be concluded that the molecules of **3**, like those of **2**, are arranged in arrays of stacked dimers. This ordering can be explained by assuming that the tapered monodendrons attached to **3** have an aligned arrangement. In this arrangement, the steric bulk from the tapered tails is only expressed in the direction perpendicular to the strongly π -stacked dimers, and it is very likely that the interactions between the aromatic rings of the tails make the packing even stronger (Figure 6.11). A remarkable aspect of the thermal behaviour of **3** is that the compound has difficulties to order itself. At a cooling rate of $10^{\circ}\text{C min}^{-1}$, **3** does not return to a crystalline state, but rather cools to an amorphous solid, without evidence of an exotherm in the DSC thermogram which corresponds to a crystallization event. At a low cooling rate, the crystallization exotherm is present, but the large degree of supercooling ($> 60^{\circ}\text{C}$) of the transition is evident of the difficult

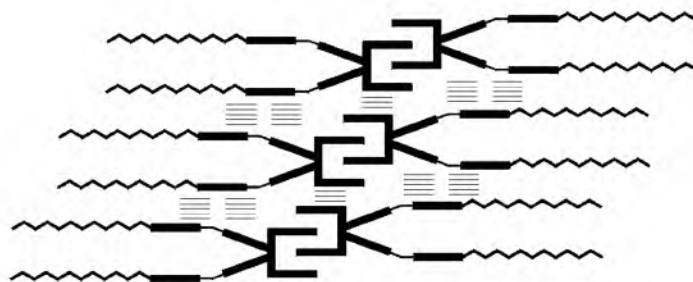


Figure 6.11 Proposed intermolecular ordering of the molecules of **3**. The π - π interactions between the aromatic rings of the dimers are highlighted. Only one of the alkyl tails of the monodendrons is shown for clarity reasons.

ordering.²¹ Similar difficulties in crystallization have been observed for related tapered monodendritic compounds.^{22,23} It has been rationalized that the presence of the alkyl chains, and in particular the *meta*-substituted ones, in combination with the high molecular weight of the compounds makes it difficult for the molecules to return to the crystalline state without extensive annealing.²² The 3-dimensional structure of **3** is sketched in Figure 6.12. Assuming that the molecules form dimers, their overall shape is that of a butterfly. It is not difficult to envisage that these ‘butterflies’, like the molecules of **1**, can form extended 2-dimensional sheets as a result of strong π - π interactions between the dimers.

In summary, it can be concluded that functionalization of a diphenylglycoluril clip with two first generation monodendrons does not induce liquid-crystallinity into the material. Bulkier alkyl tails are apparently required, as are present in clip **4**, which is functionalized with two second generation monodendrons. The behaviour of this compound will be described in Section 6.6.

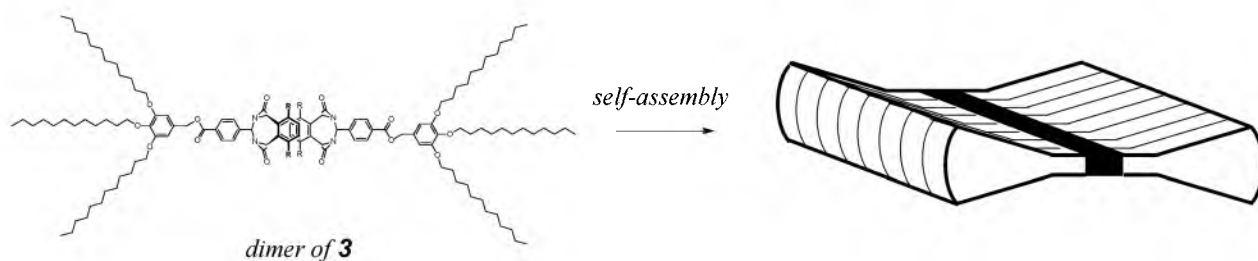


Figure 6.12 Butterfly-like shape of a dimer of **3** and the schematic ordering of its molecules into extended 2-dimensional sheets.

6.5.3 Host-guest complex of **3** and MDB

To investigate the consequences of disrupting the dimeric structure of **3**, dihydroxybenzene guest molecules were bound in its cavity. An equimolar mixture of the receptor and methyl 3,5-dihydroxybenzoate (**MDB**) was prepared by solvent evaporation of a solution of the two compounds in chloroform/methanol (4:1, v/v).²⁴ It was expected that dimerization of the clips would be inhibited and that a 1:1 host-guest complex would be quantitatively formed.²⁵

Upon cooling a sample of the complex from the melt (at a rate of $10^{\circ}\text{C min}^{-1}$), TOPM showed that its viscosity gradually increased without the appearance of a texture. When, however, the sample was annealed at 90°C for several hours, a non-malleable microcrystalline texture slowly evolved. Upon heating the sample from room temperature, isotropization occurred at 102 - 105°C . DSC analysis (Table 6.1) showed a broad exothermic transition at 52°C in the cooling run, which

could not be related to a process observed by TOPM. At -25°C a second exotherm, probably related to a glass-to-crystal transition, was observed. In the heating run, an endotherm at -14°C , due to the same crystal-to-glass transition was visible, followed by a T_g at 24°C . A cold crystallization was present at 58°C , followed by isotropization at 106°C . Repeated heating and cooling runs were identical, and no phase separation was observed, which is a strong indication that the host-guest complex of **3** and **MDB** is stable. In addition, the disappearance of the malleability, which was observed for uncomplexed **3**, suggests that the lamellar structure is disrupted due to binding of **MDB** within the cavity of the clip.

6.6 Physical properties of a clip with conical monodendrons

6.6.1 Thermal behaviour

Upon cooling a sample of **4** from the isotropic melt at a rate of $10^{\circ}\text{C min}^{-1}$, the appearance of a very viscous optically isotropic oil was observed by TOPM at circa 100°C . Further cooling led to a further increase in viscosity, until the material solidified into a glassy material at 93°C . Cooling of the sample at lower temperature rates or extensive annealing at various temperatures did not result in the formation of an anisotropic texture. When the sample was heated, a sudden change from a glassy material into a viscous optically isotropic liquid was observed at 94°C , followed by isotropization at 104°C . The DSC thermogram (Figure 6.13, Table 6.2) did not show any transitions relatable to the phenomena observed with TOPM in the cooling run. A large exotherm at -25°C was, however, clearly evident. Upon heating the sample from -65°C , a large endotherm at -16°C was observed, followed by a T_g at 73°C . Then a small exothermic transition at 95°C was visible, followed by an isotropization endotherm at 102°C . This correlates reasonably well with the temperature range in which the viscous isotropic liquid phase was observed by TOPM. Repeated cooling and heating runs were identical, which confirms that the observed phase transitions are reversible.

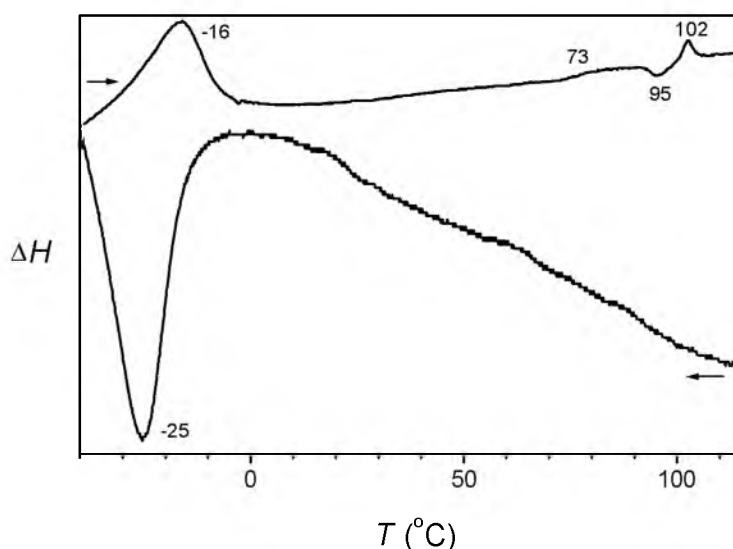


Figure 6.13 DSC thermogram of the first cooling run and second heating run of clip **4**.

Table 6.2 Observed phase transition temperatures and enthalpies of host **4**, and of the 1:1 host-guest complex of **4** and **MDB**.

Host	Transition ^a	T (°C) ^b	ΔH (kJ mol ⁻¹) ^b
4	K → K ¹	-15.8 (-24.8)	78.94 (-330.5)
	T_g	73 (—) ^c	
	K ¹ → Cub	94.74 (93) ^d	-0.97 (—) ^c
	Cub → I	102.4 (100) ^d	2.86 (—) ^c
4:MDB	K → K ¹	-19.6 (-31.6)	62.5 (-71.0)
	T_g	65 (49)	
	K ¹ → Cub	66 ^d (66) ^d	— ^c
	Cub → I	85 ^d (87) ^d	— ^c

^aK, K¹: crystalline phases; I: isotropic phase; Cub: cubic phase (tentative assignment). ^bDetermined by DSC at a temperature rate of 10°C min⁻¹, values obtained from the second heating run; in parenthesis: values obtained from the first cooling run. ^cNo transition was observed. ^dTransition only observed with TOPM.

6.6.2 Ordering of the molecules of **4**

For **4**, the observation of a viscous isotropic liquid is reminiscent of the behaviour of several other second generation monodendrons functionalized with methyl esters, carboxylic acids, etc.⁷ Its thermal properties also strongly resemble those of the polymers prepared from the styrene and methacrylate functionalized monodendrons shown in Figure 6.4b.¹³ This suggests that clip **4**, just like the aforementioned monodendrons, can form a cubic liquid-crystalline phase. The large transitions below 0°C are attributed to the melting and the crystallization of the alkyl tails, while the small exothermic peak at 95°C is associated with the formation of an enantiotropic cubic liquid-crystalline phase. Cubic phases are characterized by their optically isotropic textures and the consequence of the occurrence of this phase is that the molecules of **4**, in analogy to the other conical monodendritic compounds, are arranged in (pseudo)spherical assemblies over the whole measured temperature range. Because of the particular 3-dimensional shape of **4**, it is proposed that the clip head-groups are situated in the core of the spherical assembly and the conical monodendrons at the periphery forming a supramolecular dendrimer (Figure 6.14). The spherical assemblies can in turn organize themselves into a cubic lattice. A limited number of clip molecules (probably < 10) will be packed in such a supramolecular dendrimer, the formation of which is governed by van der Waals interactions between the alkyl tails and π -stacking interactions between the aromatic rings of the monodendrons and the clip head-groups.⁷ Additional evidence for the organization of **4** in a supramolecular dendrimer comes from the observation of a T_g -value that is higher than the observed melting temperature of the compound. Whilst the T_g in a single phase system is always lower than this temperature, they can be reversed in a microphase separated system as the cooperative motion of each phase is independent.¹³ In the case of **4**, melting and crystallization are associated with the alkyl tails, while the T_g is associated with the cooperative motion of the benzyl groups in the tails and with the interactions between the clip head-groups. No information about the precise organization of the clip head-groups within the core can be obtained from the thermal experiments, *i.e.* it remains unknown whether the cavities form dimers just like in the case of clips **1-3**. X-ray powder diffraction measurements, currently in progress, should provide conclusive evidence about the exact architecture of the self-assembly. These measurements should also give

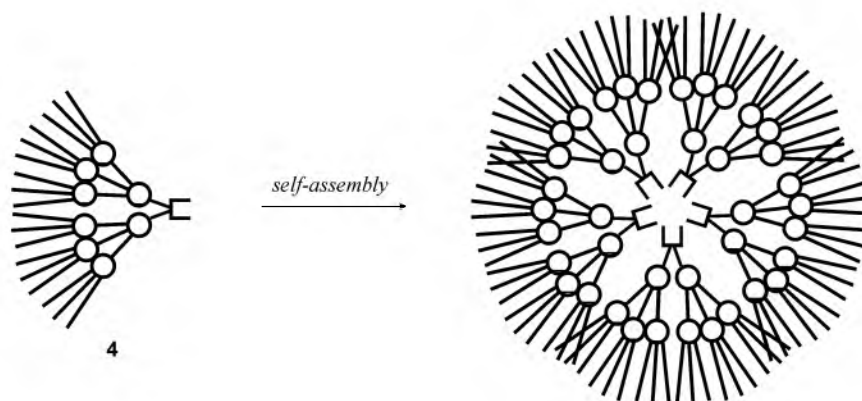


Figure 6.14 Schematic 2-dimensional representation of the self-assembly of clip molecule **4** into a spherical aggregate (supramolecular dendrimer), in which all the clip head groups are located in the core and the aliphatic tails at the periphery.

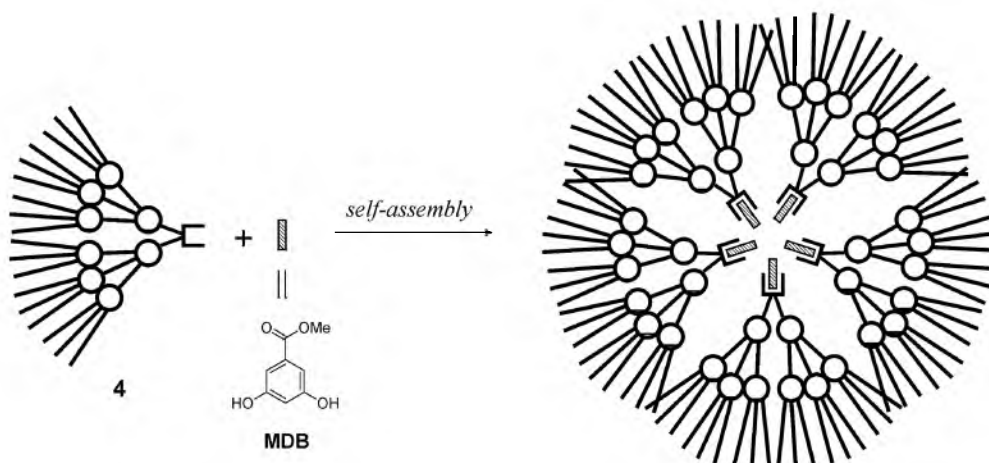


Figure 6.15 Schematic representation of the self-assembly of the host-guest complex of **4** and **MDB** into a supramolecular dendrimer, in which the guests are located in the core of the dendrimer.

information about the size of the spherical assemblies, which will in turn will enable the number of molecules of **4** in the assembly to be calculated.

6.6.3 Host-guest complex of **4** and **MDB**

If a limited number of clip molecules **4** are organized in a supramolecular dendrimer, it is of interest to investigate whether a strongly binding guest such as methyl 3,5-dihydroxybenzoate (**MDB**) can be complexed in the receptor cavities, while retaining the supramolecular dendritic structure (Figure 6.15). The 1:1 complex of **4** and **MDB** was prepared by slow evaporation of both components in a 4:1 (v/v) $\text{CHCl}_3/\text{MeOH}$ mixture, followed by cooling of the complex from the isotropic melt. The complex was studied by TOPM, which showed the appearance of an optically isotropic phase at 87°C upon cooling from the melt. The viscosity of this phase gradually increased until solidification into a glassy material occurred at 66°C . Upon heating the sample from room temperature, the glassy material turned viscous again at 66°C . This viscosity gradually decreased until isotropization occurred at 85°C . In the cooling run of the DSC thermogram (Figure 6.16, Table 6.2), no transitions related to the TOPM observed viscous phase were observed. However, a T_g at 49°C and a large exotherm at -32°C , related to crystallization of

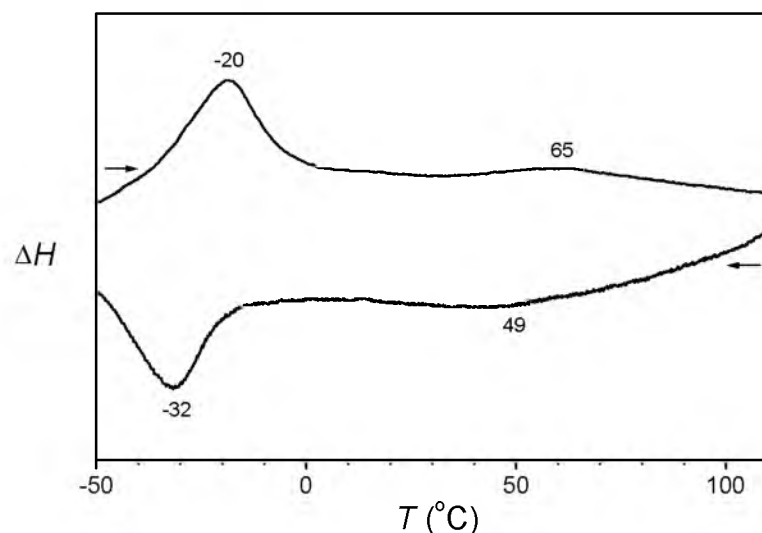


Figure 6.16 DSC thermogram of the first cooling run and second heating run of the 1:1 host-guest complex between **4** and **MDB**.

the glass, were evident. Upon heating, an endotherm at -20°C was visible, which is correlated to the crystal-to-glass transition. Although a T_g was observed at 65°C , no isotropization transition was visible by DSC. Repeated heating and cooling runs were identical, and the absence of phase separation suggests that the observed thermal behaviour can be attributed to the 1:1 host-guest complex.

The observation of an optically isotropic phase, in conjunction with the transitions observed in the DSC thermogram, together resembling the thermogram of uncomplexed **4**, suggests that the 1:1 host-guest complex of **4** and **MDB** also forms a supramolecular dendritic structure. Further evidence for the complexation of **MDB** within the cavities of **4** was obtained from reflectance FTIR measurements. The infrared spectrum of a thin film of uncomplexed **4** showed two absorptions due to the ester and urea carbonyl groups, at 1739 and 1721 cm^{-1} , respectively. In the sample of a thin film of the freshly prepared host-guest complex, neither of these vibrations was shifted. After heating the film to the isotropic melt, followed by slow cooling to 20°C , the ester carbonyl stretching vibration of **4** remained unaffected whereas the stretching vibration of the urea carbonyl function had shifted to 1718 cm^{-1} . In addition, the absorption due to the OH stretching vibration of **MDB** narrowed considerably, and shifted from 3381 to 3338 cm^{-1} . These shifts are indicative of a well-defined hydrogen bonding interaction between the two components, and the observed infrared values of the complex are almost identical to those observed for the solid-state host-guest complex between clip **1** and **MDB**.¹⁴

Although complexation of guests in **4** does not appear to severely influence the self-assembly behaviour of the clips in the supramolecular dendrimer, it can be foreseen that the size and probably also the shape of the dendritic spheres will be altered. The change in the transition temperature of the complex, compared to those of the free host support this assumption. The arrangement of the assemblies of the host-guest complex into a cubic lattice is expected to be more difficult for the host-guest complex than for the free host.

The ability of **4** to complex guests and still form supramolecular dendrimers can be of great practical interest. As can be seen in Figure 6.15, the bound guest molecules in such an assembly are in very close proximity. This opens up the possibility to use the assemblies of **4** as nanosized

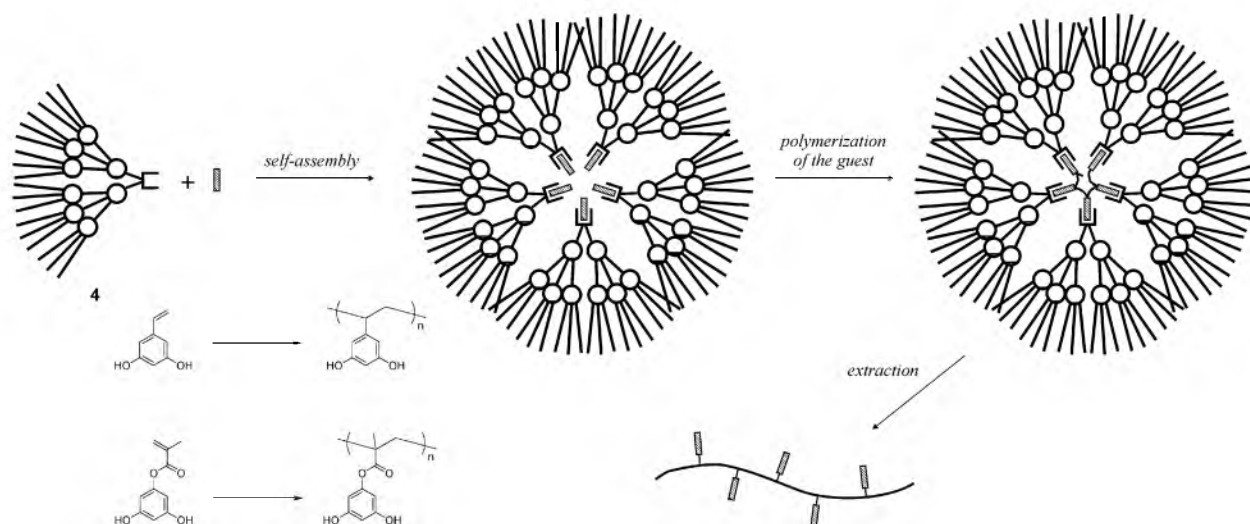


Figure 6.17 Schematic representation of the polymerization of guest molecules within a self-assembled molecular clip dendrimer.

reaction chambers, *e.g.* for the polymerization of bound guest molecules. In analogy to the polymerization of conical monodendrons (see Figure 6.4), guest molecules which are derivatized with *e.g.* vinyl or methacrylate functions can possibly be polymerized when they are complexed within a self-assembled supramolecular dendrimer of **4** (Figure 6.17). It will be particularly interesting to see whether the degree of polymerization can be controlled by the number of guests present in the superstructure. This would be an interesting method to prepare polymers or oligomers with a controlled size. After the polymerization reaction, it will be relatively easy to separate the components, *e.g.* by simple extraction of the hosts.²⁶ The latter then can be re-used in further reactions.

6.7 A library of monodendron-functionalized clips*

6.7.1 Introduction

In the previous section it was shown that by gradual expansion of the volume of the aliphatic tails connected to the clip molecules, the property of liquid-crystallinity could be introduced into the material. The critical size is reached when second generation monodendrons, which adopt a conical shape, are used. In the literature, a library of second generation monodendrons has been reported, differing in the number of tails connected to the peripheral benzene rings.²⁷ A selection of these monodendrons is shown in Chart 6.2. The effect of variation in the number and substitution pattern of the alkyl tails of the monodendrons on the liquid-crystalline properties is illustrated in the fact that the tapered monodendrons **12a** and **15a** form hexagonal phases, whereas the conical monodendrons **13a** and **14a** self-assemble into a cubic lattice. It was decided, therefore, to synthesize a library of clip molecules (Chart 6.3) which have the monodendrons shown in Chart 6.2 as tails. It was expected that in this way the liquid-crystalline properties of the clip molecules could be fine-tuned, and furthermore the number of clips required to form the supramolecular dendrimer architecture could be varied. The latter property

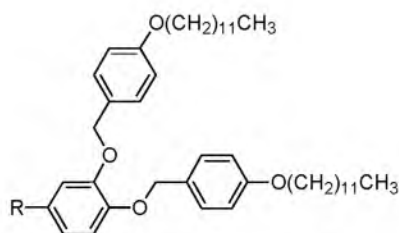
* This work was carried out in collaboration with the group of Professor Percec (Roy & Diana Vagelos Laboratories, Department of Chemistry, University of Pennsylvania, Philadelphia, USA).

is of particular interest with regard to the possible application of the hosts as reaction chambers for well-defined guest polymerization (see Section 6.6.3).

6.7.2 Synthesis

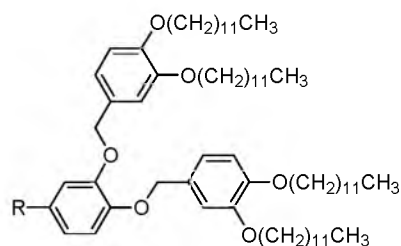
Clips **16-19** (Chart 6.3) were synthesized from clip **9** and monodendrons²⁷ **12b**, **13b**, **14b** and **15b**, respectively (Chart 6.2), following the same procedure as described for the synthesis of **3** and **4**. The clips were purified by column chromatography over basic alumina and subsequent recrystallization from acetone. The yields varied from 43 to 64%.

Chart 6.2



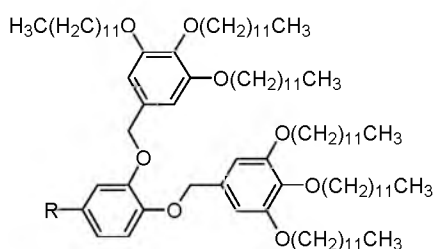
12a R = COOH

12b R = CH₂Cl



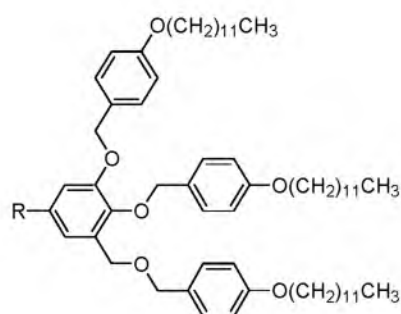
13a R = COOH

13b R = CH₂Cl



14a R = COOH

14b R = CH₂Cl



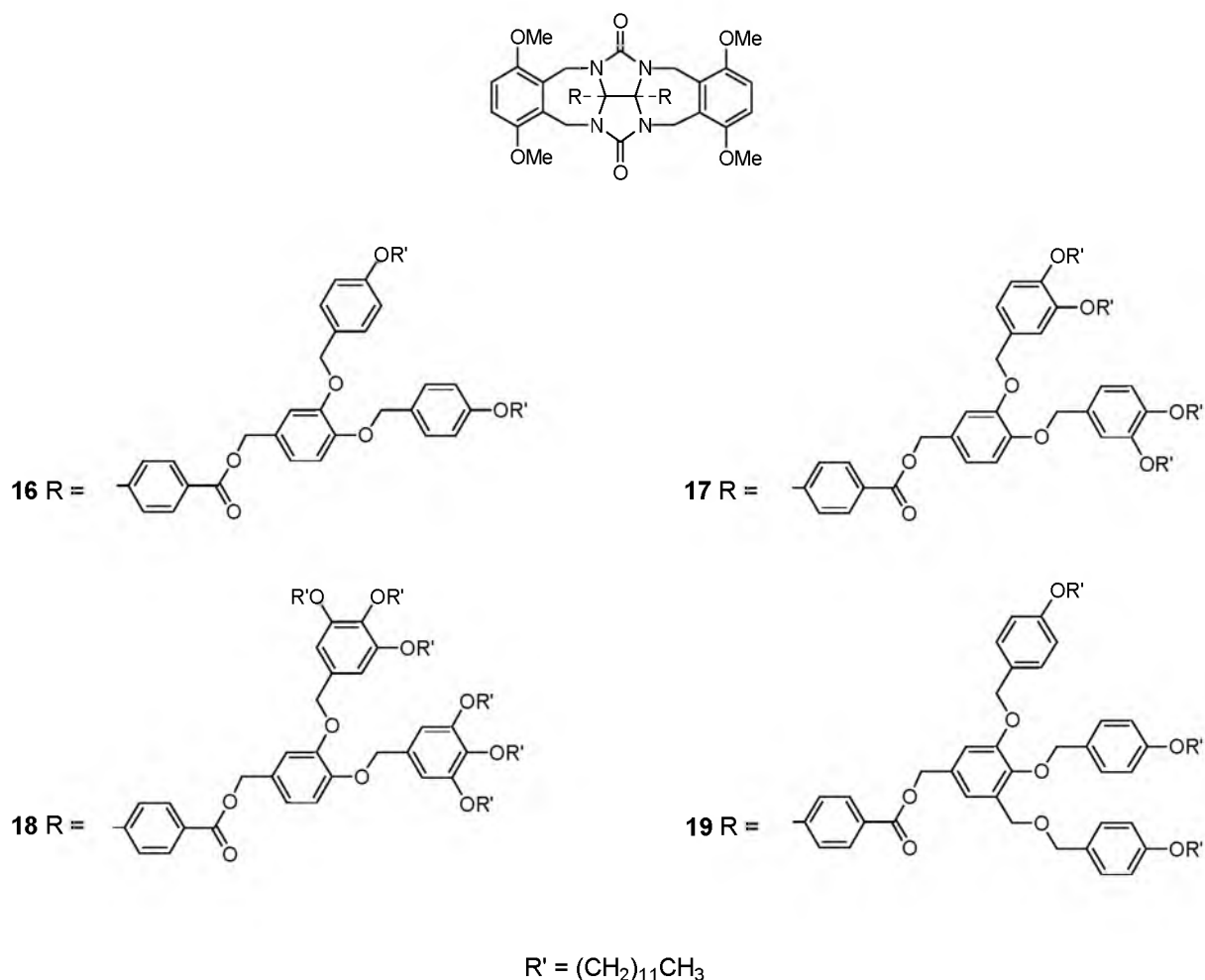
15a R = COOH

15b R = CH₂Cl

6.7.3 Thermal behaviour

The thermal behaviour of clips **16-19** was studied by TOPM. Upon cooling clip **16** from the isotropic melt, a birefringent, microcrystalline texture, which was not malleable upon the application of pressure, slowly started to evolve at 168°C. The texture remained unchanged until room temperature. Upon heating isotropization occurred at 181°C. Clips **17-19** showed a different thermal behaviour. When thin films of these three compounds were cooled from the isotropic melt, their viscosity gradually increased until a glassy material was formed. No birefringent textures were observed. Upon heating the samples from room temperature, the reverse behaviour was observed, *i.e.* at a certain temperature the viscosity of the material suddenly decreased and an isotropic oil was formed, until finally isotropization occurred.

Chart 6.3



The thermal behaviour of the compounds was further analyzed by DSC (Table 6.3). The large endotherm ($\Delta H = 45.7$ kJ/mol) observed for the isotropization of **16** at 181°C is in agreement with the texture visible by TOPM in the sense that the material is probably crystalline. The DSC thermograms of clips **17-19** are shown in Figure 6.18. They all show broad melting and crystallization transitions below 0°C , similar to those exhibited by clip **4** (see Section 6.6.1). The endotherms corresponding to isotropization are relatively small, and in the case of **18** this transition is not observed at all. Both **17** and **18** clearly exhibit glass transitions in their heating runs, at 100 and 61°C , respectively.

6.7.4 Ordering of the clips

The exact molecular ordering of clips **16-19** can only be elucidated by powder diffraction measurements. Based on the combination of TOPM and DSC observations, some speculations about the ordering of the clips can, however, already be made. It is not particularly surprising that compound **16** exhibits crystalline behaviour, since the two monodendrons attached to this clip each contain only two alkyl tails. The melting point of the clip (181°C) is, however, much higher than the melting point of the corresponding monodendron **12a** (77°C).²⁷ This implies that there are additional strong interactions between the molecules of **16**, which can be understood if

Table 6.3 Observed phase transition temperatures and enthalpies of hosts **16–19**.

Host	Transition ^a	<i>T</i> (°C) ^b	ΔH (kJ mol ⁻¹) ^b
16	K → K ¹	95.0 (90.2)	2.1 (-1.68)
	K ¹ → I	181.0 (161.4)	45.7 (-39.1)
17	K → K ¹	-17.8 (-29.0)	11.9 (-16.8)
	<i>T</i> _g	100 (—) ^c	— ^c
	K ¹ → Cub	105 ^d (106) ^d	— ^c
	Cub → I	118.3 (115.8)	2.1 (-9.7) ^e
18	K → K ¹	-27.1 (-38.3)	31.6 (-33.6)
	<i>T</i> _g	61 (—) ^c	— ^c
	K ¹ → Cub	73 ^d (72) ^d	— ^c
	Cub → I	95 ^d (92) ^d	— ^c
19	K → K ¹	-26.0 (-36.7)	15.4 (-48.9)
	K ¹ → Cub	97 ^d (90) ^d	— ^c
	Cub → I	100.3 (83.4)	9.0 (-13.1) ^e

^aK, K¹: crystalline phases; I: isotropic phase; Cub: cubic phase (tentative assignment). ^bDetermined by DSC at a temperature rate of 10°C min⁻¹, values obtained from the second heating run; in parenthesis: values obtained from the first cooling run. ^cNo transition was observed. ^dTransition only observed with POM. ^eOverlapping peaks.

the molecule forms dimers with a butterfly-like structure, similar to clip **3** (see Section 6.5). As a result of these strong interactions, extended 2-dimensional sheets can be expected to be formed by the dimeric units, resulting in a relatively high melting point and a high transition enthalpy. The occurrence of viscous optically isotropic phases, in combination with the observed series of transitions in the DSC thermograms, are a strong indication that clips **17–19** form cubic liquid-crystalline phases. The presence of *T*_g values at a higher temperature (in the case of **17** and **18**) than the melting transition points to a microphase separated nature of the molecular assemblies,¹³ implying that, in analogy to **4**, the molecules are probably organized in supramolecular dendrimers in which the clip head-groups are situated in the core and the alkyl tails at the periphery. Monodendrons **13a** and **14a** exhibit similar cubic liquid-crystalline phases and also similar isotropization points as the corresponding clips **17** and **18**. This indicates that the monodendrons and the clips self-organize as a result of the same factors, *i.e.* van der Waals interactions between the alkyl tails and the aromatic rings. In contrast to clips **17** and **18** and their respective monodendrons, monodendron **15a** exhibits a hexagonal liquid-crystalline phase (characterized by its anisotropic texture and by powder diffraction²⁷), whereas the corresponding clip **19** appears to self-assemble in an optically isotropic cubic phase. This difference in molecular organization might be attributed to the fact that in clip **19** two of the monodendritic units are in relatively close proximity to each other. Because of this they apparently cannot adopt a tapered shape anymore. As a result, **19** adopts a more conical shape, which is reflected in the fact that this compound exhibits a cubic phase.

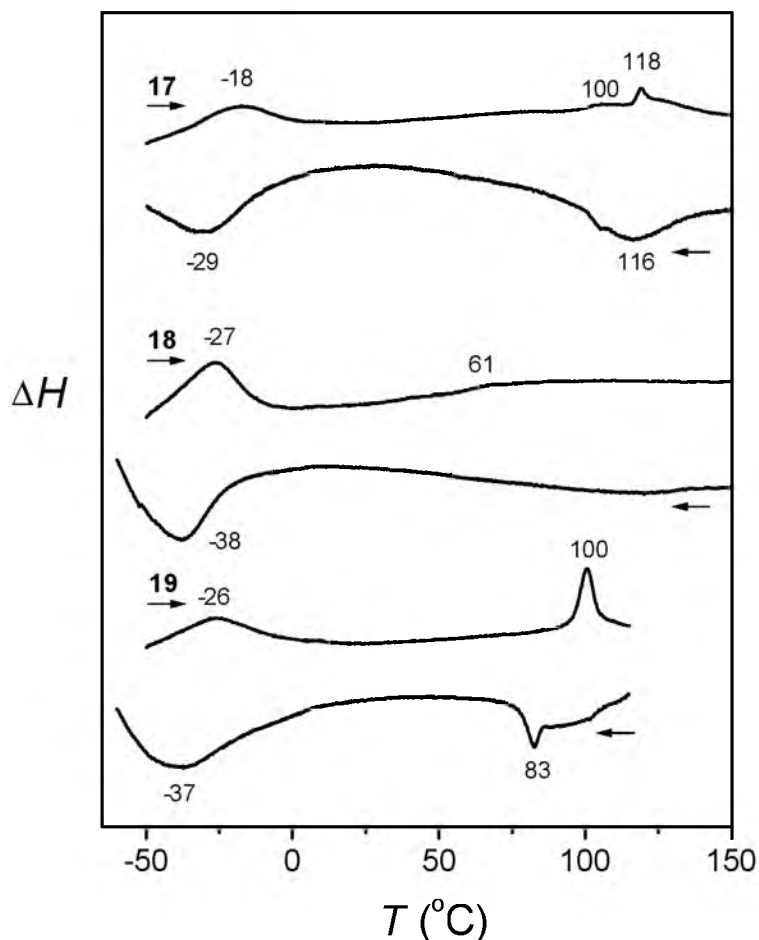


Figure 6.18 DSC thermograms of the first cooling run and second heating run of clips **17**, **18** and **19**.

6.8 Concluding remarks

In order to induce liquid-crystallinity in clips derived from diphenylglycoluril, the volume of the alkyl tails at the back of these molecules was gradually increased. When the clips were functionalized with two first generation monodendrons, which adopt a tapered shape, no liquid-crystallinity was observed, probably because the tails are not bulky enough to counterbalance the strong π - π interactions between the clip head groups. The desired effect was achieved, however, by functionalizing the clips with two *second* generation monodendrons. Due to the bulky conical shape of these units, strong π - π interactions between the clip head groups are no longer possible. Comparison of the physical properties of the compound with those of related compounds described in the literature revealed that the molecules probably arrange themselves in the form of supramolecular dendrimers. The latter dendrimers further organize themselves into rarely observed thermotropic cubic phases. The cavities of the clips in the core of the self-assembled dendrimers appear to be able to complex small guests. This opens the possibility to use the supramolecular dendrimers as confined reaction chambers, *e.g* for the controlled polymerization of polymerizable guests.

6.9 Experimental section

6.9.1 Materials and Methods

DMF was dried over BaO for one week and then vacuum distilled; the first 30% of the distillate was discarded. Dichloromethane was distilled over CaH₂. K₂CO₃ and KI were dried in an oven (150°C). Methyl 3,5-dihydroxybenzoate was recrystallized from CHCl₃. All other chemicals were used without further purification. Thermal behavior was observed under crossed polarizers using a Jeneval polarizing optical microscope connected to a Linkam THMS hot stage. Differential scanning calorimetry thermograms were recorded on a Perkin Elmer DSC 7 instrument. ESI-MS spectra were recorded on a Perkin Elmer-Sciex API 300 MS/MS mass spectrometer at the University of Eindhoven. MALDI-TOF-MS spectra were performed with a dihydroxybenzoic acid matrix on a PerSeptive Biosystems Voyager-DE-RP MALDI-TOF mass spectrometer at the Institute for Mass-Spectrometry at the University of Amsterdam. ¹H NMR dilution titrations were carried out as described in Section 3.5.2. For an overview concerning other general techniques see Section 2.6.1.

6.9.2 Thermal optical polarized microscopy and differential scanning calorimetry experiments

Approximately 5-10 mg of a clip compound was used in the DSC experiments. In the case of host-guest complexes, an amount of 5-10 mg of clip and an equimolar quantity of guest were dissolved in a mixture of CHCl₃ and MeOH (4:1, v/v). The solvent mixture was evaporated overnight under a stream of nitrogen while heating the mixture on a water bath at 40°C. Samples were studied using a polarizing microscope with crossed polarizers. DSC samples were prepared in stainless-steel large volume pans (75 µL). Unless otherwise indicated, thermograms were recorded at 10°C min⁻¹, and repeated heating and cooling runs were measured to study the stability of the material and the reproducibility of the transitions. Transition temperatures and enthalpies were generally determined from the first cooling and second heating scans.

6.9.3 Reflectance infrared experiments

Infrared samples of clip **4** and its host-guest complex with **MDB** were prepared by evaporating a drop of a CHCl₃ solution (2 mM) of the compound or complex on a gold sputtered cover glass. The resulting thin film was dried in a desiccator. Reflectance infrared spectra of the samples were recorded on a BioRad FTS-25 spectrometer with a resolution of 2.0 cm⁻¹. Spectra of the sample were taken before and after heating and subsequent cooling of the sample from the isotropic melt, which was carried out on the polarization microscope as described in section 6.9.2. The angle between the sample and the infrared beam was varied between 15 and 65°. For each spectrum 64 scans were recorded, and the optical bench of the IR apparatus was continuously purged with nitrogen. Data analysis was performed using the WIN-IR software.

6.9.4 Syntheses

The syntheses of compounds **8** and **9** have been described in Chapters 5 and 2, respectively.

N-1-(2-((4-(1,4,8,11-Tetramethoxy-6,13-dioxo-13b-(4-(((2-((1-(3,4,5-tri(dodecyloxy)phenyl)vinyl)amino)-ethyl)amino)carbonyl)phenyl)-5,7,12,13b,13c,14-hexahydro-5a,6a,12a,13a-tetraazabenz[5,6]azuleno[2,1,8-*ij*a]benzo[*f*]azulen-13-yl)benzoyl)amino)ethyl)-3,4,5-tri(dodecyloxy)benzamide (**2**):

Triethylamine (3 drops) was added to a degassed solution of **7** (229 mg, 0.319 mmol) and **8** (102 mg, 0.137 mmol) in dichloromethane (10 mL). The solution was stirred under argon for 18 h, extracted with aqueous 1 N HCl (50 mL) and the organic layer was evaporated to dryness. The residue was purified by column chromatography (first column: silica, CH₂Cl₂ /MeOH, 98:2 (v/v), second column: silica, EtOAc/hexane, 92:8, v/v). The product was dissolved in a minimal amount of chloroform and this solution was added dropwise to stirred methanol. After filtration, 265 mg (38%) of **2** was obtained as a white powder.

M.p. 192 °C; IR (KBr pellet): ν 3321 (NH), 2924, 2853 (CH₂), 1721 (urea C=O) cm⁻¹; ¹H NMR (CDCl₃ with 1 drop of CD₃OD, 300.13 MHz): δ 7.79 (s, 2H, NH), 7.45 (d, 4H, ArH glycoluril *ortho* to C(O)NH, ³J = 8.4 Hz), 7.06 (d, 4H, ArH *meta* to C(O)NH, ³J = 8.4 Hz), 6.99 (s, 4H, [OR]₃ArH), 6.76 (s, 2H, NH), 6.66 (s, 4H, ArH side-wall), 5.48 (d, 4H, NCH₂Ar *out*, ²J = 16.0 Hz), 3.93 (t, 12H, OCH₂, ³J = 5.3 Hz), 3.71 (s, 12H, OCH₃), 3.67 (d, 4H, NCH₂Ar *in*, ²J = 16.0 Hz), 3.45 (m, 8H, NCH₂), 1.76 (m, 12H, OCH₂CH₂), 1.26 (s, 108H, (CH₂)₉CH₃), 0.88 (t, 18H, CH₂CH₃, ³J = 6.6 Hz) ppm; ESI-MS: *m/z* 2106 (M + H)⁺. Anal. Calcd for C₁₂₈H₁₉₈N₈O₁₆: C, 73.04; H, 9.48; N, 5.32. Found: C, 72.84; H, 9.70; N, 5.16.

3,4,5-Tri(dodecyloxy)benzyl 4-(1,4,8,11-tetramethoxy-6,13-dioxo-13b-[4-((3,4,5-tri(dodecyloxy)benzyl)oxycarbonyl)phenyl]-5,7,12,13b,13c,14-hexahydro-5a,6a,12a,13a-tetraazabenz[5,6]azuleno[2,1,8-*ija*]benzo[*f*]-azulen-13-ylbenzoate (3):

Compound **9** (100 mg, 0.14 mmol) and K_2CO_3 (0.20 g, 1.42 mmol) were suspended in DMF (10 mL). The suspension was purged with nitrogen for 15 min., **10** (380 mg, 0.57 mmol) was added and the mixture was stirred at 100°C for 16 h. After cooling, aqueous 1 N HCl (300 ml) was added and the aqueous layer was extracted with $CHCl_3$ (2 x 50 ml). The organic layer was washed with water (300 ml), evaporated to dryness and the residue was recrystallized from methanol to yield 282 mg (33%) of **3** as a cream-white powder.

M.p. 136°C; IR (KBr pellet) ν 2980-2830 (CH_2), 1739 (ester C=O), 1721 (urea C=O), 1576, 1559, 1540, 1486, 1459, 1438, 1425 (C=C), 1307, 1264, 1218 (CH_2), 1108, 1080 (COC) cm^{-1} ; 1H NMR ($CDCl_3$, 300.13 MHz): δ 7.77 (d, 4H, ArH *ortho* to C(O)OCH₂Ar, $^3J = 8.5$ Hz), 7.16 (d, 4H, ArH *meta* to C(O)OCH₂Ar, $^3J = 8.5$ Hz), 6.65 (s, 4H, ArH side-wall), 6.59 (s, 4H, ArH *ortho* to CH₂OC(O)Ar), 5.54 (d, 4H, NCH₂Ar *out*, $^2J = 16.0$ Hz), 5.16 (s, 4H, C(O)OCH₂), 3.95 (m, 12H, OCH₂ *meta* and *para* to CH₂C(O)OAr), 3.75 (s, 12H, OCH₃), 3.72 (d, 4H, NCH₂Ar *in*, $^2J = 16.0$ Hz), 1.78 (m, 12H, OCH₂CH₂), 1.46 (m, 12H, OCH₂CH₂CH₂), 1.27 (m, 96H, O(CH₂)₃(CH₂)₈CH₃), 0.88 (m, 18H, CH₂CH₃) ppm; $^{13}C\{^1H\}$ NMR ($CDCl_3$, 50.33 MHz): δ 165.60 (ester C=O), 157.48 (urea C=O), 153.20 (ArC *meta* to CH₂OC(O)Ar), 151.03 (ArC *ipso* to OCH₃), 139.37 (ArC *ipso* to C(O)OCH₂Ar), 138.29 (ArC *ipso* to CH₂OC(O)Ar), 131.21 (ArC *para* to CH₂OC(O)Ar), 130.44 (ArC *para* to C(O)OCH₂Ar), 129.96 (ArC *ortho* to C(O)OCH₂Ar), 128.19 (ArC *meta* to C(O)OCH₂Ar), 127.06 (ArC *ipso* to CH₂N), 111.09 (ArCH *ortho* to OCH₃), 107.10 (ArC *ortho* to CH₂OC(O)Ar), 84.80 (NC(Ar)N), 73.43 (OCH₂CH₂ 4-position), 69.14 (OCH₂CH₂ 3- and 5-positions), 67.39 (CH₂OC(O)Ar), 56.79 (OCH₃), 36.93 (NCH₂Ar), 31.92 (CH₂CH₂CH₃), 30.33 (OCH₂CH₂), 29.66 (O(CH₂)₃(CH₂)₅(CH₂)₃CH₃), 29.43 (CH₂(CH₂)₂CH₃), 26.13 (O(CH₂)₂CH₂), 22.68 (CH₂CH₃), 14.11 (CH₂CH₃) ppm; FAB-MS m/z 1993 (M + H)⁺. Anal. Calcd for C₁₂₄H₁₉₀N₄O₁₆: C, 74.73; H, 9.61; N, 2.81. Found C, 74.57; H, 9.71; N, 2.87.

3,4,5-Tri((3,4,5-tri(dodecyloxy)benzyl)oxy)benzyl 4-(1,4,8,11-tetramethoxy-6,13-dioxo-13b-(4-(((3,4,5-tri((3,4,5-tri(dodecyloxy)benzyl)oxy)benzyl)oxy)carbonyl)phenyl)-5,7,12,13b,13c,14-hexahydro-5a,6a,12a,13a-tetraazabenz[5,6]azuleno[2,1,8-*ija*]benzo[*f*]azulen-13-ylbenzoate (4):

A suspension of **9** (50 mg, 0.071 mmol) and K_2CO_3 (125 mg, 0.90 mmol) in DMF (10 ml) was stirred for 15 min. Compound **11** (566 mg, 0.26 mmol) was added and the mixture was stirred overnight at 120 °C. After cooling, aqueous 1 N HCl (300 ml) was added and the aqueous layer was extracted with $CHCl_3$ (2 x 50 ml). The organic layer was washed with water (300 ml), evaporated to dryness, and the residue was purified by column chromatography (silica, EtOAc/*n*-hexane, 86:15, v/v, $R_f = 0.08$). The product was recrystallized from acetone to yield 145 mg (42%) of **4** as a cream-white powder.

Isotropization point: 102°C; IR (KBr pellet) ν 2980-2840 (CH_2), 1739 (ester C=O), 1721 (urea C=O), 1576, 1559, 1540, 1486, 1459, 1438, 1425 (C=C), 1307, 1264, 1218 (CH_2), 1108, 1080 (COC) cm^{-1} ; 1H NMR (300.13 MHz, $CDCl_3$) δ 7.78 (d, 4H, ArH *ortho* to CO₂CH₂Ar, $^3J = 8.5$ Hz), 7.19 (d, 4H, ArH *meta* to CO₂CH₂Ar, $^3J = 8.5$ Hz), 6.73 (s, 4H, ArH side-wall), 6.69 (s, 4H, ArH *ortho* to CH₂, 4-position), 6.61 (s, 8H, ArH *ortho* to CH₂, 3,5-positions), 6.59 (s, 4H, ArH *ortho* to CH₂O₂CAr), 5.54 (d, 4H, NCHHAr (*out*), $^2J = 15.9$ Hz), 5.17 (s, 4H, CO₂CH₂), 4.98 (s, 8H, ArCH₂OAr, 3,5-positions), 4.94 (s, 4H, ArCH₂OAr, 4-position), 3.92 (t, 12H, CH₂OAr 3,4,5-(4') positions, $^3J = 6.5$ Hz), 3.86 (t, 16H, CH₂OAr 3,5-(3', 5') positions, $^3J = 6.5$ Hz), 3.76 (overlapping peaks, 24H, NCH₂Ar *in*, OCH₃ and CH₂OAr 4-(3', 5') position), 1.71 (m, 36H, OCH₂CH₂), 1.27-1.46 (m, 324H, (CH₂)₉CH₃), 0.86 (t, 54H, CH₂CH₃, $^3J = 6.4$ Hz) ppm; $^{13}C\{^1H\}$ NMR (50.33 MHz, $CDCl_3$): δ 165.60 (CO₂CH₂), 157.42 (urea C=O), 153.25 (ArC *meta* to CH₂O(CO)Ar), 153.25 (ArC *meta* to CH₂, 3,5-positions), 153.05 (ArC *meta* to CH₂, 4-position), 151.25 (ArC *ipso* to OMe), 139.58 (ArC *ipso* to CO₂CH₂Ar), 138.73 (ArC *ipso* to CH₂O(CO)Ar), 137.82 (ArC *ipso* to CH₂OAr), 132.70 (ArC *para* to CH₂OAr, 4-position), 131.87 (ArC *para* to CH₂OAr, 3,5-positions), 131.21 (ArC *para* to CH₂O(CO)Ar), 130.28 (ArC *para* to CO₂CH₂Ar), 129.97 (ArC *ortho* to CO₂CH₂Ar), 128.35 (ArC *meta* to CO₂CH₂Ar), 127.34 (ArC *ipso* to CH₂N), 112.10 (CH *ortho* to OMe), 108.73 (ArC *ortho* to CH₂O(CO)Ar), 106.12 (ArC *ortho* to CH₂OAr, 4-position), 105.68 (ArC *ortho* to CH₂OAr, 3,5-positions), 84.79 (NC(Ar)N), 75.23 (OCH₂Ar, 4-position), 73.38 (OCH₂(CH₂)₁₀CH₃ 3,4,5-(4')-position), 71.76 (OCH₂Ar, 3,5-positions), 69.06 (OCH₂(CH₂)₁₀CH₃ 3,5-(3', 5')-positions), 68.82 (OCH₂(CH₂)₁₀CH₃ 4-(3', 5')-positions), 67.12 (CH₂O(CO)Ar), 57.01 (OCH₃), 37.00 (NCH₂Ar), 31.95 (O(CH₂)₉CH₂CH₂CH₃), 30.43 (OCH₂CH₂(CH₂)₉CH₃), 29.73 (O(CH₂)₃(CH₂)₅(CH₂)₃CH₃), 29.42 (O(CH₂)₈CH₂(CH₂)₂CH₃), 26.21 (O(CH₂)₂CH₂(CH₂)₈CH₃), 22.70 (O(CH₂)₁₀CH₂CH₃), 14.09 (CH₂CH₃) ppm; MALDI-TOF-MS: m/z 4841 (M)⁺. Anal. Calcd for C₃₁₀H₅₁₄N₄O₃₄: C, 76.91; H, 10.70; N, 1.16. Found: C, 76.81; H, 10.52; N, 1.44.

3,4,5-Tri(dodecyloxy)-1-benzenecarboxylic acid (5):

This compound was synthesized according to a literature procedure.⁷

3,4,5-Tri(dodecyloxy)-1-benzenecarbonyl chloride (6):

A solution of **5** (2.56 g, 3.79 mmol) in SOCl_2 (25 mL) was refluxed under nitrogen for 2 h. After cooling, the solvent was evaporated to give 2.71 g (100%) of **6** as a cream-colored and very hygroscopic solid, which was used immediately in further syntheses.

IR (KBr pellet) ν 2918, 2849 (CH_2), 1753 ($\text{C}=\text{O}$), 1468 ($\text{C}=\text{C}$) cm^{-1} ; ^1H NMR (CDCl_3 , 200.13 MHz) δ 7.32 (s, 2H, ArH), 4.05 (t, 6H, OCH_2 , $^3J = 6.0$ Hz), 1.79 (m, 6H, OCH_2CH_2), 1.27 (br s, 54H, $(\text{CH}_2)_9\text{CH}_3$), 0.88 (t, 9H, CH_2CH_3 , $^3J = 6.0$ Hz) ppm.

N-1-(2-aminoethyl)-3,4,5-tri(dodecyloxy)benzamide (7):

To a solution of 1,2-ethylenediamine (2.22 g, 37.0 mmol) and triethylamine (81 mg, 0.80 mmol) in degassed dichloromethane (100 mL) was added dropwise a solution of **6** (503 mg, 0.72 mmol) in dichloromethane (5 mL). The mixture was stirred under nitrogen for 48 h and then extracted with water (300 mL). The organic layer was evaporated to dryness. To remove the last traces of water and triethylamine, the residue was dissolved in toluene and the solution was evaporated to dryness to yield 246 mg (94%) of **7** as a cream-colored powder.

M.p. 75°C; IR (KBr pellet): ν 3279 (NH), 2921, 2852 (CH_2), 1636 (amide I), 1545 (amide II); ^1H NMR (CDCl_3 , 300.13 MHz): δ 7.19 (t, 1H, $\text{C}(\text{O})\text{NH}$, $^3J = 5.8$ Hz), 6.97 (s, 2H, ArH), 4.00 (t, 6H, OCH_2 , $^3J = 6.0$ Hz), 3.71 (m, 2H, NH_2), 3.49 (q, 2H, $\text{C}(\text{O})\text{NHCH}_2$, $^3J = 5.9$ Hz), 2.95 (t, 2H, CH_2NH_2 , $^3J = 5.9$ Hz), 1.76 (m, 6H, OCH_2CH_2), 1.26 (s, 54H, $(\text{CH}_2)_9\text{CH}_3$), 0.88 (t, 9H, CH_2CH_3 , $^3J = 6.6$ Hz) ppm; FAB-MS: m/z 718 ($\text{M} + \text{H}$)⁺. Anal. Calcd for $\text{C}_{45}\text{H}_{84}\text{N}_2\text{O}_4$: C, 75.36; H, 11.81; N, 3.91. Found: C, 75.27, H, 12.24, N, 3.57.

1-[4-(Chloromethyl)-2,6-di(dodecyloxy)phenoxy]dodecane (10):

This compound was synthesized according to a literature procedure.⁷

1-[4-[(4-(Chloromethyl)-2,6-di[3,4,5-tri(dodecyloxy)benzyl]oxyphenoxy)methyl]-2,6-di(dodecyloxy)phenoxy]-dodecane (11):

This compound was synthesized according to a literature procedure.⁷

1-4-[(4-(Chloromethyl)-2-[4-dodecyloxy]benzyl]oxyphenoxy)methyl]phenoxydodecane (12b):

This compound was synthesized according to a literature procedure.⁷

1-[4-[(4-(Chloromethyl)-2-[3,4-di(dodecyloxy)benzyl]oxyphenoxy)methyl]-2-(dodecyloxy)phenoxy]dodecane (13b):

This compound was synthesized according to a literature procedure.⁷

1-[4-[(4-(Chloromethyl)-2-[3,4,5-tri(dodecyloxy)benzyl]oxyphenoxy)methyl]-2,6-di(dodecyloxy)phenoxy]dodecane (14b):

This compound was synthesized according to a literature procedure.⁷

1-[4-(6-(Chloromethyl)-2,3-di[4-(dodecyloxy)benzyl]oxyphenoxy)phenoxy]dodecane (15b):

This compound was synthesized according to a literature procedure.⁷

3,4-Di[4-(dodecyloxybenzyl)oxy]benzyl 4-(13b-4-[(3,4-di[4-(dodecyloxybenzyl)oxy]benzyloxy)carbonyl]-phenyl-1,4,8,11-tetramethoxy-6,13-dioxo-5,7,12,13b,13c,14-hexahydro-5a,6a,12a,13a-tetraazabenz[5,6]azuleno[2,1,8-ija]benzo[f]azulen-13-yl)benzoate (16):

A mixture of DMF (20 ml) and K_2CO_3 (0.85 g, 6.1 mmol) was purged with nitrogen for 20 min. Clip **9** (355 mg, 0.503 mmol) was added and the mixture was heated to 100 °C for 15 min. Compound **12b** (1.42 g, 2.01 mmol) was added and the mixture was stirred for 48 h. The mixture was poured into ice-water (250 ml) and the resulting precipitate was isolated by filtration and purified by flash column chromatography (basic alumina, CH_2Cl_2). The product was recrystallized from acetone to yield 463 mg (45%) of **16** as a white powder.

Isotropization point: 182°C; ^1H NMR (CDCl_3 , 500.13 MHz) δ 7.76 (d, 4H, ArH *ortho* to $\text{C}(\text{O})\text{OCH}_2\text{Ar}$, $^3J = 8.5$ Hz), 7.31 (2d, 8H, ArH *ortho* to CH_2 , 3,4-positions, $^3J = 8.3$ Hz), 7.15 (d, 4H, ArH *meta* to $\text{CO}_2\text{CH}_2\text{Ar}$, $^3J = 8.5$ Hz), 7.00 (br s, 2H, ArH *ortho* to $\text{CH}_2\text{O}(\text{O})\text{CAr}$, 2-position), 6.91 (br s, 4H, ArH *meta* and *ortho* to $\text{CH}_2\text{O}_2\text{CAr}$, 6-position), 6.85 (2d, 8H, ArH *meta* to CH_2 , 4-positions, $^3J = 8.5$ Hz, $^4J = 4.5$ Hz), 6.66 (s, 4H, ArH side-wall), 5.52 (d, 4H, NCH_2Ar *out*, $^2J = 16.0$ Hz), 5.15 (s, 4H, CO_2CH_2), 5.03 (s, 8H, ArCH_2OAr , 3,4-positions), 3.93 (t, 8H, CH_2OAr 3,4-(4') positions, $^3J = 6.6$ Hz), 3.77 (overlapping peaks, 16H, NCH_2Ar *in*, OCH_3), 1.75 (m, 8H, $\text{OCH}_2\text{CH}_2(\text{CH}_2)_9\text{CH}_3$), 1.46 (m, 8H, $\text{O}(\text{CH}_2)_2\text{CH}_2(\text{CH}_2)_8\text{CH}_3$), 1.26 (m, 64H, $\text{O}(\text{CH}_2)_3(\text{CH}_2)_8\text{CH}_3$), 0.88 (t, 12H, $\text{O}(\text{CH}_2)_{11}\text{CH}_3$, $^3J = 6.4$ Hz) ppm; $^{13}\text{C}\{^1\text{H}\}$ NMR (CDCl_3 , 75.47 MHz) δ 165.62 (ester $\text{C}=\text{O}$), 158.89 (urea $\text{C}=\text{O}$), 157.52, 151.03, 149.26, 149.05 (all ArC *ipso* to OCH_2 and OCH_3), 139.36, 130.43, 129.97, 129.13, 128.95, 128.71,

128.18, 127.05, 121.84, 115.64, 115.02, 114.41, 111.90 (all ArC), 84.83 (NC(Ar)N), 71.23, 71.13, 68.02, 66.92 (all ArCH₂O), 56.78 (OCH₃), 36.95 (NCH₂Ar), 31.91 (CH₂CH₂CH₃), 29.62, 29.43, 29.29, 26.06 ((CH₂)₈CH₂CH₂CH₃), 22.69 (CH₂CH₃), 14.12 (CH₂CH₃) ppm. Anal. Calcd for C₁₂₈H₁₆₆N₄O₁₈: C, 75.04; H, 8.17; N, 2.73. Found: C, 74.98; H, 8.18; N, 2.78.

3,4-Di[(3,4-di(dodecyloxy)benzyl)oxy]benzyl 4-(13b-4-[(3,4-di[(3,4-dihydroxybenzyl)oxy]benzyloxy)carbonyl]phenyl-1,4,8,11-tetramethoxy-6,13-dioxo-5,7,12,13b,13c,14-hexahydro-5a,6a,12a,13a-tetraazabenz[5,6]azuleno[2,1,8-*ija*]benzo[*f*]azulen-13-yl)benzoate (17):

For the synthesis of this compound the same procedure was followed as described for **16**, using **9** (324 mg, 0.459 mmol), K₂CO₃ (0.822 g, 5.94 mmol) and **13b** (1.98 g, 1.84 mmol) in DMF (20 ml), to yield 816 mg (64%) of **17** as a white powder.

Isotropization point: 128°C; ¹H NMR (CDCl₃, 500.13 MHz) δ 7.77 (d, 4H, ArH *ortho* to C(O)OCH₂Ar, ³J = 8.4 Hz), 7.15 (d, 4H, ArH *meta* to C(O)OCH₂Ar, ³J = 8.4 Hz), 7.01-6.65 (overlapping peaks, 22H, ArH *meta* to CH₂, 3,4-positions, ArH *ortho* to CH₂, 3,4-positions, ArH *ortho* to CH₂OC(O)Ar, ArH *meta* to CH₂OC(O)Ar, ArH side-wall), 5.53 (d, 4H, NCH₂Ar *out*, ²J = 15.8 Hz), 5.17 (s, 4H, C(O)OCH₂), 5.03 (s, 8H, ArCH₂OAr, 3,4-positions), 3.96-3.87 (overlapping t, 16H, CH₂OAr 3,4-(3',4') positions), 3.76 (overlapping peaks, 16H, NCH₂Ar *in*, OCH₃), 1.75 (m, 16H, OCH₂CH₂), 1.27-1.46 (m, 144H, (CH₂)₉CH₃), 0.87 (t, 24H, CH₂CH₃, ³J = 6.4 Hz) ppm; ¹³C{¹H} NMR (CDCl₃, 75.47 MHz) δ 165.59 (ester C=O), 157.45 (urea C=O), 150.81 (ArC *ipso* to OCH₃), 149.19, 149.03, 148.81, 139.32, 130.43, 129.96, 129.62, 128.75, 128.17, 126.79, 121.91, 120.11, 119.95, 115.52, 115.32, 1114.95, 113.54, 113.24, 113.11, 111.69 (all ArC), 84.84 (NC(Ar)N), 71.37, 71.31, 69.28, 69.09, 66.91 (all ArCH₂O), 56.53 (OCH₃), 36.87 (NCH₂Ar), 31.90 (CH₂CH₂CH₃), 29.65, 29.47, 29.33, 26.06 ((CH₂)₈CH₂CH₂CH₃), 22.66 (CH₂CH₃), 14.09 (CH₂CH₃) ppm. Anal. Calcd for C₁₇₆H₂₆₂N₄O₂₂: C, 75.88; H, 9.48; N, 2.01. Found: C, 76.53; H, 10.27; N, 1.92.

3,4-Di[(3,4,5-tri(dodecyloxy)benzyl)oxy]benzyl 4-(13b-4-(((3,4-di[(3,4,5-(dodecyloxy)benzyl)oxy]benzyl)oxy)carbonyl)phenyl)-1,4,8,11-tetramethoxy-6,13-dioxo-5,7,12,13b,13c,14-hexahydro-5a,6a,12a,13a-tetraazabenz[5,6]azuleno[2,1,8-*ija*]benzo[*f*]azulen-13-yl)benzoate (18):

For the synthesis of this compound the same procedure was followed as described for **16**, using **9** (260 mg, 0.368 mmol), K₂CO₃ (0.832 g, 6.02 mmol) and **14b** (2.13 g, 1.47 mmol) in DMF (20 ml). Yield 830 mg (64%) of **18** as a cream-white powder.

Isotropization point: 95°C. ¹H NMR (CDCl₃, 500.14 MHz) δ 7.77 (d, 4H, ArH *ortho* to C(O)OCH₂Ar, ³J = 8.2 Hz), 7.16 (d, 4H, ArH *meta* to C(O)OCH₂Ar, ³J = 8.2 Hz), 7.02 (broad s, 2H, ArH *ortho* to CH₂OC(O)Ar, 2-position), 6.95 (2d, 4H, ArH *meta* and *ortho* to CH₂OC(O)Ar, 6-position, ³J = 8.5 Hz), 6.66, 6.64 and 6.61 (3s, 12H, ArH *ortho* to CH₂, 3,4-positions, and ArH side-wall), 5.54 (d, 4H, NCH₂Ar *out*, ²J = 15.8 Hz), 5.18 (s, 4H, CO₂CH₂), 5.02 (s, 8H, ArCH₂OAr, 3,4-positions), 3.94-3.85 (overlapping t, 24H, CH₂OAr 3,4-(3',4',5') positions), 3.77 (overlapping peaks, 16H, NCH₂Ar *in*, OCH₃), 1.73 (m, 24H, OCH₂CH₂), 1.17-1.44 (m, 216H, (CH₂)₉CH₃), 0.88 (t, 36H, CH₂CH₃, ³J = 6.4 Hz) ppm; ¹³C{¹H} NMR (CDCl₃, 75.47 MHz) δ 165.59 (ester C=O), 157.42 (urea C=O), 153.19 (ArC *ipso* to OCH₂), 150.81 (ArC *ipso* to OCH₃), 149.28, 149.04, 139.36, 137.73, 132.06, 131.95, 130.41, 129.97, 128.94, 128.21, 126.65, 122.13, 115.66, 115.07, 111.57, 105.72, 105.57 (all ArC), 84.85 (NC(Ar)N), 73.34, 71.69, 68.99, 66.88 (all ArCH₂O), 56.37 (OCH₃), 36.83 (NCH₂Ar), 31.91 (CH₂CH₂CH₃), 29.38, 26.14 ((CH₂)₈CH₂CH₂CH₃), 22.66 (CH₂CH₃), 14.08 (CH₂CH₃) ppm; FAB-MS *m/z* 3523 (M + H)⁺. Anal. Calcd for C₂₂₄H₃₅₈N₄O₂₆: C, 76.36; H, 10.24; N, 1.59. Found: C, 76.47; H, 10.44; N, 1.56.

3,4,5-Tri[(4-dodecyloxybenzyl)oxy]benzyl 4-(1,4,8,11-tetramethoxy-6,13-dioxo-13b-4-[(3,4,5-tri[(4-dodecyloxybenzyl)oxy]benzyloxy)carbonyl]phenyl)-5,7,12,13b,13c,14-hexahydro-5a,6a,12a,13a-tetraazabenz[5,6]azuleno[2,1,8-*ija*]benzo[*f*]azulen-13-yl)benzoate (19):

For the synthesis of this compound the same procedure was followed as described for **16**, using **9** (350 mg, 0.496 mmol), K₂CO₃ (0.822 g, 5.94 mmol) and **15b** (2.01 g, 2.01 mmol) in DMF (20 ml). Yield 564 mg (43%) of **19** as a cream-white powder.

Isotropization point: 107°C. ¹H NMR (CDCl₃, 400.134 MHz) δ 7.77 (d, 4H, ArH *ortho* to C(O)OCH₂Ar, ³J = 8.4 Hz), 7.30 (d, 8H, ArH *ortho* to CH₂OAr, 3,5-positions, ³J = 8.5 Hz), 7.26 (d, 4H, ArH *ortho* to CH₂OAr, 4-position, ³J = 8.5 Hz), 7.15 (d, 4H, ArH *meta* to C(O)OCH₂Ar, ³J = 8.4 Hz), 6.86 (d, 8H, ArH *meta* to CH₂OAr, 3,5-positions, ³J = 8.5 Hz), 6.74 (d, 4H, ArH *meta* to CH₂OAr, 4-position, ³J = 8.5 Hz), 6.68 and 6.64 (2s, 8H, ArH *ortho* to CH₂OC(O)Ar and ArH side-wall), 5.55 (d, 4H, NCH₂Ar *out*, ²J = 16.1 Hz), 5.15 (s, 4H, C(O)OCH₂), 4.99 (s, 8H, ArCH₂OAr, 3,5-positions), 4.91 (s, 4H, ArCH₂OAr, 4-position), 3.97-3.87 (overlapping t, 12H, CH₂OAr 3,4,5-(4') positions), 3.76 (overlapping peaks, 16H, NCH₂Ar *in*, ²J = 16.1 Hz), 3.72 (s, 12H, OCH₃), 1.75 (m, 12H, OCH₂CH₂), 1.27-1.46 (m, 108H, (CH₂)₉CH₃), 0.87 (t, 18H, CH₂CH₃, ³J = 6.4 Hz) ppm; ¹³C{¹H} NMR (CDCl₃, 75.47 MHz) δ 165.55 (ester C=O), 158.85 (urea C=O), 152.99 (ArC *ipso* to OCH₂), 150.76 (ArC *ipso* to OCH₃), 139.45, 138.58, 130.91, 130.39, 130.18, 130.02, 129.78, 129.18, 128.77, 128.25, 126.71, 114.37, 114.05, 111.64,

108.10 (all ArC), 84.87 (NC(Ar)N), 74.80, 71.10, 68.01, 67.94, 67.10 (all ArCH₂O), 56.46 (OCH₃), 36.88 (NCH₂Ar), 31.89 (CH₂CH₂CH₃), 29.43, 29.32, 26.05 ((CH₂)₈CH₂CH₂CH₃), 22.67 (CH₂CH₃), 14.10 (CH₂CH₃) ppm. Anal. Calcd for C₁₆₆H₂₂₆N₄O₂₂: C, 75.82; H, 8.66; N, 2.13. Found: C, 75.49; H, 8.93; N, 2.19.

References and notes

- ¹ For reviews about dendrimers see: Tomalia, D. A.; Durst, H. D. *Top. Curr. Chem.* **1993**, *165*, 193. Fréchet, J. M. J. *Science* **1994**, *263*, 1710. Issberner, J.; Moors, R. Vögtle, F. *Angew. Chem. Int. Ed. Engl.* **1994**, *33*, 2413. Zeng, F.; Zimmerman, S. C. *Chem. Rev.* **1997**, *97*, 1681. Smith, D. K.; Diederich, F. *Chem. Eur. J.* **1998**, *4*, 1353. Fisher, M.; Vögtle, F. *Angew. Chem. Int. Ed. Engl.* **1999**, *38*, 884. Cuadrado, I.; Moran, M.; Casado, C. M.; Alonso, B.; Losada, J. *Coord. Chem. Rev.* **1999**, *195*, 395. Bosman, A. W.; Janssen, H. M.; Meijer, E. W. *Chem. Rev.* **1999**, *99*, 1665.
- ² Kawaguchi, T.; Walker, K. L.; Wilkins, C. L.; Moore, J. S. *J. Am. Chem. Soc.* **1995**, *117*, 2159. Pollak, K. W.; Sanford, E. M.; Fréchet, J. M. J. *J. Mater. Chem.* **1998**, *8*, 519.
- ³ Huck, W. T. S.; Prins, L. J.; Fokkens, R. H.; Nibbering, N. M. M.; van Veggel, F. C. J. M.; Reinhoudt, D. N. *J. Am. Chem. Soc.* **1998**, *120*, 6240. Newkome, G. R.; He, E. F.; Moorefield, C. N. *Chem. Rev.* **1999**, *99*, 1689.
- ⁴ Newkome, G. R.; Yao, Z.; Baker, G. R.; Gupta, V. K.; Russo, P. S.; Saunders, M. J. *J. Am. Chem. Soc.* **1986**, *108*, 849. Hawker, C. J.; Farrington, P. J.; MacKay, M. E.; Wooley, K. L.; Fréchet, J. M. J. *J. Am. Chem. Soc.* **1995**, *117*, 4409. Huck, W. T. S.; van Veggel, F. C. J. M.; Kropman, B. L.; Blank, D. M. A.; Keim, E. G.; Smithers, M. M. A.; Reinhoudt, D. N. *J. Am. Chem. Soc.* **1995**, *117*, 8293. Saville, P. M.; Reynolds, P. A.; White, J. W.; Hawker, C. J.; Fréchet, J. M. J.; Wooley, K. L.; Penfold, J.; Webster, J. R. P. *J. Phys. Chem.* **1995**, *99*, 8283. Tomalia, D. A.; Baker, H.; Dewald, J.; Hall, M.; Kallos, G.; Martin, S.; Ryder, J.; Smith, P. *Macromolecules* **1996**, *19*, 2466.
- ⁵ Newkome, G. R.; Moorefield, C. N.; Baker, G. R.; Behera, R. K.; Escamilla, G. H.; Saunders, M. J. *Angew. Chem. Int. Ed. Engl.* **1992**, *31*, 917.
- ⁶ Percec, V.; Chu, P.; Ungar, G.; Zhou, J. *J. Am. Chem. Soc.* **1995**, *117*, 11441. Percec, V.; *Pure Appl. Chem.* **1995**, *67*, 2031.
- ⁷ Balagurusamy, V. S. K.; Ungar, G.; Percec, V.; Johansson, G. *J. Am. Chem. Soc.* **1997**, *119*, 1539.
- ⁸ For other examples of self-assembly of tapered monodendrons, see: Percec, V.; Tomazos, D.; Heck, J.; Blackwell, H.; Ungar, G. *J. Chem. Soc. Perkin Trans.* **1994**, *31*. Kwon, Y. K.; Chvalun, S.; Schneider, A.-I.; Blackwell, J.; Percec, V.; Heck, J. A. *Macromolecules* **1994**, *27*, 6129. Percec, V.; Johansson, G.; Ungar, G.; Zhou, J. *J. Am. Chem. Soc.* **1996**, *118*, 9855. Percec, V.; Schlueter, D. *Macromolecules* **1997**, *30*, 5783. Percec, V.; Schlueter, D.; Ungar, G.; Cheng, S. Z. D.; Zhang, A. *Macromolecules* **1998**, *31*, 1745. Beginn, U.; Zipp, G.; Möller, M. *Chem. Eur. J.* **2000**, *6*, 2016.
- ⁹ See for example: Luzzati, V.; Spegt, P. A. *Nature* **1967**, *215*, 701. Luzzati, V.; Gulik-Krzywicki, T.; Tardieu, A. *Nature* **1968**, *218*, 1031. Mariani, P.; Luzzati, V.; Delacroix, H. *J. Mol. Biol.* **1988**, *204*, 165. Seddon, J. M.; Zeb, N.; Templer, R.H.; McElhaney, R.N.; Mannock, D. A. *Langmuir* **1996**, *12*, 5250. Seddon, J. M. *Biochemistry* **1990**, *29*, 7997. Hyde, S. T. *Langmuir* **1997**, *13*, 842.
- ¹⁰ Fischer, S.; Fisher, H.; Diele, S.; Pelzl, G.; Jankowski, K.; Schmidt, R. R.; Vill, V. *Liq. Cryst.* **1994**, *6*, 855. Latterman, G.; Stauffer, G. *Mol. Cryst. Liq. Cryst.* **1990**, *191*, 199. Borisch, K.; Diele, S.; Goering, P.; Tsierske, C. *Chem. Commun.* **1996**, 237. Borisch, K.; Diele, S.; Goring, P.; Kresse, H.; Tschierske, C. *Angew. Chem. Int. Ed. Engl.* **1997**, *36*, 2087. Borisch, K.; Diele, S.; Goring, P.; Kresse, H.; Tschierske, C. *J. Mater. Chem.* **1998**, *8*, 529. Hong Cheng, X.; Diele, S.; Tschierske, C. *Angew. Chem. Int. Ed.* **2000**, *39*, 592. Felder, D.; Heinrich, B.; Guillon, D.; Nicoud, J.-F.; Nierengarten, J.-F. *Chem. Eur. J.* **2000**, *6*, 3501.
- ¹¹ Hudson, S. D.; Jung, H.-T.; Percec, V.; Cho, W.-D.; Johansson, G.; Ungar, G.; Balagurusamy, V. S. K. *Science* **1997**, *278*, 449. Percec, V.; Cho, W.-D.; Möller, M.; Prokhorova, S. A.; Ungar, G.; Yeardley, D. J. P. *J. Am. Chem. Soc.* **2000**, *122*, 4249.
- ¹² Kwon, Y. K.; Chviaun, S. N.; Blackwell, J.; Percec, V.; Heck, J. *Macromolecules* **1995**, *28*, 1552.
- ¹³ Percec, V.; Ahn, C.-H.; Ungar, G.; Yeardley, D. J. P.; Möller, M.; Sheiko, S. S. *Nature* **1998**, *391*, 161.
- ¹⁴ Holder, S. J.; Elemans, J. A. A. W.; Barberá, J.; Rowan, A. E.; Nolte, R. J. M. *Chem. Commun.* **2000**, 355. Holder, S. J.; Elemans, J. A. A. W.; Donners, J. J. J. M.; Boerakker, M. J.; Barberá, J.; de Gelder, R.; Rowan, A. E.; Nolte, R. J. M. *J. Org. Chem.* **2001**, *66*, 391.
- ¹⁵ Percec, V.; Lee, M.; Heck, J.; Blackwell, H. E.; Ungar, G.; Alvarez-Castillo, A. *J. Mater. Chem.* **1992**, *2*, 931.
- ¹⁶ Hot DMF is the only solvent in which clip **9** is slightly soluble.
- ¹⁷ Gray, G. W.; Goodby, J. W. G. in: *Smectic Liquid Crystals - Textures and Structures*, Leonard Hill, Glasgow, **1984**.

- ¹⁸ St. Pourcain, C. B. ; Griffin, A. C. *Macromolecules* **1995**, *28*, 4116.
- ¹⁹ Ungar, G.; Abramic, D.; Percec, V.; Heck, J. A. *Liq. Cryst.* **1996**, *21*, 73.
- ²⁰ McQuade, D. T.; McKay, S. L. ; Powell, D. R.; Gellman, S. H. *J. Am. Chem. Soc.* **1997**, *119*, 8528. Gung, B. W.; Zhu, Z. *J. Org. Chem.* **1997**, *62*, 2324.
- ²¹ Percec, V.; Ahn, C.-H.; Bera, T. K.; Ungar, G.; Yeardley, D. J. P. *Chem Eur. J.* **1999**, *5*, 1070.
- ²² Hoag, B. P.; Gin, D. L. *Adv. Mater.* **1998**, *10*, 1546.
- ²³ Percec, V.; Johansson, G.; Heck, J.; Ungar, G.; Batty, S. V. *J. Chem. Soc. Perkin Trans. 1*, **1993**, 1411.
- ²⁴ Methanol was added in order to fully dissolve both the clip and guest components.
- ²⁵ This assumption is based on the difference in association constant of the dimerization reaction and the host-guest complexation reaction in chloroform solution, with the former constant being several orders of magnitude smaller than the latter one.
- ²⁶ Unlike clip **4** the polymeric guest products will not dissolve in, for example, chloroform or dichloromethane.
- ²⁷ Percec, V.; Ahn, C.-H.; Cho, W.-D.; Jamieson, A. M.; Kim, J.; Leman, T.; Schmidt, M.; Gerle, M.; Möller, M.; Prokhorova, S. A.; Sheiko, S. S.; Cheng, S. Z. D.; Zhang, A.; Ungar, G.; Yeardley, D. J. P. *J. Am. Chem. Soc.* **1998**, *120*, 8619.

Chapter 7

A Conductive Molecular Clip Polymer

7.1 Introduction

Chemosensors are devices which are designed to detect a specific molecule or class of molecules.¹ Typically, a chemosensor is composed of three functional elements, *viz.* a selector (receptor) which binds the molecule to be detected, a transducer which transforms the binding reaction into a physically measurable signal, and a detector which processes this physical signal. One of the key issues in sensor development is to achieve high selectivity in combination with efficient transduction, and in this context one of the best approaches is to develop materials which combine these two items.² Functionalized π -conjugated polythiophenes are a very promising class of sensor materials which can exhibit impressive responses upon exposure to external stimuli.³ They are conductive polymers,⁴ which can undergo conformational changes when exposed to *e.g.* heat and light, giving rise to phenomena like thermochroism and photochromism.⁵ Polythiophenes can be made conductive by oxidation (p-doping), resulting in the introduction of cationic charge carriers in the material.⁴ Conformational defects in the polymer chains can reduce the conductivity and the best conductivity is obtained when the polymer has a flat, planar structure in which the thiophene units alternate with respect to each other. The sensing properties of polythiophenes are often based on a geometrical disturbance from this ideal conformation, resulting in a change in their conductivity which is typically monitored by UV-vis, fluorescence or electrochemical techniques. One of the first investigated polythiophene-based sensing materials was a polythiophene provided with crown ether side-chains. This material was designed to detect alkali metal ions (Figure 7.1a).⁶ In its conductive form, the crown ether chains are folded over the polymer backbone. Upon binding of sodium ions, the structure of the polymer backbone is forced to rearrange and as a result changes in the conductivity and in the optical properties could be measured. In this particular case, also electrostatic interactions between the bound ions and the polymer were thought to be responsible for the observed changes in properties. Increased sensing selectivities of different types of alkali metal ions were achieved by using thiophene polymers to which rigid and more preorganized calixarene receptors were attached.⁷ In a different approach, polymers of bithiophenes functionalized with nucleic acid bases such as adenine and uracil were applied as very specific sensors for the detection of the complementary nucleic acid bases (Figure 7.1b).⁸ This is a remarkable result since in these

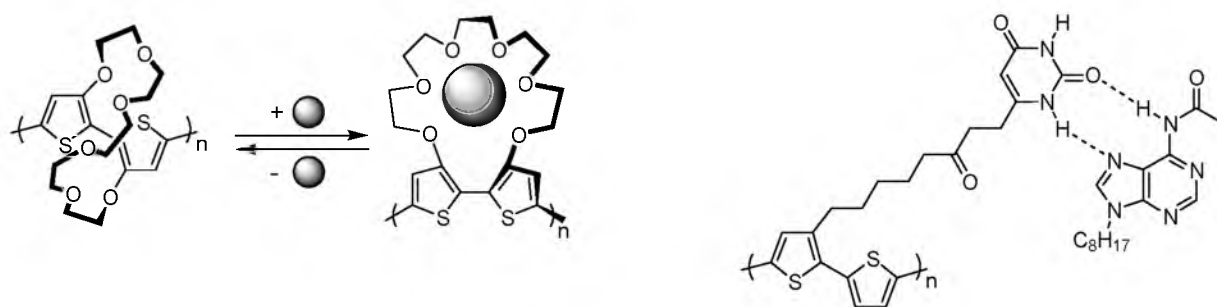


Figure 7.1 Examples of responsive thiophene-based materials.

since in these polymers an insulating alkyl chain spacer electronically decouples the receptor and the transducer part of the molecule. Apparently, this decoupling had no serious influence on the sensing properties of the material.

In this chapter we describe a polythiophene to which a molecular clip receptor⁹ is attached. Molecular clips derived from diphenylglycoluril have shown to be ideal receptors for 1,3-dihydroxybenzene guests which are complexed in the cavities of these molecules by a combination of hydrogen bonding, π - π interactions, and cavity filling effects.¹⁰ With the help of molecular modeling compound **1** (Figure 7.2) was designed. It contains a thiophene unit which is connected to the convex side of the receptor *via* two propyl spacers. Studies aimed at polymerizing **1** are presented in this chapter. To date no polymers of molecular clips have been described and it will be of interest to investigate whether such polymers can be applied in the sensing of 1,3-dihydroxybenzene guests. Studies towards this goal have been carried out and are discussed in the following sections.

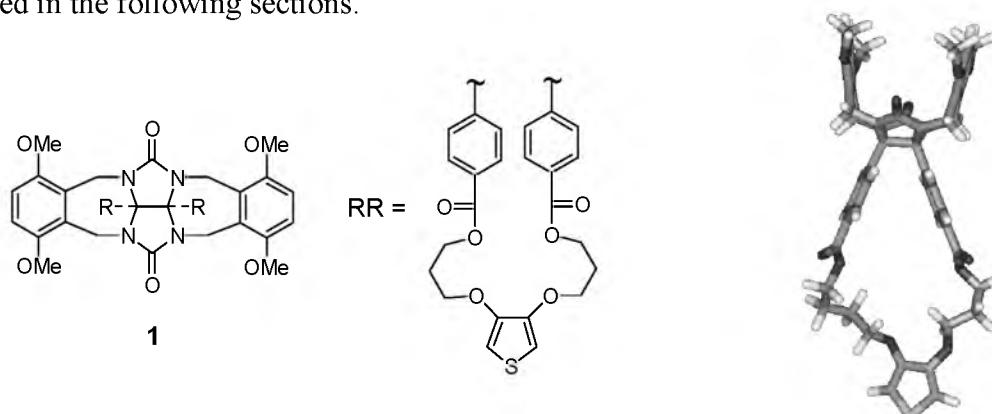
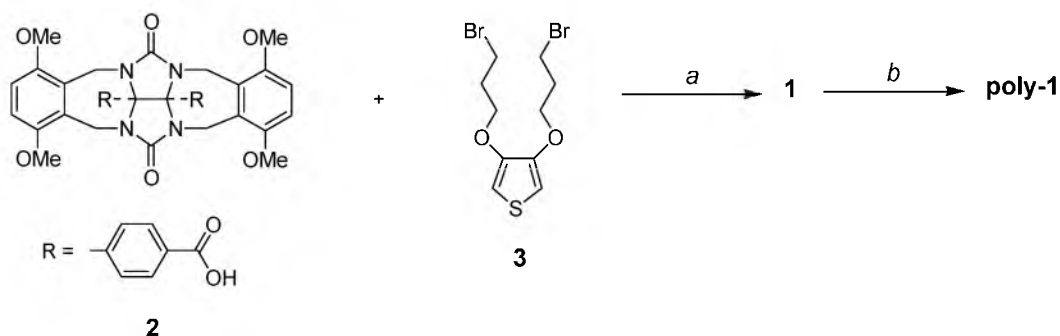


Figure 7.2 Thiophene-functionalized clip **1** and a computer-modeled structure of this molecule (protons have been omitted for clarity).

7.2 Results and discussion

7.2.1 Polythiophene synthesis and characterization

Clip molecule **1** was synthesized by heating an equimolar mixture of carboxylic acid functionalized clip **2** (see Chapter 2) and 3,4-di(3-bromopropoxy)thiophene in dimethylformamide, using potassium carbonate as a base (Scheme 7.1). Remarkably, in the



Scheme 7.1 Reagents and conditions: (a) K_2CO_3 , KI, DMF, $120^\circ C$, 5 days. (b) $FeCl_3$, CH_2Cl_2 , 1 day.

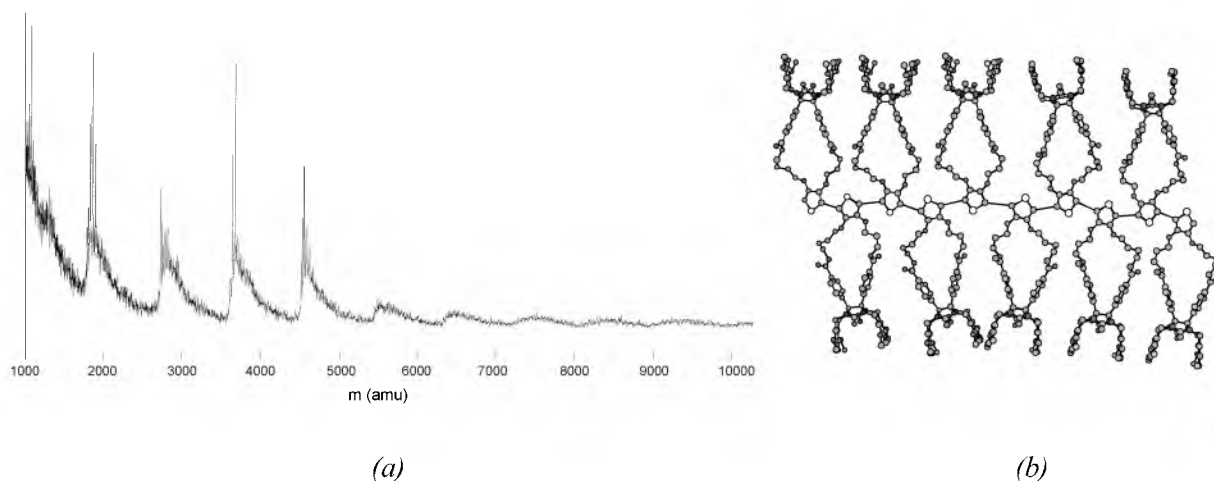


Figure 7.3 (a) Maldi-TOF mass spectrum and (b) computer modeled representation of the polymer of **1** (protons have been omitted for clarity).

crude product no polymeric material (clips linked by thiophene units) were detected, but only the desired product, unreacted **2** and a thiophene derivative of which the bromide groups had reacted to alcohols. After purification by column chromatography and precipitation of a chloroform solution of the product in diethylether, **1** was obtained in 28% yield.

Polythiophenes can be synthesized by both electrochemical and chemical oxidation, as well as through chemical coupling reactions.¹¹ In this preliminary study we did not aim at producing high molecular weight polymers of **1**, since it is well-known that the characteristic electronic and conductive properties of polythiophenes are already obtained at relatively low degrees of polymerization.¹² In fact, low molecular weight thiophene oligomers are preferred since they usually display greater crystallinity, and, as a result, may exhibit larger conductivities than disordered high molecular weight polymers.¹³ Compound **1** was polymerized by chemical oxidation using iron trichloride in dichloromethane (Scheme 7.1). A blue solid was obtained, which was hardly soluble in chloroform, but well-soluble in DMSO. 1H NMR spectroscopy in DMSO showed, in addition to sharp peaks corresponding to residual monomer or polymer end groups, broad signals under each of these sharp peaks, except underneath the thiophene proton signal. These results indicate that polymer formation had taken place. Analysis of the material by MALDI-TOF mass spectrometry confirmed this conclusion and indicated that polymers with at least 10 monomeric units of **1** were present (Figure 7.3a). A computer modeled structure of such a polymer is shown in Figure 7.3b. When it is assumed that the polymer has a flat, alternating

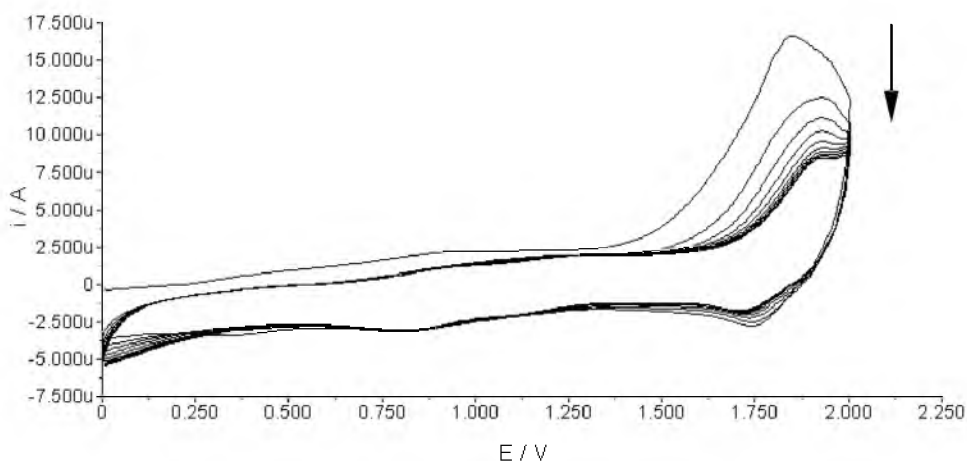


Figure 7.4 Electrochemical polymerization of thiophene monomer **1** from a CH_2Cl_2 solution (5 mM of **1**) containing TBAH (0.1 M) as the electrolyte. A gold electrode was used as the working electrode. 10 Scans were recorded between 0 and 2.0 V at a scanning rate of 100 mV s^{-1} .

conformation, it is clear that there will be a considerable amount of Van der Waals interactions between the molecular clip side-chains. Polymerization of **1** could also be accomplished by electrochemical oxidation on a gold electrode.¹⁴ To this end, monomer **1** was dissolved in dichloromethane (5 mM) and electro-oxidized at potentials above 1.0 V vs. Ag/AgNO₃. The electrochemical growth of the polymer could be observed in a series of consecutive cyclic voltammograms (Figure 7.4). During these cycles a blue material was deposited upon the gold electrode surface. As a result of this, the oxidative polymerization of residual monomer occurred increasingly slowly which was visible from the progressively decreasing current of the oxidation wave. In addition, the oxidation potential gradually shifted from 1.84 to 1.93 V, which is an indication that the conductivity of material became lower after a while.¹⁵

The chemically prepared polymer was further studied by UV-vis spectroscopy. Whilst the UV-vis spectrum of monomer **1** exhibited bands only at wavelengths lower than 300 nm (corresponding to $\pi \rightarrow \pi^*$ transitions of the aromatic rings in the molecule), the UV-vis spectrum of a film of the polymer of **1** displayed several new bands at higher wavelengths (Figure 7.5). The band at 446 nm corresponds to $\pi \rightarrow \pi^*$ transitions of the reduced, neutral form of the polymer, whereas the bands between 600 and 900 nm, the so-called polaronic bands, are characteristic of its oxidized and conductive state.¹⁶

7.2.2 Response measurements

To investigate if the polymer of **1** could be applied as a sensing material for the detection of 1,3-dihydroxybenzenes, response measurements to these analytes were carried out by UV-vis spectroscopy and cyclic voltammetry. To a chloroform-filled UV-cuvet containing a thin film of the polymer of **1** deposited on the inner walls of the cuvet resorcinol was added in small portions. Upon these additions, the intensity of band at 446 nm slowly decreased whereas the intensities of all the bands between 600 and 900 nm increased (Figure 7.5). This suggests an increase in conductivity of the polymer. No shifts in the wavelengths of the bands, which are generally related to conformational changes in the polymer backbone,⁵ were detected. When, however, 1,3-dimethoxybenzene, a guest that does not bind in the cavity of **1**, was tested instead of resorcinol, similar changes in the UV-vis spectrum were observed. Also cyclic voltammetry gave similar results as obtained with resorcinol. Upon addition of a solution of

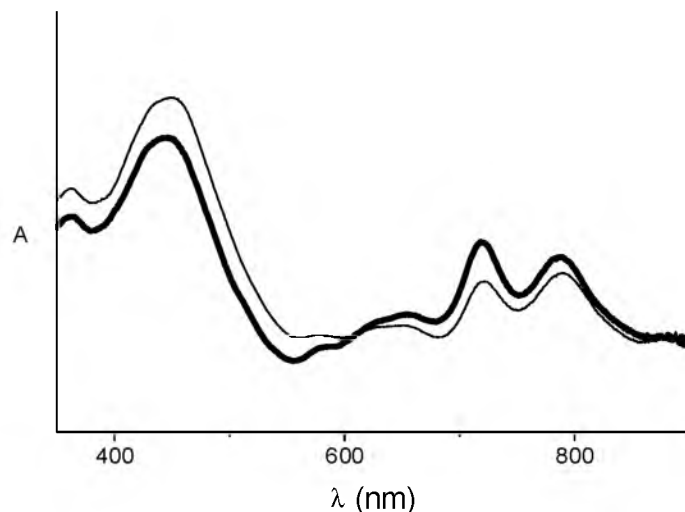


Figure 7.5 UV-vis spectra of thin films of the polymer of **1** deposited from a CHCl_3 solution on the inner walls of a cuvet. Thin solid line: polymer of **1**. Bold line: polymer of **1** in contact with a CHCl_3 solution of resorcinol (0.5 mM).

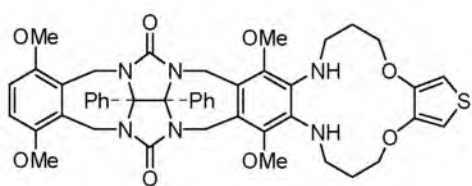
hexyl 3,5-dihydroxybenzoate (HDB) in dichloromethane (5 mM) to the polymer of **1** deposited on a gold electrode, very small variations in the current of the oxidation wave of the polymer were observed (not shown). Addition of this analyte caused no shifts in the oxidation potential. When the non-binding analyte 1,3-dimethoxybenzene was used, the changes in the cyclic voltammogram were very similar to those induced by HDB.

The results from the measurements described above may be explained as follows: when the analytes are added to the polymer, partial binding in the cavities of the clip molecules will occur which possibly lead to a response. In addition, the analytes will have a direct electrostatic interaction with the polymer backbone which also causes a response. The latter interaction was investigated by carrying out response measurements with poly(3,4-ethylenedioxythiophene) (PEDOT) as the sensor material. Addition of resorcinol, HDB or 1,3-dimethoxybenzene to this polymer caused similar, small responses in the UV-vis spectra and in the cyclic voltammograms as observed for the polymer of **1**.

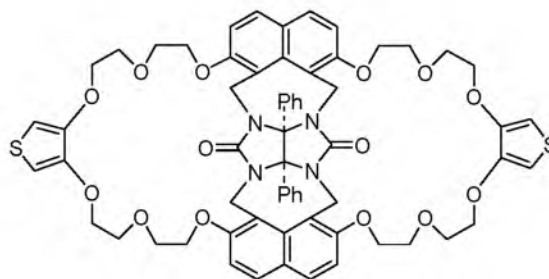
7.3 Concluding remarks

In this chapter we have demonstrated that it is possible to synthesize a conductive polythiophene which is derivatized at each repeating unit with a molecular clip. Although the synthesis of the polymer has not yet been optimized, mass spectrometry reveals that polymers of at least 10 repeating units can be obtained. Since modeling showed that there is a severe steric hindrance between the clips in the polythiophene side chains, polymers with a higher average molecular weight can probably be obtained by copolymerizing **1** with a sterically less demanding monomer, such as 3,4-ethylenedioxythiophene (EDOT).

The present functionalized polythiophene appears to be unsuitable for the selective detection of 1,3-dihydroxybenzene guests in chloroform solution. Although the addition of these guests to the polymer leads to changes in its visible spectrum and in the electrochemical



4



5

response, the addition of the non-binding guest 1,3-dimethoxybenzene causes similar responses. It is possible that the analytes give a response due to their binding in the cavities. In addition, it has been demonstrated that they cause a response as a result of a direct electrostatic interaction with the polymer backbone.

To achieve a more selective response upon binding of 1,3-dihydroxybenzenes, it will be necessary to synthesize different types of polythiophenes, *e.g.* polythiophenes in which the cavities of the clips are in closer proximity to the backbone of the polymer. Compound **4**, which can probably be synthesized from **3** and a known clip compound containing one diamino-functionalized side-wall,¹⁷ is an ideal candidate. In the polymer derived from this molecule, a bound guest has a direct π - π stacking interaction with the thiophene units. Another interesting candidate is the naphthalene-walled basket-shaped molecule **5**. It is known that upon binding of a guest this type of molecule undergoes a conformational change (see Section 1.4.2).¹⁸ In the case of **5**, this conformational change will also affect the thiophene units in the polymer and hence the properties of the material.

7.4 Experimental section

7.4.1 Materials and methods

DMF was dried over BaO for one week and then vacuum distilled; the first 30% of the distillate was discarded. K_2CO_3 and KI were dried in an oven (150°C). All other chemicals were used without further purification. Matrix Assisted Laser Desorption Ionization Time-Of-Flight (MALDI-TOF) mass spectrometry was carried out using a Perkin Elmer/PerSeptive Biosystems Voyager-DE-RP MALDI-TOF mass spectrometer. A 337 nm UV nitrogen laser producing 3 ns pulses was used in the linear and reflection mode. The samples were prepared by mixing a dichloromethane solution (1 μ L) of the sample with a solution of 2,5-dihydroxybenzoic acid (3 mg/L, 20 mL). A sample of the mixture (1 μ L) was loaded on a gold sample plate. For a description of the other general techniques see Section 2.6.1.

7.4.2 Cyclic voltammetry measurements

Polymerization experiments were carried out using a three-electrode electrochemical cell in a glove box in which a dry and oxygen-free atmosphere was maintained. A cell was used with a platinum or gold working electrode, a platinum auxiliary electrode and an Ag/AgNO₃ electrode as the reference. The latter electrode consisted of a silver wire immersed in a 0.1 M tetrabutylammonium hexafluorophosphate (TBAH) solution in CH₃CN containing 0.1 M AgNO₃. As background electrolyte a solution of TBAH (0.1 M) in CH₃CN or CH₂Cl₂ was used. The cell was calibrated before each measurement using the standard ferrocene/ferrocinium couple. Electrochemical characterization was performed using a PGSTAT 10 Eco Chemie Auto Lab instrument.

7.4.3 Syntheses

The synthesis of compound **2** has been described in Chapter 2. 3,4-Di(3-bromopropoxy)thiophene (**3**) was a kind gift of Dr A. Kros.

6,9,20,23-Tetramethoxy-30,34,40,44-tetraoxa-37-thia-3,12,14,23-tetraazadecacyclo[44.2.2.2^{25,28}.1^{3,23}.0^{2,12}.0^{2,24}.0^{5,10}.0^{14,24}.0^{16,21}.0^{35,39}]-tripentaconta-1(48),5(10),6,8,16(21),17,19,25,27,35,38,46,49,51-tetradecaene-13,29,45,53-tetraone (1):

Compounds **2** (975 mg, 1.38 mmol) and **3** (495 mg, 1.38 mmol) were suspended in degassed DMF (150 mL). K₂CO₃ (1.9 g, 13.8 mmol) and KI (10 mg) were added and the mixture was heated at 120°C for 5 days. After cooling the mixture was filtered and the filtrate was evaporated to dryness. The residue was dissolved in CH₂Cl₂ (150 mL), the solution was extracted with aqueous 1N HCl (2 × 200 mL), with aqueous 1N NaOH (200 mL), with a saturated aqueous NaCl solution (200 mL), and finally evaporated to dryness. The residue was purified by column chromatography (silica, CHCl₃/MeOH 99:1, v/v, R_f = 0.05). The product was dissolved in a minimal amount of CHCl₃ and this solution was added dropwise to stirred diethyl ether. After isolation of the precipitate and drying under vacuum, 350 mg (28%) of **1** was obtained as a white solid.

M.p. > 300°C; IR (KBr pellet) ν 3112 (ArH), 2999, 2957, 2836 (CH₂), 1713 (C=O), 1543, 1485, 1463, 1439 (C=C), 1307, 1277, 1263 (CH₂), 1106, 1077 (COC) cm⁻¹; ¹H NMR (CDCl₃, 300.13 MHz) δ 7.57 (d, 4H, ArH *ortho* to C(O)O, ³J = 8.3 Hz), 7.02 (d, 4H, ArH, ³J = 8.3 Hz), 6.67 (s, 4H, ArH *side-wall*), 6.40 (s, 2H, thiopheneH), 5.51 (d, 4H, NCH₂Ar *out*, ²J = 15.9 Hz), 4.43 (t, 4H, C(O)OCH₂, ³J = 5.9 Hz), 4.12 (t, 4H, ArOCH₂CH₂, ³J = 5.9 Hz), 3.88 (d, 4H, NCH₂Ar *in*, ²J = 15.9 Hz), 3.78 (s, 12H, OCH₃), 2.17 (m, 4H, CH₂CH₂CH₂) ppm; FAB-MS *m/z* 903 (M + H)⁺. Anal. Calcd for C₄₈H₄₆N₄O₁₂S(CHCl₃): C, 57.73; H, 4.65; N, 5.50; S, 3.15. Found: C, 57.99; H, 4.84; N, 5.44; S, 2.76.

Chemical polymerization of 1:

Compound **1** (11.5 mg, 12.7 mmol) and FeCl₃ (20 mg, 0.12 mmol) were suspended in degassed CH₂Cl₂ (10 mL). The mixture was stirred under argon for 22 h and then evaporated to dryness. The residue was suspended in water (5 mL), the precipitate was filtered off and dried under vacuum to yield a blue solid.

References and notes

- For several reviews about chemosensors, see: *Acc. Chem. Res.* **1998**, *31*, issue 5.
- For a review see: Van Veggel, F. C. J. M. in: *Comprehensive Supramolecular Chemistry*. Atwood, J. L.; Davies, J. E. D.; MacNicol, D. D.; Vögtle, F.; Reinhoudt, D. N.; Lehn, J.-M. Eds.; Elsevier Science Ltd., Pergamon: Elmsford, **1996**; Vol. 10, 171-185.
- Leclerc, M.; Faïd, K. *Adv. Mater.* **1997**, *9*, 1087.
- Swager, T. M. *Acc. Chem. Res.* **1998**, *31*, 201.
- Faïd, K.; Leclerc, M. *J. Am. Chem. Soc.* **1998**, *120*, 5274.
- Marsella, M. J.; Swager, T. M. *J. Am. Chem. Soc.* **1993**, *115*, 12214.
- Marsella, M. J.; Newland, R. J.; Carroll, P. J.; Swager, T. M. *J. Am. Chem. Soc.* **1995**, *117*, 9842. Crawford, K. B.; Goldfinger, M. B.; Swager, T. M. *J. Am. Chem. Soc.* **1998**, *120*, 5187.
- Bäuerle, P.; Emge, A. *Adv. Mater.* **1998**, *10*, 324.
- For a review about molecular clips, see: Rowan, A. E.; Elemans, J. A. A. W.; Nolte, R. J. M. *Acc. Chem. Res.* **1999**, *32*, 995.
- Sijbesma, R. P.; Kentgens, A. P. M.; Lutz, E. T. G.; van der Maas, J. H.; Nolte, R. J. M. *J. Am. Chem. Soc.* **1993**, *115*, 8999. Reek, J. N. H.; Priem, A. H.; Engelkamp, H.; Rowan, A. E.; Elemans, J. A. A. W.; Nolte, R. J. M. *J. Am. Chem. Soc.* **1997**, *119*, 9956.
- Roncali, J. *Chem. Rev.* **1992**, *92*, 711.
- Thienpont, H.; Rikken, G. L. J. A.; Meijer, E. W.; ten Hoeve, W.; Wijnberg, H. *Phys. Rev. Lett.* **1990**, *65*, 2141.
- Marsella, M. J.; Carroll, P. J.; Swager, T. M. *J. Am. Chem. Soc.* **1995**, *117*, 9832.
- A gold electrode was used instead of a platinum one because the former electrode interacts more favourably with the thiophene units.
- Kros, A. *Thesis*, University of Nijmegen, **2000**, Chapter 5.
- Chayer, M.; Faïd, K.; Leclerc, M. *Chem. Mater.* **1997**, *9*, 2902.
- Reek, J. N. H.; Elemans, J. A. A. W.; Nolte, R. J. M. *J. Org. Chem.* **1997**, *62*, 2334.
- Sijbesma, R. P.; Wijmenga, S. S.; Nolte, R. J. M. *J. Am. Chem. Soc.* **1992**, *114*, 9807. Reek, J. N. H.; Engelkamp, H.; Rowan, A. E.; Elemans, J. A. A. W.; Nolte, R. J. M. *Chem. Eur. J.* **1998**, *4*, 716.

Chapter 8

Molecular Clip Porphyrin Arrays

8.1 Introduction

The light-harvesting systems present in plants are the means by which Nature is able to very efficiently convert light into chemical energy. An important step was taken in the understanding of the process of photosynthesis when the structure of the reaction center of the purple bacterium *Rhodospseudomonas viridis* was determined as the first membrane bound protein complex.¹ More recently a further step was taken when the LH2 antenna complex of the purple bacterium *Rhodospseudomonas acidophila* was crystallized and its structure determined to 2.5 Å resolution.² The LH2 antenna system is capable of capturing light energy and diffusing it over an array of chromophores. This energy is then transferred via a multi-step process to another light harvesting complex, LH1, and then onto the photosynthetic reaction center.³ The active assembly of LH2 consists of two sets of chromophoric rings, one containing 27 bacteriochlorophyll and the other 9 carotenoid chromophores, held in place by 18 helical protein molecules. The overall architecture of LH2 resembles a hollow cylinder with a radius of 18 Å (Figure 8.1).² The system is perfectly designed to harvest light due an ideal energy gradient between the different chlorophyll units.



Figure 8.1 Cyclic arrangement of the bacteriochlorophyll and carotenoid chromophores in the crystal structure of the LH2 complex of *Rhodospseudomonas acidophila*.

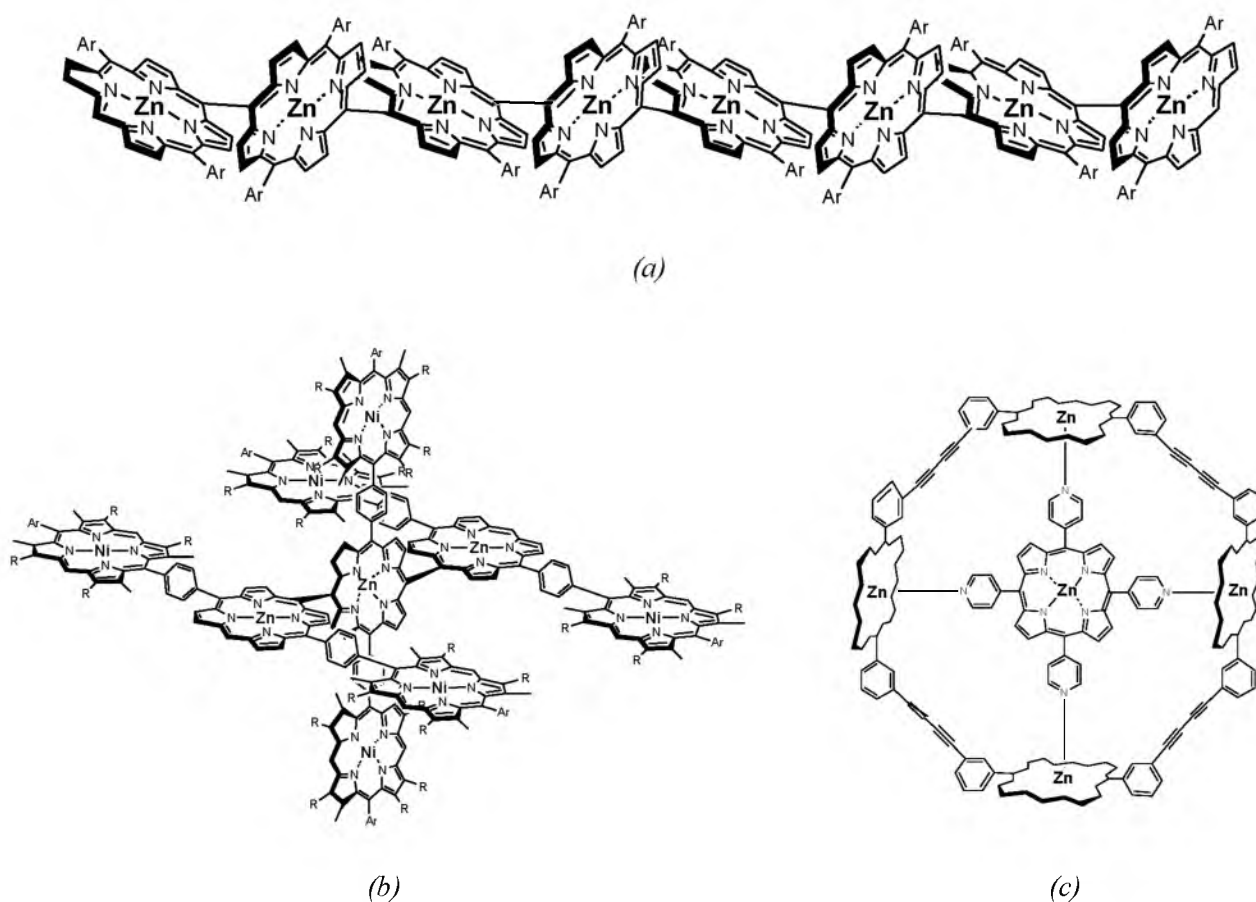


Figure 8.2 Examples of covalently connected linear and circular porphyrin arrays from (a, b) Osuka, and (c) Sanders.

In recent literature there have been numerous articles describing the construction of artificial porphyrin arrays.⁴ Many simplified models have been constructed in order to get a better understanding of the factors governing the efficient light-harvesting process carried out by the natural systems. The main purpose of the majority of these investigations was to understand the interplay between the structure of the model arrays and the efficiency of directional electronic excitation energy transfer or charge separation. The very simplest systems, synthetic bisporphyrins bridged by various spacers have been shown to be very useful for the study of the primary photosynthetic processes.⁵ More recently, effort has been directed towards the creation of higher oligomers of porphyrins, which can be arranged in a linear,^{6,7} circular,^{8,9} or dendritic¹⁰ fashion (some examples are shown in Figure 8.2). A great disadvantage of many of these covalently built systems is their elaborate and costly multistep synthesis. It is therefore that alternative approaches have been investigated, such as the self-assembly of porphyrin monomers into linear or circular arrays through strong intermolecular hydrogen bonding interactions,¹¹ self-assembly approaches involving crystal engineering methods¹² and the aggregation of ionic porphyrins in water.¹³ Recent research has shown that the linking of porphyrins by highly predictive metal-ligand interactions can be a very efficient route toward the assembly of well-defined arrays.¹⁴ Following this approach, linear,¹⁵ planar 2-dimensional¹⁶ and circular¹⁷ multiporphyrin systems have been self-assembled in structures with a precisely controlled shape and size (Figure 8.3).

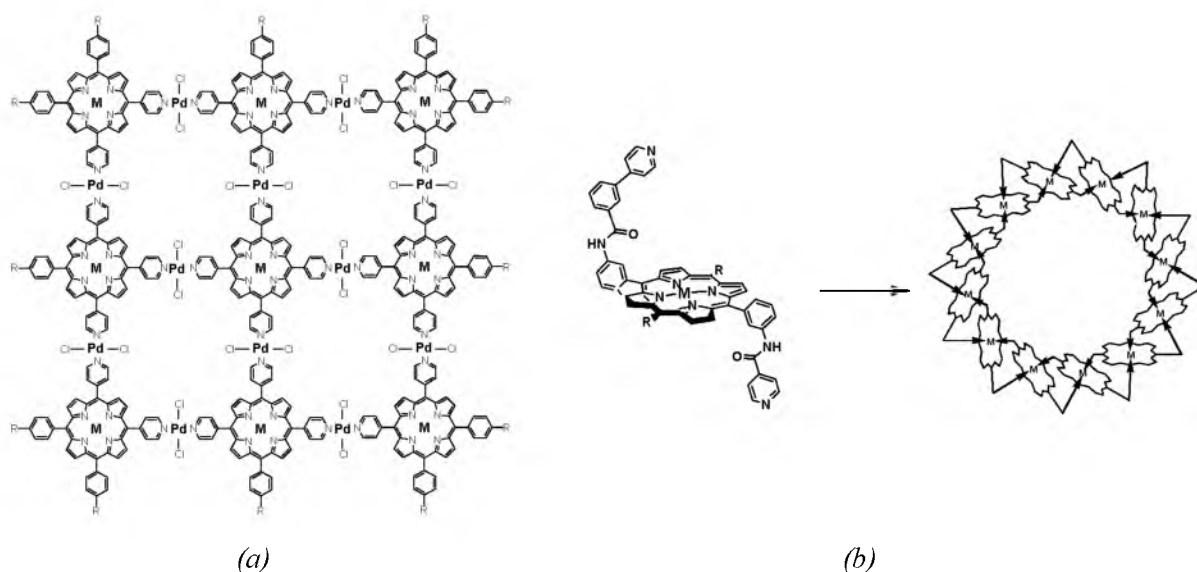


Figure 8.3 Examples of porphyrin arrays which are self-assembled through metal-ligand coordination from (a) Drain and (b) Hunter.

The research in this chapter deals with the construction of artificial porphyrin arrays by specific self-assembly utilizing molecular clip receptors.¹⁸ Three different approaches to construct porphyrin arrays were followed. The first approach makes use of the ability of clips functionalized with long hydrocarbon tails to form, upon complexation with a porphyrin guest, ordered thin films by means of melt-processing (Section 8.2). The second approach was to complex clips functionalized with porphyrins on their convex side to a central porphyrin guest (Section 8.3). In the last approach, basket-shaped molecules functionalized with two porphyrins are organized around a central porphyrin by means of a metal-templated self-assembly process (Section 8.4).

8.2 Construction of porphyrin arrays by melt-processing

8.2.1 Introduction

In Chapter 5 it has been demonstrated that clip molecules which are functionalized on their convex side with long hydrocarbon tails are able to form lamellar crystalline solids by means of dimerization of the clip head-groups and further self-assembly of these head-groups into two-dimensional sheets. It was shown that the properties of these materials can be tuned by the incorporation of guests, such as methyl 3,5-dihydroxybenzoate and 3,5-dihydroxybenzoic acid.¹⁹ The resulting lamellar materials were prepared by melt-processing, *i.e.* the appropriate amounts of host and guest were co-melted, whereupon at subsequent cooling the guests were incorporated in the solid in a well-defined manner. It was our aim to extend the possibilities of this method by the inclusion of multifunctional guests, *i.e.* porphyrins, into these lamellar solids. Host-guest complexes were therefore prepared between clips **1-3** and tetrafunctional porphyrin guest **4** (Chart 8.1), which in principle should generate a self-assembled system containing a porphyrin core surrounded by an outer coating of molecular clips (Figure 8.4).

8.2.2 Thermal behavior of the complexes in the solid state

The 4:1 complexes of clips **1-3** and porphyrin **4** were prepared by slow evaporation of solutions

Chart 8.1

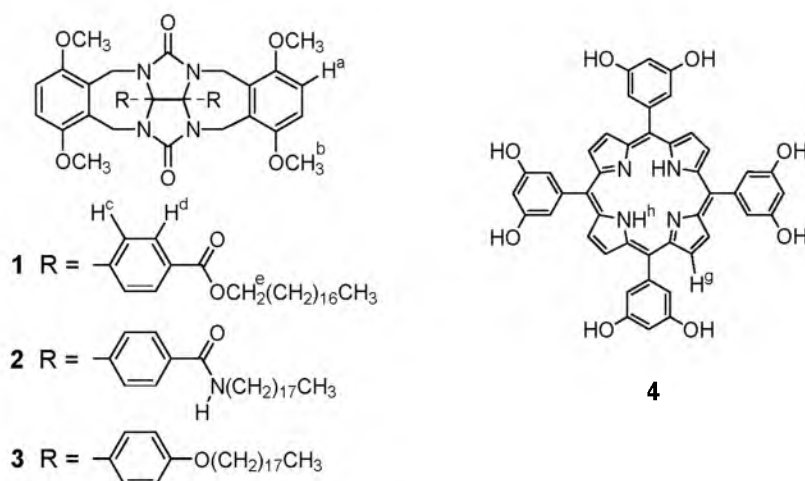


Table 8.1 Observed phase transition temperatures and enthalpies of host–guest complexes between hosts 1–3 and porphyrin guest 4.

Complex	Transition ^a	<i>T</i> (°C) ^b	ΔH (kJ mol ⁻¹) ^b
1,4	K → K ¹	105.5 (89.1)	5.7 (–2.6)
	K ¹ → I	167.8 (–) ^c	15.0 (–) ^c
2,4	K → I	218.7 (–) ^c	10.9 (–) ^c
3,4	K → K ¹	102.0 (–) ^c	13.1 (–) ^c
	K ¹ → K ²	112.6 (106.4)	13.3 (–11.8)
	K ² → K ³	198.9 (187.7)	89.6 (–53.9)
	K ³ → I	205.6 (194.8)	

^aK, K¹, K², K³: crystalline phases; I: isotropic phase. ^bDetermined by DSC, values obtained from the fourth heating run; in parenthesis: values obtained from the third cooling run. ^cNo phase transition was observed.

of the components in a mixture of chloroform and methanol (4:1, v/v).²⁰ Samples of the resulting materials were heated to the isotropization temperature with the help of the thermal optical polarized microscopy equipment, and subsequently cooled. Neither cooling of the samples at various temperature rates (10–1°C min⁻¹), nor excessive annealing at various temperatures resulted in the formation of an anisotropic texture. Instead, the materials slowly solidified into dark red glassy solids. The samples were further investigated with differential scanning calorimetry (DSC, see Table 8.1). For all the complexes, several consecutive heating and cooling runs were required to obtain identical DSC traces. This indicates that the components have difficulties to order themselves and form a homogeneous film. The observed thermal behaviour of the complexes resembled those seen for the thermal behaviour of the respective uncomplexed hosts in the sense that transitions around 100°C were followed by an isotropization transition with a much higher enthalpy 60–100 degrees higher in temperature (see Chapter 5). This suggests that all the complexes are crystalline up to isotropization. For the **1,4** complex, this conclusion

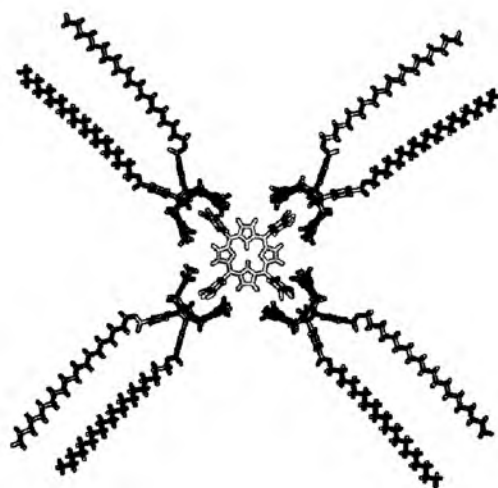


Figure 8.4 Computer modeled structure of the 4:1 host-guest complex between **1** and **4**.

was confirmed by X-ray powder diffraction (XRPD) measurements which showed a number of sharp peaks at 20 and 130°C.²¹ In analogy to the thermal behaviour of uncomplexed **1-3**, the transitions around 100°C are believed to be related to a rearrangement of the alkyl tails of the clips. At isotropization, the interactions between the molecules are broken, and the thermal parameters involved with this transition can provide information about the strength of these intermolecular interactions. While the differences in isotropization temperature (T_i) of the different complexes are comparable to the differences in T_i of the uncomplexed hosts, the isotropization enthalpy (ΔH_i) of **2₄** is somewhat smaller than that of **1₄**, suggesting that the intermolecular interactions within the former complex are somewhat weaker than those within the latter. The very high ΔH_i of **3₄**, in contrast, suggest that the intermolecular interactions within this complex are very strong.

8.2.3 UV-vis and fluorescence studies

In a large majority of reported porphyrin aggregates, the porphyrin molecules are stacked in a cofacial arrangement with an interplanar distance ranging from 3.5-4 Å.²² The formation of aggregates between porphyrins is proposed to be dominated by van der Waals interactions, whereas their intermolecular geometry is controlled by electrostatic interactions.²³ Information about the aggregation geometry can be obtained from changes in the absorption and fluorescence

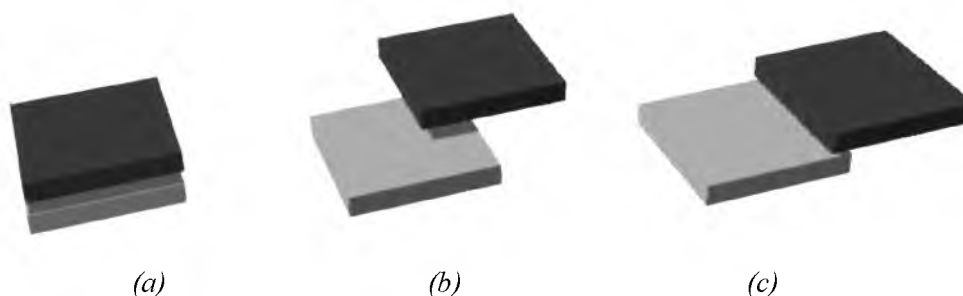


Figure 8.5 Arrangement of porphyrins in aggregates and changes in the UV-vis spectrum according to Kasha's exciton theory. (a) Face-to-face, blue shift of the Soret band. (b) Head-to-tail, red shift of the Soret band. (c) Edge-to-edge, splitting of the Soret band.

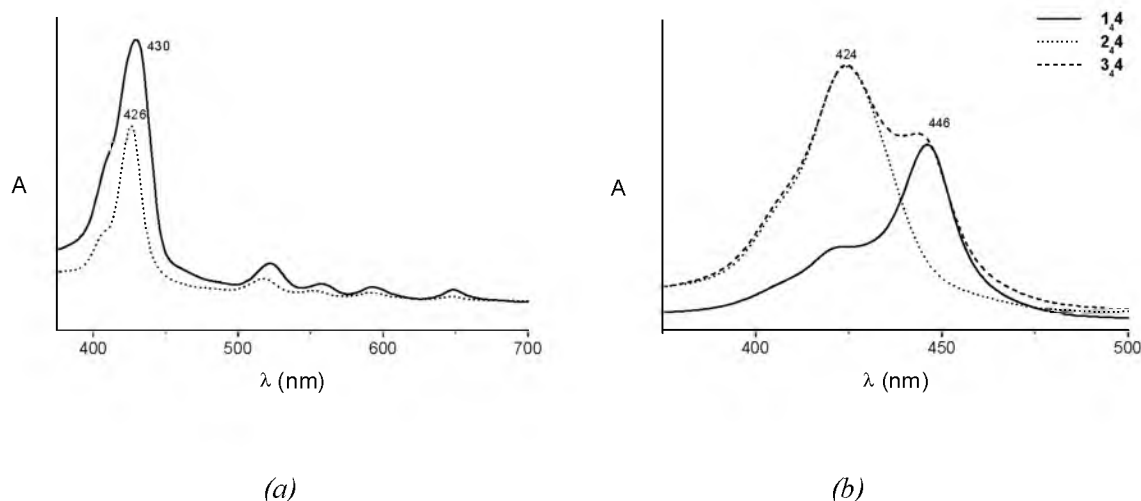


Figure 8.6 (a) UV-vis spectra of a solid film of **1₄₄** before (solid line) and after (dashed line) melt processing. (b) UV-vis spectra of the Soret band region of **1₄₄**, **2₄₄**, and **3₄₄** in chloroform

Table 8.2 Spectroscopic data of host-guest complexes **1₄₄**, **2₄₄**, and **3₄₄**.

	UV-vis				Fluorescence	
	Thin film ^a		CHCl ₃ solution ^b		CHCl ₃ solution ^b	
	$\lambda_{\text{Soret band}}/\text{nm}$	$\lambda_{\text{Q-bands}}/\text{nm}$	$\lambda_{\text{Soret band}}/\text{nm}$	$\lambda_{\text{Q-bands}}/\text{nm}$	$\lambda_{\text{em}}/\text{nm}$	I/a.u.
1₄₄	426	522, 558, 593, 648	424, 446	529, 566, 586, 641	634 ^c	8
2₄₄	422	520, 550, 592, 648	424	520, 551, 590, 647	649 ^d	25
3₄₄	429	520, 551, 593, 648	424, 444	525, 560, 588, 644	643 ^e	9

^aAfter melt-processing. ^b[Porphyrin] = 5.5×10^{-6} M. ^c $\lambda_{\text{ex}} = 446$ nm. ^d $\lambda_{\text{ex}} = 424$ nm. ^e $\lambda_{\text{ex}} = 444$ nm.

spectra of porphyrin compounds. The *exciton theory* developed by Kasha²⁴ gives a qualitative interpretation of the relative arrangement of porphyrin monomers with respect to each other. According to this theory, the interaction of the porphyrin dipoles with respect to each other induces shifts or splitting of the porphyrin Soret band, as illustrated in Figure 8.5.

To investigate the ordering of the porphyrins within **1₄₄**, **2₄₄** and **3₄₄**, UV-vis spectra were recorded of thin solid films of these complexes which were melt-processed on glass substrates (Figure 8.6a, Table 8.2). Compared to the wavelength of the Soret band of uncomplexed **4** in acetone ($\lambda_{\text{Soret}} = 424$ nm), λ_{Soret} of complexes **1₄₄** and **3₄₄** displayed a red shift in the solid films, suggesting a head-to-tail arrangement of the porphyrins. A red shift was also observed for the Soret band in a cast film of **4** ($\lambda_{\text{Soret}} = 429$ nm). Head-to-tail arrangements, however, are commonly observed for porphyrins in the solid state, for example in the crystal structure of tetrakis-*meso*-phenyl porphyrin.²⁵

When the melt-processed²⁶ complexes were dissolved in chloroform ([porphyrin] = 5.5×10^{-6} M), completely different UV-vis spectra were observed (Figure 8.6b, Table 8.2). For **1₄₄** and **3₄₄**, the Soret bands appeared to be split, whereas **2₄₄** displayed only a single band at 424 nm. According to the exciton theory, the splitting in the Soret band observed for the former two complexes would indicate an edge-to-edge arrangement of the porphyrins. The observation of two bands can, however, also be caused by the presence of both aggregated and non-aggregated

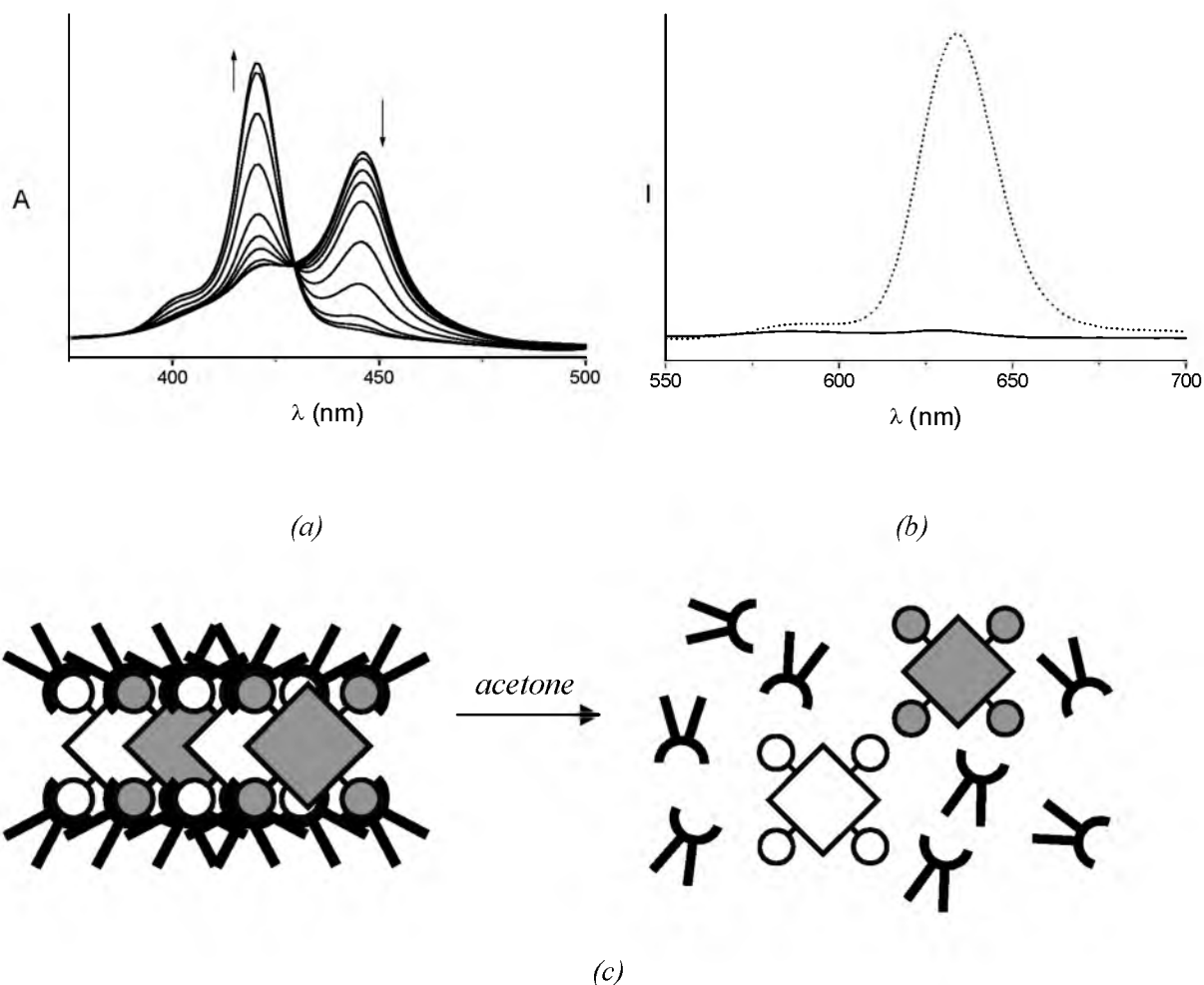


Figure 8.7 (a) UV-vis spectral changes upon the addition of acetone to a solution of **144** in chloroform. (b) Fluorescence emission spectra of **144** in chloroform ($\lambda_{\text{ex}} = 446$ nm, solid line) and of **144** in a mixture of chloroform and acetone ($\lambda_{\text{ex}} = 424$ nm, (9:1, v/v), dashed line). (c) Schematic picture of the dissociation of the aggregate and the complex upon the addition of acetone.

porphyrin molecules. This is supported by the fact that a gradual addition of acetone to the solution containing **144** caused a decrease in intensity of the band at 446 nm, while simultaneously the intensity of the band at 424 nm increased (Figure 8.7a). An isosbestic point at 430 nm was observed during this titration, which supports the above assumption that the porphyrins in pure CHCl_3 are present in either aggregated or non-aggregated form. More than 5% (v/v) of acetone was needed to fully remove the red shifted component. From these observations it is proposed that part of the porphyrin molecules in CHCl_3 solution strongly aggregate in a head-to-tail fashion, which causes a red shift in the UV-vis spectrum, while the remaining porphyrins are free. Addition of acetone to a solution of **344** had a similar effect on the porphyrin Soret band, while addition of acetone to a solution of **244** only caused a small sharpening of the Soret band at 424 nm. When the Soret bands of the complexes in CHCl_3 were excited (in the case of **144** and **344** at the highest λ_{max} values), very little fluorescence emission was observed above 600 nm (Figure 8.7b). This quenching is believed to be caused by the close proximity of the porphyrin molecules in the aggregates. Upon the addition of acetone the fluorescence emission was restored. In pure CHCl_3 the emission of **244** was substantially larger

than the emissions of the other two complexes (Table 8.2). It is proposed, therefore, that upon the addition of acetone the aggregated porphyrin complexes are broken up and only monomeric porphyrins are observed (Figure 8.7c).

8.2.4 NMR solution studies

The structures of the porphyrin complexes were further investigated by ^1H NMR spectroscopy. The results are presented in Figure 8.8 and in Table 8.3. When the ^1H NMR spectra of uncomplexed **1** and **144** (both 5 mM) are compared, it is clear that in the spectrum of the complex most of the signals are significantly broadened. In addition, the resonances of the side-wall and methoxy protons are considerably shifted upfield ($\Delta\delta = -0.8$ and -0.3 ppm, respectively, see Table 8.3). The resonances belonging to the porphyrin are significantly broadened, probably due to slow exchange on the NMR timescale. To get more detailed information about the structure of the complex, a 2D NOESY spectrum was recorded (Figure 8.8c). Several nOe contacts were observed between the porphyrin and clip protons, *e.g.* between H_g and $\text{H}_a/\text{H}_b/\text{H}_c$, and between H_h and H_b (see Chart 8.1). In addition, there appeared to be a number of very strong nOe contacts between protons of **1** which cannot be a result of *intramolecular* close contacts, such as between H_a/H_b and H_c/H_d . These results indicate that in CDCl_3 clip **1** and porphyrin **4** are complexed, and in addition that the molecules of **1** are in very close proximity to each other. When the solution of **144** was heated or diluted, the signals of the clip protons H_a and H_b and the porphyrin protons H_g shifted downfield and sharpened, whereas the porphyrin H_h signal shifted upfield. The addition of deuterio acetone induced a similar effect. The downfield shifts of the proton signals of **1** indicates breaking up of the complex with **4**.

Table 8.3 Selected NMR resonances (δ , ppm) for hosts **1–3** and their **4:1** complexes with porphyrin guest **4**.^a

	Proton ^b	1	144	2	244	3	344
Host protons	H_a	6.62	5.76	6.65	6.51	6.65	5.96
	H_b	3.74	3.46	3.70	3.62	3.76	3.48
Porphyrin protons	H_g		8.63		8.71		8.70
	H_h		-2.71		-2.84		-2.72

^a CDCl_3 solution, [porphyrin] = 5.0 mM, 298 K. ^bFor numbering see Chart 8.1.

While the ^1H NMR spectrum of **344** in CDCl_3 (5 mM) was very similar to that of **144**, the spectrum of **244** (5 mM) displayed relatively sharp signals, of which the side-wall and methoxy protons of **2** were shifted only slightly upfield ($\Delta\delta \sim -0.1$ - -0.15 ppm, Table 8.3) when compared to uncomplexed **2**. The amide NH proton signals of **2** were shifted significantly downfield ($\Delta\delta = +0.25$ ppm), which indicates their involvement in a hydrogen bonding interaction. The intensities of the proton signals of the porphyrin guest were much weaker than in the spectra of **144** and **344**. In addition, the signals of the porphyrin NH protons of **244** were shifted upfield compared to these signals in the other complexes (Table 8.3). In the 2D NOESY spectrum of **244**, only weak nOe contacts were observed between the β -pyrrole protons of **4** and the side-wall and methoxy protons of **2**.

8.2.5 Discussion

It is proposed that porphyrin **4** and host **1** form a self-assembled structure which is stabilized by a variety of intermolecular interactions, which probably act in a cooperative manner. The shifts

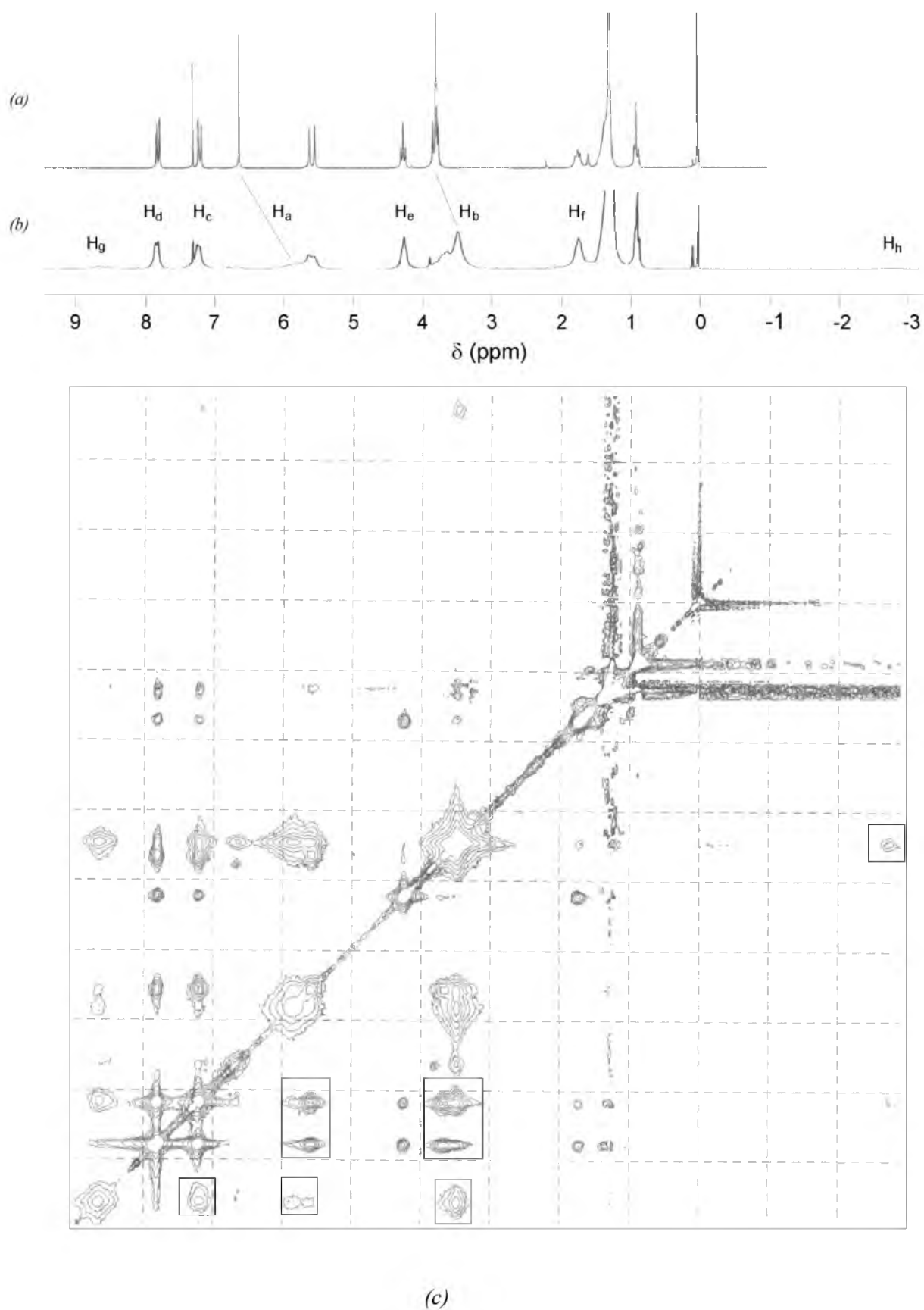


Figure 8.8 (a) ^1H NMR spectrum of 1. (b) ^1H NMR spectrum of 1,4. (c) NOESY 2D spectrum of 1,4, in which the intermolecular nOe contacts are highlighted in squares.

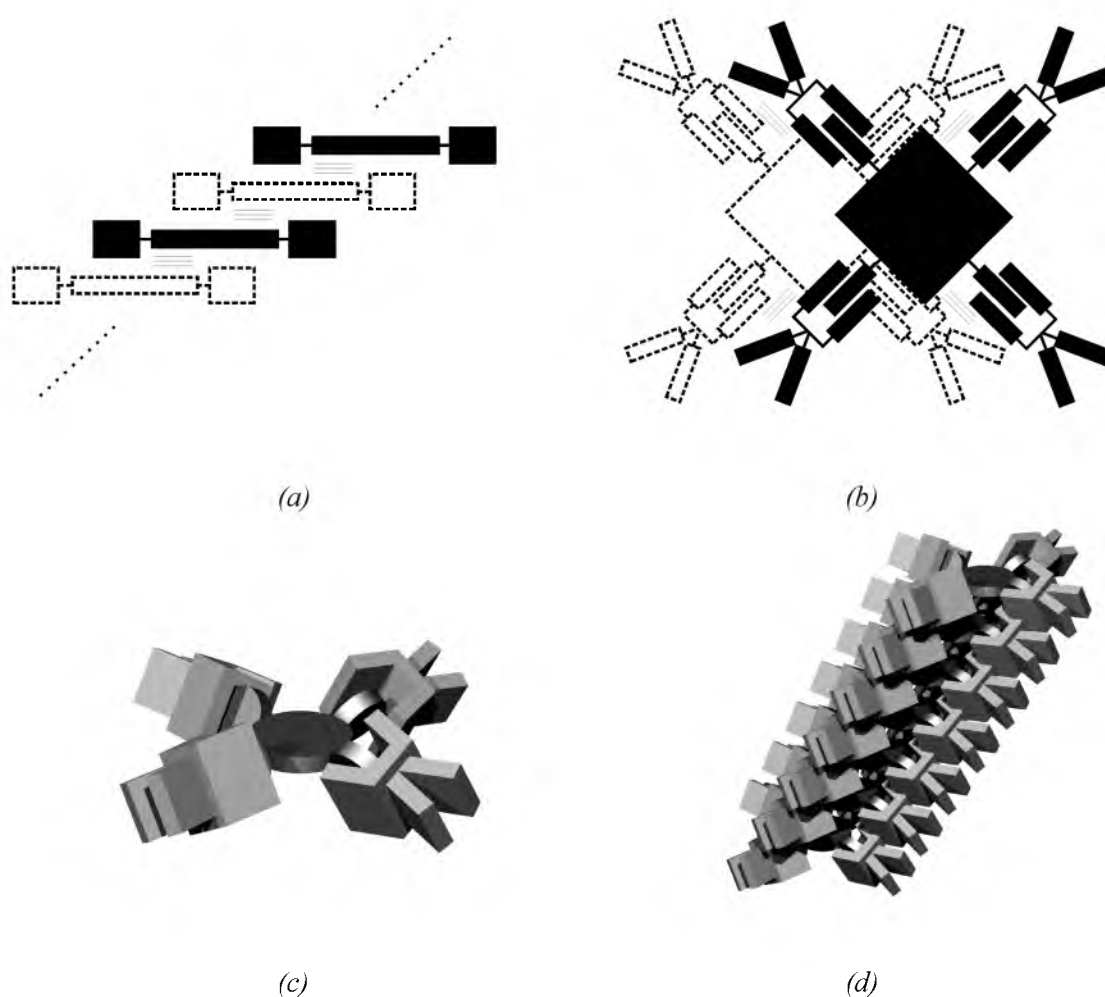


Figure 8.9 Schematic structures, based on the UV-vis, fluorescence, and NMR studies, of the ordering of the 4:1 host-guest complex between **1** and **4**. (a) Side view of the stacking of the guest porphyrins **4**. (b) Top view of two 4:1 complexes. (c) 3D structure of the 4:1 complex. (d) 3D structure of the ordering of these 4:1 complexes.

observed in the NMR spectrum indicate that the clip molecules form a complex with the dihydroxybenzene parts of the porphyrin. This complexation was also confirmed by shifts in the carbonyl stretching vibrations of the host and the relatively sharp hydroxy stretching vibration of the porphyrin dihydroxybenzene groups in the FTIR spectra in chloroform solution. In addition, both the red shift in the porphyrin Soret band in the UV-vis spectrum and the strong quenching of the fluorescence emission suggest that the porphyrins in the complex are at very close distance. A possible self-assembled structure for the 4:1 host-guest complex is illustrated in Figure 8.9. In this complex, the porphyrins are cofacially arranged in a head-to-tail fashion, which explains the UV-vis and fluorescence results. Molecular modeling indicates that such a head-to-tail arrangement allows four clip molecules to be attached to the central porphyrin. Additional stabilizing π - π stacking interactions are possible between the side-walls of the clips in adjacent 4:1 complexes. The proposed self-assembled arrangement of the host-guest complexes is in line with the strong nOe contacts which were observed in the NOESY 2D NMR spectrum. The close proximity of adjacent clips, as well as the fact that the cavities of **1** in the proposed model are partly situated above the porphyrin plane, account for the observed large

complexation induced shifts of the side-wall and methoxy protons of **1** ($\Delta\delta = -0.86$ and -0.28 ppm, respectively).²⁷

The several consecutive heating and cooling runs which were required to obtain a stable 4:1 complex of **1** and **4** in the solid state suggest that the components have difficulties to order themselves into a homogeneous layer. However, the absence of phase separation suggests that eventually each of the porphyrins is complexed to four clip molecules. It is as yet unclear how many clips are complexed to the porphyrin in chloroform solution, since the association constant between a clip and a dihydroxybenzene unit attached to a porphyrin is relatively low.²⁸ Upon strong dilution of **1** and **4** in CDCl_3 , the upfield shifted signals of the side-wall and methoxy protons of **1** shifted downfield, while the porphyrin remained completely soluble. Hence, it is not unlikely that the complexation of only *one* clip molecule **1** is sufficient to dissolve **4** in chloroform. At higher concentrations, longer head-to-tail aggregates of porphyrins are formed as indicated by UV-vis. At the periphery of these porphyrin arrays, the dihydroxybenzene functions can be progressively occupied by clip molecules, which further stabilize the aggregates by π - π interactions between adjacent clips. NMR dilution or host-guest titrations could not yet give definitive information about the stoichiometry between the components in these superstructures.

The self-assembled structure of **2** and **4** in solution is significantly different from that of **1** and **4**. The observed relatively sharp signals and the small upfield shifts in the NMR spectrum, combined with the absence of nOe contacts between different molecules of **2** in the NOESY 2D spectrum, suggest that the clips in the self-assembled structure are in a different geometry to that postulated for the **1** and **4** complex. The absence of a large red shift of the porphyrin Soret band in the UV-vis spectrum suggests also that the porphyrins in **2** and **4** are relatively far apart. This hypothesis is confirmed by the lower degree of fluorescence quenching observed for **2** and **4** compared to **1** and **4**. Since the only difference between **1** and **2** is the presence of an amide function in the latter clip, it is proposed that this group plays an active role in the self-assembly of **2** and **4**. The formation of hydrogen bonds between the amide NH functions and hydrogen bond acceptor sites in adjacent clip molecules, which was suggested by shifts in the ^1H NMR spectrum of **2** and **4**, might arrange the components of the complex in such a way that the porphyrins are further apart than in **1** and **4**.

Based on the similarities in the NMR, UV-vis and fluorescence spectra, the arrangement of the molecules of **3** and **4** in solution is proposed to be similar to that of the molecules of **1** and **4**. The large ΔH_i of **3** and **4**, however, suggests that the interactions between the constituting building blocks of this complex in the solid state are much stronger than those between the building blocks of **1** and **4**. This is attributed to a closer packing of the alkyl tails of **3** in the former complex. This difference in packing was also observed in the uncomplexed hosts **1** and **3** (see Chapter 5).

8.3 Molecular clips with porphyrin-functionalized convex sides

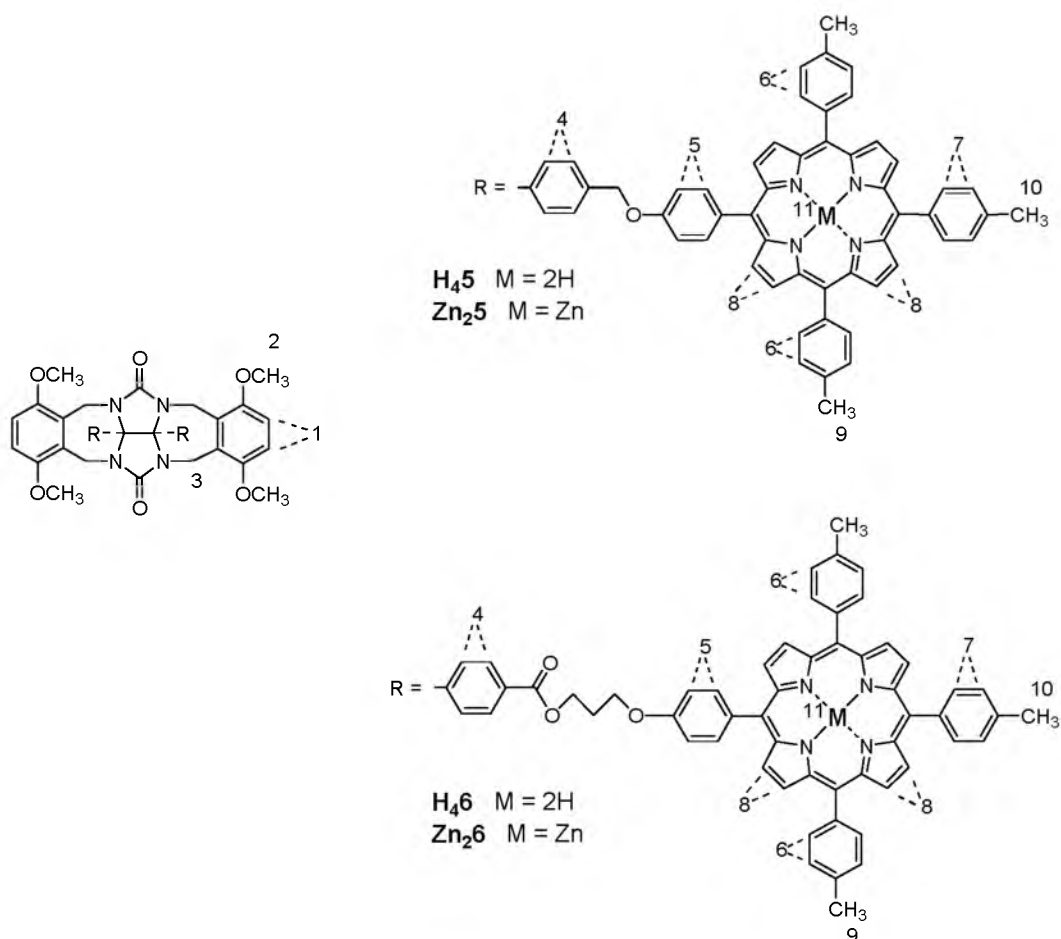
8.3.1 Introduction

In the previous section it was demonstrated that by means of melt-processing 4:1 complexes of molecular clips and a central porphyrin guest can be generated. Furthermore, it was shown that the central porphyrin guests have the propensity to stack in a head-to-tail geometry to give porphyrin arrays surrounded by a mantle of clip molecules. Following up these studies we reasoned that when the alkyl tails of the molecular clips would be replaced by porphyrins, a multiporphyrin complex would be obtained composed of a central porphyrin surrounded by 8



Figure 8.10 Computer modeled structure of the 4:1 host-guest complex between **H₄₅** and **4**.

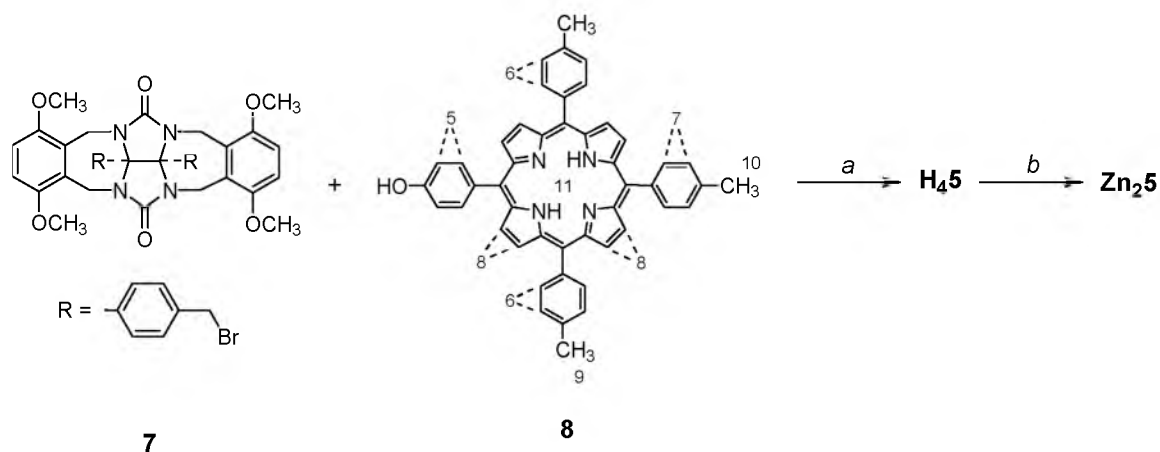
Chart 8.2



additional porphyrins (Figure 8.10). To investigate this possibility, porphyrin functionalized clips **H₄₅** and **H₄₆** (Chart 8.2) were designed and synthesized and their host-guest complexation properties with **4** studied.

8.3.2 Synthesis

Clip **H₄5** was synthesized from the benzyl bromide functionalized clip **7**²⁹ by a reaction with monohydroxy porphyrin **8** in dimethylformamide using potassium carbonate as a base (Scheme 8.1). The purification of the product was hindered by the presence of small amounts of contaminations in the starting compound **7**, *viz.* mono- and tribrominated compounds.³⁰ As a result of this, small amounts of clips functionalized with only one porphyrin were formed. It was very difficult to separate these monofunctionalized clips from **H₄5**. In addition, small amounts of unreacted porphyrin **8** remained present in the product, possibly because this molecule is easily clamped in between the two porphyrin substituents of **H₄5** as a result of intermolecular π - π stacking. By adding a small percentage of triethylamine to the eluent for column chromatography, however, it was possible to remove this impurity. A small amount of pure material could be obtained (total yield 14%). Metallation of **H₄5** with zinc acetate dihydrate in a 2:1 mixture of chloroform and methanol gave metalloclip **Zn₂5** in nearly quantitative yield, after purification by column chromatography.



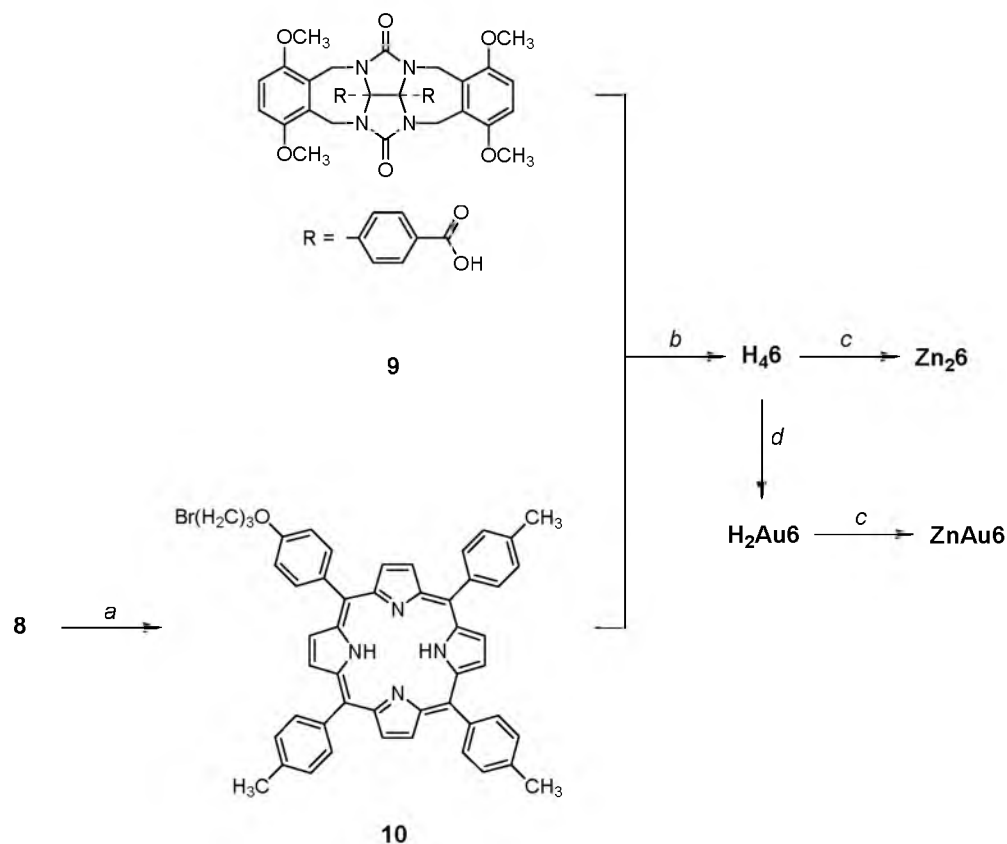
Scheme 8.1 Reagents and conditions: (a) K_2CO_3 , KI, DMF, $100^\circ C$, 64 h. (b) $Zn(OAc)_2 \cdot 2H_2O$, $CHCl_3$, MeOH, reflux, 3 h.

As a consequence of the difficulties encountered in the synthesis of **H₄5**, a second route toward porphyrin functionalized clips was designed. As starting material, dibenzoic acid functionalized clip molecule **9** (Scheme 8.2) was used (see Chapter 5), which can be easily obtained in pure form. Porphyrin **10** was obtained from **8** by alkylation with a 40-fold excess of 1,3-dibromopropane in dimethylformamide using potassium carbonate as a base (Scheme 8.2). It was then coupled to **9** in dimethylformamide using potassium carbonate as a base. Clip **H₄6** (Chart 8.2) was readily obtained in a yield of 42%, after purification by column chromatography.

8.3.3 Structure of the porphyrin functionalized clips

In the 1H NMR spectrum of **H₄5** in $CDCl_3$ all the porphyrin proton resonances exhibited significant upfield shifts (up to -0.24 ppm) when compared to their signals in reference porphyrin **8** (Table 8.4). We attribute these shifts to the influence one porphyrin experiences from the ring current of the other porphyrin.³¹ A computer-modeled representation of **H₄5** based upon the observed upfield shifts is shown in Figure 8.11. In the 1H NMR spectrum of the more flexible **H₄6**, the porphyrin proton signals were also shifted upfield with respect to **8**, but to a lesser extent than in the case of **H₄5** (Table 8.4) This suggests that in the former clip the porphyrins are further apart than in the latter.

Compound **H₄6** was converted to **Zn₂6** in nearly quantitative yield in a similar manner as described for the synthesis of **Zn₂5**.



Scheme 8.2 Reagents and conditions: (a) 1,3-Dibromopropane, K_2CO_3 , $20^\circ C$, 24 h. (b) K_2CO_3 , KI, DMF, $100^\circ C$, 64 h. (c) $Zn(OAc)_2 \cdot 2H_2O$, $CHCl_3$, MeOH, reflux, 3 h. (d) $KAuCl_4$, NaOAc, AcOH, reflux, 64 h.

Table 8.4 Assignments of proton resonances (δ , ppm) in the 1H NMR spectra of compounds **8**, **H₄5**, the 4:1 host–guest complex between **H₄5** and **4**, **H₄6** and **Zn₂6**^a

Proton set ^b	8	H₄5	(H₄5)₄	H₄6	Zn₂6
1		6.70	6.28	6.57	5.30
2		3.81	3.65	3.71	2.60
3		5.65, 3.91	5.66, 3.86	5.51, 3.77	4.14, 2.62
4		7.39, 7.26	7.35, 7.32	8.02, 7.13	7.73, 6.83
5	8.07, 7.20	7.76, 6.95	7.73, 6.91	7.88, 7.25	7.73, 7.19
6	8.09, 7.55	7.92, 7.35	7.90, 7.33	8.05, 7.50	7.98, 7.50
7	8.09, 7.55	7.85, 7.35	7.82, 7.33	8.03, 7.46	8.07, 7.52
8	8.85	8.73, 8.71, 8.69, 8.64	8.72, 8.69, 8.68, 8.62	8.81-8.77	8.88, 8.85, 8.77, 8.70
9	2.70	2.56	2.55	2.66	2.68
10	2.70	2.63	2.62	2.66	2.69
11	-2.78	-2.83	-2.82	-2.78	

^a $CDCl_3$ solution, 500 MHz, 298 K. ^bFor proton numbering see Scheme 8.1 and Chart 8.2.

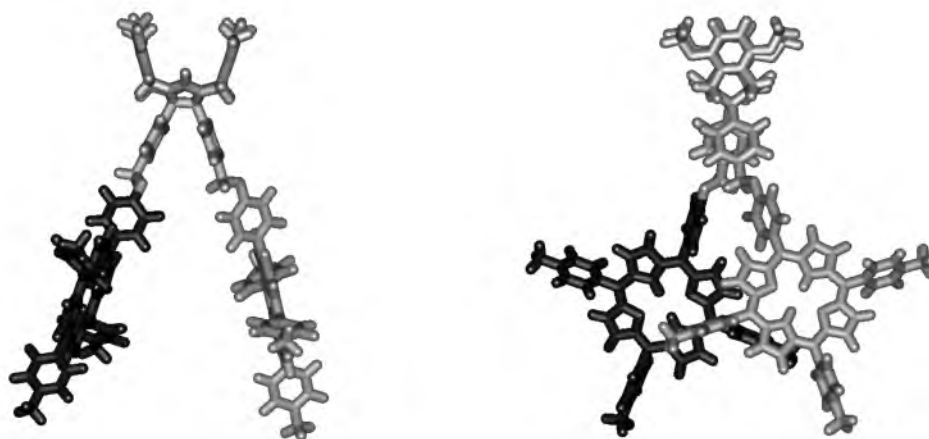


Figure 8.11 Computer modelled structure of **H₄₅** (front and side-view) based on the 2D NOESY spectrum and the observed shifts in the ¹H NMR spectrum.

The ¹H NMR spectra of the zinc porphyrin derivatives **Zn₂5** and **Zn₂6** in CDCl₃ were more difficult to interpret. In the spectrum of **Zn₂5**, sharp signals were observed only for the porphyrin protons; the signals of the cavity part were extremely broadened. In the spectrum of **Zn₂6**, however, all the NMR signals were sharp. Compared to the spectrum of **H₄₆**, very large upfield shifts were observed for the cavity proton sets H₁ ($\Delta\delta = -1.27$ ppm), H₂ ($\Delta\delta = -1.11$ ppm), H₃ ($\Delta\delta = -1.37$ and -1.15 ppm), and H₄ ($\Delta\delta = -0.29$ and -0.30 ppm) (see Table 8.4). The UV-vis spectra of both zinc porphyrin clips in CHCl₃ displayed a Soret band with a maximum at 424 nm, a value which is shifted 4 nm to the red when compared to the UV-vis spectrum of ZnTPP. The addition of methanol or acetone, which coordinated to the central zinc ion in **Zn₂5** and **Zn₂6**, returned the Soret band to 420 nm. The ¹H NMR spectra of both compounds in the presence of these ligands became similar to the NMR spectra of the respective free base analogues **H₄₅** and **H₄₆**. Combining the above observations in the UV-vis and ¹H NMR spectra, it is proposed that the porphyrins in **Zn₂5** and **Zn₂6** fold back onto the receptor cavities. This geometry change is the result of coordination of the zinc ions to the oxygen atoms of the methoxy groups of the side-walls (Figure 8.12). Molecular modeling revealed that such a backfolding is readily possible for both compounds. NMR dilution studies indicated that the coordination to the methoxy groups is intramolecular, further confirming the proposed backfolding.

For the protons near the cavity of **Zn₂5** and **Zn₂6**, larger upfield shifts than ~ -1.5 ppm would have been expected if the porphyrins are in such close proximity. Each of the zinc porphyrins, however, has the possibility to choose between *two* methoxy groups at each side-wall, rapidly interconverting between two possible geometries. For **Zn₂5**, the coordination on and off rates apparently are slower than for **Zn₂6**, which results in the observed broad signals in the NMR spectrum of the former compound.

We found that in addition to methanol and acetone also nitrogen bases can break the interaction between the porphyrin and the cavity. Addition of the ditopic base diazabicyclooctane (DABCO) to **Zn₂6**, for example, caused the formation of a very strong 1:1 complex, which was confirmed by ¹H NMR and UV-vis measurements. In this complex, the base is clamped in between the two zinc porphyrins fixing the latter substituents at the convex side of the clip (Figure 8.12c).³²

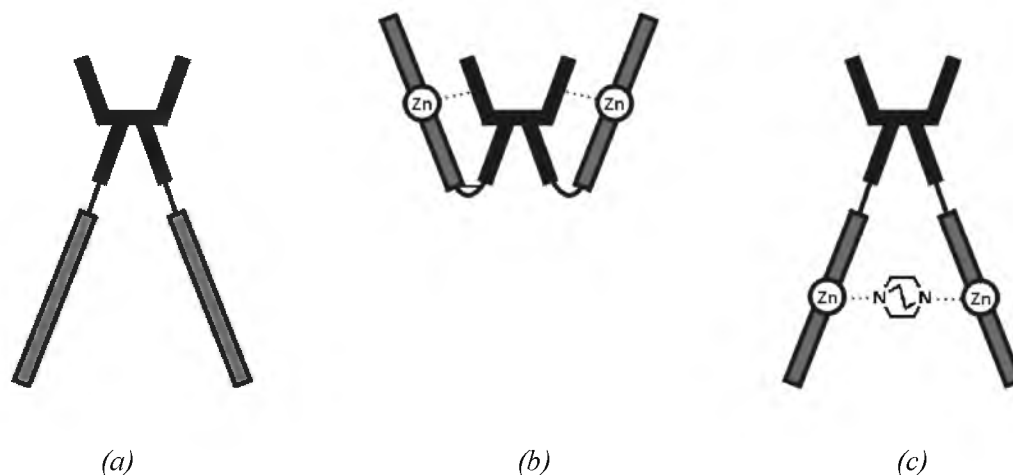


Figure 8.12 Schematic structures of porphyrin functionalized clips. (a) **H₄5** and **H₄6**. (b) **Zn₂5** and **Zn₂6**, with the porphyrin zinc ion coordinating to a methoxy group of the cavity. (c) The 1:1 complex between **Zn₂6** and DABCO.

8.3.4 Properties of the 4:1 host-guest complex of **H₄5** and **4**

Preparation of the 4:1 host-guest complex between clip **H₄5** and porphyrin **4** by melt-processing was difficult, because **H₄5** does not melt but decomposes above 400°C. It was also not possible to mix both compounds in chloroform, since **4** does not dissolve in this solvent, even in the presence of **H₄5**. An alternative method was applied, in which a solution of **H₄5** in chloroform was mixed with a solution of **4** in acetone. After slow evaporation of the solvents, the residue was sparingly soluble in chloroform. After applying the above procedure several times, however, a fully chloroform-soluble complex was obtained.

The ¹H NMR spectrum of the 4:1 complex displayed some remarkable similarities, as well as differences, with uncomplexed **H₄5** (Figure 8.13 and Table 8.4). For the complex, only very small upfield shifts were observed for the phenyl and pyrrole proton resonances of the porphyrin part of the receptors, whereas the resonances of the side-wall (H₁) and methoxy protons (H₂) of the cavity part displayed strong upfield shifts ($\Delta\delta = -0.42$ and -0.24 ppm, respectively). In addition, all signals of the cavity part of **H₄5** were significantly broadened.³³ None of the signals of the central porphyrin guest molecule could be clearly distinguished in the spectrum. To get more insight in its structure, a 2D NOESY spectrum of the complex was recorded. Apart from the expected intramolecular close contacts, strong nOe contacts were observed between H₂ and protons H₄, and between H₂ and *all* of the porphyrin protons of **H₄5** (H₅-H₁₁). These contacts can only be a result of intermolecular interactions between adjacent molecules of **H₄5** which are in close proximity. A similar behaviour was observed for the 4:1 complex between **1** and **4** (see Section 8.2), and it is proposed therefore that the 4:1 complex between **H₄5** and **4** has a comparable structure, *viz.* a stacked array of central porphyrins **4** surrounded by molecules of **H₄5** which are complexed to the dihydroxybenzene units of **4**. The Soret band in the UV-vis spectrum of this complex, however, did not display a red shift, as was observed for the complex between **1** and **4**. This implies that the central porphyrins in the complex between **H₄5** and **4** apparently do not further self-assemble to form larger arrays, as in **1₄4**, or that they are relatively far apart. Further studies will be needed to unravel the exact structure of the complex between **H₄5** and **4**.

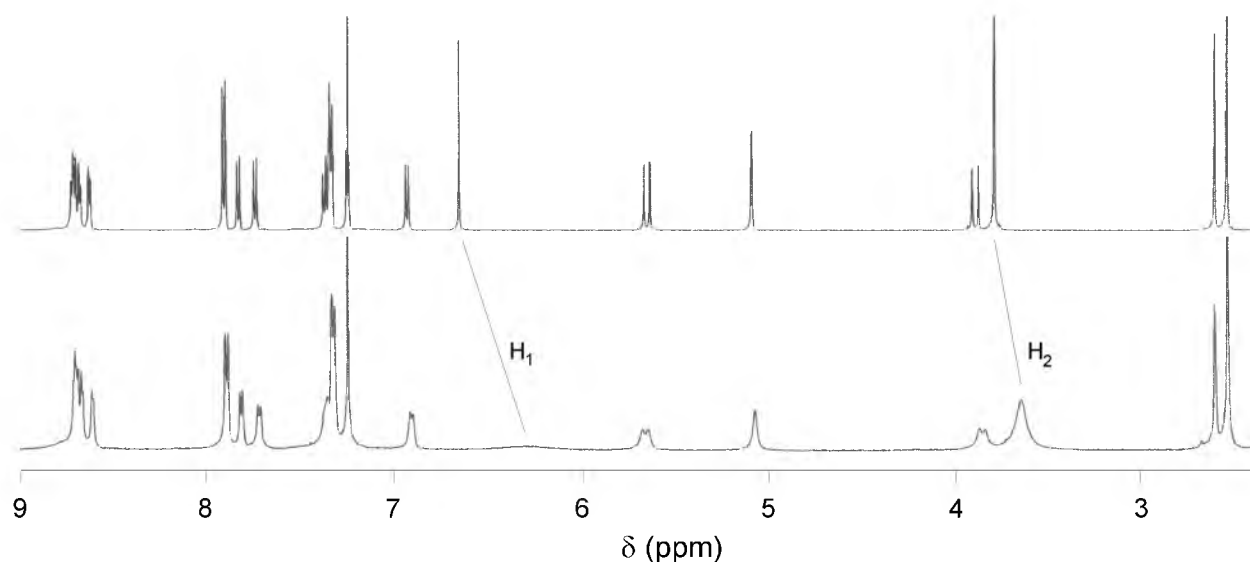
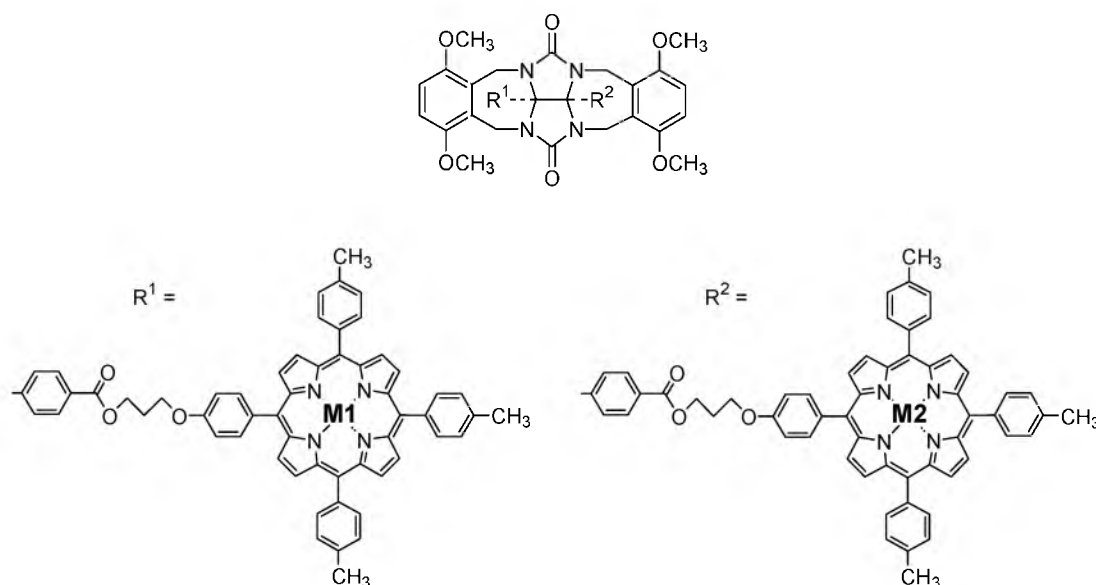


Figure 8.13 Parts of the ^1H NMR spectra (500 MHz) of porphyrin functionalized clip **H₄₅** (top) and the 4:1 host-guest complex between **H₄₅** and **4** (bottom) in CDCl_3 . For proton numbering see Chart 8.2.

8.3.5 Photophysical properties of a clip functionalized with a donor and acceptor porphyrin

After light energy has been harvested by the LH2 and LH1 antenna systems, it is eventually passed to the photosynthetic reaction center where it is converted into chemical energy through a series of electron transfer processes involving the special pair of this reaction center, two other porphyrins and a quinone molecule.³ In order to mimic parts of these electron transfer processes, we have previously constructed clip molecules containing one zinc porphyrin functionalized side-wall and one *p*-benzoquinone side-wall.³⁴ Spectroscopic studies revealed that upon excitation of the zinc porphyrin an electron was transferred to the quinone side-wall, and that this transfer was enhanced when a guest was bound in the cavity of the clip.

Chart 8.3



H₂Au6: **M1** = 2H, **M2** = AuCl

ZnAu6: **M1** = Zn, **M2** = AuCl

In Section 8.3.2 it was demonstrated that the zinc porphyrins in **Zn₂6** fold back to coordinate to the methoxy groups of the side-walls of the clip. It was decided therefore to synthesize clip **ZnAu6** (Chart 8.3) in which one of the porphyrins contains a zinc ion (donor), and the other a gold ion (acceptor). Since gold porphyrins have no affinity for methoxy oxygen atoms, **ZnAu6** was expected to adopt the structure shown in Figure 8.14a, *viz.* with only the donor zinc porphyrin backfolding onto the cavity side-wall. Upon excitation of the zinc porphyrin, it was expected that its fluorescence would be less quenched than when this porphyrin was not backfolded. In this section the effect of the addition of a resorcinol guest in the spectroscopic properties of **ZnAu6** and **ZnAu6** will be investigated. The objective was to investigate what influence these additives have on the geometry of the zinc porphyrin, and its fluorescence properties (Figure 8.14b).

Porphyrin functionalized clip **ZnAu6** was synthesized from **H₄6** by treating the latter with one equivalent of potassium tetrachloroaurate, separating the statistic product mixture, and reacting the isolated **H₂Au6** with zinc acetate dihydrate (Scheme 8.2). The desired product was obtained in an overall yield of 50%. The ¹H NMR spectrum of the compound in CDCl₃ confirmed the proposed structure (see Figure 8.14a), since the signals of protons of only *one* of the side-walls were shifted strongly upfield, indicating the proximity of the zinc porphyrin.

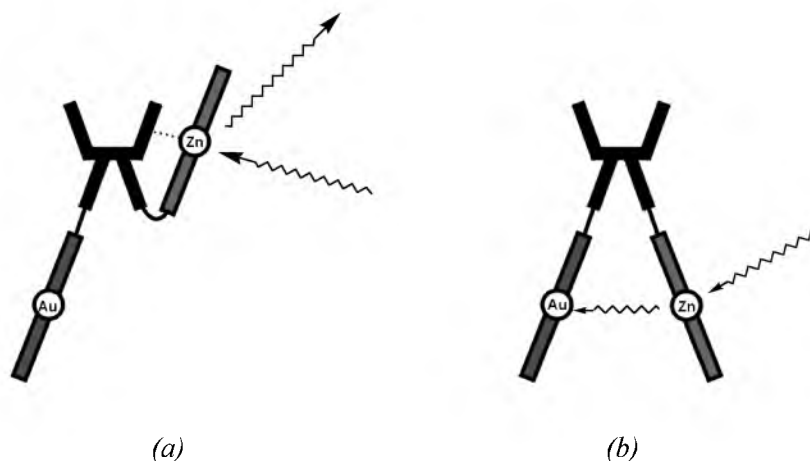


Figure 8.14 (a) Schematic structure of **ZnAu6** showing the fluorescence emission upon excitation of the zinc porphyrin. (b) Structure of **ZnAu6** in which the zinc porphyrin is flipped down, allowing the desired fluorescence quenching by the gold porphyrin upon excitation of the zinc porphyrin.

Table 8.5 Spectroscopic data for **ZnAu6** and **Zn₂6**.^a

Solvent or additive	ZnAu6			Zn₂6		
	$\lambda_{\text{Soret}}/\text{nm}$	$\lambda_{\text{em}}/\text{nm}^b$	I/a.u.	$\lambda_{\text{Soret}}/\text{nm}$	$\lambda_{\text{em}}/\text{nm}^b$	I/a.u.
CHCl ₃	420	606	309	422	607	738
CHCl ₃ /MeOH 95:5	414, 424	607	267	424	602	695
CHCl ₃ , +100 equiv. resorcinol	420	606	288	422	602	690

^a298 K, [porphyrin] = 10⁻⁶ M. ^b λ_{ex} = 430 nm.

The spectroscopic features of **ZnAu6** are summarized in Table 8.5 and compared to those of **Zn₂6**. In CHCl₃, the fluorescence emission intensity upon excitation of the zinc porphyrin was found to be smaller for **ZnAu6** than for **Zn₂6**. This is not surprising because of the presence of two zinc porphyrins in the latter compound. ¹H NMR studies revealed that in both compounds the interaction between the zinc porphyrin and the clip side-wall was broken when methanol was

added. For both compounds, the fluorescence decreased, in the case of **ZnAu6** however proportionally to a higher extent. This might be a result of the quenching properties of the gold porphyrin.³⁵ NMR spectroscopy, however, revealed that the addition of resorcinol to both compounds in chloroform did not result in a flipping down of the zinc porphyrin. The fluorescence of the zinc porphyrins was only slightly quenched, which can be attributed to quenching by the resorcinol guest itself. The degree of fluorescence quenching upon ‘flipping down’ of the zinc porphyrin is less than expected. This indicates that the donor and acceptor porphyrin are too far apart and too flexible to have a significant electronic interaction with each other. Future work will focus on studying the synthesis and photophysical properties of **ZnAu5**, in which the two porphyrins are in closer proximity.

8.4 A porphyrin templated molecular capsule

8.4.1 Introduction

Two areas of great interest within the field of supramolecular chemistry are supramolecular catalysis³⁶ and well-defined self-assembly.³⁷ As part of our studies on cytochrome P450 mimics³⁸ we have the goal to construct Mn(III) porphyrin-functionalized receptor molecules, which can carry out substrate-selective oxidation of substrates. To achieve this goal, molecular clips derived from diphenylglycoluril were functionalized with a porphyrin roof which was situated directly over the receptor cavity. In Chapter 9, the syntheses of three of these compounds,³⁹ which are currently applied as epoxidation catalysts,⁴⁰ will be described. Due to the relatively low yield of the synthesis of these molecules, their application as catalysts is somewhat hindered. Alternative synthetic routes were therefore investigated. In this section, a different approach toward the synthesis of porphyrin-capped receptors is reported, *viz.* by means of metal-templated self-assembly⁴¹ of the receptor and the catalyst, both of which can be synthesized in relatively large quantities.

A basket-shaped molecule functionalized with two pendant porphyrins, **H₄11**, was designed (Figure 8.15). Molecular modeling indicated that, after the insertion of a zinc ion, the porphyrins could self-assemble with a tetrakis-*meso*-4-pyridyl porphyrin **TPyP** molecule to form a 2:1 capsule-like complex. The latter porphyrin acts as a template, to which both receptor cavities coordinate via pyridine-zinc interactions (Figure 8.15).⁴² Modeling furthermore indicated that in this capsule 1,3-dihydroxybenzene guests could still be bound in the cavities. Such self-assembled capsules are of great interest since they can be used as confined reaction chambers for the conversion of bound guests.⁴³

8.4.2 Synthesis

Diporphyrin functionalized basket **H₄11** was synthesized following different routes (Scheme 8.3). The first route started from a basket-shaped molecule containing two propanol side-chains (**12**).⁴⁴ Chlorination of **12** with thionyl chloride, surprisingly, gave unstable products. Shifts in the ¹H and ¹³C NMR spectra suggested the presence of tetra-alkyl ammonium ions. It is proposed that the azacrown ether nitrogen atoms carry out a nucleophilic attack carbon atom containing the chloride leaving group. The close distance between these reacting sites enhances the intramolecular reaction⁴⁵ and an azetidinium ring is formed (Scheme 8.4). It turned out that this undesired reaction could be inhibited when the azacrown ether nitrogen atoms of **12** were protonated prior to chlorination. Consequently, **12** was first treated with hydrochloric acid in

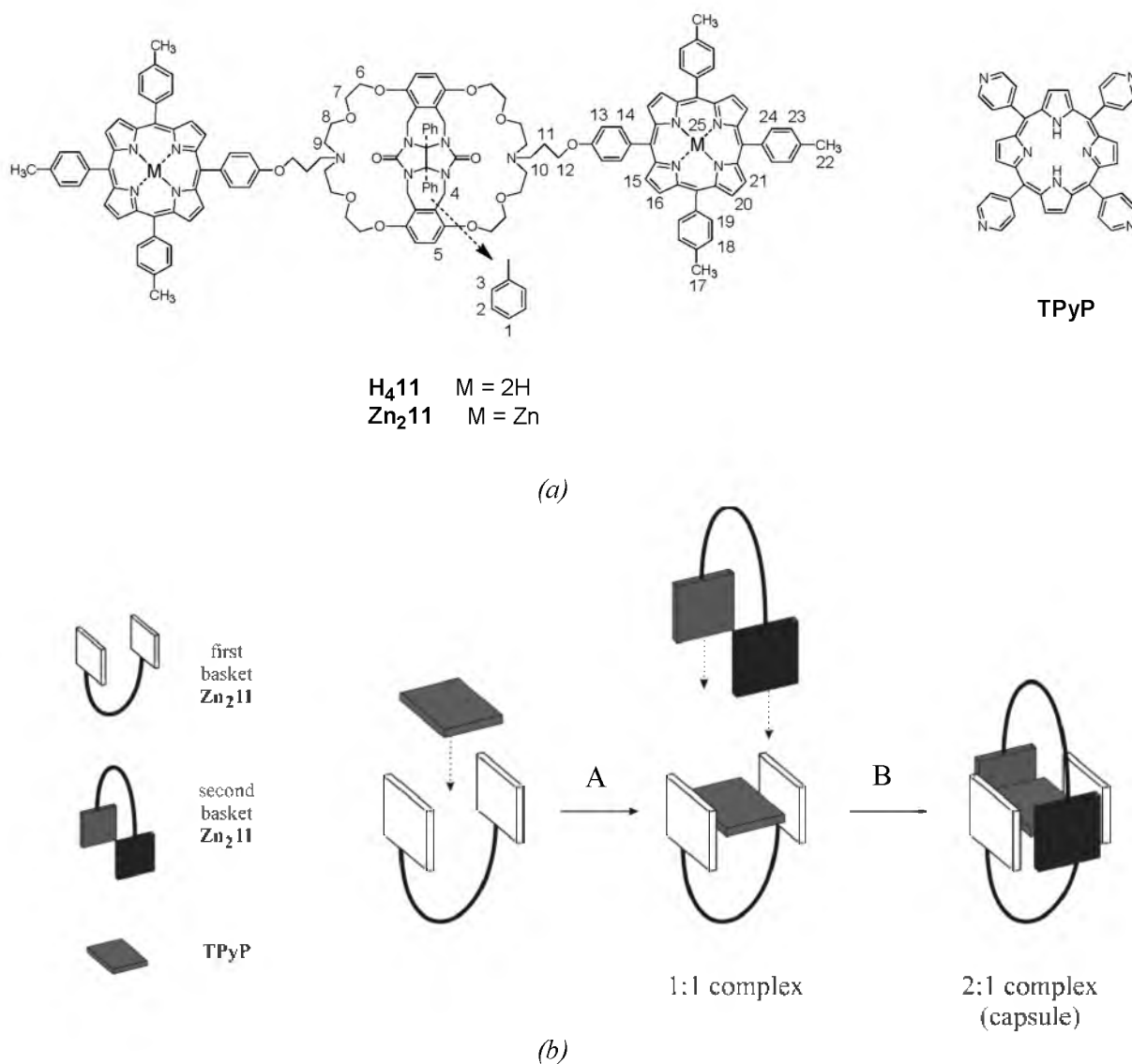
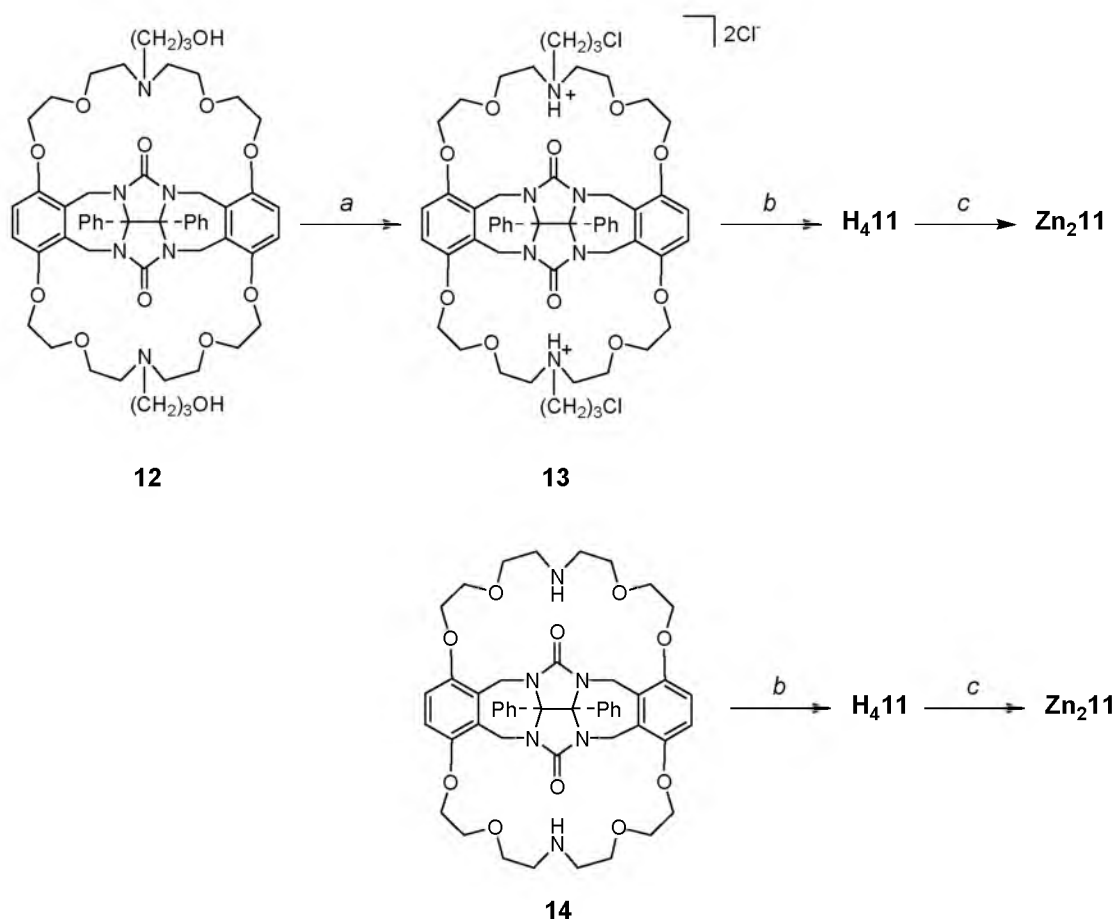
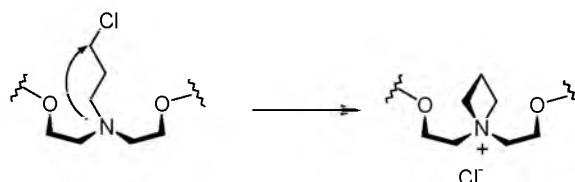


Figure 8.15 (a) Structures of $\text{H}_4\mathbf{11}$, $\text{Zn}_2\mathbf{11}$ and TPyP (b) Schematic representation of the templated self-assembly of a porphyrin-centered capsule.

methanol. Subsequent reaction of the diprotonated basket with thionyl chloride afforded the stable dichloride **13** in quantitative yield. Reaction of **13** with porphyrin **8** in dimethylformamide, using potassium carbonate as a base, gave diporphyrin basket $\text{H}_4\mathbf{11}$ in low yields (< 10%) after purification by column chromatography. However, the base used during the reaction also causes the deprotonation of the azacrown ether nitrogen atoms and hence the occurrence of the intramolecular ring closure depicted in Scheme 8.4, which results in the formation of considerable amounts of side-products. To alleviate these problems, another synthetic route to synthesize $\text{H}_4\mathbf{11}$ was developed which starts from azabasket **14**.⁴⁶ This compound was reacted with propyl bromide functionalized porphyrin **10** (see Scheme 8.2) under similar conditions as described for the reaction between **13** and **8**. Compound $\text{H}_4\mathbf{11}$ was readily obtained in a yield of 76%, after purification by column chromatography. Finally, $\text{H}_4\mathbf{11}$ was converted nearly quantitatively to $\text{Zn}_2\mathbf{11}$ by a reaction with zinc acetate dihydrate in a mixture of chloroform and methanol (2:1, v/v). The pure compound was obtained after purification by column chromatography.



Scheme 8.3 Reagents and conditions: (a) First HCl, MeOH, 30 min, then SOCl₂, 16 h. (b) **8** or **10**, K₂CO₃, KI, DMF, 100°C, 64 h. (c) Zn(OAc)₂·2H₂O, CHCl₃, MeOH, reflux, 3 h.



Scheme 8.4 Intramolecular substitution which is proposed to take place in compound **13** when its azocrown ether nitrogen atoms are not protonated. For clarity only part of one crown ether ring is shown.

8.4.3 Structural characterization

The structures of **H₄11** and **Zn₂11** were investigated with NMR spectroscopy (500 MHz). Using COSY and 2D NOESY techniques, all the signals in the spectra of these compounds could be fully assigned (Table 8.6).

In the ¹H NMR spectrum of **H₄11**, the signal of the side-wall protons (at 6.55 ppm) was shifted slightly upfield ($\Delta\delta = -0.14$ ppm) compared to this signal in basket **12**, which may be an indication that these protons are to some extent shielded by the porphyrin ring. The resonances of the phenyl groups of the diphenylglycoluril framework, which are usually unresolved (even at 500 MHz), had split up in three distinct signals and were also shifted slightly upfield. Basket

Table 8.6 Assignment of proton resonances (δ , ppm) in the ^1H NMR spectra of **H₄11** and **Zn₂11**.^a

Proton ^b	H₄11	Zn₂11	Proton	H₄11	Zn₂11
1	6.97	6.98-6.84	12	4.30	4.12
2	7.06	6.98-6.84	13	7.27	7.12
3	7.00	6.98-6.84	14	8.10	7.98
4 (in)	3.67	3.43	15	8.86	8.98-8.89
4(out)	5.62	5.26	16	8.88	8.98-8.89
5	6.55	6.38	17	2.68	2.65
6a	4.30	3.39	18	7.52	7.50
6b	4.00	3.23	19	8.07	8.09
7a	3.85-3.65	3.39	20	8.84	8.98-8.89
7b	3.85-3.65	3.09	21	8.84	8.98-8.89
8	3.85-3.65	3.00	22	2.68	2.70
9a	2.88	2.20	23	7.53	7.57
9b	2.88	1.99	24	8.08	8.14
10	2.88	2.37	25	-2.76	-
11	2.13	1.86			

^a CDCl_3 solution, 500 MHz, 298 K. ^bFor proton numbering see Figure 8.15.

Zn₂11, surprisingly, gave a much more complicated ^1H NMR spectrum. Compared to the spectrum of **H₄11**, the most remarkable differences were the resonances of the crown ether protons H₆-H₉, which were all shifted strongly upfield ($\Delta\delta = -0.6$ - -0.9 ppm). In addition, significant upfield shifts were observed for the resonances of the side-wall protons H₅ ($\Delta\delta = -0.17$ ppm), the methylene protons H₄ ($\Delta\delta = -0.24$ and -0.36 ppm), the protons of the propyl spacer (H₁₀: $\Delta\delta = -0.51$ ppm; H₁₁: $\Delta\delta = -0.27$ ppm; H₁₂: $\Delta\delta = -0.18$ ppm) and the protons of the phenyl group that links the porphyrin to the spacer (H₁₃: $\Delta\delta = -0.15$ ppm; H₁₄: $\Delta\delta = -0.12$ ppm). The very strong upfield shifts of the crown ether proton resonances suggest that these protons are proximal to the porphyrin ring.³¹ Taking all the shifts into account, a prediction of the 3-dimensional structure of the compound can be made by molecular modeling (Figure 8.16). In this structure, one of the porphyrins of **Zn₂11** covers the crown ether ring at the opposite side of the receptor, and its *meso*-phenyl group is docked between the cavity side-walls. Since average signals were observed in the NMR spectrum, the proposed geometry must be in fast equilibrium with the identical mirror image geometry in which the other porphyrin covers the opposite crown ether ring. Further evidence for the proposed geometry came from the 2D NOESY spectrum of **Zn₂11**, in which nOe contacts were visible between the side-wall protons H₅ and the *meso*-phenyl protons H₁₄, between H₅ and the β -pyrrole protons H_{15/16}, and between H_{15/16} and crown ether protons H₆ and H₇.

The driving force for the observed geometry is thought to be a coordinative interaction between the porphyrin zinc ion and the azacrown ether nitrogen atom. This geometry is supported by the UV-vis spectrum of **Zn₂11**, in which next to the porphyrin Soret band at 420 nm a shoulder was visible which was red shifted (*ca.* 8 nm) with respect to this band. This shift is characteristic for a zinc porphyrin with a coordinated amine ligand. In the proposed geometry, the second porphyrin cannot coordinate simultaneously to an azacrown ether nitrogen atom in the same molecule. It can, however, coordinate to another molecule of **Zn₂11**. At millimolar concentrations, this intermolecular process could be observed, since in the spectrum of **Zn₂11**

broad signals were visible underneath the relatively sharp signals of the intramolecular coordination complex. Upon dilution these broad signals disappeared. When a drop of methanol or acetone was added to the chloroform solution of **Zn₂11**, an NMR spectrum was obtained which closely resembled that of **H₄11**, a molecule in which the porphyrins have no coordinative interaction with the crown ethers. In addition the UV-vis spectrum displayed only a symmetrical band at 420 nm. Both these observations confirm the geometry of **Zn₂11** in pure chloroform, in which the zinc ion coordinates to the azacrown ether nitrogen atom.

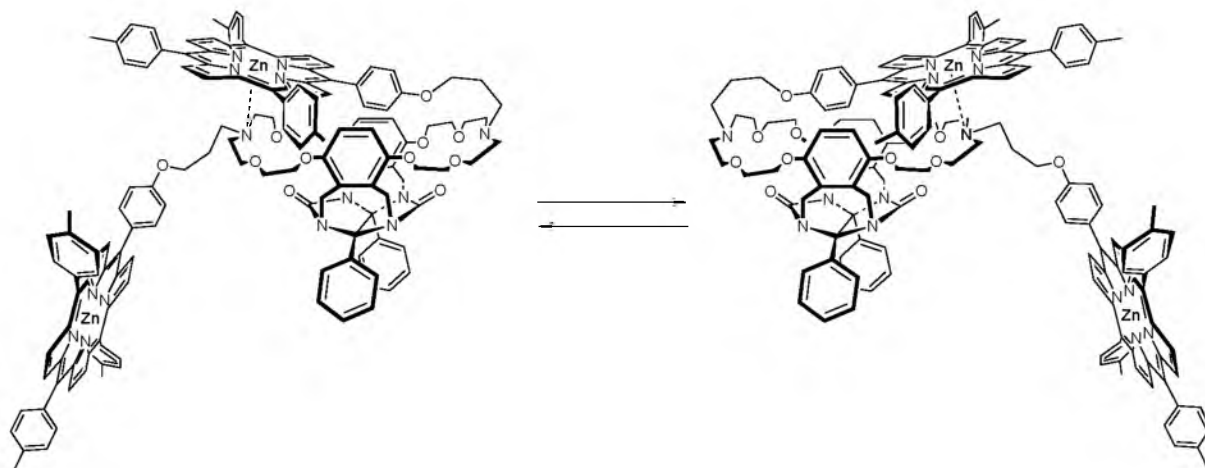


Figure 8.16 Conformational behaviour of **Zn₂11** in chloroform solution.

8.4.4 Complexes with TPyP

UV-vis and NMR studies

The complexation of **TPyP** to **Zn₂11** was studied by UV-vis and ¹H NMR spectroscopy. A UV-vis titration was carried out in which **TPyP** was added to a solution of **Zn₂11** (concentration 3.8×10^{-7} M) in chloroform. The change in absorption at 420 nm was followed. A single inflection point was observed after the addition of *one* equivalent of **TPyP** (Figure 8.17a) This indicates that at the applied concentration of **Zn₂11** only a 1:1 complex between the two components is formed. No association constant K_a could be obtained from the titration curve, due to the large number of processes that occur during the self-assembly of the molecules.⁴⁷

The complexation of **TPyP** was also investigated at millimolar concentrations with the help of 500 MHz ¹H NMR spectroscopy in CDCl₃. A titration was carried out in which **Zn₂11** was added to **TPyP**. Upon the addition of 10 equiv. of **Zn₂11** with respect to **TPyP**, the resonance of the **TPyP** pyrrole NH protons ($\delta_{\text{NH}} = -4.48$ ppm) was shifted by -1.55 ppm upfield when compared to uncomplexed **TPyP** ($\delta_{\text{NH}} = -2.93$ ppm). In addition, the β -pyridyl protons of **TPyP** were shifted upfield to 6.12 ppm ($\Delta\delta = -2.05$ ppm). The α -pyridyl protons could not be assigned. The very large complexation induced upfield shifts suggest that **TPyP** coordinates to four peripheral zinc porphyrins.^{8,48} Upon the addition of more equivalents of **Zn₂11**, the signals of the NH and β -pyridyl protons displayed smaller upfield shifts. The titration curve following the porphyrin NH resonance turned out to be somewhat S-shaped (Figure 8.17b). From this curve an inflection point can be derived, which clearly indicates a 2:1 host-guest stoichiometry in the complex between **Zn₂11** and **TPyP** at the applied concentrations. The second part of the titration curve, *i.e.* the part after the addition of one equivalent of **Zn₂11**, could be fitted to an equation

governing the association of a 1:1 complex with an association constant $K_a = 9200 \pm 500 \text{ M}^{-1}$. Considering the large upfield shifts displayed by the **TPyP** NH protons in this part of the curve, it is proposed that the measured association constant corresponds to the binding of a second **Zn₂11** molecule to the already formed 1:1 complex between **Zn₂11** and **TPyP** (process B in Figure 8.15b).

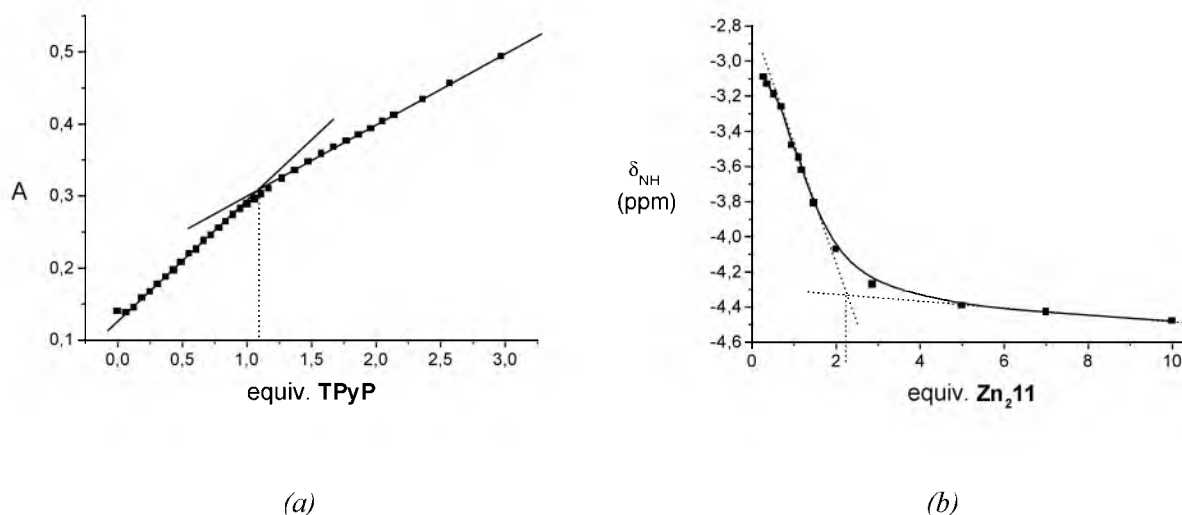


Figure 8.17 (a) Change in the absorbance at 420 nm during the UV-vis titration of **Zn₂11** with **TPyP**. (b) Shifts of the pyrrole NH protons of **TPyP** upon the addition of this compound to **Zn₂11** in CDCl_3 (500 MHz, 298 K).

During the titration, the upfield shifted resonances of the crown ether protons of **Zn₂11** shifted back downfield and a relatively simple NMR spectrum was obtained. In this spectrum, the cavity side-wall protons were shifted upfield by -0.38 ppm ($\delta = 6.17 \text{ ppm}$) when compared to their signal in the spectrum of **H₄11**. This upfield shift might be the result of a shielding effect caused by the **TPyP** molecule, which is positioned above the cavities. A 2D NOESY spectrum was recorded in order to get more insight in the orientation of the clip cavities with respect to the bound **TPyP**. No nOe effects between these components were, however, observed, indicating that they are not in close proximity.

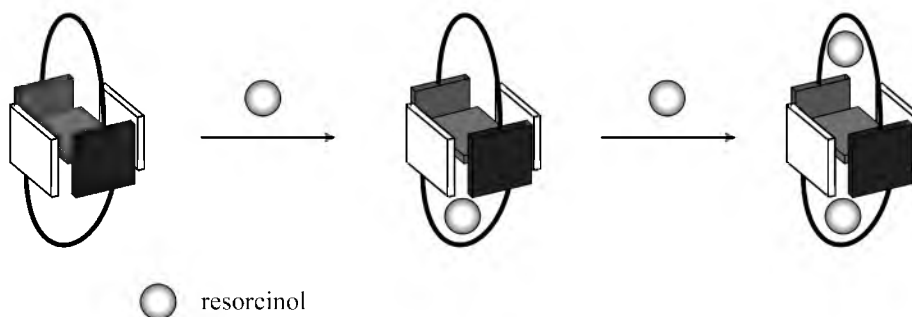


Figure 8.18 Schematic representation of the binding of one or two resorcinol guests within the cavities of the capsule-like assembly of **Zn₂11** and **TPyP**.

To investigate if the glycoluril cavities of **Zn₂11** in the complex with **TPyP** were still available for the binding of guests, resorcinol was added to a CDCl_3 solution containing **Zn₂11** and **TPyP**

in a 2:1 molar ratio. Upon the addition 10 equivalents of guest, the signals of the side-wall protons of the cavities shifted upfield by an additional -0.40 ppm ($\delta = 5.77$ ppm). Apart from small upfield shifts of the crown ether proton signals, no significant changes in the resonances of the porphyrin protons were observed. These results indicate that the guest can still bind in the cavities of the receptors, and that this binding apparently does not disturb the **TPyP** porphyrin. The upfield shift of -0.40 ppm upon the addition of resorcinol suggests that both cavities of the complex bind a resorcinol guest (Figure 8.18).²⁷ Further NMR studies need to be performed in order to obtain more information about the precise topology of this host-guest complex.

Proposed structure of the complex

Self-assembly of the **Zn₂11** and **TPyP** components can in principle give rise to several types of 1:1 and 2:1 complexes. Polymeric complexes are also conceivable, but their formation is entropically unfavourable, and not supported by the fact that at the used concentrations the signals in the ¹H NMR spectra remained sharp.

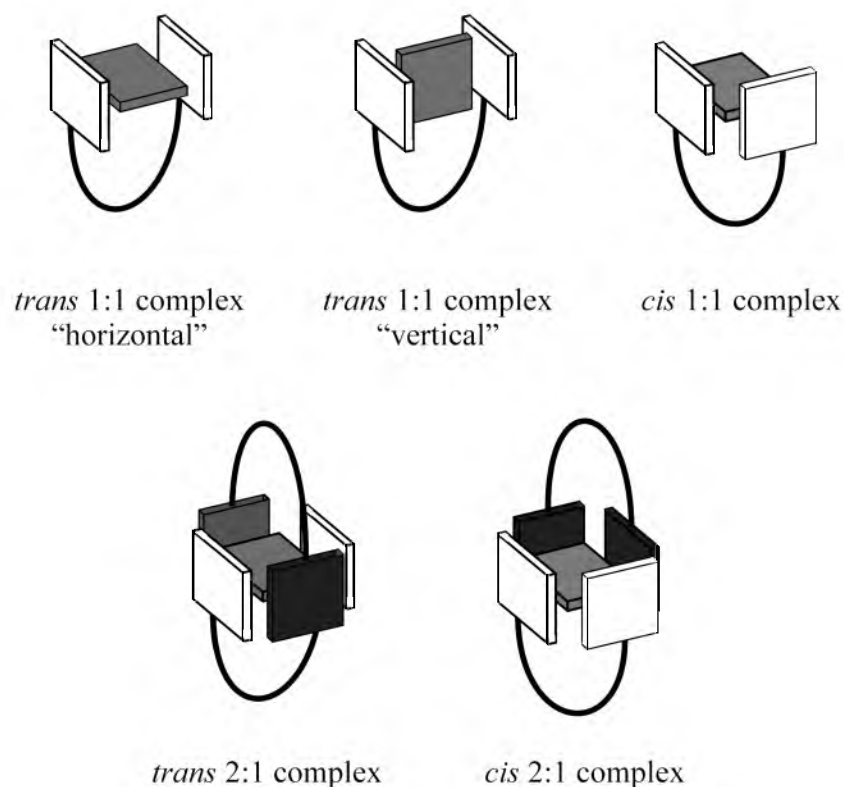


Figure 8.19 Possible 1:1 and 2:1 complexes which can be formed upon the self-assembly of **Zn₂11** and **TPyP**.

It is interesting to note that the UV-vis measurements indicated the formation of a 1:1 complex, whereas the NMR titration suggested a 2:1 complex between **Zn₂11** and **TPyP**. Apparently, the stoichiometry of the complex strongly is dependent on the concentration, *i.e.* at a concentration of 10^{-6} M only a 1:1 complex is formed, whereas at millimolar concentrations also a 2:1 complex is present. This suggests that the first molecule of **Zn₂11** binds stronger to **TPyP** than the second molecule of **Zn₂11**. This is thought to be a result of steric hindering of the two uncomplexed

pyridine ligands of **TPyP** in the 1:1 complex for an incoming second molecule of **Zn₂11**. The bound **TPyP** molecule in the 1:1 complex has the ability to rotate around the axis through the coordinated pyridine groups. In addition to the geometry in which the **TPyP** molecule covers the cavity of **Zn₂11** as a roof ("horizontal" geometry), another arrangement ("vertical" geometry) is also possible in which the edge of the porphyrin points to the direction of the cavity (Figure 8.19). In the latter geometry, one of the uncomplexed pyridine groups would be in the direct proximity of the cavity of **Zn₂11**. This geometry was, however, not observed by the NMR en NOESY 2D measurements. Many other geometries between the "horizontal" and the "vertical" ones are feasible, however, and this conformational flexibility might account for the weaker binding of a second molecule of **Zn₂11**.

In both the 1:1 and 2:1 complexes, the **Zn₂11** molecules can coordinate to **TPyP** in a "cis" or in a "trans" fashion (Figure 8.19). Molecular modeling, however, indicated that in order to adopt the *cis*-geometry a considerable rearrangement in the structure of **Zn₂11** is required. In addition, modeling showed that in the *trans*-geometry, the two zinc porphyrins of **Zn₂11** are at an ideal distance (~ 19 Å) to bind a **TPyP** molecule (the *trans*-pyridine N-N distance in the latter molecule is 15.5 Å and two average zinc porphyrin to pyridyl bond distances are 2.2 Å⁴⁹). It can therefore be expected that the *trans*-geometries are more likely to occur for both the 1:1 and 2:1 complex. Further NMR and host-guest studies are required to provide more information about the exact structures and dynamics of the different complexes.

8.5 Concluding remarks

In this chapter, three different types of porphyrin arrays based on host-guest complexes between porphyrins and molecular clips have been described. The first two types involve 4:1 complexes between clips and a central tetrafunctional porphyrin guest. Although the 4:1 complexes derived from a porphyrin and a clip with long aliphatic tails appeared to be stable in the solid state, it is as yet unclear whether this also holds for a chloroform solution. The exact stoichiometry between the host-guest components in the latter solvent is unknown. Probably only one clip needs to be complexed to the porphyrin guest in order to dissolve the complex in chloroform. It then may further self-assemble by head-to-tail stacking of the central porphyrins to form extended arrays of molecules. Additional clip molecules can be attached to the vacant dihydroxybenzene substituents of the porphyrins in the arrays. A 4:1 host-guest complex between a clip functionalized with two porphyrins and the porphyrin guest displayed similar features, but the stacking between the central porphyrins in the array was weaker. Finally, we succeeded in organizing two basket-shaped molecules with pendant zinc porphyrins around a central tetrapyrrolyl porphyrin by a metal-templated self-assembly process. Depending on the concentration of the components, 1:1 or 2:1 complexes were formed. The 1:1 complex appeared to be more stable than the 2:1 complex. Although the precise structure of the 2:1 complex is as yet unclear, its cavities can still bind dihydroxybenzene guests. The self-assembled capsule-like complex is of great interest as a potential catalyst in which the central, templating porphyrin, can have various metal centers (*e.g.* Mn(III), Ru(II), Mg(II)) which opens the possibility to selectively oxidize or polymerize bound guest molecules.

8.6 Experimental section

8.6.1 Materials and methods

DMF was dried over BaO for one week and then vacuum distilled; the first 30% of the distillate was removed. K₂CO₃ and KI were dried in an oven (150°C). Pyrrole was vacuum distilled at room temperature. Unless stated otherwise, all other chemicals were commercial materials and used without further purification. Thermal behaviour was observed with a Jeneval polarizing optical microscope connected to a Linkam THMS hot stage. Differential scanning calorimetry thermograms were recorded on a Perkin Elmer DSC 7 instrument. NMR and UV titrations were carried out as described in Chapter 9. For an overview of other general techniques see Section 2.6.1.

8.6.2 Polarized optical microscopy and differential scanning calorimetry experiments

An amount of 5-10 mg of clip and a weighted amount of guest were dissolved in a mixture of CHCl₃ and MeOH (4:1, v/v). The solvent mixture was evaporated overnight under a stream of nitrogen while heating the mixture on a water bath at 40°C. Samples were studied using a polarizing microscope with crossed polarizers. DSC samples were prepared in stainless-steel large volume pans (75 µL). Thermograms were recorded at 2-10°C min⁻¹ and repeated heating and cooling runs were measured to study the stability of the material and the reproducibility of the transitions.

8.6.3 X-ray powder diffraction experiments

X-ray powder diffraction experiments were carried out on powder samples in a pinhole camera (Anton-Paar) operating with a Ni-filtered Cu_{Kα} beam. The samples were held in Lindemann glass capillaries (1 mm diameter), and the X-ray patterns were collected on flat photographic film.

8.6.4 Solution FTIR experiments

Fourier transform infrared solution spectra were recorded on a BioRad FTS-25 spectrometer with a resolution of 2.0 cm⁻¹. Solutions of the complexes dissolved in CDCl₃ (concentration approximately 1 mM) were placed in a cuvet between two NaCl plates. The optical bench of the spectrometer was continuously flushed with dry nitrogen gas. For each spectrum 64 scans were recorded. The measured data were corrected for the solvent and analysis was performed using the WIN-IR software.

8.6.5 Fluorescence measurements

Fluorescence spectra were recorded on a Perkin Elmer luminescence spectrometer LS50B equipped with a thermostatted cuvette holder (T = 298 K). Solutions of the compounds in a 1.00 cm 4 mL quartz cuvette were purged with argon to exclude fluorescence quenching by oxygen. The excitation and emission slits were 5 and 15 nm, respectively. The emissions were recorded from 500 to 750 nm applying a scanning speed of 120 nm min⁻¹.

8.6.6 Syntheses

The syntheses of compounds **1-3** have been described in Chapter 5, and the synthesis of compound **9** in Chapter 2.

21H,23H-5,10,15,20-Tetrakis(3,5-dihydroxyphenyl)porphyrin (**4**):

This compound was synthesized according to a literature procedure.⁵⁰

Porphyrin functionalized clip **H₄5**:

Compounds **7** (61 mg, 76 µmol) and **8** (180 mg, 0.26 mmol) were dissolved in degassed DMF (20 mL), and K₂CO₃ (120 mg, 0.90 mmol) and KI (5 mg) were added. The mixture was heated under nitrogen at 100°C for 64 h. After cooling, the suspension was poured into aqueous 1 N HCl (150 mL) and the product was extracted with CH₂Cl₂ (2 x 25 mL). The organic layer was washed with a saturated aqueous NaHCO₃ solution (100 mL), with water (100 mL), and then evaporated to dryness. The product was purified by column chromatography (first column: Merck silica 60H, CH₂Cl₂/EtOH 98:2, v/v, R_f = 0.17, second column Acros silica, CH₂Cl₂/MeOH/Et₃N 198:1:1 v/v/v) to yield 21 mg (14%) of **H₄5** as a purple solid.

M.p. > 400°C (dec.); ¹H NMR (CDCl₃, 500.14 MHz) δ 8.73 (d, 4H, β-pyrroleH, ³J = 5.0 Hz), 8.71 (d, 4H, β-pyrroleH, ³J = 5.0 Hz), 8.69 (d, 4H, β-pyrroleH, ³J = 5.0 Hz), 8.64 (d, 4H, β-pyrroleH, ³J = 5.0 Hz), 7.92 (d, 4H, ArH meta to CH₃, ³J = 8.0 Hz), 7.84 (d, 4H, ArH meta to CH₃, ³J = 7.5 Hz), 7.75 (d, 4H, ArH meta to OCH₂, ³J = 8.5 Hz), 7.39 (d, 4H, ArH ortho to CH₂O, ³J = 8.0 Hz), 7.35 (d, 12H, ArH ortho to CH₃, ³J = 8.0 Hz), 7.26 (d, 4H, ArH meta to CH₂O, ³J = 8.0 Hz), 6.94 (d, 4H, ArH ortho to OCH₂, ³J = 8.5 Hz), 6.66 (s, 4H, ArH side-wall), 5.65 (d, 4H, NCH₂Ar out, ²J = 16.0 Hz), 5.09 (s, 4H, ArCH₂O), 3.90 (d, 4H, NCH₂Ar in, ²J = 16.0 Hz), 3.80 (s, 12H, OCH₃), 2.63 (s, 6H, ArCH₃), 2.56 (s, 12H, ArCH₃), -2.81 (s, 4H, NH) ppm, a complete assignment of the porphyrin proton

resonances can be found in Table 8.4; $^{13}\text{C}\{^1\text{H}\}$ NMR (CDCl_3 , 75.47 MHz) δ 158.11, 157.82 (2 \times C=O), 151.26 (ArC ipso to OCH_3), 139.15, 137.11, 135.32, 134.37, 131.01, 128.70, 127.83, 127.25, 119.99, 119.32 (all ArC), 85.18 (NC(Ar)N), 69.52 (CH_2O), 57.12 (OCH_3), 37.03 (NCH_2Ar), 21.40 (ArCH_3) ppm; FAB-MS m/z 1986 (M^+). UV-vis (CHCl_3) λ 420, 515, 548, 587, 639 nm.

Porphyrin functionalized clip **Zn₂5**:

A solution of **H₄5** (5.0 mg, 2.5 μmol) and $\text{Zn}(\text{OAc})_2 \cdot 2\text{H}_2\text{O}$ (3 mg, 14 μmol) in a mixture of CHCl_3 (1 mL) and MeOH (0.5 mL) was refluxed under nitrogen for 3 h. After cooling, the solvent was removed *in vacuo*. The residue was dissolved in CH_2Cl_2 (20 mL) and the organic layer was extracted with water (3 \times 50 mL) and evaporated to dryness. The product was purified by column chromatography (Merck silica, $\text{CH}_2\text{Cl}_2/\text{EtOH}$ 98:2, v/v, R_f = 0.22) to give 5.1 mg (96%) of **Zn₂5** as a purple solid.

M.p. > 400°C (dec.); ^1H NMR ($\text{CDCl}_3/\text{CD}_3\text{OD}$, 95/5, v/v, 300.13 MHz) δ 8.85-8.78 (m, 8H, β -pyrroleH), 7.97 (d, 12H, ArH, 3J = 7.4 Hz), 7.93 (d, 4H, ArH, 3J = 7.5 Hz), 7.44 (d, 4H, ArH, 3J = 7.4 Hz), 7.40 (d, 8H, ArH, 3J = 7.4 Hz), 7.09 (d, 4H, ArH, 3J = 7.5 Hz), 6.75 (s, 4H, ArH side-wall), 5.65 (d, 4H, $\text{NCH}_2\text{Ar out}$, 2J = 16.0 Hz), 5.18 (s, 4H, ArCH_2O), 3.91 (d, 4H, NCH_2Ar , 2J = 16.0 Hz), 3.82 (s, 12H, OCH_3), 2.60 (s, 6H, ArCH_3), 2.57 (s, 12H, ArCH_3) ppm; FAB-MS m/z 2113 ($\text{M} + \text{H}^+$). UV-vis (CHCl_3) λ 424, 551, 592 nm.

Porphyrin functionalized clip **H₄6**:

A suspension of compounds **9** (30 mg, 0.042 mmol) and **10** (80 mg, 0.106 mmol) in DMF (5 mL) was purged with nitrogen for 15 min. K_2CO_3 (100 mg, 0.72 mmol) was added and the mixture was stirred at 100°C for 64 h. After cooling, the solvent was removed *in vacuo* and the residue was dissolved in CH_2Cl_2 (50 mL). The organic layer was extracted with aqueous 1N HCl (2 \times 100 mL) with a saturated aqueous NaHCO_3 solution (100 mL) and evaporated to dryness. The product was purified by column chromatography (silica, $\text{CH}_2\text{Cl}_2/\text{MeOH}$ 199:1, v/v, R_f = 0.08) to yield 38 mg (42%) of **H₄6** as a purple crystals.

M.p. > 400°C (dec.); ^1H NMR (CDCl_3 , 500.14 MHz) δ 8.82 (s, 8H, β -pyrroleH), 8.81 (d, 4H, β -pyrroleH, 3J = 5.0 Hz), 8.79 (d, 4H, β -pyrroleH, 3J = 5.0 Hz), 8.06 (d, 8H, ArH meta to CH_3 , 3J = 8.0 Hz), 8.02 (d, 4H, ArH meta to CH_3 , 3J = 7.6 Hz), 8.00 (d, 4H, ArH meta to OCH_2 , 3J = 8.5 Hz), 7.88 (d, 4H, ArH ortho to C(O)O, 3J = 8.5 Hz), 7.50 (d, 8H, ArH ortho to CH_3 , 3J = 8.0 Hz), 7.46 (d, 4H, ArH ortho to CH_3 , 3J = 7.5 Hz), 7.23 (d, 4H, ArH meta to C(O)O, 3J = 8.5 Hz), 7.13 (d, 4H, ArH ortho to OCH_2 , 3J = 8.5 Hz), 6.61 (s, 4H, ArH side-wall), 5.51 (d, 4H, $\text{NCH}_2\text{Ar out}$, 2J = 16.0 Hz), 4.61 (t, 4H, ArOCH_2 , 3J = 6.5 Hz), 4.26 (t, 4H, C(O) OCH_2 , 3J = 6.0 Hz), 3.78 (d, 4H, $\text{NCH}_2\text{Ar in}$, 2J = 16.0 Hz), 3.73 (s, 12H, OCH_3), 2.66 (s, 18H, ArCH_3), 2.37 (m, 4H, $\text{CH}_2\text{CH}_2\text{CH}_2$), -2.79 (br s, 4H, NH) ppm; $^{13}\text{C}\{^1\text{H}\}$ NMR (CDCl_3 , 100.61 MHz) δ 165.86 (ester C=O), 158.44 (urea C=O), 157.58 (ArC ipso to OCH_2), 151.18 (ArC ipso to OCH_3), 139.55, 139.27, 127.26, 135.55, 134.78, 134.48, 133.78, 130.99, 130.52, 129.93, 128.32, 127.38, 120.06, 119.61, 112.59, 112.03 (all ArC), 84.84 (NC(Ar)N), 64.58, 62.35 (2 \times C(O) OCH_2), 56.97 (OCH_3), 37.03 (NCH_2Ar), 29.72, 28.91 (ArCH_3), 21.49 ($\text{CH}_2\text{CH}_2\text{CH}_2$) ppm; FAB-MS m/z 2134 ($\text{M} + \text{H}^+$). UV-vis (CHCl_3) λ 420, 517, 548, 588, 640 nm.

Porphyrin functionalized clip **Zn₂6**:

Starting from **H₄6** (15 mg, 7.0 μmol) and $\text{Zn}(\text{OAc})_2 \cdot 2\text{H}_2\text{O}$ (10 mg, 46 μmol), this compound was synthesized as described for **Zn₂5**. The product was purified by column chromatography (Merck silica, $\text{CH}_2\text{Cl}_2/\text{MeOH}$ 99:1, v/v, R_f = 0.33), to give 15 mg (94%) of **Zn₂6** as a purple solid.

M.p. > 400°C (dec.); ^1H NMR (CDCl_3 , 400.13 MHz) δ 8.89 (d, 4H, β -pyrroleH, 3J = 4.5 Hz), 8.85 (d, 4H, β -pyrroleH, 3J = 4.5 Hz), 8.77 (d, 4H, β -pyrroleH, 3J = 4.6 Hz), 8.70 (d, 4H, β -pyrroleH, 3J = 4.6 Hz), 8.07 (d, 4H, ArH meta to OCH_2CH_2 , 3J = 7.6 Hz), 7.99 (d, 12H, ArH meta to CH_3 , 3J = 7.4 Hz), 7.73 (d, 4H, ArH ortho to C(O)O, 3J = 8.3 Hz), 7.51 (d, 4H, ArH ortho to CH_3 , 3J = 7.4 Hz), 7.50 (d, 8H, ArH meta to CH_3 , 3J = 7.4 Hz), 7.19 (d, 4H, ArH ortho to OCH_2CH_2 , 3J = 7.6 Hz), 6.83 (d, 4H, ArH meta to C(O)O, 3J = 8.3 Hz), 5.30 (s, 4H, ArH side-wall), 4.62 (t, 4H, C(O) OCH_2 , 3J = 5.6 Hz), 4.46 (t, 4H, C(O) OCH_2 , 3J = 5.5 Hz), 4.14 (d, 4H, $\text{NCH}_2\text{Ar out}$, 2J = 16.4 Hz), 2.69 (s, 6H, ArCH_3), 2.68 (s, 12H, OCH_3), 2.62 (d, 4H, $\text{NCH}_2\text{Ar in}$, 2J = 16.4 Hz), 2.60 (s, 9H, ArCH_3), 2.38 (m, 4H, $\text{CH}_2\text{CH}_2\text{CH}_2$) ppm; FAB-MS m/z 2259 (M^+). UV-vis (CHCl_3) λ 422, 550, 592 nm.

Porphyrin functionalized clip **H₂Au6**:

A mixture of **H₄6** (10 mg, 4.6 μmol), KAuCl_4 (1.13 mg, 3 μmol) and NaOAc (5 mg, 61 μmol) in acetic acid (2 mL) was refluxed under nitrogen for 64 h. After cooling, the solvent was evaporated and the residue was dissolved in CH_2Cl_2 (10 mL). The solution was extracted with a saturated aqueous NaHCO_3 solution (25 mL), with water, and evaporated to dryness. The residue was purified by column chromatography (Merck silica, $\text{CHCl}_3/\text{MeOH}$, 9:1, v/v, R_f = 0.21) to give 7 mg (63%) of **H₂Au6** as a purple solid, which was directly used in further synthesis.

^1H NMR (CDCl_3 , 300.13 MHz) δ 9.30-9.15 (m, 8H, β -pyrroleH), 8.80-8.75 (m, 8H, β -pyrroleH), 8.07-7.93 (m, 20H, ArH), 7.87 (d, 4H, ArH, 3J = 7.0 Hz), 7.66-7.59 (m, 8H, ArH), 7.54-7.44 (m, 8H, ArH), 7.21 (d, 4H, ArH, 3J =

8.1 Hz), 7.12 (d, 4H, ArH, $^3J = 8.4$ Hz), 6.61 (s, 2H, ArH side-wall), 6.47 (s, 2H, ArH side-wall), 5.48 (d, 2H, NCH₂Ar out, $^2J = 15.9$ Hz), 5.41 (d, 2H, NCH₂Ar out, $^2J = 15.9$ Hz), 4.67-4.62 (m, 2H, C(O)OCH₂), 4.42-4.30 (m, 4H, ArOCH₂ and C(O)OCH₂), 4.04-3.98 (m, 2H, ArOCH₂), 3.77 (d, 2H, NCH₂Ar in, $^2J = 15.9$ Hz), 3.72 (s, 6H, OCH₃), 3.67 (s, 6H, OCH₃), 3.60 (d, 2H, NCH₂Ar in, $^2J = 15.9$ Hz), 2.74-2.66 (m, 18H, ArCH₃), 2.42 (m, 4H, CH₂CH₂CH₂) ppm.

Porphyrin functionalized clip ZnAu₆:

Starting from H₂Au₆ (7 mg, 3 mmol) and Zn(OAc)₂·2H₂O (5 mg, 20 mmol) in a mixture of CHCl₃ (2 mL) and MeOH (1 mL) this compound was synthesized as described for Zn₂5. The product was purified by column chromatography (Merck silica, CH₂Cl₂/MeOH, 9:1, v/v, R_f = 0.35), dissolved in CHCl₃ (2 mL) and this solution was stirred overnight with a saturated aqueous KPF₆ solution (2 mL). The organic layer was washed with water (10 mL) and evaporated to dryness to yield 6 mg (80%) of ZnAu₆ as an orange-brown solid.

M.p. > 300°C (dec.); ¹H NMR (CDCl₃, 300.13 MHz) δ 9.24-9.18 (m, 8H, β-pyrroleH), 8.86 (d, 2H, β-pyrroleH, $^3J = 4.5$ Hz), 8.83 (d, 2H, β-pyrroleH, $^3J = 4.5$ Hz), 8.75 (d, 2H, β-pyrroleH, $^3J = 4.5$ Hz), 8.69 (d, 2H, β-pyrroleH, $^3J = 4.5$ Hz), 8.07-7.93 (m, 12H, ArH), 7.79 (d, 4H, ArH, $^3J = 8.1$ Hz), 7.66-7.59 (m, 4H, ArH), 7.52-7.48 (m, 4H, ArH), 7.33-7.20 (m, 4H, ArH), 7.14-6.93 (m, 8H, ArH), 6.80 (m, 4H, ArH, $^3J = 8.1$ Hz), 6.61 (s, 2H, ArH side-wall), 5.48 (s, 2H, ArH side-wall), 5.08 (d, 2H, NCH₂Ar out, $^2J = 16.2$ Hz), 4.67-4.58 (m, 2H, C(O)OCH₂), 4.50 (m, 2H, ArOCH₂), 4.43-4.28 (m, 4H, ArOCH₂ and NCH₂Ar out), 4.10 (m, 2H, ArOCH₂), 3.45 (s, 6H, OCH₃), 3.38 (d, 2H, NCH₂Ar in, $^2J = 16.2$ Hz), 2.85 (d, 2H, NCH₂Ar in, $^2J = 16.2$ Hz), 2.79 (s, 6H, OCH₃), 2.75-2.62 (m, 18H, ArCH₃), 2.42 (m, 4H, CH₂CH₂CH₂) ppm; ¹³C{¹H} NMR (CDCl₃, 75.47 MHz) δ 164.22 (ester C=O), 156.22 (urea C=O), 150.79, 150.09, 143.89, 139.96, 139.42, 136.99, 136.03, 135.64, 134.39, 132.15, 131.60, 129.91, 128.44, 128.13, 127.28, 127.17, 123.61, 114.56, 113.90, 112.90, 112.28, 111.64 (all ArC), 85.38 (NC(Ar)N), 68.60, 64.92 (C(O)OCH₂), 62.31 (ArOCH₂), 56.87, 54.10 (OCH₃), 36.47, 35.94 (NCH₂Ar), 31.01, 29.69 (CH₂CH₂CH₂), 23.15, 21.59 (ArCH₃) ppm; FAB-MS m/z 2389 (M - PF₆)⁺; UV-vis (CHCl₃) λ 420, 524, 547, 592 nm.

13b,13c-Di[4-(bromomethyl)phenyl]-1,4,8,11-tetramethoxy-5,7,12,13b,13c,14-hexahydro-5a,6a,12a,13a-tetra-azabenzof[5,6]azuleno[2,1,8-ija]benzo[f]azulene-6,13-dione (7):

This compound was synthesized according to a literature procedure.

21H,23H-5-(4-hydroxyphenyl)-10,15,20-tris(4-methylphenyl)porphyrin (8):

A solution of *p*-tolualdehyde (2.75 g, 22.9 mmol) and *p*-hydroxybenzaldehyde (930 mg, 7.6 mmol) in propionic acid (100 mL) was heated to reflux. Pyrrole (2.05 g, 30.6 mmol) was added and the mixture was refluxed for 1 h. The mixture was cooled at 4°C for 16 h and then filtered. The purple residue was dried by suction and purified by flash column chromatography (neutral alumina act. III, gradient CH₂Cl₂-CH₂Cl₂/MeOH, 99:1, v/v) to yield 350 mg (7%) of **8** as a purple powder.

¹H NMR (CDCl₃, 300.13 MHz) δ 8.85 (s, 8H, β-pyrroleH), 8.09 (d, 6H, ArH meta to CH₃, $^3J = 7.8$ Hz), 8.07 (d, 2H, ArH meta to OH, $^3J = 8.4$ Hz), 7.55 (d, 6H, ArH ortho to CH₃, $^3J = 7.8$ Hz), 7.20 (d, 2H, ArH ortho to OH, $^3J = 8.4$ Hz), 5.01 (br s, 1H, OH), 2.70 (s, 9H, CH₃), -2.78 (br s, 2H, NH) ppm.

21H,23H-5(4-(3-bromopropoxy)phenyl)-10,15,20-tris(4-methylphenyl)porphyrin (10):

A solution of **8** (100 mg, 0.149 mmol) and 1,3-dibromopropane (1.2 g, 6.0 mmol) in DMF (25 mL) was purged with argon for 15 min. K₂CO₃ (200 mg, 1.45 mmol) was added and the mixture was stirred for 16 h. Hereafter, it was evaporated to dryness and CH₂Cl₂ (50 mL) was added to the residue. The organic layer was extracted with aqueous 1 N HCl, with a saturated aqueous NaHCO₃ solution, with water, and then evaporated to dryness. The crude product was purified by flash column chromatography (silica, CH₂Cl₂). To remove traces of DMF and 1,3-dibromopropane, the product was dissolved in a minimal amount of CH₂Cl₂ and this solution was added dropwise to stirred methanol (20 mL). After filtration, 105 mg (89%) of **10** was obtained as a purple powder.

M.p. > 300°C (dec.); ¹H NMR (CDCl₃, 400.13 MHz) δ 8.85 (s, 8H, β-pyrroleH), 8.12 (d, 2H, ArH meta to O(CH₂)₃Br, $^3J = 8.1$ Hz), 8.09 (d, 6H, ArH meta to CH₃, $^3J = 7.8$ Hz), 7.55 (d, 6H, ArH ortho to CH₃, $^3J = 7.8$ Hz), 7.27 (d, 2H, ArH ortho to O(CH₂)₃Br, $^3J = 8.1$ Hz), 4.40 (t, 2H, ArOCH₂, $^3J = 5.8$ Hz), 3.79 (t, 2H, CH₂Br, $^3J = 6.4$ Hz), 2.70 (s, 9H, CH₃), 2.52 (m, 2H, CH₂CH₂CH₂), -2.77 (s, 2H, NH) ppm; ¹³C{¹H} NMR (CDCl₃, 75.47 MHz) δ 139.29, 137.29, 135.58, 134.50, 130.99, 128.78, 127.39, 120.08, 112.70 (all ArC), 65.55 (OCH₂), 32.58 (CH₂Br), 30.15 (CH₂CH₂CH₂), 21.51 (ArCH₃) ppm; FAB-MS m/z 794 (M + H)⁺. Anal. Calcd for C₅₀H₄₁N₄OBr: C, 75.65; H, 5.21; N, 7.06. Found: C, 75.89; H, 5.07; N, 6.77.

Free base diporphyrin basket H₄11:

Method A: Compound **13** (94 mg, 85 μmol) and porphyrin **8** (160 mg, 238 μmol) were dissolved in DMF (10 mL) and K₂CO₃ (260 mg, 1.89 mmol) and KI (5 mg) were added. The mixture was heated under nitrogen at 100°C for 5

days. After cooling, the solvent was evaporated and the residue was dissolved in CH_2Cl_2 (50 mL). This solution was extracted with a saturated aqueous NaHCO_3 solution (100 mL), with water (3 x 100 mL), and then evaporated to dryness. After purification by column chromatography (ACROS silica, $\text{CH}_2\text{Cl}_2/\text{EtOH}/\text{Et}_3\text{N}$, 95:4:1, v/v/v), the product was dissolved again in CH_2Cl_2 (20 mL), extracted with a saturated aqueous NaHCO_3 solution (50 mL), with water (3 x 50 mL), and then evaporated to dryness. The resulting product was dissolved in a minimal amount of CHCl_3 , and this solution was added dropwise to hexane (15 mL), while stirring vigorously. After centrifugation, the product was dried under vacuum to give 83 mg (42%) of **H₄11** as a purple solid.

Method B:

Compounds **10** (25 mg, 32 μmol) and **14** (12 mg, 14 μmol) were dissolved in degassed DMF (3 mL). K_2CO_3 (50 mg, 36 mmol) and KI (5 mg) were added and the mixture was heated under nitrogen at 100°C for 5 days. After cooling, the product was extracted and purified as described in Method A, to yield 24 mg (76%) of **H₄11**.

M.p. > 300°C (dec.); ^1H NMR (CDCl_3 , 500.14 MHz) δ 8.88 (d, 4H, β -pyrroleH, $^3\text{J} = 4.8$ Hz), 8.86 (d, 4H, β -pyrroleH, $^3\text{J} = 4.8$ Hz), 8.84 (s, 8H, β -pyrroleH), 8.10 (d, 4H, ArH, $^3\text{J} = 8.0$ Hz), 8.08 (d, 4H, ArH, $^3\text{J} = 7.8$ Hz), 8.07 (d, 8H, ArH, $^3\text{J} = 8.0$ Hz), 7.53 (d, 4H, ArH, $^3\text{J} = 7.8$ Hz), 7.52 (d, 8H, ArH, $^3\text{J} = 8.0$ Hz), 7.27 (d, 4H, ArH, $^3\text{J} = 8.0$ Hz), 7.06 (t, 4H, ArH, $^3\text{J} = 6.9$ Hz), 7.00 (d, 4H, ArH, $^3\text{J} = 6.9$ Hz), 6.97 (t, 2H, ArH, $^3\text{J} = 6.9$ Hz), 6.55 (s, 4H, ArH side-wall), 5.62 (d, 4H, $\text{NCH}_2\text{Ar out}$, $^2\text{J} = 15.9$ Hz), 4.30 (t, 4H, ArOCH_2 , $^3\text{J} = 5.7$ Hz), 4.00 (m, 4H, ArOCH_2), 3.86 (m, 4H, $\text{ArOCH}_2\text{CH}_2$), 3.85-3.65 (m, 16H, OCH_2), 3.67 (d, 4H, $\text{NCH}_2\text{Ar in}$, $^2\text{J} = 15.9$ Hz), 2.88 (m, 12H, NCH_2), 2.68 (s, 18H, ArCH_3), 2.13 (m, 4H, $\text{CH}_2\text{CH}_2\text{CH}_2$) ppm, see Table 8.6 for exact signal assignments; $^{13}\text{C}\{^1\text{H}\}$ NMR (CDCl_3 , 75.47 MHz) δ 159.12 (urea C=O), 156.47, 151.30, 139.28, 137.27, 135.10, 134.19, 133.21, 130.97, 128.84, 128.37, 127.38, 120.05, 114.09, 112.74 (ArC), 84.62 (NC(Ar)N), 70.23, 69.96, 69.43, 66.31 (CH_2O), 54.01, 52.18 (CH_2N), 36.96 (NCH_2Ar), 27.65 ($\text{CH}_2\text{CH}_2\text{CH}_2$), 21.50 (ArCH_3) ppm; FAB-MS m/z 2303 (M + H)⁺. UV-vis (CHCl_3) λ 420, 515, 549, 585, 638 nm. Anal. Calcd for $\text{C}_{148}\text{H}_{136}\text{N}_{14}\text{O}_{12}$: C, 77.19; H, 5.95; N, 8.51. Found: C, 77.57; H, 5.93; N, 8.14.

Zinc diporphyrin basket **Zn₂11**:

Compound **H₄11** (20 mg, 8.7 μmol) and $\text{Zn}(\text{OAc})_2 \cdot 2\text{H}_2\text{O}$ (5 mg, 23 μmol) were dissolved in a mixture of CHCl_3 (2 mL) and MeOH (1 mL). The mixture was refluxed for 3 h and evaporated to dryness. The residue was dissolved in CH_2Cl_2 (20 mL) and this solution was extracted with a saturated aqueous NaHCO_3 solution (50 mL) and with water (3 x 50 mL) and evaporated to dryness. The product was dissolved in a minimal amount of CHCl_3 , and this solution was added dropwise to hexane (15 mL) while stirring vigorously. After centrifugation, the product was dried under vacuum to give 20 mg (95%) of **Zn₂11** as a purple solid.

M.p. > 300°C (dec.); ^1H NMR (CDCl_3 , 500.14 MHz) δ 8.98-8.89 (m, 16H, β -pyrroleH), 8.14 (d, 4H, ArH, $^3\text{J} = 7.5$ Hz), 7.98 (d, 4H, ArH, $^3\text{J} = 7.5$ Hz), 8.07 (d, 8H, ArH, $^3\text{J} = 7.5$ Hz), 7.57 (d, 4H, ArH, $^3\text{J} = 7.5$ Hz), 7.50 (d, 8H, ArH, $^3\text{J} = 7.5$ Hz), 7.12 (d, 4H, ArH, $^3\text{J} = 7.5$ Hz), 6.98-6.84 (m, 10H, ArH), 6.38 (br s, 4H, ArH side-wall), 5.26 (d, 4H, $\text{NCH}_2\text{Ar out}$, $^2\text{J} = 15.5$ Hz), 4.12 (m, 4H, ArOCH_2), 3.43 (d, 4H, $\text{NCH}_2\text{Ar in}$, $^2\text{J} = 15.5$ Hz), 3.39 (m, 8H, ArOCH_2), 3.23 (m, 4H, OCH_2), 3.09 (m, 4H, OCH_2), 3.00 (m, 8H, OCH_2), 2.37 (m, 4H, NCH_2), 2.20 (m, 4H, NCH_2), 1.99 (m, 4H, NCH_2), 1.86 (m, 4H, $\text{CH}_2\text{CH}_2\text{CH}_2$) ppm, see Table 8.6 for exact proton assignments; FAB-MS m/z 2428 (M)⁺. UV-vis (CHCl_3) λ 420, 429 (shoulder), 552, 594 nm. Anal. Calcd for $\text{C}_{148}\text{H}_{132}\text{N}_{14}\text{O}_{12}\text{Zn}_2$: C, 73.17; H, 5.48; N, 8.07. Found: C, 73.50; H, 5.46; N, 7.71.

8,25-Di(3-hydroxypropyl)-36,37-diphenyl-2,5,11,14,19,22,28,31-octaoxa-8,25,35,38,43,45-hexaazaocyclo[30.15.2.1^{35,38,0^{15,41}.0^{18,40}.0^{33,47}.0^{36,45}.0^{37,43}}]pentaconta-1(48),15,17,32(49),33(47),40-hexaene-44,50-dione (12):

This compound was synthesized according to a literature procedure.⁴⁴

8,25-Di(3-hydroxypropyl)-44,50-dioxo-36,37-diphenyl-2,5,11,14,19,22,28,31-octaoxa-35,38,43,45-tetraaza-8,25-diazoniaocyclo[30.15.2.1^{35,38,0^{15,41}.0^{18,40}.0^{33,47}.0^{36,45}.0^{37,43}}]pentaconta-1(48),15,17,32(49),33(47),40-hexaene dichloride (12.2HCl), and 8,25-di(3-chloropropyl)-44,50-dioxo-36,37-diphenyl-2,5,11,14,19,22,28,31-octaoxa-35,38,43,45-tetraaza-8,25-diazoniaocyclo[30.15.2.1^{35,38,0^{15,41}.0^{18,40}.0^{33,47}.0^{36,45}.0^{37,43}}]pentaconta-1(48),15,17,32(49),33(47),40-hexaene dichloride (13):

Compound **12** (22 mg, 0.022 mmol) was stirred in a mixture of methanol (5 mL) and aqueous 37% HCl (0.5 mL) for 1 h. The solvent was then evaporated and the product was dried in a desiccator over P_2O_5 for 24 h to afford **12.2HCl**. Subsequently, this compound was stirred in SOCl_2 (5 mL) for 40 h. The solvent was evaporated and the product was dried under vacuum to yield 24 mg (100%) of **3** as a white solid, which was used without further purification for further syntheses. A sample was recrystallized from methanol/diethyl ether for analysis.

12.2HCl: M.p. > 300°C; ^1H NMR (CD_3OD , 300.13 MHz) δ 7.28-7.02 (m, 10H, ArH glycoluril), 6.84 (m, 4H, ArH side-wall), 5.70-5.58 (overlapped d, 4H, $\text{NCH}_2\text{Ar out}$), 4.41 (m, 2H, CH_2O), 4.33-4.10 (m, 6H, CH_2O), 4.08-3.85 (m, 20H, CH_2O), 3.83 (d, 4H, $\text{NCH}_2\text{Ar in}$, $^2\text{J} = 16.2$ Hz), 3.67 (m, 12H, NCH_2CH_2), 2.05 (m, 4H, $\text{CH}_2\text{CH}_2\text{CH}_2$) ppm; $^{13}\text{C}\{^1\text{H}\}$ NMR (CD_3OD , 75.47 MHz) δ 159.89 (urea C=O), 152.01, 151.90 (ArC *ipso* to OCH_2), 135.08,

130.44, 130.32, 129.86, 129.48, 129.16 (all ArC), 114.47, 113.54 (ArC *para* to CH₂N), 87.33 (NC(Ph)N), 71.21, 71.09, 70.62, 67.11, 66.16 (CH₂O), 60.96, 60.51, 55.22, 54.95 (CH₂CH₂N), 38.31 (NCH₂Ar, 27.59, 26.97 (CH₂CH₂CH₂) ppm. **13**: M.p. > 300°C; ¹H NMR (CD₃OD, 300.13 MHz) δ 7.38-6.95 (m, 10H, ArH glycoluril), 6.87-6.78 (m, 4H, ArH side-wall), 5.74-5.47 (m, 4H, NCH₂Ar *out*), 4.38-3.42 (m, 40H, CH₂O, CH₂N, CH₂Cl), 3.84 (d, 4H, NCH₂Ar *in*, ²J = 16.1 Hz), 2.31 (m, 4H, CH₂CH₂CH₂) ppm; ¹³C{¹H} NMR (CD₃OD, 75.47 MHz) δ 158.86 (urea C=O), 151.84 (ArC *ipso* to CH₂N), 134.94, 130.31, 129.81, 129.5 (all ArC), 114.91, 114.58, 114.19, 113.58 (ArC *para* to CH₂N), 87.34 (NC(Ph)N), 71.62, 71.24, 70.82, 70.47, 67.21, 66.01 (CH₂O), 55.22, 54.95, 54.46, 53.99, 52.67 (CH₂N), 42.94 (CH₂Cl), 38.35 (NCH₂Ar), 27.93, 27.65, 27.38 (CH₂CH₂CH₂) ppm. FAB-MS *m/z* 1029 (M - 2Cl - H)⁺. Anal. Calcd for C₅₄H₆₈N₆O₁₀Cl₂: C, 58.80; H, 6.21; N, 7.62. Found: C, 58.99; H, 6.15; N, 7.49.

36,37-Diphenyl-2,5,11,14,19,22,28,31-octa-oxa-8,25,35,38,43,45-hexaazaocyclo-[30.15.2.1^{35,38}.0^{15,41}.0^{18,40}.-0^{33,47}.0^{36,45}.0^{37,43}]pentaconta-1(48),15,17,32(49),33(47),40-hexaene-44,50-dione (14):

This compound was synthesized according to a literature procedure.⁴⁶

References and notes

- Deisenhofer, J.; Epp, O.; Miki, K.; Huber, R.; Michel, H. *Nature* **1985**, *318*, 618.
- McDermott, G.; Prince, S. M.; Freer, A. A.; Hawthornthwaite-Lawless, A. M.; Papiz, M. Z.; Cogdell, R. J.; Isaacs, N. W. *Nature* **1995**, *374*, 517.
- Pullerits, T.; Sundström, V. *Acc. Chem. Res.* **1996**, *29*, 381. Van Grondelle, R.; Monshouwer, R.; Valkunas, L. *Pure Appl. Chem.* **1997**, *69*, 1211.
- For reviews about artificial porphyrin arrays see: Wasielewski, M. R. *Chem. Rev.* **1992**, *92*, 435. Kurreck, H.; Huber, M. *Angew. Chem. Int. Ed. Engl.* **1995**, *34*, 849. Chin-Ti, C. in: *Comprehensive Supramolecular Chemistry*. Atwood, J. L.; Davies, J. E. D.; MacNicol, D. D.; Vögtle, F.; Reinhoudt, D. N.; Lehn, J.-M. Eds.; Elsevier Science Ltd., Pergamon: Elmsford, **1996**; Vol. 5, 91. Sanders, J. K. M. in: *Comprehensive Supramolecular Chemistry*. Atwood, J. L.; Davies, J. E. D.; MacNicol, D. D.; Vögtle, F.; Reinhoudt, D. N.; Lehn, J.-M. Eds.; Elsevier Science Ltd., Pergamon: Elmsford, **1996**; Vol. 9, 131. Harriman, A.; Sauvage, J.-P. *Chem. Soc. Rev.* **1996**, *25*, 41. Ward, M. D. *Chem. Soc. Rev.* **1997**, *26*, 365. Burrell, A. K.; Wasielewski, M. R. *J. Porphyrins Phthalocyanines* **2000**, *4*, 401.
- Hunter, C. A.; Sanders, J. K. M.; Stone, A. J. *J. Chem. Phys.* **1989**, *133*, 395. Chambron, J.-C.; Harriman, A.; Heitz, V.; Sauvage, J.-P. *J. Am. Chem. Soc.* **1993**, *115*, 7419.
- Anderson, H. L. *Chem. Commun.* **1999**, 2323, and references cited therein.
- Anderson, H. L. *Inorg. Chem.* **1994**, *33*, 972. Nakano, A.; Osuka, A.; Yamazaki, I.; Yamazaki, T.; Nishimura, Y. *Angew. Chem. Int. Ed.* **1998**, *37*, 3023. Taylor, P. N.; Anderson, H. L. *J. Am. Chem. Soc.* **1999**, *121*, 11538. Aratani, N.; Osuka, A.; Kim, Y. H.; Jeong, D. H.; Kim, D. *Angew. Chem. Int. Ed.* **2000**, *39*, 1458.
- Anderson, H. L.; Anderson, S.; Sanders, J. K. M. *J. Chem. Soc. Perkin Trans. 1* **1995**, 2231.
- Mongin O.; Papamicae C.; Hoyle, N.; Gossauer, A. *J. Org. Chem.* **1998**, *63*, 5568. Biemans, H. A. M.; Rowan, A. E.; Verhoeven, A.; Vanoppen, P.; Latterini, L.; Foekema, J.; Schenning, A. P. H. J. Meijer, E. W.; de Schryver, F. C.; Nolte, R. J. M. *J. Am. Chem. Soc.* **1998**, *120*, 11054. Bampos, N.; Marvaud, V.; Sanders, J. K. M. *Chem. Eur. J.* **1998**, *4*, 335. Ambroise, A.; Li, J.; Yu, L.; Lindsey, J. S. *Org. Lett.* **2000**, *2*, 2563. Maruo, N.; Uchiyama, M.; Kato, T.; Arai, T.; Akisada, H.; Nishino, N. *Chem. Commun.* **1999**, 2057. Mongin, O.; Schuwey A.; Vallot, M. A.; Gossauer, A. *Tetrahedron Lett.* **1999**, *40*, 8347.
- Officer, D. L.; Burrell, A. K.; Reid, D. C. W. *Chem. Commun.* **1996**, 1657. Huck, W. T. S.; Rohrer, A.; Anilkumar, A. T.; Fokkens, R. H.; Nibbering, N. M. M.; van Veggel, F. C. J. M.; Reinhoudt, D. N. *New J. Chem.* **1998**, *22*, 165. Mak, C. C.; Bampos, N.; Sanders, J. K. M. *Angew. Chem. Int. Ed.* **1998**, *37*, 3020.
- Sessler, J. L.; Wang, B.; Harriman, A. *J. Am. Chem. Soc.* **1995**, *117*, 704. Drain, C. M.; Russell, K. C.; Lehn, J.-M. *Chem. Commun.* **1996**, 337.
- Krishna Kuma, R.; Balasubramanian, S.; Goldberg, I. *Inorg. Chem.* **1998**, *37*, 541. Krishna Kuma, R.; Balasubramanian, S.; Goldberg, I. *Chem. Commun.* **1998**, 1435.
- Rubires, R.; Crusats, J.; El-Hachemi, Z.; Jaramillo, T.; López, M.; Valls, E.; Farrera, J.-A.; Ribó, J. M. *New J. Chem.* **1999**, 189. Kano, K.; Fukuda, K.; Wakami, H.; Nishiyabu, R.; Pasternack, R. F. *J. Am. Chem. Soc.* **2000**, *122*, 7494.
- Hunter, C. A.; Hyde, R. K. *Angew. Chem. Int. Ed. Engl.* **1996**, *35*, 1936. Wilson, G. S.; Anderson, H. L. *Chem. Commun.* **1999**, 1539. Chichak, K.; Branda, N. R. *Chem. Commun.* **2000**, 1211.
- Burrell, A. K.; Officer, D. L.; Reid, D. C. W.; Wild, K. Y. *Angew. Chem. Int. Ed.* **1998**, *37*, 114. Michelsen, U.; Hunter, C. A. *Angew. Chem. Int. Ed.* **2000**, *39*, 764.
- Drain, C. M.; Nifiatis, F.; Vasenko, A.; Batteas, J. D. *Angew. Chem. Int. Ed.* **1998**, *37*, 3020.

- ¹⁷ Chi, X.; Guerin, A.; Haycock, R. A.; Hunter, C. A.; Sarson, L. D. *J. Chem. Soc. Chem. Commun.* **1995**, 2567.
Haycock, R. A.; Hunter, C. A.; James, D. A.; Michelsen, U.; Sutton, L. R. *Org. Lett.* **2000**, 2, 2435.
- ¹⁸ For a review about molecular clips see: Rowan, A. E.; Elemans, J. A. A. W.; Nolte, R. J. M. *Acc. Chem. Res.* **1999**, 32, 995.
- ¹⁹ Holder, S. J.; Elemans, J. A. A. W.; Barberá, J.; Rowan, A. E.; Nolte, R. J. M. *Chem. Commun.* **2000**, 355.
Holder, S. J.; Elemans, J. A. A. W.; Donners, J. J. J. M.; Boerakker, M. J.; de Gelder, R.; Barberá, J.; Rowan, A. E.; Nolte, R. J. M. *J. Org. Chem.* **2001**, 66, 391.
- ²⁰ Methanol was added in order to fully dissolve both clip and guest components.
- ²¹ At both temperatures, two sharp high-angle reflections were observed in the powder diffractogram, whereas in a liquid-crystalline phase the high-angle reflections usually are diffuse. The observed reflections correspond to a rather disorganized crystalline phase. No evidence for a columnar organization could be found.
- ²² Scheidt, W. R.; Lee, Y. J. *Structure and bonding* **1987**, 64, 1. Koehorst, R. B. M.; Hostra, U.; Schaafsma, T. J. *J. Magn. Res. Chem.* **1988**, 26, 167.
- ²³ Hunter, C. A.; Sanders, J. K. M. *J. Am. Chem. Soc.* **1990**, 112, 5525.
- ²⁴ McRae, E. G.; Kasha, M. *J. Chem. Phys.* **1958**, 28, 721. Kasha, M.; Rawls, H. R.; Ashraf El-Bayoumi, M. *Pure Appl. Chem.* **1965**, 11, 371.
- ²⁵ Silvers, S. J.; Tulinsky, A. *J. Am. Chem. Soc.* **1967**, 89, 3331.
- ²⁶ The melting and subsequent cooling of the complexes appeared to be necessary in order to be able to fully dissolve the material.
- ²⁷ The binding of a 1,3-dihydroxybenzene guest usually causes a maximal upfield shift of -0.5 ppm of the cavity side-wall protons of a molecular clip, see: Reek, J. N. H.; Elemans, J. A. A. W.; Nolte, R. J. M. *J. Org. Chem.* **1997**, 62, 2234.
- ²⁸ The binding constant between **1** and a mono-3,5-dihydroxybenzene functionalized porphyrin was determined to be $K_a = 750 \text{ M}^{-1}$.
- ²⁹ Reek, J. N. H.; Kros, A.; Nolte, R. J. M. *Chem. Commun.* **1996**, 245.
- ³⁰ It appeared to be impossible to separate these contaminations by column chromatography, HPLC or crystallization.
- ³¹ For a paper concerning the shielding and deshielding effects caused by the porphyrin ring current, see: Cross, K. J.; Crossley, M. J. *Aust. J. Chem.* **1992**, 45, 991.
- ³² The calculation of an association constant (K_a) between **Zn₂6** and DABCO was complicated due to the occurrence of reorganizations in the host upon binding of the guest. The slow exchange between the various components in the NMR spectra, however, suggested that this K_a is very high ($>10^5 \text{ M}^{-1}$).
- ³³ As a result of the observed broad signals in the NMR spectrum, an unsuccessful attempt was undertaken to freeze out the complexation processes within the 4:1 complex.
- ³⁴ Reek, J. N. H.; Rowan, A. E.; de Gelder, R.; Beurskens, P. T.; Crossley, M. J.; de Feyter, S.; de Schryver, F.; Nolte, R. J. M. *Angew. Chem. Int. Ed. Engl.* **1997**, 36, 361. Reek, J. N. H.; Rowan, A. E.; Crossley, M. J.; Nolte, R. J. M. *J. Org. Chem.* **1999**, 64, 6653.
- ³⁵ The observed quenching could, however, also be a result from the change in solvent polarity.
- ³⁶ Lehn, J.-M. *Science* **1985**, 227, 849. Feiters, M. C. in: *Comprehensive Supramolecular Chemistry*. Atwood, J. L.; Davies, J. E. D.; MacNicol, D. D.; Vögtle, F.; Reinhoudt, D. N.; Lehn, J.-M. Eds.; Elsevier Science Ltd., Pergamon: Elmsford, **1996**; Vol. 10, 267.
- ³⁷ Whitesides, G. M.; Mathias, J. P.; Seto, C. T. *Science* **1991**, 254, 1312. Philp, D.; Stoddart, J. F. *Angew. Chem. Int. Ed. Engl.* **1996**, 35, 1155.
- ³⁸ Schenning, A. P. H. J.; Hubert, D. H. W.; van Esch, J. H.; Feiters, M. C.; Nolte, R. J. M. *Angew. Chem., Int. Ed. Engl.* **1994**, 33, 2468; Schenning, A. P. H. J.; Lutje Spelberg, J. H.; Hubert, D. H. W.; Feiters, M. C.; Nolte, R. J. M. *Chem. Eur. J.* **1998**, 4, 871.
- ³⁹ Elemans, J. A. A. W.; Claase, M. B.; Aarts, P. P. M. Rowan, A. E.; Schenning, A. E.; Nolte, R. J. M. *J. Org. Chem.* **1999**, 64, 7009.
- ⁴⁰ Elemans, J. A. A. W.; Bijsterveld, E. J. A.; Rowan, A. E.; Nolte, R. J. M. *Chem. Commun.* **2000**, 2443.
- ⁴¹ For a review about metal-templated self-assembly of artificial receptors see: Linton, B.; Hamilton, A. D. *Chem. Rev.* **1997**, 97, 1669.
- ⁴² For other examples of templated assembly of porphyrins and phthalocyanines, see: Chernook, A. V.; Rempel, U.; von Borczyskowski, C.; Shulga, A. M.; Zenkevich, E. I. *Chem. Phys. Lett.* **1996**, 254, 229. Reek, J. N. H.; Schenning, A. P. H. J.; Bosman, A. W.; Meijer, E. W.; Crossley, M. J. *Chem. Commun.* **1998**, 11. Li, X.-Y.; Ng, D. K. P. *Eur. J. Inorg. Chem.* **2000**, 1845. Felluga, F.; Tecilla, P.; Hillier, L.; Hunter, C. A.; Licini, G.; Scrimin, P. *Chem. Commun.* **2000**, 1087.

- ⁴³ Kang, J.; Rebek, J., Jr. *Nature* **1997**, *385*, 50. Kang, J.; Hilmersson, G.; Santamaría, J.; Rebek, J., Jr. *J. Am. Chem. Soc.* **1998**, *120*, 3650. Kang, J.; Santamaría, J.; Hilmersson, G.; Rebek, J., Jr. *J. Am. Chem. Soc.* **1998**, *120*, 7389.
- ⁴⁴ Van Nunen, J. L. M.; Stevens, R. S. A.; Picken, S. J.; Nolte, R. J. M. *J. Am. Chem. Soc.* **1994**, *116*, 8825.
- ⁴⁵ In principle intermolecular reactions are also possible but the absence of broad signals in the NMR spectra suggests that mainly intramolecular substitution occurs.
- ⁴⁶ Smeets, J. W. H.; Sijbesma, R. P.; van Dalen, L.; Spek, A. L.; Smeets, W. J. J.; Nolte, R. J. M. *J. Org. Chem.* **1989**, *54*, 3710.
- ⁴⁷ Upon binding a **TPyP** molecule, the interaction between one of the zinc porphyrins and the azacrown ether nitrogen atom of **Zn₂11** is broken, while two new pyridine-zinc coordinative interactions are formed.
- ⁴⁸ Johnston, M. R.; Gunter, M. J.; Warrenner, R. N. *Chem. Commun.* **1998**, 2739.
- ⁴⁹ Anderson, S.; Anderson, H. L.; Bashall, A.; McPartlin, M.; Sanders, J. K. M. *Angew. Chem. Int. Ed. Engl.* **1995**, *34*, 1096.
- ⁵⁰ Van Nunen, J. L. M.; Folmer, B. F. B.; Nolte, R. J. M. *J. Am. Chem. Soc.* **1997**, *119*, 283.

Chapter 9

Porphyrin Clips

9.1 Introduction

The complexity encountered in natural enzyme systems hampers to a great extent the understanding of their exact working mechanisms, and it is therefore that one of the aims of today's supramolecular chemistry is the design of simplified enzyme mimics that display the properties of the natural systems.¹ To be an efficient enzyme mimic, the designed molecule needs to possess a binding cavity or site that is able to selectively recognize and bind a desired substrate. In the next step, this substrate has to be converted at a catalytic center in the direct proximity of the binding site. Finally, the catalyst should be able to release the converted substrate and have the ability to be regenerated. Using natural enzymes as an inspiration, several approaches to synthetic catalysts which contain a substrate binding site that recognizes substrates next to an active site have been described in the literature.²

As part of our studies to create a cytochrome P450 mimic,³ we have been interested in developing porphyrin-functionalized receptor molecules which can selectively bind substrate molecules. Numerous capped, strapped and picket-fence porphyrins have been described in the literature which have been used to study electron transfer processes and O₂ and CO binding,⁴ but these cannot simultaneously bind substrates. There are many porphyrins with functional and directed binding groups at their *meso*-phenyl substituents which allow them to recognize anions,⁵ quinones,⁶ carboxylic acids,⁷ amino acid esters,⁸ and carbohydrates.⁹ Immobilization of binding sites such as crown ethers,¹⁰ Kemp's triacid derivatives¹¹ and diamidopyridines¹² on a porphyrin platform has resulted in porphyrin hosts displaying substrate, size and shape selective properties. Relatively few porphyrins, however, possess a well-defined cavity, which can selectively recognize substrates and shield these molecules from the surrounding medium. Examples include porphyrins connected to known cavity molecules such as cyclodextrins,¹³ cyclocholates,¹⁴ calixarenes¹⁵ and cyclophanes¹⁶ (Figure 9.1). Some of these molecules contain Mn(III) and Fe(III) porphyrins which catalyze oxidation reactions and display a certain regio- or stereoselectivity.¹⁷ Substrate binding in these systems takes place in water and is predominantly governed by hydrophobic interactions and not by specific molecular recognition phenomena. A novel approach is to construct cyclic porphyrin arrays in which the porphyrins themselves form the cavity (Figure 9.2).¹⁸ In these cyclic host systems substrates possessing metal-ligand

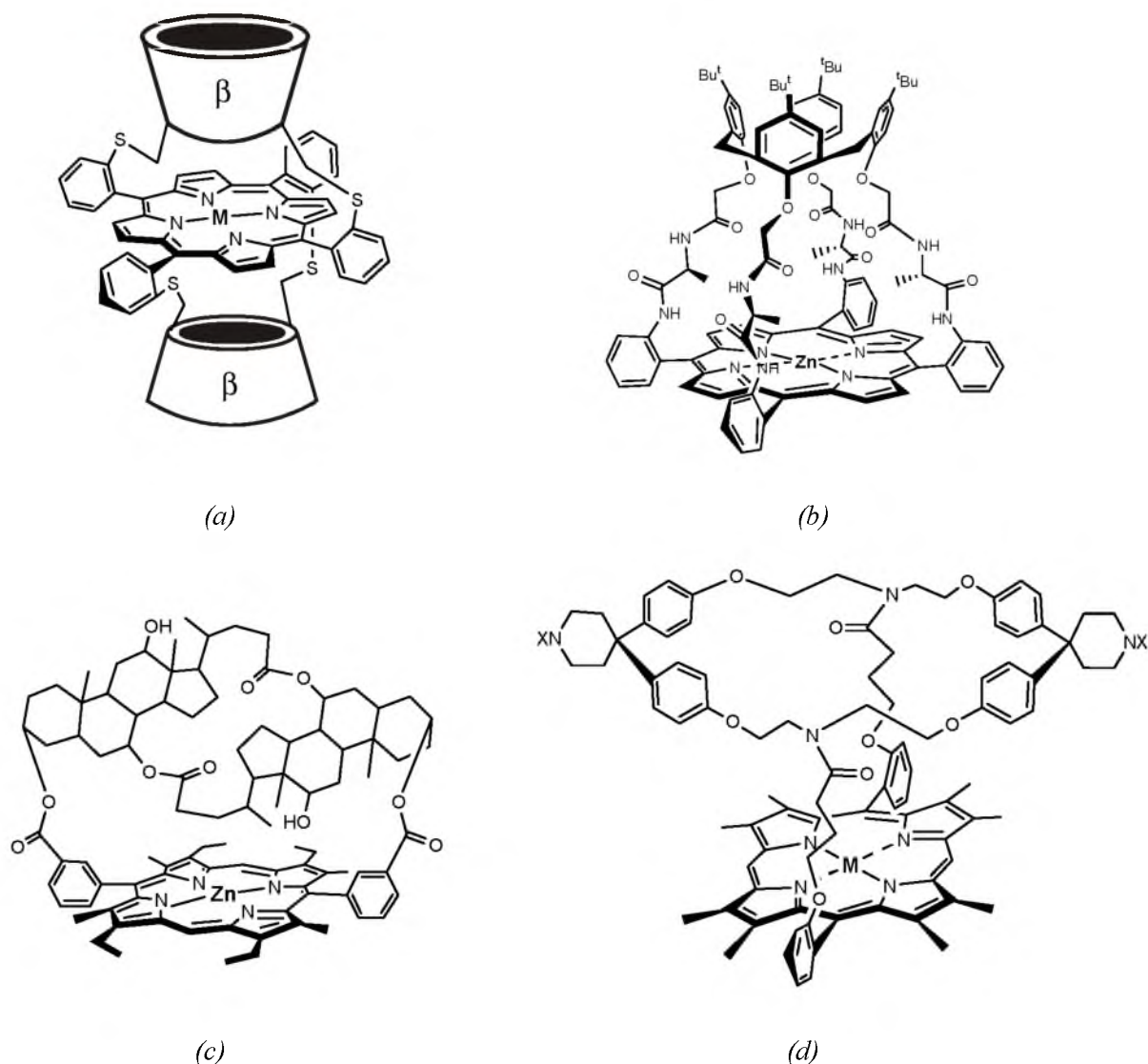


Figure 9.1 Examples of cavity-containing porphyrin molecules from (a) Ogoshi, (b) Shinkai, (c) Sanders, and (d) Diederich.

functions can be bound to the porphyrin metal and coupled to each other in a Diels-Alder reaction.

Binding of organic substrates without the aid of the porphyrin metal is rarely documented. The cyclophane-capped porphyrins of Sanders¹⁹ and the cyclophane-bridged porphyrin of Diederich are examples of such receptors, which bind substrates by directed hydrogen bonding or π - π stacking interactions, without any aid of the porphyrin metal. In addition to binding the substrate, Diederich's host is also active as a catalyst. It is capable of oxidizing bound acenaphthene molecules to acenaphthenone, however only in low turnovers.²⁰

In this chapter, the synthesis and binding properties of two new 'porphyrin clips' are described, which possess well-defined cavities with directed binding sites. It will be shown that small changes in the design of the molecules result in great differences in their conformations and in their binding affinities toward viologen, (dihydroxy)benzene, and pyridine derived guest molecules. The catalytic properties of these new porphyrin receptors will be described in Chapter 10.

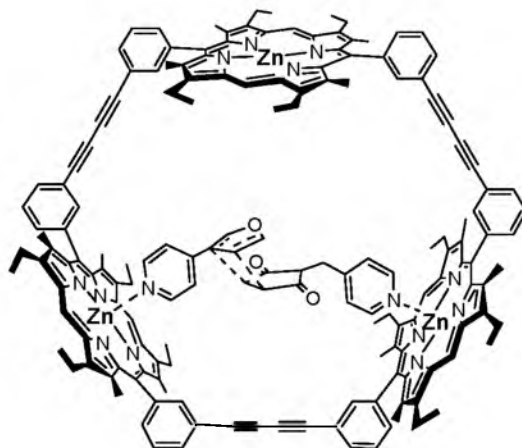
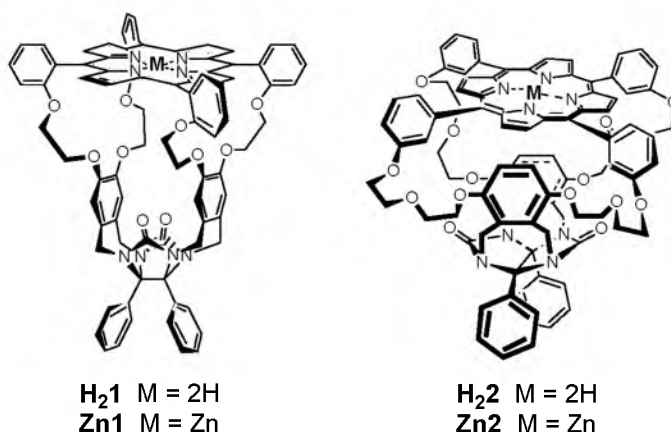


Figure 9.2 Cyclic porphyrin array of Sanders which catalyzes the Diels Alder reaction between a furan and a maleimide molecule.

9.2 Design

The receptor component of the new porphyrin hosts is the well-documented molecular clip, a molecule that can bind (di)hydroxybenzenes and viologen derivatives in organic solutions (see section 1.4). In previous work, one of the clip side-walls had already been functionalized with a porphyrin,²¹ but the application of this molecule as a catalyst in aziridination or epoxidation reactions turned out to be unsuccessful. The reason for this lack of success was attributed to an inappropriate geometry of the bound substrate with respect to the porphyrin catalyst, and to the incompatibility of the guest phenolic hydroxy substituents with the reaction conditions.²² In an alternative approach, a basket-shaped clip molecule was functionalized with a Rh^I phosphite center situated above the cavity.²³ This system proved to be an efficient hydrogenation and isomerization catalyst, showing features similar to those encountered in natural enzymes, such as substrate selectivity, Michaelis-Menten kinetics, product inhibition and rate enhancement by cooperative binding.



Based on the latter studies it was decided to prepare supramolecular catalysts in which the porphyrin is situated *above* the receptor cavity, see **1** and **2**. Molecular modeling studies predicted that in the case of clip **1** the porphyrin is rigidly held above the cavity as a result of the four short spacers which link this macrocycle to the cavity side-walls. In the case of clip **2**, the porphyrin has more conformational flexibility because of the presence of longer spacers.

9.3 Synthesis

The synthesis of **1** started from diol **3**²⁴ which was treated with *p*-toluenesulfonyl chloride in pyridine to give the ditosylate **4** in 90% yield (Scheme 9.1). This molecule was attached to tetrakis(chloromethyl)diphenylglycoluril **5**²⁵ by a Friedel Crafts alkylation reaction in 1,2-dichloroethane using tin tetrachloride as a Lewis acid catalyst. In addition to the product **6**, a mono-walled clip and decomposition products in which **6** had lost one or more tosyl groups were formed. Prolonged reaction times resulted in an increase in yield of the double-walled product, but a concomitant loss of more tosyl groups. Purification of the crude product by column chromatography was very troublesome. Recrystallization from hot toluene, however, afforded pure **6** in 62% yield. This compound was then refluxed overnight in acetonitrile with salicylic aldehyde using potassium carbonate as a base to give the tetra-aldehyde clip molecule **7** in 59% yield, after purification by column chromatography. Finally, condensation of **7** with 4 equivalents of pyrrole in dichloromethane using boron trifluoride etherate as a catalyst and subsequent oxidation of the formed porphyrinogen with *p*-chloranil afforded porphyrin clip **H₂1** in 6% yield, after purification by column chromatography and several precipitations of a chloroform solution of the product in *n*-hexane. The latter procedure proved to be necessary to remove aliphatic contaminations which are probably captured in the receptor cavity.

The starting compound for porphyrin clip **2** was tetrapodand **8** (Scheme 9.2).²³ This compound was refluxed with *m*-hydroxybenzaldehyde under Finkelstein conditions in acetonitrile using sodium carbonate as a base to give the tetra-aldehyde clip molecule **9** in 64% yield, after purification by column chromatography. Due to the less acidic nature of the hydroxy proton of the aldehyde (as compared to salicylic aldehyde in the synthesis of **7**), this reaction was only completed after 10 days. Porphyrin clip **H₂2** was synthesized from **9** in 4% yield in the same manner as described for **H₂1**.

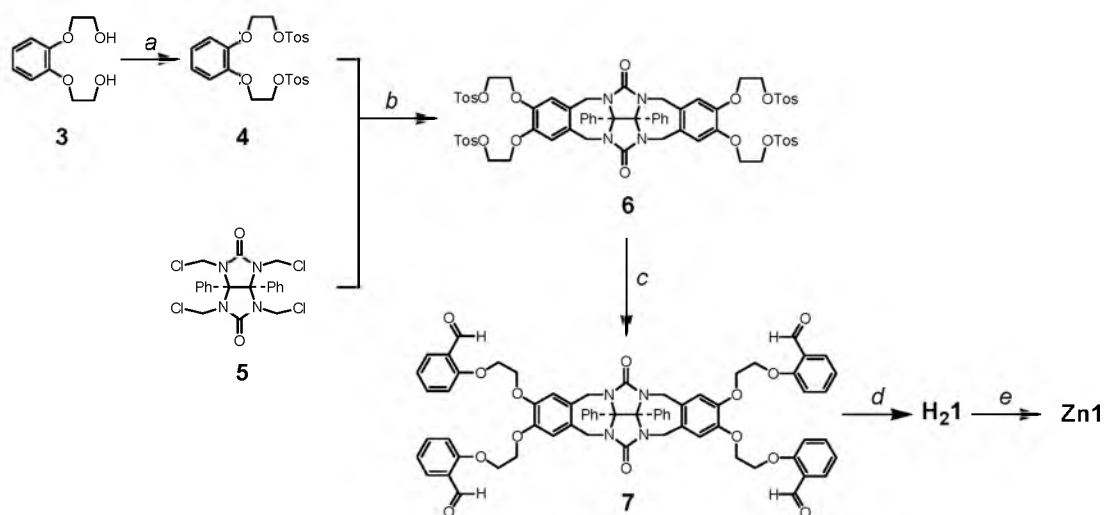
In order to shorten the synthetic route to **H₂2**, an attempt was undertaken to attach **8** *directly* to 5,10,15,20-tetrakis(*meso-m*-hydroxyphenyl)porphyrin **10**. After a reaction of **8** with **10** in acetonitrile under Finkelstein conditions using sodium carbonate as a base, porphyrin clip **H₂2** could be obtained in a yield of 6% (Scheme 9.3).²⁶

H₂1 and **H₂2** were nearly quantitatively converted to their corresponding zinc derivatives **Zn1** and **Zn2** by a reaction with excess zinc acetate dihydrate in a 2:1 mixture of chloroform and methanol. The zinc metal was complexed as a substitute for the paramagnetic Mn(III), in order to be able to use NMR spectroscopy in the structural analysis and binding properties of the compounds. Purification of the metallo-cavities was carried out by column chromatography, followed by several precipitations of the product in *n*-hexane.

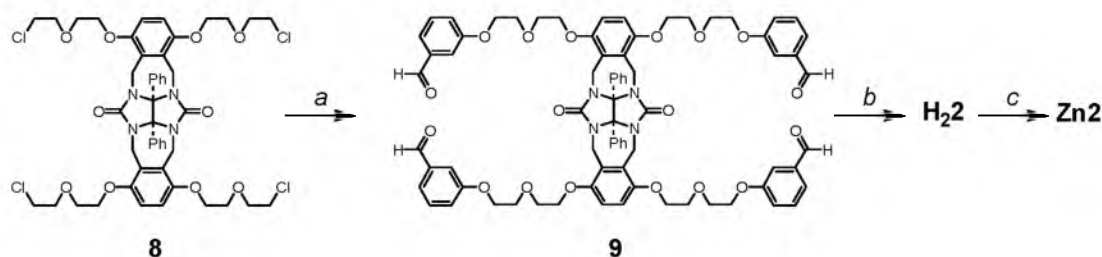
Many attempts were undertaken to grow crystals of the new porphyrin hosts. In several cases, single crystals could indeed be obtained, but in all cases they turned out to be too thin or too instable for successful X-ray analysis.

9.4 Conformational behaviour of the porphyrin clips

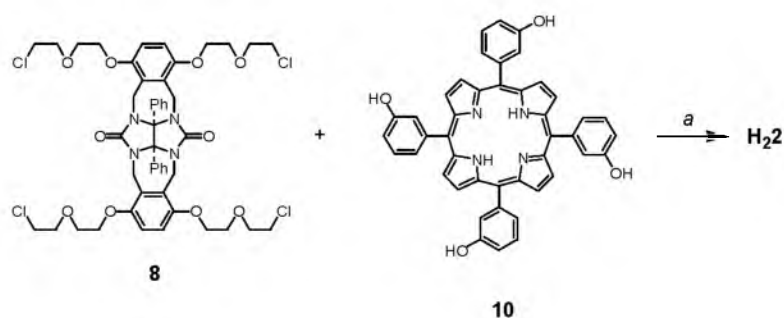
The structures of the porphyrin receptors were investigated with high resolution (500 MHz) ¹H NMR spectroscopy. Nearly all proton resonances in the spectra could be assigned with the help of COSY and 2D NOESY techniques (Figures 9.3 and 9.4).



Scheme 9.1 Synthesis of porphyrin clips **H₂1** and **Zn1**. Reagents and conditions: (a) TsCl , pyridine, 0°C , 16 h. (b) SnCl_4 , $\text{ClCH}_2\text{CH}_2\text{Cl}$, reflux, 16 h. (c) salicylic aldehyde, K_2CO_3 , CH_3CN , 16 h. (d) Pyrrole, BF_3OEt_2 , CH_2Cl_2 , 16 h, then *p*-chloranil, CH_2Cl_2 , reflux, 1 h. (e) $\text{Zn}(\text{OAc})_2 \cdot 2\text{H}_2\text{O}$, $\text{CHCl}_3/\text{MeOH}$ 2:1 (v/v), reflux, 3 h.



Scheme 9.2 Synthesis of porphyrin clips **H₂2** and **Zn2**. Reagents and conditions: (a) *m*-Hydroxybenzaldehyde, Na_2CO_3 , NaI , CH_3CN , reflux, 10 d. (b) Pyrrole, BF_3OEt_2 , CH_2Cl_2 , 16 h, then *p*-chloranil, reflux, 1 h. (c) $\text{Zn}(\text{OAc})_2 \cdot 2\text{H}_2\text{O}$, $\text{CHCl}_3/\text{MeOH}$ 2:1 (v/v), reflux, 3 h.



Scheme 9.3 Alternative synthesis of porphyrin clip **H₂2**. Reagents and conditions: (a) Na_2CO_3 , NaI , CH_3CN , reflux, 10 d.

CPK models and molecular modeling studies indicated that in clip **H₂1** the four short spacers position the porphyrin symmetrically above the clip, forming a well-defined and rigid cavity with a diameter of approximately 9 Å (Figure 9.5a). Its rigidity is confirmed by the observation of well-separated and sharp resonances for each oxyethylene proton in the ^1H NMR spectrum in

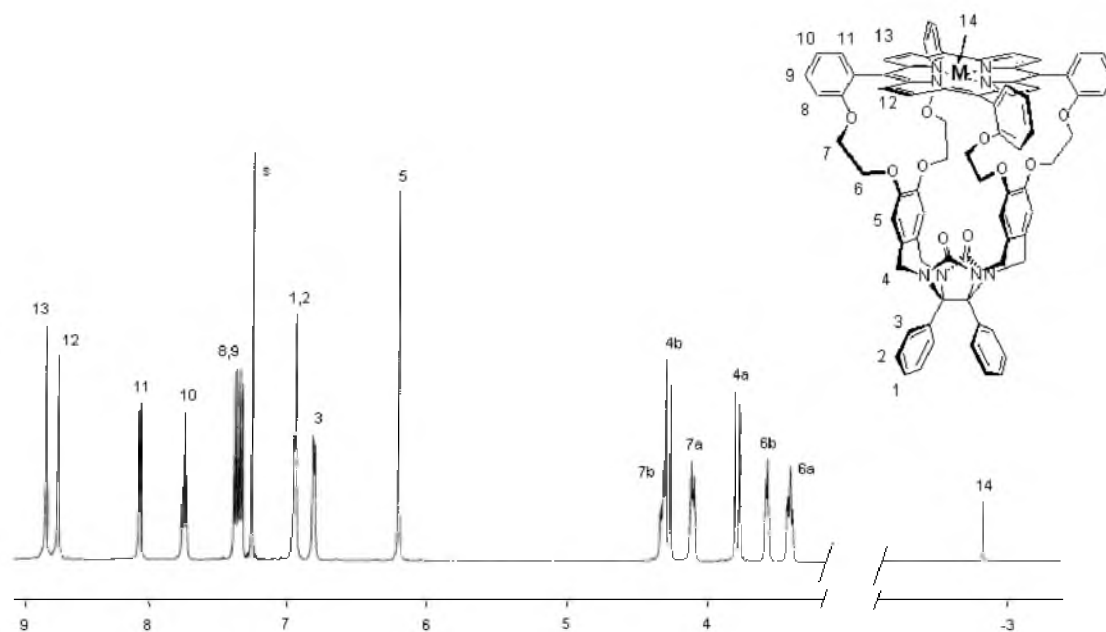


Figure 9.3 500 MHz ^1H NMR spectrum and proton assignments of porphyrin clip **H₂1** in CDCl_3 .

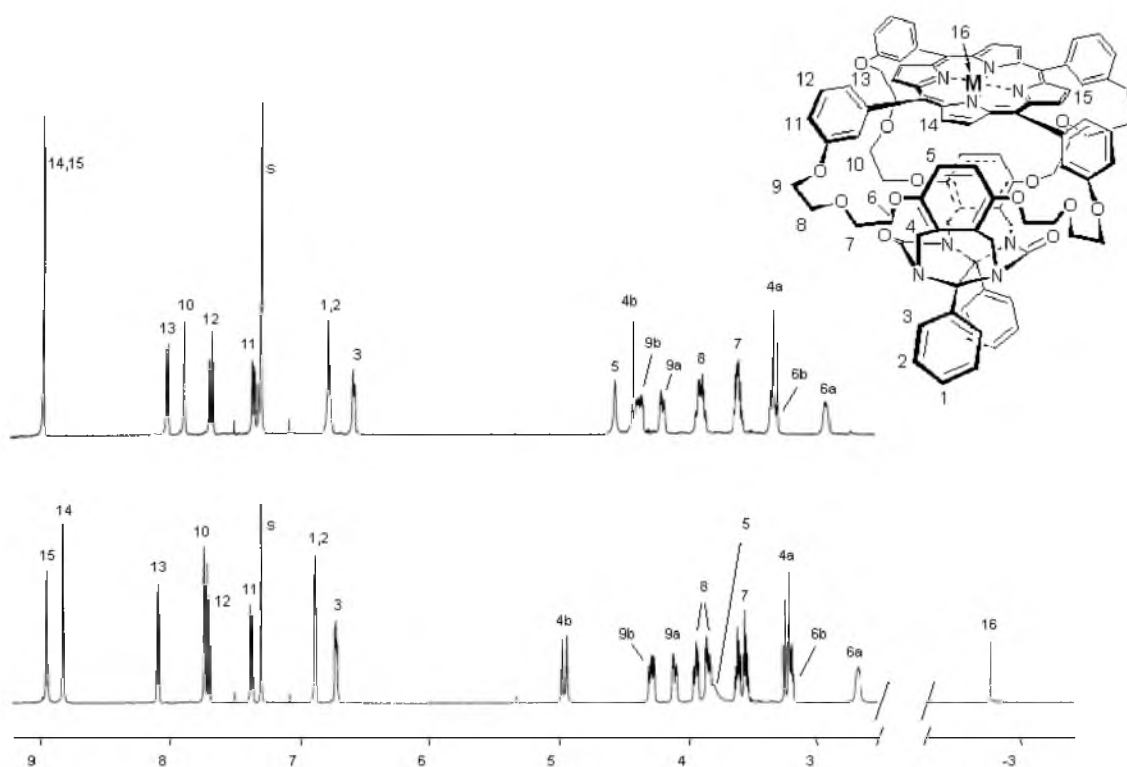


Figure 9.4 500 MHz ^1H NMR spectra and proton assignments of porphyrin clips **H₂2** (bottom) and **Zn2** (top) in CDCl_3 .

CDCl_3 (Figure 9.3). Insertion of a zinc ion caused no significant changes in the NMR spectrum and thus in the 3-dimensional structure of **Zn1**.

In **H₂2**, the spacers between the porphyrin and the clip are longer and CPK models suggested that the porphyrin has considerably more freedom of movement when compared to **H₂1**. The spacers are too short, however, to allow the porphyrin to be situated on the convex side of the

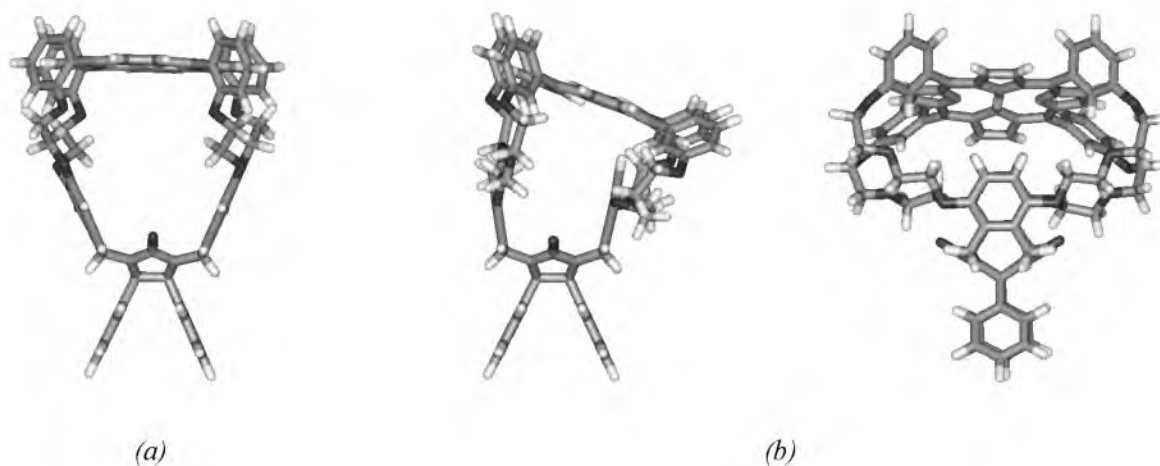


Figure 9.5 Computer calculated structures of porphyrin clips based on the *nOe* constraints in the 2D NOESY spectra. (a) **H₂₁** (b) **H₂₂** (side view and front view).

clip. If the spacers were fully extended and the porphyrin would be situated symmetrically above the clip, molecular modeling predicted that a larger cavity than the cavity of **H₂₁**, *viz.* with a diameter of approximately 10 Å, would be formed.

The NMR spectra of **H₂₂** and **Zn2** in CDCl₃ (Figure 9.4) revealed that the porphyrin roofs were not situated symmetrically above the cavity, and that the molecules are indeed more flexible than **1**. Strong upfield shifts were observed for the cavity side-wall protons H5 of **H₂₂** (at 3.8 ppm, $\Delta\delta = -2.8$ ppm compared to the shift of these protons in **9**) and for the signals of the nearby crown ether protons H6a and H6b ($\Delta\delta = -1.3$ and -0.8 ppm, respectively). These shifts indicate that the side-wall of the cavity is in the direct proximity of the porphyrin center.²⁷ The 2D NOESY spectrum of **H₂₂** revealed several *nOe* contacts between the side-wall protons H5 and the β -pyrrole protons H14, between H5 and the pyrrole NH protons H16 in the porphyrin center, and between all crown ether protons (H6 - H9) and H10/H14.

The combination of the observed *nOe* contacts and the strong upfield shifts confirms that the center of the porphyrin is situated directly above the cavity side-walls. The observed shift of the proton signal of H5 (at 3.8 ppm) is an *average* value, since it is not possible for the porphyrin center to be simultaneously situated above *both* side-walls. If the porphyrin would be locked in its position near one of the side-walls, two separate resonances for the side-wall protons of **H₂₂** should be observed and the shift of the protons covered by the porphyrin would be expected at approximately 1 ppm ($\Delta\delta \approx -5.5$ ppm). Since only one, broadened signal is observed, it can be concluded that **H₂₂** apparently exists in two conformations that interconvert rapidly on the NMR timescale. In each of the conformations, the porphyrin has to be located in a more or less *edge-to-face* geometry above one of the side-walls of the clip molecule. The well-resolved resonances for all oxyethylene protons indicate that these geometries are very well-defined. A computer-modeled structure of one of the conformations, which was calculated using the observed *nOe* contacts, is shown in Figure 9.5b. A schematic representation of the conformational behaviour of **H₂₂** is depicted in Figure 9.6a.

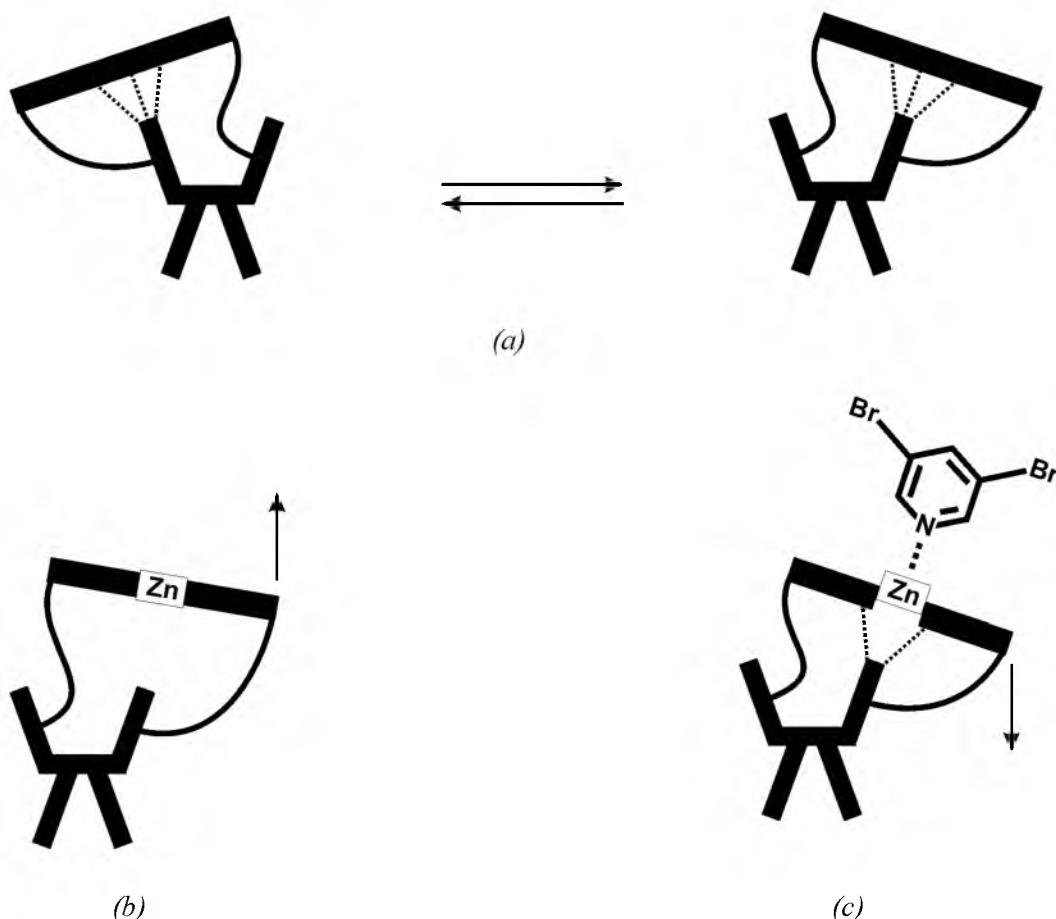


Figure 9.6 Schematic representation of the conformational behaviour of hosts **H₂2** and **Zn2** in CDCl_3 solution. The dashed lines highlight the interactions between the side-walls of the host and the porphyrin plane. (a) The two exchanging conformations of **H₂2**. (b) Lifting of the porphyrin in the case of **Zn2**. (c) Complexation of 3,5-dibromopyridine to **Zn2** which causes a lowering of the porphyrin.

The insertion of a zinc ion in **H₂2** to give **Zn2** led to some remarkable changes in the ^1H NMR spectrum of the cavity (Figure 9.4, top). The most pronounced difference observed was a downfield shift and a sharpening of the signal of the side-wall protons H5 (at 4.5 ppm, $\Delta\delta = +0.7$ ppm compared to **H₂2**). In addition, the signals of the crown ether protons H6a and H6b shifted downfield by +0.27 and +0.14 ppm, respectively. Furthermore, the resonances of oxyethylene protons H7 and H8 became less well-resolved when compared to those of **H₂2**, which is indicative of a greater flexibility in the crown ether spacers. Somewhat surprisingly, some proton resonances of the cavity skeleton exhibited large shifts (for example: H1,2: $\Delta\delta = -0.14$ ppm; H3: $\Delta\delta = -0.19$ ppm; H4b: $\Delta\delta = -0.64$ ppm). In the 2D NOESY spectrum of **Zn2** no nOe contacts between the porphyrin and cavity part were observed. Combined with the observed downfield shifts of the signals of H5, H6a and H6b, this was interpreted as indicating that the porphyrin center is not as directly sitting over the cavity side-walls as it is in **H₂2**, but is lifted upwards (see Figure 9.6b) This change in location of the porphyrin apparently also involves some reorganization in the glycoluril skeleton, which explains the observed shifts of H1 - H3 and H4b.²⁸

The dynamics of the conformational behavior of **H₂2** and **Zn2** were studied with Variable Temperature (VT) NMR. A solution of **H₂2** in CDCl_3 was cooled to 213 K, at which temperature the resonances of all protons lining the inside of the cavity (H5, H6 - H9 and H10) significantly

broadened. The solution also was heated stepwise to 328 K. Over this 115 K temperature range, several proton signals displayed large downfield shifts, *e.g.* the signals of H5 (+0.77 ppm), H6a (+0.47 ppm), and H16 (+0.16 ppm). The VT NMR studies indicated that upon increasing the temperature the interaction between the porphyrin center and the cavity side-wall is weakened. The NMR spectrum of a solution of **H₂2** in CDCl₃ at 328 K closely resembled the NMR spectrum of a solution of **Zn2** in CDCl₃ which was cooled to 240 K. Upon heating the solution of **Zn2** to 328 K, strong downfield shifts of the signals of H5 (+1.4 ppm), H6a (+0.71 ppm) and H6b (+0.46 ppm) were observed indicating a further lifting of the porphyrin away from the cavity side-wall.

The observed interaction between the porphyrin and the side-walls of **2** can be explained using predictions of π - π interactions developed by Hunter and Sanders.²⁹ This model predicts an attractive π - π interaction between two aromatic systems which are either oriented in an offset *face-to-face*, or in an *edge-to-face* geometry. The NMR measurements, in combination with molecular modeling, support the latter interaction in the case of hosts **2**, *i.e.* a rather favorable *edge-to-face* interaction between the porphyrin and the side-wall is present. An increase in solvent polarity, *e.g.* by the addition of CD₃OD or CD₃CN to the CDCl₃ solution, decreases this interaction. When a zinc ion is complexed in the porphyrin, the interaction becomes less attractive, which is attributed to a repulsive effect between the positively charged metal ion and the edge of the side-wall. This is supported by the VT NMR experiments, which showed that at lower temperatures the interaction becomes stronger in both **H₂2** and **Zn2**, and that at 240 K **Zn2** adopted an almost similar geometry as **H₂2** at 328 K. Further evidence for the difference in interaction between the porphyrin and the side-wall came from the coordination of the bulky axial ligand 3,5-dibromopyridine to the zinc ion of **Zn2**. The NMR spectrum of this complex in CDCl₃ clearly showed that the ligand coordinated exclusively on the *outside* of the cavity. In addition, the observed shifts upon coordination indicated a geometry between porphyrin and side-wall which had become almost identical to the geometry in **H₂2**, *i.e.* the interaction between porphyrin and side-wall had become more favourable. It is known that upon coordination of a pyridine ligand, the metal ion is pulled *ca.* 0.3 Å out of the porphyrin plane.²⁷ As a result, the repulsion between the porphyrin center and the side-wall in **Zn2** is reduced, and a similar geometry as observed for **H₂2** is adopted (Figure 9.6c).

9.5 Host-guest binding properties

Porphyrin clips **1** and **2** both possess a cavity that can bind guests by a variety of interactions, *viz.* by hydrogen bonding with the glycoluril carbonyl groups, by π - π interactions with the side-walls and the porphyrin roof, by hydrogen bonding and dipole interactions with the crown ether oxygen atoms of the spacers, and in the case of a metalloporphyrin clip, by complexation of ligands to the metal center. The host-guest binding properties of **1** and **2** toward a variety of guest molecules, such as viologen, dihydroxybenzene and pyridine derivatives, were therefore investigated with emphasis on the influence of the differences in cavity size and flexibility between **1** and **2** on their complexation behavior.

9.5.1 Binding of viologen derivatives

The first binding experiments were carried out with viologen derivatives (*N,N'*-disubstituted 4,4'-dipyridinium compounds), since host-guest complexes of these guests with dibenzo-crown ethers had already been described by Stoddart and coworkers.³⁰ In our group, basket-shaped receptors

had also been demonstrated to be very efficient receptors for such guests (see also section 1.4).³¹ In this section, the complexation behaviour of viologen guests **G1** and **G2** toward porphyrin hosts **1** and **2** is described, resulting in the formation of porphyrin-viologen pseudo-rotaxane structures.³² The binding of a bipyridinium cation in close proximity to the porphyrin ring opens up the possibility of an efficient photoactive interaction between the two components, which in the future may lead to potential applications in multicomponent photochemical devices.³³

Binding of viologens in hosts **1**

UV-vis titrations revealed that porphyrin clips **H₂1** and **Zn1** form exceptionally strong charge transfer³⁴ host-guest complexes with **G1** and **G2** (see Table 9.1) in acetonitrile/chloroform (1:1, v/v) solution. The complexes are stabilized by π - π interactions between the aromatic surfaces of the viologen and the *o*-xylylene side-walls and the porphyrin roof of the hosts, and by electrostatic interactions between the crown ether oxygen atoms of the host and the positive charge distributed over the *N*-methylene moieties and the 3,5-protons of the bipyridine ring of the guest.³⁵ Extra stabilization can be obtained when the guest can form additional hydrogen bonds with the carbonyl groups of the host (as in the case of **G2**). Addition of **G1** or **G2** to a solution of **H₂1** caused a decrease in intensity of the porphyrin Soret band (at 418 nm) in the UV-vis spectrum and a redshift of this band (2 nm for **G1** and 5 nm for **G2**). No significant shifts were observed in the porphyrin Q-bands. During the titration, several isosbestic points were observed, which is an indication of well-defined 1:1 host-guest complexation. Titrations of the guests with zinc tetrakis(*meso*-phenyl)porphyrin (ZnTPP) revealed no significant interactions, which confirms that binding of the guests in **H₂1** occurs within the cavity.

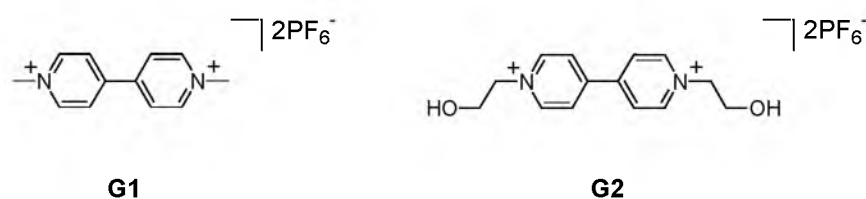


Table 9.1 Association constants K_a (M^{-1}) and binding free energies ΔG ($kJ\ mol^{-1}$, in parenthesis) of host-guest complexes between porphyrin clips and viologen guests **G1** and **G2**.^a

	H₂1	Zn1	H₂2	Zn2
G1	6.0×10^5 ^b (-32.9)	8.6×10^5 ^b (-33.8)	1100 ^c (-17.4)	5800 ^c (-20.2)
G2	7.4×10^6 ^d (-39.2)	— ^e	3500 ^c (-20.2)	1×10^4 ^b (-22.8)

^aIn $CHCl_3/CH_3CN$ (1:1, v/v) or $CDCl_3/CD_3CN$ (1:1, v/v) solution, 298 K. ^bEstimated error 30%. ^cEstimated error 10%. ^dEstimated error 50%. ^eNo reliable K_a -value could be determined, see text.

High resolution ¹H NMR experiments were carried out on the host-guest complexes in order to get exact insight in their binding geometries. At 298 K, the complex between **H₂1** and **G2** was in slow exchange on the NMR timescale with the free host, whereas for the complex between **H₂1** and **G1** sharp, averaged signals were observed. For all complexes, large complexation induced

shifts (CIS) were observed for most resonances of the protons lining the inside of the cavity of the hosts and all protons of the guests (see Table 9.2). It can be clearly seen from the CIS values that **G1** and **G2** are bound in host **1** in very different geometries. In the case of the complex between **H₂1** and **G1**, the signals of the crown ether protons H6a,b were shifted upfield, whereas all crown ether protons were shifted downfield in the complex between **H₂1** and **G2**. Furthermore, the resonance of the pyrrole NH protons in **H₂1** was shifted strongly upfield in the

Table 9.2 Selected complexation induced shift values (in ppm) of host–guest complexes between porphyrin clips **H₂1** and **H₂2** and viologen guests **G1** and **G2**.^a

Host protons ^b	Host-guest complex			
	H₂1-G1	H₂1-G2	H₂2-G1	H₂2-G2
5	-0.16	-0.12	+0.40	+1.10
6a	-0.69	+0.60	+0.19	+0.45
6b	-0.16	+0.41	+0.05	+0.29
7a	<i>c</i>	+0.43	<i>c</i>	<i>c</i>
7b	<i>c</i>	+0.67	<i>c</i>	<i>c</i>
14	-0.17	-1.16	<i>c</i>	<i>c</i>
16			-0.20	-0.46
Guest protons				
BipyH-2,6	-4.24	-3.51		
BipyH-3,5	-2.66	-1.99		
NCH ₃	-1.05			
NCH ₂ CH ₂ OH		-1.17		
NCH ₂ CH ₂ OH		-0.73		
OH		+0.16		

^aDetermined by ¹H NMR experiments in CDCl₃/CD₃CN (1:1, v/v) solution. ^bFor proton numbering see Figures 9.3 and 9.4. ^cNo significant shifts were observed.

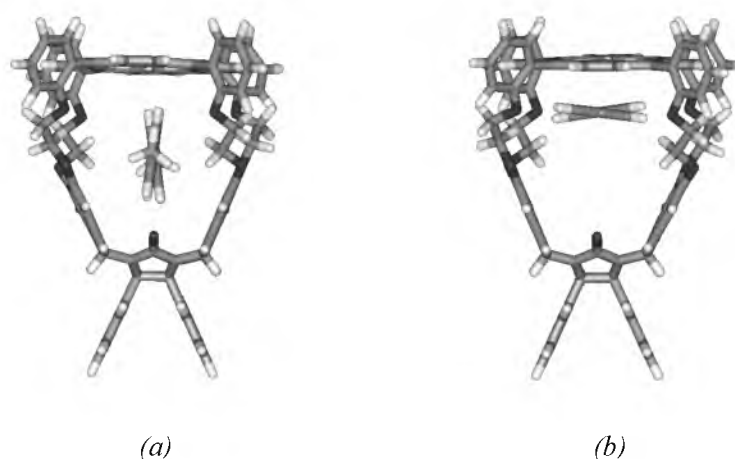


Figure 9.7 (a) Computer modeled structure of the host-guest complex between **H₂1** and **G1**. (b) Idem, of the complex between **H₂1** and **G2** (for clarity the ethanol substituent of **G2** has been omitted).

complex with **G2**, compared to only a small upfield shift of this resonance in the complex with **G1**. From these shifts it was concluded that in the complexes the aromatic surface of **G2** is

oriented parallel to the porphyrin plane, whereas the surface of **G1** is oriented more orthogonal to the plane of the porphyrin, clamped between the cavity side-walls (Figure 9.7). The latter geometry is also observed in the complex of **G1** with a molecular basket.³¹ The reason for this difference in binding geometry is attributed to the ability of **G2** to form hydrogen bonds with the carbonyl groups of the host. This additional interaction is also supported by the observed downfield shifts of the signals of the hydroxy protons in the host-guest complex. In order to accommodate the hydrogen bonds, the guest alters its orientation within the cavity. The precise orientation was confirmed by 2D NOESY experiments of the complex, in which a strong NOE was observed between the β -pyrrole protons H12 of **H21** and the NCH₂ protons of **G2**.

The complexation of a zinc ion in the center of the porphyrin did not result in significant changes in binding strength and geometry of the complexes of **H21** and **Zn1** with **G1** (Table 9.1). No reliable value for the association constant of **Zn1** with **G2** could be determined, due to coordination of the hydroxy groups of the guest to the zinc ion resulting in multiple possible complex geometries.

Binding of viologens in hosts 2

In contrast to the very strong binding of **G1** and **G2** in hosts **1**, hosts **2** had relatively low affinities for this type of guest molecules (Table 9.1). No detectable changes in the porphyrin Soret bands in the UV-vis spectra were observed upon titration of hosts **2** with **G1** or **G2**. The association constants were determined by ¹H NMR titrations in CDCl₃/CD₃CN (1:1, v/v) solution. In both **H22** and **Zn2**, **G2** is bound more strongly than **G1**, probably because of the ability of the former guest to form hydrogen bonds with the carbonyl groups of the hosts. Binding of these guests in hosts **2** occurs by an *induced-fit* mechanism: upon binding, the hosts undergo considerable conformational changes. These changes were very clearly visible in the large downfield shifts of the resonances of the crown ether protons H6a and the side-wall protons H5 (Table 9.2). These shifts suggest that, upon binding of the guest, the porphyrin is lifted from the side-walls and becomes more symmetrically situated over the cavity. Inspection of CPK models of the complex demonstrates that this lifting is in fact needed to accommodate the bipyridine rings of the guests inside the cavity. From the calculated CIS values it can be concluded that in the complex between **H22** and **G2** the porphyrin is situated more centrally over the cavity than in the complex between **H22** and **G1**. This would be expected if the mode of binding of these guests is similar to the geometries observed in the complexes with hosts **1**, *i.e.* with the bipyridinium aromatic surface oriented parallel to the porphyrin plane in the complex of **H22** with **G2** and perpendicular to it in the complex with **G1**.

The fact that **G1** and **G2** are bound weaker in **H22** than in **Zn2** is attributed to the stronger interaction between the porphyrin plane and the cavity side-wall in the former host (see section 9.3). The barrier to reorganization upon binding of a viologen guest in **H22** is larger than that for **Zn2**, which is reflected in lower association constants (K_a) for the complexes with **H22**.

Comparison of the hosts

The exceptionally high K_a -values measured for the complexes between viologens and hosts **1** are several orders of magnitude larger than the K_a -values of complexes of these guests with Stoddart's *bis*-paraphenylene-34-crown-10 macrocycle (K_a with **G1** and **G2** = 730 and 700 M⁻¹, respectively³⁰). This increase is predominantly the result of the more rigid and better preorganized cavities of hosts **1**.³⁶ The K_a -values are also an order of magnitude larger than those

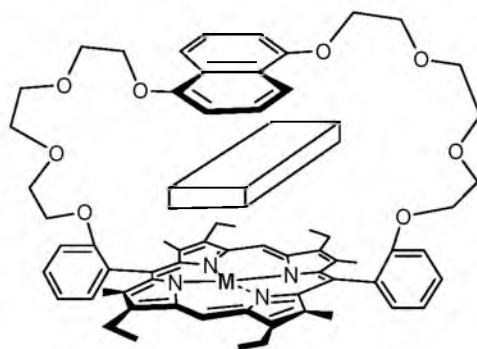
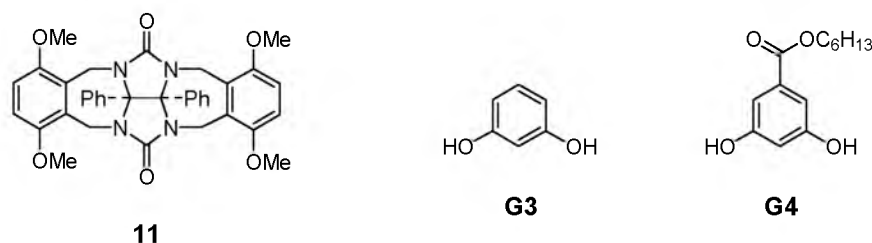


Figure 9.8 Gunter's crown ether strapped porphyrin. The block represents a complexed **G1** molecule.

observed for complexes of these guests with a crown ether basket-shaped receptor described before by our group.³¹ This is attributed to the additional interactions between the guests and the porphyrin plane in **1**. Comparably high association constants have been measured for complexes between viologen guests and the double crown ether strapped porphyrin systems studied by Gunter (Figure 9.8).³⁷ In both cases, the hosts are perfectly preorganized for the guests, stabilized by multiple interactions, and also the binding cavities are well-shielded from their environment. Hosts **1** bind viologens several orders of magnitude stronger than hosts **2** as a result of several factors: (i) **1** is much better preorganized than **2**, which, upon binding of the guests, has to undergo severe conformational changes at the expense of binding free energy; (ii) the electron donating crown ether oxygen atoms of **1** are in closer proximity to the guests than the oxygen atoms of **2**; (iii) possibly also 'cavity-effects' play a role, because **1** has a somewhat smaller and less solvated cavity which is more prone to accept a guest than **2**.

9.5.2 Binding of dihydroxybenzene derivatives

Binding experiments were also carried out with 1,3-dihydroxybenzene derivatives, which are known to be ideal guests for receptors derived from **11** (see Section 1.4).³⁸ The binding of guests **G3** and **G4** in the porphyrin hosts was investigated by ¹H NMR titrations in CDCl₃ solution and compared to the binding of these guests in the reference clip **11** (Table 9.3). Both guests appeared to form weaker host-guest complexes with the porphyrin clips than with clip **11**, which is most likely due to the fact that in **1** and **2** the porphyrin roof is to some extent sterically impeding the binding of the guests. The observed CIS values upon binding (Table 9.4) suggest that the geometry of binding is similar to that in **11**, *viz.* with the hydroxy groups of the guests directed to the carbonyl groups of the hosts.



In the ¹H NMR spectrum of the host-guest complex of **H21** with resorcinol (**G3**) the signals of the side-wall and crown ether protons of the host were shifted strongly upfield, whereas the signals of the pyrrole NH protons H14 were shifted downfield (Table 9.4). This suggests that the

Table 9.3 Association constants K_a (M^{-1}) and binding free energies ΔG (kJ mol^{-1} , in parenthesis) of host-guest complexes between various hosts and dihydroxybenzene guests **G3** and **G4**.^a

	H₂1	Zn1	H₂2	Zn2	11^b
G3	2200 (-19.1)	1400 (-17.9)	1400 (-17.9)	440 (-15.1)	2600 (-19.5)
G4	520 (-15.5)	800 (-16.6)	2100 (-19.0)	4500 (-20.8)	1.7×10^4 (-24.1)

^aIn CDCl_3 solution, estimated error 10%. ^bValues taken from ref 38.

Table 9.4 Selected complexation induced shift values (in ppm) of host-guest complexes between porphyrin clips **H₂1** and **H₂2** and dihydroxybenzene guests **G3** and **G4**.^a

Host protons ^b	Host-guest complex			
	H₂1-G3	H₂1-G4	H₂2-G3	H₂2-G4
5	-0.06	-0.01	-0.73	<i>c</i>
6a	-0.72	-0.44	-0.74	<i>c</i>
6b	-0.57	-0.03	-0.10	<i>c</i>
7a	-0.66	-0.15	<i>d</i>	<i>d</i>
7b	-0.55	-0.09	<i>d</i>	<i>d</i>
14	+0.20	-0.09	<i>d</i>	<i>d</i>
16			-0.23	-0.31

^aDetermined by ^1H NMR experiments in $\text{CDCl}_3/\text{CD}_3\text{CN}$ (1:1, v/v) solution. ^bFor proton numbering see Figures 9.3 and 9.4. ^cDue to broadening of the signal no reliable shifts could be calculated. ^dNo significant shifts were observed.

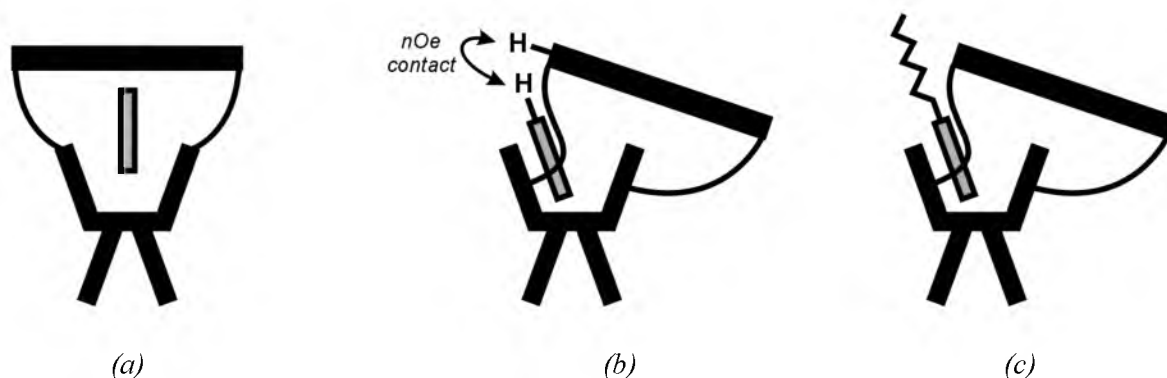


Figure 9.9 Schematic representation of the structures of the host-guest complexes between (a) **H₂1** and **G3**, (b) **H₂2** and **G3**, and (c) **H₂2** and **G4**.

aromatic ring of the guest is oriented in an *edge-to-face* geometry with respect to the plane of the porphyrin (Figure 9.9a). The CIS-values observed for the host indicated a similar geometry of binding for the complex between **G3** and **Zn1**, even though the K_a is lower. A similar *edge-to-face* interaction was observed between the porphyrin and the side-walls in clips **H₂2** and **Zn2** (see section 9.3). The proton signals of **G3** were significantly broadened and obscured by the signals of the host upon complexation.

In contrast to the downfield shift observed in the complex between **H₂1** and **G3**, the signals of the pyrrole NH protons were shifted upfield in the complex between this guest and **H₂2**. Since the other observed shifts indicated very little conformational change in the receptor upon binding of the guest, this result suggests that the NH protons in the latter complex are shielded by the aromatic ring of the guest, which must be located more or less parallel to the porphyrin plane. CPK models indicated that in this orientation the guest cannot be symmetrically bound in the cavity, but must be leaning to one of the side-walls (Figure 9.9b). Additional evidence for this geometry came from a 2D NOESY NMR experiment of the complex in CDCl₃. A strong nOe was observed between the 5-proton of **G3** and the nearby β-pyrrole protons H14 of the host (see Figure 9.9b).

The K_a -value of the complex between **Zn2** and **G3** appeared to be significantly lower than the K_a -value of the complex between **H₂2** and **G3**. In **Zn2** the porphyrin is not located precisely over the side-wall as it is in **H₂2**, but is situated farther away from the cavity. The weaker binding of the guest may be a result of steric hindrance by the porphyrin exerted on the cavity of **Zn2**.

It was expected that substitution of the 5-proton of **G3** by a bulky substituent would result in a weaker binding to **1**. Indeed, the K_a -values of the complexes between hosts **1** and hexyl 3,5-dihydroxybenzoate (**G4**) were lower than those between these hosts and **G3** (Table 9.3). The CIS values of the crown ether protons H6b and H7 in the complex between **H₂1** and **G4** were much lower than the values observed for these protons in the complex between **H₂1** and **G3** (Table 9.4). This indicates that **G4** is bound within the cavity in a different geometry than **G3**. The negative CIS value observed for the porphyrin NH protons further supports this conclusion. Molecular modeling suggested that the guest is partly bound on the outside of the cavity with only one of its phenolic hydroxy groups hydrogen bonding to one of the carbonyl groups of the host. In hosts **2** this steric effect is less severe, because the ester substituent has more room to be accommodated in the cavity. As a consequence, the K_a -values of the complexes between **G4** and these hosts are larger than those between the hosts and **G3** (Table 9.3). In addition, the electron-withdrawing character of the ester group will enhance the binding in a similar way as observed for the complex between **G4** and clip **11**.³⁸ The addition of **G4** to **H₂2** or **Zn2** resulted in severely broadened signals for the protons lining the inside of the cavities. This is probably due to a hindering of the process in which the two conformers of the hosts exchange, with the hydrocarbon chain of the guest acting as a '*supramolecular brake*' (Figure 9.9c). It turned out that this exchange process was still relatively rapid on the NMR timescale at low temperatures (218 K) and could not be frozen out.

The remarkable fact that both **Zn1** and **Zn2** bind **G4** stronger than their free base analogues (Table 9.3) implies the presence of additional stabilizing interactions, possibly between the ester carbonyl group of the guest and the zinc ion in the porphyrin center.³⁹ However, no further evidence for such an interaction could be obtained by UV-vis or IR spectroscopy.⁴⁰

9.5.3 Binding of pyridine derivatives

The presence of a metalcenter in **Zn1** and **Zn2** opened the possibility to study the binding of pyridine derivatives in these hosts. UV-vis titrations were carried out with **Zn1** and **Zn2** and pyridine guests **G5-G8** in chloroform solution. The results are presented in Table 9.5. In all

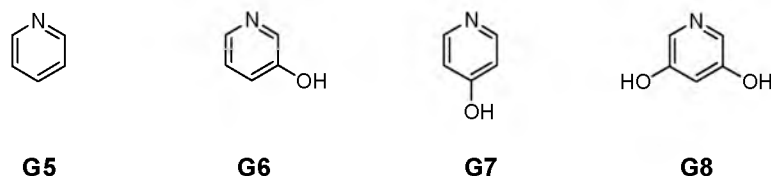


Table 9.5 Association constants K_a (M^{-1}) and binding free energies ΔG ($kJ\ mol^{-1}$, in parenthesis) of host–guest complexes between various zinc porphyrins and pyridine guests **G5**– **G8**.^a

	Zn1	Zn2	ZnTPP
G5	1.1×10^5 ^b (–28.8)	1.4×10^4 ^b (–23.6)	920 (–16.9)
G6	3.0×10^7 ^c (–42.7)	4.8×10^6 ^c (–38.1)	1300 (–17.8)
G7	2.5×10^4 ^b (–25.1)	8.0×10^4 ^b (–28.0)	1100 (–17.4)
G8	6.9×10^4 ^b (–27.6)	1.9×10^4 ^b (–24.4)	< 1

^aIn $CHCl_3$ solution. ^bEstimated error 20%. ^cEstimated error 50%.

cases, addition of these guests to the hosts caused a redshift (12 nm) of the porphyrin Soret band and also redshifts of the two Q-bands (of 18 and 13 nm, respectively), indicating coordination to the zinc centers. The CIS values in the 500 MHz 1H NMR spectra (not shown) indicated that all guests were bound within the cavities of the hosts.

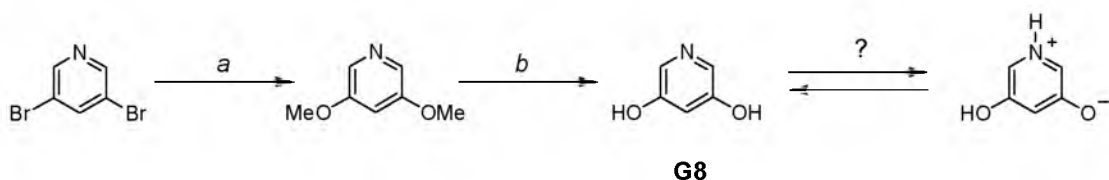
Pyridine (**G5**) is bound considerably stronger to both **Zn1** and **Zn2** (Table 9.5) than to ZnTPP ($K_a = 920\ M^{-1}$). This stronger binding is attributed to the possibility of this guest to have Van der Waals and π – π interactions with the spacers and side-walls of the host, and to the presence of a cavity effect, *i.e.* the filling of the empty cavity of the hosts, which in chloroform results in a favourable contribution to the overall binding.⁴¹ The K_a -value of the complex between **Zn1** and **G5** is one of the highest values measured for a zinc porphyrin and this guest in organic solvents.⁴² The strong binding resulted in slow exchange between bound and unbound guest on the NMR timescale.

For both **Zn1** and **Zn2**, extremely high K_a -values were measured for their complexes with 3-hydroxypyridine (**G6**) (Table 9.5). Molecular modeling revealed that this guest can coordinate with its pyridine nitrogen atom to the zinc center, and simultaneously form a strong hydrogen bond with one of the carbonyl groups of the glycoluril framework. The strength of the binding was reflected in the NMR spectra of complexes **Zn1-G6** and **Zn2-G6**. In both cases, slow exchange between the free components and the host–guest complexes was observed on the NMR timescale. In addition, many resonances of the host were split into two peaks due to the unsymmetrical mode of binding of the guest.

In contrast to the very strong binding observed for **G6**, the K_a -values of the complexes between the porphyrin hosts and 4-hydroxypyridine (**G7**) turned out to be much smaller. This can be partly attributed to an electronic effect caused by the hydroxy substituent of the guest, and to the fact that 4-hydroxypyridine can undergo a tautomeric exchange to give a pyridon.⁴³ It is surprising that **G7** forms a weaker host–guest complex with **Zn1** than with **Zn2** and even a weaker complex than **G5** with **Zn1**. Inspection of CPK models of the complex between **Zn1** and **G7** indicated that this guest can not coordinate to the zinc ion and at the same time form a hydrogen bond with one of the carbonyl groups of the host. In **Zn2** the spacers between the

cavity and the porphyrin are longer and more flexible, allowing weak coordination of **G7** to the zinc ion whilst maintaining a hydrogen bond between the hydroxy group of the guest and one of the carbonyl groups of the host.

Very strong binding was expected between the zinc containing hosts and 3,5-dihydroxypyridine (**G8**), since with this guest a coordinative bond and two additional hydrogen bonds can be formed. **G8** was synthesized by a nucleophilic aromatic substitution reaction using 3,5-dibromopyridine and sodium methoxide in methanol, followed by demethylation of the methoxy groups with boron tribromide (Scheme 9.4).



Scheme 9.4 Synthesis of 3,5-dihydroxypyridine. Reagents and conditions: (a) Na, MeOH, Cu, 5 bar, 1 week. (b) BBr₃, CH₂Cl₂, 16 h.

Surprisingly, the measured K_a -values of the complexes of this guest with **Zn1** and **Zn2** turned out to be rather low and in the same order of magnitude as the K_a -values of the complexes of these hosts with **G7**. Remarkably, **G8** did not coordinate to ZnTPP at all, and turned out to be completely insoluble in chloroform. Only upon addition of **Zn1** or **Zn2** and sonication of the resulting mixture the compound (partly) dissolved. A redshift of 11 nm in the porphyrin Soret band in the UV-vis spectrum was observed when the guest was added to a solution of **Zn1** or **Zn2** in chloroform, indicating coordination of the guest to the zinc ion. The ¹H NMR spectrum of the complexes in CDCl₃ suggested a similar host-guest binding geometry as observed for **G6**, viz. with the guest within the cavity. An explanation for the relatively weak binding of **G8** in the porphyrin clips is that this compound in chloroform solution predominantly exists in a non-binding tautomeric form, with a possible charged structure (Scheme 9.4). The melting point of **G8**, which turned out to be over 400°C, is a strong indication for this Zwitter-ionic structure. It is as yet unclear why **G8** would exist in this tautomeric form and **G6** not. An electronic effect caused by the extra OH group of **G8** might be the reason for this effect.

9.6 An approach to responsive porphyrin clips

9.6.1 Introduction

The design and synthesis of substrate selective catalysts, which mimic natural enzymes in both architecture and activity, has always been one of the goals in supramolecular chemistry.⁴⁴ Many synthetic receptor molecules have been developed which bind guests with high association constants (K_a) in organic solvents.⁴⁵ Substrate binding can be accompanied by a change in the structure of the receptor. This ‘induced-fit’ mode of binding⁴⁶ is often observed in Nature, e.g. when a substrate induces a structural reorganization in the receptor site of an enzyme, enhancing the binding. Substrate binding can be even more sophisticated when it is influenced by external stimuli.⁴⁷ In such so-called ‘responsive’ systems, binding of the substrate is regulated by conformational changes in the host which are induced, for example, by changes in the pH,⁴⁸ by

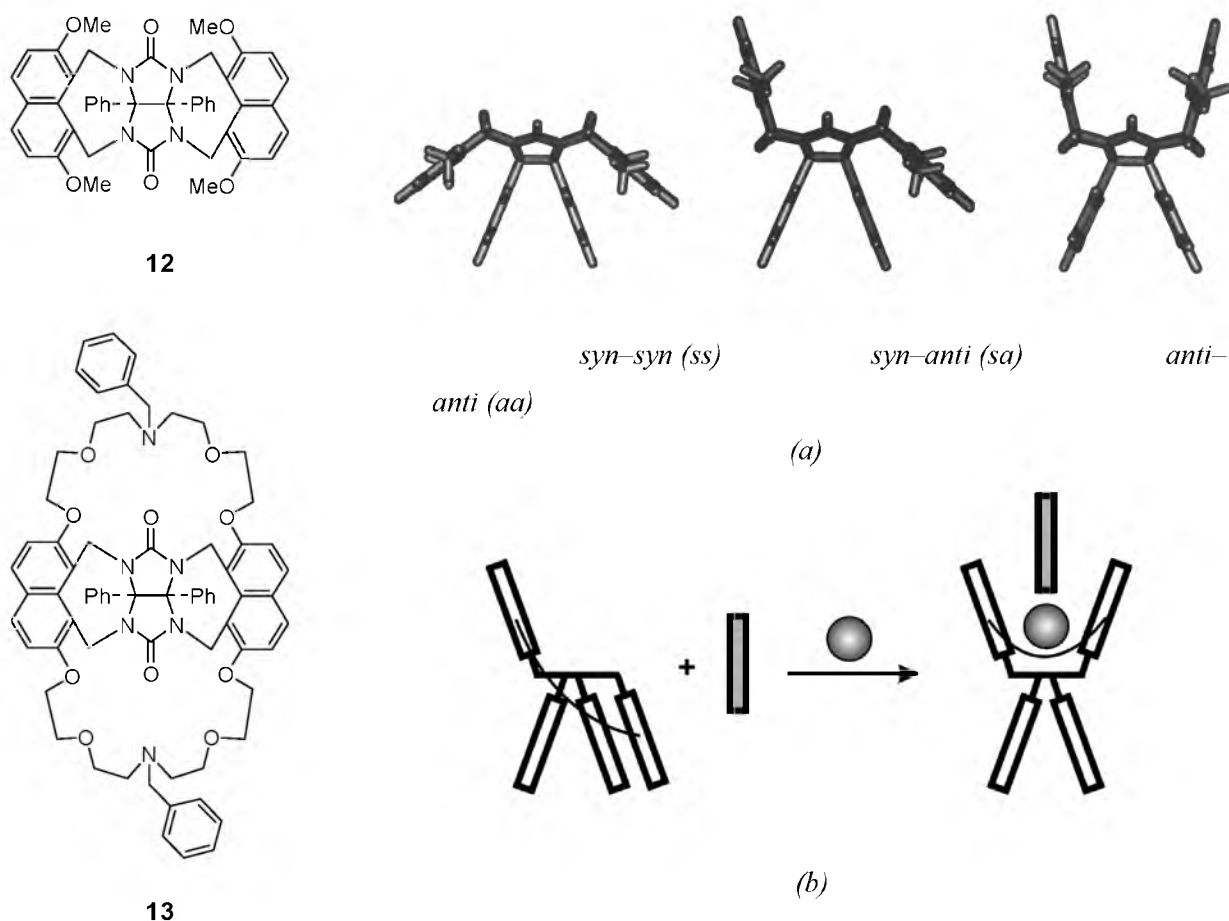


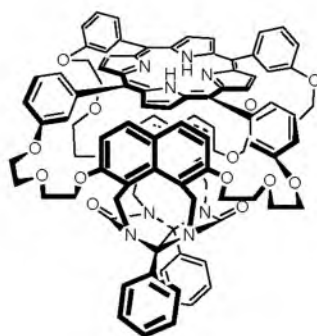
Figure 9.10 Conformational behaviour of naphthalene-walled clip molecules. (a) Three conformations adopted by **12** in chloroform solution. (b) Schematic representation of the allosteric binding of a 1,3-dinitrobenzene guest by **13** in the presence of K^+ ions.

light,⁴⁹ or by electrochemical switching.⁵⁰ Another way of regulating binding, which is observed in many proteins, is by means of the ‘allosteric effect’. In an allosteric receptor, more than one binding site is present, and binding of a guest at one site is influenced by the binding of another guest or metal ion at a second, remote site. Only few synthetic hosts working according to this principle have been described in literature,⁵¹ and examples of this type of receptors containing an adjacent catalytically active site have not been reported at all.

Previous work in the Nolte-group has shown that molecular clip **12** exists in chloroform as a mixture of three slowly interconverting conformers. These conformers differ in the orientation of the side-walls with respect to the phenyl groups on the concave side of the diphenylglycoluril framework; this orientation can be *syn* or *anti* (Figure 9.10a).⁵² Without a guest, the *syn-syn (ss)*, *syn-anti (sa)* and *anti-anti (aa)* conformers are present in populations of 89.6, 7.7, and 2.7%, respectively. Addition of a 1,3-dihydroxybenzene guest results in the ‘flipping-up’ of the naphthalene side-walls to give the *aa* conformer, thus a cavity is formed which binds the guest according to an induced-fit mechanism. Apart from dihydroxybenzene derivatives, host **12** is also capable of complexing silver(I) ions⁵³ and electron deficient guests without aromatic hydroxy groups, such as 1,3-dinitrobenzene. When two azacrown ether spacers are attached to the side-walls of **12**, to give host **13**, the *aa* conformer disappears in solution and only a mixture of *sa* (88%) and *ss* (12%) conformers is observed. However, when sodium or potassium ions which bind in the crown ether rings are added, a change in conformation takes place and the host

becomes 100% preorganized into the guest binding *aa* conformation. Depending on the solvent, 1,3-dinitrobenzene is bound 2 to 6 times more strongly in the host containing the ions than when these ions are absent (Figure 9.10b), mimicking the allosteric effect observed in enzymes.

In the present study it is our aim to construct an allosteric receptor similar to **13**, which in addition possesses a proximal catalytically active site. To this end, porphyrin-capped clip molecule **H₂14** was designed, which combines a naphthalene-walled receptor for neutral aromatic substrates with a catalytically active porphyrin. These two components are connected via a set of four crown ether-like spacers. The latter can act as the remote binding site for alkali metal ions. In this section, the synthesis, conformational behaviour, and binding properties of **H₂14** toward alkali metal ions and aromatic guests will be discussed.



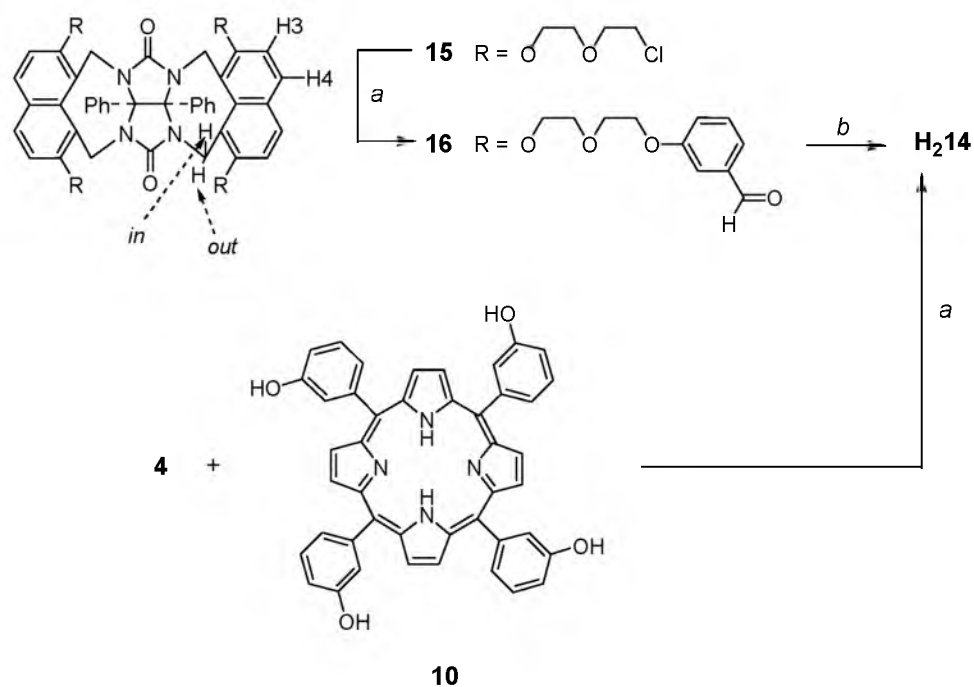
H₂14

9.6.2 Synthesis

Porphyrin clip **H₂14** could be synthesized by two different routes which are outlined in Scheme 9.5. In the first route tetrapodand **15**⁵² was reacted with *m*-hydroxybenzaldehyde under Finkelstein conditions in acetonitrile, using sodium carbonate as a base to give the tetra-aldehyde clip **17** in 67% yield, after purification by column chromatography. In CDCl₃ at room temperature, the compound appeared to exist as a mixture of three conformers, *sa*, *ss* and *aa*, in a ratio of 78:13:9. Compound **16** was further reacted with four equivalents of pyrrole under high dilution conditions in dichloromethane, using boron trifluoride etherate as a catalyst, to afford, after oxidation of the porphyrinogen with *p*-chloranil, porphyrin clip **H₂14**. This compound was obtained in 6% yield, after purification by column chromatography and precipitation in *n*-hexane. In the second route clip **15** was directly reacted with porphyrin **10** under high dilution Finkelstein conditions in acetonitrile, using sodium carbonate as a base, to give **H₂14** in a yield of 8%.

9.6.3 Conformational behaviour

The structure of **H₂14** in CDCl₃ solution was examined by high resolution NMR spectroscopy. The ¹H NMR spectrum (Figure 9.11) revealed that the host displayed a very complex conformational behaviour. The flexible crown ether spacers allow the porphyrin to move freely with regard to the receptor, but molecular modeling calculations showed that it is not possible for the porphyrin to be situated on the convex side of the clip. As was observed for **12**, the clip moiety of **H₂14** exists in three conformations which interconvert slowly on the NMR timescale; they are observed separately in the NMR spectrum. With the help of COSY and NOESY 2D spectra, most of the resonances in the spectrum could be assigned. By comparison with the



Scheme 9.5 Two possible routes for the synthesis of porphyrin clip **H₂14**. Reagents and conditions: (a) *m*-Hydroxybenzaldehyde, Na_2CO_3 , NaI , CH_3CN , reflux, 10 days. (b) Pyrrole, $\text{BF}_3 \cdot \text{OEt}_2$, CH_2Cl_2 , 16 h, then *p*-chloranil, reflux, 1 h.

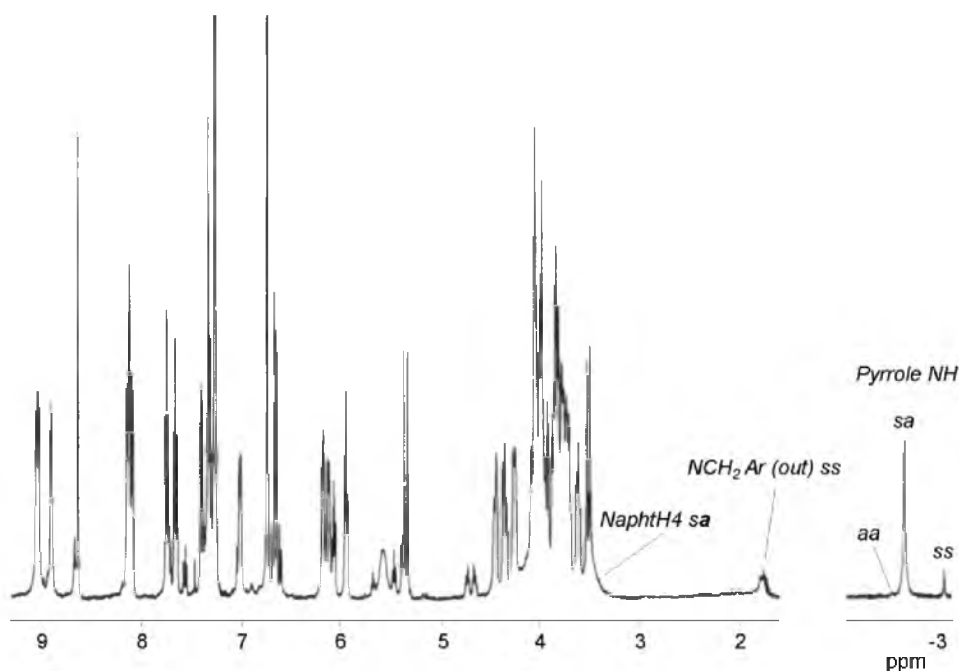


Figure 9.11 ^1H NMR spectrum of **H₂14** in CDCl_3 (500 MHz, 298K, 2 mM).

spectrum of **12** and with the help of the Johnson-Bovey tables,⁵⁴ which were used to calculate the ring current shifts, the different conformers could be identified (Table 9.6). For host **H₂14**, the *sa* conformer is the predominant one at room temperature, constituting 78% of the population, while the *ss* conformer (20%) and the *aa* conformer (2%) are less abundant species. From the strongly upfield shifted signals of the naphthalene H4 protons on the *anti*-positioned side-wall in

Table 9.6 Assignment of selected ^1H NMR signals to the conformers of **H₂14**.^a

Resonance	Conformer		
	<i>aa</i>	<i>ss</i>	<i>sa</i>
NCH ₂ <i>out</i>	5.14	1.75	5.52 (<i>s</i>) 5.36 (<i>a</i>)
NCH ₂ <i>in</i>	3.62	4.07	3.91 (<i>s</i>) 3.52 (<i>a</i>)
NaphtH-3	<i>b</i>	6.70	6.64 (<i>s</i>) 6.16 (<i>a</i>)
NaphtH-4	<i>b</i>	6.66	6.99 (<i>s</i>) 3.52 (<i>a</i>)
NH	-3.10	-2.64	-2.70

^aIn CDCl₃, 298 K, shifts are in ppm; the designations (*s*) and (*a*) are used for the CH₂ protons on the side of the molecule where the naphthyl groups have a *syn* or *anti* orientation with respect to the phenyl groups. The designations (*in*) and (*out*) are used as indicated in the structural formula of **15** (Scheme 9.5). ^bDue to overlap of signals and the low abundance of the conformer no assignment could be made.

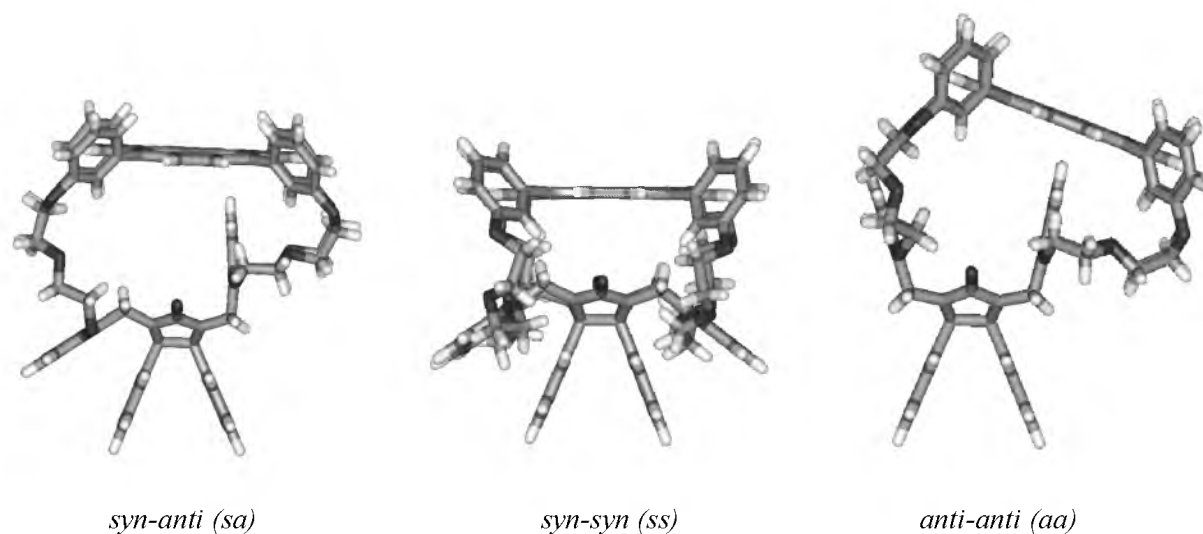
the *sa* conformer (at 3.52 ppm, $\Delta\delta = -4.2$ ppm compared to the chemical shift of these protons in **16**) it was concluded that the center of the porphyrin is positioned directly above this side-wall, in an edge-to-face geometry. In the *ss* conformer the porphyrin is situated over the glycoluril skeleton, which was indicated by the strong upfield shift of the signals of the NCH₂Ar *out*-protons (at 1.75 ppm, $\Delta\delta = -4.5$ ppm compared to **16**). Using the observed shifts and the nOe-effects in the 2D NOESY spectrum, the three-dimensional structures of the *sa* and *ss* conformers were calculated with the help of molecular modeling (Figure 9.12). Due to the low abundance of the *aa* conformer, its exact structure could not be derived from NMR shifts and it was computer modeled assuming that also in this conformer, as in the *sa*-conformer, the porphyrin is situated over (one of) the side-walls.⁵⁵ 2D exchange spectroscopy (EXSY) experiments were carried out to obtain more information about the conformational behaviour of **H₂14**. In an EXSY spectrum crosspeaks are observed between signals of conformers that exchange during the applied mixing time (τ_m). EXSY spectra of **3** in CDCl₃ were recorded at $\tau_m = 100, 500, 750,$ and 1000 ms, but no crosspeaks between the signals of different conformers were observed, indicating that the exchange between them is very slow (life times > 1 s.).

In a previous study⁵⁶ detailed information was obtained about the influence of solvation and substituents on the conformational behaviour of 1,8-connected naphthalene-walled clips. In the present study the population ratio of the different conformers of **H₂14** was compared to that of the related molecule **12**. Table 9.7 shows that in CDCl₃ at room temperature a higher ratio of the molecules of **H₂14** adopts the *ss* conformation compared to **12**. Upon heating the solution of **H₂14**, the amount of *sa* conformer decreased while the amount of *ss* conformer increased. No detectable change in the amount of *aa* conformer was observed. In contrast, hardly any changes ($< \sim 2\%$) in the ratios of conformers of **12** were observed upon a similar variation in temperature. The temperature dependent studies on **H₂14** allowed the calculation of the thermodynamic parameters for the equilibrium $ss \rightleftharpoons sa$, which are $\Delta H = 1.65 \text{ kJ mol}^{-1}$ and $\Delta S = 5.26 \text{ J mol}^{-1}$

Table 9.7 Populations of the conformers of hosts **12** and **H₂14**.^a

Host	Solvent	<i>T</i> (K)	% <i>aa</i>	% <i>sa</i>	% <i>ss</i>	$\Delta G_{sa/ss}$ (kJ mol ⁻¹) ^b
12 ^c	CDCl ₃	298	2.7	89.6	7.7	-6.08
H₂14	CDCl ₃	298	2	77	21	-3.22
	CDCl ₃	308	2	65	33	-1.74
	CDCl ₃	318	2	51	47	-0.22
	CDCl ₃	328	2	40	58	+1.01
	CDCl ₃ /CD ₃ CN 3:1 (v/v)	298	8	78	14	-4.25
	CDCl ₃ /CD ₃ CN 1:1 (v/v)	298	6	64	30	-1.88

^aRelative populations were determined by integration of the NMR spectra, estimated error is $\pm 2\%$ ^bFor the equilibrium $ss \rightleftharpoons sa$. ^cValues taken from ref 52.

**Figure 9.12** Computer modeled structures, based on the NMR spectra in CDCl₃ solution, of the 3 conformers of **H₂14**.

K⁻¹.⁵⁷ The fact that the conformational ratio of **H₂14**, in contrast to that of **12**, is severely influenced by the temperature can be attributed to the presence of the porphyrin, which is positioned in an edge-to-face geometry over the *anti*-oriented naphthalene side-wall. The ‘T-type’ π - π interaction between the two aromatic surfaces is known to be enthalpically favourable.⁵⁸ Studies on a related porphyrin clip with benzene side-walls have shown that if the temperature is increased the interaction between the porphyrin and side-wall becomes weaker (see Section 9.4). A similar behaviour is observed for **H₂14** (Table 9.7). When the temperature is increased, the interaction between the porphyrin and the naphthalene side-wall becomes weaker as follows from the strong downfield shifts of the side-wall proton signals and the small upfield shift of the signals of the porphyrin central NH protons. All observed shifts are in agreement with a process in which the porphyrin moves away from the cavity side-wall. Simultaneously, the relative amount of *ss* conformer rapidly increases at the expense of the *sa* conformer. Apparently, the interaction between the porphyrin and the *anti* oriented side-wall is required to stabilize the latter conformer. Without this interaction, the porphyrin plane collapses onto the glycoluril framework.⁵⁹ This process is believed to be entropically favourable since it reduces the amount of poorly solvated aromatic surfaces.⁶⁰ A similar behaviour was observed when at room

temperature the solvent polarity was increased, *viz.* by the addition of CD₃CN (Table 9.7). The more polar environment weakens the edge-to-face interaction between the porphyrin and the side-wall and thus favours the generation of the *ss*-conformer. The slight increase in the amount of *aa*-conformer is attributed to a better solvation of the cavity, which is able to accommodate CD₃CN molecules better than CDCl₃ molecules.

9.6.4 Binding properties

Binding of alkali metal ions

Host **H₂14** was expected to be able to complex potassium ions between its crown ether spacers (Figure 9.13). The effect of the addition of KPF₆ and KSCN on the conformational equilibrium of **H₂14** was studied by ¹H NMR spectroscopy in mixtures of CDCl₃ and DMSO-*d*₆ (9:1 and 3:1 *v/v*, respectively). In both solvent mixtures, the addition of up to 100 equivalents of KSCN or KPF₆ did not have a measurable effect on the ratio of conformers of the receptor, although the

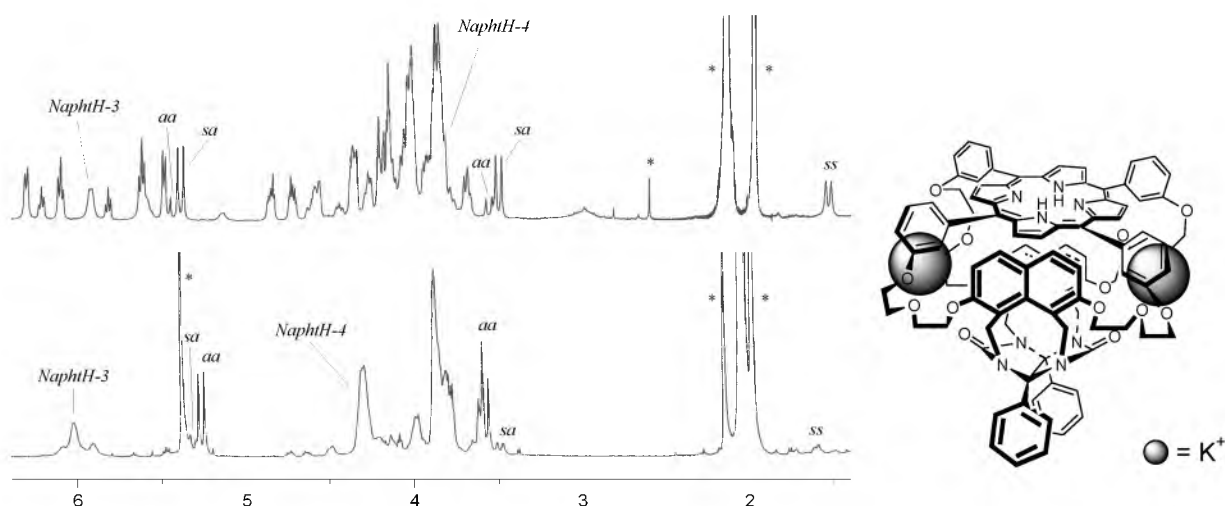


Figure 9.13 (a) ¹H NMR spectra of (methylene region) of **H₂14** in CDCl₃/CD₃CN (1:1, *v/v*) solution before (top) and after (bottom) the addition of an excess of KPF₆ (* = residual solvent) (b) Proposed structure of the complex of the *aa*-conformer of **H₂14** with two K⁺ ions.

salts completely dissolved. This is remarkable, since in the same solvent mixtures only four equivalents of these salts were needed to convert the structurally related compound **13** (Figure 9.10) into the *aa*-conformation. When, however, a solvent mixture of CDCl₃ and CD₃CN (3:1, *v/v*) was used, the addition of approximately two equivalents of KSCN or KPF₆ to **H₂14** caused more than 70% of the molecules to adopt the *aa*-conformation. Molecular modeling indicated that potassium ions can be nicely accommodated between two crown ether spacers at the sides of the cavity where the carbonyl functions are located (Figure 9.13b). In this geometry, additional electrostatic interactions between the alkali metal ions and these carbonyl functions are possible. In the NMR spectrum of a solution of **H₂14** containing an excess of KPF₆ (Figure 9.13a), the signals of the naphthalene side-wall protons were found at 6.01 and 4.32 ppm. These observed upfield shifts indicate that the porphyrin plane shields the side-walls. Since it is geometrically impossible for the porphyrin to be located above both side-walls at the same time, the complex has to be a mixture of two conformers which differ in the position of the porphyrin plane. These conformers exchange rapidly on the NMR timescale.

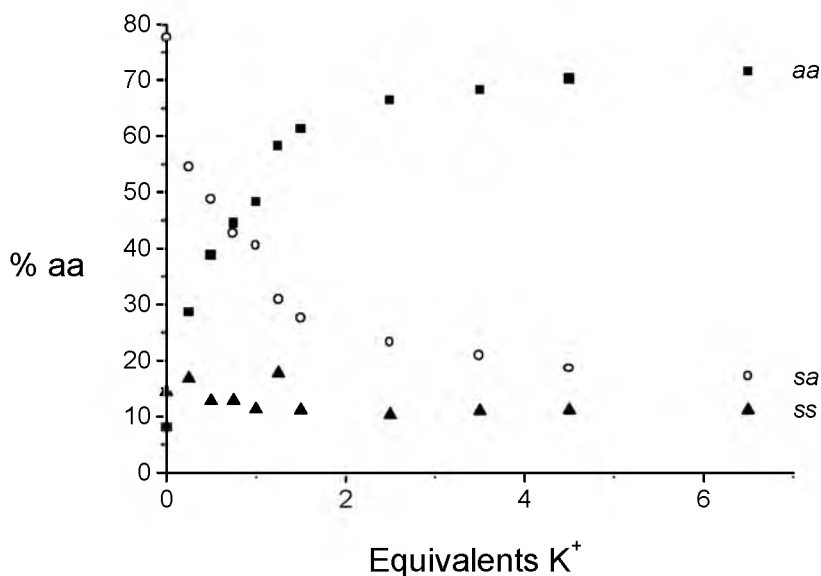


Figure 9.14 Changes in conformer populations upon the addition of KPF_6 to a solution of H_214 in $CDCl_3/CD_3CN$ (3:1, v/v).

To evaluate the strength and stoichiometry of KPF_6 binding, a 1H NMR titration was carried out. The changes in the populations of the conformers of H_214 upon addition of this salt are depicted in Figure 9.14. During the addition of KPF_6 the relative amount of *sa*-conformer decreased and that of the *aa*-conformer increased, while the amount of *ss*-conformer remained constant. Surprisingly, the titration curve obtained for the *aa*-conformer could be almost perfectly fitted when a 1:1 complex was assumed between H_214 and KPF_6 . The 1:1 association constant was determined to be $K_a = 4.3 \pm 0.5 \times 10^4 M^{-1}$. The ion binding behaviour of H_214 appears to be remarkably different from the behaviour of the related host **13**, which binds *two* K^+ ions in a strongly cooperative manner.⁵² The first ion, which induces a change to the *aa*-conformer, is bound in **13** with a relatively low association constant ($K_a = 128 M^{-1}$), making that the second ion is bound much stronger ($K_a = 5440 M^{-1}$) in the preorganized second crown ether ring. In H_214 , the first K^+ ion is apparently bound much stronger than it is in **13**. This might be due to a better fit of this ion between two of the crown ether spacers in the former host. The binding of a second K^+ ion between the two available and preorganized crown ether spacers at the other side of the $H_214:KPF_6$ complex could not be demonstrated from the NMR spectra. However, if a second K^+ ion is complexed in H_214 , it can be expected that the K_a of this binding process is several orders of magnitude higher than the K_a between H_214 and the first K^+ ion and hence can not be measured by 1H NMR techniques.⁶¹

Binding of aromatic guest molecules

The *aa*-conformers of hosts **12** and **13** are perfectly suited to form host-guest complexes with neutral guests such as dinitrobenzenes and 1,3-dihydroxybenzenes. Upon binding of these guests in **12** and **13**, the relative amount of the *aa*-conformer was found to increase. Surprisingly, porphyrin clip H_214 displayed a different binding behaviour. Upon the addition of 1,3-dinitrobenzene to a solution of H_214 in $CDCl_3$, no increase in the amount of *aa*-conformer was detected in the NMR spectrum, nor were significant shifts observed in the signals of the guest or host protons. This indicates that no host-guest complex is formed. The potentially stronger

binding guest resorcinol, which can form hydrogen bonds with the carbonyl groups of the host, also did not form a host-guest complex with **H₂14**. Only the addition of an excess of 5-cyanoresorcinol to a solution of **H₂14** resulted in very small upfield shifts in the signals of the protons of the *anti*-oriented naphthalene side-wall. No measurable increase in the amount of *aa*-conformer was, however, detected, and the shifts in the signals of the side-wall protons were too small (< 0.05 ppm) to determine a reliable association constant. A possible explanation for the inability of **H₂14** to bind these neutral aromatic guests is that the energy required to generate the *aa*-conformer is too high and cannot be overcome by the binding of the neutral guests.

Clip molecules containing crown ether rings related to **H₂14** have proved to be ideal hosts for paraquat (**G1**).⁶² Upon the addition of this guest to a solution of **H₂14** in a mixture of CDCl₃ and CD₃CN (1:1, v/v), the relative amount of *aa*-conformer rapidly increased at the expense of the amounts of both the *sa*- and *ss*-conformer, as shown by ¹H NMR. From an NMR titration experiment the association constant of the 1:1 host-guest complex was determined to be $K_a = 1.8 \pm 0.2 \times 10^4 \text{ M}^{-1}$. In the **H₂14**:**G1** complex, the signals of the side-wall protons were found at 6.50 and 4.82 ppm ($\Delta\delta \sim +0.5$ ppm compared to these signals in the **H₂14**:KPF₆ complex). In the presence of *one* equivalent of **G1**, the aromatic signals of the guest were very broad and shifted strongly upfield ($\Delta\delta \sim -1.5 - -2$ ppm) compared to the signals in the absence of **H₂14**. This indicates that **G1** binds within the cavity of the *aa*-conformer of the host. Further evidence for this came from a 2D NOESY spectrum of the complex, in which several nOe contacts were present between the guest and the side-wall protons and between the guest and crown ether protons lining the inside of the cavity. The observed downfield shift ($\Delta\delta = +0.22$ ppm) of the porphyrin NH protons of the *aa*-conformer during the titration suggests that the guest is bound in an edge-to-face geometry with respect to the porphyrin plane. Since upon binding of the guest the porphyrin has to lift up from the side-walls, the side-wall protons become deshielded, and hence their resonances should shift downfield. This was indeed observed. Molecular modeling of the complex revealed that this lifting is necessary in order to accommodate the bipyridine ring system of the guest. Combining the modeling studies with the NMR results, a binding geometry is proposed in which **G1** is bound orthogonal to the porphyrin plane and parallel to the cavity side-walls (Figure 9.15).

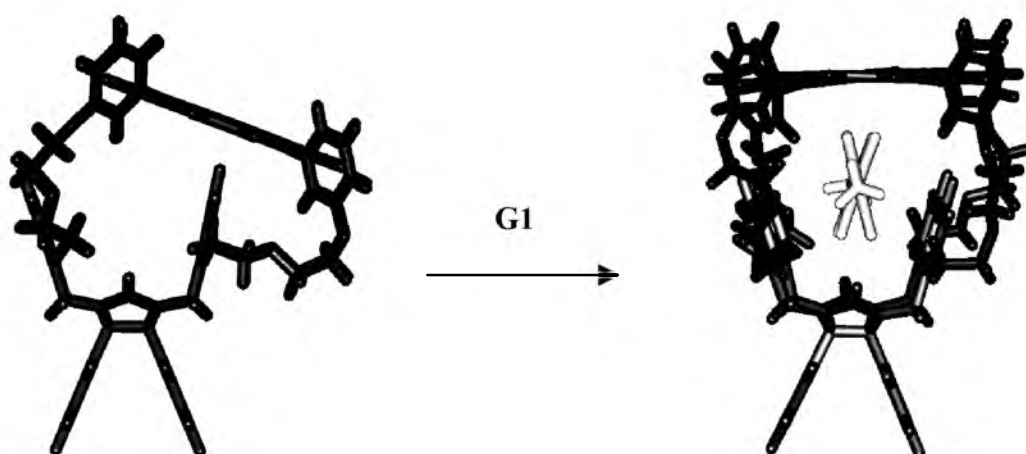


Figure 9.15 Proposed rearrangement in host **H₂14** upon binding of **G1**. The calculated geometry of the host-guest complex is shown on the right

Allosteric binding studies

To investigate the effect of preorganization of the cavity of **H₂14** on the binding of 1,3-dinitrobenzene, binding experiments of this guest in the presence of KPF₆ were carried out. To a solution of **H₂14** in CDCl₃/CD₃CN (3:1, v/v), 10 equivalents of KPF₆ were added, which caused 80% of the molecules of **H₂14** to adopt the *aa*-conformation. 1,3-Dinitrobenzene was added to this solution in small portions. In the ¹H NMR spectrum very small (< 0.05 ppm) complexation induced upfield shifts were observed for the signals of the side-wall protons of the *aa*-conformer, as well as for the guest proton signals. No shifts in the signals of the other conformers were detected, and no shifts in the dinitrobenzene signals were observed when this compound was added to a solution containing only the KPF₆ ions. These results suggest that 1,3-dinitrobenzene is weakly complexed between the naphthalene side-walls of the *aa*-conformer of **H₂14**. The observed shifts were too small to determine a reliable association constant. The weakness of binding, indicated by the small complexation induced shifts, is caused by the presence of the polar CD₃CN in the mixture, which weakens the π–π interactions between the host and guest. Stronger binding will probably be achieved in pure CDCl₃, a solvent, however, in which KPF₆ ions do not dissolve. Future work should be directed to the use of alkali metal ions that dissolve in CDCl₃, e.g. ions which have more lipophilic anions.

9.7 Concluding remarks

The results described in this chapter clearly demonstrate that the location and orientation of the porphyrin ring with regard to the receptor, imposed by the spacers between these components, has a great impact on the conformational and complexation behavior of the new host molecules. Clips **1** are far better hosts for viologen guests than clips **2**, because the former hosts have more rigid and preorganized cavities than the latter molecules. On the contrary, clips **2** are somewhat more versatile hosts than clips **1**, because they can adjust their structure upon complexation of a guest (*induced fit* binding). All porphyrin hosts display a ‘cavity-effect’, which leads to higher binding constants under appropriate conditions. For hosts **1**, which possess the more rigid and preorganized cavities, this effect is more pronounced than for hosts **2**.

It is evident that the porphyrin hosts, with their various directed binding sites, are ideal receptors for a wide variety of guest molecules. The very strong binding of viologen derivatives by **H₂1** and **Zn1** makes the host-guest complexes interesting candidates as building blocks for the synthesis of (poly)rotaxanes. Preliminary binding studies revealed that mono-cations, such as pyridinium derivatives, can also be complexed within these hosts, but with lower association constants than the viologen derivatives.⁶³

The observed strong binding of the pyridine derivatives by means of additional interactions, makes the zinc porphyrin hosts versatile receptors for pyridine containing and related natural products. A series of binding experiments was carried out with guests such as nicotinic acid, phenyl alanine, purine, and adenine (Figure 9.16). These experiments, although preliminary, revealed that these compounds can also be complexed within the cavities of **Zn1** and **Zn2**.⁶³ Finally, the strong binding of pyridine derivatives within these hosts can be utilized to increase the catalytic activity of manganese derived porphyrin clips. This will be described in Chapter 10. Naphthalene-walled porphyrin clip **H₂14** displays an interesting and rather complex conformational behaviour. The compound exists in three slowly interconverting conformers, which differ in the orientation of the side-walls: *ss* (21%), *sa* (77%), and *aa* (2%). Only the latter

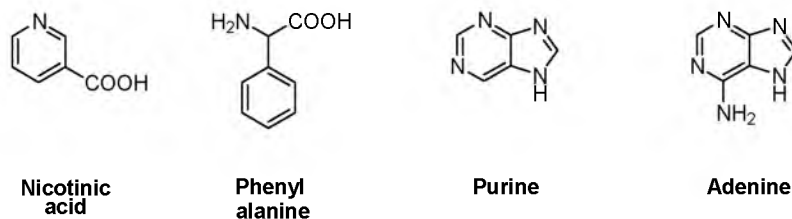


Figure 9.16 Examples of naturally occurring guest molecules which can be complexed by **Zn1** and **Zn2**.

conformer possesses a cavity suitable for aromatic guest binding. Compared to other clips with naphthalene walls the present compound contains a higher ratio of molecules in the *ss*-conformation. The porphyrin plays an active role in the conformational ratio, since it stabilizes the *sa*-conformer by favourable edge-to-face π - π interactions. An increase in the temperature or the addition of a more polar solvent weakens this interaction and results in a further increase in the amount of *ss* conformer and a concomitant decrease in the percentage of *sa*-conformer.

Potassium ions can be complexed between the crown ether spacers of **H₂14**, a process which leads to the almost complete conversion of the clip molecules into the cavity-containing *aa*-conformers. The formation of a strong 1:1 host-salt complex is observed. The expected binding of a second potassium ion could not be proven by NMR spectroscopy. Unexpectedly, **H₂14** turns out to be a very poor host for neutral 1,3-dihydroxybenzene and dinitrobenzene guests. The dication paraquat, however, is strongly bound. This guest is complexed by π - π stacking interactions with the naphthalene walls and 'T-type' π - π interactions with the porphyrin ring. In addition, the crown ether spacers help in the binding process because they attract the paraquat by favourable dipole-dipole interactions. Very weak binding of 1,3-dinitrobenzene could be observed in the presence of KPF_6 ions, which points to an allosteric binding of this guest in **H₂14**.

9.8 Experimental section

9.8.1 Materials and methods

Diethyl ether and *n*-hexane were distilled under nitrogen from sodium benzophenone ketyl. Chloroform and acetonitrile were distilled from CaCl_2 . Dichloromethane, 1,2-dichloroethane and methanol were distilled from CaH_2 . Deuteriochloroform used in the NMR titrations was vacuum distilled from P_2O_5 and stored under nitrogen. Ethyl acetate and *n*-hexane used for column chromatography were rotary evaporated prior to use. Pyrrole was vacuum distilled at room temperature immediately before use. Salicylic aldehyde was vacuum distilled and *m*-hydroxybenzaldehyde was recrystallized from water. MgSO_4 , Na_2CO_3 , K_2CO_3 and NaI were dried in an oven (150°C). Guests **G3**, **G4**, **G5**, **G6** and all other solvents and chemicals were commercial materials and used without purification. Molecular modeling calculations were performed on a Silicon Graphics Indigo II work station using the CHARMM force field.⁶⁴ For an overview of general techniques see Section 2.6.1.

9.8.2 NMR titrations

NMR titrations were carried out on Bruker AC 300 and Bruker AMX 500 instruments at 298 K. To a weighed amount of approximately 0.5 mL of a 1.0-2.0 mM stock solution of a porphyrin host in CDCl_3 (or in 1:1 (v/v) $\text{CDCl}_3/\text{CD}_3\text{CN}$) were added small amounts (25-100 μL , microsyringe) of a 5-10 mM stock solution of the guest in the same solvent, until approximately 10 equivalents of guest were present. For each titration, at least 12 data points were collected. Binding constants were determined by following several proton resonances of the host as a function of the guest concentration. The data were fitted with the computer program Grafit⁶⁵ using the following equation.⁶⁶

$$\delta_{obs} = \delta_H + \frac{\Delta_0}{2[H_{Tot}]} \left\{ [H_{Tot}] + [G_{Tot}] + \frac{1}{K_a} - \sqrt{\left[\left([H_{Tot}] + [G_{Tot}] + \frac{1}{K_a} \right)^2 - 4[H_{Tot}][G_{Tot}] \right]} \right\} \quad (1)$$

in which δ_{obs} is the observed chemical shift (in Hz) of a proton probe signal, δ_H is the chemical shift of this probe when no guest is present, $\Delta_0 = \delta_{obs} - \delta_{calc}$, in which δ_{calc} is the calculated chemical shift of the probe in the host-guest complex and K_a is the association constant. This procedure can be applied to the guest's ^1H resonances as well. After every addition of the stock solution of the guest dilution occurs. To account for this, $[H_{Tot}]$ and $[G_{Tot}]$ have to be defined as:

$$[H_{Tot}] = \frac{[H_{Stock}] \times V_0}{V_0 + V_{Add}} \quad (2)$$

$$[G_{Tot}] = \frac{[G_{Stock}] \times V_{Add}}{V_0 + V_{Add}} \quad (3)$$

in which $[H_{Stock}]$ and $[G_{Stock}]$ are the concentrations of the host and guest stock solutions, V_0 is the starting volume of the host stock solution (~ 0.5 mL) and V_{Add} the total volume of added guest stock solution.

9.8.3 UV-vis titrations

All UV titrations were carried out in duplo. CHCl_3 and CH_3CN were freshly distilled before use. To a weighed amount of approximately 1.5 mL of a 1.0-2.0 μM stock solution of the porphyrin host in CHCl_3 (or in 1:1 (v/v) $\text{CH}_3\text{CN}/\text{CDCl}_3$) were added small amounts (25-100 μL , microsyringe) of a stock solution containing the porphyrin host in the same concentration and approximately 60 μM guest, so that at the end approximately 10 equivalents of guest were present. For each titration, at least 25 data points were collected. The decrease in absorption of the B-band of the free host was plotted versus the guest concentration. The data were fitted with the computer program Grafit⁶⁵ using the following equation.⁶⁶

$$A = A_0 - \epsilon_r \left\{ \frac{1}{2} \left[[H_{Tot}] + [G_{Tot}] + \frac{1}{K_a} - \sqrt{\left[\left([H_{Tot}] + [G_{Tot}] + \frac{1}{K_a} \right)^2 - 4[H_{Tot}][G_{Tot}] \right]} \right] \right\} \quad (4)$$

in which A is the observed absorption of the B-band, A_0 is the absorption of this band when no guest is present, ϵ_r is the relative extinction coefficient, $[H_{Tot}]$ is the total host concentration, $[G_{Tot}]$ is the total guest concentration and K_a is the association constant. For each titration, several isosbestic points were observed, which is indicative of the presence of only one host-guest complex.

All ^1H NMR, COSY, and 2D NOESY and EXSY experiments on **H₂14** and its host-guest complexes were performed on a 500 MHz machine. The NMR titrations were carried out according to the procedure described in Section 2.6.2. Association constants of the host-guest complexes were measured by following the change in the conformer ratio as a function of the guest concentration. To this end, after each addition of guest as many as possible non-overlapping signals of each conformer in the spectra were integrated. Assuming that only the *aa*-conformer binds the guest, the following sets of equations were used to calculate the concentrations of the uncomplexed host and guest and that of the host-guest complex:

$$K_a = \frac{[aa \cdot G]}{[aa]_{free} \times [G]_{free}} \quad (5)$$

In this equation, $[aa \cdot G]$ is the equilibrium concentration of the complex between the *aa* conformer and the guest G , $[aa]_{free}$ the concentration of the uncomplexed *aa*-conformer, and $[G]_{free}$ the concentrations of the free guest. Assuming that the *sa*-conformer is not involved in binding of the guest, $[aa]_{free}$ can be determined with the help of the equilibrium constant $K_{sa/aa}$, which is defined by:

$$K_{sa/aa} = \frac{[sa]}{[aa]_{free}} \quad (6)$$

The constant $K_{sa/aa}$ can be determined by integration of the signals belonging to the *sa*- and *aa*-conformers in a solution of the host which contains no guest. The other concentrations in equation (5) can be calculated using equations (7) and (8):

$$[aa \cdot G] = [aa]_{tot} - [aa]_{free} \quad (7)$$

$$[G]_{free} = [G]_{tot} - [aa \cdot G] \quad (8)$$

9.8.4 Syntheses

Porphyrin clip **H₂1**:

To freshly distilled CH_2Cl_2 (250 mL) were added compound **8** (300 mg, 0.26 mmol) and pyrrole (70 mg, 1.0 mmol). The solution was purged with argon for 15 min., excluded from light, and $\text{BF}_3 \cdot \text{OEt}_2$ (50 mg, 0.35 mmol) was added. The orange solution was stirred for 16 h at room temperature. *p*-Chloranil (170 mg, 0.75 mmol) was added and the mixture was refluxed for 1 h. After cooling, the solvent was evaporated and the residue was purified by column chromatography (silica, first column $\text{CH}_2\text{Cl}_2/\text{EtOH}$ 95:5 (v/v), second column $\text{CHCl}_3/\text{MeOH}$ 99:1 (v/v)). The product was dissolved in a minimal amount of CHCl_3 and this solution was added dropwise to stirred *n*-hexane (25 mL) to yield, after centrifugation and drying of the product under vacuum, 20 mg (6%) of **H₂1** as a dark red solid.

M.p. > 400°C; IR (KBr pellet) ν 3059 (ArH), 2922, 2873 (CH_2), 1712 (C=O), 1597, 1580, 1488, 1457, 1425 (C=C, C=N), 1343, 1306, 1279, 1251, 1213 (CH_2), 1140, 1066 (COC) cm^{-1} ; ^1H NMR (CDCl_3 , 500.14 MHz) δ 8.75 (s, 4H, β -pyrroleH), 8.66 (s, 4H, β -pyrroleH), 8.07 (d, 4H, ArH, $^3J = 7.3$ Hz), 7.75 (t, 4H, ArH, $^3J = 8.0$ Hz), 7.37 (t, 4H, ArH, $^3J = 7.4$ Hz), 7.34 (d, 4H, ArH, $^3J = 8.4$ Hz), 6.97-6.91 (m, 6H, ArH), 6.83-6.78 (m, 4H, ArH), 6.20 (s, 4H, ArH side-wall), 4.30-4.20 (m, 4H, CH_2O), 4.24 (d, 4H, $\text{NCH}_2\text{Ar out}$, $^2J = 15.8$ Hz), 4.09-4.01 (m, 4H, CH_2O), 3.74 (d, 4H, $\text{NCH}_2\text{Ar in}$, $^2J = 15.8$ Hz), 3.53-3.43 (m, 4H, CH_2O), 3.37-3.30 (m, 4H, CH_2O), -2.72 (br s, 4H, NH) ppm, see Figure 9.3 for the exact assignment of all proton resonances; $^{13}\text{C}\{^1\text{H}\}$ NMR (CDCl_3 , 75.47 MHz) δ 158.76 (urea C=O), 156.99, 146.60, 135.75, 133.63, 131.90, 129.82, 129.57, 128.45, 128.10, 119.82, 115.21, 111.93 (ArC), 84.76 (NC(Ph)C), 67.43, 66.87 (CH_2O), 44.39 (NCH_2Ar) ppm; UV-vis (CHCl_3) λ/nm , log ($\epsilon/\text{M}^{-1}\text{cm}^{-1}$) 418 (5.63), 485 (3.44), 515 (4.27), 548 (3.82), 587 (4.02), 639 (3.70); FAB-MS m/z 1345 (M + H)⁺. Anal. Calcd for $\text{C}_{84}\text{H}_{64}\text{N}_8\text{O}_{10}$: C, 74.97; H, 4.79; N, 8.33. Found: C, 74.84; H, 4.93; N, 8.32.

Porphyrin clip **Zn1**:

To a degassed solution of **H₂1** (20 mg, 0.015 mmol) in a mixture of CHCl_3 (2 mL) and MeOH (1 mL) was added $\text{Zn}(\text{OAc})_2 \cdot 2\text{H}_2\text{O}$ (8.0 mg, 0.036 mmol). The mixture was excluded from light and refluxed under nitrogen for 3 h. After cooling, the solvent was evaporated and the residue was dissolved in CH_2Cl_2 (10 mL). The organic layer was washed with water (2 x) and concentrated *in vacuo*. After purification by column chromatography ($\text{CH}_2\text{Cl}_2/\text{MeOH}$, 97:3, v/v) 20 mg (95%) of **Zn1** was obtained as a purple solid.

M.p. > 400°C; IR (KBr pellet) ν 3052 (ArH), 2923, 2853 (CH_2), 1712 (C=O), 1634, 1577, 1450, 1425 (C=C, C=N), 1339, 1277, 1248, 1212 (CH_2), 1119, 1063 (COC) cm^{-1} ; ^1H NMR (CDCl_3 , 500.14 MHz) δ 8.89 (s, 4H, β -pyrroleH), 8.77 (s, 4H, β -pyrroleH), 8.10 (d, 4H, ArH, $^3J = 6.6$ Hz), 7.74 (t, 4H, ArH, $^3J = 7.2$ Hz), 7.38 (t, 4H, ArH, $^3J = 7.5$ Hz), 7.34 (d, 4H, ArH, $^3J = 8.2$ Hz), 7.00-6.92 (m, 6H, ArH), 6.85-6.74 (m, 4H, ArH), 6.17 (s, 4H, ArH), 4.27-4.15 (m, 4H, CH_2O), 4.19 (d, 4H, NCH_2Ar , $^2J = 15.6$ Hz), 4.09-3.99 (m, 4H, CH_2O), 3.72 (d, 4H, NCH_2Ar , $^2J = 15.6$ Hz), 3.57-3.47 (m, 4H, CH_2O), 3.35-3.23 (m, 4H, CH_2O) ppm, see Figure 9.3 for the exact assignment of all proton resonances; $^{13}\text{C}\{^1\text{H}\}$ NMR (CDCl_3 , 75.47 MHz) δ 158.87 (urea C=O), 150.13, 149.88, 146.63, 135.56, 133.66, 132.72, 131.44, 130.89, 129.90, 129.36, 128.50, 128.11, 119.87, 116.14, 115.41, 112.16 (ArC), 84.76 (NC(Ph)N), 67.50, 67.02 (CH_2O), 44.33 (NCH_2Ar) ppm; UV-vis (CHCl_3) λ/nm (log($\epsilon/\text{M}^{-1}\text{cm}^{-1}$)): 420 (5.6), 545 (4.1). FAB-MS m/z 1409 (M + H)⁺. Due to the limited amount of compound no satisfactory elemental analysis could be obtained.

Porphyrin clip **H₂2**:

Route A: Starting from pyrrole (61 mg, 0.91 mmol), **9** (300 mg, 0.23 mmol) and $\text{BF}_3 \cdot \text{OEt}_2$ (50 mg, 0.35 mmol) in freshly distilled CH_2Cl_2 , this compound was synthesized as described for **H₂1**. The crude product was purified by column chromatography (silica, first column $\text{CHCl}_3/\text{MeOH}$ 97:3 (v/v), second column gradient elution EtOAc/*n*-hexane 1:1 (v/v) - EtOAc/*n*-hexane 3:1 (v/v)). The product was dissolved in a minimal amount of CHCl_3 and this solution was added dropwise to stirred *n*-hexane (25 mL) to yield, after centrifugation and drying of the product under vacuum, 12 mg (4%) of **H₂2** as a dark red solid.

Route B: Compounds **8** (200 mg, 0.202 mmol) and **10** (137 mg, 0.202 mmol) were dissolved in freshly distilled acetonitrile (600 mL). Na_2CO_3 (1.0 g, 9.4 mmol) and NaI (2.0 g, 13.3 mmol) were added and the mixture was refluxed under nitrogen for 10 days. After cooling, the solvent was evaporated and the residue was suspended in

CH₂Cl₂ (100 mL). The organic layer was extracted with aqueous 1 N HCl (200 mL), with a saturated aqueous NaHCO₃ solution (200 mL), and with water and finally evaporated to dryness. After purification by column chromatography (see route A), 18 mg (6%) of **H₂2** was obtained.

M.p. > 400°C; IR (KBr pellet) ν 3056 (ArH), 2927, 2860 (CH₂), 1710 (C=O), 1630, 1585, 1485, 1458 (C=C, C=N), 1296, 1263 (CH₂), 1132, 1080 (COC) cm⁻¹; ¹H NMR (CDCl₃, 500.13 MHz) δ 8.92 (s, 4H, β -pyrroleH), 8.80 (s, 4H, β -pyrroleH), 8.06 (d, 4H, ArH, ³J = 7.3 Hz), 7.71 (br s, 4H, ArH), 7.68 (t, 4H, ArH, ³J = 7.9 Hz), 7.35 (dd, 4H, ArH, ³J = 8.2 Hz, ⁴J = 2.3 Hz), 6.85 (m, 6H, ArH), 6.70 (m, 4H, ArH), 4.92 (d, 4H, NCH₂Ar out, ²J = 16.1 Hz), 4.24 (m, 4H, CH₂O), 4.09 (m, 4H, CH₂O), 3.85 (m, 8H, CH₂O), 3.8 (br s, 4H, ArH), 3.55 (m, 8H, CH₂O), 3.21 (d, 4H, NCH₂Ar in, ²J = 16.1 Hz), 3.20 (m, 4H, CH₂O), 2.68 (m, 4H, CH₂O), -2.70 (br s, 2H, NH) ppm, see Figure 9.4 for the exact assignment of all proton resonances; ¹H NMR (CDCl₃:CD₃CN 1:1, v/v, 500.13 MHz) δ 8.92 (s, 4H, β -pyrroleH), 8.85 (s, 4H, β -pyrroleH), 8.03 (d, 4H, ArH, ³J = 7.3 Hz), 7.82 (br s, 4H, ArH), 7.71 (t, 4H, ArH, ³J = 7.9 Hz), 7.34 (dd, 4H, ArH, ³J = 8.2 Hz, ⁴J = 2.3 Hz), 6.85 (m, 6H, ArH), 6.70 (m, 4H, ArH), 4.65 (d, 4H, NCH₂Ar out, ²J = 16.1 Hz), 4.35 (m, 4H, CH₂O), 4.16 (m, 4H, CH₂O), 3.85 (m, 12H, CH₂O and ArH), 3.55 (m, 8H, CH₂O), 3.16 (d, 4H, NCH₂Ar in, ²J = 16.1 Hz), 3.16 (m, 4H, CH₂O), 2.64 (m, 4H, CH₂O), -2.78 (br s, 2H, NH) ppm; ¹³C{¹H} NMR (75 MHz, CDCl₃) δ 158.00 (urea C=O), 156.90, 149.35, 143.30, 133.86, 132.91, 129.83, 128.18, 127.97, 127.56, 127.14, 126.02, 121.69, 120.18, 116.37, 111.56 (ArC), 84.52 (NC(Ph)N), 70.74, 69.76, 68.74, 68.11 (CH₂O), 36.40 (NCH₂Ar) ppm; UV-vis (CHCl₃) λ /nm (log(ϵ /M⁻¹cm⁻¹)): 420 (5.6), 515 (4.2), 549 (4.0), 588 (3.7), 644 (3.6); FAB-MS m/z 1521 (M + H)⁺. Due to the limited amount of compound no satisfactory elemental analysis could be obtained.

Porphyrin clip Zn2:

Starting from **H₂2** (20 mg, 0.013 mmol) and Zn(OAc)₂·2H₂O (7.2 mg, 0.032 mmol), this compound was synthesized as described for **Zn1**. After purification by column chromatography (silica, EtOAc/*n*-hexane 2:1 (v/v)), the product was dissolved in a minimal amount of CHCl₃ and this solution was added dropwise to stirred *n*-hexane (25 mL) to yield, after centrifugation and drying the product under vacuum, 20 mg (96%) of **Zn2** as a purple solid.

M.p. > 400°C; IR (KBr pellet) ν 3055 (ArH), 2925, 2858 (CH₂), 1710 (C=O), 1632, 1598, 1584, 1480, 1450, 1430 (C=C, C=N), 1301, 1299, 1259 (CH₂), 1132, 1068 (COC) cm⁻¹; ¹H NMR (CDCl₃, 500 MHz) δ 8.96 (s, 4H, β -pyrroleH), 8.94 (s, 4H, β -pyrroleH), 7.98 (d, 4H, ArH, ³J = 7.4 Hz), 7.85 (br s, 4H, ArH), 7.65 (t, 4H, ArH, ³J = 7.5 Hz), 7.33 (dd, 4H, ArH, ³J = 8.3 Hz, ⁴J = 2.3 Hz), 6.71 (m, 6H, ArH), 6.51 (m, 4H, ArH), 4.59 (s, 4H, ArH), 4.32 (m, 4H, CH₂O), 4.28 (d, 4H, NCH₂Ar, ²J = 15.6 Hz), 4.18 (m, 4H, CH₂O), 3.85 (m, 8H, CH₂O), 3.55 (m, 8H, CH₂O), 3.30 (d, 4H, NCH₂Ar, ²J = 15.6 Hz), 3.34 (m, 4H, CH₂O), 2.95 (m, 4H, NCH₂O) ppm, see Figure 9.4 for the exact assignment of all proton resonances; ¹H NMR (CDCl₃:CD₃CN 1:1, v/v, 500.14 MHz) δ 8.97 (s, 4H, β -pyrroleH), 8.92 (s, 4H, β -pyrroleH), 8.01 (d, 4H, ArH, ³J = 7.4 Hz), 7.96 (br s, 4H, ArH), 7.70 (t, 4H, ArH, ³J = 7.5 Hz), 7.34 (dd, 4H, ArH, ³J = 8.3 Hz, ⁴J = 2.3 Hz), 6.88 (m, 6H, ArH), 6.72 (m, 4H, ArH), 4.76 (s, 4H, ArH), 4.72 (d, 4H, NCH₂Ar, ²J = 15.6 Hz), 4.56 (m, 4H, CH₂O), 4.27 (m, 4H, CH₂O), 3.88 (m, 8H, CH₂O), 3.58 (m, 8H, CH₂O), 3.20 (d, 4H, NCH₂Ar, ²J = 15.6 Hz), 3.15 (m, 4H, CH₂O), 3.00 (m, 4H, NCH₂O) ppm; ¹³C{¹H} NMR (CDCl₃, 75 MHz) δ 157.22 (urea C=O), 156.89, 150.23, 149.62, 134.28, 132.11, 131.92, 127.84, 127.62, 127.31, 126.61, 121.68, 120.96, 115.83, 112.44 (ArC), 84.36 (NC(Ph)N), 70.74, 70.02, 68.62 (CH₂O), 36.49 (NCH₂Ar) ppm; UV-vis (CHCl₃) λ /nm (log(ϵ /M⁻¹cm⁻¹)): 420 (5.6), 546 (4.2); FAB-MS m/z 1585 (M + H)⁺. Due to the limited amount of compound no satisfactory elemental analysis could be obtained.

2-[2-(2-Hydroxyethoxy)phenoxy]-1-ethanol (3):

This compound was synthesized according to a literature procedure.²⁴

2-[2-(2-[(4-Methylphenyl)sulfonyl]oxyethoxy)phenoxy]ethyl 4-methyl-1-benzenesulfonate (4):

A cooled solution (0°C) of **3** (7.0 g, 37 mmol) in pyridine (25 mL) was purged with argon for 15 min. *p*-Toluenesulfonyl chloride (14.8 g, 78.2 mmol) was added in small portions over a period of 2 h, while stirring the mixture. The suspension was stored overnight at 4°C, and then poured into crushed ice (100 mL). After the ice had melted, aqueous 6 N HCl (25 mL) was added and the product was extracted with CH₂Cl₂ (2 x 50 mL). The combined organic layers were dried with MgSO₄, filtered and evaporated to dryness. The residue was recrystallized from toluene to yield 16.0 g (90%) of **4** as a white solid.

M.p. 86°C; IR (KBr pellet) ν 3078 (ArH), 2963, 2884 (CH₂), 1597, 1505, 1459 (C=C), 1358 (CH₃), 1175 (S=O), 1018 (COC) cm⁻¹; ¹H NMR (CDCl₃, 300.13 MHz) δ 7.80 (d, 4H, ArH *ortho* to SO₂, ³J = 8.3 Hz), 7.33 (d, 4H, ArH *meta* to SO₂, ³J = 8.3 Hz), 6.93-6.87 (m, 2H, ArH, *meta* to OCH₂), 6.84-6.78 (m, 2H, ArH, *ortho* to OCH₂), 4.33-4.30 (m, 4H, ArOCH₂CH₂) 4.17-4.14 (m, 4H, ArOCH₂CH₂), 2.43 (s, 6H, CH₃) ppm; ¹³C{¹H} NMR (CDCl₃, 75.47 MHz) δ 148.42 (ArC *ipso* to SO₂), 145.01 (ArC *ipso* to OCH₂), 132.85 (ArC *ipso* to CH₃), 129.92 (ArC *ortho* to SO₂), 127.91 (ArC *meta* to SO₂), 122.60 (ArC *meta* to OCH₂), 116.33 (ArC *ortho* to OCH₂), 68.22 (ArOCH₂CH₂), 67.30

(ArOCH₂CH₂), 21.59 (CH₃) ppm; EI-MS *m/z* 506 (M)⁺. Anal. Calcd for C₂₄H₂₆O₆S₂: C, 56.90; H, 5.17; S, 12.66. Found: C, 56.95; H, 4.94; S, 12.80.

1,3,4,6-Tetrakis(chloromethyl)tetrahydro-3a,6a-diphenyl-imidazo[4,5-*d*]imidazole-2,5(1*H*, 3*H*)dione (5):

This compound was synthesized according to a literature procedure.²⁵

2-[3,9,10-Tri(2-[(4-methylphenyl)sulfonyl]oxyethoxy)-6,13-dioxo-13b,13c-diphenyl-5,7,12,13b,13c,14-hexahydro-5a,6a,12a,13a-tetraazabenz[5,6]azuleno[2,1,8-*ija*]benzo[*f*]azulen-2-yl]oxyethyl 4-methyl-1-benzenesulfonate (6):

Compounds **4** (5.0 g, 10 mmol) and **5** (2.2 g, 4.5 mmol) were dissolved in freshly distilled 1,2-dichloroethane (100 mL). SnCl₄ (4 mL, 32 mmol) was added and the mixture was refluxed under nitrogen for 16 h. After cooling, aqueous 6 N HCl (25 mL) was added and the mixture was refluxed for another 30 min. After cooling, CH₂Cl₂ (75 mL) was added and the organic layer was washed with aqueous 1 N HCl (3 x 100 mL) and water and evaporated to dryness. The crude product was recrystallized from toluene to yield 3.8 g (62%) of **6** as a white solid.

M.p. 110°C; IR (KBr pellet) ν 3064 (ArH), 2925, 2853 (CH₂), 1712 (C=O), 1599, 1457 (C=C), 1354, 1305 (CH₂), 1098 (S=O) cm⁻¹; ¹H NMR (CDCl₃, 300.13 MHz) δ 7.69 (d, 8H, ArH *ortho* to SO₂, ³J = 9.0 Hz), 7.17 (d, 8H, ArH *meta* to SO₂, ³J = 9.0 Hz), 7.15-7.02 (m, 10H, ArH glycoluril), 6.67 (s, 4H, ArH side-wall), 4.65 (d, 4H, NCH₂Ar *out*, ²J = 15.8 Hz), 4.21 (t, 8H, ArOCH₂CH₂, ³J = 7.3 Hz), 4.09 (d, 4H, NCH₂Ar *in*, ²J = 15.8 Hz), 4.01-3.85 (m, 8H, ArOCH₂CH₂), 2.36 (s, 6H, CH₃) ppm; ¹³C{¹H} NMR (CDCl₃, 75.47 MHz) δ 157.70 (urea C=O), 146.77 (ArC *ipso* to SO₂), 144.87 (ArC *ipso* to OCH₂), 133.52 (ArC glycoluril), 132.62 (ArC *ipso* to CH₃), 130.07 (ArC *ipso* to CH₂N), 129.82 (ArC *ortho* to SO₂), 128.91, 128.73, 128.19 (ArC glycoluril), 127.81 (ArC *meta* to SO₂), 117.11 (ArC *ortho* to OCH₂), 85.39 (NC(Ar)N), 68.22 (ArOCH₂CH₂), 66.78 (ArOCH₂CH₂), 44.73 (NCH₂Ar), 21.58 (CH₃) ppm; FAB-MS *m/z* 1355 (M + H)⁺. Anal. Calcd for C₆₈H₆₆N₄O₁₈S₄: C, 60.25; H, 4.91; N, 4.13; S, 9.46. Found: C, 60.12; H, 4.87; N, 4.22; S, 9.12.

2-[2-(3,9,10-Tri(2-(2-formylphenoxy)ethoxy)-6,13-dioxo-13b,13c-diphenyl-5,7,12,13b,13c,14-hexahydro-5a,6a,12a,13a-tetraazabenz[5,6]azuleno[2,1,8-*ija*]benzo[*f*]azulen-2-yloxy)ethoxy]benzaldehyde (7):

A suspension of **6** (2.1 g, 1.6 mmol), salicylic aldehyde (0.82 g, 6.7 mmol) and K₂CO₃ (0.85 g, 6.2 mmol) in freshly distilled acetonitrile (100 mL) was refluxed under nitrogen for 16 h. After cooling, the mixture was filtered and the filtrate was evaporated to dryness. The residue was dissolved in CH₂Cl₂ (50 mL). This solution was extracted with aqueous 0.5 N NaOH (2 x 100 mL), with water (100 mL) and evaporated to dryness. The residue was purified by column chromatography (CHCl₃/MeOH 197:3 (v/v)). The resulting off-white product was dissolved in a minimal amount of CHCl₃, and this solution was added dropwise to stirred diethylether (100 mL). After filtration, the product was dried under vacuum to yield 1.10 g (59%) of **7** as a white solid.

M.p. 107°C; IR (KBr pellet) ν 3068 (ArH), 2923, 2867 (CH₂), 1685 (C=O), 1598 (C=C), 1457 (CH), 1282, 1244, 1102 (COC) cm⁻¹; ¹H NMR (CDCl₃, 300.13 MHz) δ 10.30 (s, 4H, ArCHO), 7.70 (dd, 4H, ArH *ortho* to CHO, ³J = 7.9 Hz, ⁴J = 1.8 Hz), 7.43 (td, 4H, ArH *meta* to CHO and *para* to OCH₂, ³J = 7.9 Hz, ⁴J = 1.8 Hz), 7.21-7.07 (m, 10H, ArH glycoluril), 6.95-6.70 (m, 8H, ArH *para* to CHO, ArH *meta* to CHO and *ortho* to OCH₂), 6.89 (s, 4H, ArH side-wall), 4.76 (d, 4H, NCH₂Ar *out*, ²J = 15.9 Hz), 4.24-4.17 (m, 4H, ArOCH₂CH₂), 4.17 (d, 4H, NCH₂Ar *in*, ²J = 15.9 Hz), 4.15-4.08 (m, 4H, ArOCH₂CH₂) ppm; ¹³C{¹H} NMR (CDCl₃, 75.47 MHz) δ 189.71 (CHO), 160.99 (urea C=O), 157.81 (ArC *ortho* to CHO and *ipso* to OCH₂), 147.38 (ArC side-wall *ipso* to OCH₂), 135.83 (ArC *ipso* to CHO), 133.50 (ArC glycoluril), 131.05 (ArC *ipso* to CH₂N), 128.89, 128.73, 128.24 (ArC glycoluril), 127.98 (ArC *ortho* to CHO), 125.04 (ArC *para* to CHO), 120.99 (ArC *meta* to CHO and *para* to OCH₂), 116.80 (ArC *ortho* to CH₂N), 113.10 (ArC *meta* to CHO and *ortho* to OCH₂), 85.45 (NC(Ph)N), 67.68, 67.41 (CH₂O), 44.81 (NCH₂Ar) ppm; MS (FAB) *m/z* 1155 (M + H)⁺. Anal. Calcd for C₆₈H₅₈N₄O₁₄·0.5CHCl₃: C, 67.72; H, 4.85; N, 4.61. Found: C, 67.83; H, 4.86; N, 4.89.

5,7,12,13b,13c,14-Hexahydro-1,4,8,11-tetrakis[2-(2-chloroethoxy)-ethoxy]-13b,13c-diphenyl-6*H*,13*H*-5a,6a,-12a,13a-tetraazabenz[5,6]-azuleno[2,1,8-*ija*]benzo[*f*]azulene-6,13-dione (8):

This compound was synthesized according to a literature procedure.²⁵

3-(2-2-[(4,8,11-Tri-2-[2-(3-formylphenoxy)ethoxy]ethoxy)-6,13-dioxo-13b,13c-diphenyl-5,7,12,13b,13c,14-hexahydro-5a,6a,12a,13a-tetraazabenz[5,6]azuleno[2,1,8-*ija*]benzo[*f*]azulen-1-yl]oxy]ethoxy)ethoxy]benzaldehyde (9):

A mixture of **8** (0.50 g, 0.50 mmol), Na₂CO₃ (1.6 g, 15 mmol), NaI (5.0 g, 33 mmol) and *m*-hydroxybenzaldehyde (0.50 g, 4.1 mmol) in freshly distilled acetonitrile (100 mL) was refluxed under nitrogen for 10 days. After cooling, the mixture was filtered and the filtrate was evaporated to dryness. Water (100 mL) was added to the residue and the resulting suspension was extracted with CHCl₃ (3 x 50 mL). The combined organic layers were extracted with

aqueous 0.5 N NaOH (2 x 100 mL) and evaporated to dryness. After column chromatography (silica, CHCl₃/EtOH 97:3 (v/v)), 0.43 g (64%) of **9** was obtained as a white solid.

M.p. 212°C; IR (KBr pellet) ν 3052, 3044 (ArH), 2925, 2873 (CH₂), 1705 (C=O), 1596, 1584 (C=C), 1484, 1460, 1427 (CH), 1263, 1135, 1086 (COC) cm⁻¹; ¹H NMR (CDCl₃, 500.14 MHz) δ 9.95 (s, 4H, CHO), 7.43 (d, 4H, ArH *ortho* to CHO and *para* to OCH₂, ³J = 7.5 Hz), 7.39 (s, 4H, ArH *ortho* to CHO and *ortho* to OCH₂), 7.38 (t, 4H, ArH *para* to CHO and *ortho* to OCH₂, ³J = 7.5 Hz), 7.19-7.13 (m, 4H, ArH *meta* to CHO), 7.09-7.01 (m, 10H, ArH glycoluril), 6.63 (s, 4H, ArH side-wall), 5.59 (d, 4H, NCH₂Ar *out*, ²J = 15.8 Hz), 3.74 (d, 4H, NCH₂Ar *in*, ²J = 15.8 Hz), 4.08-3.81 (m, 32H, CH₂O) ppm; ¹³C{¹H} NMR (CDCl₃, 75.47 MHz) δ 192.21 (CHO), 159.41 (urea C=O), 157.80, 150.72, 137.76, 133.83, 129.96, 128.55, 128.33, 128.14, 122.97, 121.96, 114.25, 113.55 (ArC), 85.28 (NC(Ar)N), 70.47, 69.73, 67.81 (CH₂O), 37.02 (NCH₂Ar) ppm; FAB-MS *m/z* 1331 (M + H)⁺. Anal. Calcd for C₇₆H₇₄O₁₈N₄(CH₃CH₂OH): C, 68.01; H, 5.85; N, 4.07. Found: C, 68.19; H, 6.06; N, 4.08.

21H,23H-5,10,15,20-tetrakis(3-hydroxyphenyl)porphyrin (**10**):

A solution of *m*-hydroxybenzaldehyde (1.82 g, 14.9 mmol) in propionic acid (100 mL) was heated to reflux. Pyrrole (1.0 g, 14.9 mmol) was added, the mixture was refluxed for 1 h, and then cooled overnight at 4°C. The crude product was filtered off and dried by suction. Purification by column chromatography (silica, CHCl₃/MeOH, 9:1, v/v) yielded 400 mg (16%) of **10** as a purple powder, which was immediately used in further synthesis.

¹H NMR (CDCl₃/CD₃OD, 9:1 (v/v), 300.13 MHz) δ 8.93 (br s, 8H, β -pyrroleH), 7.71 (d, 4H, PhH-6, ³J = 5.1 Hz), 7.70 (br s, 4H, PhH-4), 7.57 (t, 4H, PhH-2, ³J = 7.8 Hz), 7.27 (d, 4H, PhH-5, ³J = 5.4 Hz). The NH and OH protons were not detected.

5,7,12,13b,13c,14-Hexahydro-1,4,8,11-tetramethoxy-13b,13c-diphenyl-6H,13H-5a,6a,12a,13a-tetraazabenz-[5,6]azuleno[2,1,8-*ija*]benz[*f*]azulene-6,13-dione (**11**):

This compound was synthesized according to a literature procedure.²⁵

Porphyrin clip **H₂14**:

Route A: To CH₂Cl₂ (250 mL) were added compound **16** (150 mg, 0.105 mmol) and pyrrole (28 mg, 0.42 mmol). The solution was purged with argon for 15 min., excluded from light, and BF₃•OEt₂ (50 mg, 0.35 mmol) was added. The orange solution was stirred for 16 h at room temperature. *p*-Chloranil (85 mg, 0.38 mmol) was added and the mixture was refluxed for 1 h. After cooling, the solvent was evaporated and the residue was purified by column chromatography (first column: silica, CH₂Cl₂/EtOH 95:5, v/v; second column: silica, EtOAc/*n*-hexane, 1:1, v/v). The resulting product was dissolved in a minimal amount of CHCl₃ and this solution was added dropwise to stirred *n*-hexane. A precipitate was formed which was collected by centrifugation and dried under vacuum. Yield 10 mg (6%) of **H₂14** as a purple solid.

Route B: Compounds **16** (100 mg, 0.070 mmol) and **10** (48 mg, 0.070 mmol) were dissolved in CH₃CN (300 mL). Na₂CO₃ (0.5 g, 4.7 mmol) and NaI (1.0 g, 6.7 mmol) were added and the mixture was refluxed under nitrogen for 10 days. After cooling, the inorganic salts were filtered off, the solvent was evaporated and the residue was suspended in CH₂Cl₂ (100 mL). The organic layer was extracted with aqueous 1 N HCl (200 mL), with a saturated aqueous NaHCO₃ solution (200 mL), with water and then evaporated to dryness. After purification (see route A), 9 mg (8%) of **H₂14** was obtained.

M.p. > 400°C; ¹H NMR (CDCl₃, 500.13 MHz) **sa-conformer:** δ 9.04 (d, 2H, β -pyrroleH, ³J = 5.0 Hz), 9.01 (s, 2H, β -pyrroleH), 8.89 (d, 2H, β -pyrroleH, ³J = 5.0 Hz), 8.64 (s, 2H, β -pyrroleH), 8.13 (d, 2H, ArH, ³J = 6.5 Hz), 8.12 (br s, 2H, ArH), 8.08 (d, 2H, ArH, ³J = 7.0 Hz), 7.74 (t, 2H, ArH, ³J = 8.0 Hz), 7.65 (t, 2H, ArH, ³J = 7.0 Hz), 7.39 (dd, 2H, ArH, ³J = 8.5 Hz, ⁴J = 1.5 Hz), 7.35 (br s, 2H, ArH), 7.32 (dd, 2H, ArH, ³J = 8.5 Hz, ⁴J = 1.5 Hz), 6.99 (d, 2H, NaphtH-4, ³J = 8.5 Hz (*sa*)), 6.74 (s, 5H, ArH), 6.64 (d, 2H, NaphtH-3, ³J = 8.5 Hz (*sa*)), 6.16 (d, 2H, NaphtH-3, ³J = 8.5 Hz (*sa*)), 6.16 (d, 2H, ArH, ³J = 8.0 Hz), 6.06 (t, 1H, ArH, ³J = 7.0 Hz), 5.93 (t, 2H, ArH, ³J = 8.0 Hz), 5.52 (br s, 2H, NCH₂Ar *out* (*sa*)), 5.36 (d, 2H, NCH₂Ar *out*, ²J = 16.5 Hz (*sa*)), 4.48-4.43 (m, 2H, CH₂O), 4.38-4.33 (m, 2H, CH₂O), 4.27-4.21 (m, 2H, CH₂O), 4.13-3.60 (m, 28H, CH₂O and NCH₂Ar *in* (*sa*)), 3.52 (d, 2H, NCH₂Ar *in*, ²J = 16.5 Hz (*sa*)) 3.52 (br s, 2H, NaphtH-4), -2.70 (s, 2H, NH) ppm; **ss-conformer:** δ 9.01 (s, 4H, β -pyrroleH), 8.64 (s, 4H, ArH), 8.61 (s, 4H, β -pyrroleH), 7.71 (d, 4H, ArH, ³J = 7.5 Hz), 7.55 (t, 4H, ArH, ³J = 8.0 Hz), 7.34 (d, 4H, ArH, ³J = 7.5 Hz), 6.66 (d, 4H, NaphtH-4, ³J = 8.0 Hz), 6.70 (d, 4H, NaphtH-3, ³J = 8.0 Hz), 5.67 (t, 2H, ArH, ³J = 7.5 Hz), 5.46 (t, 4H, ArH, ³J = 7.5 Hz), 5.38 (d, 4H, ArH, ³J = 7.5 Hz), 4.74 (m, 2H, CH₂O), 4.66 (m, 2H, CH₂O), 4.07 (d, 4H, NCH₂Napht *in*, ²J = 15.5 Hz), 4.07-3.60 (m, 28H, CH₂O), 1.75 (d, 4H, NCH₂Napht *out*, ²J = 15.5 Hz), -3.10 (s, 2H, NH) ppm; **aa-conformer:** δ 5.14 (d, 4H, NCH₂Napht *out*, ²J = 16.0 Hz), 3.62 (d, 4H, NCH₂Napht *in*, ²J = 16.0 Hz), -2.64 (s, 2H, NH) ppm, other signals could not be assigned due to overlap with the signals of the other conformers and due to the low abundance of the conformer; ¹³C{¹H} NMR (CDCl₃, 75.47 MHz) δ 157.85, 157.62, 157.01 (urea C=O), 155.73 (ArC *ipso* to OCH₂), 143.51, 143.32, 140.02, 138.18, 135.77, 132.83, 131.95, 130.05, 129.53, 129.30, 128.84, 127.48, 126.60, 126.18, 125.38, 124.61, 124.00, 123.33, 120.01, 117.01, 116.32,

115.88, 115.50, 114.31, 113.77 (all ArC), 83.98 (NC(Ar)N), 73.74, 71.66, 71.14, 70.32, 70.04, 69.85, 69.26, 69.09, 68.08, 67.75, 66.39 (all CH₂O), 38.60, 35.89 (NCH₂Ar) ppm; FAB-MS *m/z* 1621 (M + H)⁺. UV-vis (CHCl₃) λ/nm (log(ε/M⁻¹cm⁻¹)): 420 (5.6), 516 (4.2), 549 (4.0), 588 (3.7), 644 (3.5).

1,6,8,13-tetra[2-(2-chloroethoxy)ethoxy]-14b,14c-diphenyl-14b,14c-dihydro-15H-6b,7a,13b,14a-tetraazanaphtho[1'',8'':4',5',6']cyclohepta[3,4]pentaleno[1,6-ab]phenalene-7,14-dione (15):

This compound was synthesized according to a literature procedure.⁵²

Tetra-aldehyde clip 16:

A suspension of **15** (320 mg, 0.293 mmol), *m*-hydroxybenzaldehyde (400 mg, 3.30 mmol), Na₂CO₃ (2.0 g, 19 mmol) and NaI (3.0 g, 20 mmol) in CH₃CN (100 mL) was refluxed under nitrogen for 10 days. After cooling, the inorganic salts were filtered off and the filtrate was evaporated to dryness. The residue was dissolved in CHCl₃ (50 mL) and the organic layer was extracted with aqueous 0.5 N NaOH (100 mL), with water (100 mL), and subsequently evaporated to dryness. After purification by column chromatography (CH₂Cl₂/EtOH 97:3, v/v) 280 mg (67%) of **16** was obtained as a white solid.

M.p. 212°C; ¹H NMR (CDCl₃, 500.14 MHz) δ 9.94 (s, 4H, CHO (*ss*)), 9.92 and 9.88 (2s, 4H, CHO (*sa*)), 9.80 (s, 4H, CHO (*aa*)), 7.72 (d, 2H, NaphtH-4, ³J = 9.0 Hz (*sa*)), 7.48–6.83 (m, ArH (all conformers)), 7.38 (d, 2H, NaphtH-4, ³J = 8.8 Hz (*sa*)), 7.28 (d, 2H, NaphtH-3, ³J = 9.0 Hz (*sa*)), 7.20 (d, 2H, NaphtH-3, ³J = 8.8 Hz (*sa*)), 7.01 (d, 4H, NaphtH-4, ³J = 7.0 Hz (*ss*)), 6.82 (d, 4H, NaphtH-3, ³J = 7.0 Hz (*ss*)), 6.50 (d, 2H, ArH, ³J = 7.5 Hz (*sa*)), 6.31 (d, 4H, ArH, ³J = 7.5 Hz (*ss*)), 6.28 (d, 4H, NCH₂Napht *out*, ²J = 15.2 Hz (*ss*)), 6.24 (t, 1H, ArH, ³J = 7.5 Hz (*sa*)), 6.14 (t, 2H, ArH, ³J = 7.5 Hz (*sa*)), 6.09 (t, 2H, ArH, ³J = 7.5 Hz (*ss*)), 6.08 (d, 2H, NCH₂Napht *out*, ²J = 14.5 Hz (*sa*)), 6.01 (d, 2H, NCH₂Napht *out*, ²J = 14.5 Hz (*sa*)), 5.94 (t, 4H, ArH, ³J = 7.5 Hz (*ss*)), 5.85 (d, 4H, NCH₂Napht *out*, ²J = 16.0 Hz (*aa*)), 5.10 (d, 4H, NCH₂Napht *in*, ²J = 15.2 Hz (*ss*)), 4.77 (d, 2H, NCH₂Napht *in*, ²J = 14.5 Hz (*sa*)), 4.65–4.87 (m, CH₂O, all conformers), 4.02 (d, 2H, NCH₂Napht *in*, ²J = 14.5 Hz (*sa*)), 3.89 (d, 4H, NCH₂Napht *in*, ²J = 16.0 Hz (*aa*)) ppm; ¹³C {¹H} NMR (CDCl₃, 75.47 MHz) □ 192.06 (CHO), 159.19, 158.82 (urea C=O), 157.69, 156.00 (ArC *ipso* to OCH₂), 137.72, 135.57, 135.01, 131.92, 131.65, 130.87, 130.75, 130.03, 128.96, 128.58, 128.25, 127.91, 127.37, 126.51, 126.29, 125.25, 124.92, 124.60, 123.46, 123.40, 123.18, 121.93, 118.48, 117.01, 114.15, 113.86, 113.64, 113.30, 113.01, 112.35 (all ArC), 84.14, 83.02 (NC(Ar)N), 70.61, 70.38, 70.26, 70.16, 69.91, 69.57, 67.98, 67.80 (all CH₂O), 39.81 (NCH₂Ar, *ss*-conformer), 39.18 and 36.47 (NCH₂Ar *sa*-conformer) ppm; FAB-MS *m/z* 1431 (M + H)⁺. Anal. Calcd for C₈₄H₇₈N₄O₁₈: C, 70.48; H, 5.49; N, 3.91. Found: C, 70.10; H, 5.60; N, 4.17.

(*N,N'*)-Dimethyl-4,4'-bipyridinium dihexafluorophosphate (G1):

This compound was synthesized by the dropwise addition of the commercially available dichloride salt, dissolved in a minimal amount of water, to a saturated solution of NH₄PF₆ in water. After filtration, the product was dried under vacuum to quantitatively yield **G1** as a white solid.

(*N,N'*)-Di(2-ethanol)-4,4'-bipyridinium dihexafluorophosphate (G2):

4,4'-Bipyridine (3.7 g, 24 mmol) and 2-bromoethanol (16 g, 0.13 mol) were dissolved in acetonitrile (75 mL). The mixture was refluxed under nitrogen for 24 h. After cooling, the precipitate was filtered off, washed with diethylether and dried under vacuum. The product was dissolved in a minimal amount of water and this solution was then added to a stirred saturated aqueous NH₄PF₆ solution, to yield 6.0 g (47%) of **G2** as a white solid.

M.p. 185°C; ¹H NMR (300 MHz, CDCl₃/CD₃CN, 1:1 (v/v)) δ 9.39 (d, 4H, BipyH-3,5,3',5', ³J = 7.2 Hz), 8.85 (d, 4H, BipyH-2,6,2',6', ³J = 7.2 Hz), 5.05 (t, 4H, NCH₂, ³J = 5.1 Hz), 4.68 (t, 2H, OH, ³J = 5.2 Hz), 4.24–4.17 (m, 4H, CH₂OH) ppm; FAB-MS *m/z* 391 (M - PF₆)⁺. Anal. Calcd for C₁₄H₁₈N₂O₂P₂F₁₂: C, 31.36; H, 3.38; N, 5.22. Found: C, 31.18; H, 3.39; N, 5.18.

Hexyl 3,5-dihydroxybenzoate (G7):

This compound was synthesized according to a literature procedure.⁶⁷

3,5-Dimethoxyipyridine:

This compound was synthesized according to a modified literature procedure.⁶⁸ Na (570 mg, 24.7 mmol) was carefully dissolved in methanol (100 mL) and 3,5-dibromopyridine (1.0 g, 4.2 mmol) was added. Copper powder (10 mg) was added and the mixture was transferred to a pressure vessel and stirred at a pressure of 5 bar for 1 week. After filtration, the mixture was evaporated to dryness. The residue was dissolved in water (100 mL) and this solution was extracted with diethyl ether (4 x 50 mL). The combined organic layers were evaporated to dryness and the residue was purified by column chromatography (silica, Et₂O/Et₃N 98:2 (v/v)). The product was purified from traces of Et₃N by azeotropic co-evaporation with toluene to yield 308 mg (52%) of 3,5-dimethoxyipyridine as a

yellowish oil.

¹H NMR (CDCl₃, 200.13 MHz) δ 7.95 (d, 2H, PyH-2,6, ⁴J = 2.4 Hz), 6.73 (t, 1H, PyH-4, ⁴J = 2.4 Hz), 3.84 (s, 6H, OCH₃).

3,5-Dihydroxypyridine (G8):

A solution of 3,5-dimethoxypyridine (211 mg, 1.52 mmol) in freshly distilled CH₂Cl₂ (6 mL) was cooled to -70°C. A 1 N BBr₃ solution in CH₂Cl₂ (9 mL) was carefully added, and the mixture was stirred under nitrogen for 16 h during which time it was allowed to warm to room temperature. Water (10 mL) was added dropwise and the mixture was evaporated to dryness. The residue was washed with CHCl₃ and the residue was purified by column chromatography (silica, CHCl₃/MeOH 9:1 (v/v)) and subsequent sublimation (0.05 Torr, 200°C), to yield **G8** (128 mg, 76%) as a white, very hygroscopic solid which was stored under nitrogen at -18°C.

M.p. > 400°C; ¹H NMR (CDCl₃/CD₃OD 1:4 (v/v), 200.13 MHz) δ 7.61 (d, 2H, PyH-2,6, ⁴J = 2.4 Hz), 6.70 (t, 1H, PyH-4, ⁴J = 2.4 Hz), the OH protons were not detected; EI-MS *m/z* 111 (M)⁺.

References and notes

- Lehn, J.-M. *Science* **1985**, 227, 849.
- Feiters, M. C. in: *Comprehensive Supramolecular Chemistry*. Atwood, J. L.; Davies, J. E. D.; MacNicol, D. D.; Vögtle, F.; Reinhoudt, D. N.; Lehn, J.-M. Eds.; Elsevier Science Ltd., Pergamon: Elmsford, **1996**; Vol. 10, 267-360.
- Schenning, A. P. H. J.; Hubert, D. H. W.; van Esch, J. H.; Feiters, M. C.; Nolte, R. J. M. *Angew. Chem. Int. Ed. Engl.* **1994**, 33, 2468. Schenning, A. P. H. J.; Lutje Spelberg, J. H.; Hubert, D. H. W.; Feiters, M. C.; Nolte, R. J. M. *Chem. Eur. J.* **1998**, 4, 871.
- For reviews see: Collman, J. P. *Acc. Chem. Res.* **1977**, 10, 265. Baldwin, J. P.; Perlmutter, P. *Top. Curr. Chem.* **1984**, 121, 181. Momenteau, M.; Reed, C. A. *Chem. Rev.* **1994**, 94, 659.
- Beer, P. D.; Drew, M. G. B.; Jagessar, R. *J. Chem. Soc. Dalton Trans.* **1997**, 881.
- Aoyama, Y.; Asakawa, M.; Matsui, Y.; Ogoshi, H. *J. Am. Chem. Soc.* **1991**, 113, 6233. Hayashi, T.; Miyahara, T.; Koide, N.; Kato, Y.; Masuda, H.; Ogoshi, H. *J. Am. Chem. Soc.* **1997**, 119, 7281.
- Takeuchi, M.; Imada, T.; Shinkai, S. *J. Am. Chem. Soc.* **1996**, 118, 10658. Takeuchi, M.; Imada, T.; Shinkai, S. *Angew. Chem. Int. Ed. Engl.* **1998**, 37, 2096.
- Ogoshi, H.; Kuroda, Y.; Mizutani, T.; Hayashi, T. *Pure Appl. Chem.* **1996**, 68, 1411. Mizutani, T.; Wada, K.; Kitagawa, S. *J. Am. Chem. Soc.* **1999**, 121, 11425.
- Mizutani, T.; Kurahashi, T.; Murakami, T.; Matsumi, N.; Ogoshi, H. *J. Am. Chem. Soc.* **1997**, 119, 8991. Rusin, O.; Král, V. *Chem. Commun.* **1999**, 2367.
- Hamilton, A. D.; Lehn, J.-M.; Sessler, J. L. *J. Am. Chem. Soc.* **1986**, 108, 5158.
- Lindsey, J. S.; Kearney, P. C.; Duff, R. J.; Tjivikua, P. T.; Rebek, J., Jr. *J. Am. Chem. Soc.* **1988**, 110, 6575.
- Shipps, G., Jr.; Rebek, J., Jr. *Tetrahedron Lett.* **1994**, 35, 6823.
- Kuroda, Y.; Hiroshige, T.; Sera, T.; Shirowa, Y.; Tanaka, H.; Ogoshi, H. *J. Am. Chem. Soc.* **1989**, 111, 1912. Kuroda, Y.; Hiroshige, T.; Ogoshi, H. *J. Chem. Soc. Chem. Commun.* **1990**, 1594. Breslow, R.; Zhang, X.; Huang, Y. *J. Am. Chem. Soc.* **1997**, 119, 4535. Chen, W.-H.; Yan, J.-M.; Tagashira, Y.; Yamaguchi, M.; Fujita, K. *Tetrahedron Lett.* **1999**, 40, 891.
- Bonar-Law, R. P.; Mackay, L. G.; Sanders, J. K. M. *J. Chem. Soc. Chem. Commun.* **1993**, 456.
- Kobayashi, N.; Mizuno, K.; Osa, T. *Inorg. Chim. Acta.* **1994**, 224, 1. Nagasaki, T.; Fujishima, H.; Shinkai, S. *Chem. Lett.* **1994**, 989. Nagasaki, T.; Fujishima, H.; Takeuchi, M.; Shinkai, S. *J. Chem. Soc. Perkin Trans. 1* **1995**, 1883. Rudkevich, D. M.; Verboom, W.; Reinhoudt, D. N. *Tetrahedron Lett.* **1994**, 35, 7131. Rudkevich, D. M.; Verboom, W.; Reinhoudt, D. N.; *J. Org. Chem.* **1995**, 60, 6585. Arimura, T.; Ide, S.; Sugibara, H.; Murata, S.; Sessler, J. L. *New J. Chem.* **1999**, 23, 977. Dudic, M.; Lhoták, P.; Král, V.; Lang, K.; Stibor, I. *Tetrahedron Lett.* **1999**, 40, 5949.
- Benson, D. R.; Valentekovich, R.; Knobler, C. B.; Diederich, F. *Tetrahedron* **1991**, 47, 2401. Benson, D. R.; Valentekovich, R.; Tam, S. W.; Diederich, F. *Helv. Chim. Acta* **1993**, 76, 2034.
- Kuroda, Y.; Sera, T.; Ogoshi, H. *J. Am. Chem. Soc.* **1991**, 113, 2793. Weber, L.; Imiolczyk, I.; Haufe, G.; Rehorek, D.; Hennig, H. *J. Chem. Soc. Chem. Commun.* **1992**, 301. Weber, L.; Hommel, R.; Behling, J.; Haufe, G.; Hennig, H. *J. Am. Chem. Soc.* **1994**, 116, 2400.
- Hunter, C. A.; Leighton, P.; Sanders, J. K. M. *J. Chem. Soc. Perkin Trans. 1* **1989**, 547. Hunter, C. A.; Meah, M. N.; Sanders, J. K. M. *J. Am. Chem. Soc.* **1990**, 112, 5773. Anderson, H. L.; Hunter, C. A.; Meah, M. N.; Sanders, J. K. M. *J. Am. Chem. Soc.* **1990**, 112, 5780. Walter, C. J.; Anderson, H. L.; Sanders, J. K. M. *J. Chem. Soc.*

- Chem. Commun.* **1993**, 458. Mackay, L. G.; Wylie, R. S.; Sanders, J. K. M. *J. Am. Chem. Soc.* **1994**, *116*, 3141.
- Walter, C. J.; Sanders, J. K. M. *Angew. Chem. Int. Ed. Engl.* **1995**, *34*, 217. Anderson, H. L.; Walter, C. J.; Vidal-Ferran, C. J.; Hay, R. A.; Lowden, P. A.; Sanders, J. K. M. *J. Chem. Soc. Perkin Trans. 1* **1995**, 2275.
- Anderson, H. L.; Anderson, S.; Sanders, J. K. M. *J. Chem. Soc. Perkin Trans. 1* **1995**, 2231. Marty, M.; Clyde-Watson, Z.; Twyman, L. J.; Nakash, M.; Sanders, J. K. M. *Chem. Commun.* **1998**, 265.
- ¹⁹ Bonar-Law, R. P.; Sanders, J. K. M. *J. Chem. Soc. Chem. Commun.* **1994**, 474. Bonar-Law, R. P. *J. Am. Chem. Soc.* **1995**, *117*, 12397.
- ²⁰ Benson, D. R.; Valentekovich, R.; Diederich, F. *Angew. Chem.* **1990**, *102*, 213.
- ²¹ Reek, J. N. H.; Elemans, J. A. A. W.; Nolte, R. J. M. *J. Org. Chem.* **1997**, *62*, 2234.
- ²² Reek, J. N. H. Ph. D. Thesis, Nijmegen, The Netherlands, **1996**.
- ²³ Coolen, H. K. A. C.; van Leeuwen, P. W. N. M.; Nolte, R. J. M. *Angew. Chem. Int. Ed. Engl.* **1992**, *31*, 905.
- Coolen, H. K. A. C.; van Leeuwen, P. W. N. M.; Nolte, R. J. M. *J. Am. Chem. Soc.*, **1995**, *117*, 11906. Coolen, H. K. A. C.; van Leeuwen, P. W. N. M.; Nolte, R. J. M. *J. Org. Chem.* **1996**, *61*, 4739.
- ²⁴ Landini, D.; Montanari, F.; Rolla, F. *Synthesis* **1978**, 223-225.
- ²⁵ Sijbesma, R. P.; Nolte, R. J. M. *Recl. Trav. Chim. Pays-Bas* **1993**, *112*, 643-647
- ²⁶ Recent work revealed that also **H₂1** can be synthesized in approximately 25% yield by directly reacting **6** and **5,10,15,20-tetrakis(meso-o-hydroxyphenyl)porphyrin**. Bijsterveld, E. J. A., unpublished results.
- ²⁷ For a paper concerning (de)shielding effects caused by the porphyrin ring current, see: Cross, K. J.; Crossley, M. *J. Aust. J. Chem.* **1992**, *45*, 991.
- ²⁸ Most probably the rotation of the crown ether spacers, caused by the lifting of the porphyrin, is responsible for these conformational changes, see: Schuurman, R. J. W. Ph. D. Thesis, **1994**.
- ²⁹ Hunter, C. A.; Sanders, J. K. M. *J. Am. Chem. Soc.* **1990**, *112*, 5525.
- ³⁰ See for example: Stoddart, J. F. *Pure Appl. Chem.* **1988**, *60*, 467, and references cited therein. Ashton, P. R.; Philp, D.; Reddington, M.; Slawin, A. M. Z.; Spencer, N.; Stoddart, J. F.; Williams, D. J. *J. Chem. Soc. Chem. Commun.* **1991**, 1680. Anelli, P. L.; Ashton, P. R.; Ballardini, R.; Balzani, V.; Delgado, M.; Gandolfi, M. T.; Goodnow, T. T.; Kaifer, A. E.; Philp, D.; Pietraszkiewicz, M.; Prodi, L.; Reddington, M. V.; Slawin, A. M. Z.; Spencer, N.; Stoddart, J. F.; Vicent, C.; Williams, D. J. *J. Am. Chem. Soc.* **1992**, *114*, 193. Ashton, P. R.; Ballardini, R.; Balzani, V.; Boyd, S. E.; Credi, M. T.; Gandolfi, M. T.; Gomez-Lopez, M.; Iqbal, S.; Philp, D.; Preece, J. A.; Prodi, L.; Ricketts, H. G.; Stoddart, J. F.; Tolley, M. S.; Venturi, M.; White, A. J. P.; Williams, D. *J. Chem. Eur. J.* **1997**, *3*, 152.
- ³¹ Schenning, A. P. H. J.; de Bruin, B.; Kooijman, H.; Spek, A. L.; Nolte, R. J. M. *Angew. Chem. Int. Ed. Engl.* **1995**, *34*, 2132.
- ³² Part of this work has appeared as a preliminary communication: Rowan, A. E.; Aarts, P. P. M.; Koutstaal, K. W. *M. Chem. Commun.* **1998**, 611.
- ³³ Gunter, M. J.; Hockless, D. C. R.; Johnston, M. R.; Skelton, B. W.; White, A. H. *J. Am. Chem. Soc.* **1994**, *116*, 4810.
- ³⁴ For the complex a charge transfer band around 400-430 nm in the UV-vis spectrum is expected (see ref. 33), which, due to its low extinction coefficient, is obscured by the strongly absorbing Soret band of the porphyrin hosts.
- ³⁵ Calculations on **G1** have shown that the positive charge density is concentrated on the methyl groups and on the carbon atoms *ortho* and *para* to the nitrogen atom of the bipyridinium ring. This makes the protons on these carbon atoms more acidic and as a result more prone to CH \cdots O or CH \cdots π hydrogen bonding interactions, see ref. 31.
- ³⁶ Moore, S. S.; Cram, D. J. *J. Am. Chem. Soc.* **1977**, *99*, 2564.
- ³⁷ Gunter, M. J.; Jaynes, T. P.; Johnston, M. R.; Turner, P.; Chen, Z. *J. Chem. Soc. Perkin Trans I* **1998**, 1945.
- ³⁸ Reek, J. N. H.; Priem, A. H.; Engelkamp, H.; Rowan, A. E.; Elemans, J. A. A. W.; Nolte, R. J. M. *J. Am. Chem. Soc.* **1997**, *119*, 9956.
- ³⁹ It is well-known that a ligand (e.g. water, methanol, or an aldehyde) can axially coordinate to a zinc porphyrin. The increase in K_a -value for the complex between **Zn2** and **G4** when compared to the complex with **G3** is significantly larger than for the complexes in which **H₂2** is involved, implying some further stabilizing interactions.
- ⁴⁰ Shifts in the carbonyl stretching vibrations of the guest in the infrared spectrum were difficult to observe due to overlap with the carbonyl stretching vibrations of the host molecules.
- ⁴¹ This 'cavity-effect' was already observed in host **11** (see ref. 38) and apparently also plays an important role in the case of the porphyrin cavities. Similar cavity effects have been reported, amongst others, for the so-called 'picnic-basket' porphyrins, see: Collman, J. P.; Brauman, J. I.; Fitzgerald, J. P.; Hampton, P. D.; Namata, Y.;

- Sparapany, J. W.; Ibers, J. A. *J. Am. Chem. Soc.* **1988**, *110*, 3477. Collman, J. P.; Brauman, J. I.; Fitzgerald, J. P.; Sparapany, J. W.; Ibers, J. A. *J. Am. Chem. Soc.* **1988**, *110*, 3486.
- ⁴² Similar high values were found for the binding of pyridine to zinc picket fence porphyrins in toluene solution. See: Imai, H.; Kyuno, E. *Inorg. Chem.* **1990**, *29*, 2416. Imai, H.; Nakagawa, S.; Kyuno, E. *J. Am. Chem. Soc.* **1992**, *114*, 6719. Uemori, Y.; Takinami, S.; Takahashi, A.; Munakata, H.; Imai, H.; Nakagawa, S.; Kyuno, E. *Inorg. Chim. Acta* **1994**, *225*, 157. Imai, H.; Munakata, H.; Takahashi, A.; Nakagawa, S.; Uemori, Y. *Chem. Lett.* **1997**, 819.
- ⁴³ 4-Pyridon is known to self-assemble in chloroform to yield hydrogen-bonded oligomers. The breaking up of these oligomers costs energy which will lead to a lower association constant, see: Beak, P.; Covington, J. B.; Smith, S. G.; Matthew White, J.; Zeigler, J. M. *J. Org. Chem.* **1980**, *45*, 1354.
- ⁴⁴ Lehn, J.-M. *Science* **1985**, *227*, 849. Feiters, M. C. in: *Comprehensive Supramolecular Chemistry*. Atwood, J. L.; Davies, J. E. D.; MacNicol, D. D.; Vögtle, F.; Reinhoudt, D. N.; Lehn, J.-M. Eds.; Elsevier Science Ltd., Pergamon: Elmsford, **1996**; Vol. 10, 267-360.
- ⁴⁵ Cram, D. J. *Angew. Chem.* **1988**, *100*, 1041.
- ⁴⁶ Koshland, D. E. Jr. *Proc. Natl. Acad. Sci. U.S.A.* **1958**, *44*, 98.
- ⁴⁷ Review: Nabeshima, T. *Coord. Chem. Rev.* **1996**, *148*, 151.
- ⁴⁸ Echegoyen, L. E.; Yoo, H. K.; Gatto, V. J.; Gokel, G. W.; Echegoyen, L. *J. Am. Chem. Soc.* **1989**, *111*, 2440.
- ⁴⁹ Shinkai, S. *Top. Curr. Chem.* **1984**, *121*, 67. Arad-Yellin, R.; Green, B. S. *Nature* **1994**, *371*, 320.
- ⁵⁰ Beer, P. D. *Chem. Soc. Rev.* **1989**, *18*, 409. Nabeshima, T.; Furusawa, H.; Yano, Y. *Angew. Chem. Int. Ed. Engl.* **1994**, *33*, 1750.
- ⁵¹ Rebek, J. Jr.; Costello, T.; Marshall, J.; Wattlely, R.; Gadwood, R. C.; Onan, K. *J. Am. Chem. Soc.* **1985**, *107*, 7481. Ebmeyer, F.; Rebek, J. Jr. *Angew. Chem.* **1990**, *102*, 1191. Schneider, H. -J.; Ruf, D. *Angew. Chem.* **1990**, *102*, 1192. Haino, T.; Katsutani, Y.; Aki, H.; Fukazawa, Y. *Tetrahedron Lett.* **1998**, *39*, 8133. Kubo, ??; Murai, J.; Yamanaka, J.; Tokita, S.; Ishimara, Y. *Tetrahedron Lett.* **1999**, *40*, 6019. Al-Sayah, M. H.; Branda, N. R. *Angew. Chem. Int. Ed.* **2000**, *39*, 945. Ikeda, M.; Tandia, T.; Takeuchi, M.; Shinkai, S. *Org. Lett.* **2000**, *2*, 1803.
- ⁵² Sijbesma, R. P.; Wijmenga, S. S.; Nolte, R. J. M. *J. Am. Chem. Soc.* **1992**, *114*, 9807.
- ⁵³ Reek, J. N. H.; Sijbesma, R. P.; Nolte, R. J. M. *Tetrahedron Lett.* **1994**, *35*, 2801.
- ⁵⁴ Johnson, C. S., Jr.; Bovey, F. A. *J. Chem. Phys.* **1958**, *29*, 1012.
- ⁵⁵ Elemans, J. A. A. W.; Claase, M. B.; Aarts, P. P. M.; Rowan, A. E.; Schenning, A. P. H. J.; Nolte, R. J. M. *J. Org. Chem.* **1999**, *34*, 7009.
- ⁵⁶ Reek, J. N. H.; Engelkamp, H.; Rowan, A. E.; Elemans, J. A. A. W.; Nolte, R. J. M. *Chem. Eur. J.* **1998**, *4*, 716.
- ⁵⁷ A plot of $\ln(K(ss \rightleftharpoons sa))$ versus $1/T$ gave a straight line.
- ⁵⁸ Hunter, C. A.; Sanders, J. K. M. *J. Am. Chem. Soc.* **1990**, *112*, 5525.
- ⁵⁹ A similar collapsing has been observed before in the case of a palladium complex which was connected via flexible crown ether spacers to a diphenylglycoluril molecule. See: Niele, F. G. M.; Nolte, R. J. M. *J. Am. Chem. Soc.* **1988**, *110*, 172.
- ⁶⁰ The cavities of the *aa* and the *sa* conformers are too small to accommodate chloroform molecules.
- ⁶¹ NMR titrations are not suitable to study binding processes with $K_a > 1 \times 10^5 \text{ M}^{-1}$.
- ⁶² Schenning, A. P. H. J.; de Bruin, B.; Kooijman, H.; Spek, A. L.; Nolte, R. J. M. *Angew. Chem. Int. Ed. Engl.* **1995**, *34*, 2132. Rowan, A. E.; Aarts, P. P. M.; Koutstaal, K. W. M. *Chem. Commun.* **1998**, 611.
- ⁶³ Elemans, J. A. A. W. Unpublished results.
- ⁶⁴ CHARMM version 22.0. Revision 920911, Resident and Fellows of Harvard College, **1984**, **1992**, with the use of template charges.
- ⁶⁵ © Erithacus Software Ltd., **1989-1992**, by Robin J. Leatherbarrow.
- ⁶⁶ Tsukube, H.; Furuta, H.; Takeda, Y.; Kudo, Y.; Inoue, Y.; Liu, Y.; Sakamoto, H.; Kimura, K. in *Comprehensive Supramolecular Chemistry*, Atwood, J. L.; Davies, J. E. D.; MacNicol, D. D.; Vögtle, F.; Ripmeester, J. A.; Lehn, J.-M. Eds., Elsevier Science Ltd., Pergamon **1996**, Vol. 8, 425-482.
- ⁶⁷ Reek, J. N. H.; Rowan, A. E.; Crossley, M. J.; Nolte, R. J. M. *J. Org. Chem.* **1999**, *64*, 6653.
- ⁶⁸ Den Hertog, H. J.; Van Ammers, M.; Schukking, S. *Recl. Trav. Chim. Pays-Bas* **1955**, *74*, 1171.

Chapter 10

Porphyrin Clips as Epoxidation Catalysts

10.1 Introduction

The mono-oxygenase Cytochrome P450 (Figure 10.1) selectively binds substrates in the direct proximity of an Fe(III) protoporphyrin IX molecule. It catalyzes the reductive activation of molecular oxygen and the incorporation of one of the oxygen atoms into the bound substrate and reduction of the other one to water.¹ In the human body the enzyme is of fundamental importance since it is involved in the oxidation of a variety of xenobiotics, resulting in their excretion. Much research has been devoted to the elucidation of the complicated working mechanisms of the enzyme, and it is therefore that several simplified synthetic models have been constructed.² Many of these utilize inexpensive and more reactive Mn(III) porphyrins as catalysts in association with a wide variety of oxygen donors, such as iodosylarenes,³ hydrogen peroxide,⁴ alkylhydroperoxides,⁵ periodate,⁶ peracids,⁷ peroxomonosulfates,⁸ hypochlorites,^{9,10} and molecular oxygen in combination with a reducing agent.¹¹

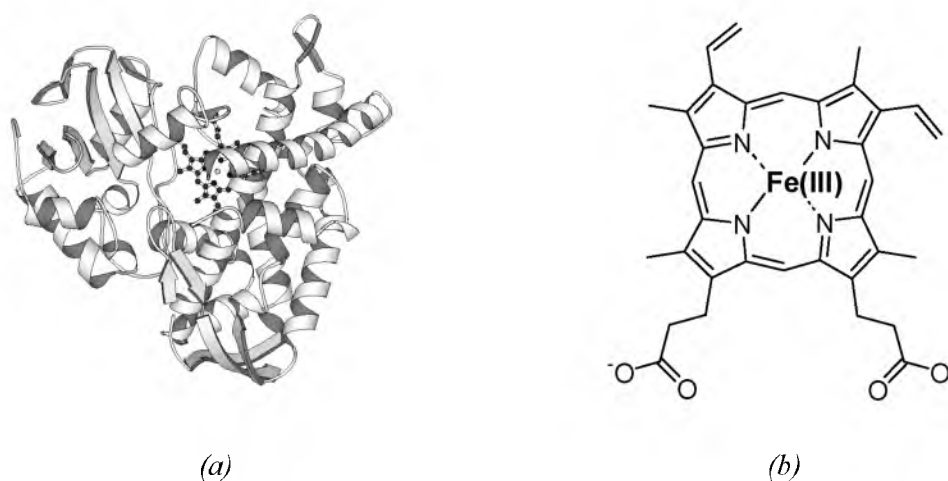


Figure 10.1 (a) X-ray crystal structure of Cytochrome P450 from *Pseudomonas Putidas*, highlighting the porphyrin prosthetic group. (b) Structure of Fe(III) protoporphyrin IX.

Porphyrin catalysts have been functionalized with straps or caps to establish an environment in which the oxygen transfer from the metal to the substrate is under steric control.¹² Following this approach, regio- and stereoselective¹³ oxidation has been achieved, in which in the latter case for example *cis*-stilbene has been oxidized to the *cis*- and *trans*-epoxides with a major preference for the production of the former isomer.¹⁴ Other approaches involve the coupling of a metalloporphyrin to a known cavity molecule. Porphyrin-functionalized cyclodextrins¹⁵ and cyclophanes¹⁶ have been synthesized which selectively bind substrates and oxidize them with enhanced rates or regio- and stereoselectivities (see also Chapter 9).

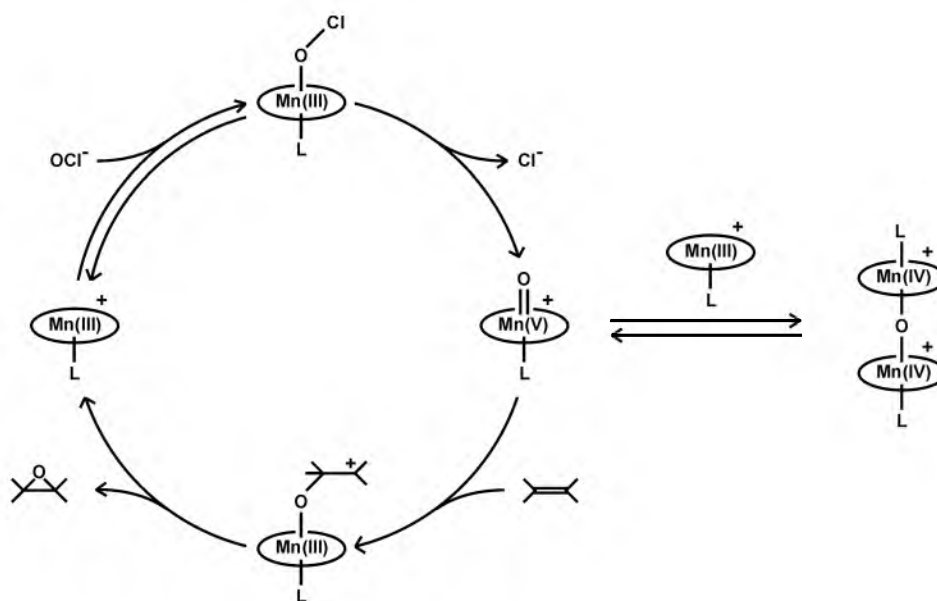
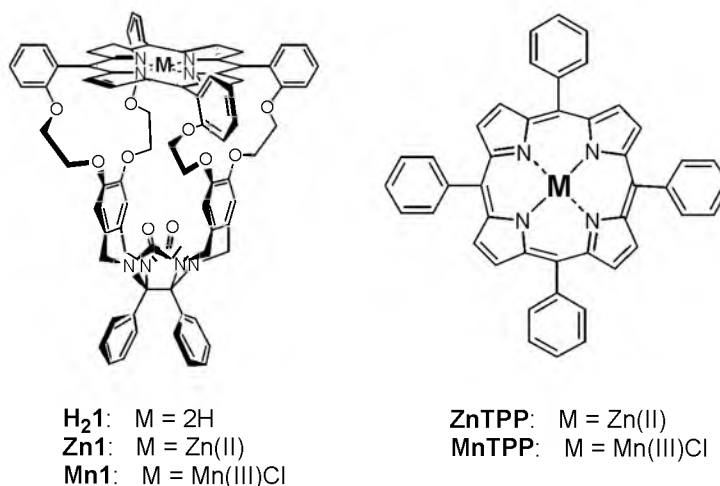


Figure 10.2 Catalytic cycle of the epoxidation of olefins catalyzed by the Mn(III) porphyrin / NaOCl system.

Several studies towards alkene oxidation utilizing a manganese porphyrin catalyst and NaOCl as oxidant in the biphasic water-dichloromethane system have been carried out by our group.^{17,18} These studies have led to the proposal of the reaction mechanism outlined in Figure 10.2. It starts with the coordination of a hypochlorite ion to the manganese center. The consecutive splitting-off of the chloride anion is believed to be the rate-determining step.¹⁹ The resulting active particle has been proposed to be a [(P)Mn(V)=O]⁺ species (P = porphyrin), which can react with an incoming alkene substrate to yield the epoxide product, after which the [(P)Mn(III)]⁺ catalyst is regenerated. An undesired side-reaction in this catalytic cycle is the decomposition of the catalyst by reaction of the [(P)Mn(V)=O]⁺ species with a [(P)Mn(III)]⁺ complex, resulting in the formation of a μ-oxobridged [(P)Mn(IV)-O-(P)Mn(IV)]²⁺ dimer. This dimer is unreactive in further catalytic epoxidation reactions and gradually decomposes, which is evident from the decolourization of the brown reaction mixture.

In this chapter, initial catalytic epoxidation studies are described using the cavity-containing manganese porphyrin clip **Mn1** (Chart 10.1) as the catalyst. This molecule consists of a well-documented molecular clip²⁰ equipped with a porphyrin roof situated symmetrically above the clip cavity.²¹ Whilst the free base host **H₂1** has been applied in the construction of rotaxanes,²² it was our intention to utilize its Mn(III) derivative as an olefin epoxidation catalyst. The catalytic

Chart 10.1



properties of **Mn1**, applying the biphasic dichloromethane/aqueous NaOCl system previously used by our group^{17,18} and other groups,⁹ will be compared to those of **MnTPP** with regard to catalyst activity and stability.

10.2 Synthesis

Porphyrin clip **Mn1** (Chart 10.1) was synthesized from its free base analogue **H₂1** (see Chapter 9) by a standard metallation reaction with manganese diacetate tetrahydrate in dimethylformamide. The metalloclip was obtained in nearly quantitative yield after purification by column chromatography and precipitation in *n*-hexane.

10.3 Catalytic reactions

10.3.1 Strong binding of axial ligands

The Fe(III) protoporphyrin in Cytochrome P450 features axial coordination by a cysteine thiolate ligand, which is believed to be essential in the splitting of the O-O bond of bound molecular oxygen.²³ Most of the synthetic mimics of the enzyme, however, utilize more stable pyridine, imidazole, or phenolate derivatives to increase the activity and stereoselectivity of the catalytic center. In previous studies in which **MnTPP** was used as the catalyst, it turned out that axial ligands enhanced the activity of the catalyst, since their electron donating properties facilitate the formation and stabilization of the reactive high-spin Mn(V)-oxo species (see Figure 10.2).²⁴ A drawback was that for optimal results a large excess (500 equivalents) of axial ligand was required, because of the relatively weak binding of the latter to the porphyrin metal. Previous work has revealed, however, that host **Zn1** complexes pyridine derivatives within its cavity with very high association constants due to stabilizing π - π interactions and cavity filling effects (see Chapter 9). In chloroform, pyridine is complexed by **Zn1** with an association constant of $K_a = 1.1 \times 10^5 \text{ M}^{-1}$, a value which is several orders of magnitude larger than the association constant

Chart 10.2

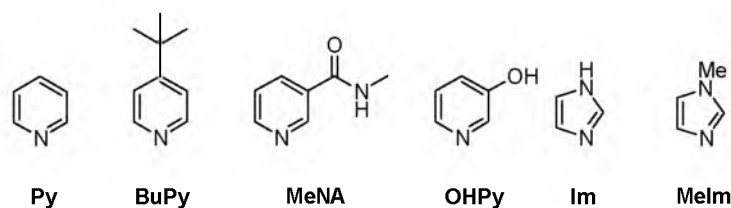


Table 10.1 Association constants K_a (M^{-1}) and binding free energies ΔG ($kJ\ mol^{-1}$, in parenthesis) of host-guest complexes between **Zn1** or **ZnTPP** and various axial ligands.^a

Ligand ^b	Porphyrin	
	Zn1	ZnTPP
Py	1.1×10^5 ^c (-28.8)	920 ^{d,e} (-16.9)
BuPy	625 ^{d,e} (-15.9)	1.5×10^4 ^b (-23.8)
MeNA	6.1×10^4 ^c (-27.3)	2.7×10^3 ^e (-19.6)
OHPy	3.0×10^7 ^f (-42.7)	1.3×10^3 ^e (-17.8)
Im	3.2×10^5 ^c (-31.4)	— ^g
MeIm	7.0×10^4 ^c (-27.6)	— ^g

^aIn $CHCl_3$ solution, 298 K. ^bSee chart 12.1 for abbreviations. ^cEstimated error 20%. ^dEstimated error 10%. ^eIn $CDCl_3$ solution. ^fEstimated error 50%. ^gNot determined.

of this ligand with **ZnTPP** ($K_a = 920\ M^{-1}$). To investigate whether also other ligands would bind strongly in the cavity of the porphyrin clip, binding studies of various pyridine and imidazole derivatives (Chart 10.2) with **Zn1** were carried out and compared to binding of these ligands with the reference compound **ZnTPP**. The zinc complexes were studied instead of the paramagnetic Mn(III) complexes, in order to be able to use NMR spectroscopy in the structural analysis and binding properties of the compounds.²⁵ The results are summarized in Table 10.1. In contrast to the strong binding of **Py** in **Zn1**, the K_a between the bulky ligand 4-*t*-butylpyridine (**BuPy**) and this host is low. This is attributed to the fact that **BuPy** can only bind to the outside of **Zn1** and hence does not experience the stabilizing effects of the cavity, which **Py** does. This binding at the outside of the cavity was also evident from the absence of any shifts of the receptor side-wall and crown ether spacer proton signals in the NMR spectrum upon addition of the ligand. As can be seen in Table 10.1, *meta*-substitution of the pyridine ring with a hydroxy group (**OHPy**) causes an enormous increase in binding strength because this ligand can coordinate with its pyridine nitrogen atom to the zinc center, and simultaneously form a strong hydrogen bond with one of the carbonyl groups of **Zn1**. In contrast to **OHPy**, *N*-methylnicotinamide (**MeNA**) complexes much weaker to **Zn1** because of a less favourable geometry of the hydrogen bond between the NH-function of the guest and the carbonyl group of the host. Its binding constant is similar to that of **Py**. Imidazole (**Im**) forms a stronger complex with **Zn1** than pyridine, which is not unexpected since the latter ligand is a weaker nucleophile. Molecular modeling studies revealed that **Im** is too small to coordinate to the zinc ion and at the same time form a hydrogen bond with one of the carbonyl groups of the clip. This makes that its binding constant is lower than that of **OHPy**. A clear drop in binding strength was observed, however, when *N*-methylimidazole (**MeIm**) instead of **Im** was used as the ligand in **Zn1**.

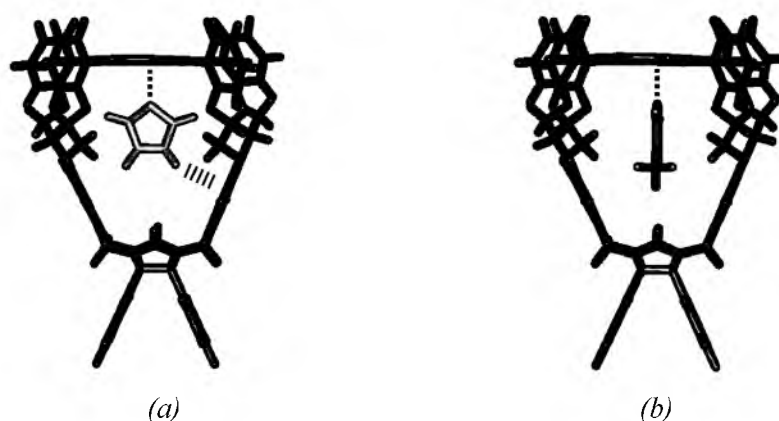


Figure 10.3 (a) Computer-modeled host-guest geometry of the complex between **Zn1** and **Im**, illustrating the possible $N-H \cdots \pi$ interaction between one side-wall of the host and the guest. (b) Idem for the host-guest complex between **Zn1** and **MeIm**.

Surprisingly, the ^1H NMR spectra of the 1:1 host-guest complexes between **Zn1** and the two imidazoles in CDCl_3 were completely different. In the spectra of the complex between **Zn1** and **MeIm**, all crown ether proton signals and the cavity side-wall proton signals were shifted strongly upfield when compared to these signals in the free host. This points to a host-guest geometry in which the aromatic surface of **MeIm** is oriented parallel to the cavity side-walls of **Zn1** (Figure 10.3b), similar to the geometry of the host-guest complexes between **Zn1** and the pyridine ligands. In contrast to this, in the complex between **Zn1** and **Im** the crown ether and side-wall proton signals were only slightly upfield shifted. This suggests that the aromatic surface of **Im** is oriented perpendicular to the aromatic surface of the cavity side-walls (Figure 10.3a). It is not unlikely that the reason for this deviating geometry is the presence of an $N-H \cdots \pi$ interaction²⁶ between one of the cavity side-walls²⁷ and the **Im** NH proton.²⁸

The strong binding of axial ligands in **Zn1** is of great interest with regard to the catalytic epoxidation reactions using the manganese analogue as the catalyst, since it can be expected that only one equivalent of such a ligand will be needed to achieve a 99+% binding to the porphyrin metal. To investigate this, catalytic epoxidation reactions were carried out with host **Mn1** and porphyrin **MnTTP** as reference compound (Figure 10.4, Approach A). The results are described in the following section.

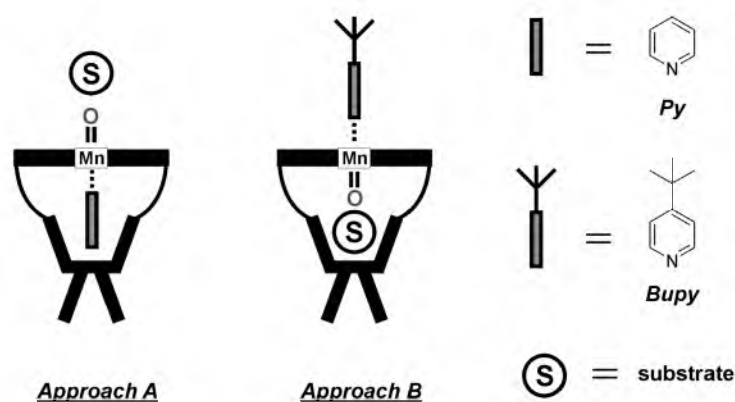


Figure 10.4 Two approaches in which **Mn1** is used as an epoxidation catalyst in combination with **Py** or **Bupy** as the axial ligand.

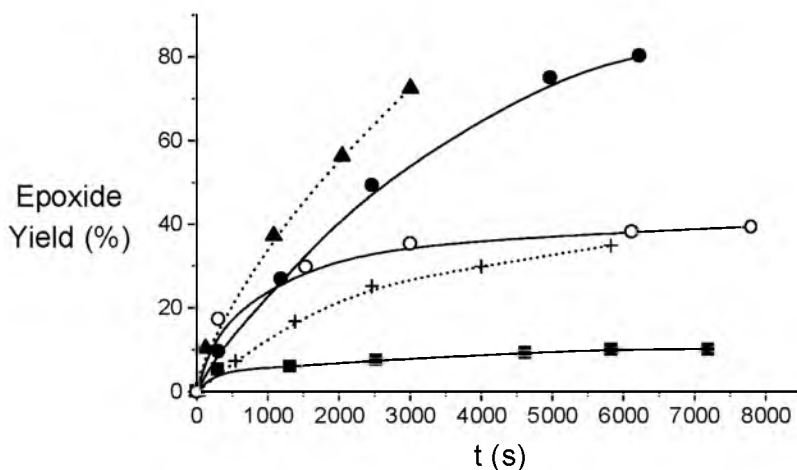


Figure 10.5 Epoxidation of α -pinene using one equivalent of an axial ligand. **Mn1-Im** (\blacktriangle), **Mn1-Py** (\bullet), **Mn1-OHPy** (\circ), **Mn1-MeIm** ($+$), **MnTPP-Py** (\blacksquare).

10.3.2 Activation of the catalyst

The effect of the supramolecular activation of **Mn1** by *one* equivalent of **Py**, compared to **MnTPP** using standard conditions (see experimental section) was studied in the epoxidation of α -pinene (Table 10.2, Figure 10.5). **Mn1** was found to display a 10 fold higher initial rate than **MnTPP**. As a result of this it required more than 10 hours for the reaction to be completed in the case of **MnTPP**, whereas it took only 2 hours in the case of **Mn1**.²⁹ Further experiments revealed that in the epoxidation of α -pinene the initial epoxidation rate is related to the binding constant of the axial ligand, *i.e.* the rate increases when the K_a -value of the ligand (measured by the related host **Zn1**) becomes higher (Table 10.3). It is remarkable that the most strongly binding ligand **OHPy** gives the highest initial rate, but also the lowest yield after 3 h. A reason for this might be the gradual expulsion of the ligand out of the cavity of **Mn1** due to deprotonation by the strongly basic OCl^- species. This deprotonation apparently does not occur when **Im** is used, and in the case of this ligand the epoxidation reaction was complete within 1 hour, yielding 82% of epoxide. In addition to a high epoxidation rate, an advantage of the strong binding of **Im** is that its degradation (by oxidation), which in other systems has been observed to occur at already relatively low concentrations,^{18,30} is minimal. Apparently, its binding in the cavity of **Mn1** protects it from this undesired reaction. The **Mn1-MeIm** system, finally, displayed a lower epoxidation rate than the **Mn1-Py** system, which is in line with the difference in binding strengths between these ligands.

Table 10.2 Epoxidation of α -pinene using **Mn1** or **MnTPP** as the catalyst.^a

Axial ligand	Catalyst			
	Mn1		MnTPP	
	Rate ^b	Yield ^c	Rate ^b	Yield ^c
Py (1 equiv.)	12.0	81	1.2	10
Bupy (500 equiv.)	10.9	82	12.9	80

^aStandard reaction conditions. ^bInitial rate, $\times 10^5 / \text{mol dm}^{-3} \text{ s}^{-1}$, estimated error 10%. ^cYield (%) after 3 h.

Table 10.3 Effect of axial ligand binding strength on the initial rate and epoxide yield in the epoxidation of α -pinene catalyzed by **Mn1**.^a

Axial ligand (1 equiv.)	K_a (M^{-1}) with Zn1	Rate ^b	Yield ^c
Py	1.1×10^5	12.0	81
OHPy	3.0×10^7	34.0	44
Im	3.2×10^5	17.0	82
MeIm	7.0×10^4	7.7	38

^aStandard reaction conditions. ^bInitial rate, $\times 10^5 / mol\ dm^{-3}\ s^{-1}$, estimated error 10%. ^cYield (%) after 3 h.

10.3.3 Stabilization of the catalyst

A major drawback of the **MnTPP** catalyst is its instability. This has been attributed to the formation of $[(P)Mn(IV)-O-Mn(IV)(P)]^{2+}$ μ -oxo dimeric structures (Figure 10.2), which are unreactive in further catalysis and decompose due to electrophilic attack on the electron-rich *meso*-positions of the porphyrin ring. When a reactive substrate is present, it generally competes successfully with a $[(P)Mn(III)X]^+$ molecule for the reactive Mn(V)-oxo species. When, however, all the substrate is converted, the catalyst rapidly decomposes which is visible from the bleaching of the brown reaction mixture. This decomposition also occurred in the case of the systems of **Mn1** with one equivalent of a strongly binding axial ligand present. To prevent this decomposition, the bulky axial ligand **Bupy** was used in combination with **Mn1**. It was rationalized that coordination of this ligand (which does not fit within the cavity of the catalyst) would efficiently prevent μ -oxo dimer formation, also after all of the substrate had been converted, since the other face of the porphyrin is protected by the receptor cavity (Figure 10.4, Approach B). Indeed, when the epoxidation of α -pinene using **Mn1** was carried out in the presence of 500 equivalents of **Bupy** (Table 10.2), catalyst destruction was prevented. This was already indicated by the fact that the organic layer retained its brown colour, even after stirring the reaction mixture in the absence of substrate for more than a week. More importantly, however, was the observation that freshly added portions of substrate were epoxidized with similar initial rates as the first portion without an apparent deterioration of the catalyst, thus allowing high turnover numbers per **Mn1** molecule (> 1000).³¹ When **MnTPP** was used as the catalyst in combination with **Bupy** under the same conditions, this stabilization did not occur and the catalyst decomposed rapidly.

10.3.4 Preliminary kinetic studies

The brown colour of the catalytic epoxidation mixtures is a characteristic feature of high-valent (IV or V) manganese porphyrins.³² To investigate the kinetic behaviour of **Mn1** and **MnTPP** upon treatment with NaOCl, UV-vis experiments in which the amount of axial ligand was varied were carried out. When a solution of **Mn1** in CH_2Cl_2 , without an axial ligand present, was thoroughly mixed with an aqueous NaOCl solution, the colour of the organic solution instantaneously turned from green into brown. This was accompanied by several changes in the UV-vis spectrum, the most important ones being a blueshift of the porphyrin Soret band from 480 to 426 nm and the formation of a new band at 552 nm. Based on similar measurements by Van der Made,³³ Groves,³⁴ and Bruice,³⁵ the structure (P)Mn(IV)-OCl is proposed for the formed species. Upon standing of the mixture, the intensities of the bands at 426 and 552 nm gradually decreased with a concomitant increase in intensity of the band at 480 nm, corresponding to the

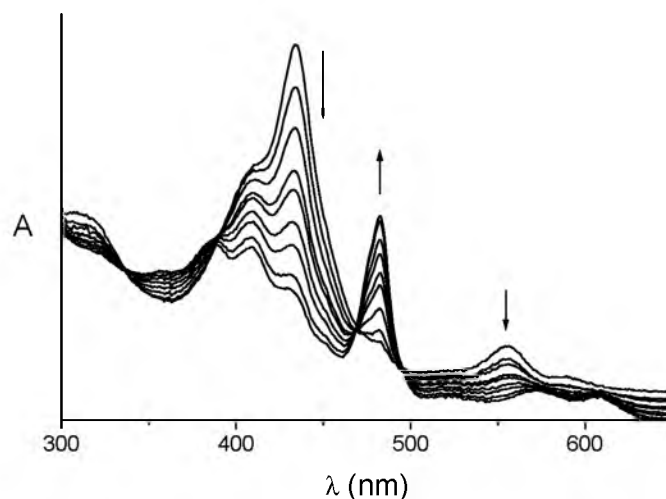


Figure 10.6 UV-vis absorption spectral changes observed upon standing of a CH_2Cl_2 solution of **Mn1** without an axial ligand present, after mixing with an aqueous NaOCl solution.

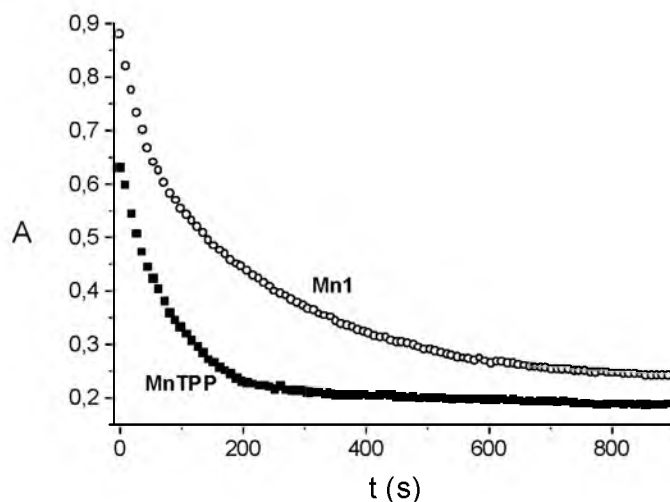


Figure 10.7 Decay of the Soret band of the $(P)\text{Mn(IV)-OCl}$ species of **Mn1** and **MnTPP** (without axial ligand).

$[(P)\text{Mn(III)}]^+$ species (Figure 10.6). The presence of several isosbestic points during this process indicates that the conversion does not involve the accumulation of any intermediates. The decay process was monitored by recording UV-vis spectra of the organic solution at small time intervals (of 9 s.). An identical experiment was carried out with **MnTPP** as the porphyrin. The absorption of the bands corresponding to the $(P)\text{Mn(IV)-OCl}$ species plotted versus time gave characteristic curves (Figure 10.7), which could be fitted to a single exponential decay.³⁶ From the k_{decay} -values (Table 10.4) it can be seen that the OCl^- complex of **Mn1** decays much slower than that of **MnTPP**, suggesting that the former complex is more stable under the applied reaction conditions. This might be a result of the stabilizing effect of the cavity in which the OCl^- ion is preferentially complexed within the cavity of **Mn1**. Another possibility is that in

Table 10.4 First order rate constants for the decay of the (P)Mn(IV)-OCl species of **Mn1** and **MnTPP** in the presence of different axial ligands.^a

Axial ligand	Number of equivalents	$k_{\text{decay}}/10^{-3} \text{ s}^{-1}$	
		Mn1	MnTPP
Without axial ligand	0	2.13	4.93
Py	5	1.49	— ^b
Py	25	1.34	— ^b
Py	50	1.03	5.12
Py	500	2.21	2.27
Py	5000	2.41	2.81
Bupy	500	4.38	2.19
Bupy	5000	5.86	3.70

^aEstimated error 10%, ^bNot determined.

the case of **Mn1** simultaneously with the binding of OCl⁻ a Na⁺ counter ion is bound between the crown ether spacers of the complex, which implies that the host acts as its own phase-transfer catalyst. When **Py** was used as an axial ligand, the k_{decay} -values of **Mn1** in all cases were lower than those of **MnTPP** (Table 10.4). For both **Mn1-Py** and **MnTPP-Py**, there appears to be a minimum in the k_{decay} -value (Table 10.4). These minima roughly correspond to a 1:1 binding of the ligand to the metal.³⁷ The measured k_{decay} -values suggest that the **Py-Mn1-OCl** species is more stable than its **MnTPP** analogue. This might be the result of the very strong binding of **Py** in **Mn1**. When **Bupy** is used as the axial ligand, the k_{decay} -values of the complexes of OCl⁻ with **Mn1** are higher than those with **MnTPP**. Assuming that the outside of the cavity of **Mn1** is shielded by the **Bupy** ligand, the decreased stability of the **Mn1-Bupy** complex can be explained by a repulsion between the OCl⁻ ion and the crown ether spacers of the host. This explanation is, however, in contrast with the abovementioned stabilization of the complex by cavity effects. Detailed kinetic studies will be necessary to unravel the exact factors that cause the differences between the two catalysts.

10.4 Concluding remarks

In this chapter it is demonstrated that by a unique supramolecular effect only one equivalent of a strongly binding axial ligand is needed to activate the **Mn1** catalyst for the epoxidation of simple olefins. In a different approach, coordination of a bulky axial ligand on the outside of **Mn1** strongly enhances the stability of the catalyst by protecting it from oxidative decomposition. Current research is focused on the functionalization of Mn(III) porphyrins with molecular clip receptors on both faces, so that the effects of supramolecular activation and catalyst protection can be combined.³⁸

It is worthwhile to investigate whether **Mn1** can be applied as a substrate-selective catalyst, *i.e.* by actively binding substrates in its cavity and subsequently converting and releasing them. A substrate like 3,5-dihydroxystyrene would be an excellent candidate for this, although related research has demonstrated that aromatic hydroxy substituents in many cases are not compatible with the oxidation reaction conditions.³⁹ Other substrate candidates are viologen derivatives. In the previous chapter it has been shown that **Zn1** is an excellent host for these guests, and preliminary UV-vis and NMR experiments have revealed that these guests are also complexed

by **Mn1**.⁴⁰ After quarterarization of the N-atoms of 4,4'-dipyridines with side-chains containing olefinic double bonds, the obtained compounds should be suitable as substrates in epoxidation reactions catalyzed by **Mn1**.

10.5 Experimental section

10.5.1 Materials and methods

DMF was dried over BaO for one week and then vacuum distilled; the first 30% of the distillate was removed. Dichloromethane was distilled from CaH₂. Pyridine was distilled from KOH pellets. ¹H NMR and UV-vis host-guest complexation studies were carried out as described in Chapter 9. For an overview concerning general techniques see Section 2.6.1.

10.5.2 Catalytic epoxidation reactions

The epoxidation of alkenes by Mn(III) porphyrin catalysts and NaOCl was performed in a two-phase water-dichloromethane system. As an internal standard for the GLC-analyses 1,3,5-tri-*t*-butylbenzene (an inert molecule which cannot block the cavity of **Mn1**) was used. The reaction conditions were as follows: to a CH₂Cl₂ solution (0.65 mL) in a Schlenk tube containing the substrate (0.626 M), the catalyst (2.5 mM), the phase transfer catalyst tetrabutylammonium chloride (5 mM), the appropriate amount of axial ligand, and the internal standard (1,3,5-tri-*t*-butyl benzene (0.17 M) was added an aqueous NaOCl solution (2 mL, 0.6 M). The mixture was stirred at a constant high rate under nitrogen for 3 h, and during the course of the reaction samples were taken from the organic layer which were analyzed by GLC and ¹H NMR. The epoxidation products were identified by comparison with authentic samples.

10.5.3 UV-vis kinetic studies

A UV cuvet containing a solution of **MnTPP** or **Mn1** in CH₂Cl₂ (1.5 mL, 9 × 10⁻⁶ M⁻¹) was thoroughly mixed with an aqueous NaOCl solution (1.5 mL, 0.6 M). The CH₂Cl₂ and aqueous layer were separated and over a period of 15 min. every 9 s a UV-vis spectrum was recorded of the organic solution. The decay of the absorption of the Mn(IV) species (between 425 and 435 nm) versus time was fitted to a standard mono-exponential decay function. The measurements were carried out *in duplo*.

10.5.4 Synthesis

The syntheses of porphyrin compounds **H₂1** and **Zn1** are described in Chapter 9.

Porphyrin clip **Mn1**:

A degassed solution of **H₂1** (25 mg, 19 μmol) in DMF (2 mL) was heated to reflux. Mn(OAc)₂·4H₂O (10 mg, 41 μmol) was added and the mixture was refluxed under nitrogen for 2 h. After cooling, the solvent was evaporated to dryness and the residue was dissolved in CHCl₃ (10 mL). A saturated aqueous NaCl solution (10 mL) was added and the mixture was stirred vigorously for 16 h. The organic layer was extracted with water (3 × 50 mL) and evaporated to dryness. The residue was purified by column chromatography (silica, CHCl₃/MeOH, 9:1, v/v, R_f = 0.17). The product was dissolved in a minimal amount of CHCl₃ and this solution was added dropwise to stirred *n*-hexane. After centrifugation, the product was dried under vacuum to yield 26 mg (97%) of **Mn1** as dark green needles.

M.p. > 400°C; IR (KBr pellet) ν 3048 (ArH), 2923, 2854 (CH₂), 1696 (C=O), 1600, 1580, 1513, 1462, 1449, 1427 (C=C), 1308, 1279, 1249, 1204 (CH₂), 1107, 1064, 1010 (COC) cm⁻¹; UV-vis (CH₂Cl₂) λ/nm (log(ε/M⁻¹cm⁻¹)): 346 (4.55), 375 (4.66), 409 (4.54), 450 (3.70), 480 (4.96), 527 (3.40), 586 (3.54), 617 (3.50); FAB-MS *m/z* 1397 (M - Cl)⁺.

5,10,15,20-Tetraphenylporphyrinato manganese chloride (**MnTPP**):

This compound was synthesized according to a standard procedure.¹⁸

References and notes

¹ For reviews see: Ortiz de Montellano, P. R., Ed. *Cytochrome P450: Structure, Mechanism and Biochemistry*, 2nd edn. Plenum Press: New York, 1995. Dawson, J. H.; Sono, M. *Chem. Rev.* 1987, 87, 1255. Gunter, M. J.; Turner, P. *Coord. Chem. Rev.* 1991, 108, 115.

- ² For a review see: Feiters, M. C.; Rowan, A. E.; Nolte, R. J. M. *Chem. Soc. Rev.* **2000**, *29*, 375.
- ³ Groves, J. T.; Kruper, W. J.; Haushalter, R. C. *J. Am. Chem. Soc.* **1980**, *102*, 6375. Hill, C. L.; Schardt, B. C.; *J. Am. Chem. Soc.* **1980**, *102*, 6374. Castellino, A. J.; Bruice, T. C. *J. Am. Chem. Soc.* **1988**, *110*, 158. Collman, J. P.; Braman, J. I. *J. Am. Chem. Soc.* **1990**, *112*, 5356. Baciocchi, E.; Boschi, T.; Cassioli, L.; Galli, C.; Jaquinod, L.; Lapi, A.; Paolesse, R.; Smith, K. M.; Tagliatesta, P. *Eur. J. Org. Chem.* **1999**, 3281.
- ⁴ Battioni, P.; Renaud, J. P.; Bartoli, J. F.; Reina-Artiles, M.; Fort, M.; Mansuy, D. *J. Am. Chem. Soc.* **1988**, *110*, 8462.
- ⁵ Mansuy, D.; Battioni, P.; Renaud, J. P. *J. Chem. Soc. Chem. Commun.* **1984**, 1255.
- ⁶ Suslick, K. S.; Acholla, F. V.; Cook, B. R. *J. Am. Chem. Soc.* **1987**, *109*, 2818.
- ⁷ Yuan, L. C.; Bruice, T. C. *J. Am. Chem. Soc.* **1986**, *108*, 1643.
- ⁸ De Poorter, B.; Meunier, B. *J. Chem. Soc. Perkin Trans 2* **1985**, 1735. Cagnina, A.; Campestrini, S.; Di Furia, F.; Ghiotto, P. *J. Mol. Catal. A* **1998**, *130*, 221.
- ⁹ Meunier, B.; Guilmet, E.; de Carvalho, M.-E.; Poilblanc R. *J. Am. Chem. Soc.* **1984**, *106*, 6668.
- ¹⁰ Collman, J. P.; Brauman, J. L.; Meunier, B.; Hayashi, T.; Kodadek, T. *J. Am. Chem. Soc.* **1985**, *107*, 2000. Montanari, F.; Penso, M.; Quici, S.; Vigano, P. *J. Org. Chem.* **1985**, *50*, 4888.
- ¹¹ Tabushi, I.; Koga, N. *J. Am. Chem. Soc.* **1979**, *101*, 6456. Groves, J. T.; Ungashe, S. B. *J. Am. Chem. Soc.* **1990**, *112*, 7796. Schenning, A. P. H. J.; Lutje Spelberg, J. H.; Hubert, D. H. W.; Feiters, M. C.; Nolte, R. J. M. *Chem. Eur. J.* **1998**, *4*, 871.
- ¹² For reviews see: Meunier, B. *Chem Rev.* **1992**, *92*, 1411. Feiters, M. C. in: *Comprehensive Supramolecular Chemistry*. Atwood, J. L.; Davies, J. E. D.; MacNicol, D. D.; Vögtle, F.; Reinhoudt, D. N.; Lehn, J.-M. Eds.; Elsevier Science Ltd., Pergamon: Elmsford, **1996**; Vol. 10, pp. 267-360. Collman, J. P.; Fu, L., *Acc. Chem. Res.* **1999**, *32*, 455.
- ¹³ For a review see: Collman, J. P.; Zhang, X.; Lee, V. J.; Uffelman, E. S.; Brauman J. I. *Science* **1993**, *261*, 1404.
- ¹⁴ Meunier, B.; de Carvalho, M.-E.; Bortolini, O.; Momenteau, M. *Inorg. Chem.* **1988**, *7*, 161.
- ¹⁵ Tabushi, I. *Coord. Chem. Rev.* **1988**, *86*, 1. Kuroda, Y.; Sera, T.; Ogoshi, H. *J. Am. Chem. Soc.* **1991**, *113*, 2793. Weber, L.; Hommel, R.; Behling, J.; Haufe, G.; Hennig, H. *J. Am. Chem. Soc.* **1994**, *116*, 2400. Breslow, R.; Huang, Y.; Zhang, X., *J. Am. Chem. Soc.*, **1997**, *119*, 4535.
- ¹⁶ Benson, D. R.; Valentekovich, R.; Diederich, F. *Angew. Chem. Int. Ed. Engl.* **1990**, *29*, 191; *Angew. Chem.* **1990**, *102*, 213. Benson, D. R.; Valentekovich, R.; Knobler, C. B.; Diederich, F. *Tetrahedron* **1991**, *47*, 2401. Benson, D. R.; Valentekovich, R.; Tam, S.-W.; Diederich F. *Helv. Chim. Acta* **1993**, *76*, 2034.
- ¹⁷ Razenberg, J. A. S. J.; Nolte, R. J. M.; Drenth, W. *Recl. Trav. Chim. Pays-Bas* **1986**, *105*, 103. Nolte, R. J. M.; Razenberg, J. A. S. J.; Schuurman, R. J. W. *J. Am. Chem. Soc.* **1986**, *108*, 2751.
- ¹⁸ Van der Made A. W.; Nolte R. J. M.; Drenth W. *Recl. Trav. Chim. Pays-Bas* **1990**, *9*, 537.
- ¹⁹ Van der Made, A. W.; Groot, P. M. F. C.; Nolte, R. J. M.; Drenth, W. *Recl. Trav. Chim. Pays-Bas* **1989**, *108*, 73.
- ²⁰ For a review about molecular clips see: Rowan, A. E.; Elemans, J. A. A. W.; Nolte R. J. M. *Acc. Chem. Res.* **1999**, *32*, 995.
- ²¹ Elemans, J. A. A. W.; Claase, M. B.; Aarts, P. P. M.; Rowan, A. E.; Schenning, A. P. H. J.; Nolte, R. J. M. *J. Org. Chem.* **1999**, *64*, 7009.
- ²² Rowan, A. E.; Aarts, P. P. M.; Koutstaal K. W. M. *Chem. Commun.* **1998**, 611.
- ²³ Dawson, J. H. *Science* **1988**, *240*, 433.
- ²⁴ Van der Made, A. W.; Nolte R. J. M. *J. Mol. Catal.* **1984**, *26*, 333.
- ²⁵ In general binding constants of pyridine and imidazole ligands with Zn(II) porphyrins are slightly higher than with Mn(III) porphyrins.
- ²⁶ For other examples of N-H $\cdots\pi$ interactions see: Adams, H.; Carver, F. J.; Hunter, C. A.; Osborne, N. J. *Chem. Commun.* **1996**, 2529. Nakanaga, T.; Ito, F. *J. Phys. Chem. A* **1999**, *103*, 5440.
- ²⁷ In addition to an NH $\cdots\pi$ interaction, also a C $\cdots\pi$ interaction is possible between the imidazole 4-proton and the other side-wall of the host, see Figure 12.3a.
- ²⁸ Unfortunately the **Im** proton signals in the spectrum of the complex were very broad, which prohibited their use as a diagnostic tool for the determination of the binding geometry of the ligand.
- ²⁹ Control experiments showed that rate enhancement exhibited by the **Mn1-Py** system is not caused by steric or electronic effects of the *meso*-phenyl 2-alkoxy groups of the porphyrin clip, see: Elemans, J. A. A. W.; Bijsterveld, E. J. A.; Rowan, A. E.; Nolte, R. J. M. *Chem. Commun.* **2000**, 2443.
- ³⁰ Campestrini, S.; Di Furia, F.; Ghiotto, P.; Novello, F.; Travaglini, C. *J. Mol. Catal.* **1996**, *105*, 17.
- ³¹ More than 4 portions of substrate were oxidized without an apparent decomposition of the catalyst. It then, however, became difficult to measure a reliable rate of conversion due to phase separation between the solvent and the epoxidation products.

- ³² Carnieri, N.; Harriman, A.; Porter, G.; Kalyanasundaram, K. *J. Chem. Soc. Dalton Trans.* **1982**, 1231. Speer, L. O.; Leone, A.; Maliyackel, A. C.; Otvos, J. W.; Calvin, M. *Inorg. Chem.* **1988**, 27, 2401.
- ³³ Van der Made, A. W. *Thesis*, Univeristy of Nijmegen, **1988**.
- ³⁴ Groves, J. T.; Stern, M. K. *J. Am. Chem. Soc.* **1988**, 110, 6828. Groves, J. T.; Lee, J.; Marla, S. S. *J. Am. Chem. Soc.* **1997**, 119, 6269.
- ³⁵ Arasasingham, R. D.; He, G.-X.; Bruice, T. C. *J. Am. Chem. Soc.* **1993**, 115, 7985.
- ³⁶ When $\ln[A]_t/[A]_0$ is plotted against t , a first order reaction will give a straight line with a slope equal to $-k_{\text{decay}}$. For all the decay processes studied, indeed a straight line was observed up to >75% conversion.
- ³⁷ It can be calculated that at the applied concentrations approximately 50 equivalents of **Py** are needed to achieve a 98+% binding of the ligand to **Mn1**, assuming a K_a -value around 10^5 M^{-1} . In the case of **MnTPP**, more equivalents of **Py** are needed due to the weak binding of the ligand when compared to **Mn1**. The increase in k_{decay} at higher concentrations of **Py** is attributed to the formation of hexacoordinate $[(\text{P})\text{Mn}(\text{III})(\text{Py})_2]^+$ species.
- ³⁸ Bijsterveld, E. J. A. Unpublished results.
- ³⁹ Gosling, P. A.; *Thesis*, University of Nijmegen, **1996**. Reek, J. N. H. *Thesis*, University of Nijmegen, **1996**.
- ⁴⁰ Elemans, J. A. A. W. Unpublished results.

Summary

During the last two decades molecular clips based on glycoluril have been successfully applied as receptors for small aromatic molecules in organic solvents. The recent discovery of the ability of these clips to form dimers, in which the cavity of one clip binds a side-wall of its neighbour and *vice-versa*, opened up the possibility to use them as self-recognizing building blocks for the construction of nanometer-sized assemblies. The major part of this thesis deals with the construction of such self-assembled architectures in water and in the solid state. Molecular clips which are derivatized at their convex side with benzoic acid, phenol and bipyridine functions have been prepared. The cavities of these clips are unaffected and remain available for the binding of a guest or another clip molecule. The functional groups at their convex side can be used for derivatization with, for example, metal centers, long aliphatic chains, and porphyrins.

The benzoic acid functionalized clips become water-soluble by deprotonation of the carboxylic acid groups. The self-association behaviour of the resulting benzoate salts in water appeared to be strongly dependent on the counter ions. In the case of sodium ions, the clips self-associate to form dimers exclusively, whereas in the case of ammonium ions nanometer-sized aggregates are obtained containing millions of molecules. The latter phenomenon is attributed to the fact that the ammonium ions are capable of forming hydrogen bonds between the benzoate groups, and act as a 'glue', holding the clips together to yield a large self-assembled structure.

The bipyridine-functionalized clips were used as ligands in ruthenium-bipyridine complexes. In water, these complexes were found to interact with each other in various geometries, e.g. head-to-head and head-to-tail, depending on the size and substitution pattern of the clip cavity. A naphthalene-walled derivative was shown to form highly defined rectangular aggregates, which under the appropriate conditions grew further, in a hierarchical self-assembly process, to give 'cigar-like' structures. By varying the temperature, the size and shape of the aggregates could be controlled. At high temperatures, the aggregates formed were more monodisperse in size than those formed at low temperatures, which can be attributed to a self-repair mechanism in the aggregate growth, reminiscent of self-repair processes occurring in Nature.

Benzoic acid and phenol functionalized clips were functionalized with long aliphatic chains, the idea being that upon dimerization of the cavities rod-like mesogens would be formed. Although the materials displayed characteristic features of liquid crystals, such as a smectic-like optical texture and malleability, differential scanning calorimetry and powder diffraction measurements revealed that they were not liquid crystals but 'plastic' crystalline materials arranged in a lamellar geometry. Strong interactions between the aromatic surfaces of the clip dimers, which prevent their movement with respect to each other, are the reason for this behaviour. The lamellae can be broken by the complexation of a strong binding guest, which disrupts the dimeric structure, and be restored by the complexation of a bifunctional guest containing a carboxylic acid substituent. Due to the latter substituent the host-guest complexes dimerize and the lamellar architecture is reformed.

Summary

The glycoluril clips were made truly liquid-crystalline by attaching branched (dendritic) instead of straight alkyl tails to the convex side of the cavities. The bulkiness of these tails prevents strong interactions between the clip headgroups. As a result, the clips were found to self-assemble into cubic liquid-crystalline phases, composed of supramolecular dendritic structures, which appeared to be capable of binding guests in their core without disrupting the liquid-crystalline phase.

A benzoic acid clip was synthesized containing a thiophene unit on its convex side. Upon polymerization of this unit, a conducting polymer with pendant clip side-chains was obtained. The goal of this research was to use the thiophene-clip polymer as a sensor for aromatic guest molecules. The polymer did not give a selective response, however, and this was attributed to the occurrence of non-selective van der Waals interactions between the polymer chain and the analyte molecules.

Two different approaches to construct porphyrin arrays based on molecular clips have been developed. The first involves the complexation of four clip molecules with long aliphatic tails to a central porphyrin ring which was functionalized with four dihydroxybenzene substituents. The complexes formed displayed plastic crystalline properties in the solid state, and gave aggregated structures in solution. These aggregates are stabilized by numerous interactions, e.g. between the guest porphyrins and between the clips that are complexed to them. A similar 1:4 complex was formed between the guest porphyrin and four clips that were functionalized at their convex side with two porphyrin molecules, resulting in the formation of a nonameric porphyrin array. The second approach involved the templated assembly of two molecular baskets, each provided with two zinc porphyrins, around a central tetrapyrrolyl porphyrin. The resulting 2:1 capsule complex contained two receptor cavities which are separated by a potential catalytically active central porphyrin.

In the final two chapters the synthesis, binding properties and catalytic behaviour of clips equipped with a porphyrin roof are described. Three different porphyrin clips were synthesized, which varied in the flexibility of the cavity side-walls or in the length of the spacer between the cavity and the porphyrin. The (zinc) porphyrin derivatives appeared to have a very high affinity for viologen guests and pyridine ligands. A manganese porphyrin clip was prepared which also displayed a very high affinity for the pyridine molecules. Due to the very strong binding of the pyridine axial ligand in the cavity of the manganese porphyrin clip was very active in the catalytic epoxidation of olefins. When instead of pyridine the bulky axial ligand 4-*t*-butylpyridine, which does not fit in the cavity of the clip, was used, the porphyrin catalyst appeared to be protected for oxidative degradation.

Samenvatting

Moleculaire clips afgeleid van glycoluril worden al zo'n 20 jaar gebruikt als receptoren voor aromatische gastmoleculen. Enkele jaren geleden werd ontdekt dat deze clips ook kunnen dimeriseren, waarbij de zijwand van één clipmolecuul wordt gebonden in de holte van zijn buurman en vice-versa. Deze eigenschap maakt het mogelijk om clips te gebruiken als bouwstenen, die via zelfherkenning kunnen aggregeren tot superstructuren van nanometer grootte. De studies die in dit proefschrift zijn beschreven omvatten voornamelijk de vorming van dergelijk superstructuren in water en in de vaste fase. De convexe zijden van de clipmoleculen zijn voorzien van substituenten, zoals benzoëzuur, fenol en bipyridine. Als gevolg hiervan blijven de holtes van deze clips onveranderd en dus beschikbaar voor de binding van gasten of het vormen van dimeren, terwijl de convexe zijden verder gefunctionaliseerd kunnen worden met bijvoorbeeld metaalcentra, lange alifatische staarten of porfyrimoleculen.

Clips gefunctionaliseerd met benzoëzuur-groepen konden wateroplosbaar worden gemaakt door deprotonering van de zuurfuncties. De zelfassociatie van de benzoaatzouten van de clips in water bleek sterk afhankelijk te zijn van het soort tegenionen. De natriumzouten bleken enkel dimeren te vormen, terwijl de ammoniumzouten goed-gedefinieerde nanostructuren gaven die waren opgebouwd uit miljoenen clipmoleculen. Dit verschil kan worden verklaard uit het feit dat de ammoniumionen waterstofbruggen kunnen vormen met de benzoaatgroepen en op deze manier de clips aan elkaar kunnen 'lijmen', terwijl de natriumionen dit niet kunnen.

De met bipyridine-groepen gefunctionaliseerde clips zijn gebruikt om complexen te vormen met ruthenium-ionen. Het bleek dat de verkregen complexen in water op verschillende manieren met elkaar kunnen binden, één en ander afhankelijk van de grootte van de holte en het substitutiepatroon van de wanden van de clip. Een clip met naftaleenwanden gaf in water zeer goed gedefinieerde rechthoekige aggregaten, die veelal verder aggregaerden, volgens een hiërarchisch groeiproces, in 'sigaarachtige' structuren. De grootte en de vorm van de rechthoekige aggregaten kon worden gecontroleerd door de temperatuur waarbij ze gemaakt worden te variëren. Bij relatief hoge temperatuur waren de gevormde aggregaten meer monodispers in grootte dan bij lage temperatuur, hetgeen verklaard kan worden door een hogere mate van zelfreparatie tijdens de aggregaatgroei, een proces dat ook wordt waargenomen in de natuur.

Glycoluril clips zijn gefunctionaliseerd met lange alifatische staarten met het idee dat de dimeren van deze moleculen zich zouden kunnen gedragen als typische staafvormige mesogenen en vloeibaar kristallijne fasen zouden kunnen vormen. Hoewel de materialen enkele karakteristieke mesogene eigenschappen vertoonden, zoals een smectische optische structuur en plasticiteit, toonden fysische metingen aan dat ze geen vloeibare kristallen waren maar kristallijne structuren, geordend in lamellaire patronen. Het optreden van sterke interacties tussen de

aromatische delen van de clips, die voorkomen dat de dimeren ten opzichte van elkaar kunnen bewegen, bleek hiervoor de oorzaak te zijn. De lamellaire patronen konden worden verbroken door gasten in de clips te binden, waardoor de vorming van dimeren onmogelijk werd. De lamellaire structuur kon weer hersteld worden door een gast met een carbonzuurfunctie toe te voegen. Met deze gast kunnen opnieuw dimere structuren ontstaan, waardoor de oorspronkelijke ordening terugkeert.

De clips konden echt vloeibaar kristallijn worden gemaakt door deze te functionaliseren met vertakte in plaats van rechte alkylstaarten. Door hun sterische omvang voorkwamen deze de aggregatie van de zijwanden van de clips. De clips bleken nu dendriem-achtige structuren te vormen, waarbij de holtes van de clips zich in het centrum van de dendrimeren bevinden en de alkylstaarten in de periferie. Deze supramoleculaire dendrimeren kunnen gasten binden zonder dat het vloeibaar kristallijne gedrag wordt verbroken.

Een clipverbinding met een thiofeengroep is gesynthetiseerd en gepolymeriseerd. Na polymerisatie werd een geleidend polymeer verkregen dat clip-zijketens bevatte. Het doel van dit onderzoek was het ontwikkelen van een sensormateriaal voor de detectie van aromatische verbindingen. Helaas bleek het polymeer geen selectieve respons op diverse aromatische moleculen te geven. Naast dihydroxybenzenen bleken ook dimethoxybenzenen - moleculen die niet in de holtes binden - een respons te vertonen.

Twee methoden zijn uitgewerkt om porfyriene-aggregaten te verkrijgen op basis van moleculaire clips. De eerste methode ging uit van de binding van vier clipmoleculen met lange alifatische staarten aan een centrale porfyriene die voorzien was van vier dihydroxybenzeensubstituenten. Complexen van deze porfyriene met de clips bleken in de vaste fase 'plastic' kristallen te vormen, en aggregaten in oplossing. Laatstgenoemde aggregaten werden gestabiliseerd door een samenspel van interacties tussen de componenten, zoals stapeling van de gastporfyriene en interacties tussen de clips die eraan zijn gecomplexeerd. Een analoog 1:4-complex kon worden gevormd door uit te gaan van het gastporfyriene en hier vier clips aan te binden die aan hun convexe zijde gefunctionaliseerd waren met twee porfyriene. Dit resulteerde in de vorming van porfyriene-nanameren. Een tweede methode om porfyriene-aggregaten te maken betrof de coordinatie van twee mandvormige clipmoleculen die gefunctionaliseerd waren met twee zinkporfyriene aan een centrale tetrapyridine porfyriene. Op deze manier werd een capsule-achtig complex verkregen dat twee receptorholtes bevatte die gescheiden worden door de centrale porfyriene.

In de laatste twee hoofdstukken van dit proefschrift wordt de synthese, het bindingsgedrag en de katalytische eigenschappen van clips die gefunctionaliseerd zijn met een porfyriene-'dak' beschreven. Drie porfyrieneclips werden gesynthetiseerd die verschilden in de flexibiliteit van de wanden van de holte en de lengte van de bindingen tussen de clip en het porfyriene. De (zink) porfyrieneclips bleken zeer sterk viologen en pyridineliganden te binden. Vanwege de zeer sterke binding van pyridine in de holte van een mangaanporfyrieneclip bleek de laatstgenoemde verbinding te worden geactiveerd als katalysator voor de epoxidatie van olefines. Wanneer, in plaats van pyridine, 4-t-butylpyridine werd gebruikt - een ligand dat niet in de holte van de clip past - kon de porfyrienekatalysator beschermd worden tegen oxidatieve ontleding.

List of Publications

The crystal and molecular structure of a clip-shaped molecule with two different side-walls

W. P. Bosman, J. M. M.; Smits, R. de Gelder, J. N. H. Reek, J. A. A. W. Elemans, R. J. M. Nolte, *J. Chem. Cryst.* **1997**, *27*, 75–79.

Synthesis, conformational analysis, and binding properties of molecular clips with two different side-walls

J. N. H. Reek, J. A. A. W. Elemans, R. J. M. Nolte, *J. Org. Chem.* **1997**, *62*, 2234–2243.

Binding features of molecular clips. Separation of the effects of hydrogen bonding and π - π interactions

J. N. H. Reek, A. H. Priem, H. Engelkamp, A. E. Rowan, J. A. A. W. Elemans, R. J. M. Nolte, *J. Am. Chem. Soc.* **1997**, *119*, 9956–9965.

Conformational behaviour and binding properties of naphthalene-walled clips

J. N. H. Reek, H. Engelkamp, A. E. Rowan, J. A. A. W. Elemans, R. J. M. Nolte, *Chem Eur. J.* **1998**, *4*, 716–722.

Bipyridine functionalized molecular clips. Self-assembly of their ruthenium complexes in water

J. A. A. W. Elemans, R. de Gelder, A. E. Rowan, R. J. M. Nolte, *Chem. Commun.* **1998**, 1553–1554.

Porphyrin clips derived from diphenylglycoluril. Synthesis, conformational analysis and binding properties

J. A. A. W. Elemans, M. B. Claase, P. P. M. Aarts, A. E. Rowan, A. P. H. J. Schenning, R. J. M. Nolte, *J. Org. Chem.* **1999**, *64*, 7009–7016.

Molecular and supramolecular objects from glycoluril

A. E. Rowan, J. A. A. W. Elemans, R. J. M. Nolte, *Acc. Chem. Res.* **1999**, *32*, 995–1006.

Host-guest complexes with tunable solid-state properties

S. J. Holder, J. A. A. W. Elemans, J. Barberá, A. E. Rowan, R. J. M. Nolte, *Chem. Commun.* **2000**, 355–356.

Self-assembled architectures from glycoluril

J. A. A. W. Elemans, A. E. Rowan, R. J. M. Nolte, *Ind. Eng. Chem. Res.* **2000**, *39*, 3419–3428.

A host-guest epoxidation catalyst with enhanced activity and stability

J. A. A. W. Elemans, E. J. A. Bijsterveld, A. E. Rowan, R. J. M. Nolte, *Chem. Commun.* **2000**, 2443–2444.

List of publications

Lamellar organic thin films through self-assembly and molecular recognition

S. J. Holder, J. A. A. W. Elemans, J. J. J. M. Donners, M. J. Boerakker, R. de Gelder, J. Barberá, A. E. Rowan, R. J. M. Nolte, *J. Org. Chem.* **2001**, *66*, 391–399.

Self-association and self-assembly of molecular clips in water

J. A. A. W. Elemans, R. R. J. Slangen, A. E. Rowan, R. J. M. Nolte, *J. Incl. Phenom. Macrocyclic Chem.* **2001**, in press.

Hierarchical self-assembly of rigid metallohosts. Towards discrete nanostructures

J. A. A. W. Elemans, A. E. Rowan, R. J. M. Nolte, *J. Am. Chem. Soc.*, submitted.

Self-association and self-assembly of molecular clips in solution and in the solid state

J. N. H. Reek, A. E. Rowan, J. A. A. W. Elemans, R. de Gelder, P. T. Beurskens, R. J. M. Nolte, Manuscript in preparation.

A porphyrin cavity with induced-fit binding properties

J. A. A. W. Elemans, A. E. Rowan, R. J. M. Nolte, Manuscript in preparation.

Controlled self-assembly of rigid facial amphiphiles

J. A. A. W. Elemans, R. R. J. Slangen, R. de Gelder, M. C. Feiters, A. E. Rowan, R. J. M. Nolte, Manuscript in preparation.

Supramolecular dendrimers with molecular recognition properties

J. A. A. W. Elemans, M. J. Boerakker, W.-D. Cho, A. E. Rowan, V. Percec, R. J. M. Nolte, Manuscript in preparation.

A self-assembled porphyrin capsule

J. A. A. W. Elemans, V. F. Slagt, A. E. Rowan, R. J. M. Nolte, Manuscript in preparation.

Host-guest multiporphyrin architectures

J. A. A. W. Elemans, A. E. Rowan, R. J. M. Nolte, Manuscript in preparation.

Bedankt...

Op deze laatste en meestgelezen pagina's wil ik de mensen bedanken die onmisbaar zijn geweest bij de totstandkoming van dit proefschrift. Naast de overeenkomst met een eigenschap van de moleculen waar dit boekje over gaat, symboliseert de handdruk op de kaft ook de dank voor al de hulp die ik in de jaren gehad hebt.

Allereerst wil ik 'de baas', mijn promotor Prof. Roeland Nolte, bedanken. Beste Roeland, de vrijheid die ik van jou in mijn werk kreeg is uniek en heb ik altijd ontzettend kunnen waarderen. Voor de problemen die ik tegen kwam, of het nu op het chemische of het persoonlijke vlak was, stond je deur altijd open en wist je meestal een voor de hand liggende oplossing te vinden. Daarnaast koppelde je het uiterlijk van mijn vreemde aggregaatjes aan soms dubieuze equivalenten uit het 'alledaagse leven'. Ook je vrouw Helma wil ik bedanken voor de altijd weer gezellige babbeltjes.

Ik heb er nooit een dag spijt van gehad dat ik Dr. Alan Rowan als copromotor heb gevraagd. Alan, jouw inbreng in dit proefschrift is van onschatbare waarde geweest. Na elk inspirerend half uurtje brainstormen over chemistry (en over schapen) had ik weer een maand of drie werk dat volgens jou in "laten we zeg...in two weekjes from now" wel af kon zijn. Many thanks, en ik hoop dat we er nog het nodige vervolg aan kunnen geven in de toekomst.

Ik heb het geluk gehad dat ik in een tijd gepromoveerd ben dat er nog voldoende studenten waren die een stage bij ons op de afdeling kwamen lopen. Maar liefst zes daarvan durfden het aan dat onder mijn 'deskundige leiding' te komen doen.

Na een jaar zelf prutsten stapte Vincent 'Chesteaux' Slagt de aiokamer binnen om een hoofdvakje te komen doen. Zo'n 365 paarse kolommen later was het doelmolecuul bijna daar maar helaas nét niet. Toch heeft jouw noeste arbeid het nodige inzicht verschaft in porfmandchemie, zodat het gewenste resultaat er nu alsnog ligt. Je imitaties van 2-Unlimited-Ray en de wens om net zulk haar te krijgen als Tony Little zal ik niet snel vergeten.

Een paar maanden later kreeg Vincent gezelschap van Ralf Slangen. Ralf, razendsnel synthetiseerde jij een hele batterij aan water-oplosbare clips bij elkaar, waarop je vervolgens ook een scala aan meetapparatuur los liet. Ik had er geen omkijken naar en aan het eind van elke dag lag er weer een stapeltje mooie EM-foto's klaar. Uiteraard heb ik het ook bijzonder gewaardeerd dat je gedurende je stage je haar steeds korter knipte. Daarnaast bedacht je samen met je labgenoot de wildste ideeën, al wacht ik er nog steeds op wanneer de 'moleculaire tractor' nu eens klaar is voor het land.

Menno Claase, jou kende ik al uit mijn grijze studentenverleden en ik was dan ook blij dat je na je ziekte nog een half jaartje wilde komen meten aan een molecuul wat je eerder al gemaakt had, en wat ik gelukkig nog uit een kastje heb getrokken. Dat je vervolgens zo'n 50 titraties deed met anderhalve korrel materiaal mag een voorbeeld zijn voor alle organisch chemici, aangezien die altijd zo graag willen kunnen 'scheppen'.

Jack Donners kende ik ook al en ik wist dat er in ieder geval een brok luidruchtig enthousiasme in huis kwam. Jij zette staarten aan de clips, maar de teleurstelling was groot toen bleek dat de moleculen niet vloeibaar kristallijn waren. Dat dat geen probleem hoeft te zijn bewijst Hoofdstuk 5 en een mooie publicatie. Als het over de chemie ging stond de zuurkast-ruit razendsnel vol met

Bedankt...

ideeën, te veel om uit te voeren. Alleen het destilleren van pyrrool, styreen, het demethyleren van porfo's, en het halen van een vat mét stikstof leverde nogal eens problemen op.

Mark Boerakker had een jaar voordat hij begon al een hangplek op ons lab bij zijn 'vrienden', en na wat onzinpraat van mijn kant was hij al snel gestrikt om échte 'liquid-clippalline mysterials' te komen maken. Jouw stage kan je het best omschrijven als een bijzonder efficiënte: na 4 maanden waren de moleculen gemaakt, 4 maanden later waren de metingen klaar, en daarna vertrok je ook nog eens 2 maanden naar Cleveland om in de groep van Prof. Percec de puntjes op de i te gaan zetten.

Claudia Bokel was de laatste uit de rij. Alhoewel je onderzoek niet altijd even vlot verliep, neem ik toch mijn petje af voor het feit dat je een scheikundestudie durft te combineren met olympische aspiraties in de schermsport. Ook is mijn mening over onze oosterburen door jou wat genuanceerd. Maar ik verwacht wel dat je over 3 jaar in Athene, als een echt 'Siegertuuup', even wat eremetaal aan de degen gaat prikken.

Patrick Aarts, alhoewel je niet voor mij hebt gewerkt, heb ik toch een groot deel van je fraaie resultaten mogen verwerken in Hoofdstuk 9 en in een publicatie. Maar goed dat we dat rode bandje op de kolom op die vrijdagmiddag (!) in '95 nog hebben opgevangen, toen jij al in de Limbo-express op weg naar huis was. Tenslotte wil ik Frank van der Reijden, (opnieuw) Vincent Slagt, Jurry Hannink, Joost van der Rijt en Pieter de Witte bedanken voor het schrijven van hoofdvakscripties, die mij het nodige literatuur-zoekwerk bespaarden.

Als meubelstuk van de afdeling heb ik een groot aantal collega's zien gaan en komen. Toen ik begon liep de 'oude garde' er nog rond: Patricia, Hanny, Appie, Joost (ex-clippappa), René, Rudi, Nico, Gerben, Fokke, en Bert. Daarna kwam de lichte die de rest van mijn tijd de aiokamer op practicumzaal VII met me gedeeld heeft: Rob, Jantien, Edward (sterke partner in epoxidatie), Vera (7 keer), Gerald (starkeprietske-twarre), Marga (BMW), Johan (Schwulert de Stevige), en Ruud ("dát beweert ik"). 'Die van boven', Peter (schreeuwlillekerd), Hans, Bastienne, Bart en Femke, en 'die van de overkant', Pieter (boem), Jurry (plaatjesmaker), Jeroen (ex-clipbroertje), Aurélie, en Dennis (paranimf die iets onafhankelijk schijnt te kunnen). En 'de buitenlanders', Simon Webb, Bea ("ainonofing"), Cristina, Joan, Kelly, Isabelle, Palli, Peter en Mariangela. Verder alle collega's van de 3e. Hans ("op 'n gegeven moment") en Wim (met sigaar) maakten als echte mannen-met-baarden met hun sterke verhalen menig koffiepauze tot een feest. Tenslotte alle studenten die het lab in de jaren bevolkt hebben. Iedereen bedankt voor de vele retraites, labuitstapjes, volleybalpartijtjes (auw!), (foute-) film, bowl-, snooker-, en brotj-swarma-bij-Achmat-avondjes, en voor het feit dat ik mijn dagen kon kleuren door lekker op jullie te kankeren en jullie in de maling te nemen. Bij deze mijn welgemeende excuses daarvoor, krijg ik nou een lief en aardig liedje?

Speciaal woordje van dank voor twee mannen van het eerste uur. Alexander Kros, mannetje-met-het-kastanjebruine haar (sorry maar het is echt roodblond), al in '93 knoeiden we samen aan clips, later in de vorm van vrijdagmiddagreacties onder de dekmantel van 'De Boeren'. Verder hebben de jaarlijkse Bossche Bollen, je ietwat dubieuze omgang met je studenten, en die avondse rode ouwemannenkoekbliktank een onuitwisbare indruk achtergelaten. Als de dag van gisteren weet ik nog dat Bas Kokke in '94 het lab binnenstapte als een verlegen knulletje. Nooit heeft schijn meer bedrogen! Het LBPM-gehalte van foute films kon niet hoog genoeg zijn, maar ik ben wel blij dat we elkaars voorliefde voor (Piet Bambergen)-humor en goede muziek (zoals Beegees, Heino en Dré) koden delen. Wie anders als paranimf!

I have been very lucky that Dr. Simon Holder has worked with me in the liquid-crystalline clip project. Dear Simon, many thanks for all the work, and for making me understand something about materials chemistry. Many thanks also to Wook-Dong Cho and Prof. Virgil Percec (University of Pennsylvania, USA), for their collaboration in the work of the dendrimer clips. I would like to acknowledge Prof. Joaquín Barberá (University of Zaragoza, Spain) for carrying out several powder diffraction measurements.

Op alle verdiepingen van het UL was ik wel eens lastig, en iedereen die me daar geholpen heeft wil ik graag dankzeggen. Soms kwam ik nog wel eens op het 'oude nest' van 'anorg' waar bijgekletst kon worden met Jan, Reinout, en Bas, en niet te vergeten Paul, met wie het altijd fijn onzin uitkramen was in ongeschoren toestand achter een onwillige NMR. Dr. Martin Feiters, bedankt voor je belangstelling en je hulp met de poedermetingen. Prof. Vlieg, Dr. Meekes en Dr. van Enkevort van de afdeling Vastestofchemie wil ik bedanken voor het brainstormen over de aggregaatgroei, en Dr. Peter Christianen, Marius Boamfa, en Igor Shklyarevskiy van het Magnetenlab voor hun poging de 'sigaren' uit te lijnen.

Geen proefschrift zonder analytische ondersteuning. Chris Kroon stond altijd klaar om me van chemicaliën te voorzien, en Wim van Luyn zorgde voor de bestellingen daarvan. Jos Joordens was behulpzaam als ik weer eens een NMR had laten vastlopen, om hem een jasje aan te trekken, of op het laatste moment 'even' een poster uit te draaien. René Aben, dank voor de hulp met de hoge druk. Daarnaast wil ik graag Ad Swolfs (NMR), Peter van Galen (FABjes), Pieter van der Meer (computers) en Helene Amatdjais-Groenen (EAs) bedanken. Joost van Dongen (TUE) en Roel Fokkens (UvA) wil ik bedanken voor electrospray en MALDI-TOF metingen. Huub Geurts heeft mij ingewijd in de electronenmicroscopie en stond altijd klaar ('service met een S'). Met Dr. René de Gelder van de afdeling kristallografie heb ik altijd plezierig samengewerkt, en ook in dit boekje zijn weer enkele mooie kristalstructuren terug te vinden. Sandra Tijdink en vooral Désirée van der Weij waren onmisbaar met hun secretariële ondersteuning.

Ik ben altijd blij geweest dat als ik de deur van het lab achter me dicht trok, die 'andere' wereld er ook nog was. Alhoewel men soms niet helemaal beseft dat wat ik deed al lang geen 'school' meer was ("maar wanneer studeer je nou af?"), waardeer ik toch de interesse van mijn familie, vrienden en kennissen, die er, en dat is het allerbelangrijkste, op allerlei manieren voor hebben gezorgd dat mijn kop niet altijd naar chemie stond en ervoor gezorgd hebben dat 'thuis' ook thuis was.

Mijn ouders hebben me de kans gegeven en gestimuleerd om verder te leren en daar ben ik hen uitermate dankbaar voor. Helaas heeft mijn vader deze voltooiing niet meer kunnen meemaken. Mam, jou bedank ik voor 'het-er-altijd-zijn' en dat je mij geleerd hebt om in moeilijke tijden de zaken te kunnen relativeren. Uiteraard is dit proefschrift aan jullie opgedragen.

Curriculum Vitae

Hans Elemans werd geboren in Nijmegen op 5 juli 1970. Na het behalen van het diploma Gymnasium- β aan het Elshof College te Nijmegen werd in 1988 begonnen aan een studie Scheikunde aan de Katholieke Universiteit Nijmegen, alwaar in 1989 het propaedeutisch examen werd afgelegd. In 1994 werd het doctoraaldiploma behaald, met als uitgebreide hoofdrichting Fysisch Organische Chemie (Prof. Dr. R.J.M. Nolte), en als uitgebreide nevenrichting Anorganische Chemie (Prof. Dr. Ir. J.J. Steggerda). Na te hebben voldaan aan zijn verplichtingen voor het Ministerie van Defensie was de auteur van 1995-1999 in dienst als AIO aan de Katholieke Universiteit Nijmegen. Gedurende deze periode heeft hij onder leiding van Prof. Dr. R.J.M. Nolte en Dr. A.E. Rowan het in dit proefschrift beschreven onderzoek verricht. Sinds 1 januari 2001 is hij in dienst van het NSR-RIM instituut als postdoctoraal onderzoeker in een verbindingsfunctie tussen de afdelingen Experimentele Vastestoffysica en Organische Chemie.